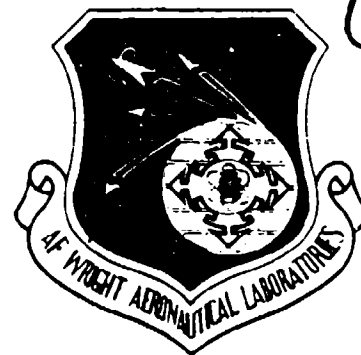


AFWAL-TR-88-4146

**DTIC FILE COPY**  
**ADVANCED CUMULATIVE DAMAGE  
MODELING**



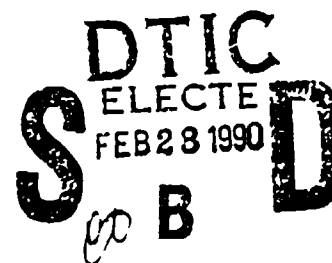
R.H. VanStone, O.C. Gooden, and D.D. Krueger

GE Aircraft Engines  
Advanced Technology Operation  
Cincinnati, Ohio 45215

September 1988

Final Report for Period December 1984 - September 1986

Approved for Public Release; Distribution is Unlimited



MATERIALS LABORATORY  
AIR FORCE WRIGHT AERONAUTICAL LABORATORIES  
AIR FORCE SYSTEMS COMMAND  
WRIGHT-PATTERSON AIR FORCE BASE, OHIO 45433-6533

90 02 26 140

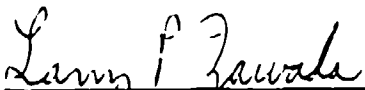
AD-A218 555

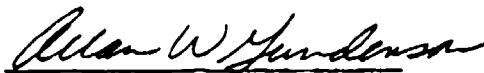
## NOTICE

WHEN GOVERNMENT DRAWINGS, SPECIFICATIONS, OR OTHER DATA ARE USED FOR ANY PURPOSE OTHER THAN IN CONNECTION WITH A DEFINITELY GOVERNMENT-RELATED PROCUREMENT, THE UNITED STATES GOVERNMENT INCURS NO RESPONSIBILITY OR ANY OBLIGATION WHATSOEVER. THE FACT THAT THE GOVERNMENT MAY HAVE FORMULATED OR IN ANY WAY SUPPLIED THE SAID DRAWINGS, SPECIFICATIONS, OR OTHER DATA, IS NOT TO BE REGARDED BY IMPLICATION, OR OTHERWISE IN ANY MANNER CONSTRUED, AS LICENSING THE HOLDER, OR ANY OTHER PERSON OR CORPORATION; OR AS CONVEYING ANY RIGHTS OR PERMISSION TO MANUFACTURE, USE, OR SELL ANY PATENTED INVENTION THAT MAY IN ANY WAY BE RELATED THERETO.

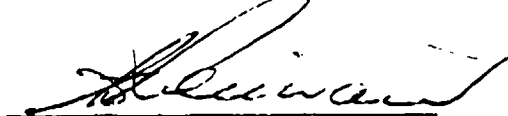
THIS REPORT HAS BEEN REVIEWED BY THE OFFICE OF PUBLIC AFFAIRS (ASD/PA) AND IS RELEASABLE TO THE NATIONAL TECHNICAL INFORMATION SERVICE (NTIS). AT NTIS IT WILL BE AVAILABLE TO THE GENERAL PUBLIC INCLUDING FOREIGN NATIONS.

THIS TECHNICAL REPORT HAS BEEN REVIEWED AND IS APPROVED FOR PUBLICATION.

  
LARRY E. ZAWADA, Project Engr  
Materials Research Engineer  
Materials Behavior Branch

  
ALLAN W. GUNDERSON  
Tech Area Manager  
Materials Behavior Branch

FOR THE COMMANDER

  
WALTER H. REIMANN, Branch Chief  
Materials Behavior Branch  
Metals and Ceramics Division

IF YOUR ADDRESS HAS CHANGED, IF YOU WISH TO BE REMOVED FROM OUR MAILING LIST, OR IF THE ADDRESSEE IS NO LONGER EMPLOYED BY YOUR ORGANIZATION PLEASE NOTIFY WRDC/MLLN, WRIGHT-PATTERSON AFB, OH 45433-6533 TO HELP MAINTAIN A CURRENT MAILING LIST.

COPIES OF THIS REPORT SHOULD NOT BE RETURNED UNLESS RETURN IS REQUIRED BY SECURITY CONSIDERATIONS, CONTRACTUAL OBLIGATIONS, OR NOTICE ON A SPECIFIC DOCUMENT.

UNCLASSIFIED

SECURITY CLASSIFICATION OF THIS PAGE

## REPORT DOCUMENTATION PAGE

1. REPORT SECURITY CLASSIFICATION <b>Unclassified</b>			1b. RESTRICTIVE MARKINGS <b>None</b>	
2a. SECURITY CLASSIFICATION AUTHORITY			3. DISTRIBUTION/AVAILABILITY OF REPORT <b>Approved for public release; distribution unlimited.</b>	
2b. DECLASSIFICATION/DOWNGRADING SCHEDULE				
4. PERFORMING ORGANIZATION REPORT NUMBER(S)			5. MONITORING ORGANIZATION REPORT NUMBER(S) <b>AFWAL-TR-88-4146</b>	
6a. NAME OF PERFORMING ORGANIZATION <b>GE Aircraft Engines Advanced Technology Operation</b>		6b. OFFICE SYMBOL (if applicable)	7a. NAME OF MONITORING ORGANIZATION <b>Air Force Wright Aeronautical Laboratories Materials Laboratory (AFWAL/MLLN)</b>	
6c. ADDRESS (City, State, and Zip Code) <b>1 Neumann Way, Cincinnati, Ohio 45215</b>			7b. ADDRESS (City, State, and Zip Code) <b>Wright-Patterson Air Force Base Ohio 45433-6533</b>	
8a. NAME OF FUNDING/SPONSORING ORGANIZATION <b>Wright Aeronautical Laboratories</b>		8b. OFFICE SYMBOL (if applicable) <b>AFWAL/MLLN</b>	9. PROCUREMENT INSTRUMENT IDENTIFICATION NUMBER <b>F33615-84-C-5032</b>	
8c. ADDRESS (City, State, and Zip Code) <b>Air Force Systems Command Wright-Patterson AFB, OH 45433-6523</b>			10. SOURCE OF FUNDING NUMBERS	
			PROGRAM ELEMENT NO. <b>62102F</b>	PROJECT NO. <b>2420</b>
11. Title (Include Security Classification) <b>Advanced Cumulative Damage Modeling</b>				
12. PERSONAL AUTHOR(S) <b>R.H. VanStone, O.C. Gooden, and D.D. Krueger</b>				
13a. TYPE OF REPORT <b>Final</b>		13b. TIME COVERED <b>FROM 12-13-84 TO 9/31/86</b>		14. DATE OF REPORT (Yr., Mo., Day) <b>September 1988</b>
15. PAGE COUNT <b>345</b>				
16. SUPPLEMENTARY NOTATION <b>This is the Final Report for Contract F33615-84-C-5032 and summarizes work performed between 13 December 1984 and 31 September 1986</b>				
17. COSATI CODES			18. SUBJECT TERMS (Continue on reverse if necessary and identify by block number)	
FIELD	GROUP	SUB. GR.	<b>Fatigue, life prediction, time-dependent, fatigue crack growth, cycle-dependent fatigue, interpolative model, fracture mechanics, superposition model</b>	
11	06			
13	13			
19. ABSTRACT (Continue on reverse if necessary by block number) <b>Crack growth in the near-threshold and Paris regimes (Regions I and II) were measured in single edge notch specimens of Rene' 95 and Alloy 718 as a function of test temperature, R-ratio, hold time, frequency, and overpeak ratio. The results obtained at 649°C were modeled using an interpolation and interpolation + superposition model. Both models accurately predicted the time dependent crack growth of these materials. The interpolation + superposition model appeared to be a better model because the interpolation model made unrealistic predictions outside the range of data obtained in this investigation. The overpeak retardation was predicted using a modified Willenborg model. A residual life computer code (ACDCYCLE), which can be run on an IBM personal computer, was written to make predictions of crack growth rates and residual lives. Fractography and several other types of crack growth tests, including tests in a high vacuum environment, were performed and showed that time</b>				
20. DISTRIBUTION/AVAILABILITY OF ABSTRACT UNCLASSIFIED/UNLIMITED <input checked="" type="checkbox"/> SAME AS RPT <input type="checkbox"/> DTIC USERS <input type="checkbox"/>			21. ABSTRACT SECURITY CLASSIFICATION <b>Unclassified</b>	
22a. NAME OF RESPONSIBLE INDIVIDUAL <b>Larry P. Zawada</b>			22b. TELEPHONE NUMBER (Include Area Code) <b>(513) 255-1352</b>	
			22c. OFFICE SYMBOL <b>WRDC/MLLN</b>	

**UNCLASSIFIED**

SECURITY CLASSIFICATION OF THIS PAGE

19. Abstract (Continued)

dependent crack growth in nickel-base superalloys is highly dependent on a complex interaction between creep, fatigue, and environment.

**UNCLASSIFIED**

SECURITY CLASSIFICATION OF THIS PAGE



### ACKNOWLEDGEMENTS

The authors of this report would like to acknowledge the assistance of K.C. Cooper, E.D. Deaton, T.E. Wallrauch, and R.C. Volmer for instrumenting and performing the crack growth tests in this investigation. We also deeply appreciated the support and helpful suggestions of our management, J.H. Laflen and A.M. Johnson. R.B. Ashbrook, M.J. Cannon, L. Piazza, and B. Shivar were instrumental in performing the microscopy during the mechanisms studies. We are also indebted to M.F. Henry of GE Corporate Research and Development, who developed the modification of the potential drop system used in this investigation and provided us with a prototype version. We also appreciated the many helpful comments provided by T. Nicholas of the Air Force Materials Laboratory.



Accession For	
NTIS GRA&I	<input checked="checked" type="checkbox"/>
DTIC TAB	<input type="checkbox"/>
Unannounced	<input type="checkbox"/>
Justification	
By	
Distribution/	
Availability Codes	
Dist	Avail and/or Special
A-1	

## TABLE OF CONTENTS

<u>Section</u>	<u>Page</u>
1.0 INTRODUCTION	1
2.0 LITERATURE REVIEW	5
2.1 Creep-Fatigue-Environment Interactions	5
2.1.1 Crack Growth	6
2.2 Crack Growth Curves	7
2.2.1 Paris Law	8
2.2.2 Sinh Curve	10
2.2.3 Sigmoidal Curve	12
2.3 Time-dependent Crack Growth Models	15
2.3.1 Interpolative Models	15
2.3.2 Superposition Models	17
2.3.3 Retardation Models	21
3.0 MISSION ANALYSIS	25
4.0 MATERIALS AND EXPERIMENTAL TECHNIQUES	47
4.1 Materials	47
4.1.1 Rene'95	47
4.1.2 Alloy 718	50
4.1 Single Edge Notch Specimen	56
4.2 Test Specimen Machining And Orientation	58
4.3 Potential Drop Test Method	59
4.4 Test Description And Data Analysis	59
4.4.1 Threshold Tests	61
4.4.2 Constant $\Delta K$ Tests	65
4.5 Vacuum Test Method	67

<u>Section</u>	<u>Page</u>
5.0 EXPERIMENTAL RESULTS	71
5.1 Rene'95 Crack Growth Results	71
5.1.1 Rene'95 Constant $\Delta K$ Tests	71
5.1.2 Rene'95 Threshold Tests	90
5.1.3 Rene'95 Static Crack Growth	110
5.1.4 Rene'95 Retardation Tests	113
5.2 Alloy 718 Crack Growth Results	127
5.2.1 Alloy 718 Constant $\Delta K$ Tests	127
5.2.2 Alloy 718 Threshold Tests	131
5.2.3 Alloy 718 Static Crack Growth	143
5.2.4 Alloy 718 Retardation Tests	143
6.0 MECHANISM STUDIES	153
6.1 Approach of Mechanism Studies	153
6.1.1 Fractographic Examination	153
6.1.2 Vacuum Tests	153
6.1.3 Metallographic Sectioning Experiments	154
6.1.4 Characterization of Crack Tip Damage Zones	154
6.2 Fractography of Specimens Testee in Air	154
6.2.1 Rene'95: Region II Observations	155
6.2.2 Rene'95: Region I Observations	167
6.2.3 Rene'95: Retardation Test Observations	167
6.2.4 Alloy 718: Region II Hold Time Observations	170
6.3 Vacuum Results	170
6.3.1 Rene'95 Vacuum crack Growth Results	175
6.3.2 Alloy 718 Vacuum crack Growth Results	180
6.3.3 Rene'95 Vacuum Test Fractographic Observations	180
6.3.4 Alloy 718 Vacuum Test Fractographic Observations	184
6.3.5 Discussion of Vacuum Results	188
6.4 Metallographic Sectioning Studies	192
6.5 Mechanism testing program	195
6.6 Discussion	203

<u>Section</u>	<u>Page</u>
7.0 CRACK GROWTH MODELING	200
7.1 Crack Growth Models	207
7.1.1 Interpolation Model Of Threshold Values	208
7.1.2 Interpolation Model	208
7.1.3 Superposition Model	208
7.1.4 Retardation Model	210
7.2 Advanced Cumulative Damage Cycle (ACDCYCLE) Computer Code	221
7.2.1 ACDCYCLE Options	224
7.2.2 ACDCYCLE Input and Output	225
7.3.3 Residual Life Calculations	227
7.3 Modeling of Rene'95 at 649°C	230
7.3.1 Rene'95 Threshold model	232
7.3.2 Rene'95 Interpolation Model	232
7.3.3 Rene'95 Interpolation + Superposition Model	236
7.3.4 Comparison of Predicted and Measured Crack Growth	239
7.3.5 Retardation model	254
7.4 Modeling of Alloy 718 At 649°C	264
7.4.1 Alloy 718 Threshold Model	266
7.4.2 Alloy 718 Interpolation + Superposition Model	266
7.4.3 Comparison of Predicted and Measured Crack Growth	274
7.4.4 Retardation Model	276
8.0 SUMMARY AND CONCLUSIONS	285
9.0 REFERENCES	289
APPENDIX A: STATISTICAL ANALYSIS OF RENE'95 CONSTANT $\Delta K$ DATA	297
APPENDIX B: STATISTICAL ANALYSIS OF RENE'95 OVERPEAK HOLD TIME DATA	303
APPENDIX C: STATISTICAL ANALYSIS OF ALLOY 718 CONSTANT $\Delta K$ DATA	313
APPENDIX D: STATISTICAL ANALYSIS OF ALLOY 718 OVERPEAK HOLD TIME DATA	317

## LIST OF FIGURES

<u>Figure</u>	<u>Caption</u>	<u>Page</u>
2.1	Schematic drawing of fatigue crack growth curve showing Regions I, II, and III.	9
2.2	Schematic drawing of sinh crack growth curve.	11
2.3	Schematic drawing of sigmoidal or Knaus crack growth curve.	13
2.4	Variation in $t_{eff} / t$ with R-ratio and Paris exponent (n) for loading ramps as predicted by the linear superposition model.	20
3.1	Example of a mission with frequent changes in rotor speed.	26
3.2	Example of a mission with changes in rotor speed and cruise conditions.	27
3.3	Example of a mission consisting primarily of cruise conditions.	28
3.4	Variation of normalized stress with time for (a) actual mission and (b) simplified mission.	30
3.5	Variation of temperature with time for (a) actual mission and (b) simplified mission.	31
3.6	Variation of stress ratio with temperature for eighteen missions.	34
3.7	Variation of stress ratio of ramp segments with temperature.	35

<u>Figure</u>	<u>Caption</u>	<u>Page</u>
3.8	Variation of (a) ramp time with temperature and (b) stress ratio with ramp time for individual segments of eighteen missions.	36
3.9	Variation of (a) ramp time with temperature and (b) stress ratio with ramp time for increasing load segments of eighteen missions.	38
3.10	Variation of hold time with temperature for eighteen missions.	39
3.11	Variation of hold times in excess of 10 seconds and 510°C with temperature.	40
3.12	Variation of underpeak ratio (stress ratio) of hold times with temperature greater than 510°C with temperature.	41
3.13	Variation of overpeak ratios of hold times with temperatures in excess of 510°C with temperature	43
3.14	Variation in overpeak ratio with (a) temperature and (b) stress ratio for loading and unloading segments ( $R < 0.9$ ).	44
4.1	Microstructure of Rene'95 forging as shown with (a) low magnification optical micrograph, (b) high magnification optical micrograph, and (c) TEM replica micrograph.	51
4.2	Optical micrographs of Alloy 718 plate at (a) low and (b) high magnifications. The rolling direction is displayed horizontally and the plate thickness direction is shown vertically.	54

<u>Figure</u>	<u>Caption</u>	<u>Page</u>
4.3	Optical micrographs of Alloy 718 plate at (a) low and (b) high magnifications. The plate width direction is displayed horizontally and the plate thickness direction is shown vertically.	55
4.4	Buttonhead single edge notch (SEN) specimen	57
4.5	Schematic diagram of SEN specimen DC potential drop test apparatus.	60
4.6	Typical K-history for a threshold crack growth test.	62
4.7	Influence of K-shed rate on near-threshold crack growth rates measured in Rene'95 specimens cycled at 649°C and R=0 with a 300 second hold time.	64
4.8	Typical variation of $K_{max}$ and frequency in a $\Delta K$ -Controlled frequency test	66
4.9	Influence of test control mode on Region II crack growth rates measured in Rene'95 specimens cycled at R=0 with a 300 second hold time.	68
5.1	Variation of (a) $K_{max}$ with crack length and (b) crack length with cycles during constant $\Delta K$ hold time test on Rene'95 at 649°C and R=0.	74
5.2	Results of the statistical analysis of constant $\Delta K$ hold time test on Rene'95 at 649°C with R=0.	75
5.3	Results of the constant $\Delta K$ hold time test on Rene'95 at 649°C with R=0.	77

<u>Figure</u>	<u>Caption</u>	<u>Page</u>
5.4	Results of the constant $\Delta K$ hold time test on Rene'95 with R=0 at (a) 538°C and (b) 593°C.	78
5.5	Variation of crack growth rate with hold time measured in Rene'95 constant $\Delta K$ tests with R=0 at (a) 538°C and (b) 593°C.	79
5.6	Results of the constant $\Delta K$ hold time tests on Rene'95 at 593°C with (a) R=0.5 and (b) R=0.8.	81
5.7	Results of the constant $\Delta K$ hold time tests on Rene'95 at 649°C with (a) R=0.5 and (b) R=0.8.	82
5.8	Variation of crack growth rate with hold time measured in Rene'95 constant $\Delta K$ tests at 593°C with (a) R=0.5 and (b) R=0.8.	83
5.9	Variation of crack growth rate with hold time measured in Rene'95 constant $\Delta K$ tests at 649°C with (a) R=0.5 and (b) R=0.8.	84
5.10	Results of the constant $\Delta K$ frequency tests on Rene'95 at 593°C with (a) R=0.0, (b) R=0.5, and (c) R=0.8.	85
5.11	Results of the constant $\Delta K$ frequency tests on Rene'95 at 649°C with (a) R=0.0, (b) R=0.5, and (c) R=0.8.	87
5.12	Comparison of results of 593°C Rene'95 constant $\Delta K$ tests cycled at 20 cpm, 300 second cycle period, and 300 second hold time with (a) R=0.0, (b) R=0.5, and (c) R=0.8.	88
5.13	Comparison of results of 649°C Rene'95 constant $\Delta K$ tests cycled at 20 cpm, 300 second cycle period, and 300 second hold time with (a) R=0.0, (b) R=0.5, and (c) R=0.8.	89



<u>Figure</u>	<u>Caption</u>	<u>Page</u>
5.14	Results of 649°C Rene'95 threshold tests with 3 second cycle period and different R-ratios as a function of (a) $\Delta K$ and (b) $K_{max}$ .	91
5.15	Results of 593°C Rene'95 threshold tests with 3 second cycle period and different R-ratios as a function of (a) $\Delta K$ and (b) $K_{max}$ .	92
5.16	Comparison of 593 and 649°C Rene'95 threshold tests with 3 second cycle period for R-ratios of (a) $R=0.0$ and (b) $R=0.8$ .	94
5.17	Results of Rene'95 threshold tests with $R=0$ and different hold times at (a) 593°C and (b) 649°C.	95
5.18	Results of 649°C Rene'95 threshold tests with $R=0$ and different test frequencies.	96
5.19	Variation of $(K_{th})_{max}$ in Rene'95 at 649°C with R-ratio and (a) hold time and (b) test frequency.	98
5.20	Comparison of crack growth rates measured in threshold and constant $\Delta K$ tests of Rene'95 at 649°C and $R=0$ for cycle periods of (a) 3 seconds, (b) 30 seconds, and (c) 300 seconds.	101
5.21	Comparison of crack growth rates measured in threshold and constant $\Delta K$ tests of Rene'95 at 649°C and $R=0$ for hold times of (a) 30 seconds and (b) 300 seconds.	103
5.22	Comparison of crack growth rates measured in threshold and constant $\Delta K$ tests of Rene'95 at 649°C and $R=0.5$ for cycle periods of (a) 3 seconds and (b) 300 seconds.	104

<u>Figure</u>	<u>Caption</u>	<u>Page</u>
5.23	Comparison of crack growth rates measured in threshold and constant $\Delta K$ tests of Rene'95 at 649°C and R=0.5 for a hold time of 300 seconds.	105
5.24	Comparison of crack growth rates measured in threshold and constant $\Delta K$ tests of Rene'95 at 649°C and R=0.8 for cycle periods of (a) 3 seconds and (b) 300 seconds.	106
5.25	Comparison of crack growth rates measured in threshold and constant $\Delta K$ tests of Rene'95 at 649°C and R=0.8 for hold times of (a) 4 seconds, (b) 30 seconds, and (c) 300 seconds.	107
5.26	Comparison of crack growth rates measured in threshold and constant $\Delta K$ tests of Rene'95 at 593°C and R=0.0 for hold times of (a) 0 seconds and (b) 300 seconds.	108
5.27	Comparison of crack growth rates measured in threshold and constant $\Delta K$ tests of Rene'95 at 593°C and R=0.8 for hold times of (a) 0 seconds and (b) 300 seconds.	109
5.28	Results of Rene'95 static crack growth tests at 649°C.	111
5.29	Results of Rene'95 static crack growth tests at 593°C.	112
5.30	Schematic showing multiple retardation cycles with hold times of 0, 4, and 30 seconds.	115
5.31	Variation of crack growth rate with distance in Rene'95 at 649°C with a 300 second hold time at R=0 preceded by a 50% overpeak.	117
5.32	Results of 649°C multiple overpeak hold time tests on Rene'95 R=0 for overpeaks of (a) 10%, (b) 20%, and (c) 50%.	118

<u>Figure</u>	<u>Caption</u>	<u>Page</u>
5.33	Results of 649°C multiple overpeak hold time tests on Rene'95 R=0.5 for overpeaks of (a) 10% and (b) 20%.	119
5.34	Results of 593°C multiple overpeak hold time tests on Rene'95 R=0 for overpeaks of (a) 10% and (b) 20%.	121
5.35	Results of 593°C multiple overpeak hold time tests on Rene'95 R=0.5 for overpeaks of (a) 10% and (b) 20%.	122
5.36	Variation of crack growth rate with hold time measured in 649°C multiple overpeak hold time tests on Rene'95 with R=0 for overpeaks of (a) 10%, (b) 20%, and (c) 50%.	123
5.37	Variation of crack growth rate with hold time measured in 649°C multiple overpeak hold time tests on Rene'95 with R=0.5 for overpeaks of (a) 10% and (b) 20%.	124
5.38	Variation of crack growth rate with hold time measured in 593°C multiple overpeak hold time tests on Rene'95 with R=0 for overpeaks of (a) 10% and (b) 20%.	125
5.39	Variation of crack growth rate with hold time measured in 593°C multiple overpeak hold time tests on Rene'95 with R=0.5 for overpeaks of (a) 10% and (b) 20%.	126
5.40	Variation of crack length with cycles during constant $\Delta K$ hold time test on Alloy 718 at 649°C with R=0.	129
5.41	Variation of crack length with cycles during transitions from 300 second hold time to 0 second hold time during constant $\Delta K$ hold time test on Alloy 718 at 649°C with R=0 for 300 second hold time $K_{max}$ values of (a) 18 MPa/m and (b) 31 MPa/m.	130

<u>Figure</u>	<u>Caption</u>	<u>Page</u>
5.42	Results of the Constant $\Delta K$ hold time tests on Alloy 718 at 593°C with (a) R=0.0, (b) R=0.5, and (c) R=0.8.	132
5.43	Results of the Constant $\Delta K$ hold time tests on Alloy 718 at 649°C with (a) R=0.0, (b) R=0.5, and (c) R=0.8.	133
5.44	Variation of crack growth rate with hold time measured in Alloy 718 constant $\Delta K$ tests at 593°C with (a) R=0.0, (b) R=0.5, and (c) R=0.8.	134
5.45	Variation of crack growth rate with hold time measured in constant Alloy 718 $\Delta K$ tests at 649°C with (a) R=0, (b) R=0.5, and (c) R=0.8.	135
5.46	Results of 649°C Alloy 718 threshold tests with 3 second cycle period and different R-ratios as a function of (a) $\Delta K$ and (b) $K_{max}$ .	136
5.47	Comparison of 593 and 649°C Alloy 718 threshold tests with 3 second cycle period for R=0.0.	137
5.48	Results of Alloy 718 threshold tests with R=0 and different hold times at 649°C.	139
5.49	Variation of $(K_{th})_{max}$ in Alloy 718 at 649°C with R-ratio and hold time.	140
5.50	Comparison of crack growth rates measured in threshold and constant $\Delta K$ tests of Alloy 718 at 649°C and R=0 for a 300 second hold time cycle.	141
5.51	Comparison of crack growth rates measured in threshold and constant $\Delta K$ tests of Alloy 718 at 649°C and R=0.8 for hold times of (a) 4 seconds, (b) 30 seconds, and (c) 300 seconds.	142

<u>Figure</u>	<u>Caption</u>	<u>Page</u>	
5.52	Results of Alloy 718 static crack growth tests at 649°C.	144	
5.53	Results of Alloy 718 static crack growth tests at 593°C.	145	
5.54	Results of 649°C multiple overpeak hold time tests on Alloy 718 with R=0 for overpeaks of (a) 10% and (b) 20%.	148	•
5.55	Results of 649°C multiple overpeak hold time tests on Alloy 718 with R=0.5 for overpeaks of (a) 10% and (b) 20%.	149	•
5.56	Variation of crack growth rate with hold time measured in 649°C multiple overpeak hold time tests on Alloy 718 with R=0 for overpeaks of (a) 10% and (b) 20%.	150	
5.57	Variation of crack growth rate with hold time measured in 649°C multiple overpeak hold time tests on Alloy 718 with R=0.5 for overpeaks of (a) 10% and (b) 20%.	151	
6.1	SEM micrographs showing Region II fracture morphology of constant $\Delta K$ , R=0 Rene'95 specimens tested in air and conditions of (a) 538°C, low $K_{max}$ , 4 second hold time cycle, (b) 538°C, low $K_{max}$ , 300 second hold time cycle, (c) 593°C, high $K_{max}$ , 4 second hold time cycle, and (d) 593°C, high $K_{max}$ , 300 second hold time cycle.	158	
6.2	SEM micrographs showing Region II fracture morphology of constant $\Delta K$ , R=0 Rene'95 specimen tested in air at 649°C and conditions of (a) high $K_{max}$ , 4 second hold time cycle, (b) high $K_{max}$ , 30 second hold time cycle, and (c) high $K_{max}$ , 300 second hold time cycle.	159	•

<u>Figure</u>	<u>Caption</u>	<u>Page</u>
6.3	SEM micrographs showing Region II fracture morphology of constant $\Delta K$ , R=0 Rene'95 specimen tested in air at 538°C and conditions of (a) intermediate $K_{max}$ , 4 second hold time cycle, (b) intermediate $K_{max}$ , 300 second hold time cycle, (c) high $K_{max}$ , 4 second hold time cycle, and (d) high $K_{max}$ , 300 second hold time cycle.	161
6.4	SEM micrographs showing Region II fracture morphology of constant $\Delta K$ , R=0 Rene'95 specimens tested in air at 593°C and conditions of (a) low $K_{max}$ , 30 second cycle period and (b) low $K_{max}$ , 30 second hold time cycle.	163
6.5	SEM micrographs showing Region II fracture morphology of constant $\Delta K$ Rene'95 specimens tested in air at 593°C and conditions of (a) R=0, intermediate $K_{max}$ , 3 second cycle period and (b) R=0.8, intermediate $K_{max}$ , 3 second cycle period.	166
6.6	SEM micrographs showing threshold arrest morphology of K-shed, R=0 Rene'95 specimens tested in air at 649°C and conditions of (a) 3 second cycle period and (b) 30 second hold time cycle.	168
6.7	SEM micrographs showing the fracture surface of constant $\Delta K$ , R=0 Rene'95 hold time specimens tested in air at 649°C and conditions of (a) 20% overpeak and (b) no overpeak.	169
6.8	SEM micrographs showing Region II fracture morphology of constant $\Delta K$ , R=0 Alloy 718 specimen tested in air at 593°C and conditions of (a) low $K_{max}$ , 4 second hold time cycle, (b) low $K_{max}$ , 30 second hold time cycle, and (d) low $K_{max}$ , 300 second hold time cycle.	171

<u>Figure</u>	<u>Caption</u>	<u>Page</u>
6.9	SEM micrographs showing Region II fracture morphology of constant $\Delta K$ , R=0 Alloy 718 specimen tested in air at 593°C and conditions of (a) intermediate $K_{max}$ , 4 second hold time cycle, (b) intermediate $K_{max}$ , 300 second hold time cycle, (c) high $K_{max}$ , 4 second hold time cycle, and (d) high $K_{max}$ , 300 second hold time cycle.	172
6.10	SEM micrographs showing Region II fracture morphology of constant $\Delta K$ , R=0 Alloy 718 specimen tested in air at 649°C and conditions of (a) intermediate $K_{max}$ , 4 second hold time cycle, (b) intermediate $K_{max}$ , 300 second hold time cycle, (c) high $K_{max}$ , 4 second hold time cycle, and (d) high $K_{max}$ , 300 second hold time cycle.	173
6.11	Crack growth data from 3 second period Rene'95 vacuum tests with different R-ratios as a function of (a) $\Delta K$ and (b) $K_{max}$ .	176
6.12	Comparison of Rene'95 crack growth rates measured in air and vacuum for tests cycled at 593°C with R=0 and 4 second hold time.	177
6.13	Comparison of Rene'95 crack growth rates measured in air and vacuum for tests cycled at 649°C with (a) R=0 and 0 second hold time, (b) R=0.8 and 0 second hold time, and (c) R=0 and 300 second hold time.	178
6.14	Influence of hold time on Rene'95 crack growth rates at 649°C with R=0 in (a) air and (b) vacuum.	179
6.15	Influence of test temperature on Rene'95 crack growth rates at R=0 and 0 second hold time in (a) air and (b) vacuum.	181

<u>Figure</u>	<u>Caption</u>	<u>Page</u>
6.16	Comparison of Alloy 718 crack growth rates measured in air and vacuum for tests cycled at 649°C with R=0 and (a) 0 second hold time and (b) 300 second hold time.	182
6.17	Influence of hold time on Alloy 718 crack growth rates at 649°C with R=0 in (a) air and (b) vacuum.	183
6.18	SEM micrographs showing Region II fracture morphology of K-increase, R=0 Rene'95 specimens tested in vacuum at 649°C and conditions of (a) low $K_{max}$ , 3 second cycle period, (b) intermediate $K_{max}$ , 3 second cycle period, (c) low $K_{max}$ , 300 second hold time cycle, and (d) intermediate $K_{max}$ , 300 second hold time cycle.	185
6.19	SEM micrographs showing Region II fracture morphology of K-increase, R=0 Alloy 718 specimen tested in vacuum at 649°C with a 3 second cycle period; (a) low $K_{max}$ , (b) intermediate $K_{max}$ , and (c) high $K_{max}$ .	186
6.20	SEM micrograph showing Region II fracture morphology for constant $\Delta K$ , R=0 Alloy 718 specimen tested in air at 649°C with a 3 second cycle period (low $K_{max}$ level).	187
6.21	SEM micrograph showing Region II fracture morphology of K-increase, R=0 Alloy 718 specimen tested in vacuum at 649°C with a 300 second hold time cycle (intermediate K level).	189
6.22	Comparison of Rene'95 crack growth rates measured at 649°C for R=0 cycling with 0 second hold time in air and vacuum and 300 second hold time in vacuum.	190



<u>Figure</u>	<u>Caption</u>	<u>Page</u>
6.23	Comparison of Alloy 718 crack growth rates measured at 649°C for R=0 cycling with 0 second hold time in air and vacuum and 300 second hold time in vacuum.	191
6.24	Optical micrographs showing crack in K-shed, R=0 Rene'95 specimen tested in air at 649°C with a 300 second hold time cycle; (a) low magnification view of entire crack, (b) high magnification view of crack in arrest region (unetched microstructure), and (c) high magnification view of crack in arrest region (etched microstructure).	193
6.25	Optical micrographs showing crack in K-shed, R=0 Alloy 718 specimen tested in air at 649°C with a 300 second hold time cycle; (a) low magnification view of entire crack, (b) high magnification view of crack in arrest region (unetched microstructure), and (c) and (d) high magnification views of crack in arrest region (etched microstructure).	194
6.26	Variation of damage zone size with R-ratio and $K_{max}$ for Alloy 718 cycled at 593°C with a 300 second hold time.	196
6.27	Variation of crack length with cycles for damage zone experiment in air.	198
6.28	Variation of damage zone size with hold time, material, and test temperature as measured in damage zone experiment in air.	199
6.29	Variation of crack length with cycles for the transition from 300 second hold time to 20 cpm cycling for (a) air/air cycling, (b) vacuum/vacuum cycling, (c) vacuum/air cycling, and (d) air/vacuum cycling.	200

<u>Figure</u>	<u>Caption</u>	<u>Page</u>
7.1	Sigmoidal crack growth rate curve adjusted to permit static crack growth below the static crack growth threshold.	211
7.2	Schematic diagram of superposition model including a static crack growth threshold.	214
7.3	Schematic diagram of modified Willenborg retardation model	218
7.4	Application of static retardation to constant amplitude, constant frequency tests.	220
7.5	Application of static retardation to overpeak hold time test cycle.	222
7.6	Schematic example of a mission analyzed by ACDCYCLE.	228
7.7	Comparison of 649°C Rene'95 (a) hold time and (b) frequency threshold data with predictions from the interpolation threshold model.	234
7.8	Cyclic crack growth curve used in the 649°C Rene'95 superposition model.	238
7.9	Static crack growth curve used in the 649°C Rene'95 superposition model.	240
7.10	Comparison of experimental data with predictions from interpolation model (I) and interpolation + superposition model (I+S) for Rene'95 tested at 649°C with R=0.0 and hold times of (a) 4 seconds, (b) 30 seconds, and (c) 300 seconds.	242

<u>Figure</u>	<u>Caption</u>	<u>Page</u>
7.11	Comparison of experimental data with predictions from interpolation model (I) and interpolation + superposition model (I+S) for Rene'95 tested at 649°C with R=0.5 and hold times of (a) 4 seconds, (b) 30 seconds, and (c) 300 seconds.	243
7.12	Comparison of experimental data with predictions from interpolation model (I) and interpolation + superposition model (I+S) for Rene'95 tested at 649°C with R=0.8 and hold times of (a) 4 seconds, (b) 30 seconds, and (c) 300 seconds.	245
7.13	Comparison of experimental data with predictions from interpolation model (I) and interpolation + superposition model (I+S) for Rene'95 tested at 649°C with R=0.0 and cycle periods of (a) 3 seconds, (b) 30 seconds, and (c) 300 seconds.	246
7.14	Comparison of experimental data with predictions from interpolation model (I) and interpolation + superposition model (I+S) for Rene'95 tested at 649°C with R=0.5 and cycle periods of (a) 3 seconds, (b) 30 seconds, and (c) 300 seconds.	247
7.15	Comparison of experimental data with predictions from interpolation model (I) and interpolation + superposition model (I+S) for Rene'95 tested at 649°C with R=0.8 and cycle periods of (a) 3 seconds, (b) 30 seconds, and (c) 300 seconds.	248
7.16	Predictions of crack growth rates in Rene'95 at 649°C with (a) hold time and (b) cycle period (frequency) using the superposition model.	250
7.17	Predictions of crack growth rates in Rene'95 at 649°C with (a) hold time and (b) cycle period (frequency) using the interpolation model.	252

<u>Figure</u>	<u>Caption</u>	<u>Page</u>
7.18	Comparison of crack growth predictions for R=0 hold time and frequency cycling of Rene'95 at 649°C using the (a) superposition and (b) interpolation models.	253
7.19	Comparison of 649°C Rene'95 crack growth predictions for R=0 hold time cycles with 0.005 and 1.5 second loading ramps using the (a) superposition and (b) interpolation models.	255
7.20	Variation of $\Phi$ with $K_{O1}$ for 649°C Rene'95 hold time overpeak tests with 10% overpeaks.	257
7.21	Comparison of predicted and observed cycles to propagate through individual segments of 649°C Rene'95 hold time overpeak tests with R-ratios of (a) 0.0 and (b) 0.5.	258
7.22	Comparison of ACDCYCLE predictions with experimental crack growth rates in 649°C, R=0.0 Rene'95 hold time overpeak tests with 300 second hold times and (a) 10%, (b) 20%, and (c) 50% overpeaks.	260
7.23	Comparison of ACDCYCLE predictions with experimental crack growth rates in 649°C, R=0.5 Rene'95 hold time overpeak tests with 300 second hold times and (a) 10% and (b) 20%.	261
7.24	Comparison of ACDCYCLE predictions with experimental crack growth rates in 649°C, R=0.0 Rene'95 test with a cycle period of 300 seconds.	263
7.25	Comparison of ACDCYCLE predictions with experimental crack growth rates in 649°C, R=0.0 Rene'95 test with a hold time of 300 seconds.	265
7.26	Comparison of 649°C Alloy 718 hold time threshold data with predictions from the interpolation threshold model.	268

<u>Figure</u>	<u>Caption</u>	<u>Page</u>
7.27	Static crack growth curve used in the 649°C Alloy 718 superposition model.	271
7.28	Comparison of cyclic and superposition ACDCYCLE predictions with Alloy 718 crack growth data measured during a R=0, 0 second hold time test in air.	272
7.29	Comparison of cyclic and superposition ACDCYCLE predictions with Alloy 718 crack growth data measured during a R=0.5, 0 second hold time test in air.	273
7.30	Comparison of experimental data with predictions from interpolation + superposition model for Alloy 718 tested at 649°C with R=0.0 and hold times of (a) 0 seconds, (b) 4 seconds, (c) 30 seconds, and (d) 300 seconds.	275
7.31	Comparison of experimental data with predictions from interpolation + superposition model for Alloy 718 tested at 649°C with R=0.5 and hold times of (a) 0 seconds, (b) 4 seconds, (c) 30 seconds, and (d) 300 seconds.	277
7.32	Comparison of experimental data with predictions from interpolation + superposition model for Alloy 718 tested at 649°C with R=0.8 and hold times of (a) 0 seconds, (b) 4 seconds, (c) 30 seconds, and (d) 300 seconds.	278
7.33	Variation of $\phi$ with $K_{01}$ for 649°C Alloy 718 hold time overpeak tests with 10% overpeaks.	279
7.34	Comparison of predicted and observed cycles to propagate through individual segments of 649°C Alloy 718 hold time overpeak tests with R-ratios of (a) 0.0 and (b) 0.5.	281

<u>Figure</u>	<u>Caption</u>	<u>Page</u>
7.35	Comparison of ACDCYCLE predictions with experimental crack growth rates in 649°C, R=0.0 Alloy 718 hold time overpeak tests with 300 second hold times and (a) 10% and (b) 20% overpeaks.	282
7.36	Comparison of ACDCYCLE predictions with experimental crack growth rates in 649°C, R=0.5 Alloy 718 hold time overpeak tests with 300 second hold times and (a) 10% and (b) 20% overpeaks.	283
A.1	Statistical analysis results of Rene'95 constant $\Delta K$ hold time crack growth data from specimen cycled at 538°C with a R-ratio of 0.0.	298
A.2	Statistical analysis results of Rene'95 constant $\Delta K$ hold time crack growth data from specimens cycled at 593°C with R-ratios of (a) 0.0, (b) 0.5, and (c) 0.8.	299
A.3	Statistical analysis results of Rene'95 constant $\Delta K$ frequency crack growth data from specimens cycled at 593°C with R-ratios of (a) 0.0, (b) 0.5, and (c) 0.8.	300
A.4	Statistical analysis results of Rene'95 constant $\Delta K$ hold time crack growth data from specimens cycled at 649°C with R-ratios of (a) 0.0, (b) 0.5, and (c) 0.8.	301
A.5	Statistical analysis results of Rene'95 constant $\Delta K$ frequency crack growth data from specimens cycled at 649°C with R-ratios of (a) 0.0, (b) 0.5, and (c) 0.8.	302
B.1	Statistical analysis results of crack growth data from Rene'95 specimen AF73 cycled at 593°C with a 10% overpeak and R-ratio of 0.0 having hold times of (a) 0, (b) 4, (c) 30, and (d) 300 seconds.	304

<u>Figure</u>	<u>Caption</u>	<u>Page</u>
B.2	Statistical analysis results of crack growth data from Rene'95 specimen AF28 cycled at 593°C with a 20% overpeak and R-ratio of 0.1 having hold times of (a) 0, (b) 4, (c) 30, and (d) 300 seconds.	305
B.3	Statistical analysis results of crack growth data from Rene'95 specimen AF73 cycled at 593°C with a 10% overpeak and R-ratio of 0.5 having hold times of (a) 0, (b) 4, (c) 30, and (d) 300 seconds.	306
B.4	Statistical analysis results of crack growth data from Rene'95 specimen AF43 cycled at 593°C with a 20% overpeak and R-ratio of 0.5 having hold times of (a) 0, (b) 4, (c) 30, and (d) 300 seconds.	307
B.5	Statistical analysis results of crack growth data from Rene'95 specimen AF68 cycled at 649°C with a 10% overpeak and R-ratio of 0.0 having hold times of (a) 0, (b) 4, (c) 30, and (d) 300 seconds.	308
B.6	Statistical analysis results of crack growth data from Rene'95 specimen AF29 cycled at 649°C with a 20% overpeak and R-ratio of 0.0 having hold times of (a) 0, (b) 4, (c) 30, and (d) 300 seconds.	309
B.7	Statistical analysis results of crack growth data from Rene'95 specimen AF34 cycled at 649°C with a 50% overpeak and R-ratio of 0.0 having hold times of (a) 0, (b) 4, (c) 30, and (d) 300 seconds.	310
B.8	Statistical analysis results of crack growth data from Rene'95 specimen AF75 cycled at 649°C with a 10% overpeak and R-ratio of 0.5 having hold times of (a) 0, (b) 4, (c) 30, and (d) 300 seconds.	311

<u>Figure</u>	<u>Caption</u>	<u>Page</u>
B.9	Statistical analysis results of crack growth data from Rene'95 specimen AF35 cycled at 649°C with a 20% overpeak and R-ratio of 0.5 having hold times of (a) 0, (b) 4, (c) 30, and (d) 300 seconds.	312
C.1	Statistical analysis results of Alloy 718 constant $\Delta K$ hold time crack growth data from specimens cycled at 593°C with R-ratios of (a) 0.0, (b) 0.5, and (c) 0.8.	314
C.2	Statistical analysis results of Alloy 718 constant $\Delta K$ hold time crack growth data from specimens cycled at 649°C with R-ratios of (a) 0.0, (b) 0.5, and (c) 0.8.	315
D.1	Statistical analysis results of crack growth data from Alloy 718 specimen A13-02 cycled at 649°C with a 10% overpeak and R-ratio of 0.0 having hold times of (a) 4, (b) 30, and (c) 300 seconds.	319
D.2	Statistical analysis results of crack growth data from Alloy 718 specimen A13-14 cycled at 649°C with a 20% overpeak and R-ratio of 0.0 having hold times of (a) 4, (b) 30, and (c) 300 seconds.	320
D.3	Statistical analysis results of crack growth data from Alloy 718 specimen A13-32 cycled at 649°C (1200°F) with a 10% overpeak and R-ratio of 0.5 having hold times of (a) 4, (b) 30, and (c) 300 seconds.	321
D.4	Statistical analysis results of crack growth data from Alloy 718 specimen A13-05 cycled at 649°C (1200°F) with a 20% overpeak and R-ratio of 0.5 having hold times of (a) 4, (b) 30, and (c) 300 seconds.	322



## LIST OF TABLES

<u>Table</u>	<u>Title</u>	<u>Page</u>
3.1	Conditions for Task II Testing	45
4.1	Composition of Rene'95 Disk	48
4.2	Test Ring Properties of Rene'95 Disk	49
4.3	Composition of Alloy 718 Plate	52
5.1	Rene'95 Simple Cycle Test Matrix	72
5.2	Rene'95 593°C Threshold Data	100
5.3	Rene'95 Overpeak Test Matrix	114
5.4	Alloy 718 Simple Cycle Test Matrix	128
5.5	Alloy 718 Overpeak Cycle Test Matrix	146
6.1	Rene'95 Simple Cycle Specimens Evaluated in Fractographic Studies	156
6.2	Summary Of Rene'95 R=0 Fractography Results For Hold Time Test Specimens	157
6.3	Summary Of Rene'95 593°C, R=0 Hold Time and Frequency Fractographic Observations	164
6.4	Vacuum Crack Growth Specimens	174
6.5	Crack Curvature Data	202

<u>Table</u>	<u>Title</u>	<u>Page</u>
7.1	Application of Retardation Constants	223
7.2	Sequence Of Mission Analysis In ACDCYCLE Using Interpolation Crack Growth Model	229
7.3	Sequence Of Mission Analysis In ACDCYCLE Using Interpolation + Superposition Crack Growth Model	231
7.4	Constants for 649°C Rene'95 Interpolation Threshold Model	233
7.5	Constants for 649°C Rene'95 Interpolation Model	235
7.6	Constants for 649°C Rene'95 Superposition Model	237
7.7	Constants for 649°C Alloy 718 Interpolation Threshold Model	267
7.8	Constants for 649°C Alloy 718 Superposition Model	270

## 1.0 INTRODUCTION

Improving combat maneuverability and engine efficiency are of critical importance in the design of current and future military aircraft. Improving combat maneuverability will require an engine with rapid acceleration and deceleration capabilities coupled with higher thrust-to-weight ratios and correspondingly higher operating combustor exit temperatures. Higher engine efficiency will also require hotter engine operating temperatures. Resulting service-loading spectra will include a large variety of load applications. These load applications may include fatigue cyclic loadings, sustained loads for various times, or a combination of the two.

Analytical and experimental studies have been performed under fatigue loading and sustained loading alone, but the behavior of materials due to the interactions between fatigue and sustained loads is complex and not yet well understood. As temperatures and design stresses increase, time-dependent material behavior becomes increasingly important. It is well recognized that time-dependent behavior in typical nickel-base superalloys is an environmentally enhanced phenomenon; nonetheless, this time-dependence and sustained-load interactions must be considered for some materials being utilized or developed for advanced Air Force engines. Present crack growth predictive capability has been demonstrated or applied for primarily time-independent situations. It is the purpose of this program to improve significantly the capability for predicting crack growth at elevated temperatures, including time-dependent material behavior.

The objective of this program was to develop a mathematical model capable of predicting crack growth in advanced turbine disk alloys under operating conditions that produce time-dependent and cycle-dependent effects. Crack growth models were developed to determine crack growth rates of nickel-base superalloys in advanced Air Force engine turbine disks under spectrum loading conditions representative of anticipated service in a wide variety of missions. Model development was limited to isothermal conditions where time-dependent crack growth can occur (that is, where hold time and frequency effects play important roles in crack-growth behavior). In support of this

activity, an extensive experimental program was performed to determine material properties and to better understand the mechanisms which control time-dependent crack growth.

The program was accomplished with the following four tasks:

- Task I - Definition of typical mission spectra and range of loading conditions.
- Task II - Generation and assembly of complete baseline crack growth data on Rene'95 and limited baseline data on Alloy 718.
- Task III - Development of crack growth models and incorporation into computer code for numerical calculations.
- Task IV - Evaluation of governing mechanisms and application of this information to model development.

The work in Task I concentrated on surveying the missions or anticipated missions in advanced military aircraft. This survey included various high pressure turbine disk locations where loading and temperature profiles were significantly different. These stress/temperature/time histories were selected from analyses of the Joint Advanced Fighter Engine. In reviewing these analyses, emphasis was placed on conditions which would lead to time-dependent crack growth. Based on this Task I survey, the range of Task II testing conditions was selected.

In Task II, the crack growth properties of extruded plus isothermally forged powder metallurgy Rene' 95 and cast plus wrought Alloy 718 were measured over a range of temperatures, stress ratios, test frequencies, hold times, and overpeak loading patterns. The Region II crack growth rates were determined using buttonhead single edge notch specimens by applying segments of constant stress intensity factor where the crack length was monitored using a DC potential drop technique. This method was selected to provide a cost-effective test method, with determination of good statistical data, along

with identification of transient behavior. The near-threshold crack growth rates were determined using a K-shed technique. The data obtained in this program were modeled in Task III and were used to select test conditions for the Task IV mechanism tests.

In Task III, data obtained during the Task II on Rene' 95 and Alloy 718 were modeled. Both totally interpolative and a combination of interpolative and superposition models were developed. Based on these analyses and understanding of the crack growth mechanisms obtained during Task IV, the best crack growth model was identified and documented. At the end of this task, a personal computer (PC) crack growth prediction computer program was written and delivered to the Air Force Materials Laboratory.

The purpose of Task IV was to identify the elevated crack growth mechanisms of nickel-base superalloys. Extensive fractographic examinations were performed on the specimens tested in Task II. This information was used to evaluate the underlying mechanisms. In addition, high vacuum and other types of tests were performed to better understand the role of environment and other factors which result in time-dependent crack growth. These results were used to assist in the selection of the crack growth models in Task III.

## 2.0 LITERATURE REVIEW

The objective of the investigation described in this report was to develop an improved model for time-dependent crack growth in nickel-base superalloys for the range of conditions experienced in the turbines of advanced aircraft engines. There has been a significant amount of research performed on these and similar alloys. This section of the report will summarize that work and set the background for both the experimental and model development portions of this investigation. The literature survey has been divided into sections on creep - fatigue - environment interactions, crack growth rate curve relationships, and the models used to predict time-dependent crack growth.

### 2.1 CREEP - FATIGUE - ENVIRONMENT INTERACTIONS

It has been known for several decades that there is a complex creep - fatigue - environment damage mechanism which occurs during the high temperature cyclic loading of engineering materials. This was ably demonstrated by Coffin and his coworkers<sup>(1,2)</sup> where the elevated temperature fatigue life of smooth fatigue specimens tested in laboratory air diminished significantly as test frequency was reduced. This effect, to a large extent, disappeared when the tests were performed in a high vacuum environment. These types of observations led to the development of frequency modified fatigue laws<sup>(1,3-5)</sup> and strain range partitioning fatigue models<sup>(6-8)</sup>.

The effects of environment on the rupture behavior of nickel-base alloys was probably first demonstrated by Chang<sup>(9)</sup> who showed that rupture specimens exposed in air under no applied stress had lower rupture ductility than companion specimens tested without the pre-exposure. These types of experiments were performed using several nickel-base superalloys. Cracks nucleated at the specimen surface and exhibited an intergranular failure mode. This behavior was the subject of more exhaustive research which has been reviewed by Woodford and Bricknell<sup>(10)</sup>. It has been shown that the embrittlement behavior is very complex and results, in part, from the

diffusion of oxygen along grain boundaries. Therefore the response of a given material is highly dependent on the local chemistry and structure of grain boundaries.

### 2.1.1 Crack Growth

The growth of cracks has been studied in numerous investigations at universities<sup>(11-15)</sup>, government laboratories<sup>(16-24)</sup>, and industrial laboratories<sup>(25-32)</sup>. The materials evaluated included several commercial alloys, but the most popular alloy investigated was Alloy 718, a  $\gamma$ - $\gamma''$  superalloy. Testing conditions included a variety of different wave forms as well as constant or static load (no fatigue component). The investigations studied the influence of test temperature, R-ratio, test frequency, hold time, overpeak, microstructure (alloy, product form, and heat treatment), and/or fracture mode. Starting with the initial work of Solomon<sup>(25)</sup>, it has been shown that the presence of laboratory air greatly accelerates the growth of cracks, particularly for static loading and low frequency or hold time cyclic tests<sup>(12-14,18,29)</sup>. The most thorough evaluation of environment was the study by Floreen and Kane<sup>(29)</sup> where the crack growth of Alloy 718 was measured in several different environments. The results of that study strongly suggested that oxygen is the species which makes air such a damaging environment.

Many of the studies showed that for high frequency conditions, the testing environment does not significantly influence the crack growth rates<sup>(16,20,23-25,26)</sup>. This has led to the terminology of cycle dependent and time-dependent regimes, corresponding to conditions where propagation is dominated by static or cyclic crack growth, respectively. It was also shown that as the material experienced more time-dependent crack growth rates, the fracture path often changed from a transgranular to a intergranular mode.

Several investigations<sup>(14,19,27)</sup> have shown that there is a significant difference in time-dependent crack growth between different alloys. Cowles, Warren, and Haake<sup>(31)</sup> showed that seven aircraft engine disk alloys had similar crack growth rates for 20 cpm (0.33 Hz) continuous cycling at 649°C. The crack growth rates of these alloys accelerated significantly during 900

second hold time cycles and differed by a factor of 100 between the different alloys. These data can be correlated with a variety of parameters including grain size, ultimate tensile strength, and chromium content, but the true source of the accelerated growth associated with creep - fatigue - environment interactions is not known or understood. James<sup>(30)</sup> investigated several different product forms of Alloy 718 and showed that uniform coarse grained material had slower crack growth rates than uniformly fine grained Alloy 718. Processing conditions with a duplex, necklace microstructure were superior to either of the uniform grain sizes. A similar conclusion was reached by Bain and Pelloux<sup>(14)</sup> for Rene'95.

There have also been several investigations supporting the occurrence of a competition between environmentally-assisted crack advance and crack tip blunting (and stress redistribution) caused by creep<sup>(15,16,18)</sup>. There is also significant evidence of specimen thickness effects where more rapid crack growth occurs in the center of through crack specimens than at the surface<sup>(33,34)</sup>.

It has been observed that there can be a significant amount of time-dependent crack growth during elevated temperature service. The amount of growth is highly dependent on the temperature, environment, alloy/microstructure, and loading cycle. Although several suggestions have been made, the mechanisms by which this accelerated crack growth can occur are not well understood.

## 2.2 CRACK GROWTH CURVES

Numerous mathematical relationships have been proposed to describe the relationship between cyclic crack growth rate ( $da/dN$ ) and the value of the range of the Irwin stress intensity factor ( $\Delta K$ ) or some value of effective value of  $K$  ( $K_{eff}$ ). Three basic relationships have been used to describe the response of nickel-base superalloys - the Paris, sinh, and sigmoidal equations. This section will describe each of these and their implications and limitations.



The crack growth response of engineering materials is usually represented in a plot of the logarithm of crack growth rate ( $da/dN$ ) as a function of the logarithm of  $\Delta K$  or  $K_{eff}$ . For the remainder of this section no distinction will be made between  $\Delta K$  and  $K_{eff}$  and they will be referred to as just  $K$ . Figure 2.1 shows a schematic representation of a typical fatigue crack growth curve. This curve has three main sections as labeled in this figure. Region I is the near-threshold regime where decreasing  $K$  results in a sharp decrease in crack growth rates as the threshold value,  $K_{th}$ , is approached. Region III is the upper end of the curve with rapid crack growth rates which approach the cyclic toughness,  $K_C$ . Region II exists between these two regimes and typically has a linear response between crack growth rate and  $K$  using the log-log representation shown in Figure 2.1.

All three models consider variation in the logarithmic properties as shown in Figure 2.1. In order to avoid lengthy equations, the crack growth rates will sometimes be rewritten using the terms  $x$  and  $y$  where

$$y = \log da/dN \quad (2.1)$$

$$x = \log K \quad (2.2)$$

This representation presents the schematic curve in Figure 2.1 using linear rather than logarithmic coordinates.

### 2.2.1 Paris Law

Paris<sup>(35)</sup> was the first to show that the growth of fatigue cracks could be described using linear elastic fracture mechanics. In his original work, he noted that there was a linear relationship between the logarithm of crack growth rate and  $K$ . He proposed describing these Region II crack growth rates using a relationship which has come to be known as the Paris Law. This can be described as

$$da/dN = A K^b \quad (2.3)$$

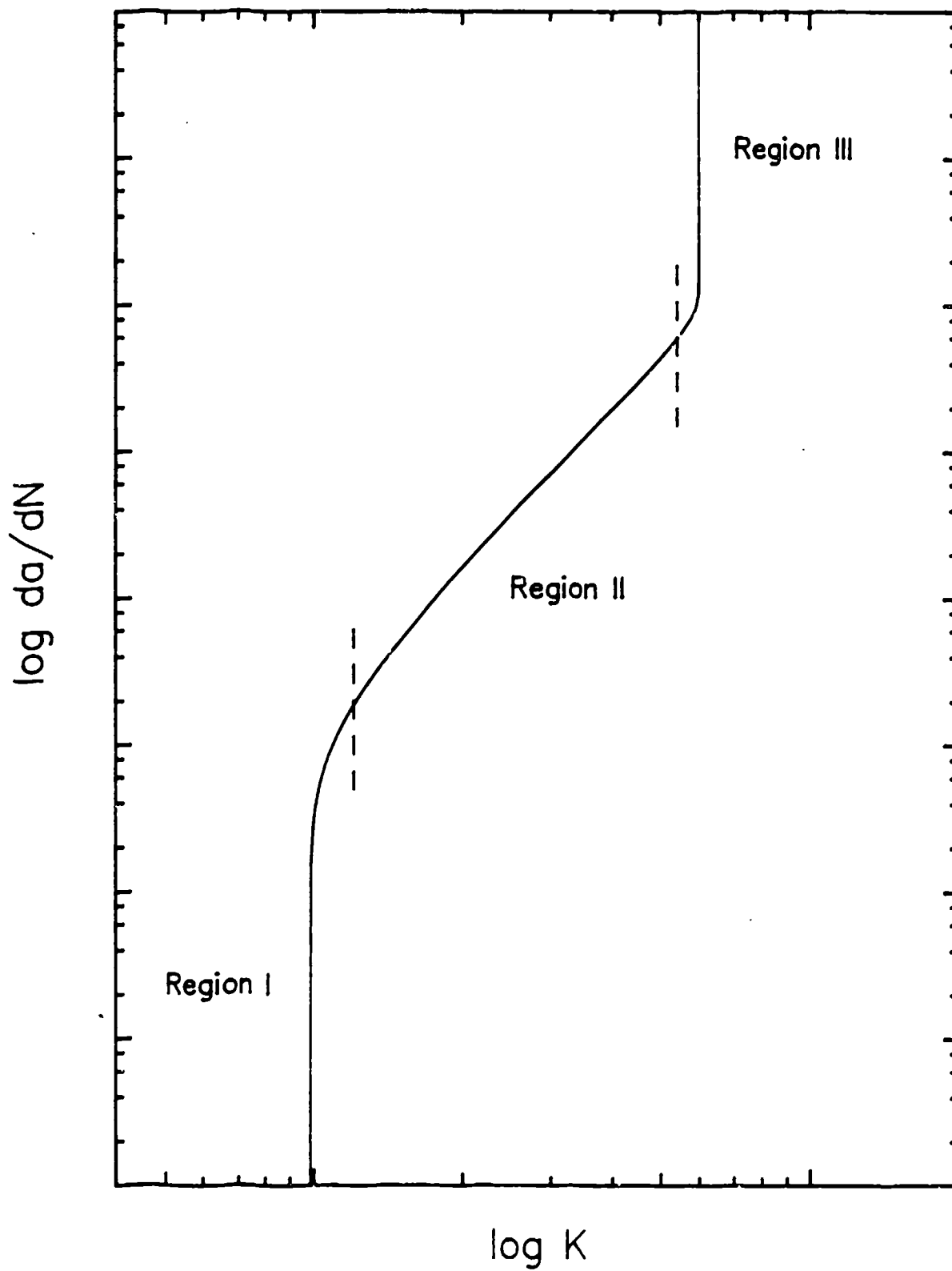


Figure 2.1: Schematic drawing of fatigue crack growth curve showing Regions I, II, and III.

where the values of A and b are constants determined from the experimental data. This relationship can also be represented as

$$y = \log A + b x \quad (2.4)$$

using the definitions of x and y in Equations 2.1 and 2.2.

The Paris relationship adequately defines the Region II portion of the crack growth rate curve. It can be combined with values of  $K_{th}$  and  $K_c$  to provide endpoints to the curve representing the lower and upper limits of crack growth, respectively; however, the transition regions between the near-threshold and near-toughness are not represented by the Paris model.

#### 2.2.2 Sinh Curve

The sinh model was developed at Pratt and Whitney<sup>(36-38)</sup> and has been used to describe the crack growth rate of several structural materials including high strength nickel-base superalloys. The hyperbolic sine (sinh) crack growth equation is

$$\log (da/dN) = C_1 \sinh (C_2 (\log K + C_3)) + C_4 \quad (2.5)$$

or using the definitions of x and y given in Equations 2.1 and 2.2

$$y = C_1 \sinh (C_2 (x + C_3)) + C_4 \quad (2.6)$$

An example of a sinh growth curve is shown schematically in Figure 2.2. An inflection point occurs at an x value of  $(-C_3)$  and a y value of  $C_4$ . This model has no mathematical definition of  $K_{th}$  or  $K_c$  and a value of  $da/dN$  can be determined for any value of K. The curvature of the sinh curve is identical in the near-threshold and near-toughness regime since the sinh function is symmetric. The parameters  $C_1$  and  $C_2$  scale the x and y axes, respectively.

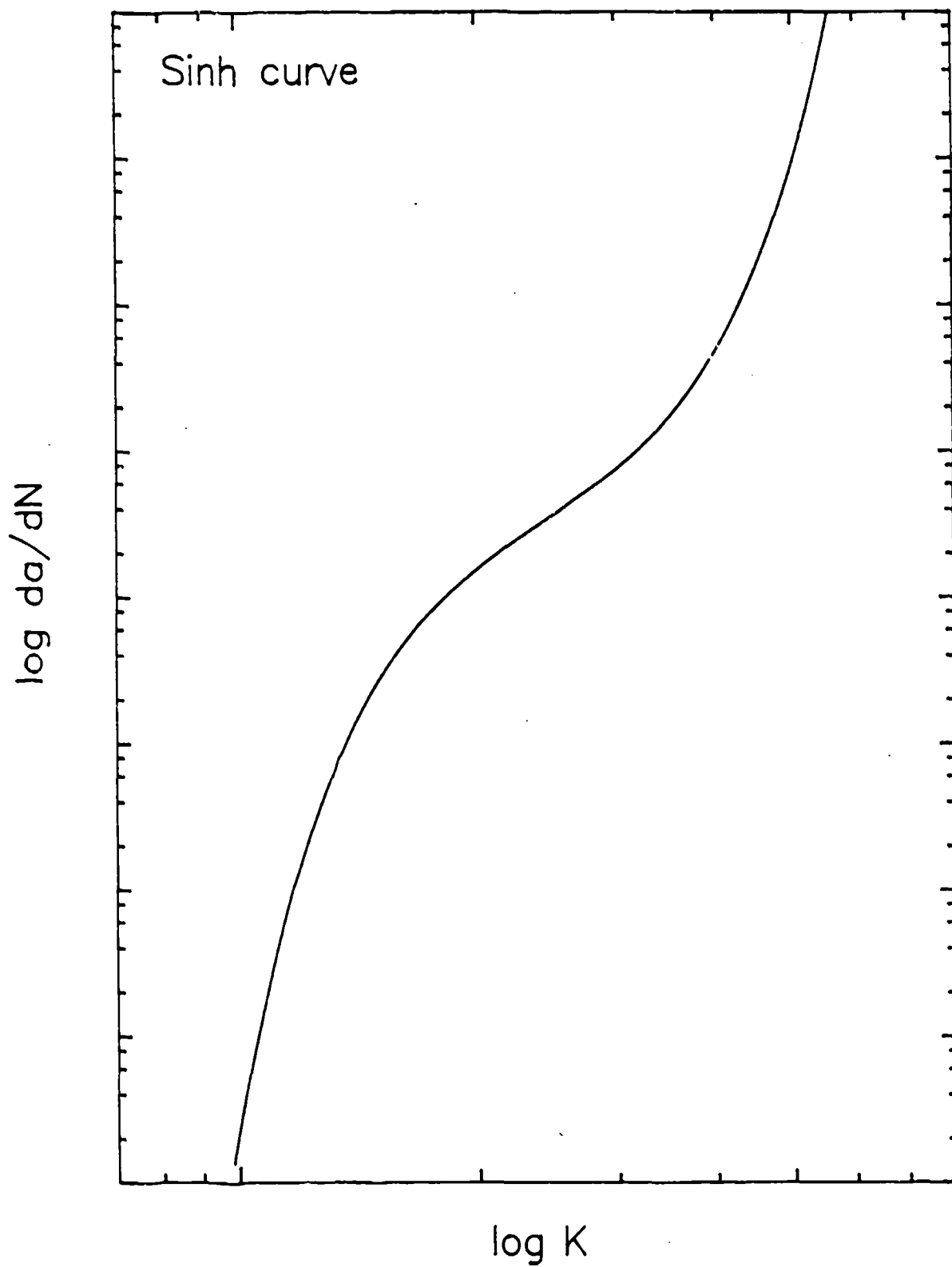


Figure 2.2: Schematic drawing of sinh crack growth curve.

The slope of the sinh curve is

$$\frac{dy}{dx} = C_1 C_2 \cosh (C_2 (x + C_3)) \quad (2.7)$$

At the inflection point ( $x_i = -C_3$ ) the slope equals  $C_1 C_2$ .

Wallace, et.al.<sup>(36)</sup> defined  $C_1$  to be a material constant. The values of  $C_2$ ,  $C_3$ , and  $C_1$  were described as a function of the test parameters and were determined from the position ( $x_i$  and  $y_i$ ) and slope of the crack growth curve at the inflection point.

### 2.2.3 Sigmoidal Curve

The sigmoidal crack growth relationship was originally developed at GE Aircraft Engines by Knaus<sup>(39)</sup> and first reported in the open literature by Coles, et.al.<sup>(28)</sup>. The form of this relationship is

$$da/dN = \exp (B) \left[ \frac{K}{K_{th}} \right]^P \left[ \log \frac{K}{K_{th}} \right]^Q \left[ \log \frac{K_c}{K} \right]^D \quad (2.8)$$

where B, P, Q, and D are constants for a given set of experimental conditions; and  $K_{th}$  and  $K_c$  are the threshold and cyclic toughness stress intensity factors, respectively. Figure 2.3 shows a schematic drawing of the sigmoidal crack growth curve.

Using the definitions of x and y given above and defining

$$x_0 = \log K_{th} \quad (2.9)$$

$$\text{and } x_f = \log K_c, \quad (2.10)$$

the sigmoidal relationship can be rewritten as

$$y = B + P(x - x_0) + Q \log (x - x_0) + D \log (x_f - x) \quad (2.11)$$

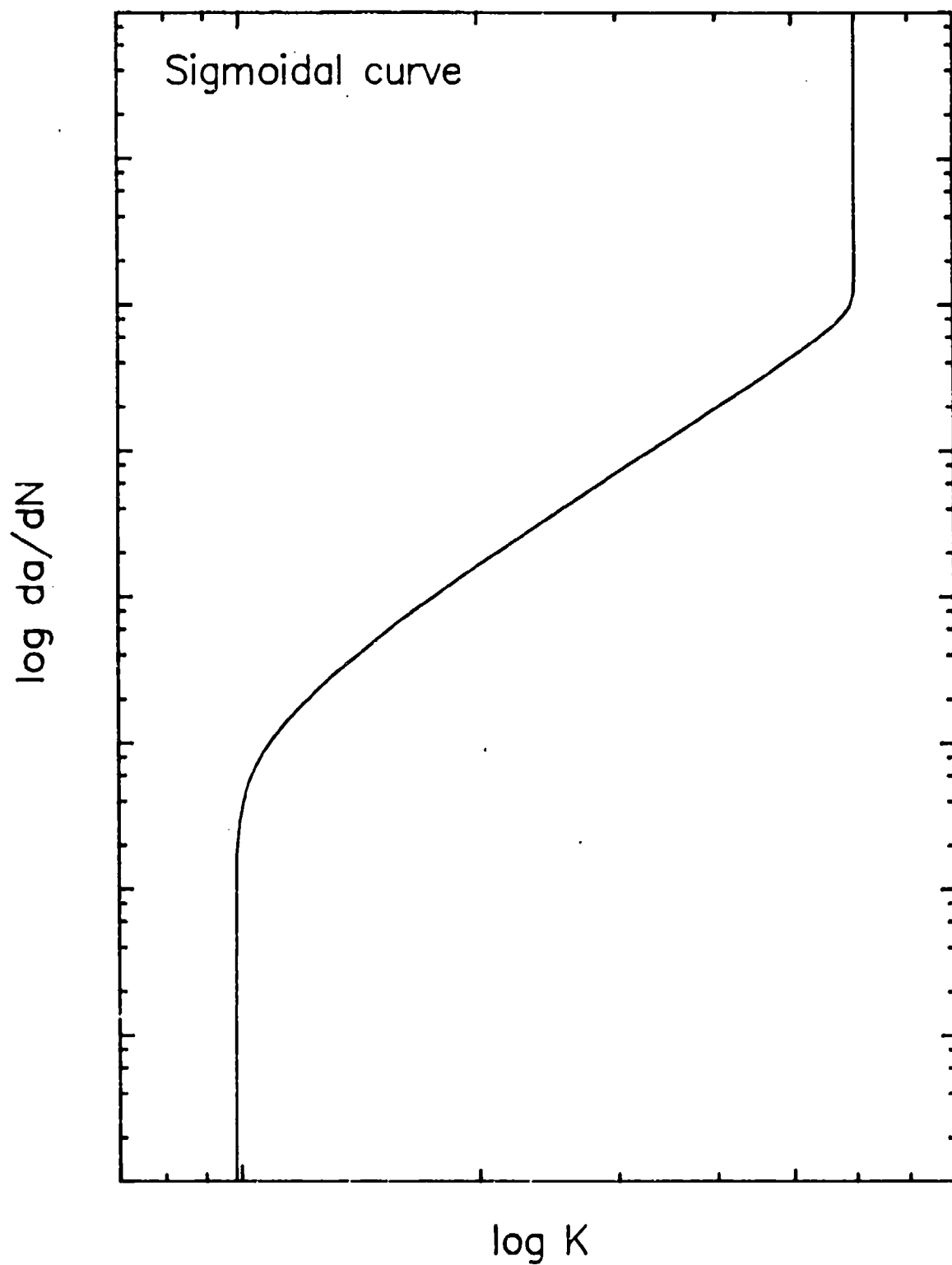


Figure 2.3: Schematic drawing of sigmoidal or Knaus crack growth curve.

The first term, B, translates the curve up the y axis. The slope of the curve is controlled by P and the curvature in the near-threshold and near-toughness regime is controlled by Q and D, respectively. In most cases, the value of D is negative. The sigmoidal curve has a form identical to the Paris relationship when Q and D are set to zero and  $K_{th}$  equals unity ( $x_0 = 0$ ).

The slope of the sigmoidal curve is

$$dy/dx = P + Q/(x-x_0) - D/(x_f-x) \quad (2.12)$$

The inflection point ( $x_1$ ) can be determined by setting  $d^2y/dx^2$  to zero and by rearranging

$$x_1 = (x_f\sqrt{Q} + x_0\sqrt{-D}) / (\sqrt{Q} + \sqrt{-D}) \quad (2.13)$$

The major advantage of the sigmoidal curve over the sinh model is that values for both the crack growth threshold and cyclic toughness are defined. The sigmoidal relationship also independently defines the curvature in the transition between both Regions I and II and Regions II and III. These are not adjustable in either of the other crack growth curve equations. This comparison of the sigmoidal and sinh models is, to some extent, slightly unfair. The sigmoidal equation has six adjustable parameters while the sinh model only has four. Thus, one would expect an inherently better fit for the sigmoidal than sinh model. The near-threshold and near-toughness transitions in the sinh model are dependent on an unadjustable functional form, in this case the hyperbolic sine. On the other hand, the sigmoidal equations models those regimes with the help of the constants Q and D. This leads to more flexibility in accurately modeling the crack growth response over the entire range of crack growth rates. The principal deficiency of the sigmoidal relationship is the inter-dependency of the six constants.

## 2.3 TIME-DEPENDENT CRACK GROWTH MODELS

There are two basic types of models which have been used to predict the time-dependent crack growth response of nickel-base superalloys: interpolative and superposition models. Interpolative models describe the constants in the crack growth rate equations as a function of the cycling variables (R, frequency, hold time, etc.) while superposition models separately account for the cycle-dependent and time-dependent parts of the crack growth. Each type of model will be considered separately.

### 2.3.1 Interpolative Models

Two interpolative models have been used to analyze elevated temperature crack growth of nickel-base superalloys. An interpolative sinh model was developed by Sims, et.al.<sup>(38)</sup> while an interpolative sigmoidal model was developed by Utah<sup>(32)</sup>. These two interpolative models were developed to represent the influence of temperature, hold time, frequency, and R-ratio on the constants in the appropriate crack growth equation. In both cases, the material constants were derived largely on the basis of Region II data.

Both models were calibrated using the movement of the inflection point in the crack growth rate curve. For the case of the sinh equation, Sims, et.al.<sup>(38)</sup> set the value of  $C_1$  to a constant. The movement of the inflection point was controlled by the variations in  $C_3$  and  $C_4$ , the values of  $x$  and  $y$  at the inflection point. The slope of the curve was controlled by the slope at the inflection point ( $C_2$ ).

Utah<sup>(32)</sup> developed a interpolative model of the sigmoidal equation by establishing relationships for the variation of  $K_{th}$  ( $\exp x_0$ ) and  $K_c$  ( $\exp x_f$ ) with test parameters and setting the value of  $Q$  to a constant. This was done in the absence on near-threshold crack growth data. The remaining sigmoidal constants ( $B$ ,  $P$ , and  $D$ ) were evaluated by the movement and slope of the inflection point. The constant  $D$  was evaluated from the  $x_1$  value of the inflection point.  $P$  was then calculated from the slope of the crack growth rate curve at the inflection point and the value of  $B$  was determined by the



absolute crack growth rate at the inflection point. Equations were constructed using regression analysis to describe the variation of the six sigmoidal terms with temperature, stress ratio, frequency, and hold time.

Both interpolative models accurately predict the response of cracks in Region II under the combined influence of test temperature, stress ratios, frequencies, and hold times, but may be inaccurate in the near-threshold regime. This low crack growth rate regime can be very important for the high R-ratio conditions which frequently occur in military aircraft. The interpolative models are also difficult to interpret in terms of crack growth mechanisms.

The models just described can be thought of as total interpolative models where all the constants in the crack growth equation are described as a function of the cycle parameters. There is also another type of interpolative model where the effect of R-ratio (mean stress) is modeled by transforming the values of  $\Delta K$  and R into a single value of  $K_{eff}$ . This changes the values on the log K (x) scale rather than the values of the crack growth equation constants. One successful example of this type of model is the relationship first proposed by Walker<sup>(40)</sup>

$$K_{eff} = K_{max} (1-R)^m \quad (2.14)$$

where m is known as the Walker exponent

When m is zero,  $K_{eff}$  equals  $K_{max}$ ; but when m is unity,  $K_{eff}$  equals  $\Delta K$ . In reality, the Walker exponent is an empirical factor which accounts for mean stress and closure effects without knowing their magnitude or the exact contribution from each effect. The crack growth curve can then be defined in terms of  $K_{eff}$  rather than  $\Delta K$ .

The Walker approach was modified by Van Stone<sup>(41)</sup> to include the use of a separate Walker exponent for positive and negative R-ratios ( $m^+$  and  $m^-$ , respectively). This approach was used to model a large range of HIP-compacted Rene'95 Region II data to a single crack growth curve for R-ratios ranging

from -1.22 to 0.75. Subsequently this approach has been used to successfully account for the influence of R-ratio on the Region I and II crack growth rates for a wider range of alloys including extruded and isothermally forged Rene'95, Alloy 718, and Direct Aged Alloy 718<sup>(42-44)</sup>. These investigations showed that the crack growth rates of these materials under 0.33 Hz (20cpm) cycling conditions could be collapsed to a single population of data which can be converted to a set of crack growth equation constants<sup>(43)</sup>.

### 2.3.2 Superposition Models

The time-dependent crack growth response of materials can also be described using a superposition model where the total crack growth rate is described as the sum of the cyclic crack growth and the time-dependent crack growth

$$da/dN = (da/dN)_c + \Delta a \quad (2.15)$$

where

- $da/dN$      = total crack growth rate
- $(da/dN)_c$  = cyclic crack growth rate
- and  $\Delta a$      = time dependent crack growth rate

This type of model was first proposed by Wei and Landes<sup>(45)</sup> for the modeling of room temperature corrosion fatigue of high-strength steels above the stress corrosion cracking threshold for the environments evaluated. This type of model was discussed more fully by Gallagher and Wei<sup>(46)</sup> and was applied for the first time to elevated temperature time-dependent crack growth of superalloys by Solomon<sup>(47)</sup>.

Elevated temperature crack growth which occurs under constant load conditions is frequently called creep crack growth. This appears to be an accurate description for the growth of cracks in pipe line and pressure vessel steels where extensive creep deformation occurs as the cracks grow. This terminology presumes that the growth of the crack is controlled by the far field creep deformation. As first noted by Larsen and Nicholas<sup>(20)</sup>, this may

not be an accurate description for the environmentally sensitive crack growth in nickel-base superalloys at elevated temperature. This type of environmentally assisted cracking appears to be phenomenologically similar to the stress corrosion cracking of steels, titanium, and aluminum alloys at low temperatures, even though the crack tip deformation and fracture mechanisms are quite different. For these reasons, this type of crack growth will be called sustained-load or static crack growth through the remainder of this report in order to avoid any misconception as to the mechanisms associated with this behavior.

Speidel<sup>(48)</sup> and Sadananda and Shahinian<sup>(17)</sup> reported that the hold time and low frequency crack growth response of Alloy 718 at elevated temperatures could be modeled as a time-dependent crack growth. Examination of Equation 2.15 shows that this can be predicted using a superposition approach when  $(da/dN)_c$  is small relative to  $\Delta a$ .

Utah<sup>(32)</sup> noted that one of the most difficult conditions to predict using an interpolation model was the combination of high mean stress, high temperature, low frequency, and long hold times. Under these conditions, a significant amount of the crack growth can occur from the constant high stress portion of the cycle only, with only a limited contribution from the cyclic component of stress. It appears that a superposition model would be able to predict the crack growth in this type of cycle better than an interpolation model.

Christoff<sup>(21)</sup> extended the superposition model by assuming that static crack growth obeyed a Paris type relationship

$$da/dt = C K^n \quad (2.16)$$

If  $K$  can be written as a function of time,  $f(t)$ , this equation can be rearranged and integrated over the time interval of a loading segment ( $t$ ) to determine the crack growth increment  $\Delta a$ :

$$\Delta a = \int da = C \int f(t)^n dt \quad (2.17)$$

Christoff<sup>(21)</sup> performed closed form integration for the cases of either (1) constant K or (2) linear variations of K with time. For constant K conditions

$$\Delta a = A K^n t \quad (2.18)$$

The result for a linear variation of K with time is dependent on t, n, and the R-ratio

$$\Delta a = C ((1 - R)^{(n+1)}/(n+1)) K_{\max}^n t \quad (2.19)$$

Comparison of Equations 2.18 and 2.19 show that they can both be expressed by the following relationship:

$$\Delta a = A K^n t_{\text{eff}} \quad (2.20)$$

$$\text{where } t_{\text{eff}} = t \text{ for hold times} \quad (2.21)$$

$$\text{and } t_{\text{eff}} = ((1 - R)^{(n+1)}/(n+1)) t \text{ for loading ramps} \quad (2.22)$$

The variation of the ratio between  $t_{\text{eff}}$  and t as defined in Equation 2.22 is shown in Figure 2.4 as a function of R and n. As R increases,  $K_{\min}$  approaches  $K_{\max}$  resulting in a larger value of K over the cycle and thus a higher  $t_{\text{eff}}$  and larger amounts of static crack growth. In the limit as R approaches unity, a loading ramp closely approximates a hold time so  $t_{\text{eff}} / t$  is unity as described in Equation 2.21. The value of n describes the slope of the static crack growth curve. Increasing n results in a larger difference in crack growth rates between  $K_{\min}$  and  $K_{\max}$  for a constant R ratio. The influence of n diminishes with increasing R because higher R ratio result in a smaller range of K.

This model assumes that there is no threshold value of K below which cracks will not grow. This approach has been used by Nicholas and co-workers<sup>(20,22,23)</sup> to predict the growth of cracks in nickel-base superalloys. They showed that this approach works well under some circumstances, but not so well under others. The most notable exceptions were

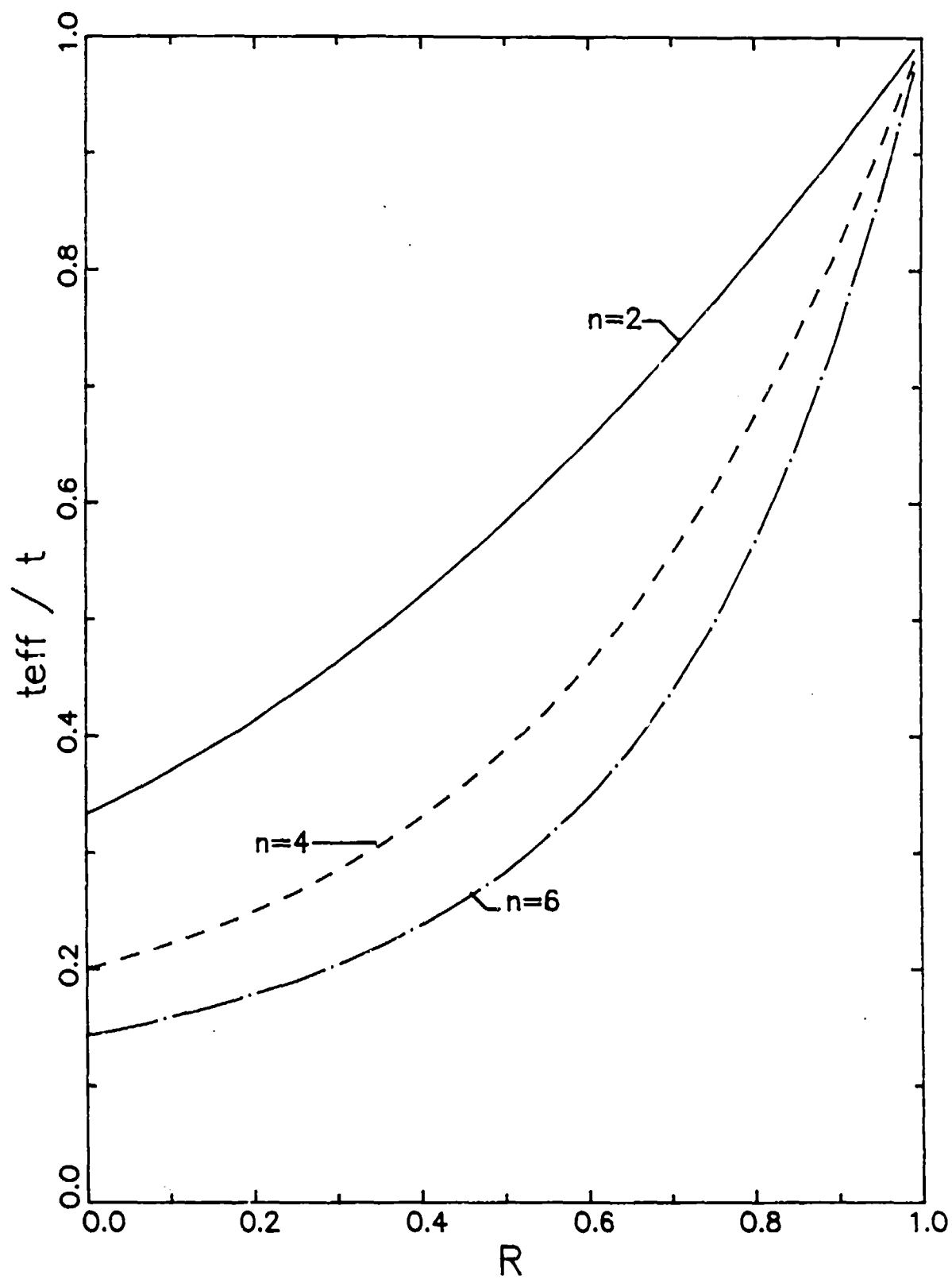


Figure 2.4: Variation in  $t_{eff} / t$  with R-ratio and Paris exponent ( $n$ ) for loading ramps as predicted by the linear superposition model.

low R-ratio loading ramps. It has been concluded that only the loading portion of cycles result in crack growth; however, this observation tends to break down for high R-ratio cycling. The superposition model does not tend to accurately predict the growth of cracks when the load or  $K$  is held at values below the maximum level. This will be discussed in the following section.

### 2.3.3 Retardation Models

It is well known that if a crack experiences a mission where a single maximum load cycle is significantly greater than the other load maxima, the crack growth rate is diminished or retarded relative to what would be anticipated had the overpeak not occurred. This behavior is known as overpeak retardation. This can be caused by a variety of mechanisms. The most frequently mentioned is the development of a compressive zone ahead of the crack. This is caused by the creation of a larger crack tip plastic zone during the overpeak and the subsequent unloading. When the load is removed, the material unloads in an elastic fashion to a more compressive local stress than was present prior to the overpeak. The crack growth will be slower until it grows through the more compressive stress zone. The amount of crack growth retardation and the distance over which it occurs increases with the size of the plastic zone, which is related to the magnitude of the overpeak  $K$ .

There are three basic types of retardation models: one which predicts the number of delay cycles until a crack again grows at its non-retarded rate, models which reduce the crack growth rate, and models which reduce the effective value of  $K$  and, in turn, reduce crack growth rates. An example of the latter type will be reviewed here because this type of model has been successfully applied to the crack growth of nickel-base superalloys under cyclic<sup>(49)</sup> and time-dependent<sup>(50)</sup> conditions.

One of the most frequently used retardation models is that developed by Willenborg<sup>(51)</sup>. The Willenborg model is very simple in concept. A value of reduced  $K$  is calculated and is dependent on the value of the overpeak, the current  $K$  (load), and various measures of the crack tip plastic zone.

$$K_{red} = (K_{01} \sqrt{[(r_{01} - \Delta)/r_{01}] - K_{max}})^{\phi} \quad (2.23)$$

where  $K_{red}$  - reduced value of  $K$

$K_{01}$  - value of  $K$  at the overpeak

$K_{max}$  - maximum value of  $K$  being reduced

$r_{01}$  - overpeak plastic zone (calculated from  $K_{01}$ )

$r_p$  - current plastic zone (calculated from  $K_{max}$ )

$\Delta$  - distance of crack propagation since overpeak ( $a - a_{01}$ )

$\phi$  - retardation constant

with the restriction that  $K_{red}$  is positive.

The only adjustable variable in the expression is the retardation constant  $\phi$ . The maximum value of  $K_{red}$  occurs when  $\Delta$  is zero and equals  $(K_{01} - K_{max})^{\phi}$ . For elastic unloading the value of  $K_{red}$  should never exceed  $K_{01} - K_{max}$  so the value of the constant  $\phi$  should never exceed unity.

The plastic zone sizes are assumed to follow the usual relationship in linear elastic fracture mechanics where they vary with the square of  $K$ . Using this relationship and setting the value of the expression within the brackets to zero ( $K_{red} = 0$ ) results in

$$\Delta_{max} = r_{01} - r_p \quad (2.24)$$

where  $r_p$  is the plastic zone size associated with the current maximum value of  $K_{max}$ . The meaning of this is that the values of  $K$  are reduced over the distance  $\Delta_{max}$  from the crack length where the overpeak occurred.

For cyclic loading, the value of  $K_{red}$  is applied to both the minimum and maximum loads resulting in a change in  $K_{max}$  and  $R$  but not in the range of  $K$

$$(K_{max})_{red} = K_{max} - K_{red}$$

$$(K_{min})_{red} = K_{min} - K_{red}$$

$$\begin{aligned} (R)_{red} &= (K_{min})_{red} / (K_{max})_{red} \\ &= (K_{min} - K_{red}) / (K_{max} - K_{red}) \end{aligned} \quad (2.25)$$

The amount of relative retardation diminished as the R-ratio increased because, for the most part, the cyclic crack growth rates for nickel base superalloys are controlled by  $\Delta K$  for high R-ratios ( $m^+ \approx 1$ ) while for negative R-ratios the growth is controlled by  $K_{max}$ . As shown in Equation 2.25, this model does not alter  $\Delta K$  but may have a significant effect on  $K_{max}$ . This, in part, may be the reason that some of the missions analyzed by Larsen, et. al. (37) do not show much benefit of retardation.

Weerasooriya and Nicholas(50) showed that a relatively small overpeak, combined with a hold time in a single cycle, could dramatically reduce the acceleration in crack growth rates associated with hold times in Alloy 718. If the K of the overpeak was more than 25 percent higher than the K of the hold, the crack growth rates were the same as those observed if the cycle had not included the hold time. This is very significant because for a cyclic case, a 25 percent overpeak would result in a relatively small reduction in crack growth rates. These results were modeled using a Willenborg type model(50).



### 3.0 MISSION ANALYSIS

The objective of this task was to review the missions of advanced military aircraft engines and identify the ranges of temperature, frequencies, hold times, stress ratios, overpeaks, and underpeaks in these turbines. These results were used to select the experimental conditions investigated in this program.

The primary emphasis of this task was to analyze a range of missions used in an advanced fighter engine. A total of 18 missions were analyzed. These included 9 different types of missions for two different locations. The locations selected were in the rim region of a high pressure turbine disk (HPTD). These regions were selected due to the combination of elevated temperature and high stress which would make them have a high susceptibility to time-dependent crack growth behavior.

A combined thermal-mechanical finite element analysis was performed on the HPTD using COMALL-A, a computer code developed at GEAE. The thermal and mechanical stresses were computed separately. These analyses resulted in calculation of the stresses in one second increments throughout each mission. The stresses shown in this report are the sum of the mechanical and thermal stresses. For each mission, the stresses are normalized by the maximum stress in that cycle.

Examples of a typical mission stress spectrum are shown in Figures 3.1 through 3.3. These particular missions were selected to illustrate conditions with relatively frequent changes in rotor speed (Figure 3.1), combination of cruise and rotor speed changes (Figure 3.2), and large segments of cruise component (Figure 3.3). During cruise conditions, the stresses are relatively constant resulting in what will be called a hold time cycle for the remainder of this report. These figures illustrate that typical advanced fighter missions operate with high mean stresses (high R) and frequently have overpeaks associated with hold times. The variations in stress occur over relatively short periods of time. On this basis, crack growth during hold times is more important than low frequency tests.

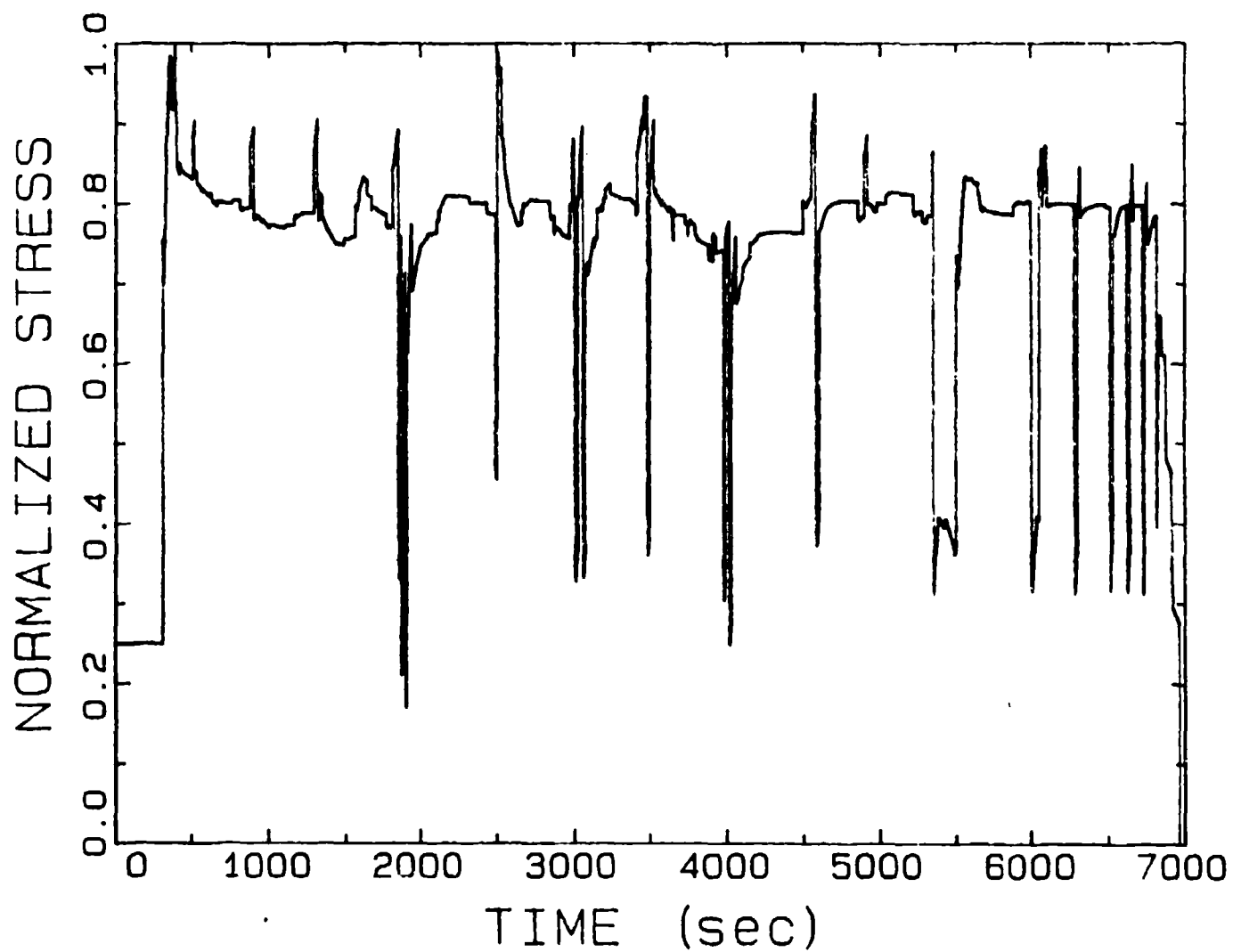


Figure 3.1: Example of a mission with frequent changes in rotor speed.

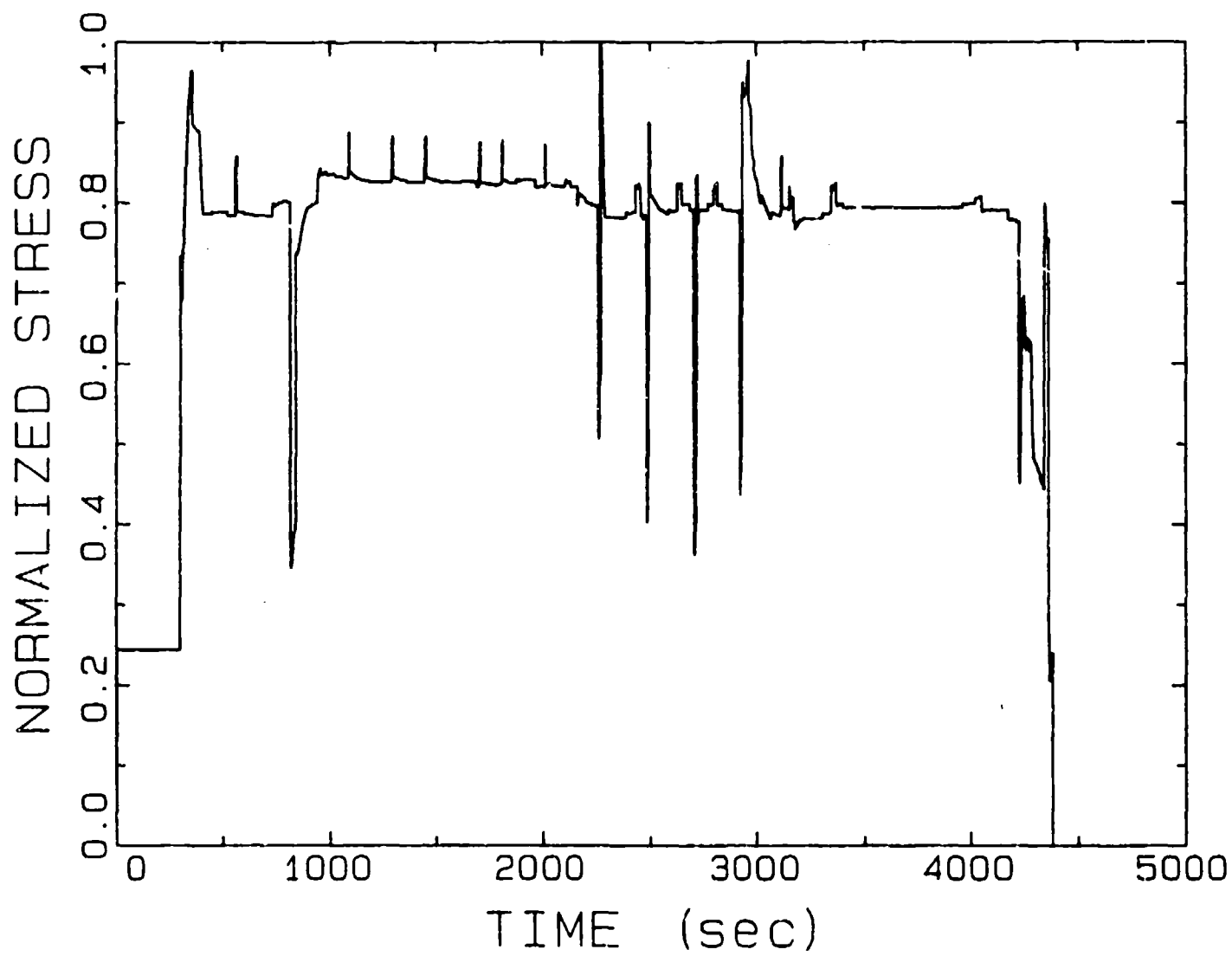


Figure 3.2: Example of a mission with changes in rotor speed and cruise conditions.

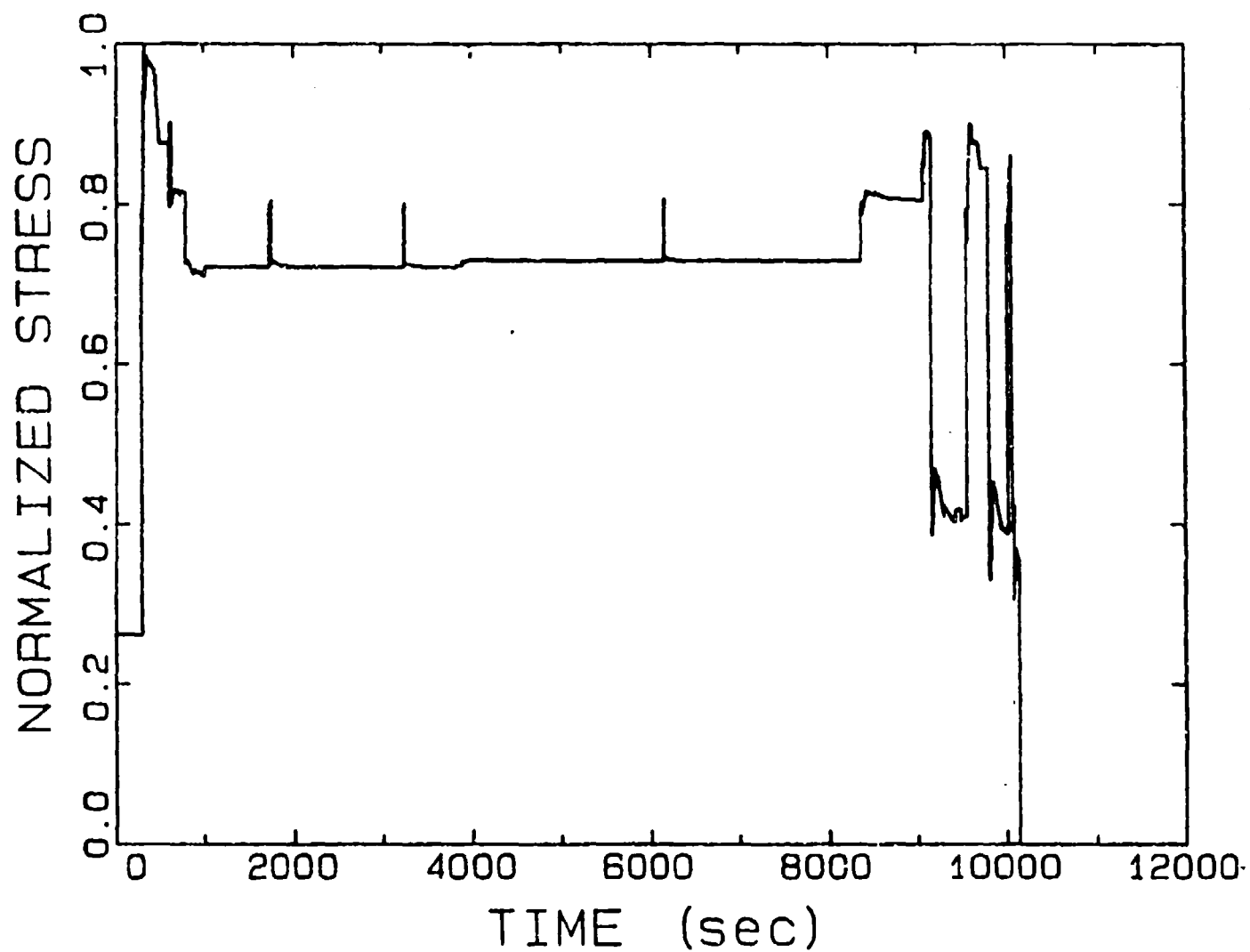
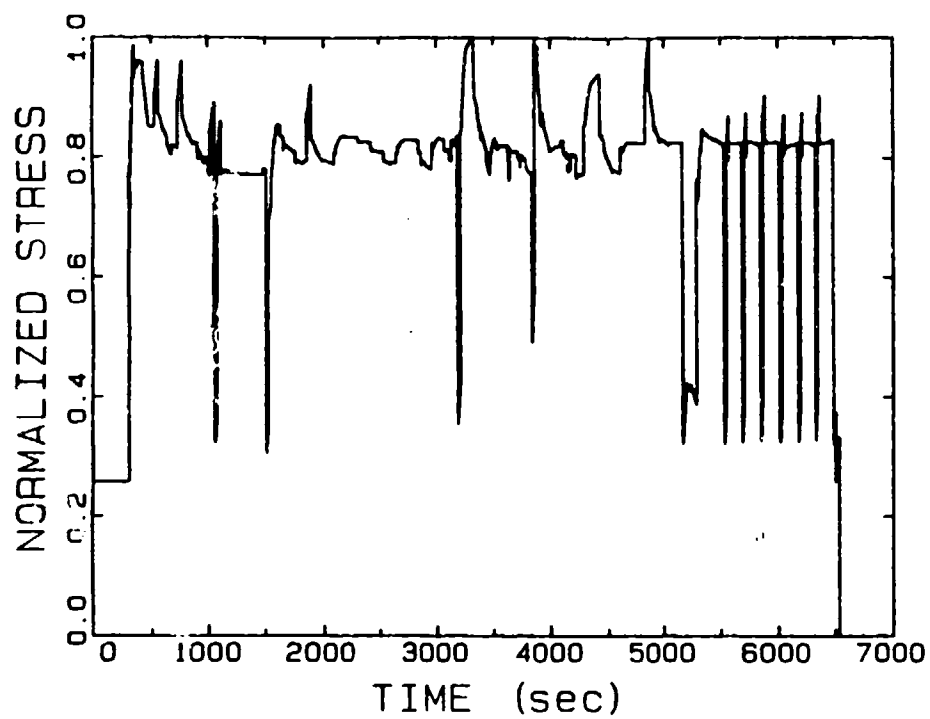


Figure 3.3: Example of a mission consisting primarily of cruise conditions.

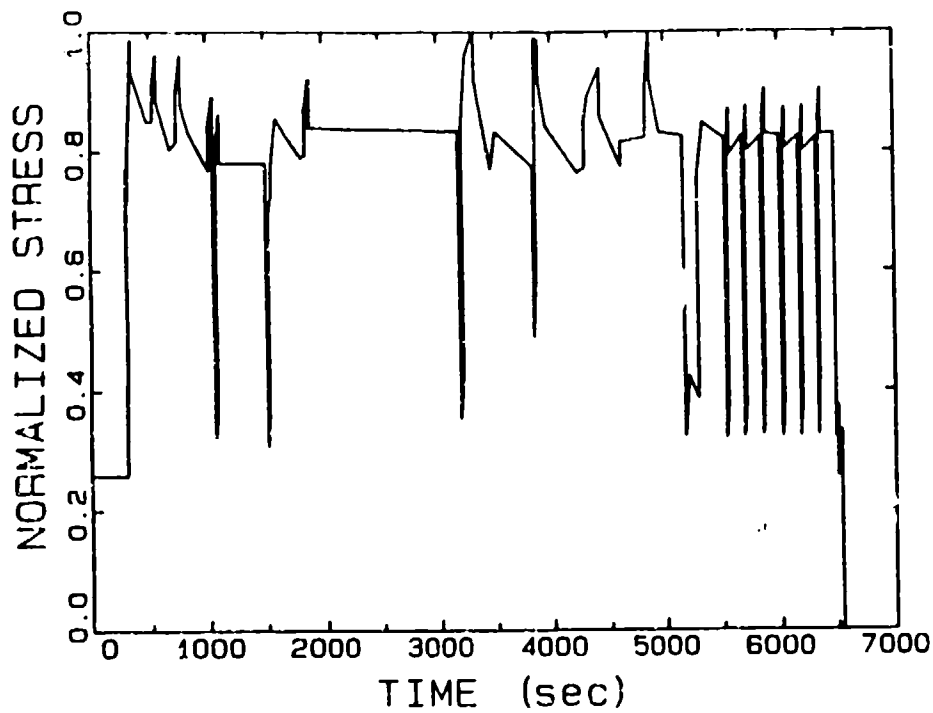
It was rather difficult to identify the critical features of these missions by visual inspection so two computer programs were written to analyze these missions. The first program revised the COMALL-A results with one stress-temperature data set for one second increments to a sequence of longer, linear segments. The second program was a sorting routine where any particular type of cycle can be extracted from the mission profiles. Each of these programs and the analysis of the eighteen missions are discussed in the following sections.

The approach used in the simplification program was to first eliminate data points where the variation in stress was small. This was accomplished by starting at the first data point and searching for the next stress value different by more than 5 percent. This process was repeated throughout the entire mission. This revised mission was further simplified by eliminating data points which were in a relatively constant stress-time ramp. Points which had variations in slope by a factor in excess of 0.75 and less than 1.5 from the previous slope were eliminated. Figure 3.4a shows a plot of normalized stress (stress/maximum stress in mission) for the mission used to develop this software. This particular mission was 6543 seconds long (6543 data points). The resulting simplified mission is shown in Figure 3.4b and contains 123 data points. This simplified mission portrays the main characteristics of the actual mission. The major weakness of the simplified mission approach is that the plus or minus 5 percent deviation in stress can result in treating 10 percent variations of stress as a hold time segment. A good example of this is shown between 2000 and 3000 seconds in Figure 3.4. Figures 3.5a and 3.5b show the variation in temperature during the actual and simplified mission respectively. As in the case of the stress, the mission simplification technique also seems to model the temperature variation rather well. Each of the eighteen missions was simplified in this fashion.

A second computer program was written to analyze the individual components of these simplified missions. This program first identified the parts of the mission which were hold time segments. Any segment which had a stress ratio ( $R = \text{minimum stress} / \text{maximum stress}$ ) greater than 0.95 was considered to be a hold time. This criterion is consistent with the 5 percent

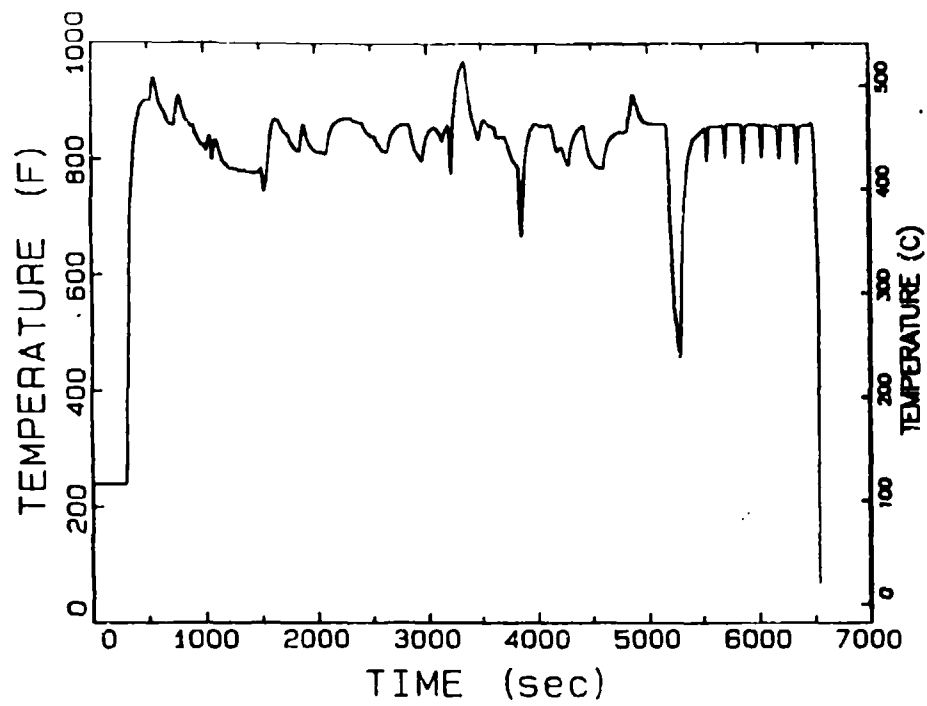


(a)

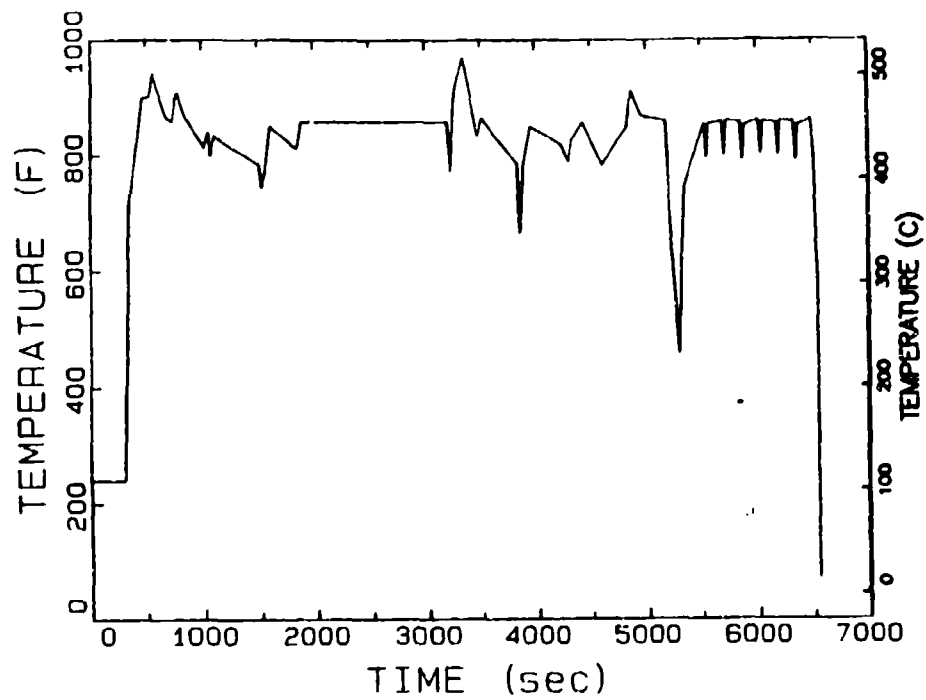


(b)

Figure 3.4: Variation of normalized stress with time for (a) actual mission and (b) simplified mission.



(a)



(b)

Figure 3.5: Variation of temperature with time for (a) actual mission and (b) simplified mission.

variation in load technique used in the mission simplification program. The mission points corresponding to local load maximums or minimums were also identified. This program permits analysis of the simplified mission in three ways:

1. Segment
2. Peak-Hold-Peak
3. Peak-to-Peak (excluding hold times)

The first technique analyzes each segment in the simplified missions and resulted in no additional simplification. The second technique simplifies the mission by considering consecutive loading segments as a single loading ramp. A similar assumption was made for unloading segments. The third technique eliminated hold times. Each of these techniques was used to determine the range of loading parameters associated with these missions.

The following parameters were identified or calculated for the resimplified missions:

1. Loading mode (increasing load, decreasing load, or hold time)
2. Stress ratio (R)
3. Duration of segment
4. Average temperature of segment
5. Temperature change during segment
6. Overpeak ratio
7. Underpeak ratio

The overpeak ratio compares the maximum of an increasing load or hold time segment with the preceeding local maximum stress (load reversal). The underpeaks were calculated using the previous local minimum stress.

The experimental portion of this investigation measured the variation in crack growth rates with cycle type (frequency, hold time, etc.). The primary emphasis of this program was on modeling of time-dependent crack growth so it is crucial to perform tests over the temperature range where variations in



crack growth rate can be detected. The experimental data reported in Section 5 showed that it was difficult to measure significant changes in crack growth rates with cycle type at temperatures lower than 538°C (1000°F).

Figure 3.6 shows the variation in stress ratio with temperature. In this and subsequent figures in this section, the different symbols (x and triangle) represent data from the two analyzed locations. As noted previously, the R values in these missions are very high. Based on these results and the lower bound temperature of 538°C (1000°F) the temperatures selected for the crack growth tests were 538, 593, and 649°C (1000, 1100, and 1200°F). The selected values of R were 0, 0.5, 0.8, and 1.0. The R-value of unity corresponds to static load testing conditions. The filled circles connected by solid lines indicate the test conditions selected for experimental evaluation. The same symbol notation is used in all subsequent figures in this section. The stress ratios shown in Figure 3.6 are based on elastic finite element analyses. Notched configurations are the most highly stressed conditions and frequently require elastic-plastic analysis. Localized plastic deformation results in lower values of maximum and minimum stresses and hence lower values of R.

The results in Figure 3.6 include hold times and individual segments. The data of the eighteen missions were also edited to eliminate hold time data (R greater than 0.95) and simplified using the peak-to-peak simplification technique. The variation of R with temperature for those editing modes are shown in Figure 3.7. These data suggest that the selected experimental conditions bracket a significant range of duty cycles.

In order to select the cycle frequencies to be evaluated, the missions were evaluated using both the peak-to-peak and segment editing mode. The first evaluation used the peak-to-peak editing mode. Figure 3.8 shows the variation of ramp time with temperature and R. The data in Figure 3.8a shows that the ramp times vary from 1 to approximately 550 seconds. Based on this information the ramp times selected for experimental evaluation were 1.5, 15, and 150 seconds which corresponds to cycle periods of 3, 30 and 300 seconds. Figure 3.8b shows that the selected stress ratios are appropriate for the

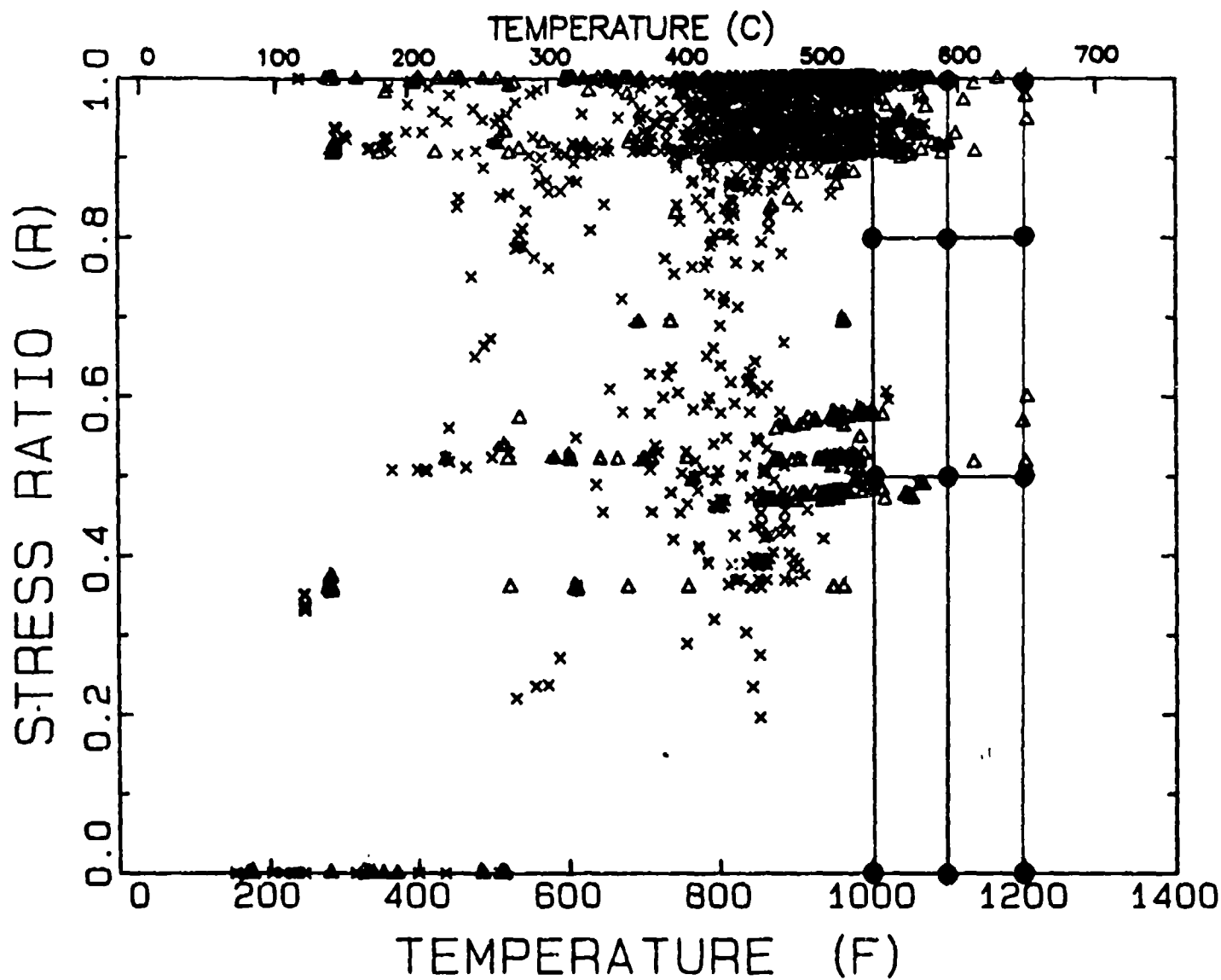


Figure 3.6: Variation of stress ratio with temperature for eighteen missions.

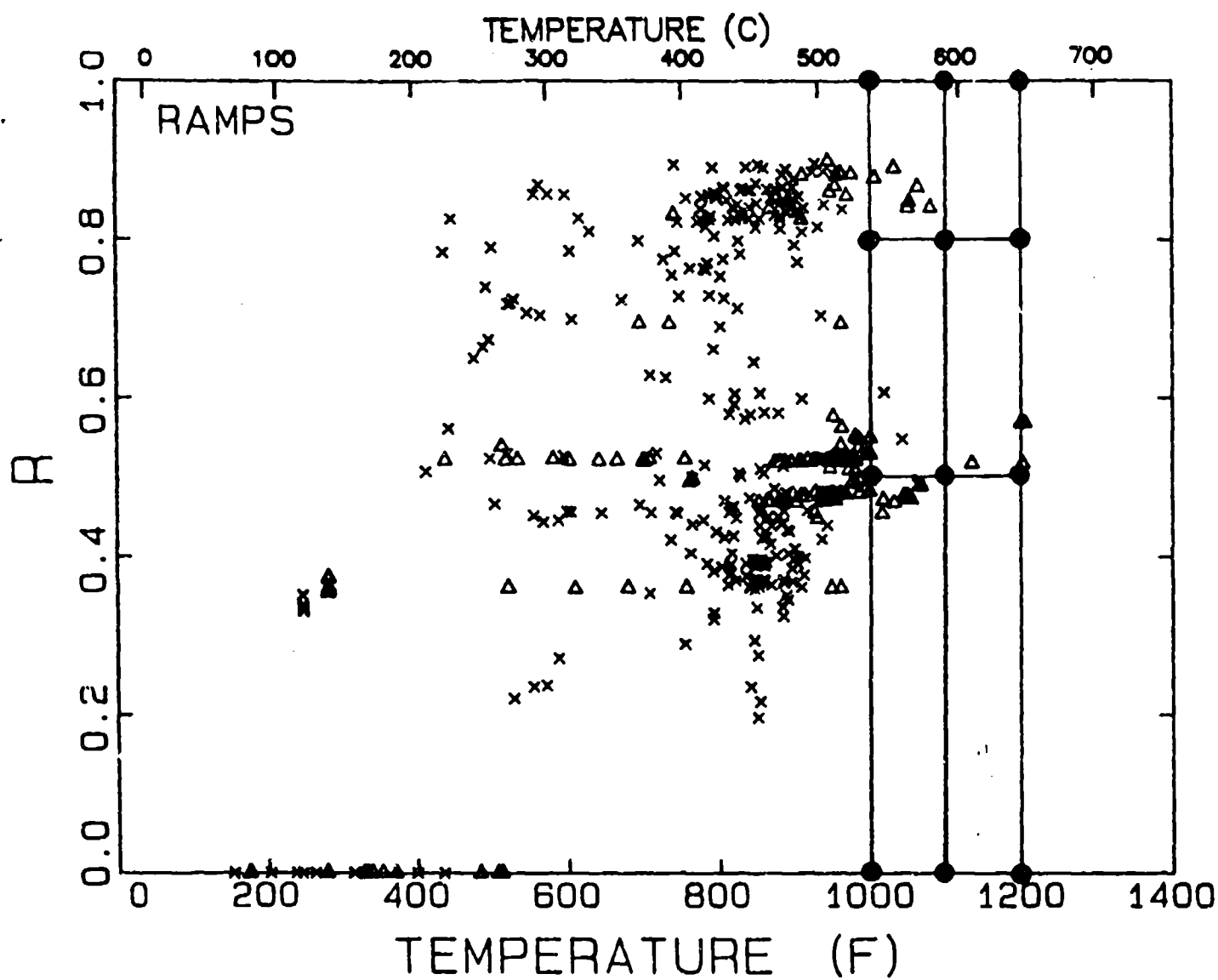
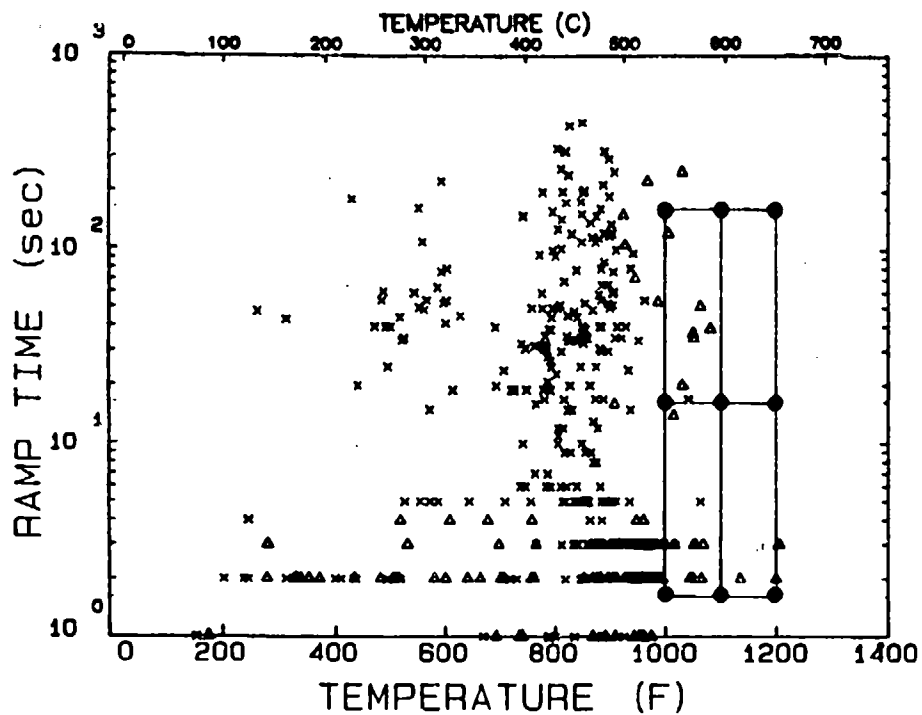
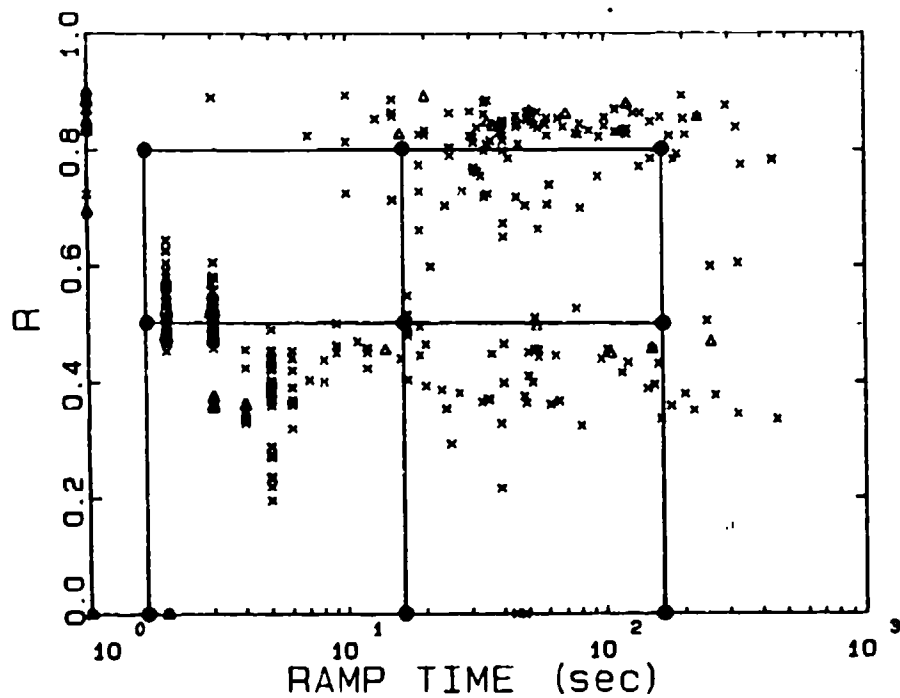


Figure 3.7: Variation of stress ratio of ramp segments with temperature.



(a)



(b)

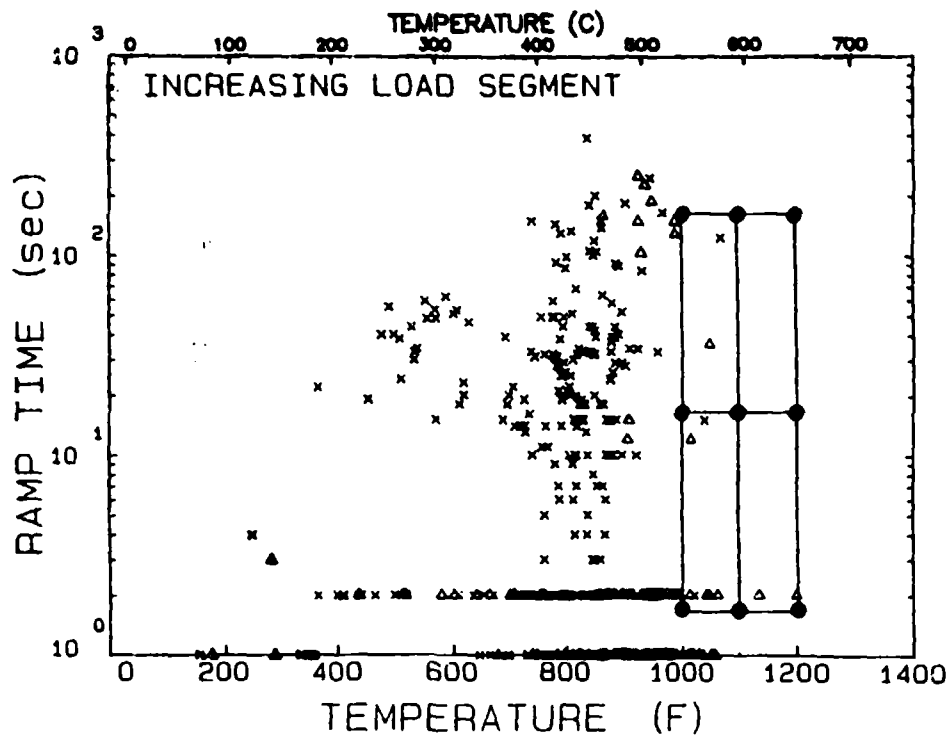
Figure 3.8: Variation of (a) ramp time with temperature and (b) stress ratio with ramp time for individual segments of eighteen missions.

slower frequencies especially when considering the potential decrease in R with elastic-plastic analysis.

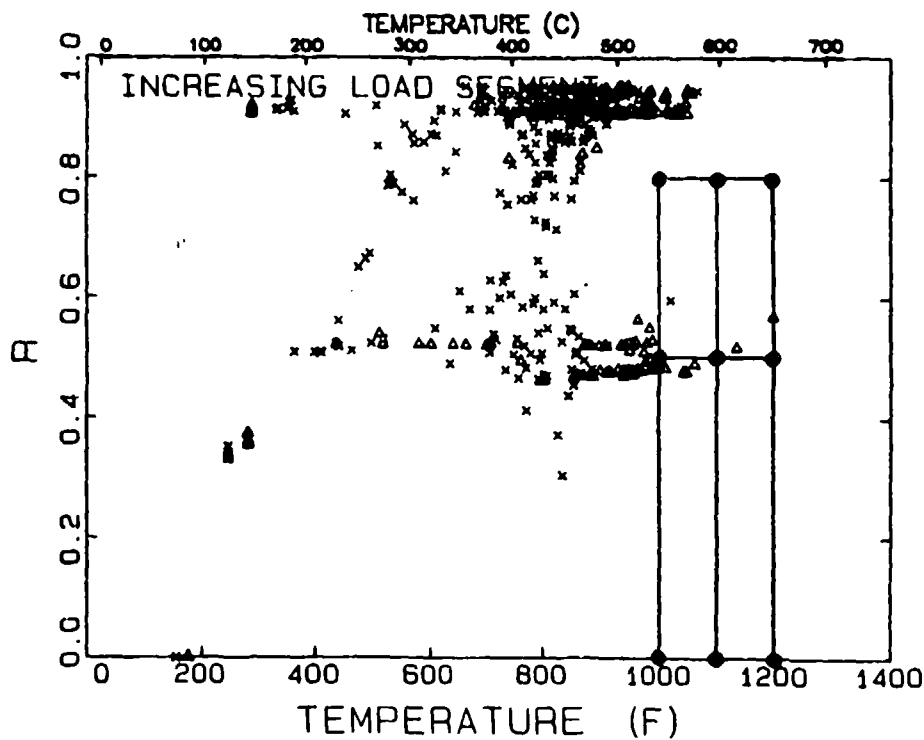
Figure 3.9 shows similar data to Figure 3.8 but for only the increasing segment mode. Figure 3.9b shows two distinct populations of data - (1) variable R for ramp times less than 5 seconds and (2) ramp times of up to 400 seconds at high R ratios. The first case corresponds to true loading and unloading while a large portion of the second case largely represents conditions approaching hold times. The selected conditions at stress ratios of zero and 0.5 for ramp times of 15 and 150 seconds are not important to the mission but are important for the development of time dependent crack growth models.

Figure 3.10 shows the variation of hold time length with temperature for these 16 missions. The box shown in this figure encloses the region investigated in this program. The testing conditions include hold times of 0 (continuously cycled), 4, 30, and 300 seconds. Figure 3.10 shows that there are hold times in excess of 300 seconds but due to test time restrictions and modeling development requirements this seems adequate. Figure 3.11 shows an expanded version of Figure 3.10 for temperatures in excess of 510°C (950°F) and hold times longer than 10 seconds. This shows that these testing conditions bracket a significant range of data. Figure 3.11 also shows that only 5 hold times are at temperatures in excess of 593°C (1100°F). If engine temperatures increase, which is typical for improved versions of a given engine, the range of temperatures evaluated will still encompass a large amount of the hold time population.

The underpeaks calculated for hold times is based on the previous local minimum so that the underpeak ratio can be considered to be the stress ratio associated with a hold time. Figure 3.12 shows a plot of underpeak ratio with temperature for hold times in excess of 10 seconds at temperatures above 510°C (950°F). In this plot underpeaks in excess of unity indicate that the hold time was preceded by an overpeak. Overpeaks will be discussed later in this section. The data in Figure 3.12 shows a large population of underpeaks ratio between 0.8 and 1.0 as well as in the vicinity of 0.5. Underpeak ratios near



(a)



(b)

Figure 3.9: Variation of (a) ramp time with temperature and (b) stress ratio with ramp time for increasing load segments of eighteen missions.

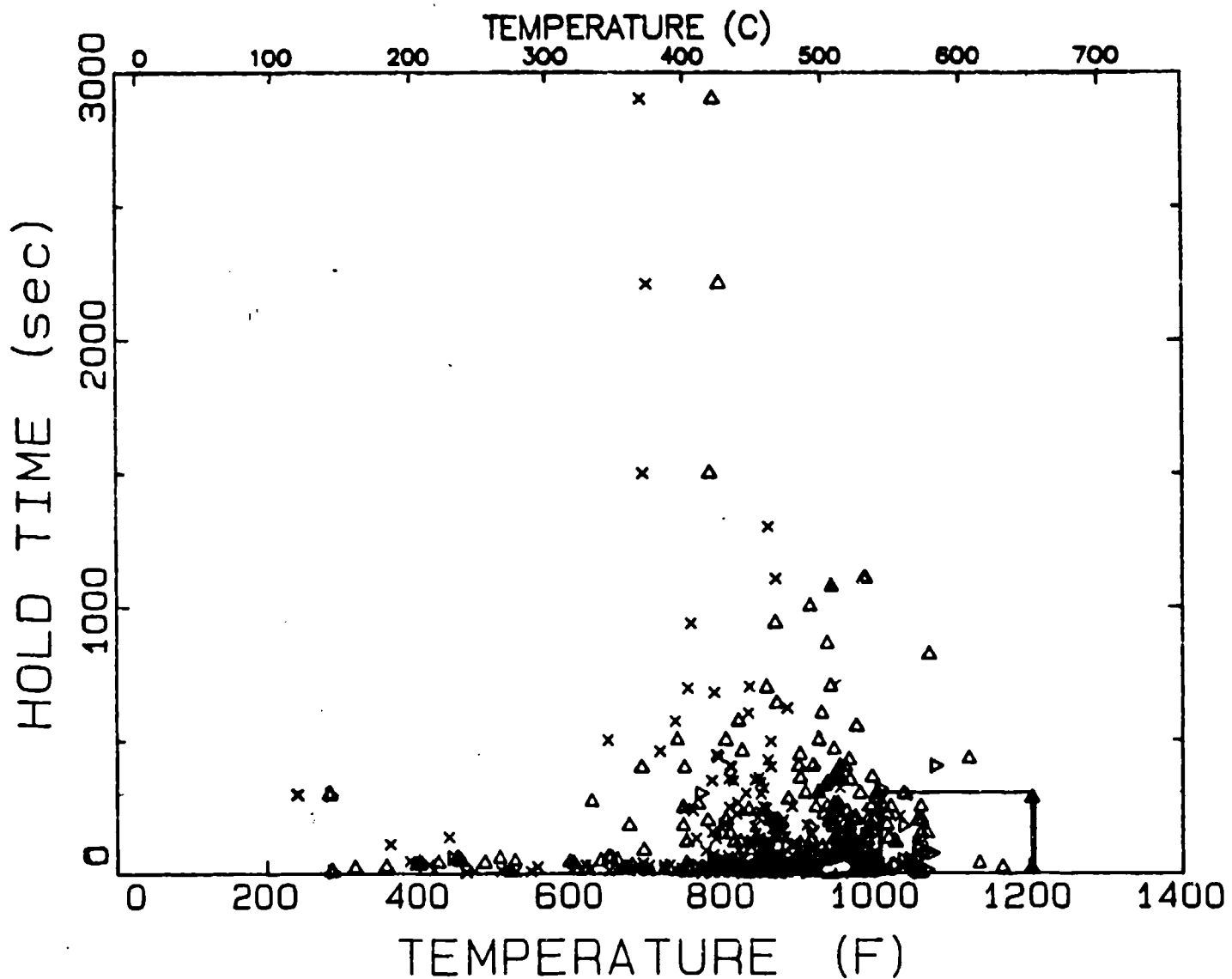
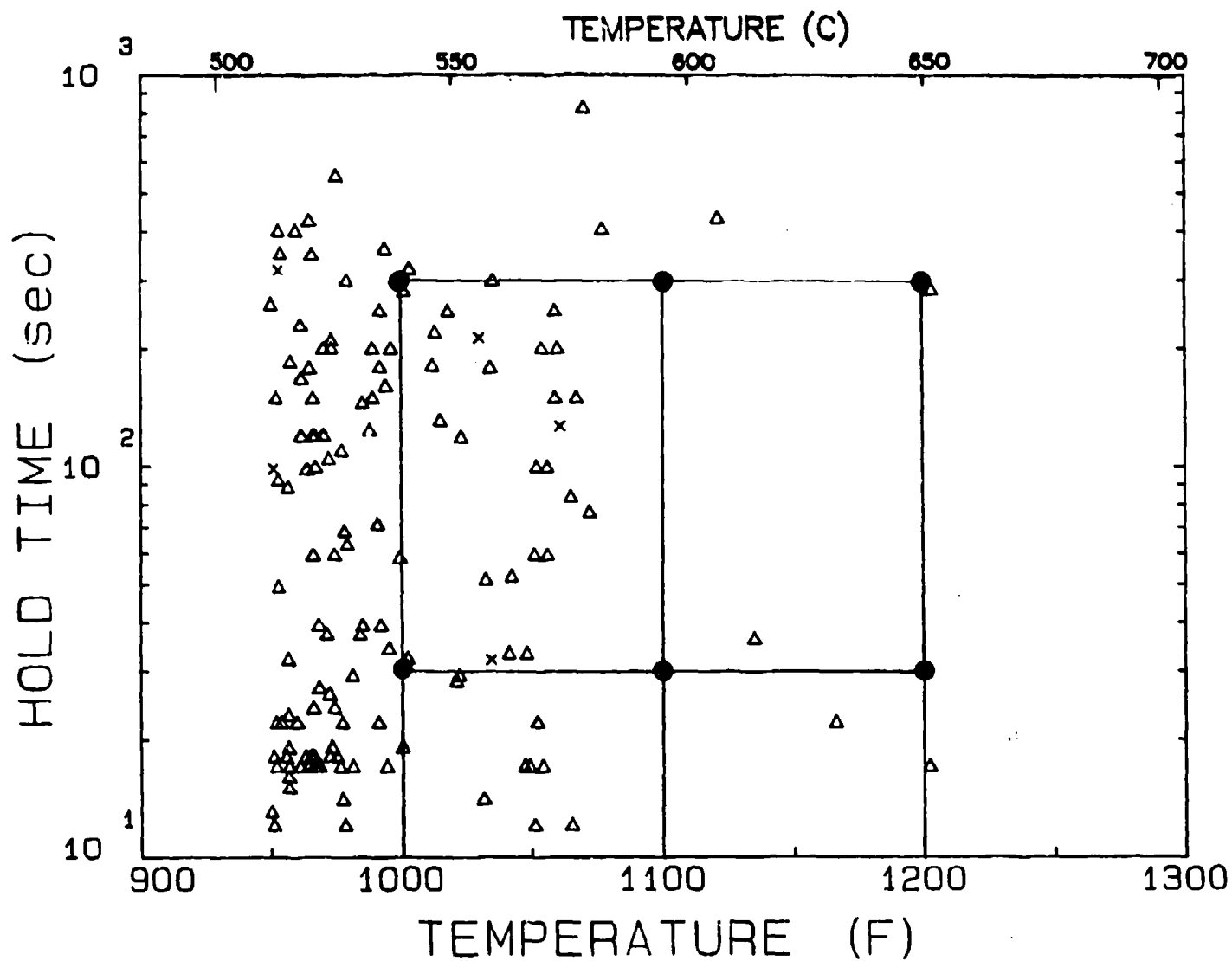


Figure 3.10: Variation of hold time with temperature for eighteen missions.





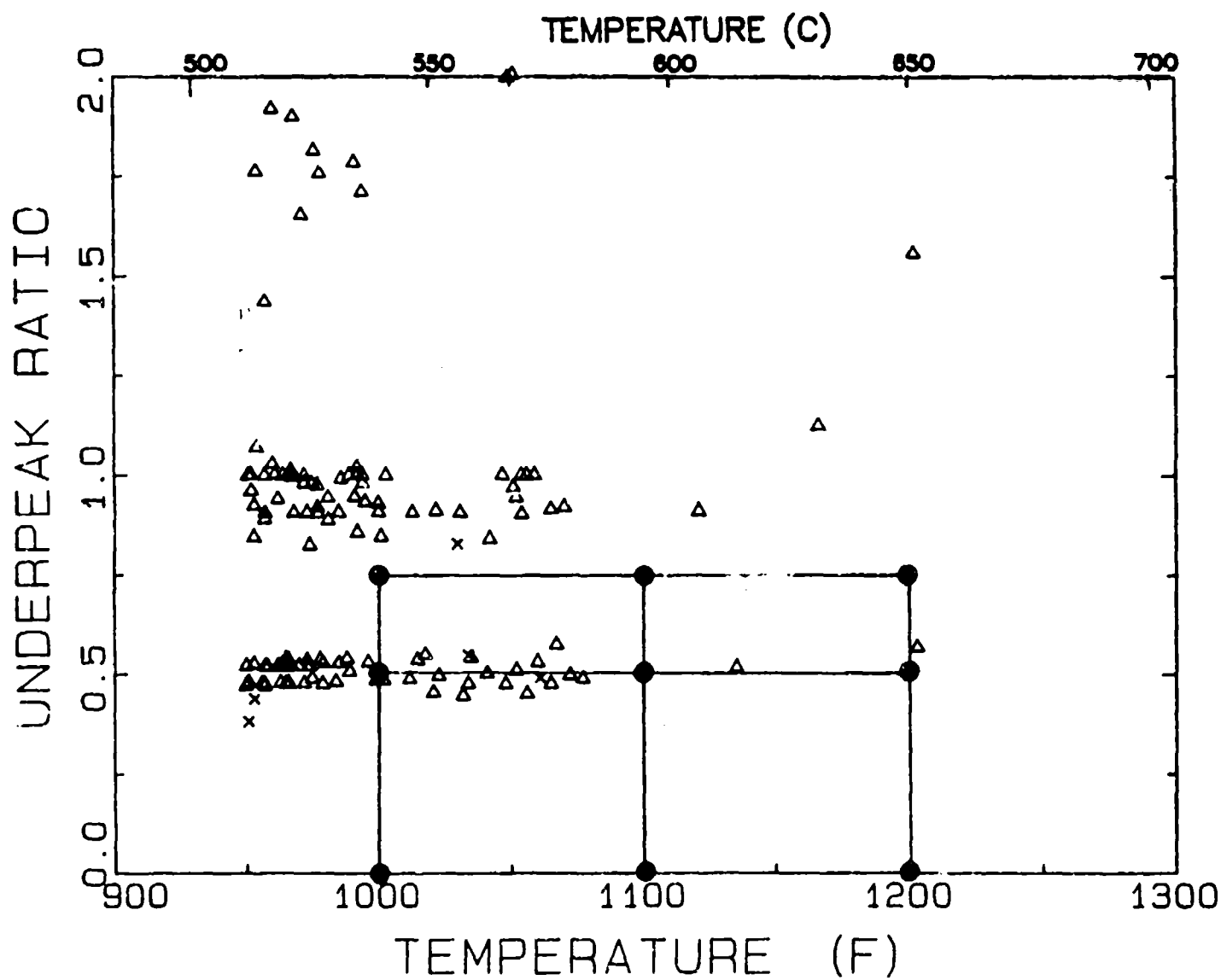


Figure 3.12: Variation of underpeak ratio (stress ratio) of hold times with temperature greater than 510°C with temperature.

unity were assessed with the static load tests. The remaining test conditions seem to bracket the mission points.

Figure 3.13 shows the overpeak ratios for the same hold time population shown in Figure 3.12. There seem to be two populations of overpeaks - one between 1.0 and 1.2 and another at approximately 2.0. Weerasooriya and Nicholas<sup>(50)</sup> have shown that overpeak ratios of 1.25 totally eliminate the degrading influence of hold times in Alloy 718 at 649°C (1200°F). Overpeak ratios of 1.1, 1.2, and 1.5 were investigated to cover the conditions shown in Figure 3.13.

The 18 simplified missions were edited using the peak-to-peak mode to consider to range of overpeaks for loading and unloading segments. These missions were further edited to eliminate ramps with stress ratios in excess of 0.9 to avoid cycles which approximate hold times. Figure 3.14 shows the overpeak ratios as a function of temperature and stress ratio. As for the case of hold times, the strategy of evaluating overpeak ratios of 1.1 to 1.5 seems to be a reasonable approach.

The conditions selected for the experimental test program are listed in Table 3.1. These conditions encompass a large variety of mission spectrum, include a range of conditions where time-dependent crack growth occurs, and provides the wide range of experimental variables necessary for the development of an advanced time dependent crack growth model.

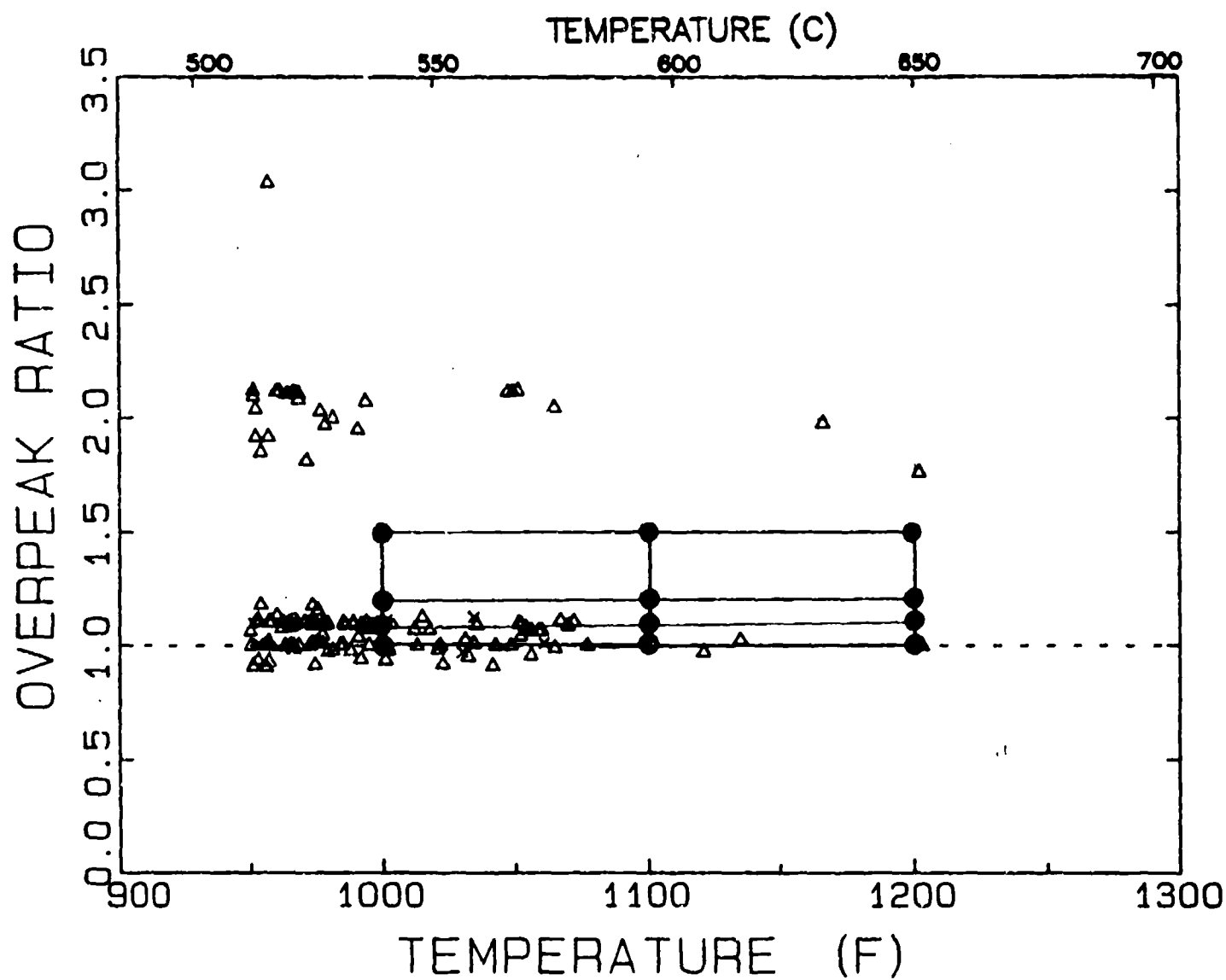
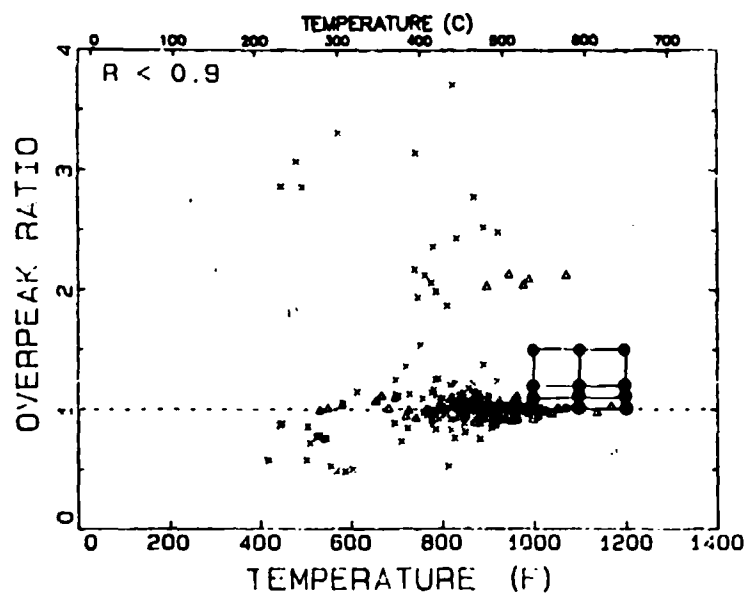
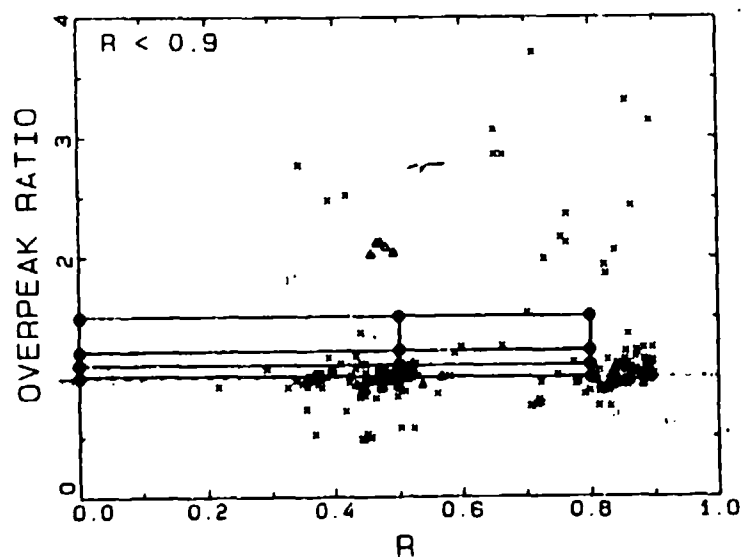


Figure 3.13: Variation of overpeak ratios of hold times with temperatures in excess of 510°C with temperature



(a)



(b)

Figure 3.14: Variation in overpeak ratio with (a) temperature and (b) stress ratio for loading and unloading segments ( $R < 0.9$ ).

**Table 3.1: Conditions for Task II Testing**

<b>Temperature</b>	538, 593, 649°C (1000, 1100, 1200°F)
<b>Stress Ratio (R)</b>	0, 0.5, 0.8, and 1.0
<b>Ramp Cycle Period</b>	3, 30, and 300 seconds
<b>Hold Times</b>	0, 4, 30, and 300 seconds
<b>Overpeak Ratio</b>	1.1, 1.2, and 1.5

#### 4.0 MATERIALS AND EXPERIMENTAL TECHNIQUES

This section of the report describes the materials evaluated and the experimental techniques used to determine the crack growth properties in this investigation. Sources and examples of error in the crack growth experiments are also presented.

##### 4.1 MATERIALS

Two materials were selected for this investigation: powder metallurgy Rene'95 processed by extrusion plus isothermal forging (E+IF), and cast plus wrought (C+W) Alloy 718. The E+IF processing technique for Rene'95 was developed to attain a fine grain size for high tensile strength and good LCF life<sup>(52)</sup>. E+IF Rene'95 was selected as the primary material for this study because it is widely used in military high pressure turbine disk applications. It has also been the subject of recent fracture mechanics modeling and processing-microstructure-property investigations (43,53).

The second material, C+W Alloy 718, is currently used in a variety of aircraft engine applications including compressor, low pressure turbine, and high pressure turbine disks. The fatigue crack growth behavior of this alloy has probably been more extensively studied than any other nickel-base superalloy(18,24,28,29,50,54-57).

##### 4.1.1 Rene'95

All Rene'95 specimens for this investigation were removed from the rim region of a single F101/F110 high pressure turbine disk forging. The E+IF Rene'95 disk was processed using argon atomized powder from Special Metals heat BN84056. As shown in Table 4.1, the composition of this heat meets all specification requirements. Powder from the -150 mesh yield was consolidated into extruded billet by Cameron Iron Works. Ladish Company prepared the billet and performed the isothermal forging. The forged disk was heat treated at 1107°C (2025°F) for one hour, oil quenched, and aged at 760°C (1400°F) for eight hours. Table 4.2 lists the tensile, creep and stress rupture properties

Table 4.1: Composition Of Rene'95 Disk  
(Weight Percent)

<u>Element</u>	<u>Specification</u>	<u>Heat Analysis</u>
C	0.04-0.09	0.06
Mn	0.15 Max	0.02
Si	0.20 Max	0.07
S	0.015 Max	0.004
P	0.015 Max	>0.01
Cr	12.0-14.0	13.38
Fe	0.50 Max	0.16
Co	7.00-9.00	8.51
Mo	3.30-3.70	3.47
Nb	3.30-3.70	3.68
Ti	2.30-2.70	2.49
Al	3.30-3.70	3.52
B	0.006-0.015	0.007
W	3.30-3.70	3.45
Zr	0.03-0.07	0.04
O	0.010 Max	>0.0082
N	0.005 Max	>0.0041
H	0.001 Max	>0.0004
V		0.10
Hf		0.01
Cu		0.024
Ta		0.05
Ni	Balance	

Table 4.2: Test Ring Properties Of Rene'95 Disk

<u>Tensile Properties</u>		
	<u>Room Temperature</u>	<u>649°C (1200°F)</u>
0.2% Offset Yield Strength (MPa)	1261	1109
Ultimate Tensile Strength (MPa)	1702	1426
Tensile Elongation (%)	20.0	9.0
Reduction in Area (%)	24.0	12.0
 <u>Rupture Properties</u>		
	<u>649°C (1200°F) 965 MPa (140 ksi)</u>	
Hours to Failure	173.6	
Rupture Elongation (%)	6.0	



obtained from the test ring location. These properties are typical for this component.

Optical metallography and transmission electron microscopy (TEM) replica techniques were used to study the microstructure of a typical test specimen from the E+IF Rene'95 disk rim. The optical micrographs of Figure 4.1 show that the grain structure is very uniform with a grain size of about 5  $\mu\text{m}$ . Although large, primary  $\gamma'$  precipitates are present at grain boundaries as shown in the high magnification optical micrograph, Figure 4.1b, the precipitate distribution is more clearly evident in the TEM replica micrograph of Figure 4.1c. Three size ranges of the  $\gamma'$  precipitate are present. The large grain boundary primary  $\gamma'$  results from precipitation of this phase during the extrusion, forging, and heat treatment procedures. These  $\gamma'$  particles are typically 2-3  $\mu\text{m}$  in size. Particles of an intermediate size (0.2  $\mu\text{m}$ ) are located within the grains and form during cooling after the 1107°C exposure. The third size range of  $\gamma'$  consists of very small precipitates, several hundred angstroms in size, which form on aging. These fine precipitates are barely discernible in the TEM micrograph and are distributed uniformly among the intermediate  $\gamma'$ . This microstructure is typical of E+IF Rene'95.

#### 4.1.2 Alloy 718

The Alloy 718 used in this investigation was obtained from commercially available hot-rolled plate. This material is the same as that used in a NASA-sponsored investigation of elastic-plastic fatigue crack growth(58). The plate had a nominal thickness of 22.2 mm (0.875 in.) and was procured in 2 pieces, each measuring 381 mm (15 in.) by 406 mm (16 in.). Both plates were produced by Cabot Corporation from heat 2180-1-9836. The ladle composition and specification for Alloy 718 are compared in Table 4.3. The composition falls within the specified limits.

The Alloy 718 plate material was procured in the mill annealed condition. Heat treatment was subsequently performed by the GE Engineering Material Technology Laboratory (EMTL) using a standard solution plus duplex age

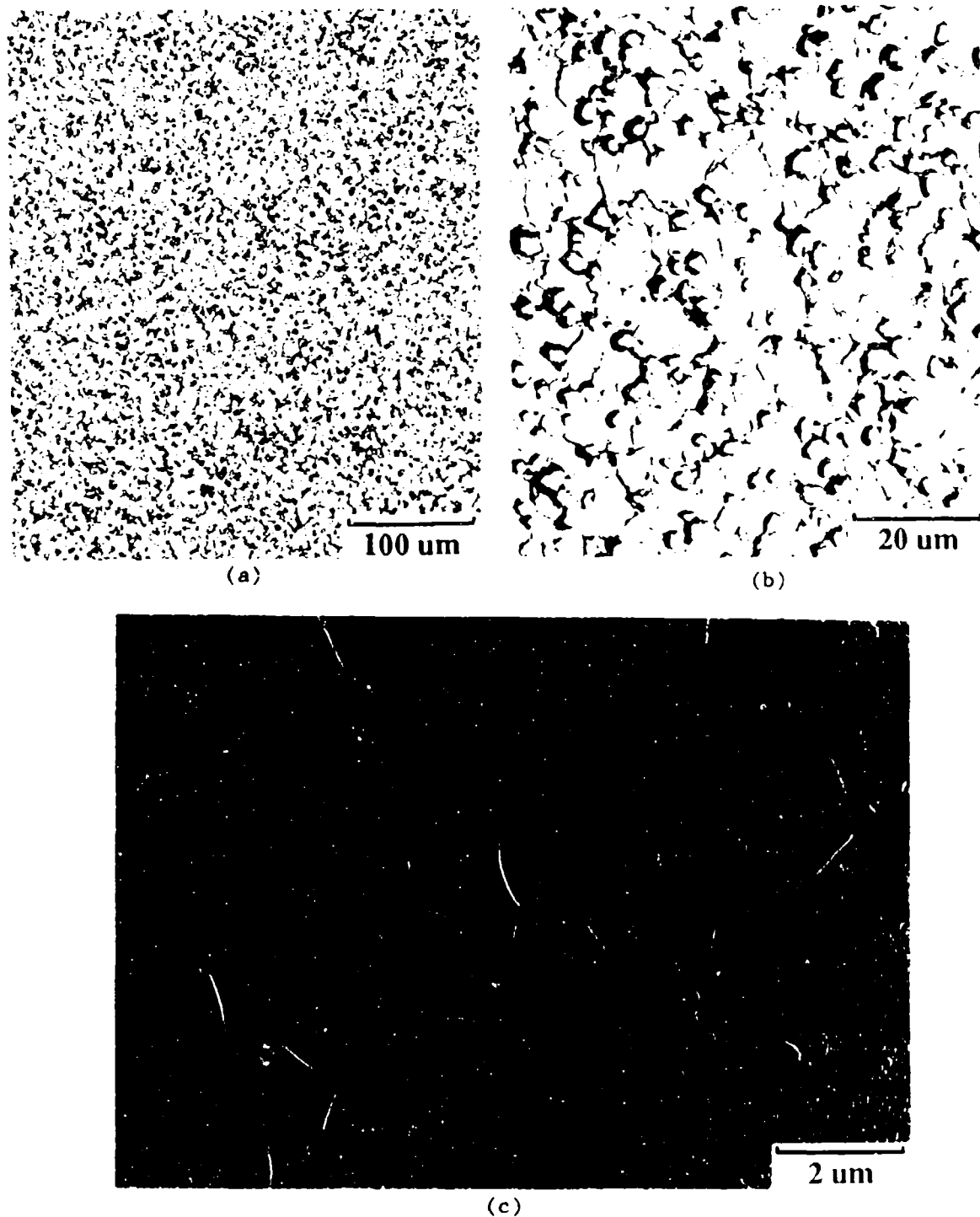


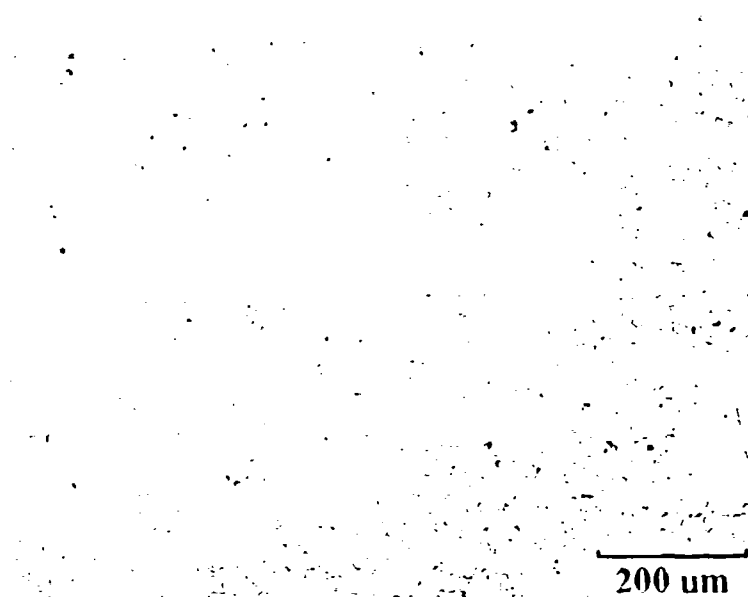
Figure 4.1: Microstructure of Rene'95 forging as shown with (a) low magnification optical micrograph, (b) high magnification optical micrograph, and (c) TEM replica micrograph.

Table 4.3: Composition Of Alloy 718 Plate  
(Weight Percent)

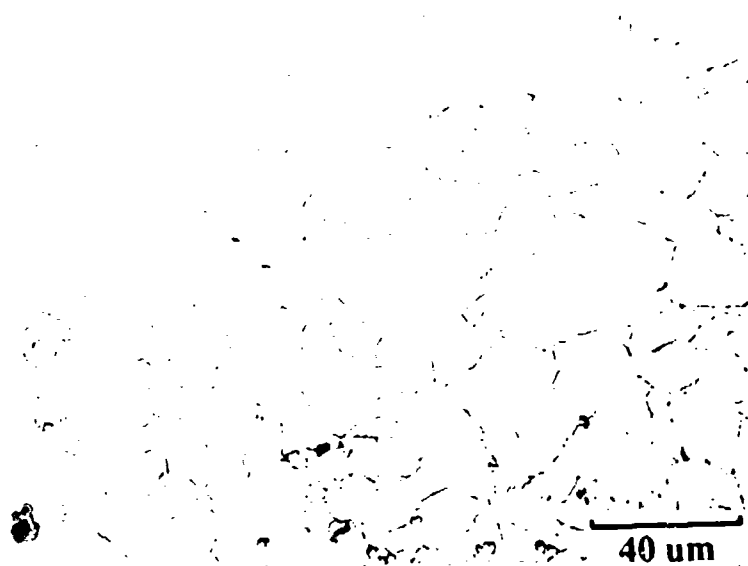
<u>Element</u>	<u>Specification</u>	<u>Ladle Analysis</u>
C	0.02-0.08	0.06
Mn	0.35 Max	0.17
Si	0.35 Max	0.17
S	0.015 Max	0.002
P	0.015 Max	0.006
Cr	17.0-21.0	17.92
Fe	15.0-21.0	18.32
Co	1.0 Max	0.10
Mo	2.80-3.30	3.03
Nb+Ta	4.75-5.50	5.11
Ti	0.75-1.15	1.12
Al	0.30-0.70	0.45
B	0.006 Max	0.002
Cu	0.30 Max	0.03
Ni	50.0-55.0	53.63

treatment for Alloy 718. After solution treatment at 968°C (1775°F) for one hour and cooling to room temperature, the plates were aged at 718°C (1325°F) for eight hours, cooled at 56°C/hr. (100°F/hr.) to 621°C (1150°F), and aged at this temperature for an additional eight hours. Tensile, creep, and cyclic properties for the Alloy 718 plate were determined over the temperature range from room temperature to 649°C (1200°F). The results were typical of Alloy 718 and have been reported elsewhere<sup>(58)</sup>

Optical metallography was used to characterize the grain structure of a typical test specimen from the Alloy 718 plate after full heat treatment. Figure 4.2 shows low and high magnification optical micrographs which illustrate the microstructure of the Alloy 718 plate in the plane containing the rolling and plate thickness directions. The rolling direction is displayed horizontally in these micrographs. The microstructure observed in the plane containing the plate width and thickness direction is shown in Figure 4.3 where the plate width is shown horizontally. These micrographs exhibit a duplex grain structure where large, elongated, unrecrystallized grains are surrounded by fine recrystallized grains. These fine grains are the predominant feature and measure about 20  $\mu\text{m}$  in size. The unrecrystallized grains are elongated parallel to the rolling direction and measure as large as 50 by 200  $\mu\text{m}$  in size. Stringers of fine carbide and nitride particles are also evident in Figure 4.3b. At high magnification, one of the precipitate phases present in Alloy 718 can be seen at the grain boundaries in the form of small, discontinuous, acicular particles. This is the orthorhombic  $\text{Ni}_3\text{Cb}$  phase which precipitates during rolling and solution treatment procedures. The strengthening phase in Alloy 718, ordered  $\text{DO}_{22}$   $\text{Ni}_3(\text{Cb}, \text{Ti}, \text{Al}) \gamma''$ , is not visible in the optical micrographs and can only be studied using TEM thin foil techniques. For fully heat treated Alloy 718 materials, these precipitates are disc-shaped with a diameter of several hundred Angstroms. Alloy 718 also contains a small amount of spherical-shaped  $\gamma'$  precipitates, with a similar diameter<sup>(55,59)</sup>.



(a)



(b)

Figure 4.2: Optical micrographs of Alloy 718 plate at (a) low and (b) high magnifications. The rolling direction is displayed horizontally and the plate thickness direction is shown vertically.

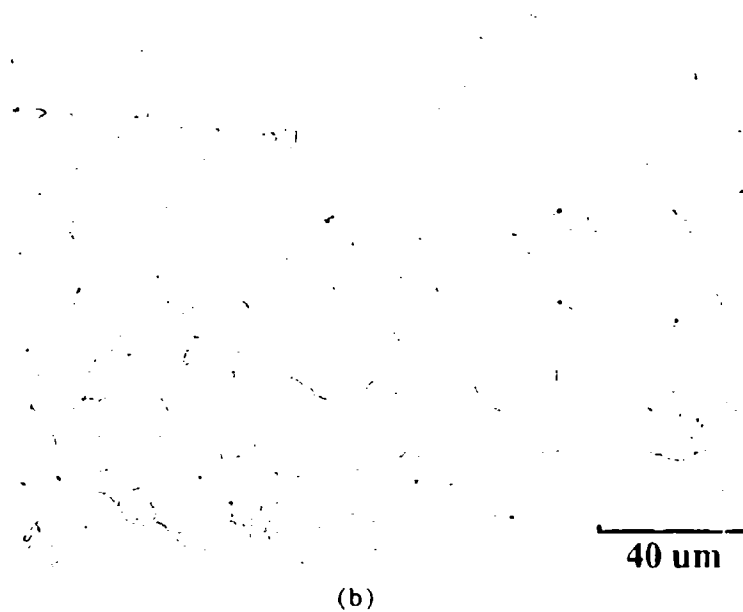
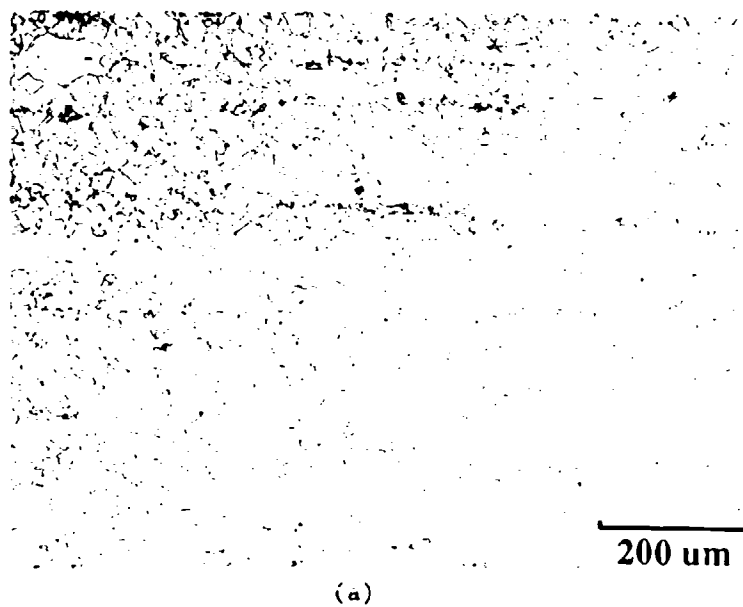


Figure 4.3: Optical micrographs of Alloy 718 plate at (a) low and (b) high magnifications. The plate width direction is displayed horizontally and the plate thickness direction is shown vertically.

From the preceding description of microstructure, it is evident that although both Rene'95 and Alloy 718 materials can be described as nickel-base superalloys, they have different strengthening precipitates and microstructures.

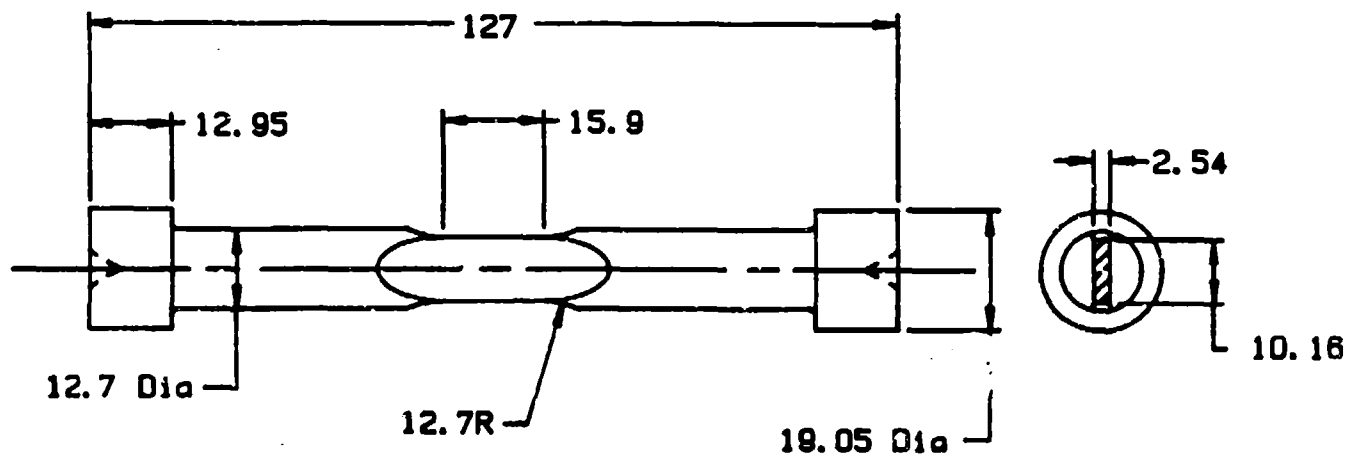
#### 4.1 SINGLE EDGE NOTCH SPECIMEN

A buttonhead single edge notch (SEN) specimen was used in the crack growth experiments. Figure 4.4 shows the drawing of this specimen. The gage section of this specimen has a thickness of 2.54 mm (0.1 inch) and a width of 10.2 mm (0.4 inch). Pin-loaded SEN specimens with this gage section geometry have previously been used by GEAE to determine the crack growth properties of a wide variety of superalloys over a range from room temperature to 980°C (1800°F)(42,43,55,60). The modification of the specimen from pin to buttonhead loading was originally made to accommodate cyclic loading with compressive loads(56).

The buttonhead geometry was selected for this investigation because the usable extent of crack length for the buttonhead geometry is greater than that for the pin-loaded specimen. Elevated temperature crack growth of a nickel base superalloy measured in a pin-loaded SEN specimen for crack length to specimen width ratio ( $a/W$ ) greater than 0.5 did not agree with other data for the same material(42). The K-solution for this specimen is valid to the larger crack lengths, but assumes free rotation between the loading pin and the specimen. The discrepancy in crack growth rates described above was probably caused by oxidation of the loading pins and specimen which prevented the free rotation at this location. The analysis of the buttonhead geometry assumes no such rotation so the usable extent of crack length is much larger.

The value of  $K$  for the buttonhead SEN specimen was calculated using the solution developed by Harris(61) for restrained bending in a single edge notch specimen.

$$K = \sigma \sqrt{\pi a} \left( 5 / \sqrt{20 - 13 (a/W) - 7 (a/W)^2} \right) \quad (5.1)$$



Dimensions are millimeters.

Figure 4.4: Buttonhead single edge notch (SEN) specimen



The validity of this relationship was verified by Malik and Gilbert<sup>(62)</sup>, who calculated K-values using both influence functions and J-integrals from the elastic finite element analysis of the buttonhead SEN specimen<sup>(58)</sup>. They found that their results agreed within several percent to those calculated using the equation developed by Harris.

#### 4.2 TEST SPECIMEN MACHINING AND ORIENTATION

The Rene'95 test specimens were removed from the rim portion of the high pressure turbine disk. This region of the disk was selected for the mission analysis (Section 3.0) because it experiences high operating temperatures during service. Removal of specimens from this region assured that the microstructure represented the appropriate area of interest in the disk. In order to increase material availability from this location, the Rene'95 crack growth specimens were fabricated by inertia welding. The 5 cm (2 inch) long gage blanks had a radial orientation and were removed with from the outer 10 cm (4 inch) of the disk. The gage sections were inertia welded to Alloy 718 buttonhead blanks. The inertia welded assembly was then machined into the buttonhead SEN geometry. The inertia weld blanks were marked so that SEN gage sections would be be machined to have crack growth in the the circumferential direction of the disk.

The Alloy 718 specimens were not fabricated from inertia welded assemblies. The specimens were oriented so that the loading axis was parallel to the longitudinal direction in the plate and the cracks grew in the transverse direction.

Prior to testing, a 0.25 mm (0.01 inch) deep electric discharge machined (EDM) crack starter notch was placed in each specimen. Each notch was centered in the gage length and traversed the 2.54 mm (0.1 inch) thickness of the gage length.

#### 4.3 POTENTIAL DROP TEST METHOD

Crack lengths were monitored using a direct current electric potential drop technique<sup>(63)</sup> adapted to the SEN geometry by Wilcox and Henry<sup>(64)</sup>. The test technique is shown schematically in Figure 4.5. Direct current was passed through the specimen. Potential leads located approximately 0.4 mm (0.016 inch) above and below the EDM notch/crack were used to obtain the potential values using either an on-off<sup>(63)</sup> or reversing potential<sup>(65)</sup> technique. The microcomputer monitored the potential and converted it to potential using the SEN potential solution developed by Johnson<sup>(66)</sup>. The microcomputer also controlled the test permitting either load- or K control testing. Potential data is taken on almost every cycle. After a predetermined number of cycles known as the block size, the potential data was averaged and stored on a floppy disk for post-test analysis. For K-controlled tests, the loads required to obtain the desired K-value was calculated at the end of each block of cycles using the Harris solution<sup>(61)</sup> and the loads are adjusted.

Henry and coworkers<sup>(67)</sup> have improved this test method so that the microcomputer can also control the cycle period and hold time. This modification permitted preprogramming of the several test segments so that the operator does not have to manually adjust the test machine function generator when the cycle frequency or hold time changed for a given test specimen.

#### 4.4 TEST DESCRIPTION AND DATA ANALYSIS

The crack growth tests in this investigation fall into two classifications -- threshold tests and constant  $\Delta K$  tests. The latter type of test was performed to evaluate the influence of R-ratio, hold time, cycle frequency, and overpeak cycling on Region II (Paris law) crack growth rates. Each classification of test will be described separately.

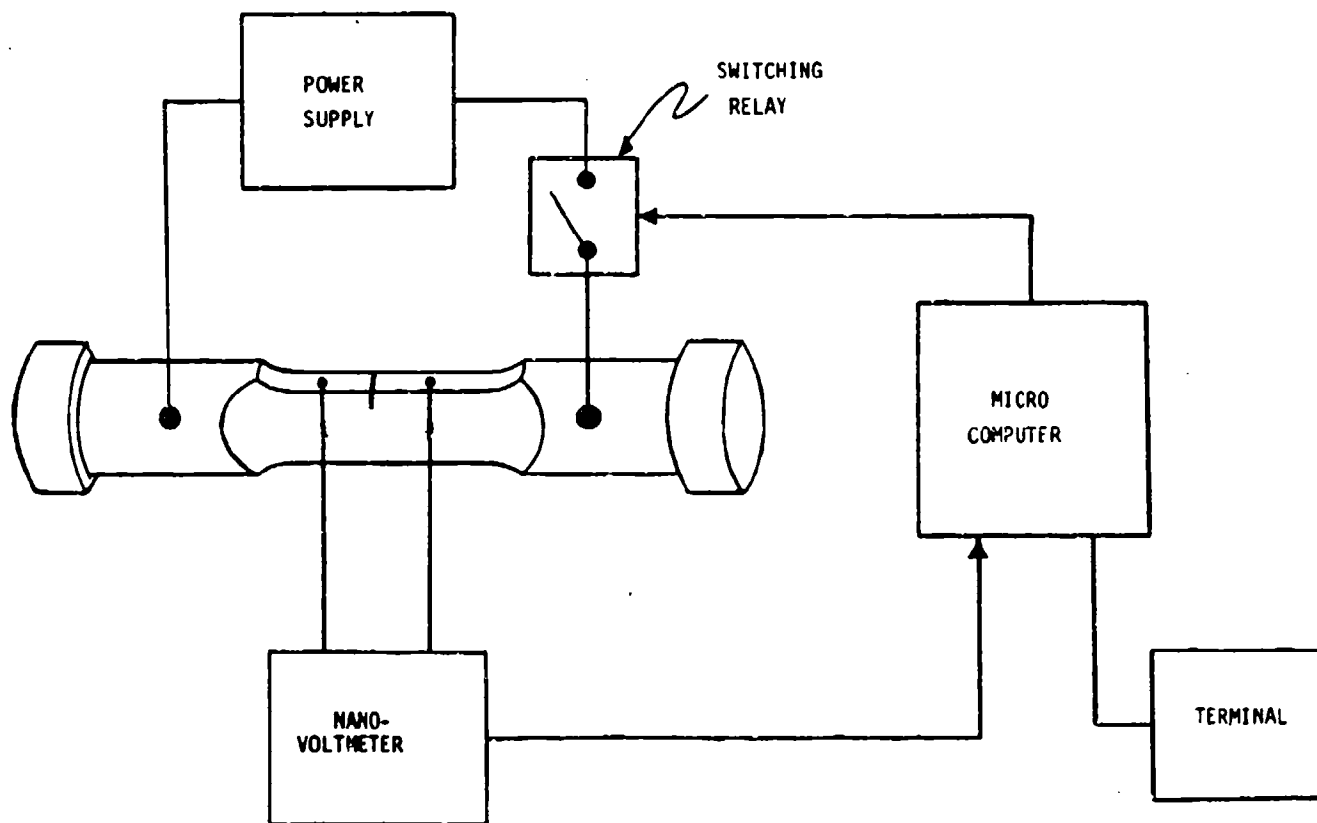


**Figure 4.5:** Schematic diagram of SEN specimen DC potential drop test apparatus.

#### 4.4.1 Threshold Tests

The threshold tests were performed at constant values of temperature, R-ratio, and cycle type (frequency or hold time). In these tests, the specimen was precracked and then cycled in a decreasing K mode until the crack growth rates approached  $1 \times 10^{-7}$  mm/cycle ( $4 \times 10^{-9}$  inch/cycle). In some tests, the specimen was then cracked in an increasing K mode (constant load or  $\Delta K/\Delta a$ ) to determine Region II crack growth rates. Figure 4.6 shows an example of the K-crack length history for this type of test. The K-shed routine was performed by controlling a shed rate constant C.

$$C = 1/K \text{ (dK/da)} \quad (4.2)$$

The value of C used in this investigation was -1.18/mm (-30/inch). This value was selected based on the work of Henry(67) and shed rate experiments described later in this section. The increasing K portion of the tests was performed so that the value of K increased linearly with crack length (dK/da = constant). In most tests, the crack was grown from a  $K_{max}$  value of several MPa/m above the measured threshold value to a  $K_{max}$  value of approximately 55 MPa/m over a distance of approximately 1.3 mm (0.05 inch).

After each test, the specimen was broken at room temperature and the crack lengths were measured on the fracture surface. Many of the tests in this investigation exhibited rather severe tunneling where the crack length at the center of the specimen was significantly longer than at the surface. This has been reported previously during elevated temperature hold time(34) and static(33) crack growth tests on nickel base superalloys. The crack length was measured at both free surfaces and three equally spaced positions across the specimen width. The average of the internal three positions was used as the crack length in the potential and K calculations.(68)

The data obtained during the K-shed and increasing K portions of the threshold tests were analyzed separately. The load and potential drop data was reaveraged so that 50 to 100 data points were obtained from each part of the test. The measured crack lengths, potential data, and load data were then

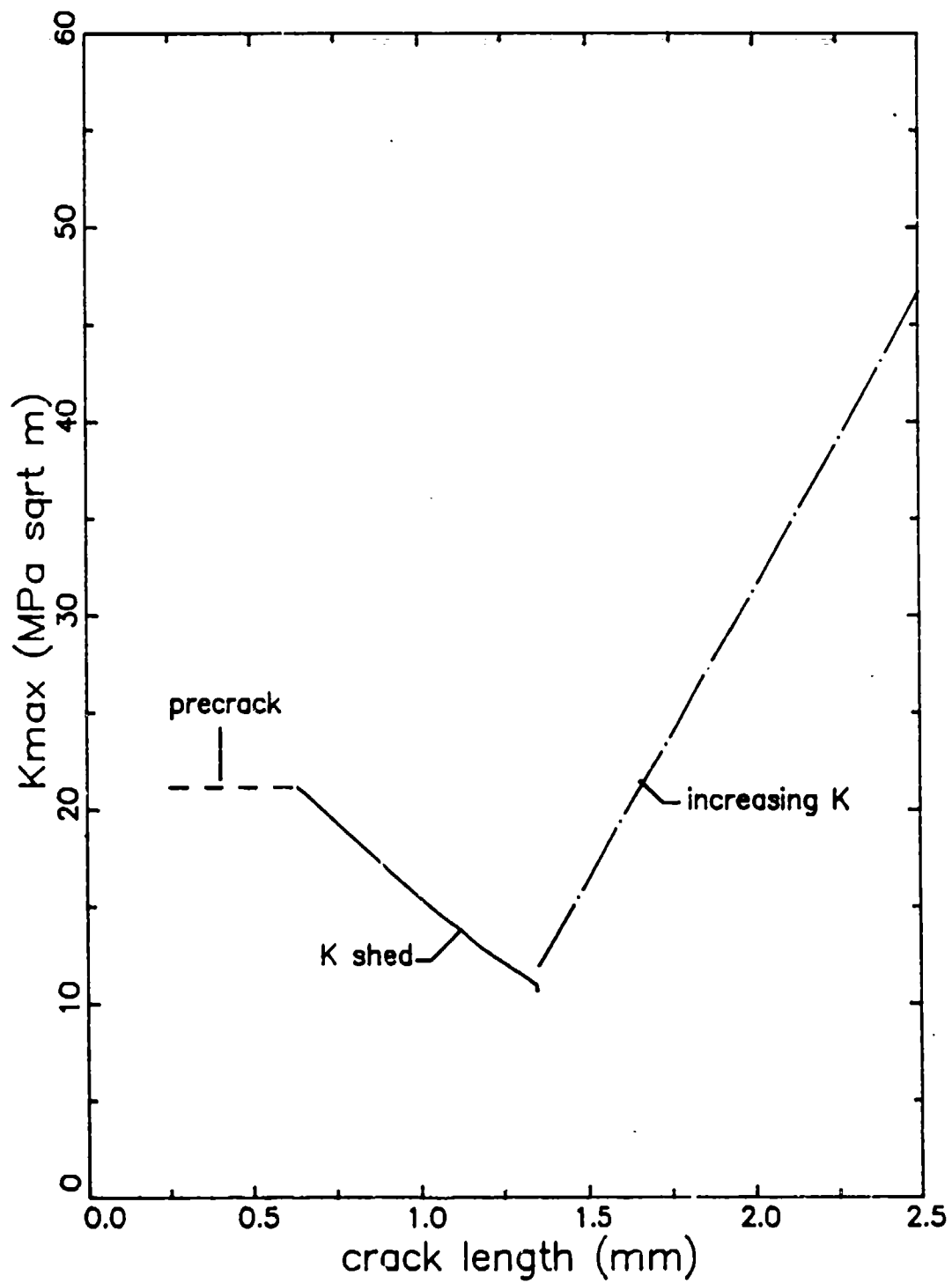


Figure 4.6: Typical K-history for a threshold crack growth test.

analyzed using the appropriate potential and K solutions. The measured crack lengths were used to correct the crack lengths as predicted using the potential solution<sup>(68)</sup>. The crack growth rates were calculated using the seven point sliding polynomial technique. An expanded description of this data analysis procedure was reported by Krueger<sup>(69)</sup>.

The ASTM standard test method<sup>(68)</sup> for determining near-threshold crack growth rates recommends that the value of the shed rate constant C should not be less than  $-0.078/\text{mm}$  ( $-2/\text{inch}$ ). The use of higher shed rates (more negative values of C) is permitted if it can be shown that the higher shed rate does not adversely affect the ability to measure near-threshold crack growth rates. The influence of shed rate on crack growth rates results primarily from overpeak retardation. If K is shed too rapidly, some overpeak retardation may occur resulting in artificially high values of threshold. Henry<sup>(67)</sup> demonstrated for nickel-base superalloys that the value of C must be less than  $-1.57/\text{mm}$  ( $-40/\text{inch}$ ) to influence the threshold values measured for 0.33 Hz cycling (20 cpm). Zawada and Nicholas<sup>(70)</sup> have also demonstrated that the value of C can be reduced substantially from that recommended by ASTM for nickel-base superalloys.

The influence of overpeak retardation is much greater for crack growth during hold times than for continuous cycling. This was previously demonstrated by Weerasooriya, et.al.<sup>(50)</sup> in Alloy 718 and was also documented in this program as will be described in Section 5. This raises the issue of whether the shed rate might have to be lower for tests where hold times or low test frequencies are being evaluated. This factor was evaluated by comparing near-threshold crack growth rates for specimens shed with C values of  $-0.39$  and  $-1.18/\text{mm}$  ( $-10$  and  $-30/\text{inch}$ ). Two Rene'95 threshold tests were performed at  $649^\circ\text{C}$  ( $1200^\circ\text{F}$ ) at an R-ratio of zero using a cycle with a 1.5 second loading ramp, a 300 second hold time, and a 1.5 second unloading ramp. This condition was selected because it is a condition which exhibits a significant retardation effect in combination with hold times and because this loading cycle results in a high value of threshold. The comparison of the tests with the two values of C is shown in Figure 4.7. This range of shed rates does not appear to influence the ability to measure near-threshold crack growth rates.

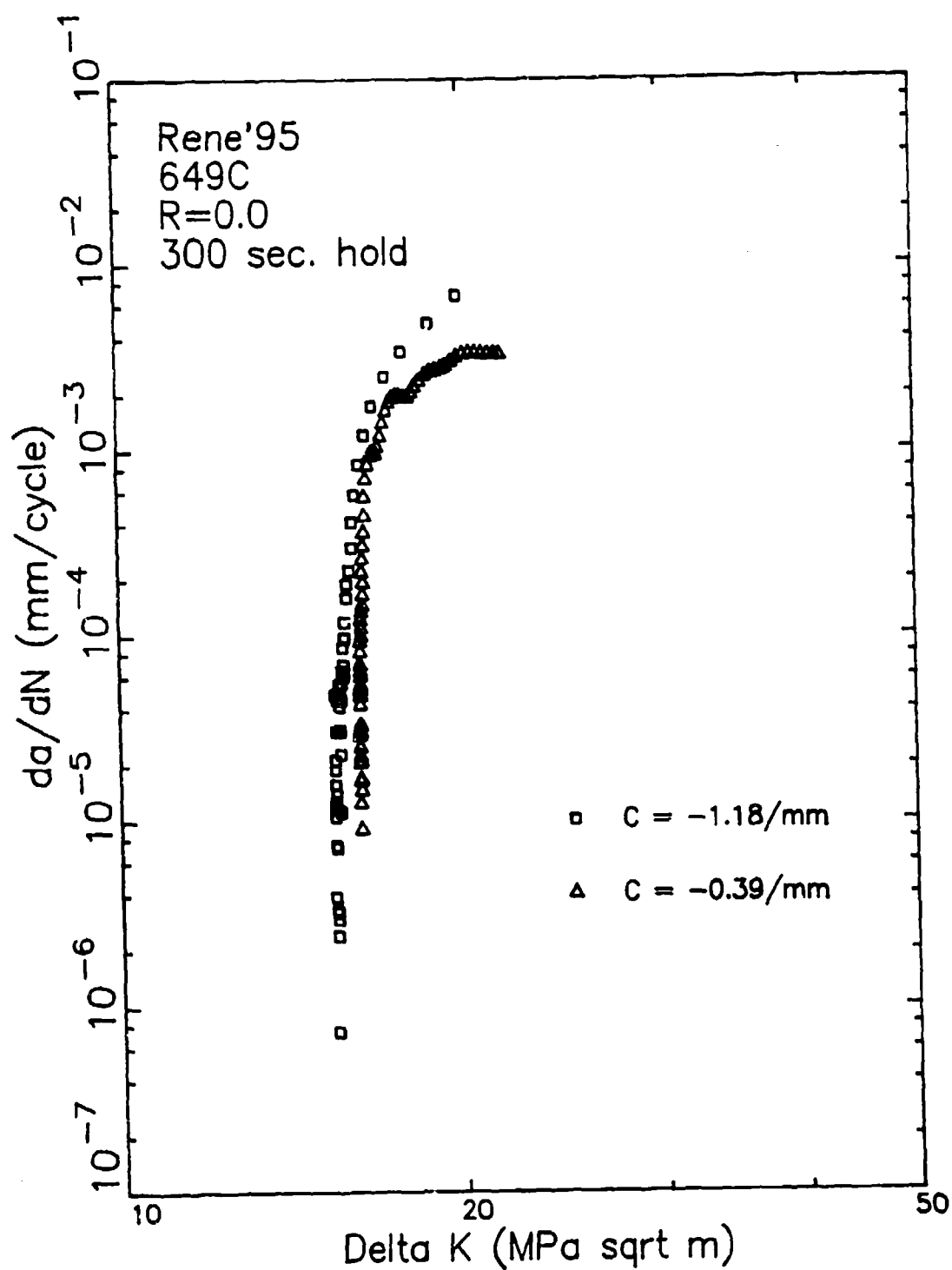


Figure 4.7: Influence of K-shed rate on near-threshold crack growth rates measured in Rene'95 specimens cycled at 649°C and R=0 with a 300 second hold time.

As a result, all other threshold tests in this investigation were performed with a shed rate (C) of  $-1.18/\text{mm}$  ( $-30/\text{inch}$ ).

#### 4.4.2 Constant $\Delta K$ Tests

The other type of test contained several segments of crack growth under constant  $\Delta K$  conditions. Within each of the constant  $\Delta K$  segments, several combinations of frequency or hold times were evaluated. Figure 4.8 shows a schematic history of a typical constant  $\Delta K$  test performed during this investigation. The R-ratio and test temperature were fixed for a given test. The nine segments shown in Figure 4.8 comprise a three by three matrix of  $K_{\text{max}}$  and test frequency. One of the objectives of this type of test was to obtain improved statistical crack growth data relative to that obtained in a more conventional test where K changes as the crack grows. This type of test also improves the efficiency of testing because the influence of several variables can be evaluated in a single test specimen.

The cyclic load and potential data obtained during each segment (constant  $K_{\text{max}}$  and frequency or hold time) were averaged to a total of approximately 25 data points. The data from the individual segments were combined, when necessary, into data files which corresponded to test segments where the initial and final crack lengths were measured on the fractured specimen. These data were then analyzed using the same software used to analyze the near-threshold tests. If necessary, these files were then separated so that individual files existed for each constant K and cycle frequency or hold time.

Data from each constant  $K_{\text{max}}$  and cycle frequency or hold time segment were analyzed statistically. The crack length (a) and cycle (N) data were analyzed using linear least squares regression analysis. The cyclic crack growth rate ( $da/dN$ ) was determined by calculating the slope of the fit between a and N. The standard deviation of this slope was calculated using standard statistical analysis. The error in K was calculated using the standard deviation in K.



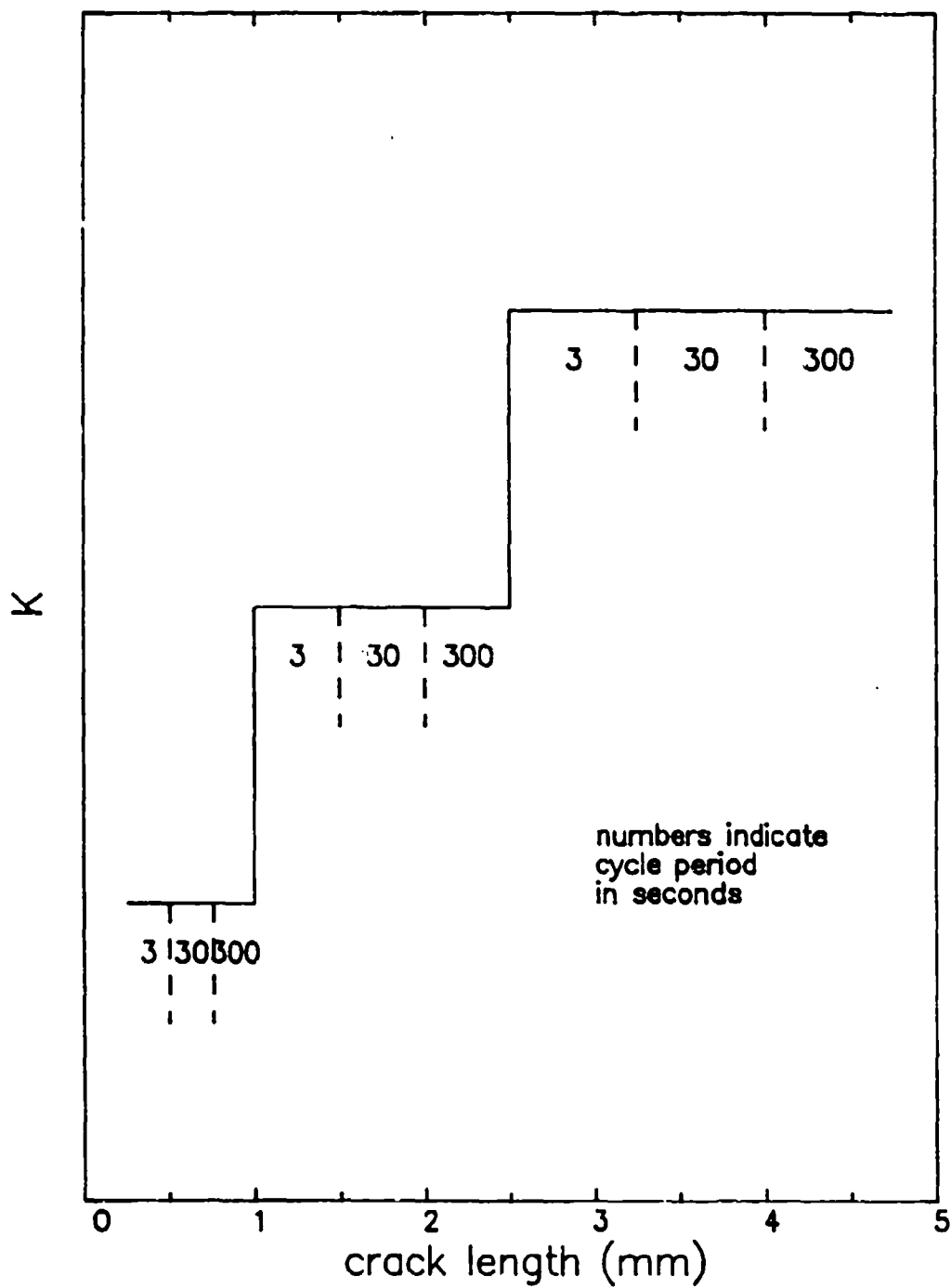


Figure 4.8: Typical variation of  $K_{max}$  and frequency in a  $\Delta K$ -Controlled frequency test

A given segment in these constant  $\Delta K$  tests was in reality a combination of many load controlled test segments. Within a block size the cycles are load controlled. When crack growth occurs during a hold time, the crack is growing under load control and not constant  $\Delta K$  control. The loads are adjusted between each block of data. This results in no difficulty for relatively low crack growth rates, but for high crack growth rates there can be a significant load drop between cycle blocks, possibly resulting in retardation. The possibility of this behavior was investigated in Rene'95 by measuring the crack growth rates under constant  $\Delta K$  control, increasing  $\Delta K$  control, and constant load control conditions. The condition selected for this evaluation was 649°C (1200°F) cycling with an R-ratio of zero and a 300 second hold time. The ramps on either side of the hold time lasted 1.5 seconds each. The results of these tests are shown in Figure 4.9. The increasing  $\Delta K$  and constant load data agree, however they are almost an order of magnitude faster than the constant  $\Delta K$  test results. This suggests that a significant amount of retardation occurred at these very rapid crack growth rates. This behavior was not discovered until very late in the test program after the constant  $\Delta K$  tests had been completed. The impact of this behavior for the constant  $\Delta K$  tests will be discussed and modeled in Section 7.

#### 4.4 VACUUM TEST METHOD

The vacuum crack growth tests were performed in a vacuum system at GEAE's Mechanical Testing Laboratory. The vacuum system is a double walled stainless steel vacuum chamber. The system was initially evacuated using a mechanical roughing pump. The high vacuum was attained using a combination of a cryopump and an ion pump. The pressure within the vacuum chamber was monitored with an ion gage. A mass spectrometer probe is also located within the system to identify the species present in the chamber. The probes for both of these devices are located within the main chamber, approximately 15 cm from the specimen, and thus should accurately monitor the testing environment. When a vacuum of approximately  $4 \times 10^{-8}$  mm was reached, the inner walls of the chamber and the specimen were heated to approximately 200°C (400°F). This hot outgassing procedure was continued until the pressure in the chamber was approximately  $2 \times 10^{-8}$  mm. The specimen was then induction heated to the

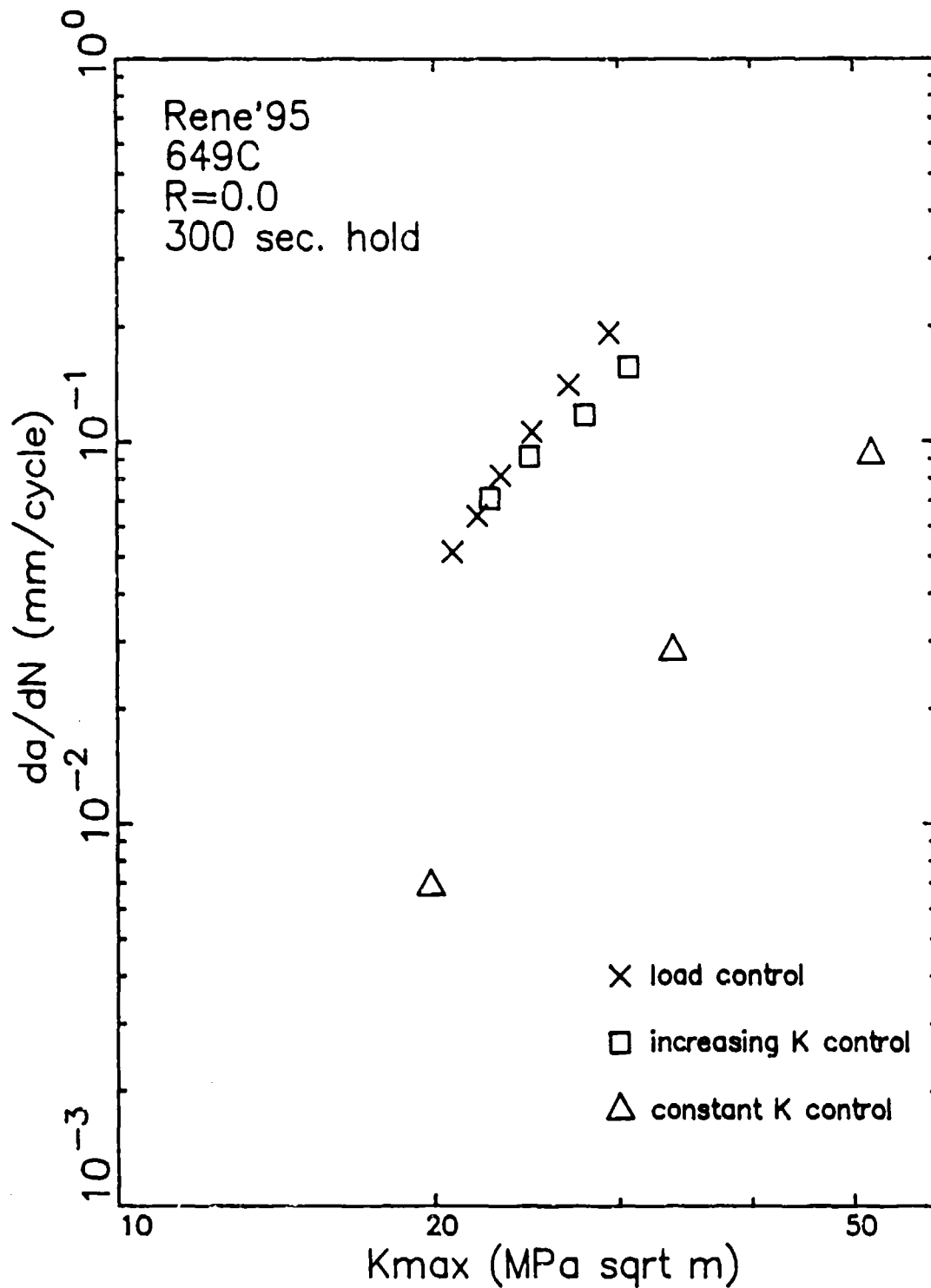


Figure 4.9: Influence of test control mode on Region II crack growth rates measured in Rene'95 specimens cycled at R=0 with a 300 second hold time.

desired temperature. This initially increased the pressure, but the test was not started until the pressure again reached  $2 \times 10^{-8}$  mm. During the test, the quality of the vacuum improved, usually reaching approximately  $5 \times 10^{-9}$  mm. The crack length was monitored using a DC potential drop system. This system was identical to the one used in air except for three differences: the specimen instrumentation contained no materials which outgas, a ceramic insert was placed in the load train between the specimen and the test machine to eliminate dual current paths, and the software used to perform the test was modified to account for the tare loads induced by the pressure difference.

Induction heating generally increases the noise in potential data by close to an order of magnitude. The higher level of noise associated with induction heating is on the same level as the differences in potential values measured during near-threshold crack growth testing. All threshold test specimens are heated in resistance furnaces to avoid this difficulty. The use of induction heating in the vacuum system prevented the measurement of near-threshold crack growth rates in vacuum.

## 5.0 EXPERIMENTAL RESULTS

This section of the report describes the experimental results of the baseline crack growth rate tests. All these tests were performed in laboratory air using the experimental techniques described in Section 4.3. The results of the vacuum crack growth tests are reported in Section 6.

This section has two major parts - one for the Rene'95 results and a second part for those on Alloy 718. Within each of those parts, there are individual sections on constant  $\Delta K$  (Region II), threshold (Regions I and II), static, and overpeak retardation tests. The results will be displayed and compared and inferences will be made as to the applicability of a superposition model. The quantitative application of both interpolative and superposition crack growth models to these data is presented in Section 7.0.

### 5.1 RENE'95 CRACK GROWTH RESULTS

Table 5.1 lists the Rene'95 baseline tests performed in this investigation. There are a wide number of variables (temperature, R-ratio, hold time, cycle frequency, and test control mode). The results will be presented in separate sections on constant  $\Delta K$ , threshold, static, and overpeak tests in order to facilitate the description of the influence of each variable.

#### 5.1.1 Rene'95 Constant $\Delta K$ Test Results

The baseline tests can be described as either frequency or hold time tests. The frequency tests were performed with cycle periods of 3, 30, or 300 seconds. The loading and unloading ramp times were equal so that the load increased during the first half of the cycle period and decreased during the second half. Throughout the text, these tests will be described in terms of their cycle period. The hold time tests were performed with a 1.5 second loading ramp, a hold time at maximum load, and a 1.5 second unloading ramp. The duration of hold times evaluated were 4, 30, and 300 seconds. The loading and unloading ramps increased the cycle period by 3 seconds over the duration

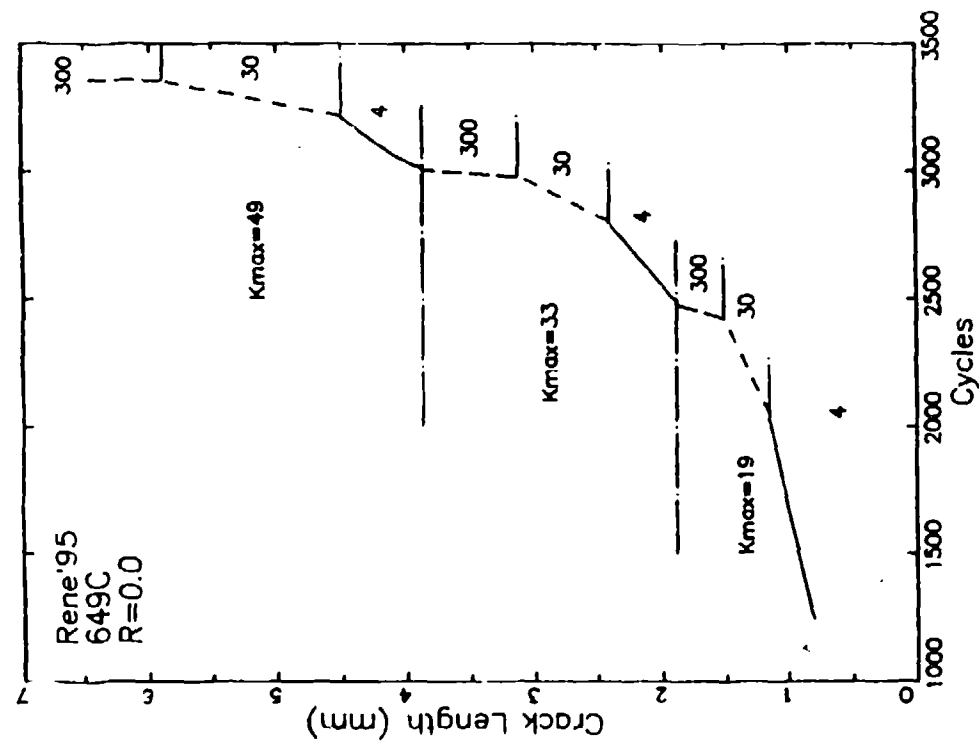
Table 5.1: Rene'95 Simple Cycle Test Matrix

Test Number	Temperature (°C)	R	Test Type	Variable
AF19	538	0.0	constant $\Delta K$	hold time
AF45	593	0.0	constant $\Delta K$	hold time
AF49	593	0.0	constant $\Delta K$	hold time
AF54	593	0.0	constant $\Delta K$	frequency
AF62	593	0.0	threshold	3 sec. cycle
AF77	593	0.0	threshold	300 sec. hold
AF44	593	0.5	constant $\Delta K$	hold time
AF66	593	0.5	constant $\Delta K$	frequency
AF59	593	0.8	constant $\Delta K$	hold time
AF12	593	0.8	constant $\Delta K$	frequency
AF13	593	0.8	threshold	3 sec. cycle
AF46	593	0.8	threshold	300 sec. hold
AF50	593	static	threshold	
AF70	593	static	constant load	
AF03	649	0.0	constant $\Delta K$	hold time
AF05	649	0.0	constant $\Delta K$	frequency
AF14	649	0.0	threshold	3 sec. cycle
AF63	649	0.0	threshold	30 sec. hold
AF06	649	0.0	threshold	300 sec. hold
AF53	649	0.0	threshold	300 sec. hold
AF18	649	0.0	threshold	30 sec. cycle
AF10	649	0.0	threshold	300 sec. cycle
AF15	649	0.5	constant $\Delta K$	hold time
AF51	649	0.5	constant $\Delta K$	frequency
AF09	649	0.5	threshold	3 sec. cycle
AF16	649	0.5	threshold	300 sec. hold
AF23	649	0.5	threshold	300 sec. cycle
AF72	649	0.8	constant $\Delta K$	hold time
AF38	649	0.8	constant $\Delta K$	frequency
AF55	649	0.8	threshold	3 sec. cycle
AF08	649	0.8	threshold	4 sec. hold
AF21	649	0.8	threshold	30 sec. hold
AF30	649	0.8	threshold	300 sec. hold
AF40	649	0.8	threshold	300 sec. hold
AF69	649	0.8	threshold	300 sec. cycle
AF17	649	static	threshold	
AF60	649	static	constant load	
AF65	649	static	constant load	

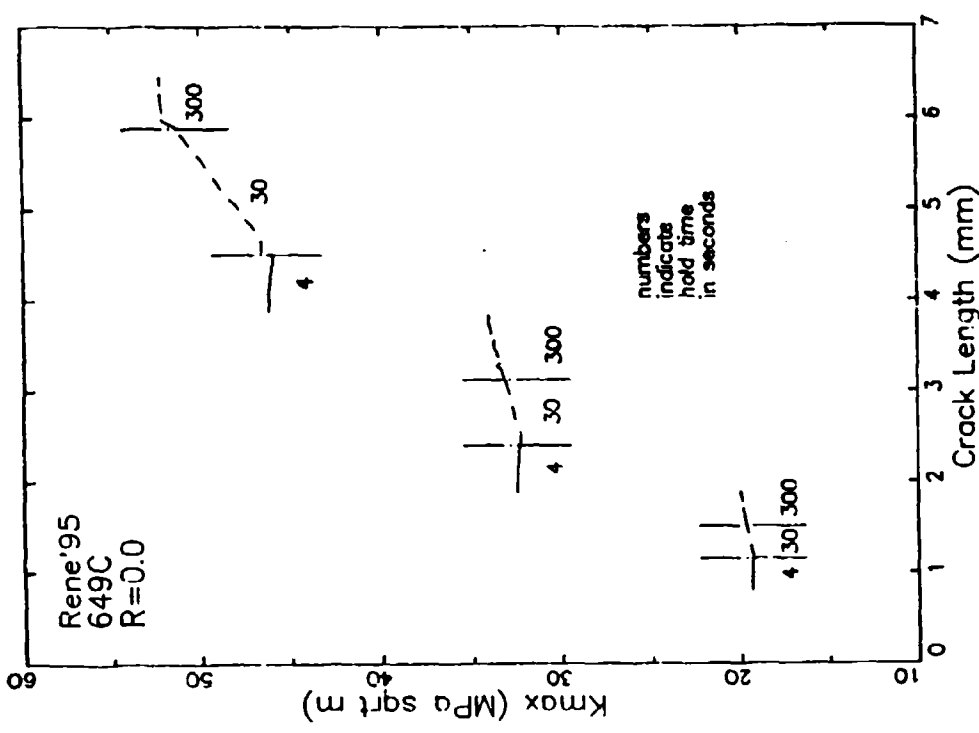
of the hold time. These tests will be referred by the length of the hold time. The loading and unloading ramps in the 3 second period test were identical to those in the hold time tests. Because of this flexibility the 3 second period results will sometimes be referred to as 0 second hold time data.

Constant  $\Delta K$  tests were performed to evaluate the influence of either test frequency or hold time. The test temperature and R-ratio was held constant for a given test. Most of the Rene'95 constant  $\Delta K$  tests had 9 segments which evaluated a three by three matrix of  $\Delta K$  levels and either frequency or hold time. The potential drop microcomputer attempted to perform tests at three levels of maximum K ( $K_{max}$ ), however the exact level of  $K_{max}$  varied from this due to inaccuracies in the initial notch depth, and the crack tunneling behavior discussed previously. The tests were analyzed using post-test crack length measurements. The resulting values of  $K_{max}$  were not always constant during a given segment. This is illustrated in Figure 5.1a for a 649°C Rene'95 hold time test with an R-ratio of zero. This figure show the variation of  $K_{max}$  with crack length. The numbers indicate the hold time in seconds for that segment. The crack length increment in a given segment was increased with higher  $K_{max}$  values to avoid extremely small number of cycles in a given constant  $\Delta K$  segment. In general, the value of  $K_{max}$  was close to constant in a given segment, however, there were some cases such as that shown for the 30 second hold time cycle with a  $K_{max}$  of approximately 50 MPa/m where the value of  $K_{max}$  increased during the  $\Delta K$ -controlled segment. Figure 5.1b shows the resulting variation in crack length with cycles for this test.

The average and standard deviation of  $K_{max}$  was determined from the values of  $K_{max}$  calculated for a given segment. The average and standard deviation of the crack growth rate for a given segment was calculated from the slope and standard deviation of variation of the crack length with cycles. The results of this test are shown in Figure 5.2 using the typical log-log plot of the variation of crack growth rate with  $K_{max}$ . A rectangle was constructed for each test segment which enclosed the range of plus or minus one standard deviation in both crack growth rate and  $K_{max}$ . The other lines on the graph connect the average values for segments with the same value of hold time. For



(a)



(b)

Figure 5.1: Variation of (a)  $K_{max}$  with crack length and (b) crack length with cycles during constant  $\Delta K$  hold time test on Rene'95 at 649°C and R=0.



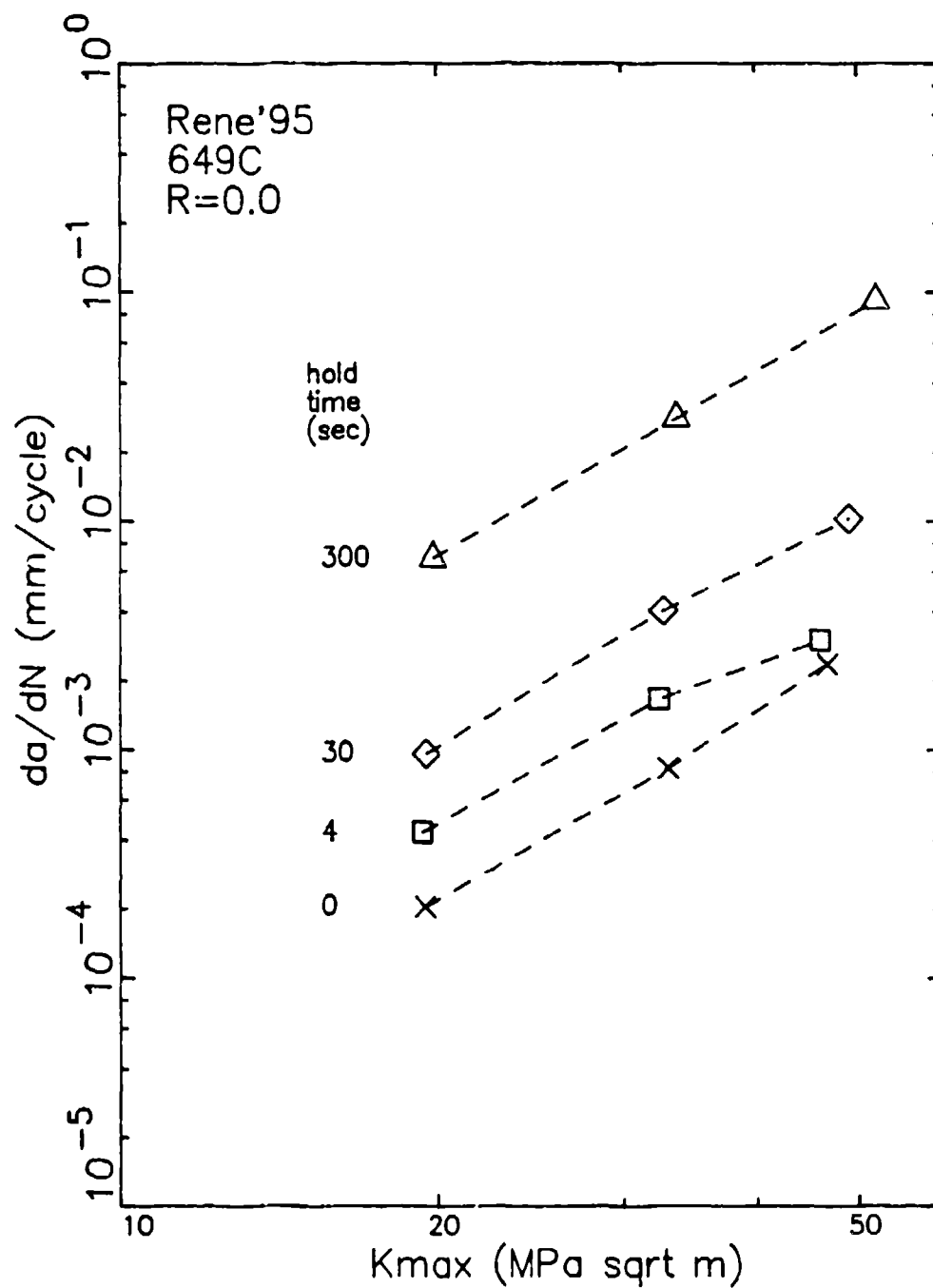


Figure 5.2: Results of the statistical analysis of constant  $\Delta K$  hold time test on Rene'95 at 649°C with R=0.

most of the segments of this test, the standard deviations were very small and the rectangle appears to be a small point. The most noticeable exceptions were for the 300 second hold time segments at the higher two levels of  $K_{max}$ . In these cases, there was a much larger variation in  $K_{max}$  than in crack growth rate. The standard deviations displayed in this figure were typical for those determined in this investigation. The results for the other Rene'95  $\Delta K$ -controlled tests showing the standard deviations are given in Appendix A. This analysis procedure was been used on all the constant  $\Delta K$  tests performed in this investigation. Due to the low standard deviations, the constant  $\Delta K$  test results will be reported in the text of the report using large symbols as shown in Figure 5.3. The data in this figure includes that shown in Figure 5.2 along with the results from a 3 second cycle period in a constant  $\Delta K$  frequency test.

The results of constant  $\Delta K$  hold time tests with a R-ratio of zero at 538 and 593°C are shown in Figures 5.4a and 5.4b, respectively. Comparison of the data in Figures 5.3 and 5.4 show the strong effect of temperature on time-dependent crack growth. At 538°C, a range of hold times from 4 to 300 seconds results in, at worst, a factor of two difference in crack growth rates. This factor is approximately 4 and 20 for 593 and 649°C, respectively. There also appears to be a substantially different behavior at 538°C relative to the higher two temperatures. The results at 593°C (Figure 5.4b) and 649°C (Figure 5.3) show that increasing hold times accelerate fatigue crack growth rates. The 538°C results (Figure 5.4a) show this acceleration at low values of  $K_{max}$ , but with increasing  $K_{max}$ , increasing hold times decrease the crack growth rates. The behavior at 538°C may be related to the competition between the environmentally-assisted crack growth and the localized blunting of the crack tip by creep deformation. Evidence of this competition was observed in other tests and will be discussed more fully in the Section 6.

The data shown in Figures 5.3 and 5.4 are replotted in Figure 5.5 where the crack growth rates are shown as a function of the hold time duration. The values of  $K_{max}$  shown in this and subsequent figures are presented in units of MPa/m. These figures show both  $da/dN$  and hold time on linear axes because according to the superposition model, the crack growth rate at a given set of

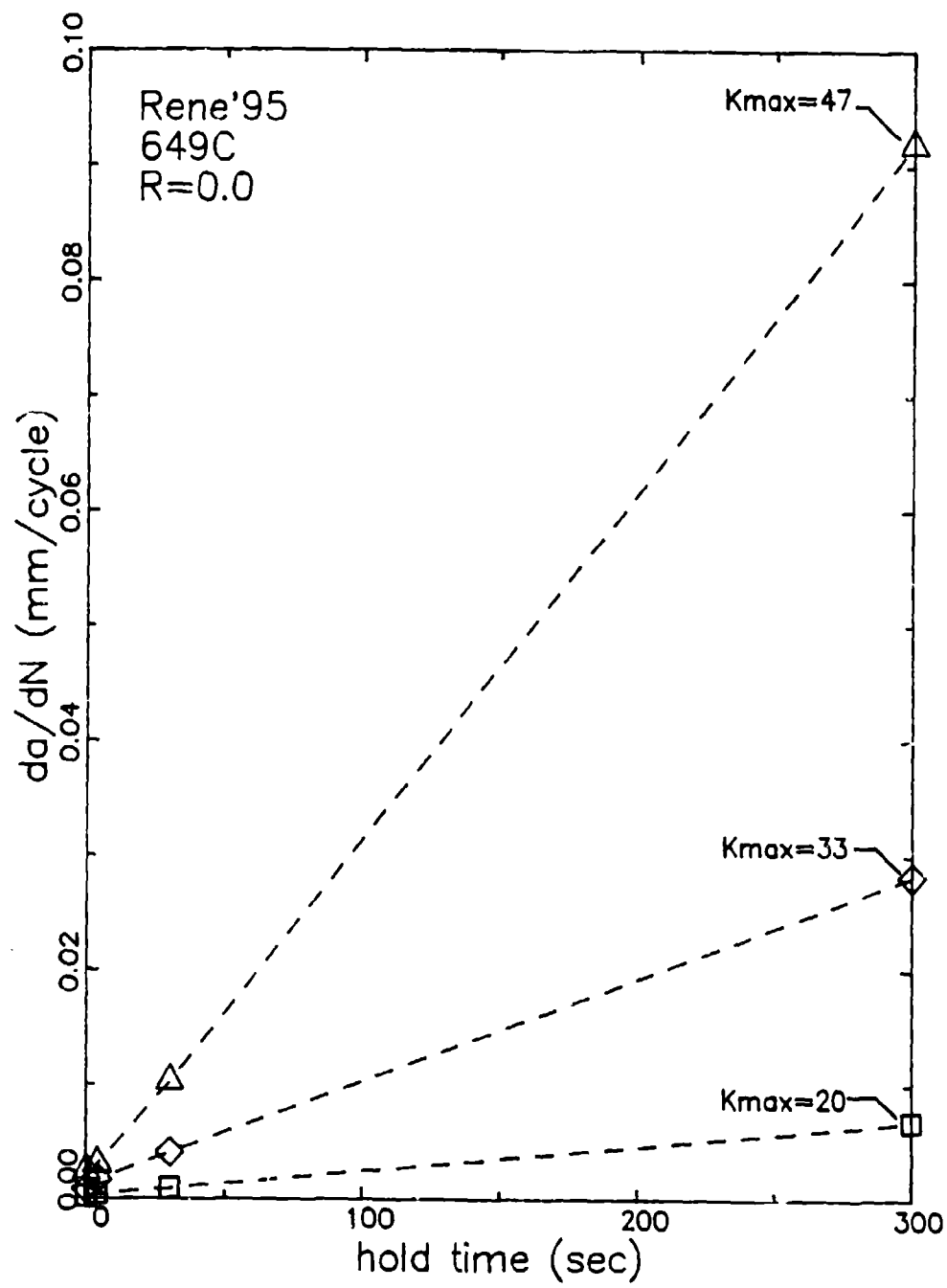


Figure 5.3: Results of the constant  $\Delta K$  hold time test on Rene'95 at 649°C with R=0.

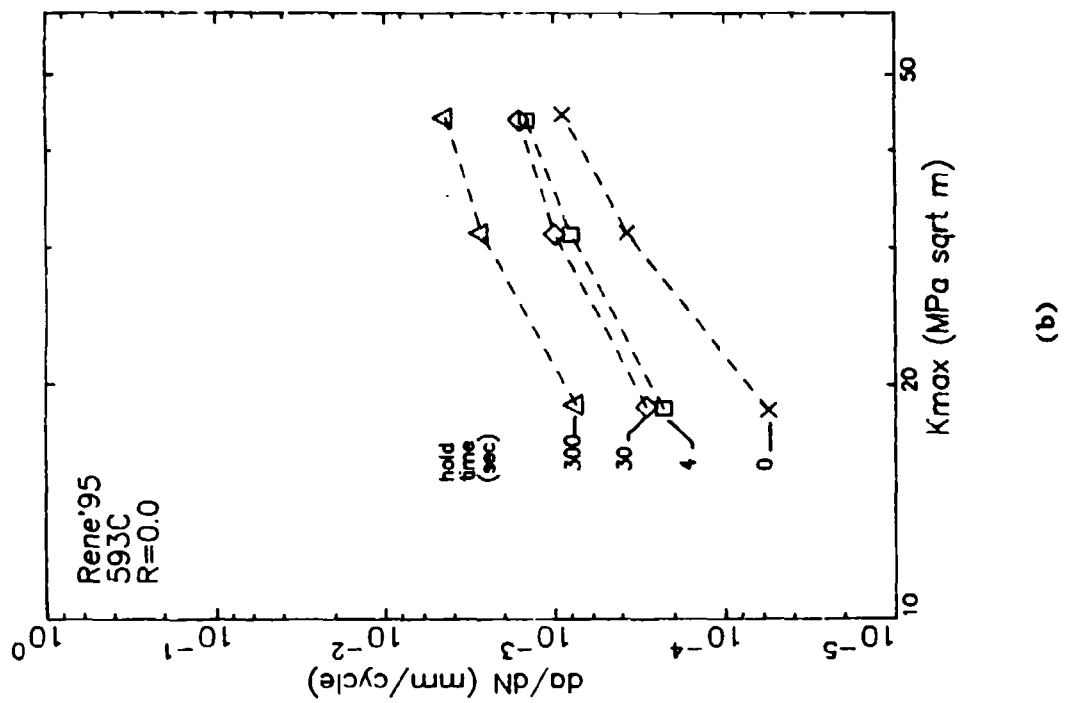
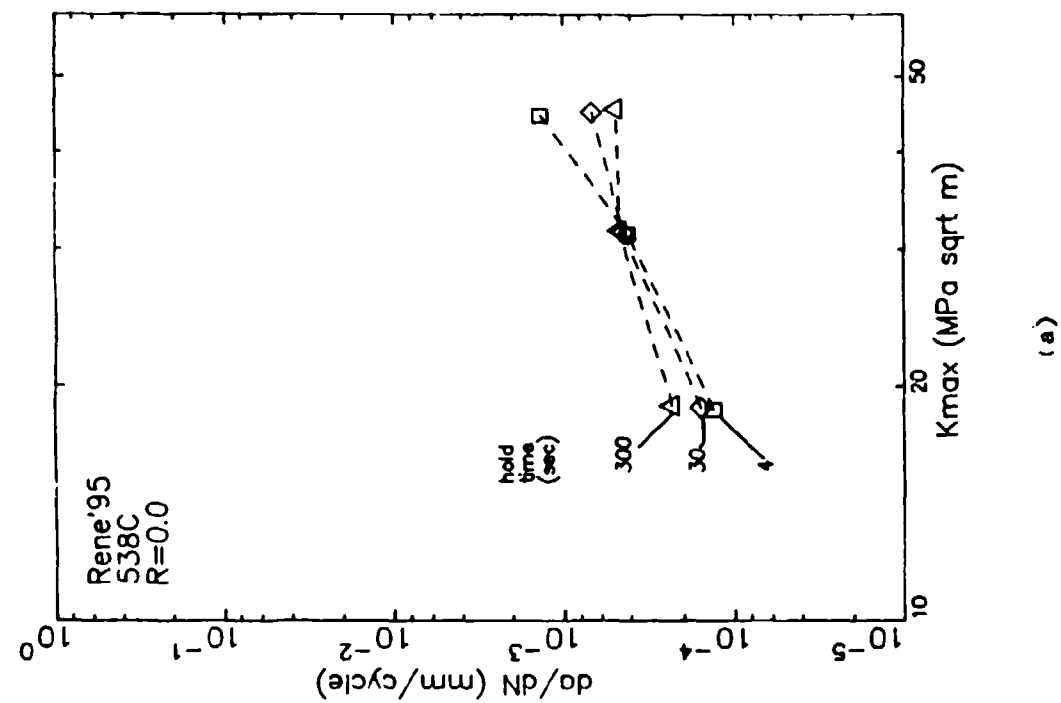
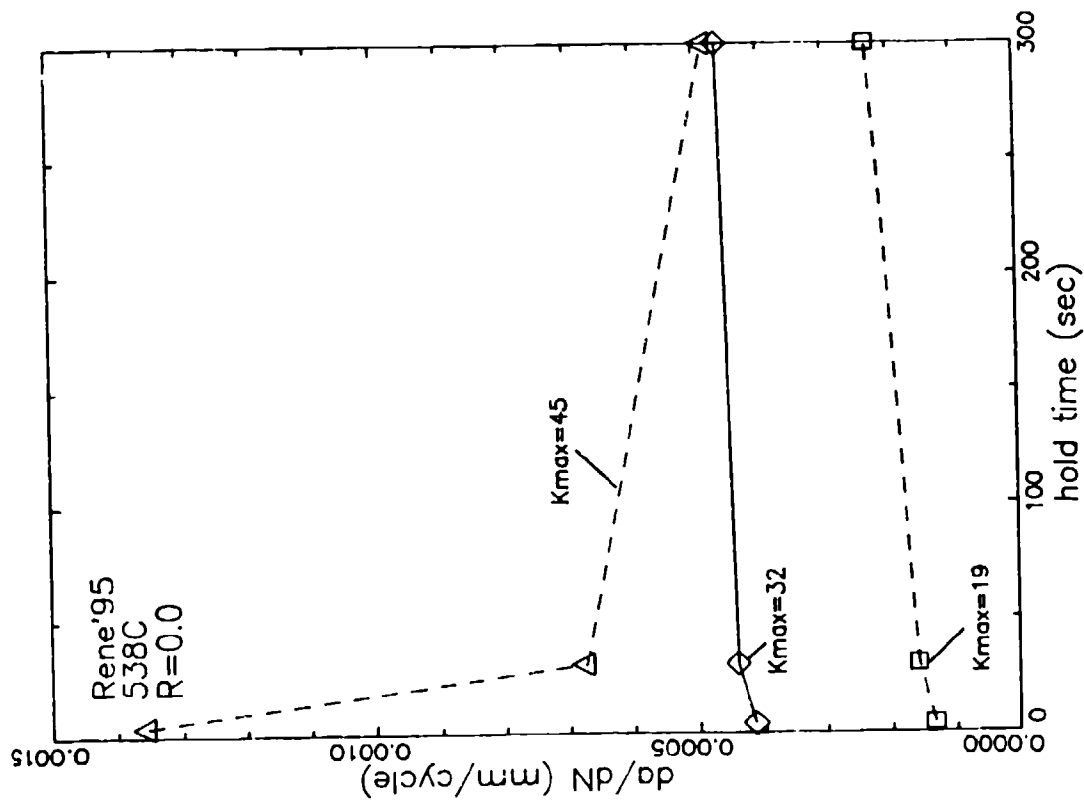
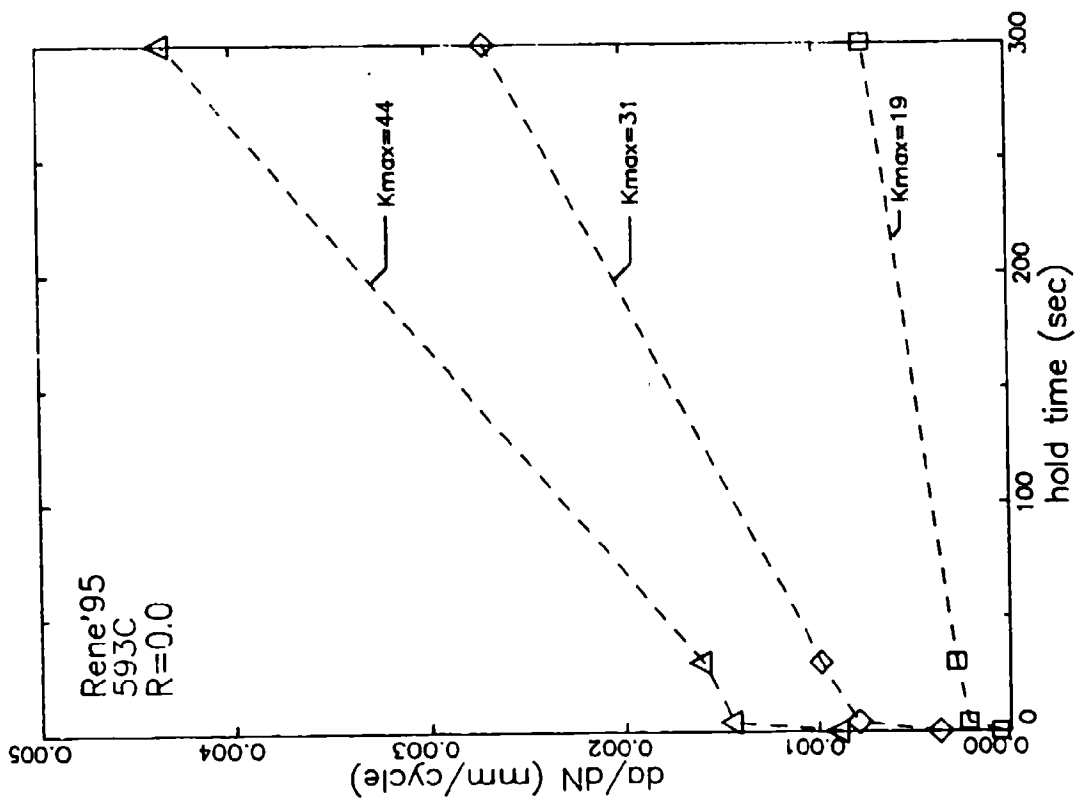


Figure 5.4: Results of the constant  $\Delta K$  hold time test on Rene'95 with  $R=0$  at (a) 538°C and (b) 593°C.



(a)



(b)

Figure 5.5: Variation of crack growth rate with hold time measured in Rene'95 constant AK tests with  $R=0$  at (a) 538°C and (b) 593°C.

loading conditions ( $\Delta K$  and  $R$ ) is proportional to the hold time. The slope of the variation of crack growth rate with hold time should equal the static crack growth rate ( $da/dt$ ) for the value of  $K$  during the hold time ( $K_{max}$ ). Figures 5.5b and 5.5c show this linear variation for the 593 and 649°C tests. Increasing  $K_{max}$  increases the slope of the crack growth rate - hold time dependency much as one would expect for static crack growth. These data qualitatively agree with the trends predicted by the superposition model. This was not the case for the 538°C test as shown in Figure 5.5a suggesting that the mechanism of time-dependent crack growth is different at this temperature.

The influence of hold time on the crack growth rates was also evaluated for  $R$ -ratios of 0.5 and 0.8 at temperatures of 593 and 649°C. Those results are shown in Figures 5.6 and 5.7, respectively. These results are shown as a function of  $K_{max}$  because if the crack growth is dominated by static crack growth, the time-dependent part will be controlled by the  $K$  during the hold time or  $K_{max}$ . Like the  $R=0$  results, both increasing temperature and increasing hold times result in faster crack growth rates. These results are replotted in Figures 5.8 and 5.9 where the variation of crack growth rate is shown as a function of hold time on linear axes. These results, like those for the  $R=0$  tests at these temperatures, show an approximately linear variation of crack growth rate with hold time as predicted by the linear superposition model.

The influence of cycle period was evaluated at 593 and 649°C for  $R$ -ratios of 0, 0.5, and 0.8. The results of the 593°C tests are shown in Figure 5.10. When  $R=0$  (Figure 5.10a), cycle period has little effect at low values of  $K_{max}$ , but accelerates the crack growth rates at higher  $K_{max}$  levels. This effect can be seen to a lesser extent at  $R=0.5$  (Figure 5.10b). It was not possible to evaluate crack growth at low  $K_{max}$  values for  $R=0.8$  due to the high threshold value for this cycling condition. Comparison of the data in these figures shows that the influence of cycle period seems to increase with  $R$ -ratio and is particularly large for  $R=0.8$  testing conditions. The influence of  $R$ -ratio on the crack growth data shown in Figure 5.10 agrees qualitatively with a

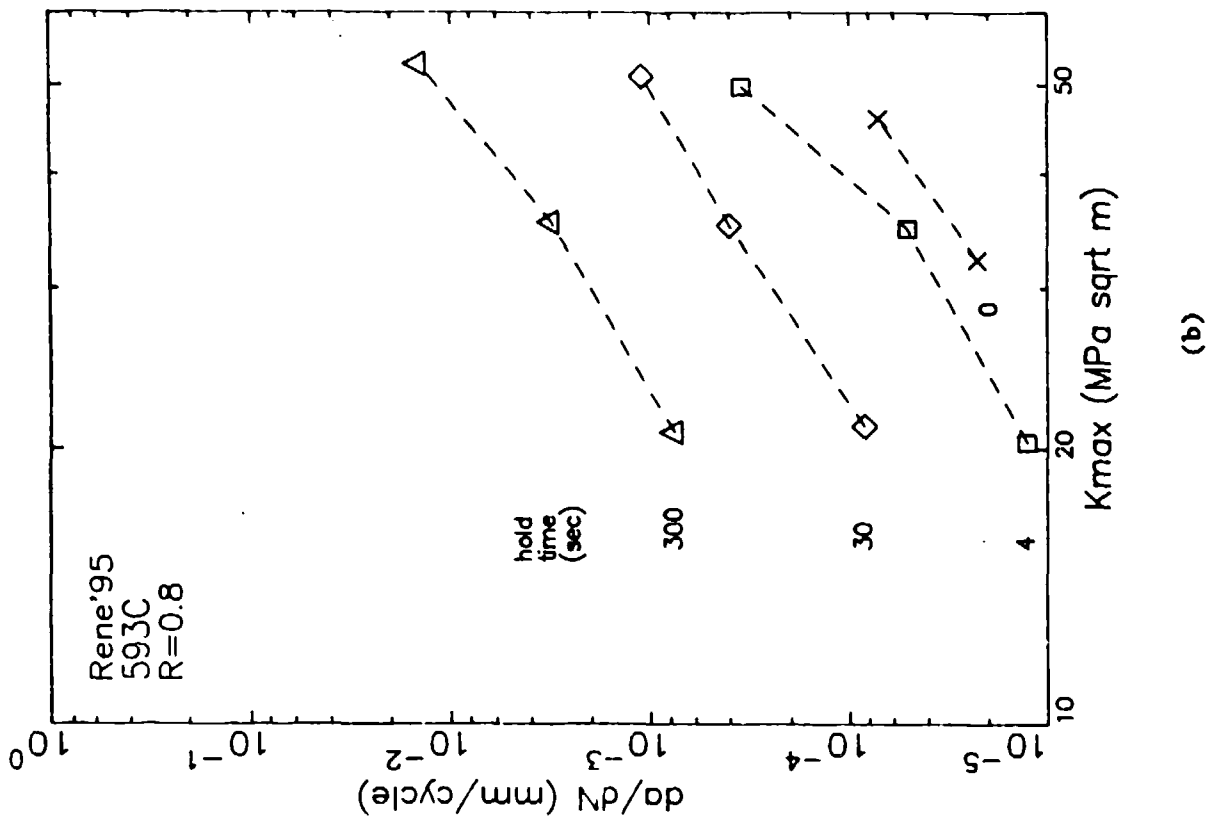
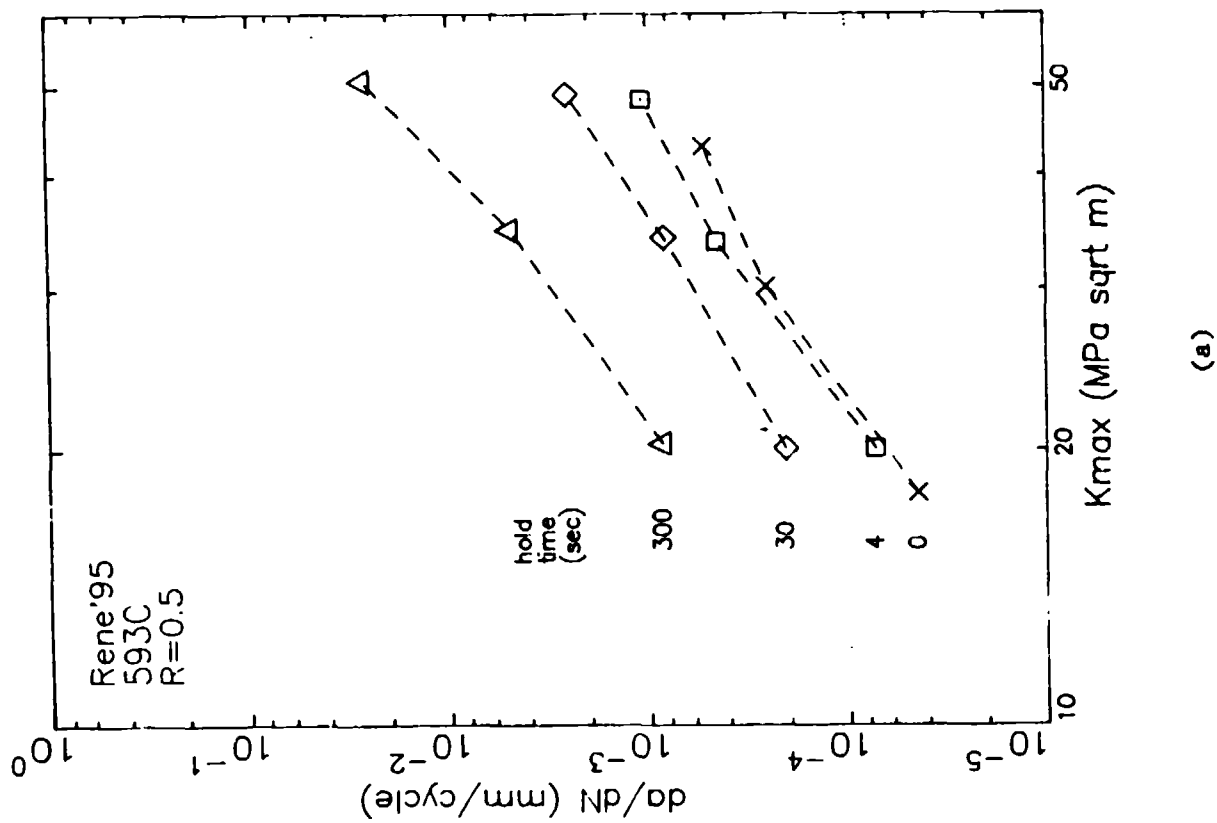


Figure 5.6: Results of the constant  $\Delta K$  hold time tests on Rene'95 at 593°C with (a)  $R=0.5$  and (b)  $R=0.8$ .

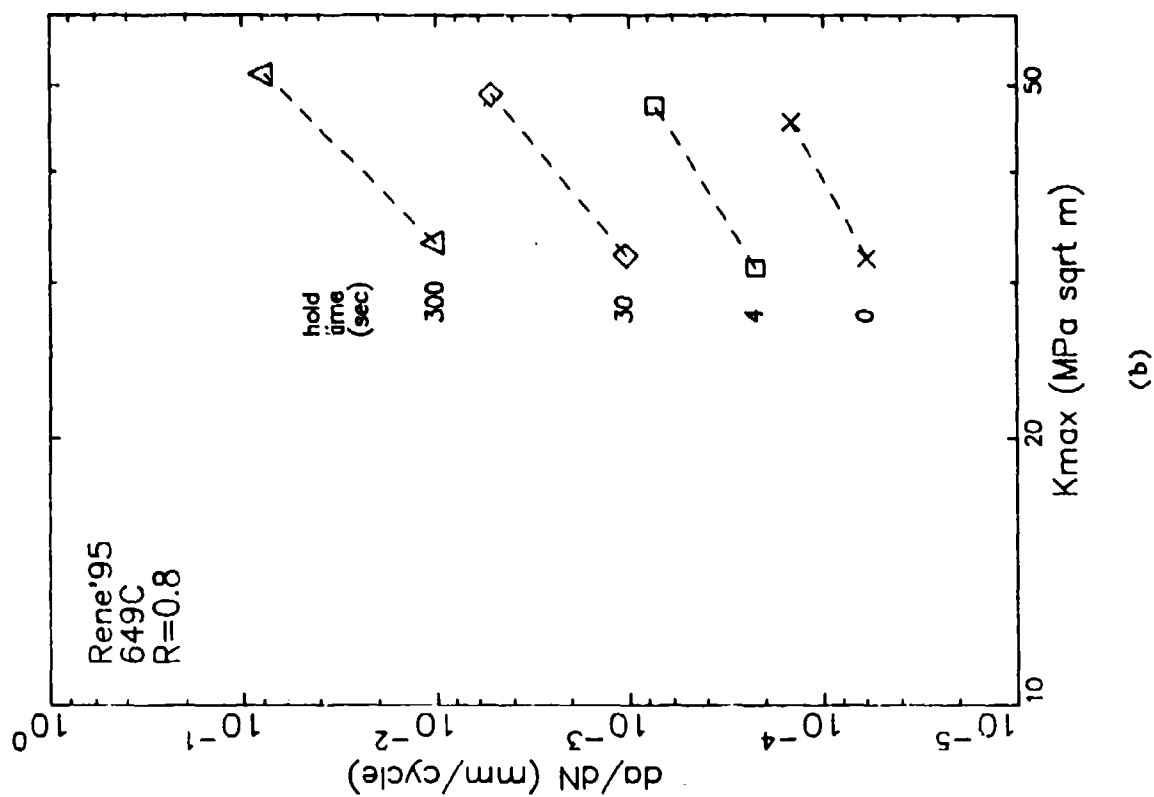
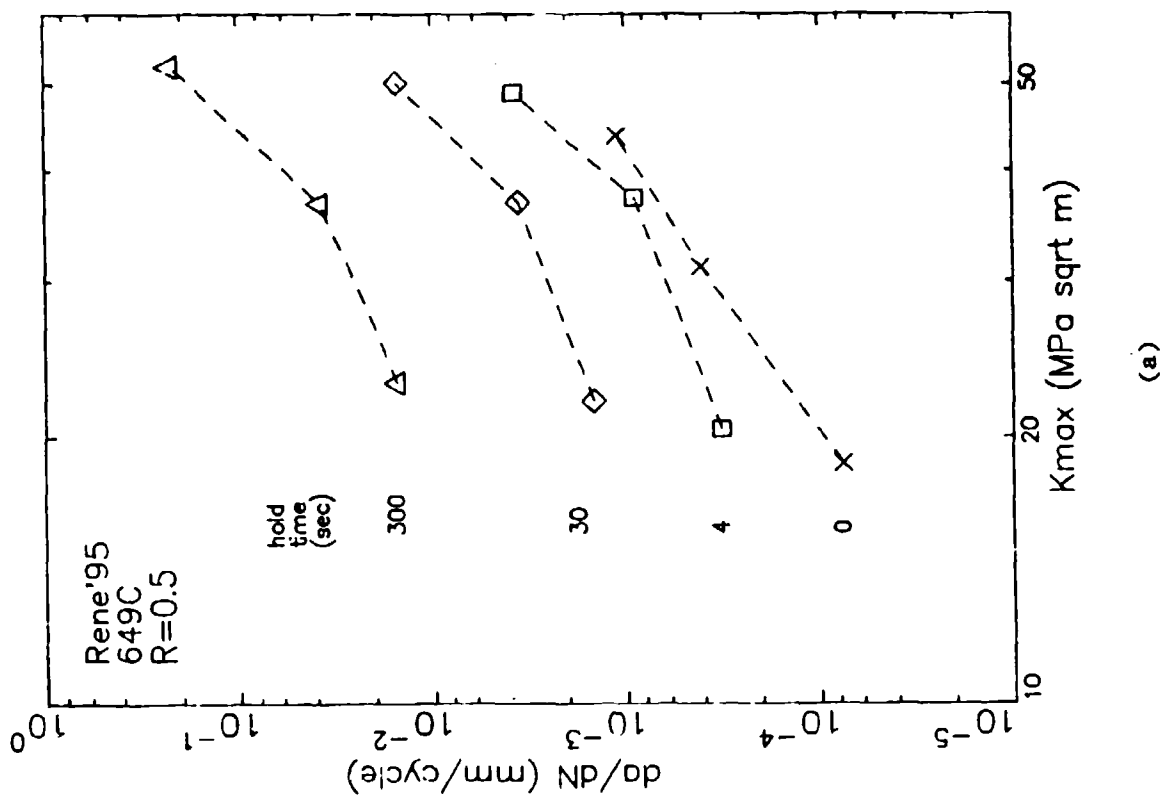


Figure 5.7: Results of the constant  $\Delta K$  hold time tests on Rene'95 at 649°C with (a)  $R=0.5$  and (b)  $R=0.8$ .



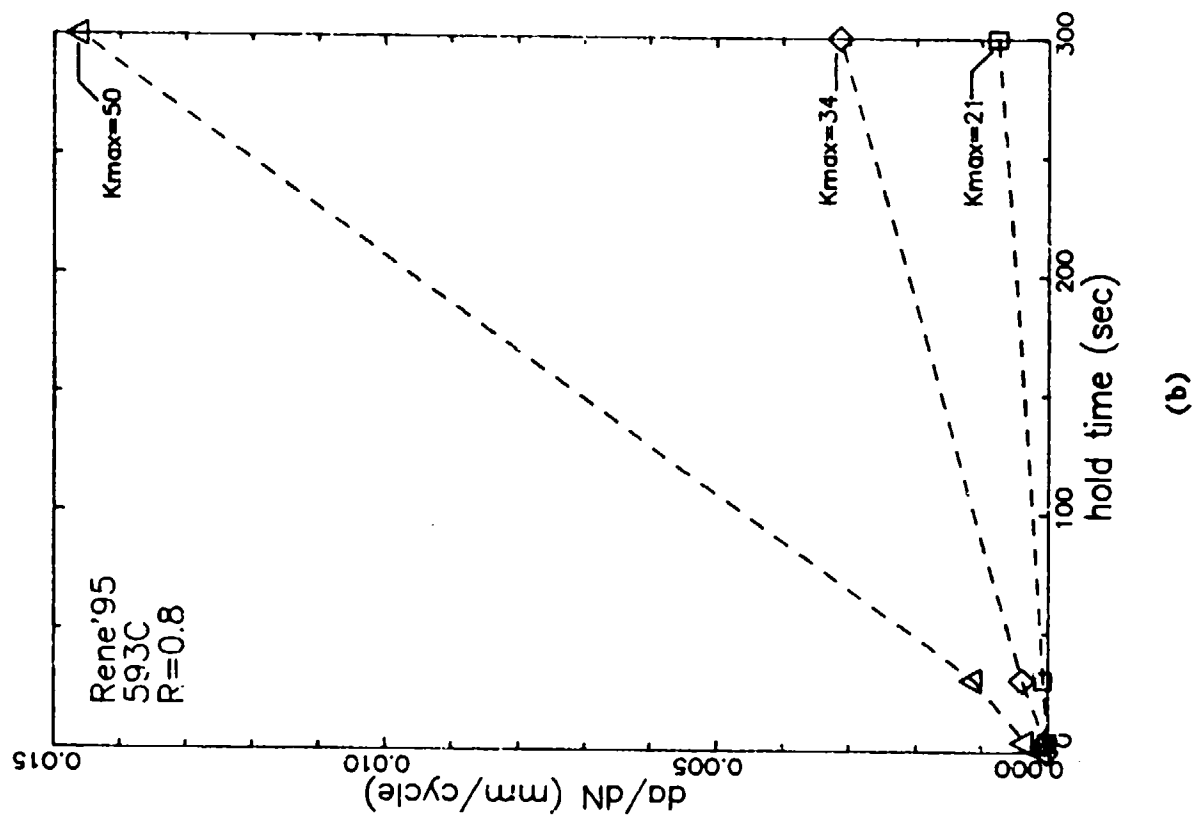
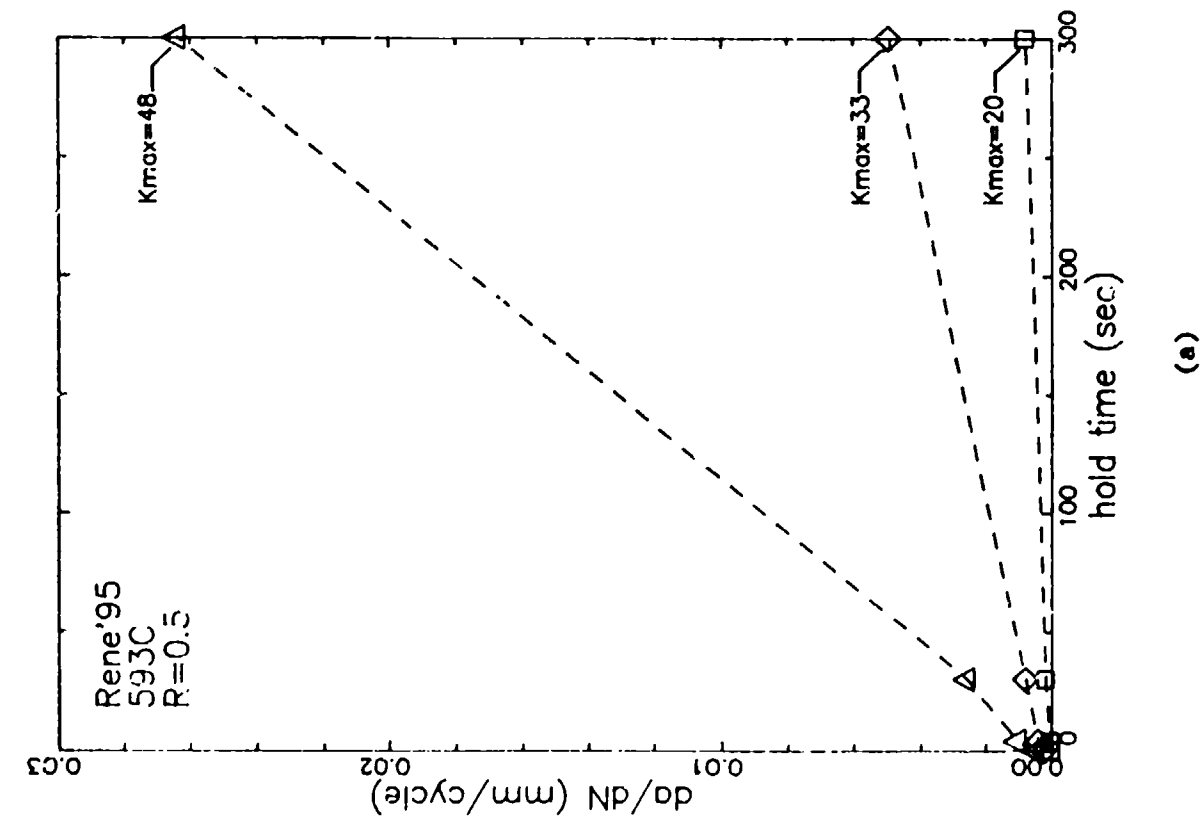
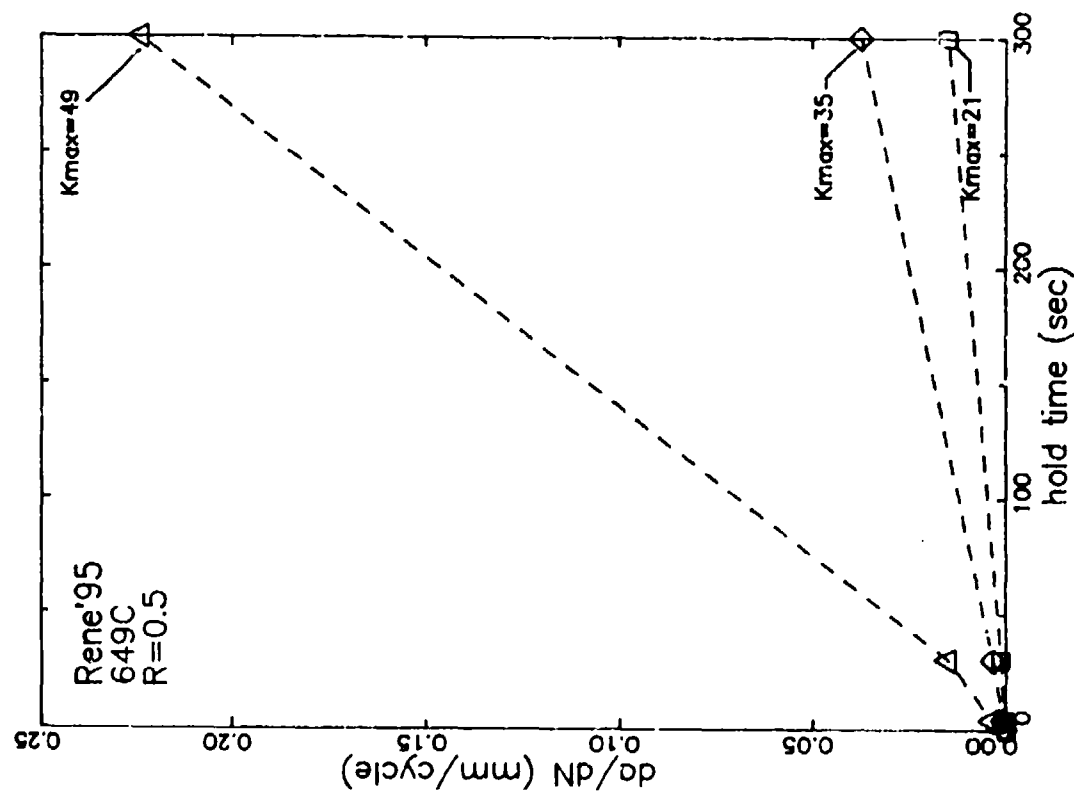
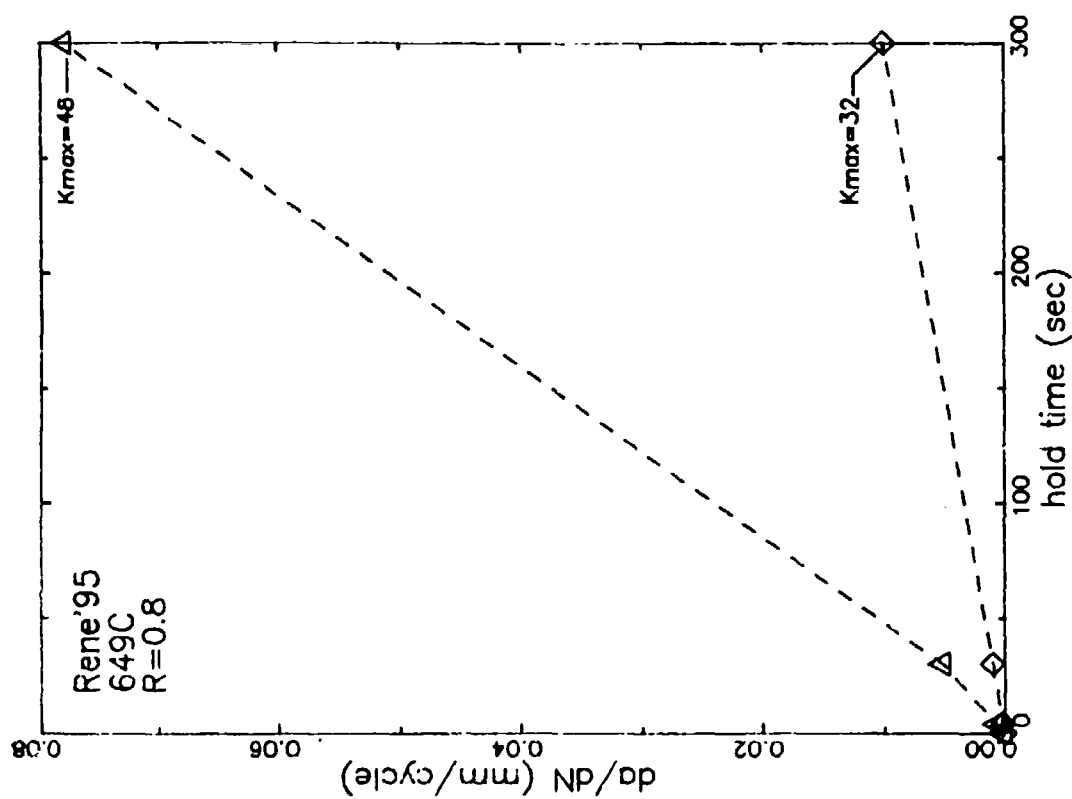


Figure 5.8: Variation of crack growth rate with hold time measured in Rene'95 constant  $\Delta K$  tests at 593°C with  
(a)  $R=0.5$  and (b)  $R=0.8$ .

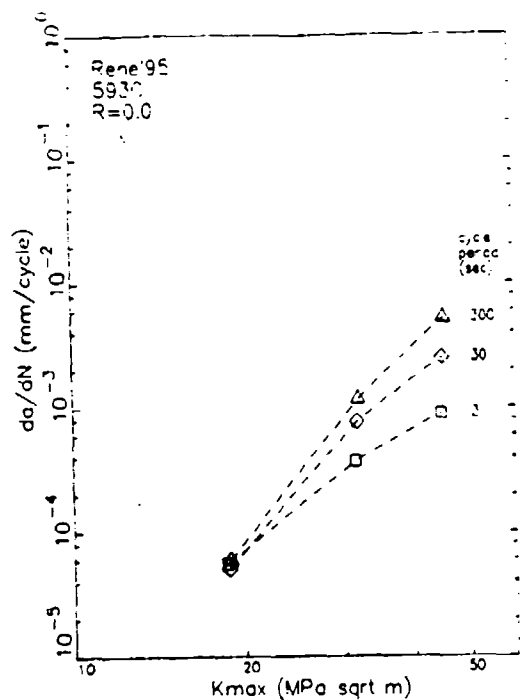


(a)

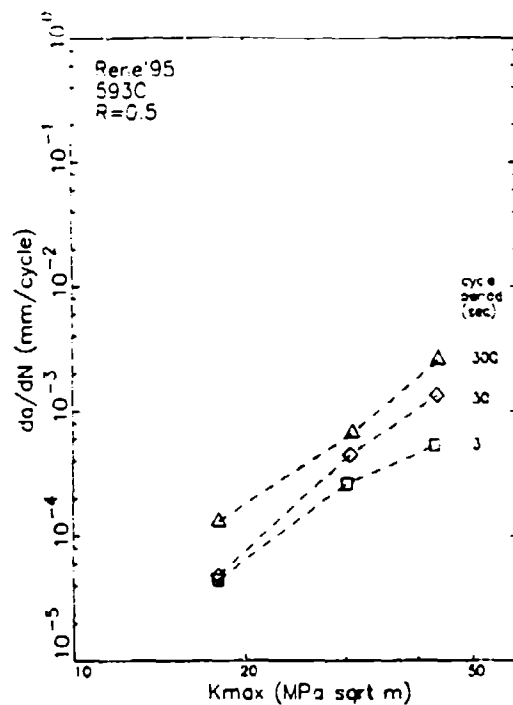


(b)

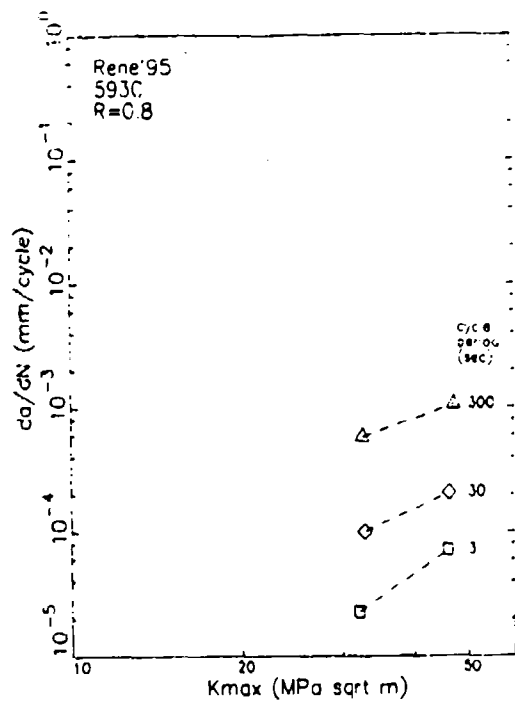
Figure 5.9: Variation of crack growth rate with hold time measured in Rene'95 constant  $\Delta K$  tests at 649°C with (a)  $R=0.5$  and (b)  $R=0.8$ .



(a)



(b)



(c)

Figure 5.10:

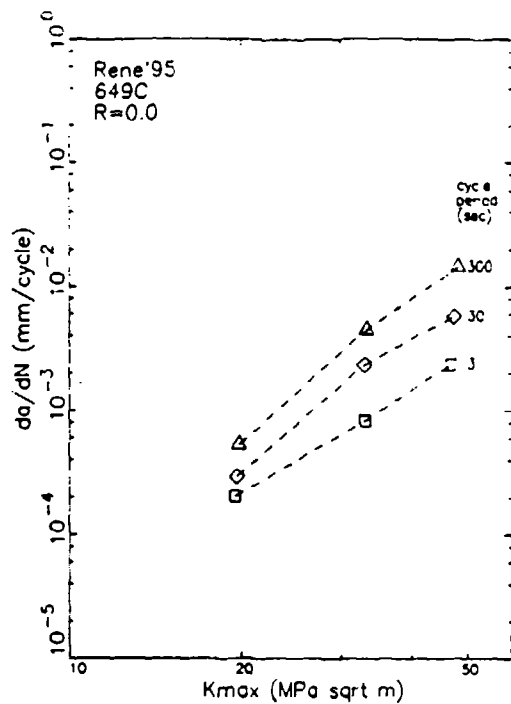
Results of the constant  $\Delta K$  frequency tests on Rene'95 at 593°C with (a)  $R=0.0$ , (b)  $R=0.5$ , and (c)  $R=0.8$ .

superposition model which predicts a large impact of test frequency with increasing R-ratio as shown in Figure 2.4.

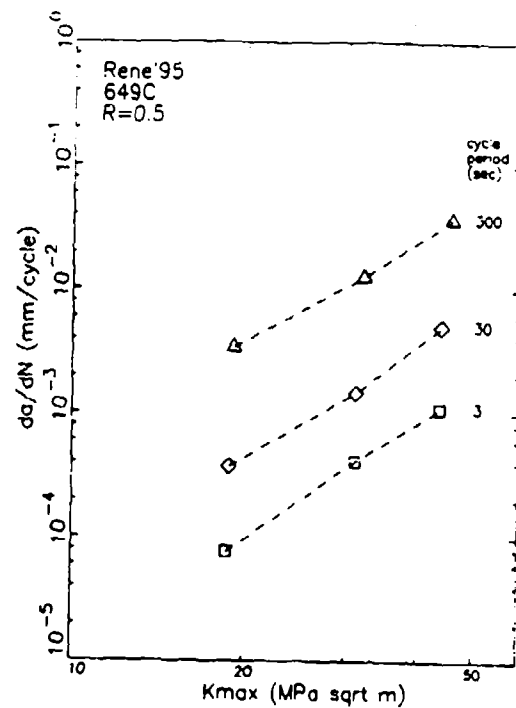
Figure 5.11 shows the results from the constant  $\Delta K$  frequency tests performed at 649°C with three R-ratios. As with the hold time results, increasing temperature resulted in a higher influence of cycle time (period or hold time) on the crack growth rates. The accelerating effect of R-ratio was also observed at 649°C for R-ratios of 0.5 and 0.8. The 649°C frequency data does not show the pronounced  $K_{max}$ -level dependency at R=0 as was observed at the lower test temperature.

The influence of cycle type (frequency or hold time) can be evaluated by direct comparisons of 300 second period data with the 300 second hold time data. The duration of the hold time cycle was 303 seconds due to the 3 seconds required for loading and unloading which is within one percent of the cycle duration of the 300 second cycle period (frequency) test. Figure 5.12 compares the results of the 593°C tests with 3 second cycle period, 300 second cycle period, and 300 second hold time cycles for all three R-ratios. These data show that the difference in crack growth rates between the 300 second frequency and hold time cycles diminishes with increasing R-ratio. This would be anticipated from the superposition model (Figure 2.4) because the minimum load (or  $K_{min}$ ) increases with the R-ratio. The complex situation for R=0 cycling may be related to the presence of a static crack growth threshold. At low values of  $K_{max}$  (or  $\Delta K$  for R=0 cycling), a significant portion of the low frequency cycle may be below the static threshold. The impact of the static threshold is diminished as the value of  $K_{max}$  is increased and a larger portion of the cycle exceeds the static threshold.

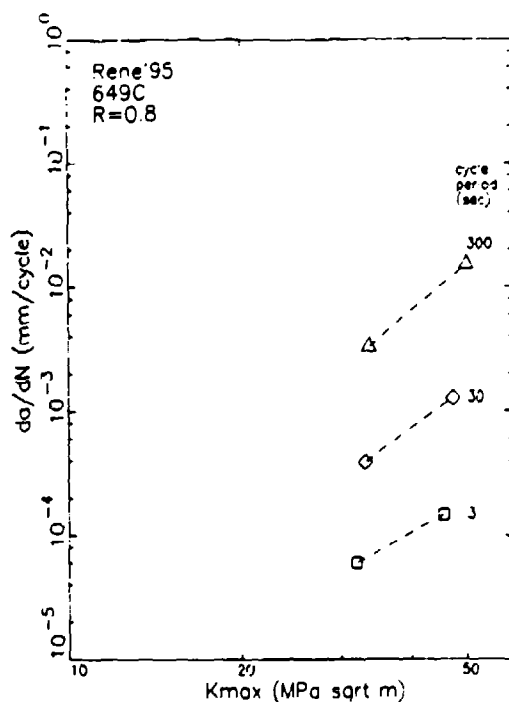
Figure 5.13 compares the results from the 20 cpm, 300 second cycle period (ramp), and 300 second hold time cycles performed during the constant  $\Delta K$  tests performed at 649°C. Qualitatively these results are similar to those shown in Figure 5.12 for the lower test temperature.



(a)



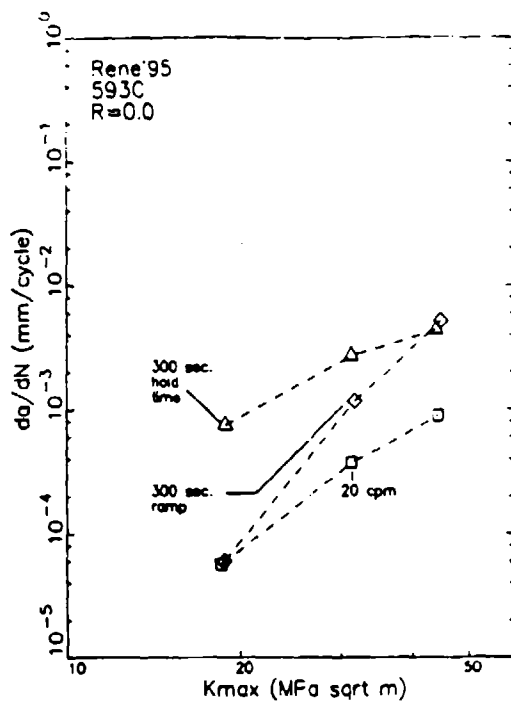
(b)



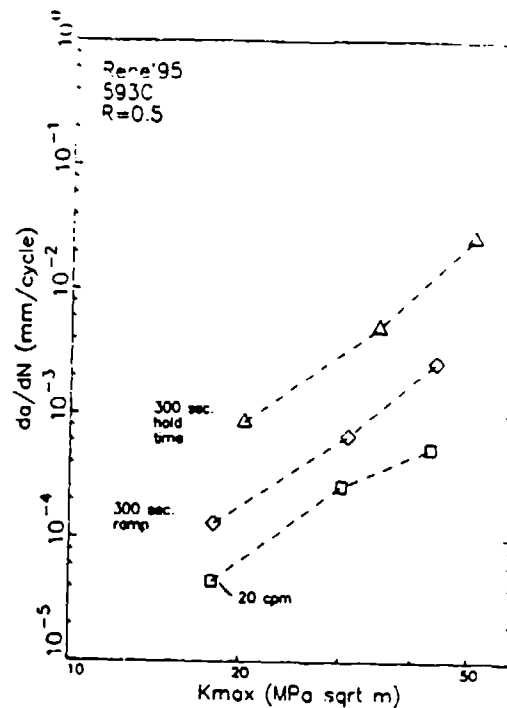
(c)

Figure 5.11:

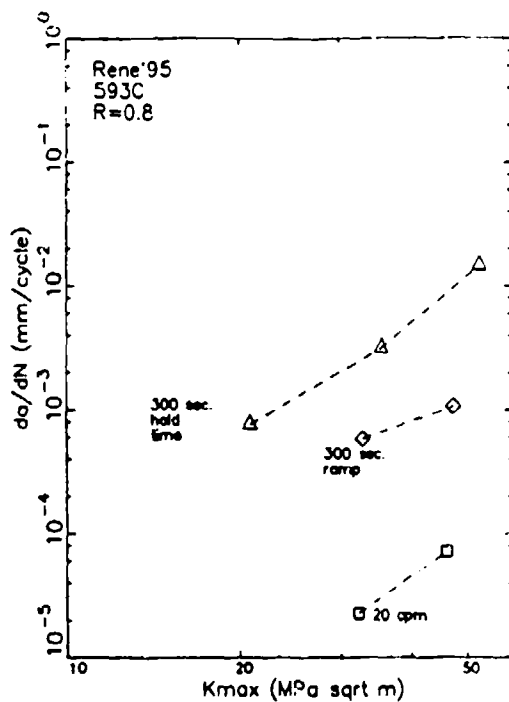
Results of the constant  $\Delta K$  frequency tests on Rene'95 at 649°C with (a)  $R=0.0$ , (b)  $R=0.5$ , and (c)  $R=0.8$ .



(a)



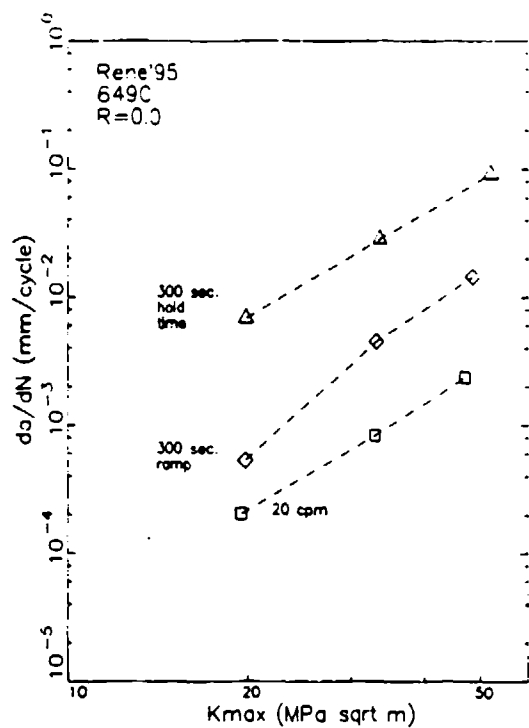
(b)



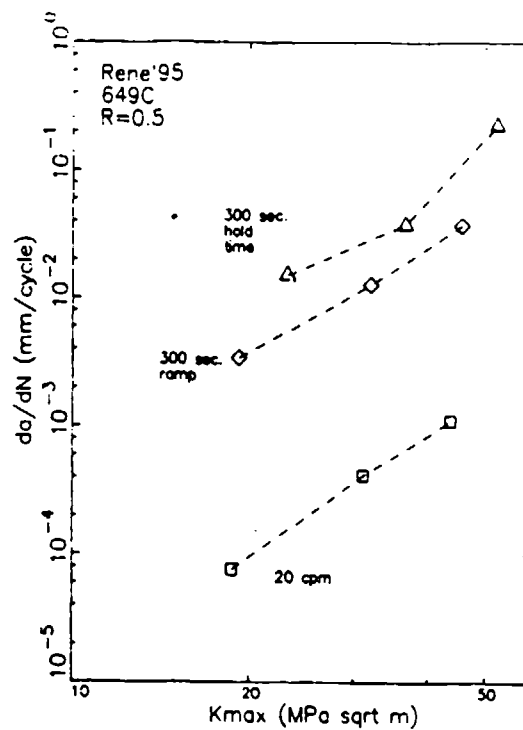
(c)

Figure 5.12:

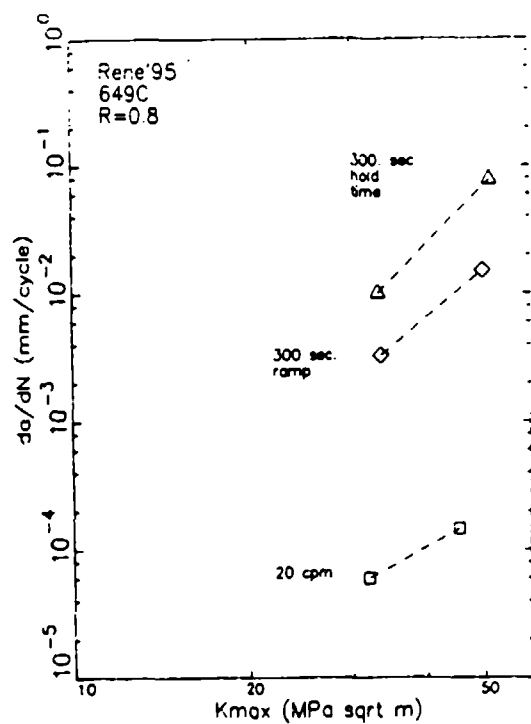
Comparison of results of 593°C  
Rene'95 constant  $\Delta K$  tests cycled at  
20 cpm, 300 second cycle period, and  
300 second hold time with (a)  $R=0.0$ ,  
(b)  $R=0.5$ , and (c)  $R=0.8$ .



(a)



(b)



(c)

Figure 5.13:

Comparison of results of 649°C  
Rene'95 constant  $\Delta K$  tests cycled at  
20 cpm, 300 second cycle period, and  
300 second hold time with (a)  $R=0.0$ ,  
(b)  $R=0.5$ , and (c)  $R=0.8$ .

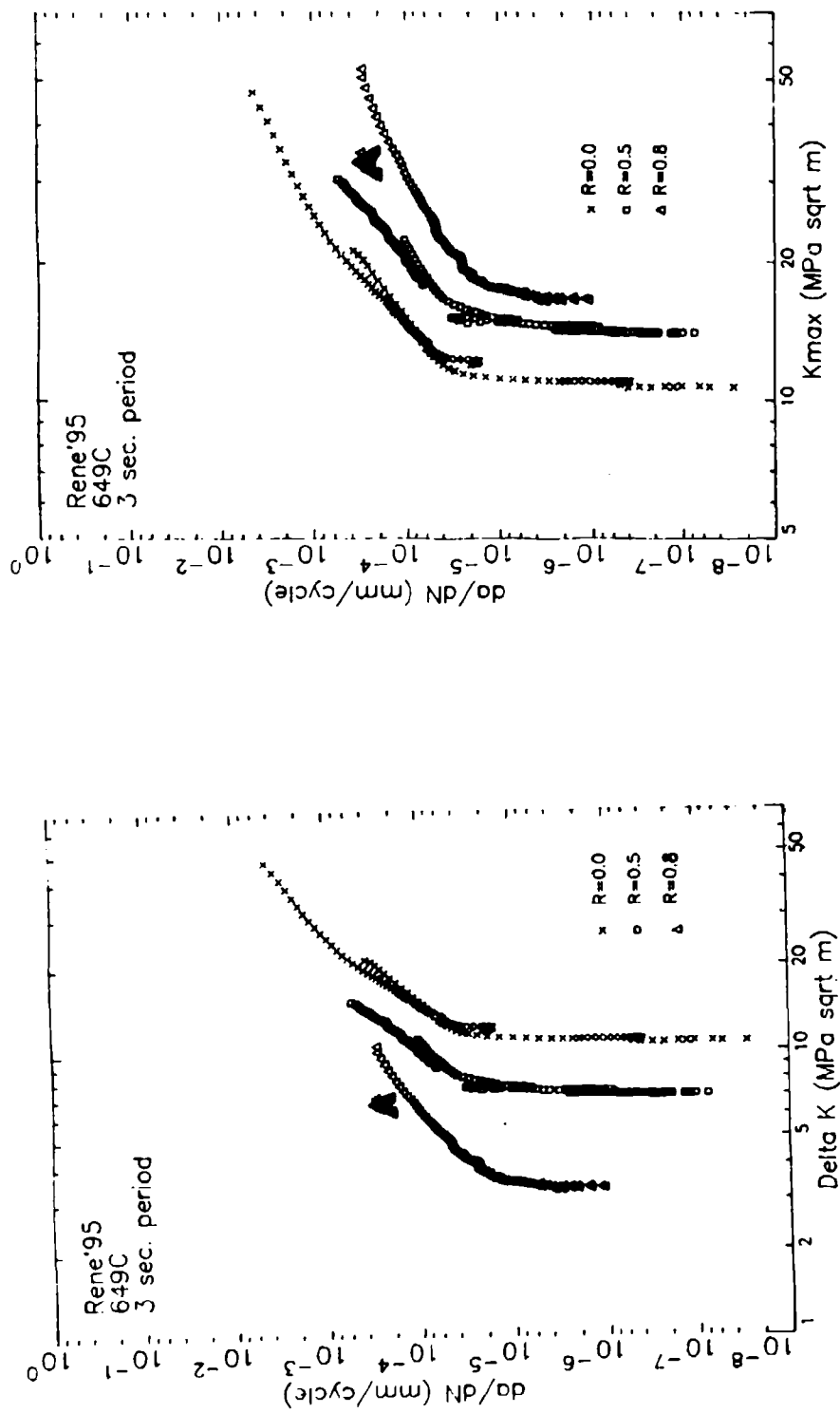
### 5.1.2 Rene'95. Threshold Test Results

The near threshold data were determined using a  $\Delta K$ -shed approach as previously described in Section 4.4.1. Some of these tests were also conducted using an increasing  $\Delta K$  mode to obtain Region II data. The results from both the  $\Delta K$ -shed and increasing  $\Delta K$  data are presented in this section. The last part of this section compares these data to those obtained under constant  $\Delta K$  control conditions. Threshold tests were performed on selected cycling conditions as listed in Table 5.1. Most of these tests were performed at 649°C with a fewer number at 593°C.

Near-threshold tests on Rene'95 at 649°C tests with a 3 second cycle period were performed with R-ratios of 0, 0.5, and 0.8. The results of these tests are shown as a function of  $\Delta K$  and  $K_{max}$  in Figures 5.14a and 5.14b, respectively. Increasing the R-ratio results in more rapid crack growth. The crack growth rate data for the various R-ratio conditions are almost parallel. These data cannot be normalized using either  $\Delta K$  or  $K_{max}$ . This is the situation often observed for nickel-base superalloys under relatively rapid frequencies<sup>(42,43,44)</sup>. The lateral translation in data with R-ratio can often be modeled using the Walker model<sup>(40)</sup>. As described previously, this model defines an effective K ( $K_{eff}$ ) which, for positive R-ratios, is between the values of  $\Delta K$  and  $K_{max}$ . The significance of this approach relative to the linear superposition model is that the cyclic component of crack growth is controlled by  $K_{eff}$  while the time-dependent portion is controlled by  $K_{max}$ . It is important to note that, for primarily cyclic conditions, the value of maximum K at threshold  $(K_{th})_{max}$  increases with R-ratio as shown in Figure 5.14b.

Near-threshold crack growth tests with 3 second cycle periods were also performed at 593°C with R-ratios of 0 and 0.8. The results from those tests are shown as a function of  $\Delta K$  and  $K_{max}$  in Figure 5.15a and 5.15b, respectively. The response at this temperature is similar to that shown in Figure 5.14 for 649°C.

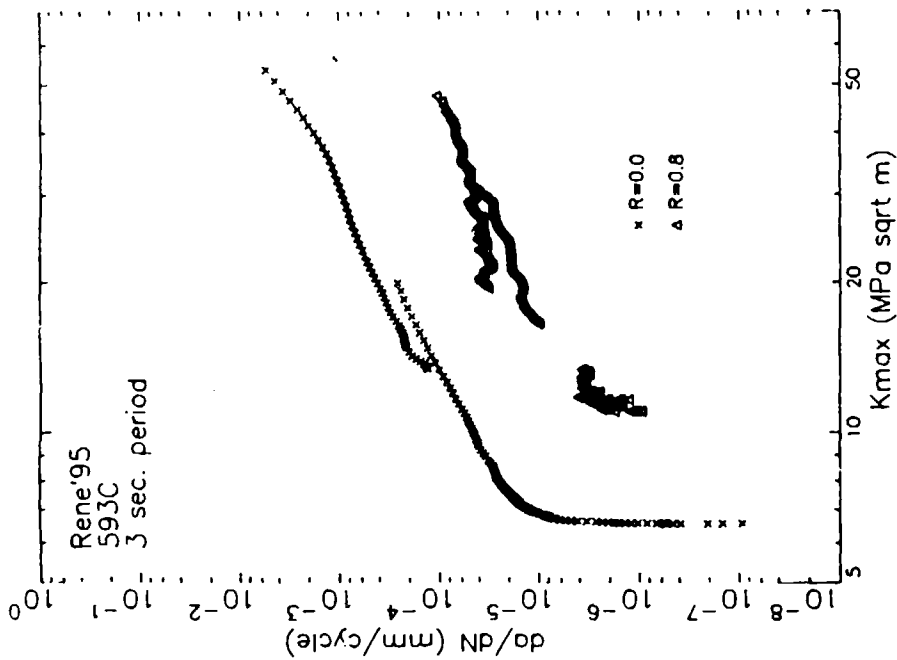




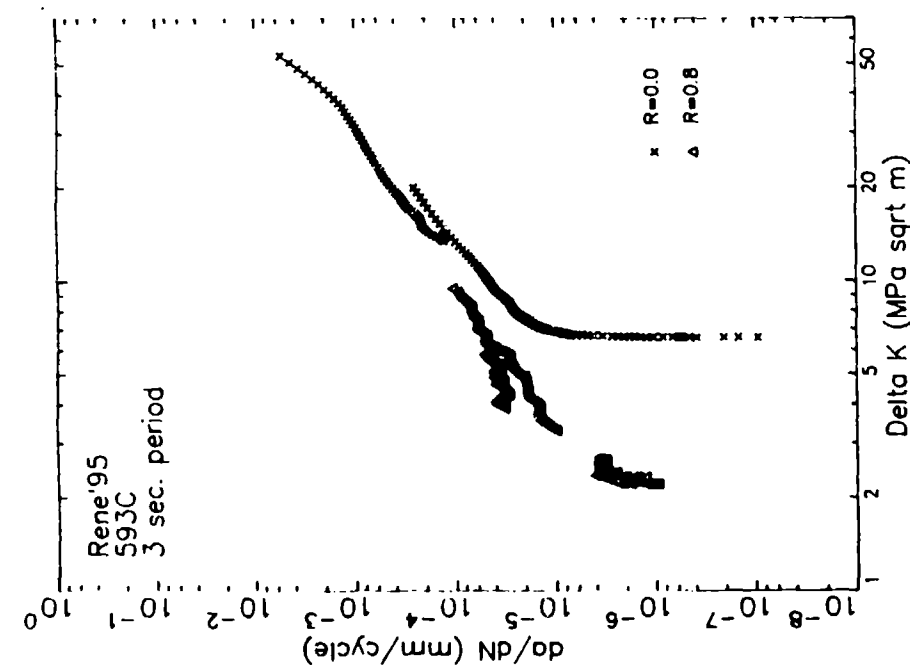
(a)

(b)

Figure 5.14: Results of 649°C Rene'95 threshold tests with 3 second cycle period and different R-ratios as a function of (a)  $\Delta K$  and (b)  $K_{max}$ .



(a)



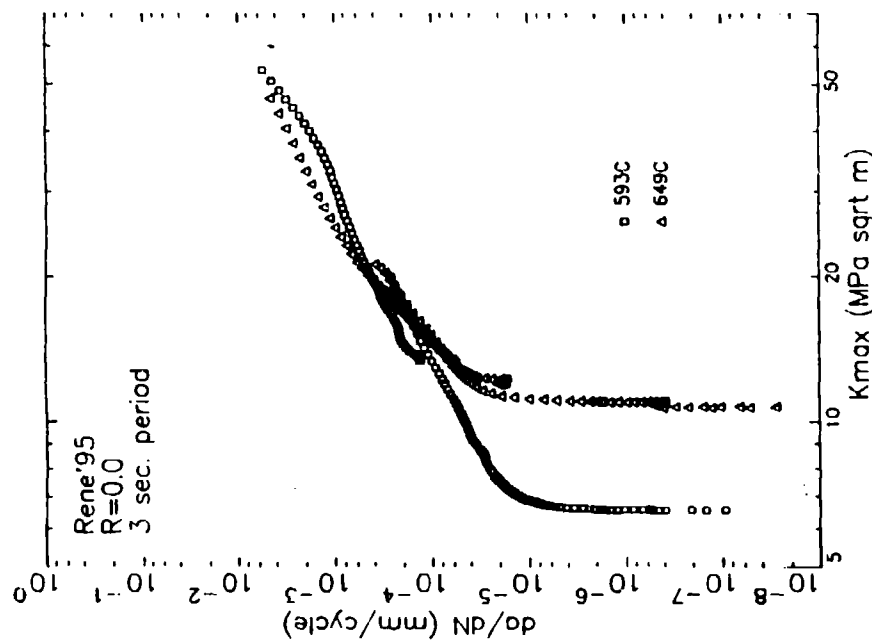
(b)

Figure 5.15: Results of 593°C Rene'95 threshold tests with 3 second cycle period and different R-ratios as a function of (a)  $\Delta K$  and (b)  $K_{max}$ .

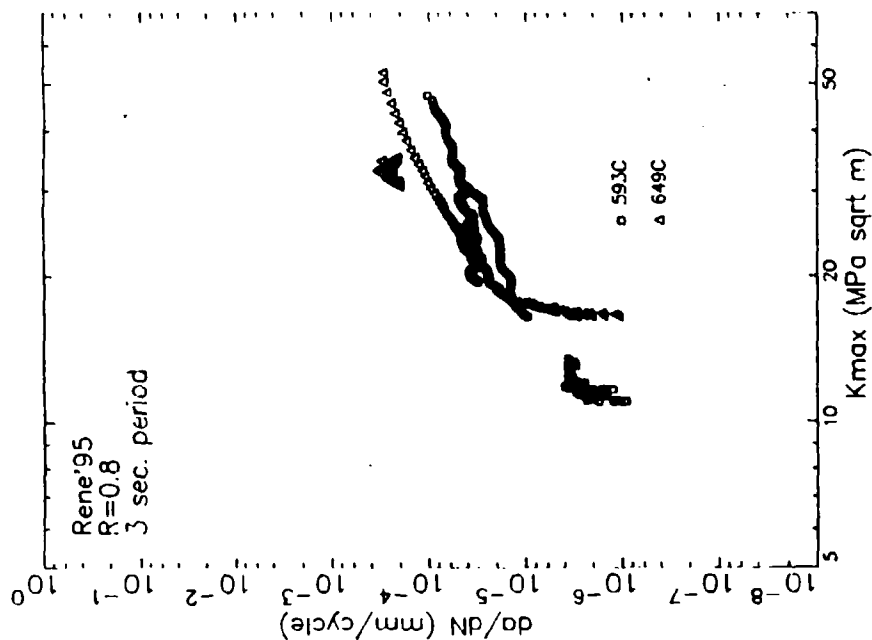
The R=0 and R=0.5 data shown in Figures 5.14a are nearly parallel over the entire range of  $\Delta K$ , however there appears to be a larger shift between the R=0.8 and R=0 near-threshold data than is observed for the Region II data. A similar effect is observed for the 593°C data shown in Figure 5.15a. There are several explanations for this behavior including oxide- or roughness-induced closure and time-dependent crack growth<sup>(44)</sup>.

Over the temperature range from room temperature to 760°C, increasing temperature results in both accelerated Region II crack growth rates and decreasing threshold values for nickel-base superalloys<sup>(42,44)</sup>. This is illustrated using the Rene'95 3 second cycle period tests at 593 and 649°C for R-ratios of 0 and 0.8 in Figures 5.16a and 5.16b, respectively. There is a relatively small change in Region II crack growth rates over this relatively small temperature range, but a rather substantial difference in near-threshold behavior. It has been suggested that the cause for the increase in cyclic threshold value with temperature is localized crack tip blunting and stress redistribution by creep deformation<sup>(42,44)</sup>. The large temperature-induced changes in threshold values at both high and low R ratios strongly suggests that the threshold behavior in these materials is not dominated by oxide-induced closure<sup>(42,44)</sup>. This further implies that the larger shift of the R=0.8 near-threshold data relative to the lower R-ratio data is caused by time-dependent crack growth.

Figure 5.17 shows the crack growth data from the hold time threshold tests for R=0 at 593 and 649°C. At both temperatures, increasing hold time duration increases the crack growth threshold and the Region II crack growth rates. The latter behavior was observed previously in the constant  $\Delta K$  tests. The influence of cycle period on the 649°C near-threshold crack growth behavior is shown in Figure 5.18. Increasing cycle period (decreasing frequency) also results in increased threshold values and Region II crack growth rates. This effect can be qualitatively rationalized by the crack tip blunting and/or stress redistribution arguments made for the temperature crossover effect<sup>(42,44)</sup>. As the cycle time is increased, there is more time available for creep deformation of the material near the crack tip. If creep blunting or stress redistribution, in part, controls the near threshold

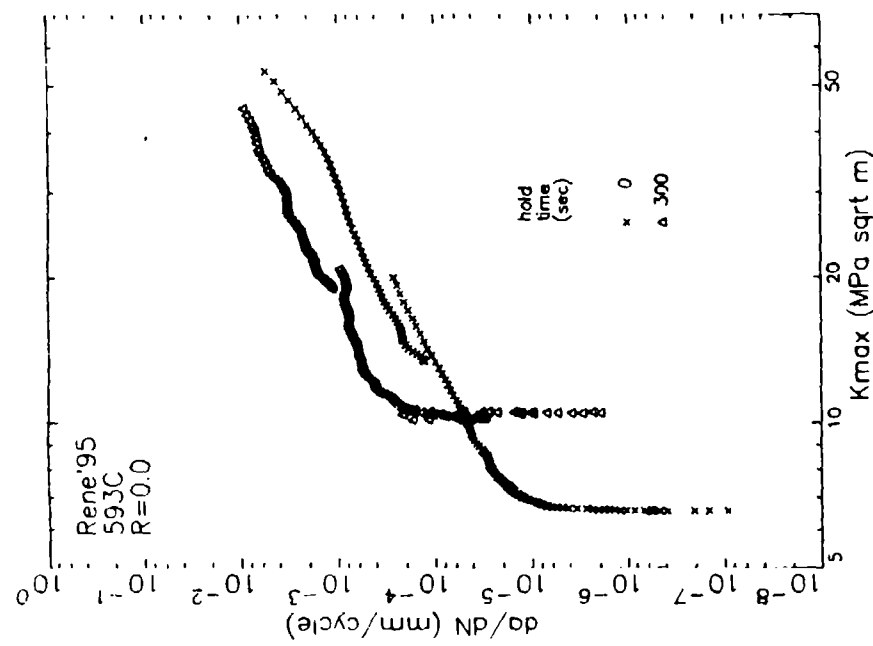


(a)

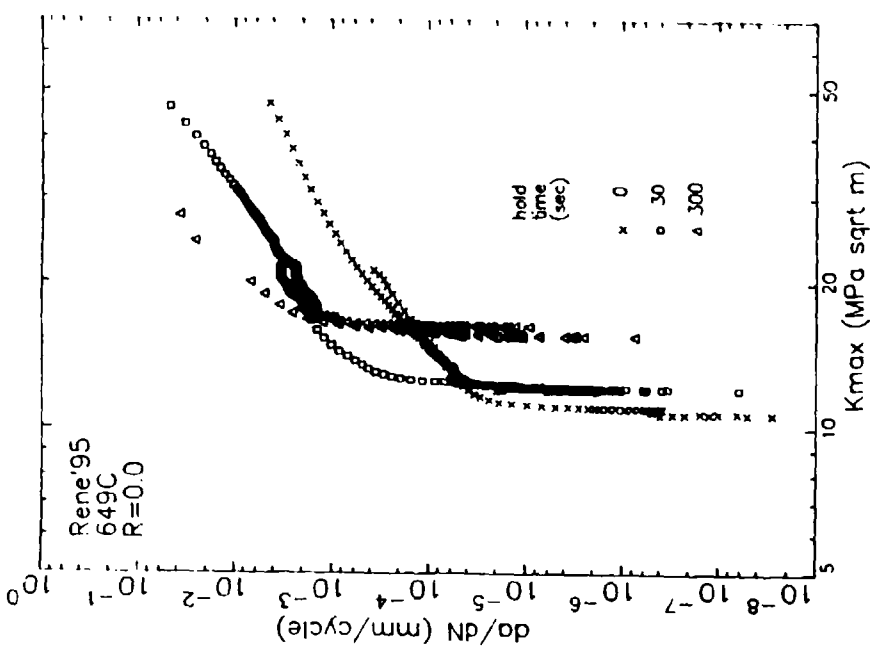


(b)

Figure 5.16: Comparison of 593 and 649°C Rene'95 threshold tests with 3 second cycle period for R-ratios of (a) R=0.0 and (b) R=0.8.



(a)



(b)

Figure 5.17: Results of Rene'95 threshold tests with R=0 and different hold times at (a) 593°C and (b) 649°C.

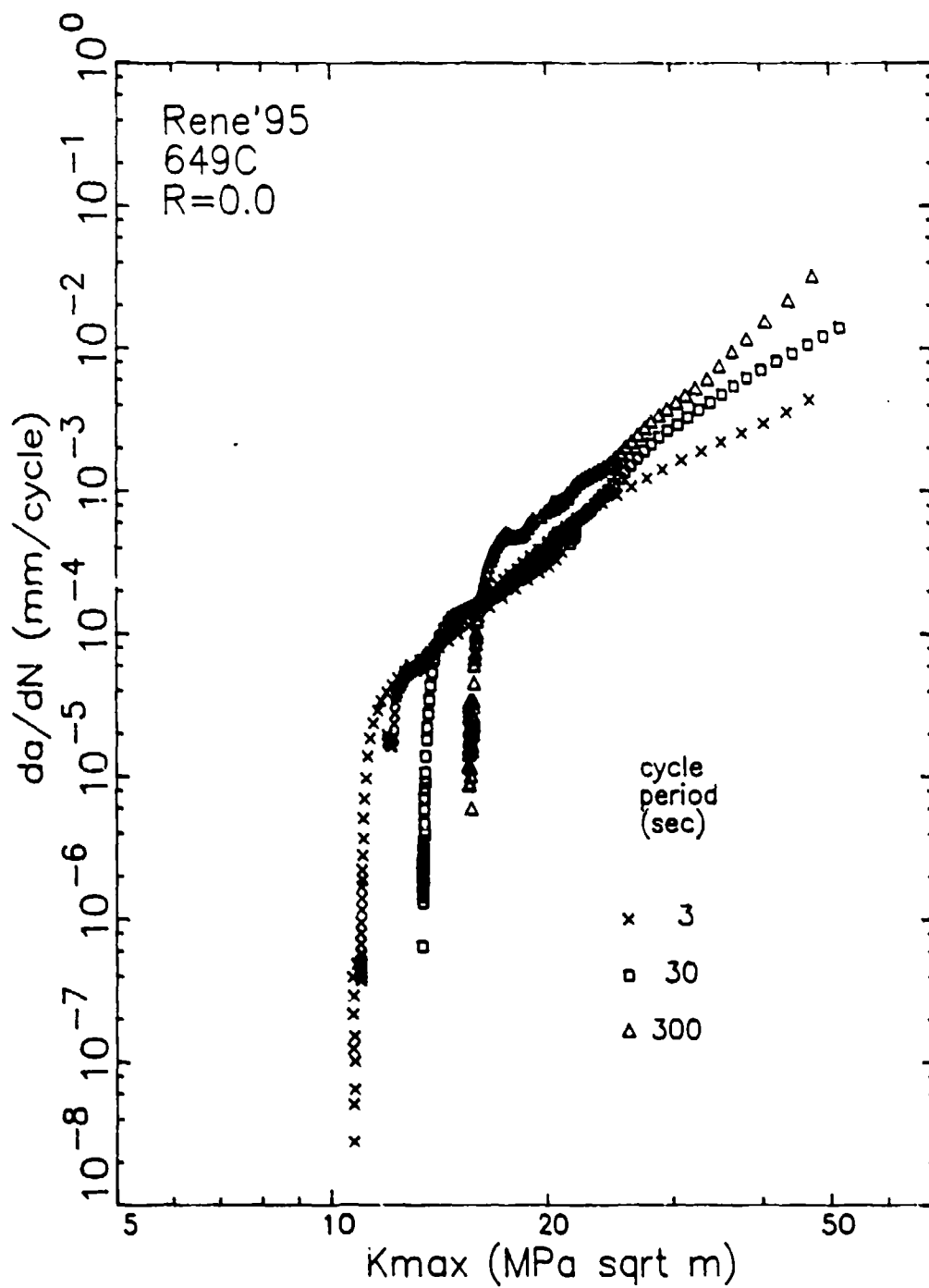
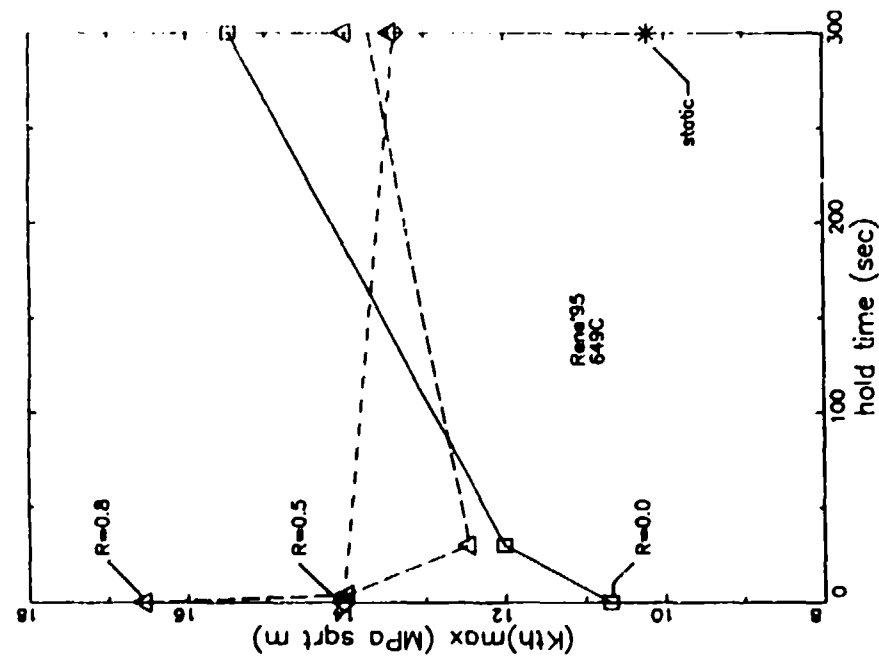


Figure 5.18: Results of 649°C Rene'95 threshold tests with R=0 and different test frequencies.

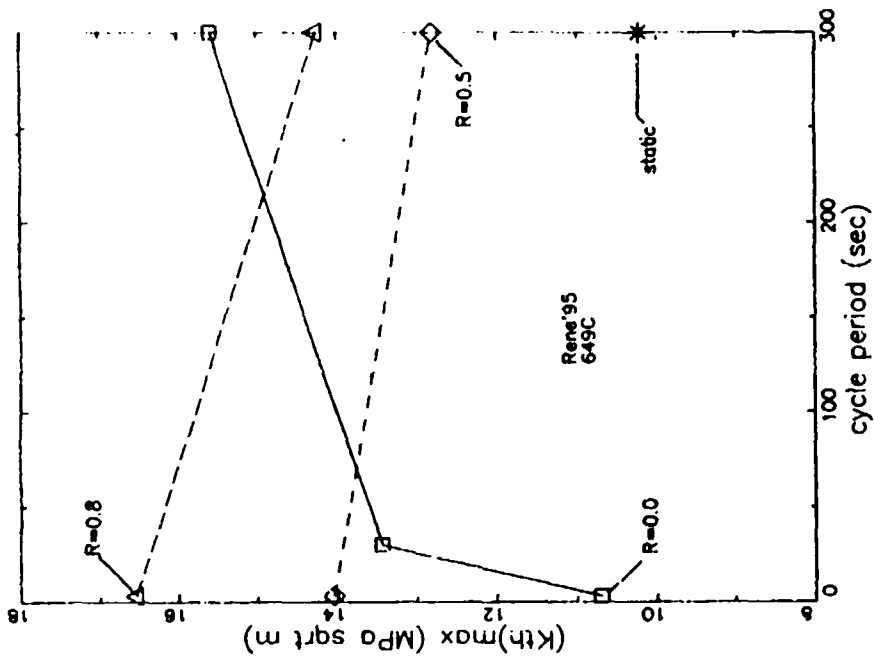
behavior, one would expect increasing values of threshold with increasing cycle period and/or hold time.

The results shown in Figures 5.17 and 5.18 were only for R=0 test conditions. The effect of R-ratio on the threshold values are shown in Figure 5.19. In this figure, the maximum value of K at the threshold,  $(K_{th})_{max}$ , is shown as a function of either hold time (Figure 5.19a) or cycle period (Figure 5.19b). The data from tests with different R-ratios are shown with different symbols. Results from the same R-ratio are connected with lines to illustrate the trends in the data. Also shown in this figure is the static crack growth threshold value as indicated by an asterisk on the right side of each figure. One would expect that as the cycle period or hold time increases, that the values of  $(K_{th})_{max}$  should approach the static threshold value. For R=0, increasing cycle time increases  $(K_{th})_{max}$  as shown in Figures 5.17 and 5.18 and the values are much larger than the static threshold. The R=0.8 hold time tests show a very interesting trend. At short hold times,  $(K_{th})_{max}$  drops quickly and seems to be approaching the static threshold. The value of  $(K_{th})_{max}$  for 300 second hold times is greater than that for a 30 second hold time illustrating that the  $(K_{th})_{max}$  passes through a minimum value with increasing hold time. Based on the available data, it can only be shown that this minimum occurs somewhere between 4 and 300 second hold times. There were insufficient near-threshold tests performed for R=0.5 hold time, R= .5 frequency, and R=0.8 frequency cycling conditions to determine if the minimum also occurs for these situations. The observation of the minimum in  $(K_{th})_{max}$  for the R=0.8 hold time tests strongly suggests that there are two competing crack growth mechanisms operating in the near-threshold regime. One mechanism results in the decrease in  $(K_{th})_{max}$  for small hold times and the other results in  $(K_{th})_{max}$  values greater than the static threshold value for long hold times. The potential mechanisms which may cause this behavior will be discussed in Section 6.

It is very interesting to compare the R=0 data for 20 cpm cycling conditions (3 second period or 0 hold time) with the results for 300 second cycle periods or hold times. For nominally cyclic crack growth (20 cpm), the value of  $(K_{th})_{max}$  increases with R-ratio as was illustrated in Figure 5.14.



(a)



(b)

Figure 5.19: Variation of  $(K_{th})_{max}$  in Rene'95 at 649°C with R-ratio and (a) hold time and (b) test frequency.



For the long hold times, the values of  $(K_{th})_{max}$  are ordered differently with  $R=0$  having the highest value followed by the  $R=0.8$  then the  $R=0.5$  values. These changes in the ordering of the threshold values further illustrate the complexity of the local crack growth mechanisms resulting in the variations in  $(K_{th})_{max}$  shown in Figure 5.19.

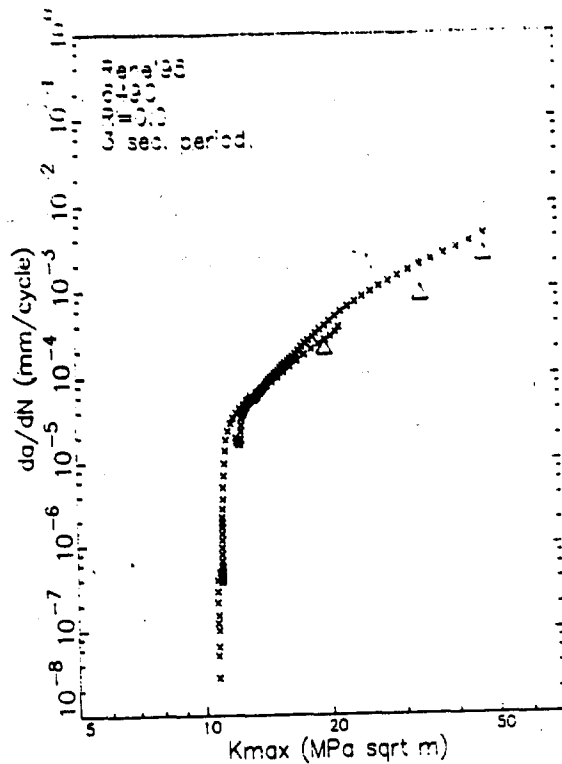
Four near-threshold crack growth rate tests were performed at  $593^{\circ}\text{C}$  comprising a two by two matrix of  $R$ -ratio (0 and 0.8) and hold time (0 and 300 seconds). The  $(K_{th})_{max}$  results for these four tests are listed in Table 5.2. The influence of hold time for the  $R=0$  tests is the same as that shown in Figure 5.17a for the higher temperature. The magnitude, however, is not as great as those observed at  $649^{\circ}\text{C}$ . There are insufficient data to determine if  $(K_{th})_{max}$  passes through a maximum for  $R=0.8$  cycling conditions. At an  $R$ -ratio of 0.8, the value of  $(K_{th})_{max}$  increased with hold time. This result is different from the  $649^{\circ}\text{C}$  results (Figure 5.19) in that increasing hold time increases the threshold value at both  $R$ -ratios and at both hold times the  $R=0.8$  test had the higher value of  $(K_{th})_{max}$ . It is not clear whether different mechanisms are occurring at the two temperatures or if there has been a relative change in the kinetics of the two competing processes.

The previous section concentrated on crack growth threshold estimated from the  $\Delta K$ -shed test results. The Region II crack growth rate tests showed the same trends observed in the constant  $\Delta K$  tests which were reported the previous section. For the remainder of this section, the results of the Region I and II crack growth rates determined in threshold tests (increasing and decreasing  $\Delta K$ ) will be compared to those determined in the constant  $\Delta K$  tests. The results of the threshold tests will be shown with small "x" symbols while the constant  $\Delta K$  test results will be indicated with large triangles.

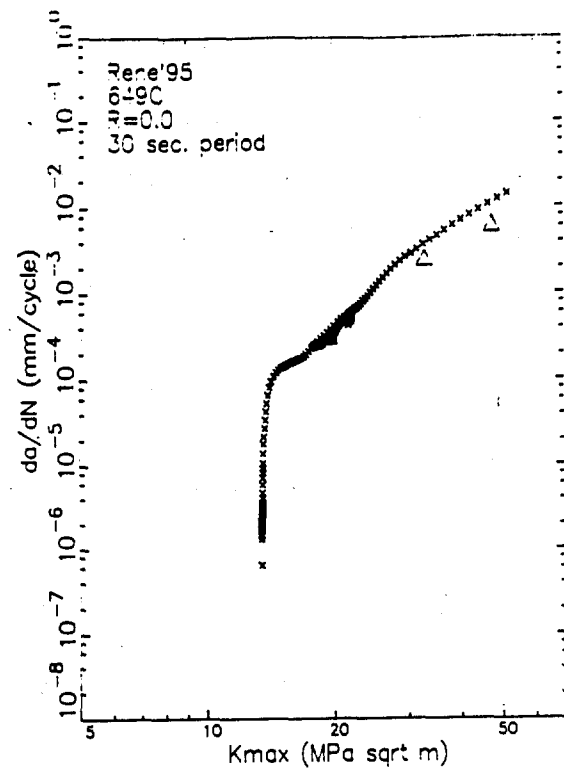
Figure 5.20 shows the results of the  $649^{\circ}\text{C}$  tests with a  $R$ -ratio of zero and different values of cycle frequency. The results of the two types of tests are similar; however, the constant  $\Delta K$  results are slightly lower than those measured during the increasing  $\Delta K$  portion of the threshold tests.

Table 5.2: Rene'95 593°C Threshold Data

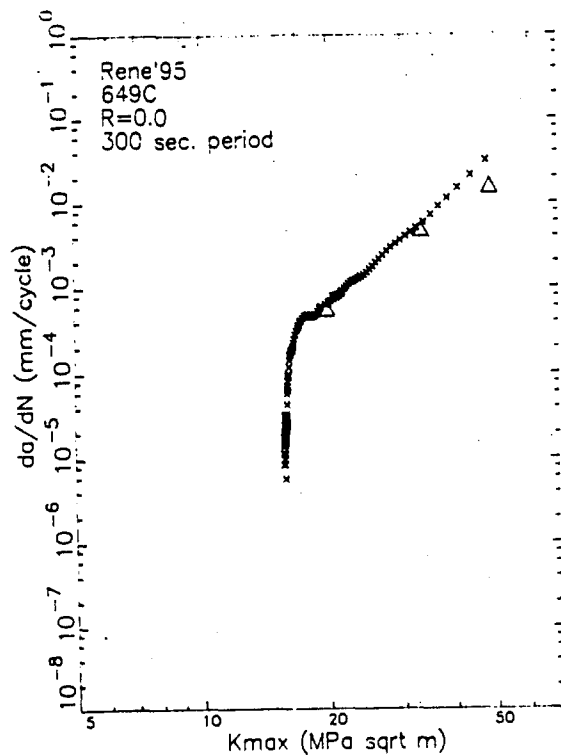
Test Number	R	Hold Time (sec)	(K <sub>th</sub> ) <sub>max</sub> (MPa/m)
AF62	0.0	0	6.56
AF77	0.0	300	11.00
AF13	0.8	0	10.47
AF46	0.8	300	12.83



(a)



(b)



(c)

Figure 5.20:

Comparison of crack growth rates measured in threshold and constant  $\Delta K$  tests of Rene'95 at 649°C and  $R=0$  for cycle periods of (a) 3 seconds, (b) 30 seconds, and (c) 300 seconds.

Figure 5.21 shows the results of the 649°C hold time tests performed with a R-ratio of zero. Also included in Figure 5.21b are the load shed results with a shed rate constant C of -0.39mm (-10/inch) previously shown in Figure 4.7 and the Region II constant load and increasing  $\Delta K$  results previously shown in Figure 4.9. The data in Figure 5.21 show that the constant  $\Delta K$  results are significantly lower than the results from the constant load or increasing  $\Delta K$  results. The influence of test control mode is greater for the hold time test specimens than the frequency test specimens.

The results determined for the 649°C tests performed with a R-ratio of 0.5 are shown in Figures 5.22 and 5.23. Both cycle frequency tests are displayed in the first figure while the 300 second hold time data are shown in the latter figure. Note that there is only increasing  $\Delta K$  data for the 300 second period test (Figure 5.22b). When data were obtained for both control modes, the constant  $\Delta K$  data was lower than the increasing  $\Delta K$  data. Comparison of the data in Figures 5.22a and 5.23 does not show the effect of cycle period or hold time observed in the R=0 tests. As noted previously, a large part of the difference in the control modes is believed to be related to retardation. The constant  $\Delta K$  tests are in fact tests with blocks of cycles performed under constant load conditions. If this is true, the retardation effect will be related to the number of cycles performed between load adjustments (block size). The implications of the block size will be examined in more detail in Section 7.

The results from the R=0.8 test at 649°C with varying test frequency and hold times are shown in Figures 5.24 and 5.25. Again the results show that lower crack growth rates were measured in the constant  $\Delta K$  tests.

The results of the four 593°C threshold tests are listed in Table 5.2 and are compared with the corresponding constant  $\Delta K$  tests in Figures 5.26 and 5.27. The R=0 results are shown in Figure 5.26 and the R=0.8 data are given in Figure 5.27. As in the lower temperature tests, the crack growth data measured in the constant  $\Delta K$  tests are lower than the rates measured under increasing  $\Delta K$  conditions.

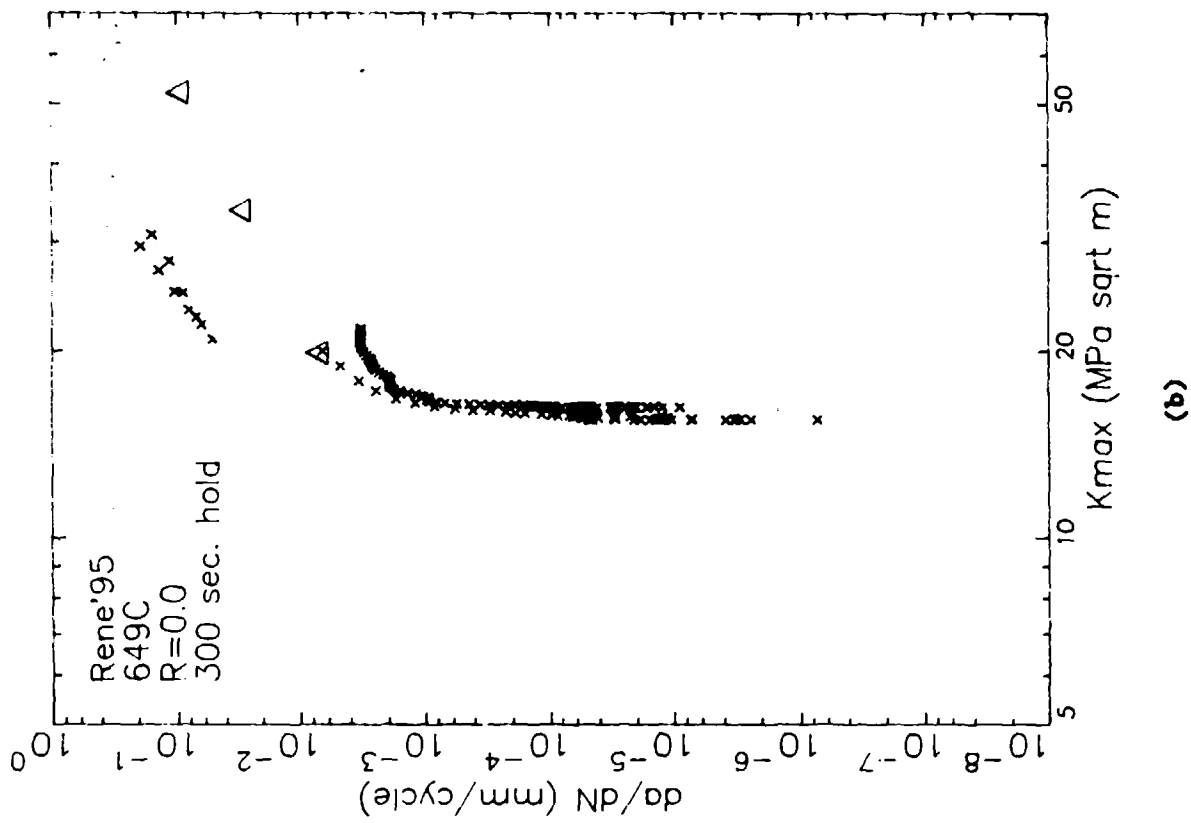
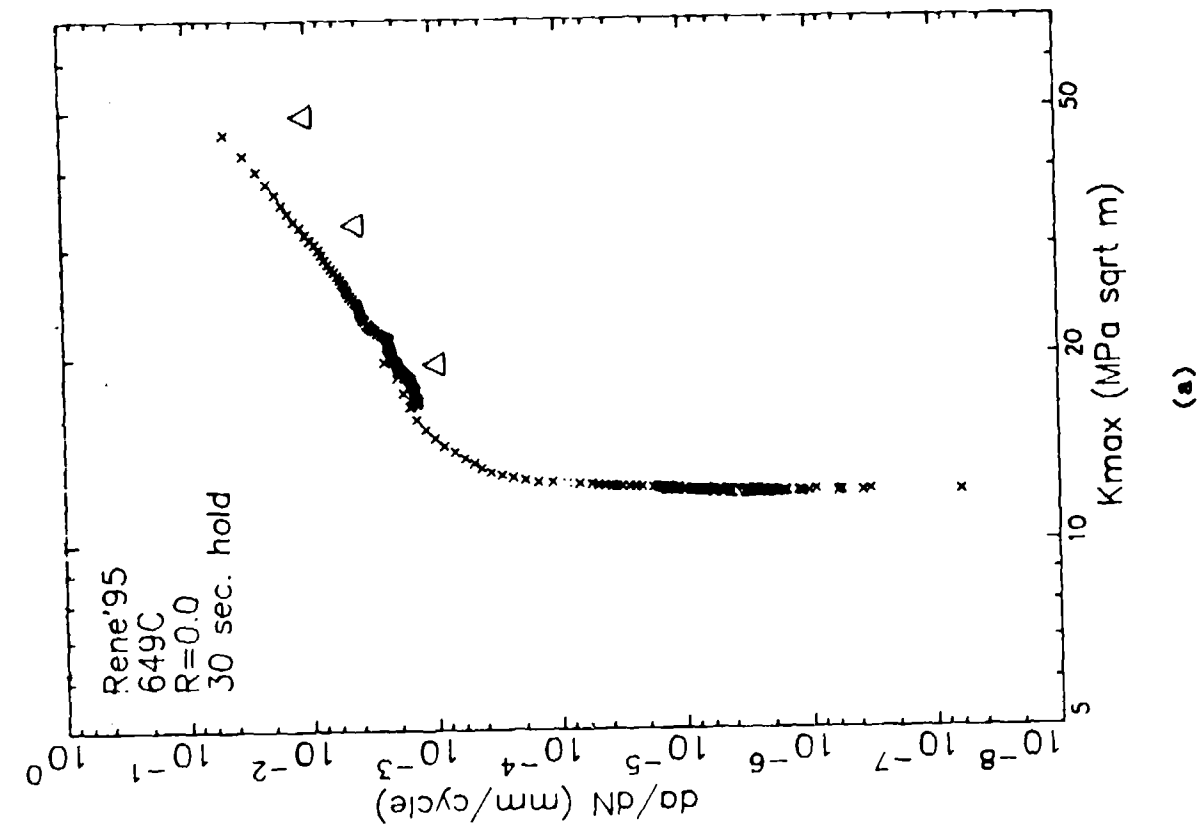
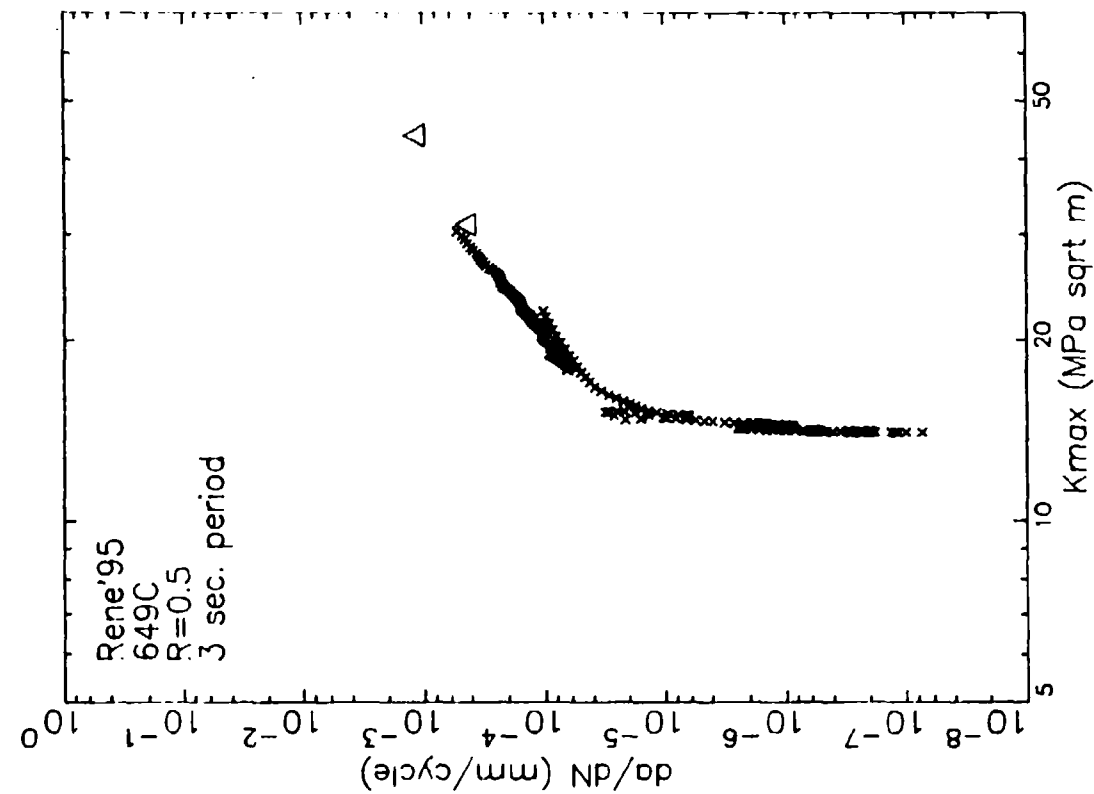
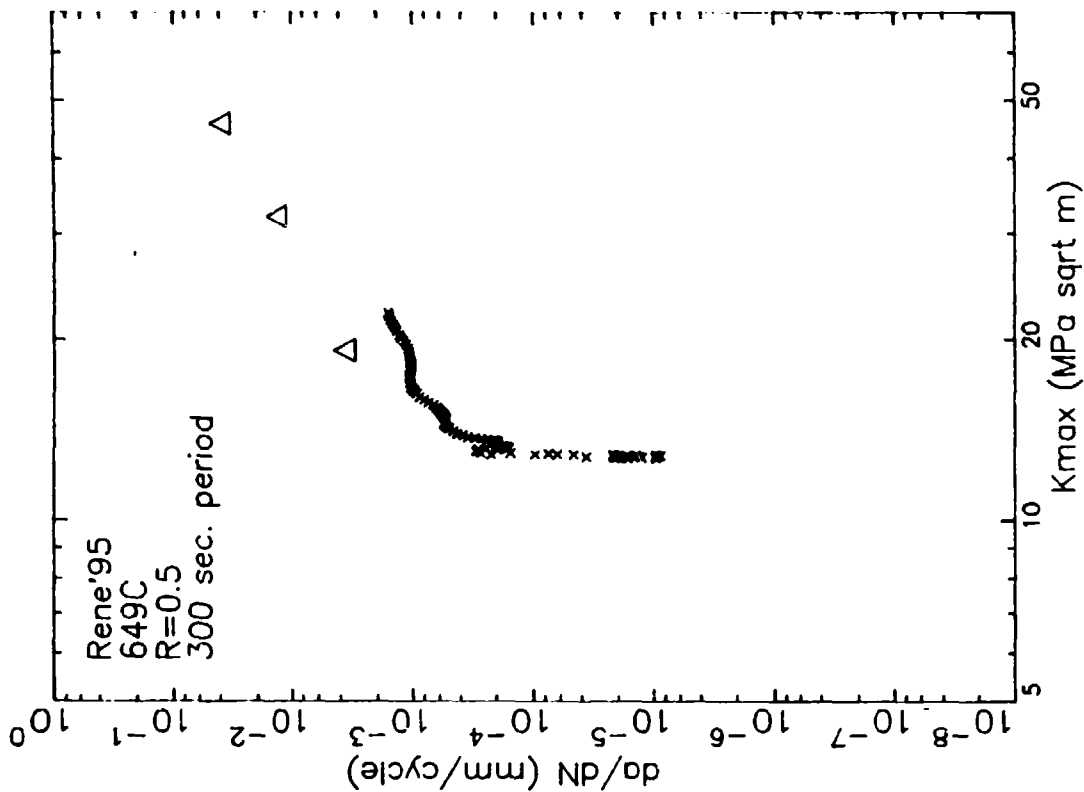


Figure 5.21: Comparison of crack growth rates measured in threshold and constant  $\Delta K$  tests of Rene'95 at 649°C and R=0 for hold times of (a) 30 seconds and (b) 300 seconds.



(a)



(b)

Figure 5.22: Comparison of crack growth rates measured in threshold and constant  $\Delta K$  tests of Rene'95 at 649°C and  $R=0.5$  for cycle periods of (a) 3 seconds and (b) 300 seconds.

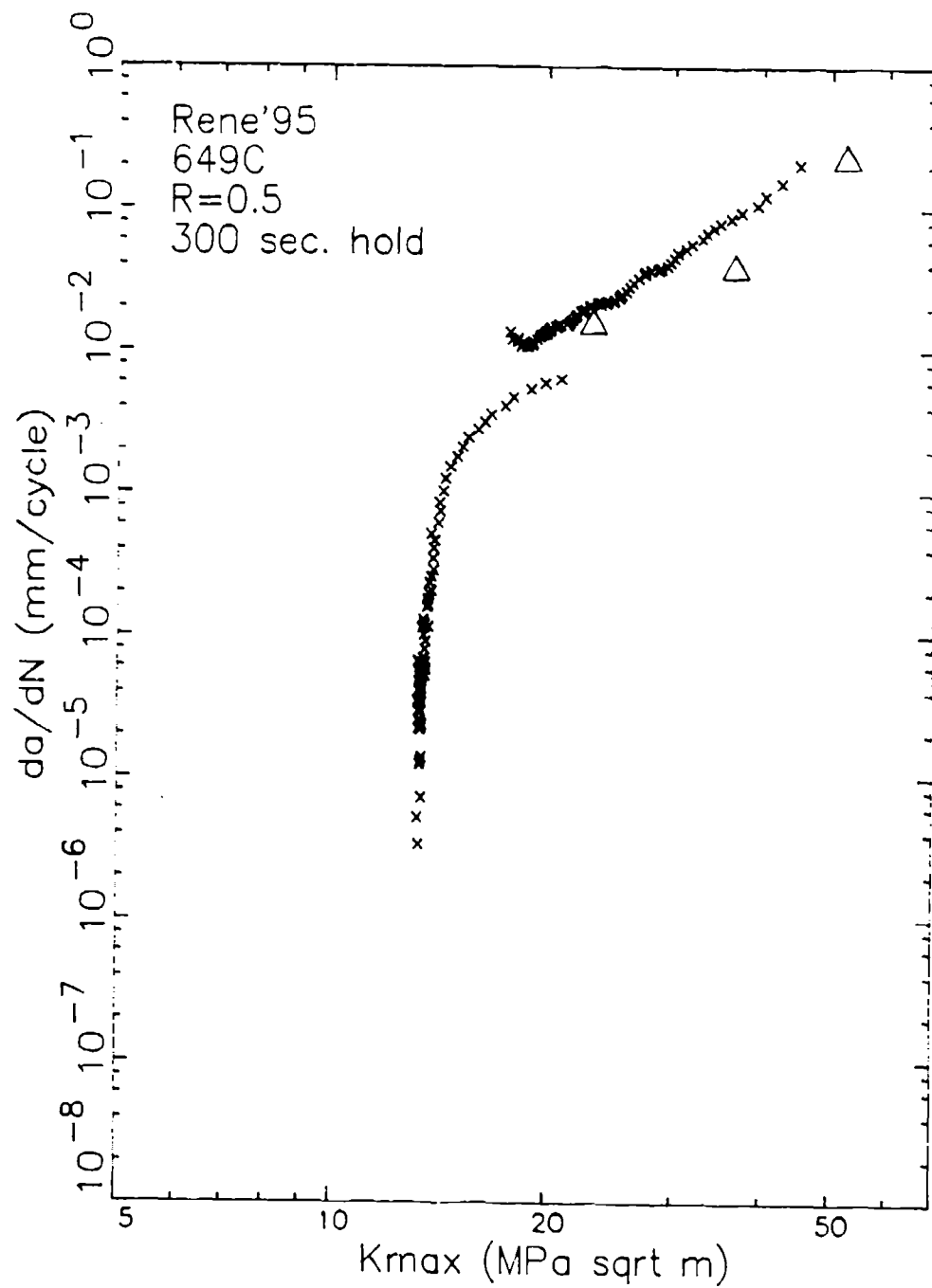


Figure 5.23: Comparison of crack growth rates measured in threshold and constant  $\Delta K$  tests of Rene'95 at 649°C and R=0.5 for a hold time of 300 seconds.

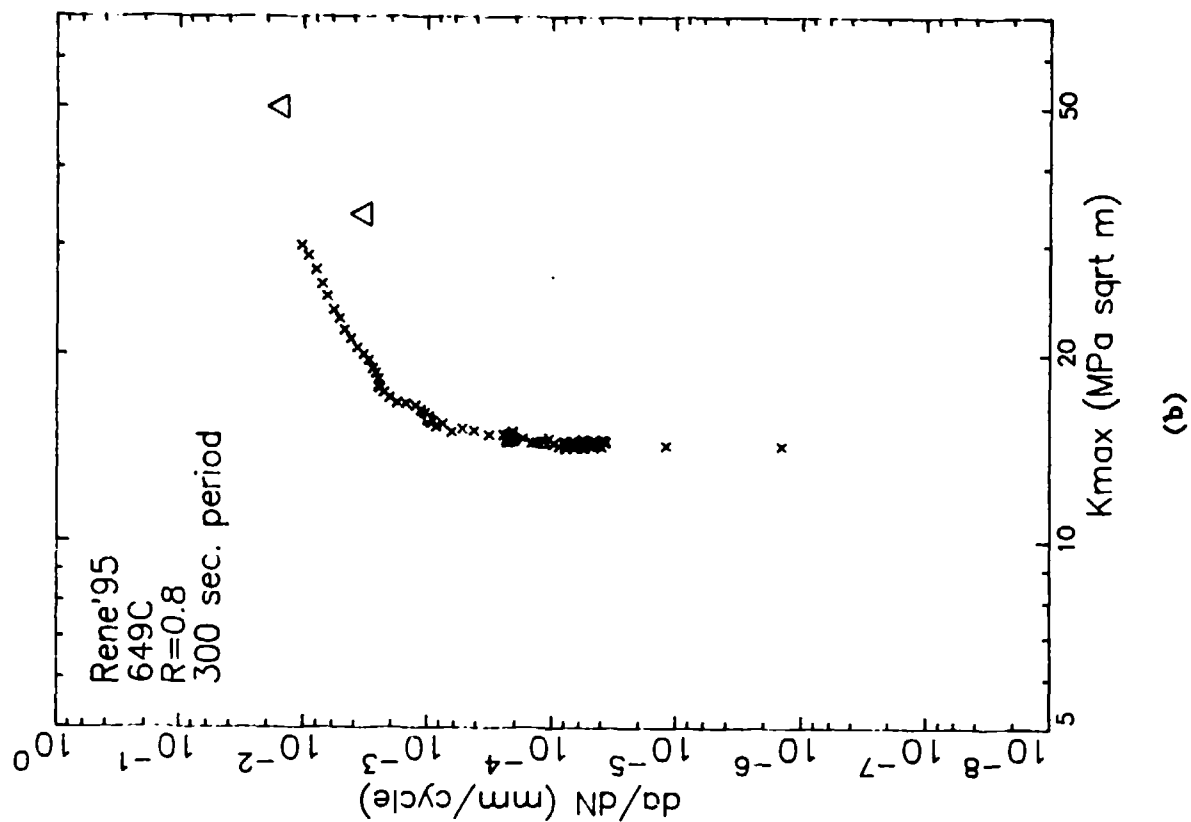
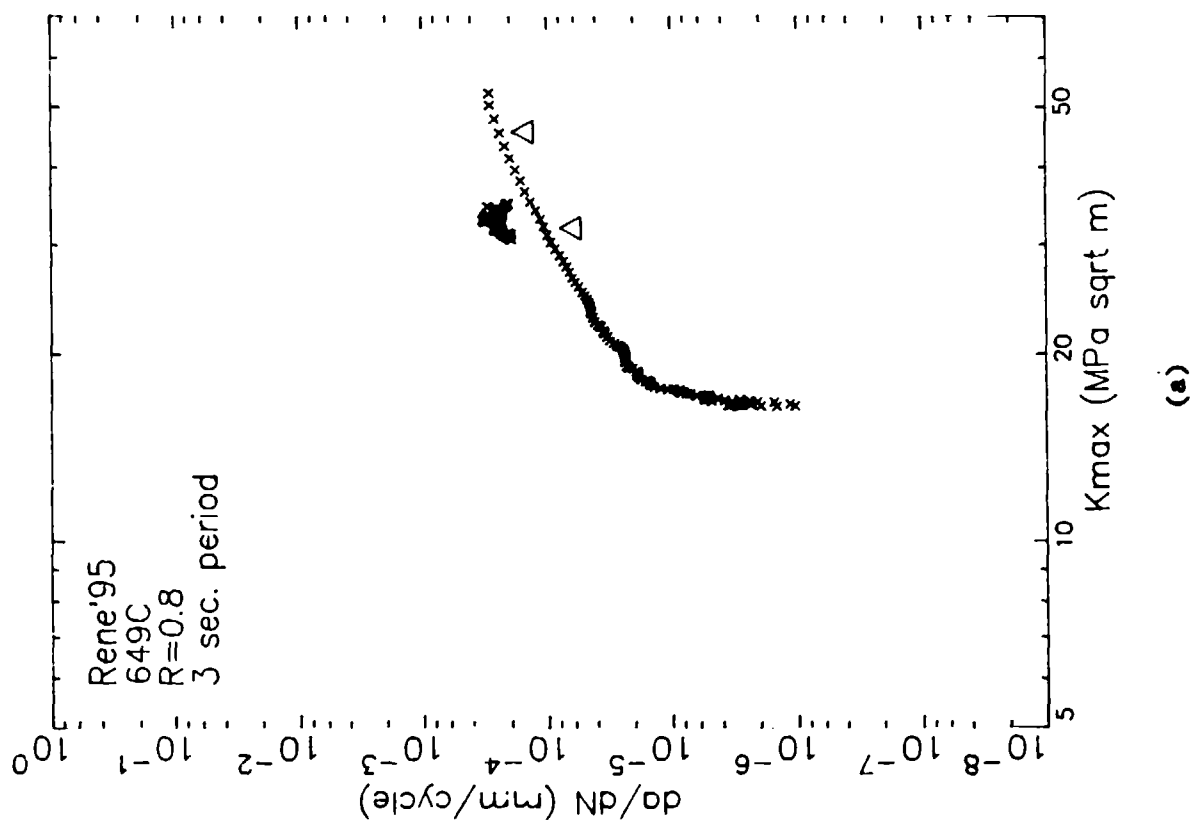
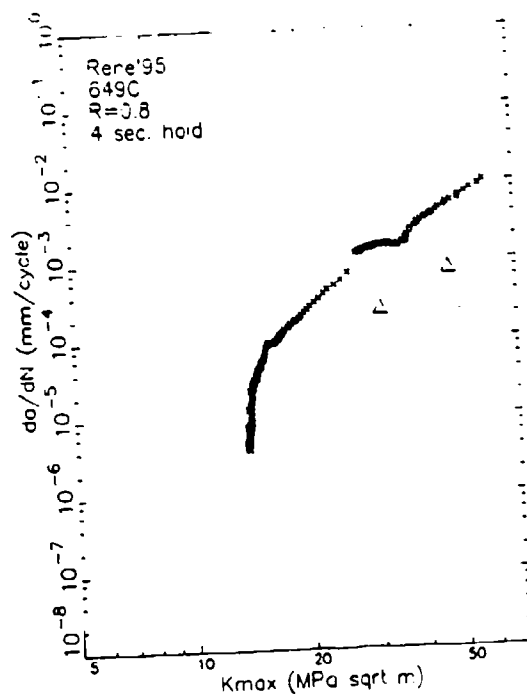
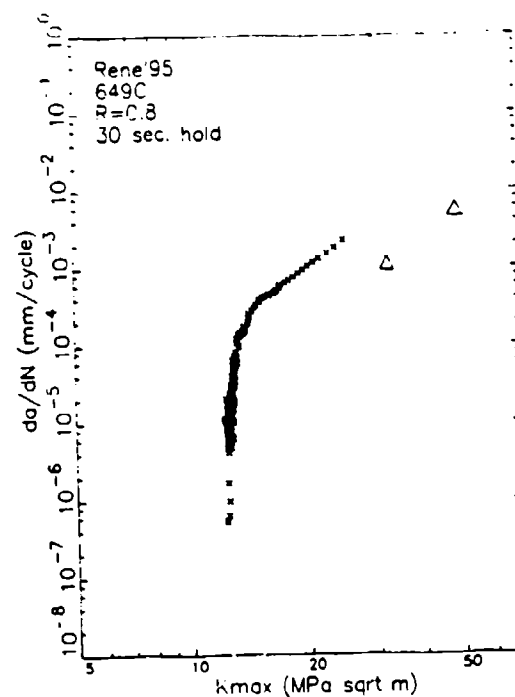


Figure 5.24: Comparison of crack growth rates measured in threshold and constant  $\Delta K$  tests of Rene'95 at 649°C and R=0.8 for cycle periods of (a) 3 seconds and (b) 300 seconds.

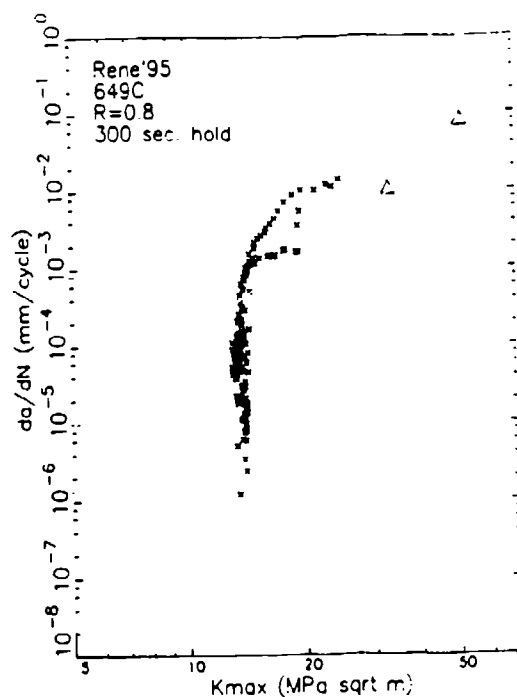




(a)



(b)



(c)

Figure 5.25:

Comparison of crack growth rates measured in threshold and constant  $\Delta K$  tests of Rene'95 at 649°C and  $R=0.8$  for hold times of (a) 4 seconds, (b) 30 seconds, and (c) 300 seconds.

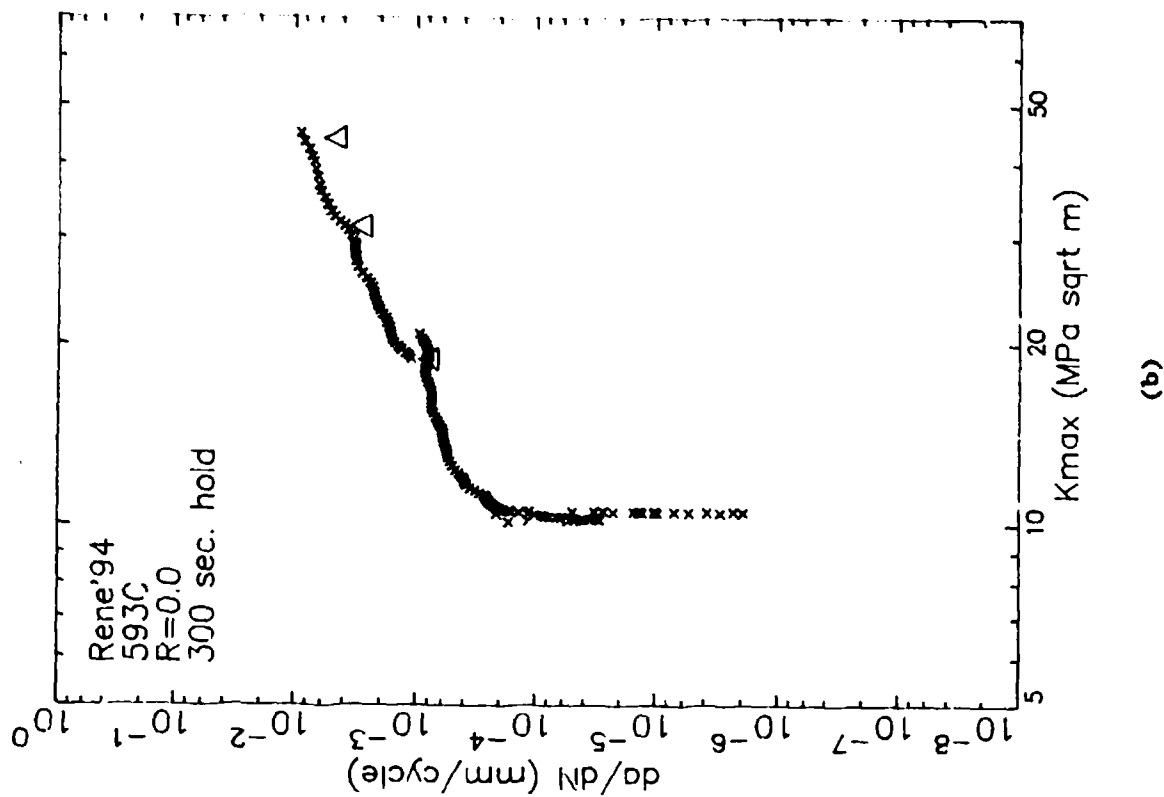
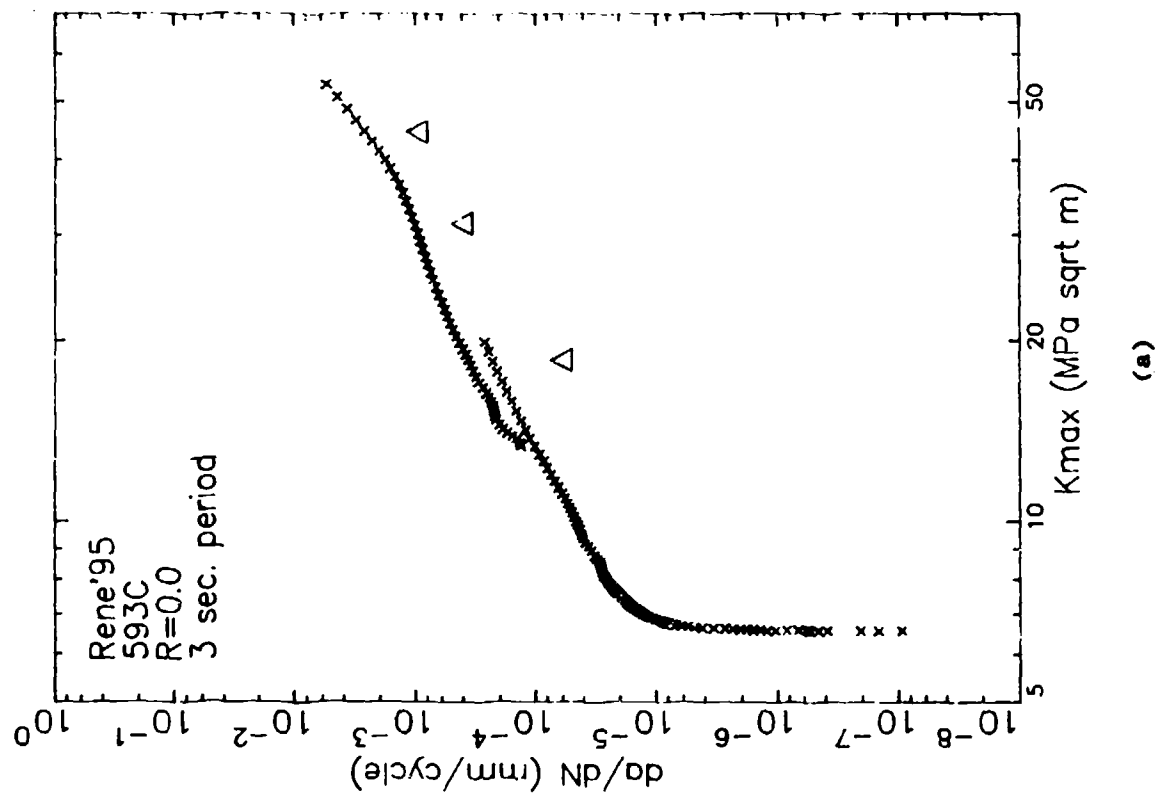
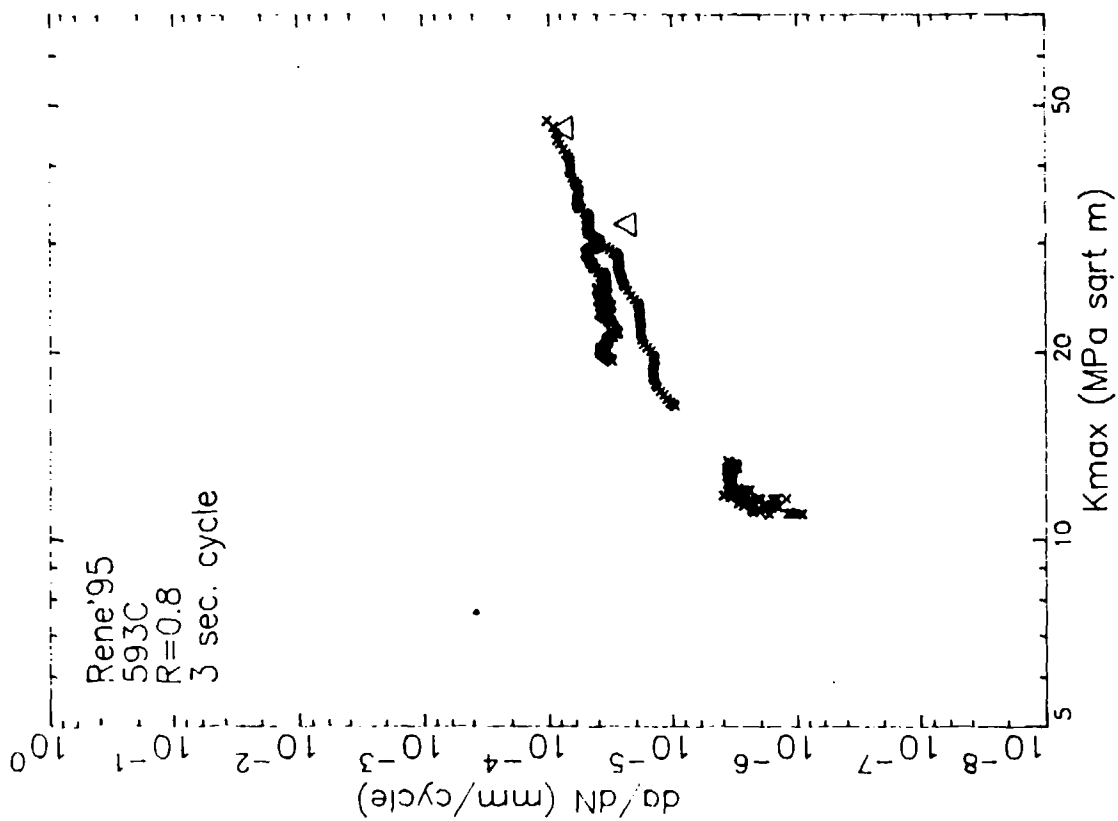
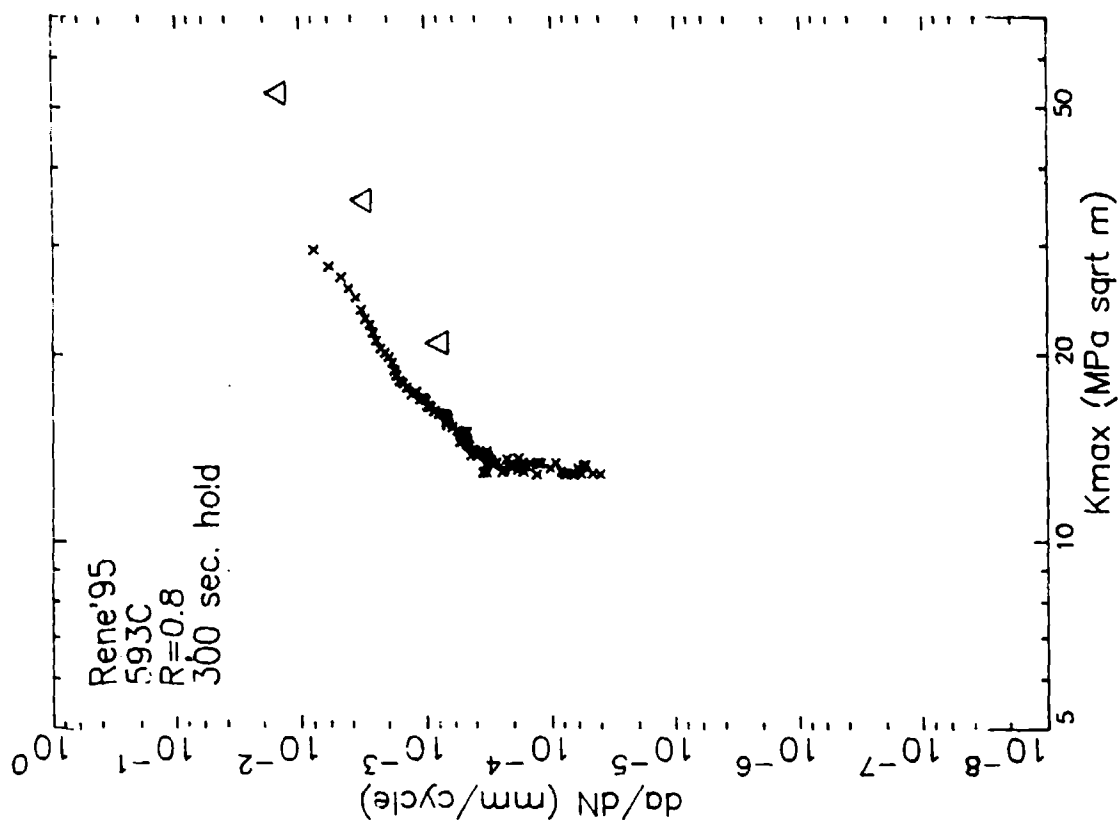


Figure 5.26: Comparison of crack growth rates measured in threshold and constant  $\Delta K$  tests of Rene'95 at 593°C and R=0.0 for hold times of (a) 0 seconds and (b) 300 seconds.



(a)



(b)

Figure 5.27: Comparison of crack growth rates measured in threshold and constant  $\Delta K$  tests of Rene'95 at 593°C and R=0.8 for hold times of (a) 0 seconds and (b) 300 seconds.

The comparisons shown in Figures 5.20 through 5.27 have clearly illustrated that crack growth rates measured in an increasing  $\Delta K$  mode exceed those determined under constant  $\Delta K$  conditions. This discrepancy is larger for hold time tests than the frequency tests and also tends to increase with increasing R ratio. The lower crack growth measurements in the constant  $\Delta K$  tests may be due to retardation induced by load drops between load control cycles in a given cycle block. For these reasons, the agreement of the crack growth predictions from the models described later in this report will rely more heavily on the increasing  $\Delta K$  rather than the constant  $\Delta K$  data.

#### 5.1.3 Rene'95, static crack growth

Static crack growth tests were performed on Rene'95 test specimens at 593 and 649°C (1100 and 1200°F). Individual tests were conducted using a  $\Delta K$ -shed and load control modes. These tests were actually run as fatigue tests with a R-ratio of 0.995 and a cycle period of 3 seconds. This approach was used so that the load could be adjusted frequently during the  $\Delta K$ -shed tests.

The results of one  $\Delta K$ -shed and two constant load tests performed at 649°C are shown in Figure 5.28. The constant load data show an apparent threshold at the start of each test. These data may be indicative of transient behavior between the R=0 precrack and the static (R=1) constant load portion of the test. Sadinanda and Shahanian<sup>(16)</sup> have reported a similar type of behavior in constant load tests performed on Alloy 718. The  $\Delta K$ -shed tests had responses typical of threshold tests. The static threshold data previously shown in Figure 5.19 were determined from this test. There is a spread by a factor of approximately three between these crack growth rates. This will become significant when applying the superposition model because the data shown in Figure 5.28 were used to determine the constants for the static crack growth curve.

Figure 5.29 shows the results from a single  $\Delta K$ -shed and constant load test performed at 593°C. Unfortunately, the  $\Delta K$ -shed test was stopped before near-threshold data were obtained. The constant load data in this figure show the apparent threshold also observed in the constant load tests performed at

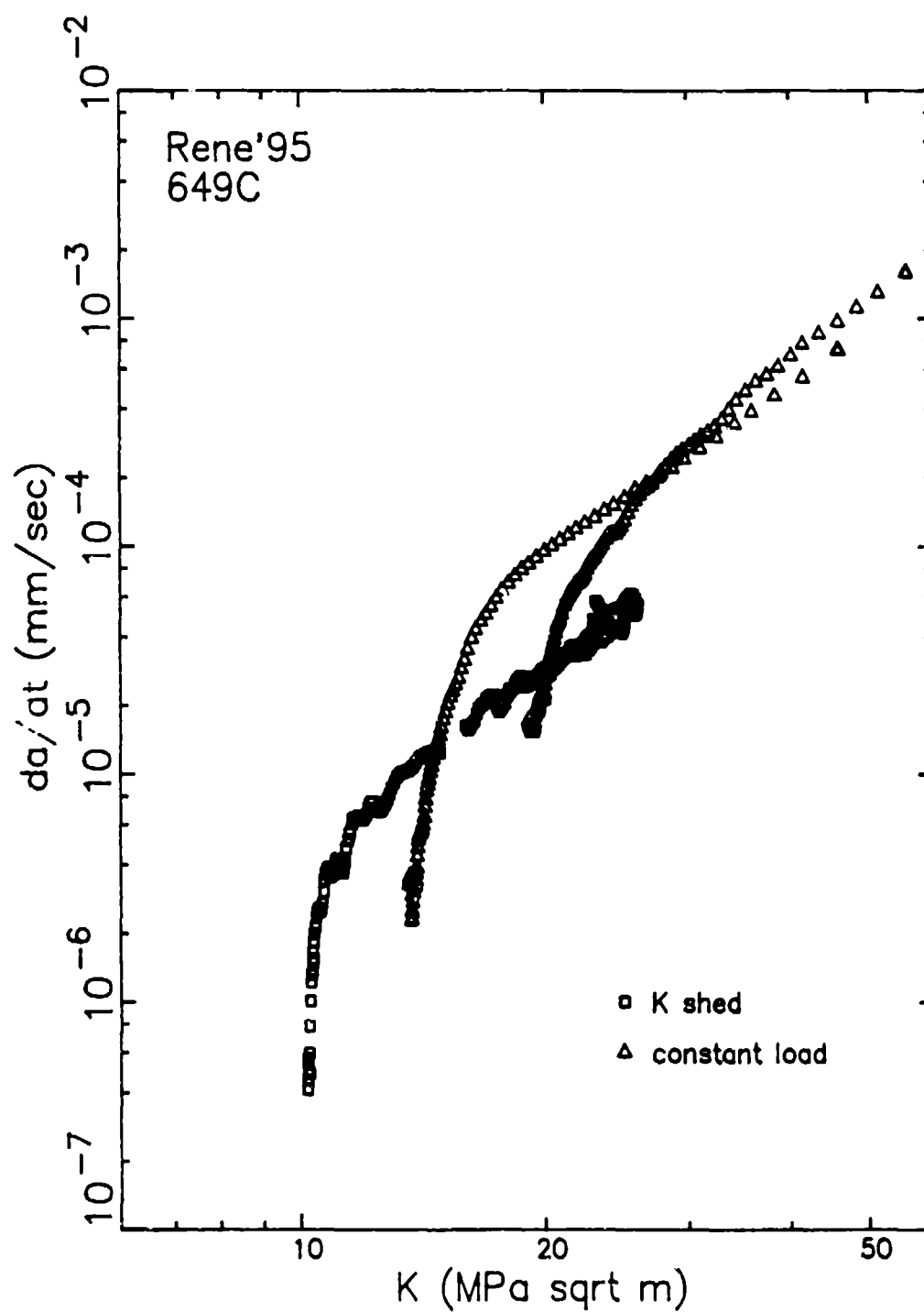


Figure 5.28: Results of Rene'95 static crack growth tests at 649°C.

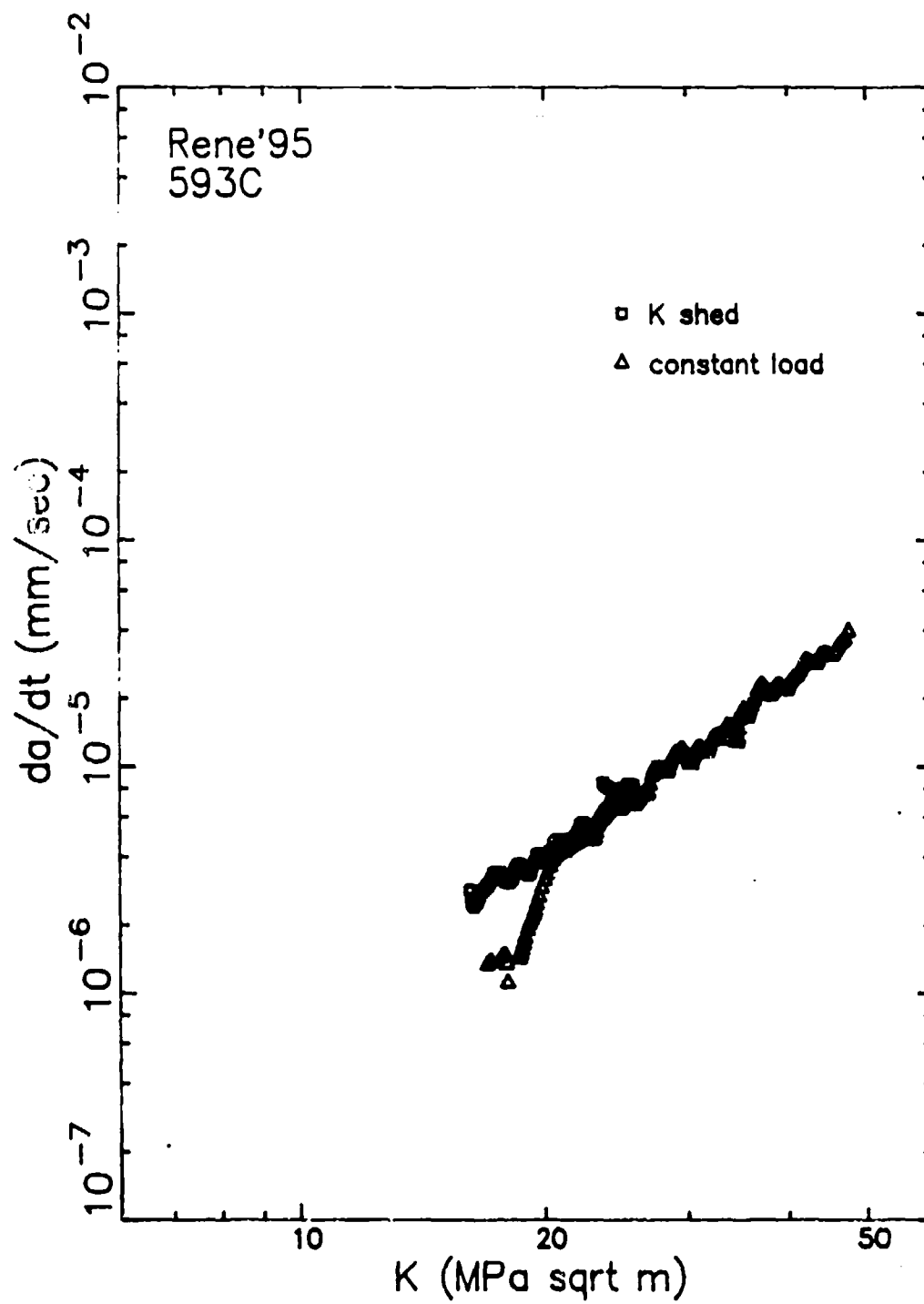


Figure 5.29: Results of Rene'95 static crack growth tests at 593°C.

the higher test temperature. Comparison of the data in Figures 5.28 and 5.29 shows that increasing the temperature by 55°C (100°F) results in an increase of static crack growth rates by an order of magnitude. The amount of scatter between test specimens is significantly higher for the 649°C tests than the 593°C tests.

#### 5.1.4 Rene'95 Retardation Tests

Retardation tests were performed to determine the influence of overpeaks in suppressing crack growth during hold times at stresses below the maximum value. The mission survey analysis (Section 3.0) showed that overpeaks ranging from almost zero to 100 percent occur during engine operation.

The Rene'95 retardation test matrix is given in Table 5.3. Two different types of constant  $\Delta K$ -control tests were used to evaluate overpeaks. single overpeak and multiple overpeak tests. Single overpeak tests were performed at 593 and 649°C (1100 and 1200°F) with a R-ratio of zero. After a single overpeak, repetitive cycles with hold times of 0.30 and 300 seconds were performed until the crack had advanced a minimum of 0.25 mm (0.01 inch). At this point, another overpeak was applied and the process was repeated. In a single test overpeak values of 10, 20, and 50 percent were evaluated.

The multiple overpeak tests were also performed using  $\Delta K$  control. Examples of some of the multiple overpeak cycles are shown in Figure 5.30 where, in some cases, a hold time occurs at a K value intermediate to the minimum and maximum K during the decreasing load ramp. All cycles performed in this fashion had a loading ramp of 7.5 seconds and an unloading ramp of 7.5 seconds. The 15 second cycle was used because the equipment used to generate the command signal for the test machine had to be programmed in even increments of time. The relatively slow ramp was necessary in order to accurately control the loading ramps in cycles with 300 second hold times. The cycles were defined by the overpeak ratio, R-ratio, and hold time. The R-ratio was defined as the ratio of minimum K to K during the hold time ( $K_{hold}$ ). The overpeak value was represented as the percentage that the overpeak  $K_{max}$  is in excess of  $K_{hold}$ . The hold time interrupted the decreasing

Table 5.3: Rene'95 Overpeak Test Matrix

<u>Test Number</u>	<u>Temperature (°C)</u>	<u>R</u>	<u>Overpeak Ratio</u>
AF58	593	0.0	variable
AF73	593	0.0	1.1
AF28	593	0.0	1.2
AF36	593	0.5	1.1
AF43	593	0.5	1.2
AF56	649	0.0	variable
AF68	649	0.0	1.1
AF29	649	0.0	1.2
AF34	649	0.0	1.5
AF75	649	0.5	1.1
AF35	649	0.5	1.2



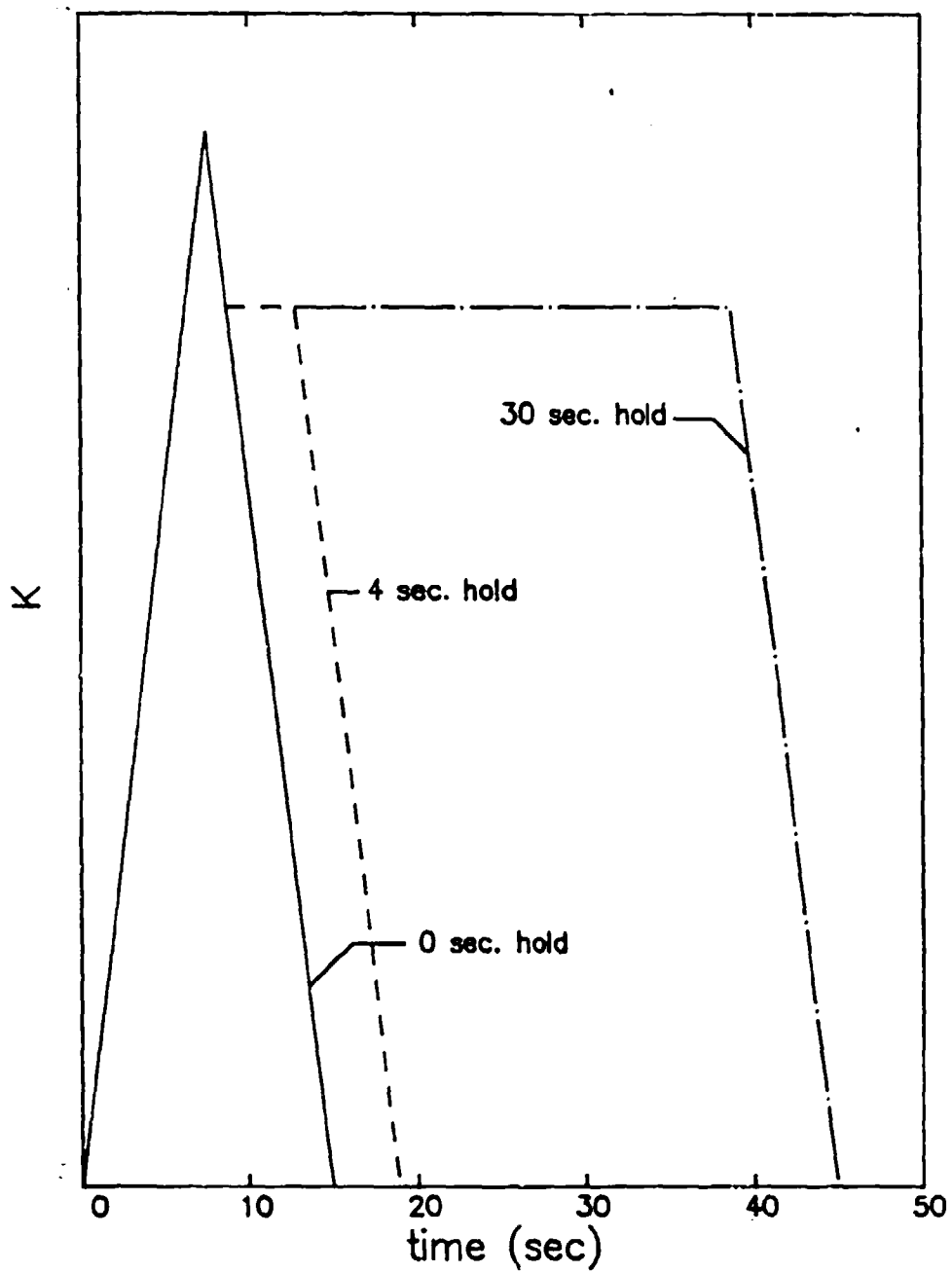


Figure 5.30: Schematic figure showing multiple retardation cycles with hold times of 0, 4, and 30 seconds.

load ramp so that the unloading rates before and after the hold time were identical. The cycles shown in Figure 5.30 have an R-ratio of zero, a 20% overpeak, and hold times of 0, 4, and 30 seconds. An individual test was performed with constant R and overpeak ratios. At least two and, in most cases, three values of  $K_{hold}$  were evaluated in a given specimen. For each value of  $K_{hold}$ , hold times of 0, 4, 30, and 300 seconds were evaluated.

In the single overpeak tests, the crack growth rate was retarded after the application of each overpeak. Figure 5.31 shows an example of this type of data as observed in a Rene'95 specimen tested at 649°C. A minimum in crack growth rate was observed at half the plastic zone size of the cyclic condition prior to the overpeak,  $(r_p)_{old}$ . The extent of the retardation zone was twice the plastic zone size of the overload cycle,  $(r_p)_{ol}$ . These values are identical to those identified in single overpeak tests of nickel-base superalloys under 3 second frequency (20 cpm) cycling conditions<sup>(49)</sup>. The magnitude and size of the crack growth retardation zone increased with the overpeak K level. It was difficult to assess the impact of combinations of overpeaks and hold times in single overpeak tests.

The results of the R=0, 649°C multiple overpeak tests on Rene'95 are shown in Figure 5.32. These data are shown as a function of  $K_{hold}$ , the K during the hold time. The degree of retardation increases with overpeak ratio and  $K_{hold}$ . In tests with 50% overpeaks, there is no influence of hold time (Figure 5.32c). A similar comment can be made for 20% overpeak tests where the  $K_{hold}$  is in excess of 30 MPa/m. Even at lower  $K_{hold}$  levels, comparison of tests with 10 and 20% overpeaks (Figures 5.32a and 5.32b, respectively) show much less influence of hold time on crack growth rates for 20% overpeaks. This very strong effect of overpeaks on time-dependent crack growth is similar to that reported by Weerasooriya and Nicholas<sup>(50)</sup> for Alloy 718. The remainder of the test conditions were restricted to overpeak ratios of 10 and 20 percent due to the absence of time-dependency for 50% overpeaks.

Figure 5.33 shows the results of the R=0.5 overpeak tests performed on Rene'95 specimens at 649°C. The trends shown with overpeak ratio,  $K_{hold}$ , and hold times are similar to those shown for the lower R-ratio in Figure 5.32.

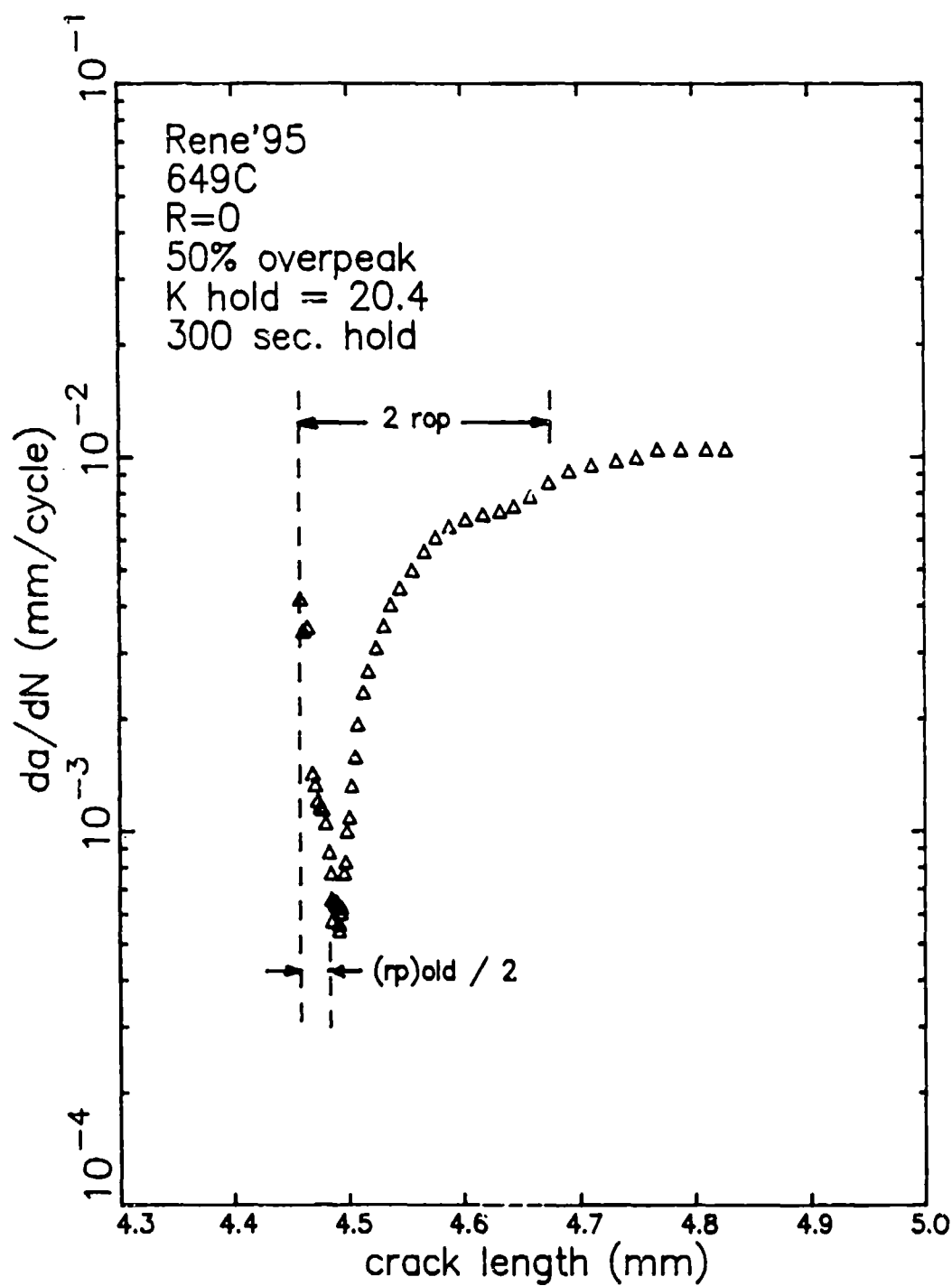
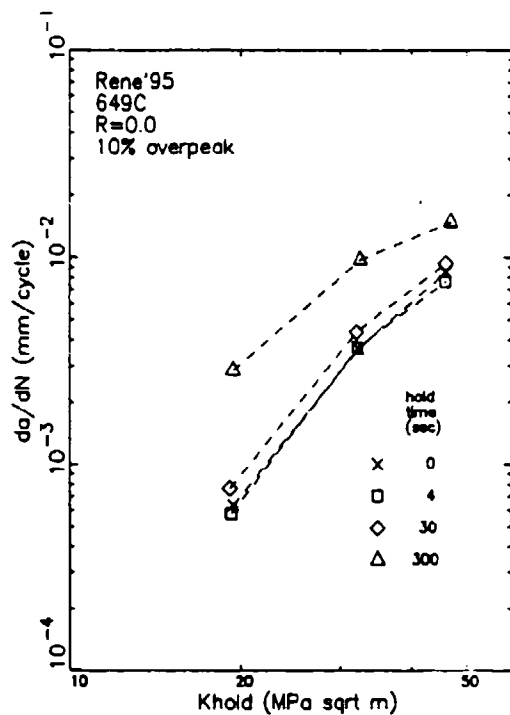
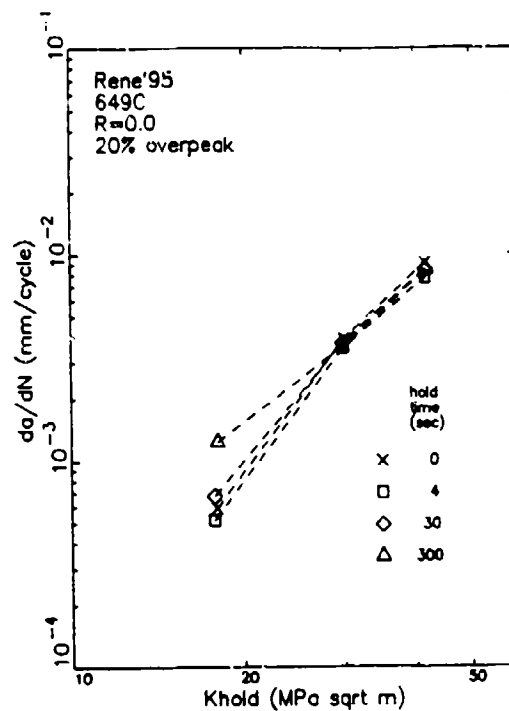


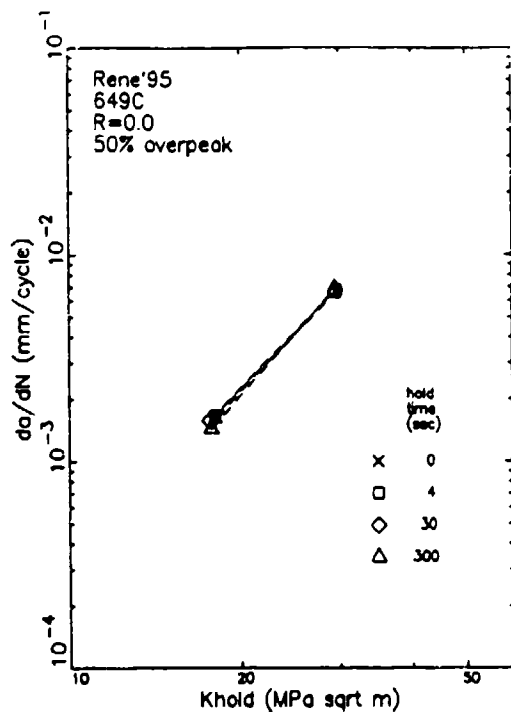
Figure 5.31: Variation of crack growth rate with distance in Rene'95 at 649°C with a 300 second hold time at R=0 preceded by a 50% overpeak.



(a)



(b)



(c)

Figure 5.32:

Results of 649°C multiple overpeak hold time tests on Rene'95 with R=0 for overpeaks of (a) 10%, (b) 20%, and (c) 50%.

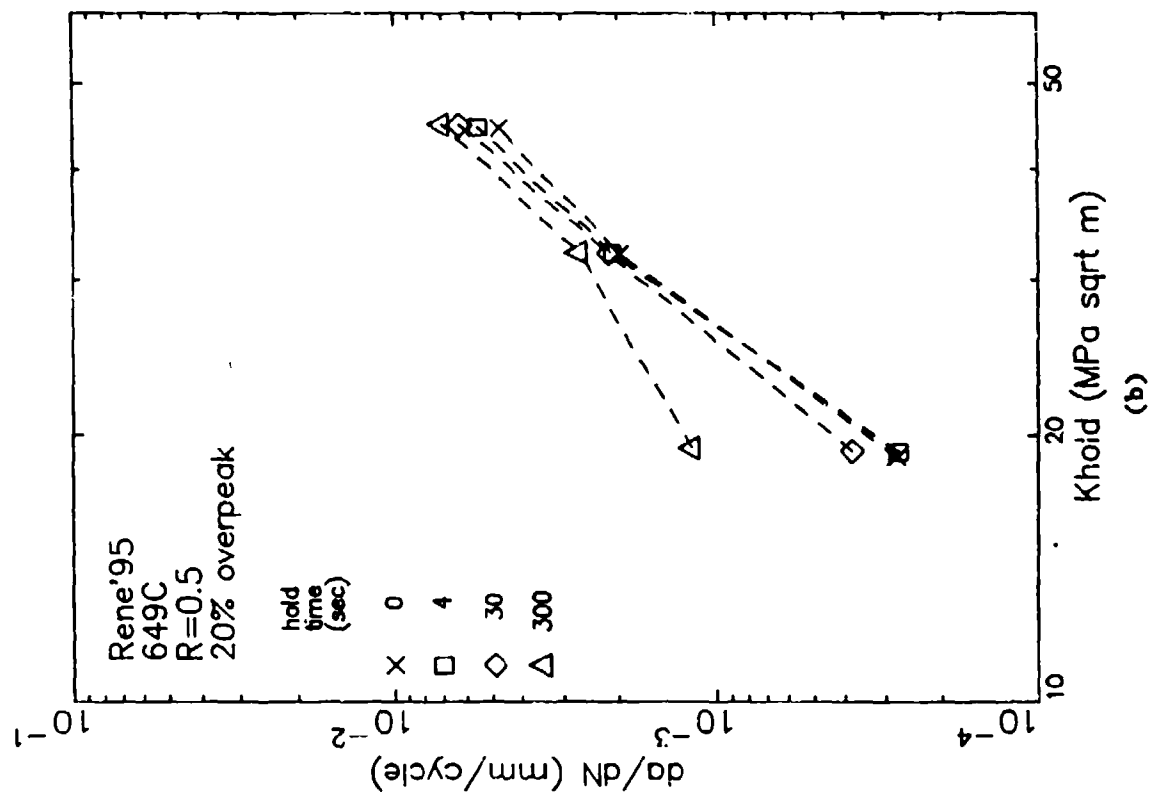
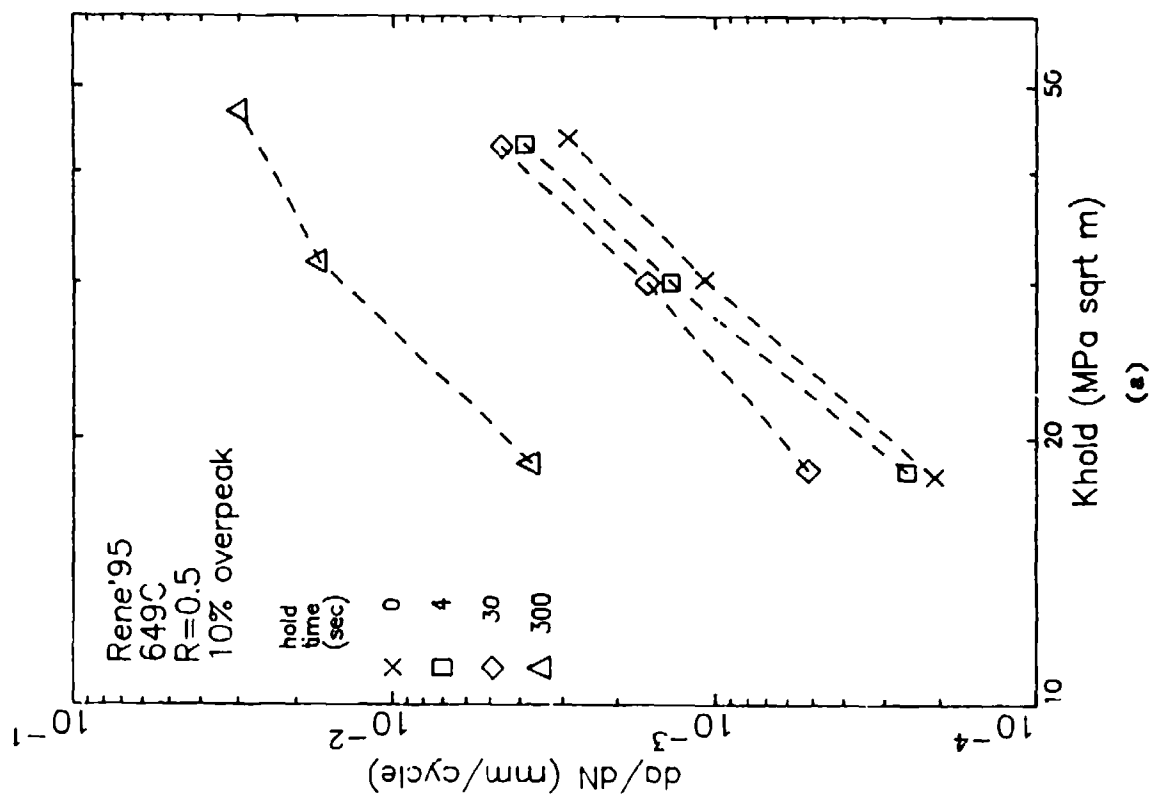


Figure 5.33: Results of 649°C multiple overpeak hold time tests on Rene'95 with R=0.5 for overpeaks of (a) 10% and (b) 20%.

The results for the 593°C multiple overpeak tests with R=0 and R=0.5 are shown in Figures 5.34 and 5.35, respectively. The trends in these tests were the same as observed in the 649°C tests. Significant benefits of retardation also occur at 593°C in Rene'95.

The results presented in Figures 5.31 through 5.35 show that a 20% overpeak is far more potent in retarding time-dependent crack growth than a 10% overpeaks. There is no indication of the amount of retardation which may occur with 10% overpeaks because the 15 second ramp time used in the overpeak tests was not experimentally evaluated during the non-overpeak testing program. To gain more insight into the effect of overpeak retardation on crack growth during hold times, the overpeak crack growth rate data were plotted against the hold time duration using linear axes. This procedure was used in Figures 5.5, 5.8, and 5.9 for the non-overpeak constant  $\Delta K$  hold time tests, where the crack growth rate varied in an almost linear fashion with hold time and the slope of the linear relationship increased with  $K_{max}$ . The results of the 649°C, R=0 overpeak test data are replotted on these linear axes in Figure 5.36. This representation reinforces the observation that increasing overpeak ratio suppresses time-dependent crack growth. The results for the 10% overpeak ratio test (Figure 5.36a) show the linear behavior for all three values of  $K_{hold}$ . The slopes of the linear behavior for the two higher value of  $K_{hold}$  (32 and 46 MPa/m) appear to be nearly identical. This illustrates that even though there is time dependency for these conditions, increasing values of  $K_{hold}$  result in less time-dependent crack growth even for overpeak ratios of 10%. A similar trend is observed for the R=0.5 overpeak tests performed at 649°C as illustrated in Figure 5.37.

The results from the 593°C multiple overpeak tests with R-ratios of 0.0 and 0.5 are shown in Figures 5.38 and 5.39, respectively using linear crack growth and hold time axes. As was observed for the higher test temperature, there is evidence that a 10% overpeak at 593°C decreases the amount of time dependent crack growth observed in Rene'95.

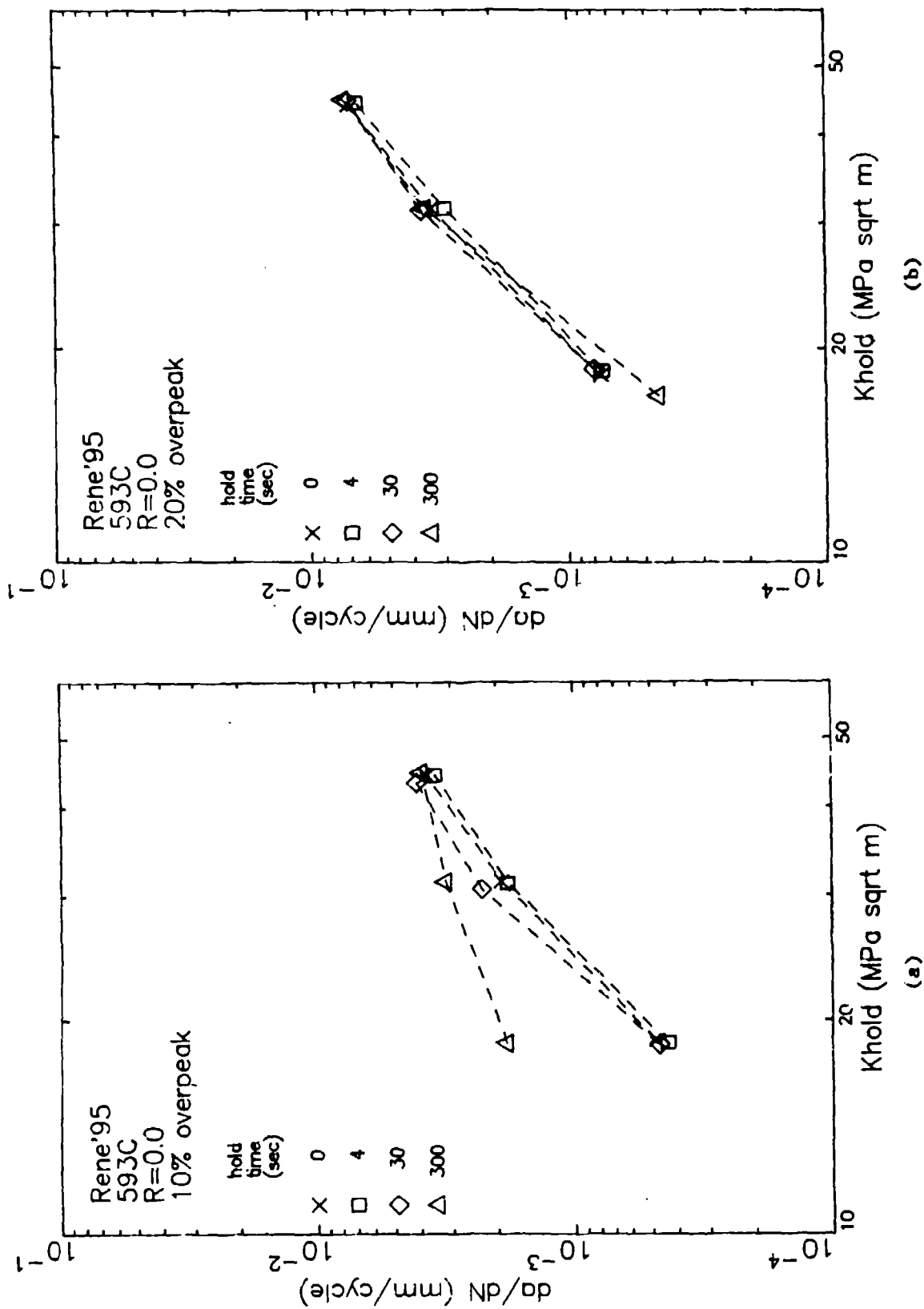


Figure 5.34: Results of 593°C multiple overpeak hold time tests on Rene'95 with R=0 for overpeaks of (a) 10% and (b) 20%.

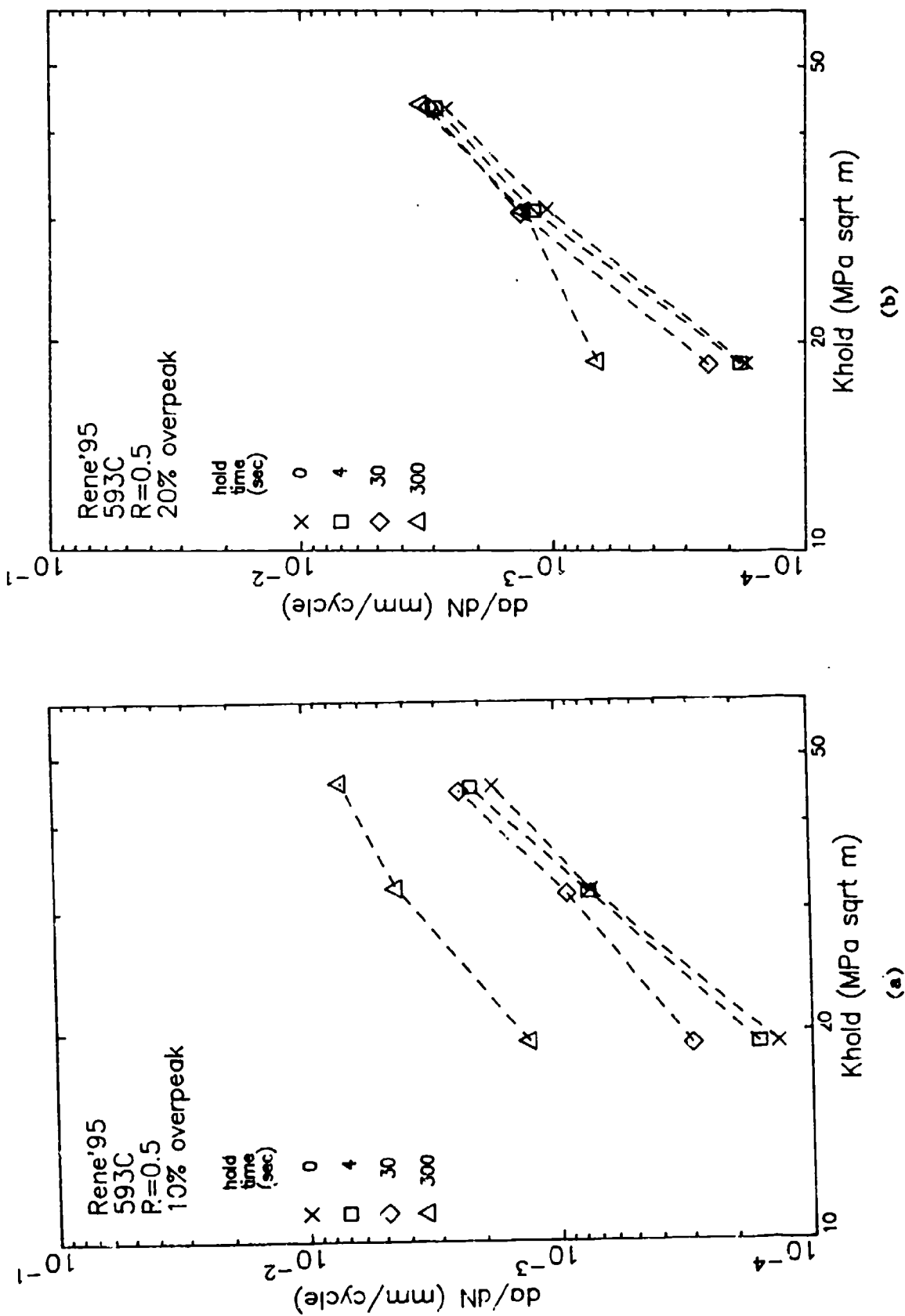
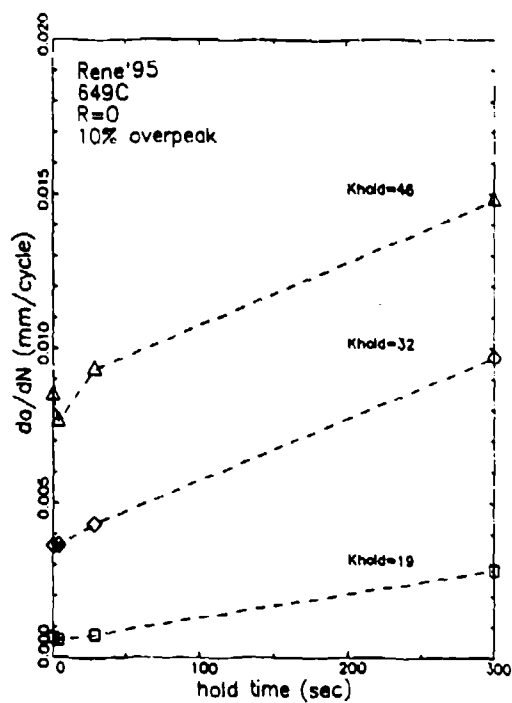
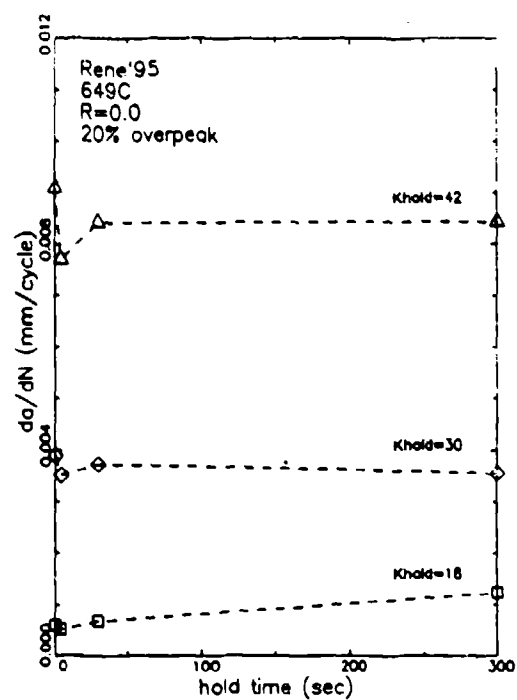


Figure 5.35: Results of 593°C multiple overpeak hold time tests on Rene'95 with R=0.5 for overpeaks of (a) 10% and (b) 20%.

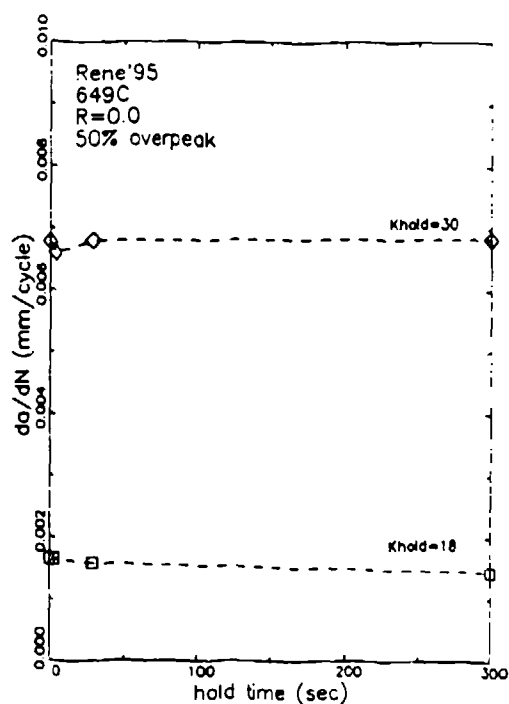




(a)



(b)



(c)

Figure 5.36:

Variation of crack growth rate with hold time measured in 649°C multiple overpeak hold time tests on Rene'95 with R=0 for overpeaks of (a) 10%, (b) 20%, and (c) 50%.

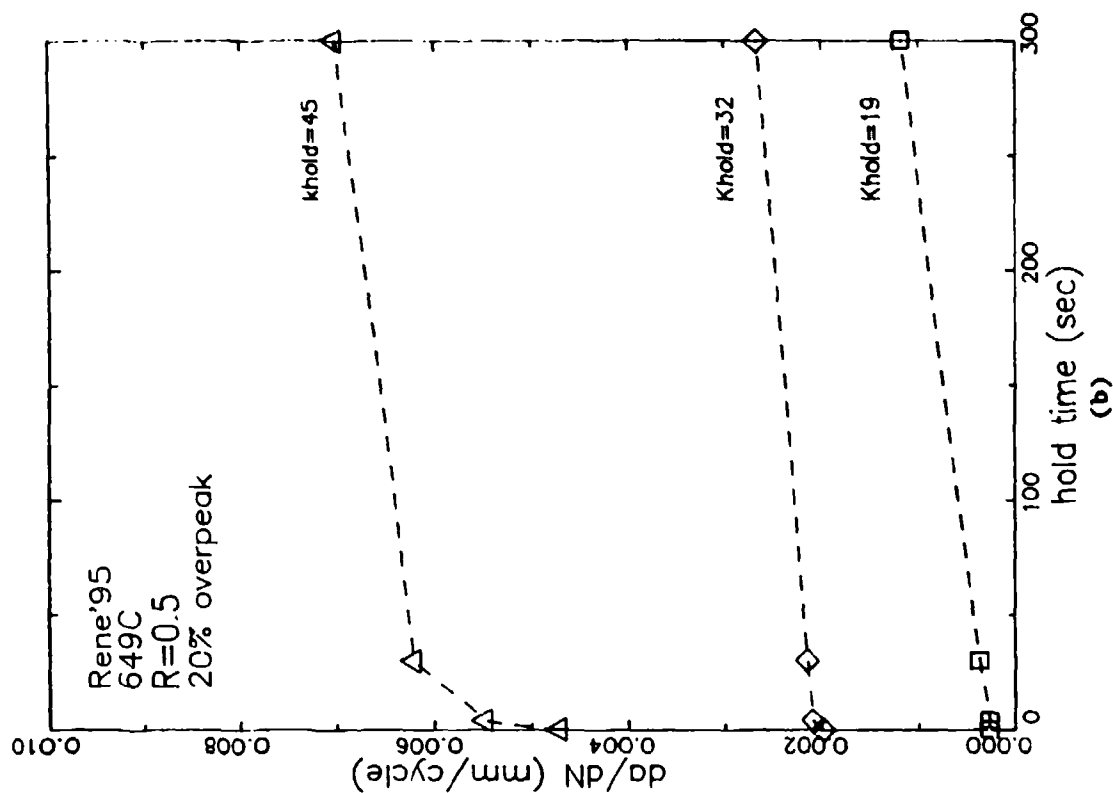
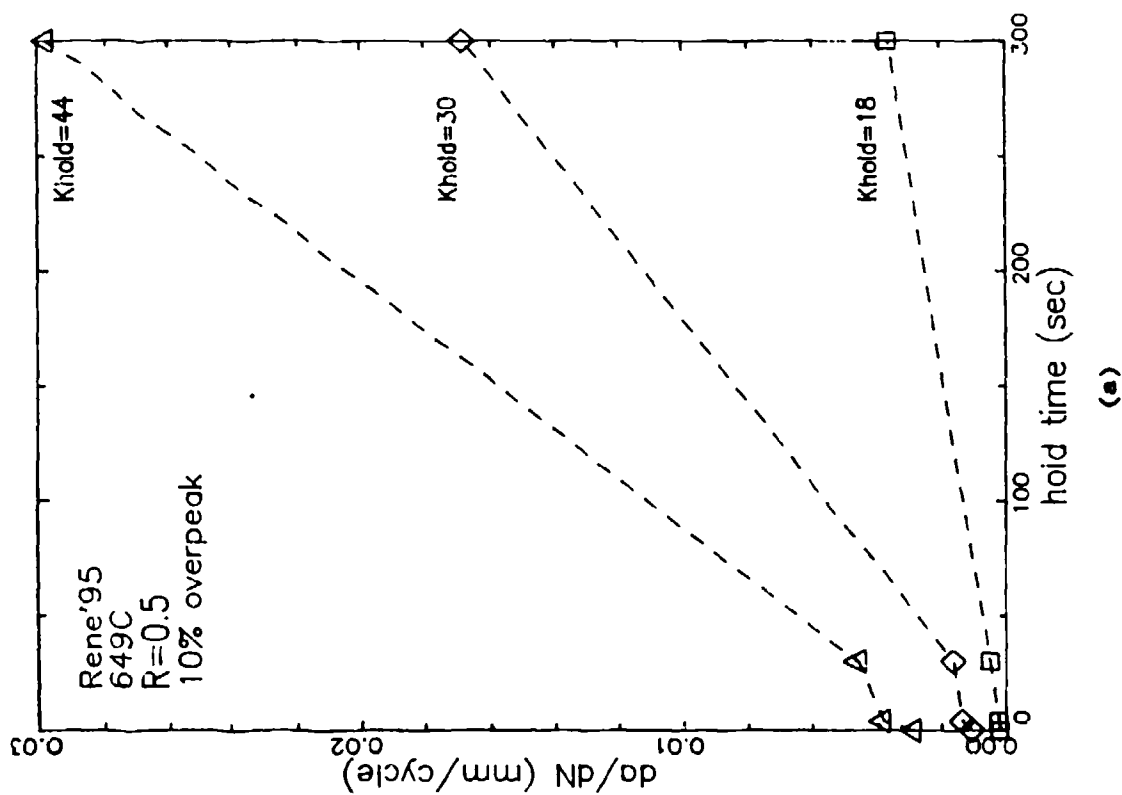


Figure 5.37: Variation of crack growth rate with hold time measured in 649°C multiple overpeak hold time tests on Rene'95 with  $R=0.5$  for overpeaks of (a) 10% and (b) 20%.

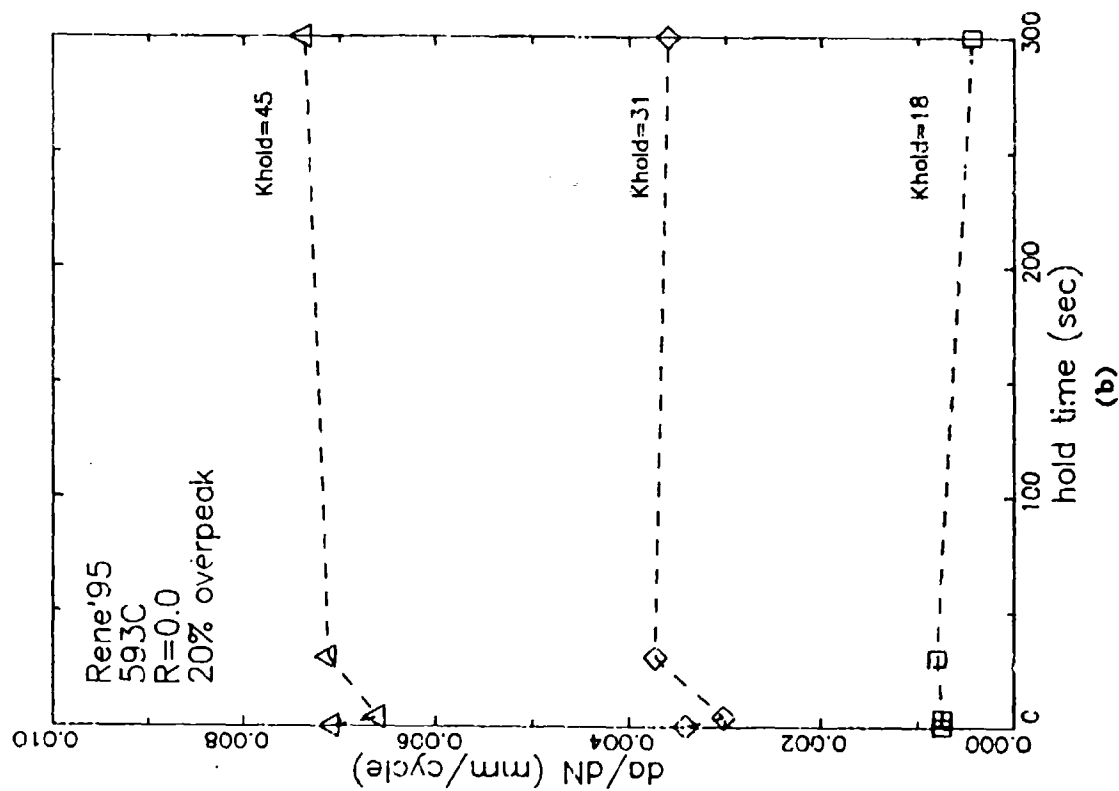
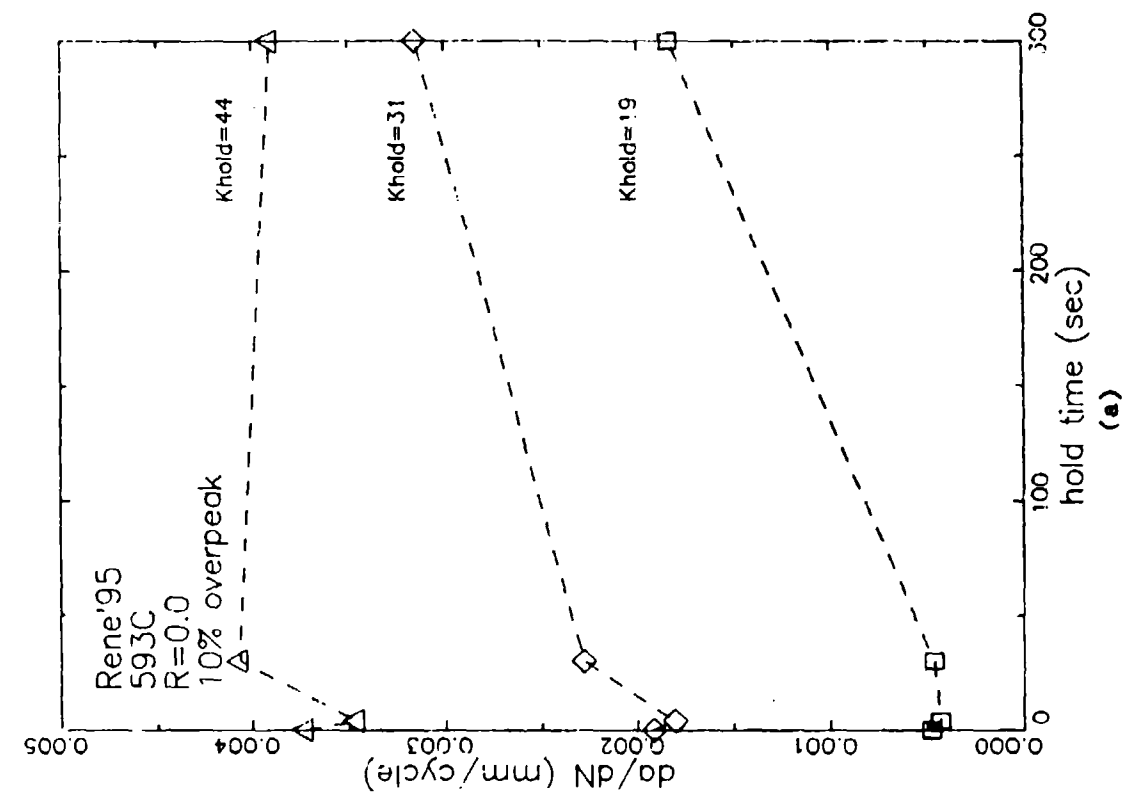


Figure 5.38: Variation of crack growth rate with hold time measured in 593°C multiple overpeak hold time tests on Rene'95 with  $R=0$  for overpeaks of (a) 10% and (b) 20%.

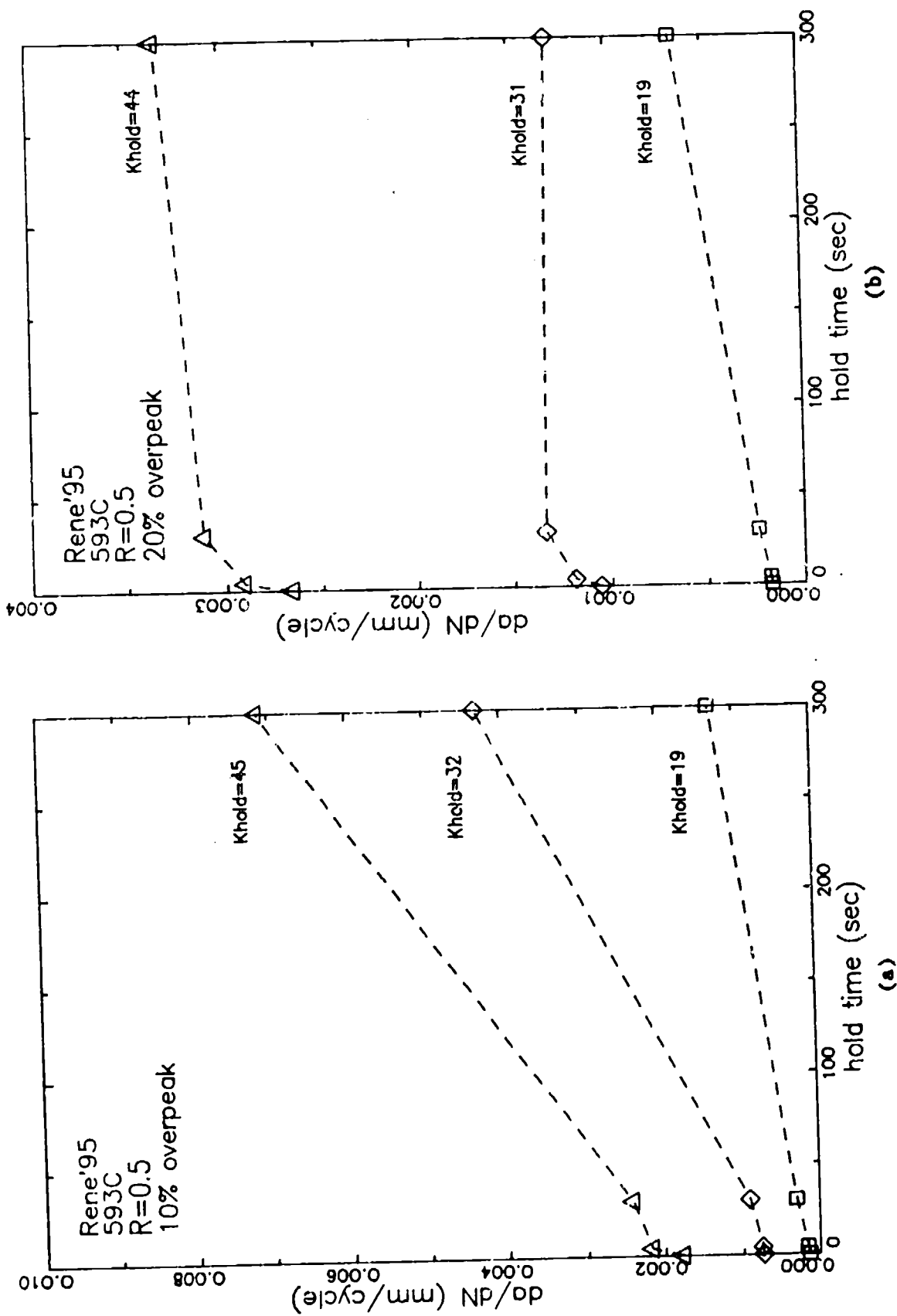


Figure 5.39: Variation of crack growth rate with hold time measured in 593°C multiple overpeak hold time tests on Rene'95 with R=0.5 for overpeaks of (a) 10% and (b) 20%.

## 5.2 ALLOY 718 CRACK GROWTH RESULTS

The test matrix for Alloy 718 was approximately half as extensive as that of Rene'95. Crack growth rates in Alloy 718 were measured at 593 and 649°C, but only the influence of hold time was evaluated. The Alloy 718 baseline test matrix is listed in Table 5.4. The Alloy 718 results will be presented in separate sections on constant  $\Delta K$ , threshold, static, and retardation tests. These data are shown using the same variables used for presenting the Rene'95 data. The rationale for presenting the data in this fashion was described in the previous section and will not be repeated here.

### 5.2.1 Alloy 718 Constant $\Delta K$ Test Results

The Alloy 718 constant  $\Delta K$  tests were performed as a function of hold time. Due to the absence of constant  $\Delta K$  frequency tests, crack growth during a zero second hold time segment was also evaluated in these tests. This resulted in a total of 12 constant  $\Delta K$  segments for each test specimen (3 levels of  $K_{max}$  x 4 hold times). Figure 5.40 shows the variation of crack length with cycles for the Alloy 718 specimen tested at 649°C with a R-ratio of 0.0. At first glance, these results seem to be very similar to those reported for Rene'95; however, in the 0 second hold time segments which follow 300 second hold time cycling at a lower  $K_{max}$ , there is transient crack growth behavior. These results are shown more clearly in Figure 5.41. In both cases, the growth during the zero second hold time cycle was initially very high and then decreased to a steady state condition. This was observed in the Alloy 718 constant  $\Delta K$  tests independent of temperature and R-ratio and precluded the accurate determination of crack growth rates during the 0 second hold time segments. Consequently, those results will not be reported. These types of transient behavior have been observed in IN100 by Larsen and Nicholas<sup>(20)</sup>. The transient behavior was studied in more detail during the mechanism experiments and are reported in Section 6.

The Alloy 718 constant  $\Delta K$  test results were analyzed statistically using the techniques described for the Rene'95 tests. The results of the statistical analyses are reported in Appendix C. In all subsequent figures,

Table 5.4: Alloy 718 Simple Cycle Test Matrix

<u>Test Number</u>	<u>Temperature (°C)</u>	<u>R</u>	<u>Test Type</u>	<u>Variable</u>
A13-17	593	0.0	constant $\Delta K$	hold time
A13-09	593	0.0	threshold	3 sec. cycle
A13-07	593	0.5	constant $\Delta K$	hold time
A13-11	593	0.8	constant $\Delta K$	hold time
A13-10	593	static	threshold	
A13-24	649	0.0	constant $\Delta K$	hold time
A13-28	649	0.0	threshold	300 sec. hold
A13-06	649	0.0	threshold	3 sec. cycle
A13-37	649	0.5	constant $\Delta K$	hold time
A13-20	649	0.5	threshold	3 sec. cycle
A13-12	649	0.8	constant $\Delta K$	hold time
A13-14	649	0.8	threshold	4 sec. hold
A13-32	649	0.8	threshold	30 sec. hold
A13-05	649	0.8	threshold	300 sec. hold
A13-02	649	0.8	threshold	3 sec. cycle
A13-19	649	static	threshold	
A13-35	649	static	constant load	

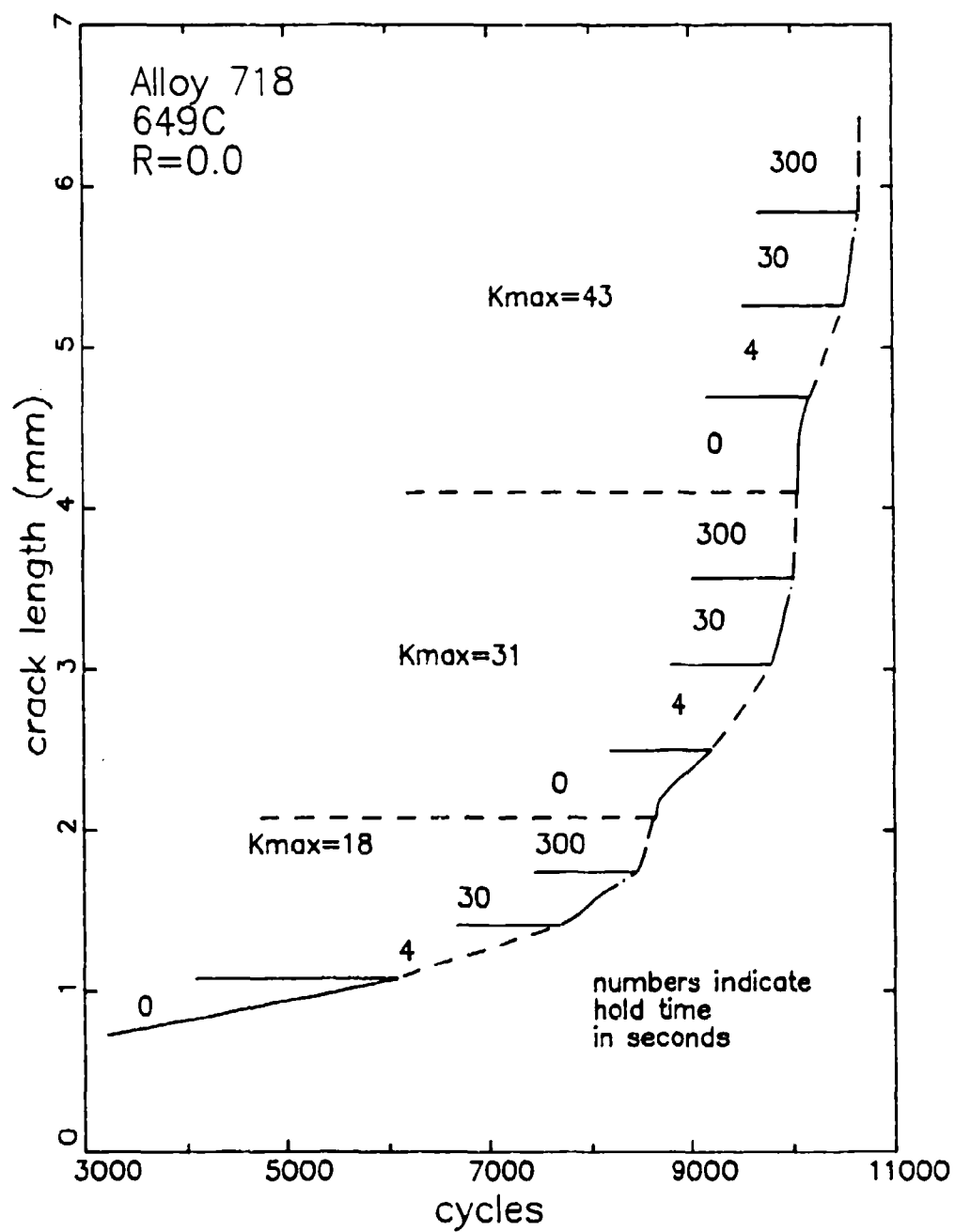


Figure 5.40: Variation of crack length with cycles during constant  $\Delta K$  hold time test on Alloy 718 at 649°C with R=0.

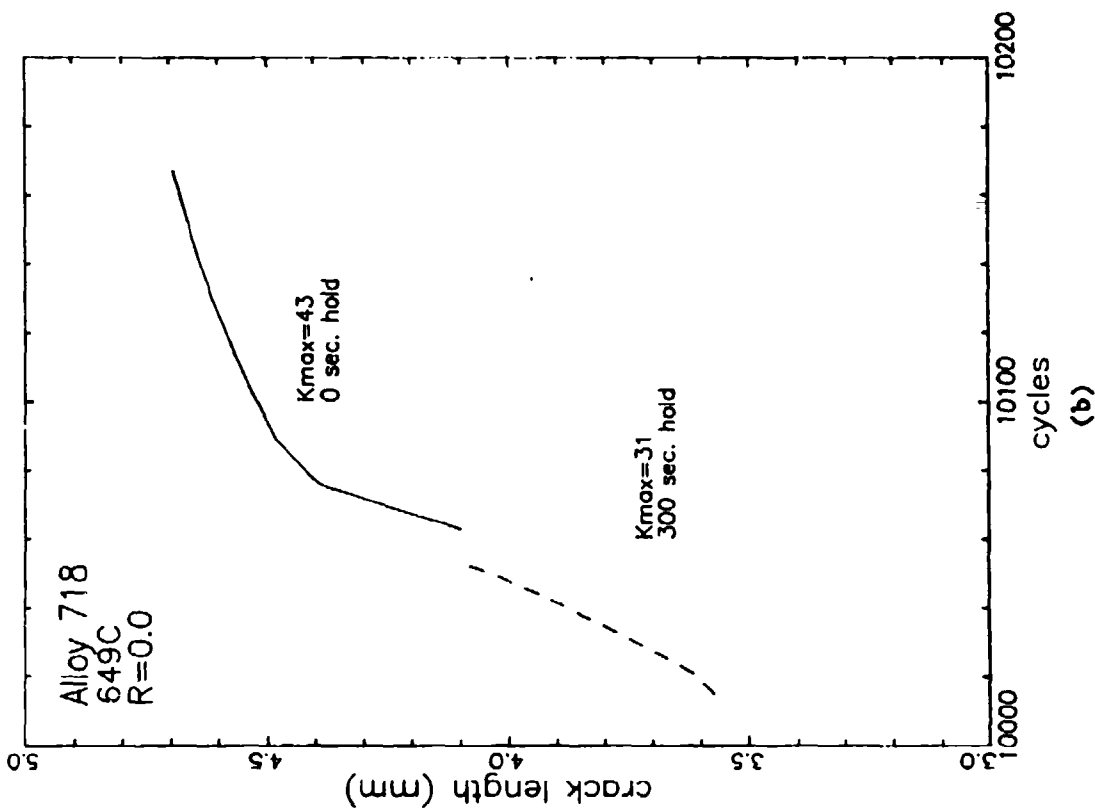
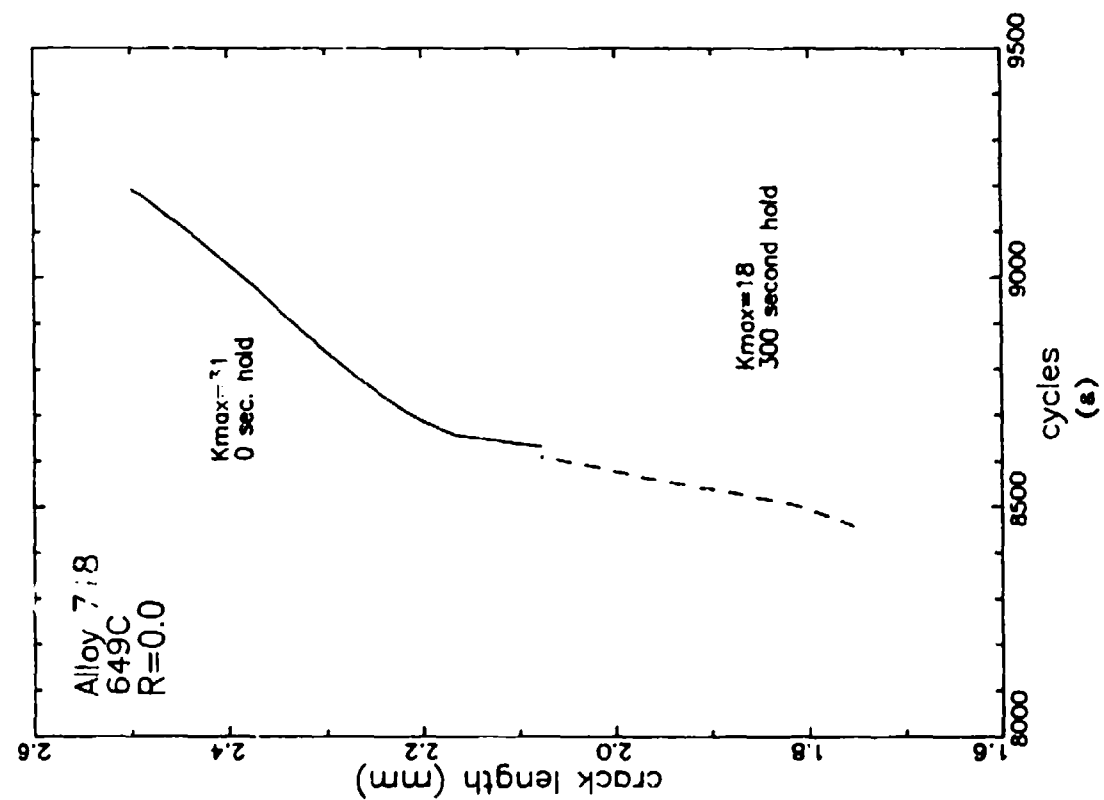


Figure 5.41: Variation of crack length with cycles during transitions from 300 second hold time to 0 second hold time during constant  $\Delta K$  hold time test on Alloy 718 at 649°C with  $R=0$  for 300 second hold time  $K_{max}$  values of (a) 18 MPa/m and (b) 31 MPa/m.



the large symbols correspond to the average values of  $K_{max}$  and crack growth rate from the constant  $\Delta K$  tests.

The results of the Alloy 718 593°C constant  $\Delta K$  tests are given in Figure 5.42. Increasing hold times accelerates the crack growth rates. There is a larger difference in crack growth rates between 4 and 30 second hold times with increasing R-ratio.

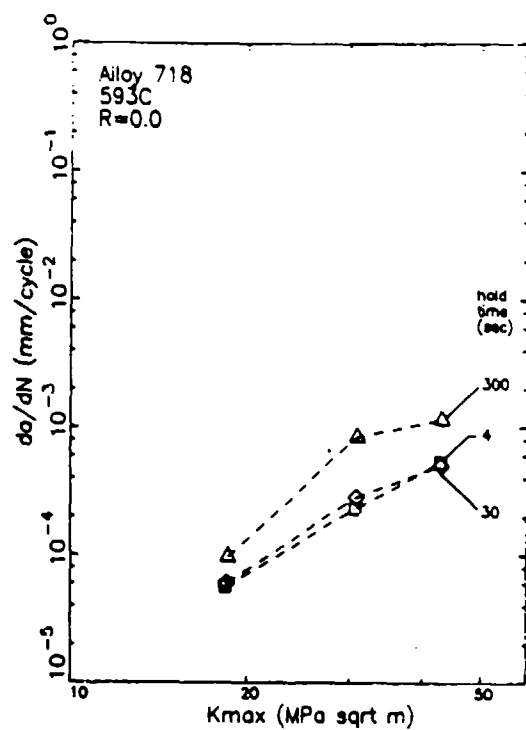
The results of the constant  $\Delta K$  tests performed at 649°C are shown in Figure 5.43. This shows the types of trends observed in the 593°C results except that there is a smaller influence of R-ratio for the 4 second hold time data. No data is shown for the 4 second hold time at the highest  $K_{max}$  level because the transient zone was so large that it also influenced this segment of crack growth rate.

The crack growth rates from the 593 and 649°C Alloy 718 constant  $\Delta K$  tests are replotted on linear axes as a function of hold time in Figures 5.44 and 5.45, respectively. The results for both temperatures show that the crack growth rates are proportional to hold time. This effect is qualitatively predicted from the superposition model.

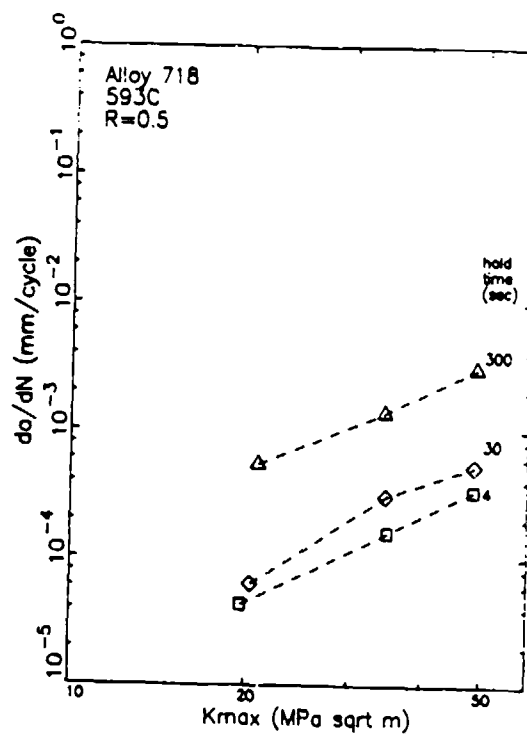
#### 5.2.2 Alloy 718. Threshold Test Results

The threshold tests performed on Alloy 718 are listed in Table 5.4. A few tests were performed at 593°C, but the majority of the threshold tests were conducted at 649°C. The influence of R-ratio on the 649°C Alloy 718 0 second hold time (3 second cycle) hold time tests are shown as a function of  $\Delta K$  and  $K_{max}$  in Figures 5.46a and 5.46b, respectively. At a constant value of  $\Delta K$ , crack growth rate increases with R-ratio while the opposite trend is observed for constant values of  $K_{max}$ . The data for the different R-ratios are roughly parallel which suggests that they could be modeled using the Walker model. These trends are very similar to those observed in Rene'95.

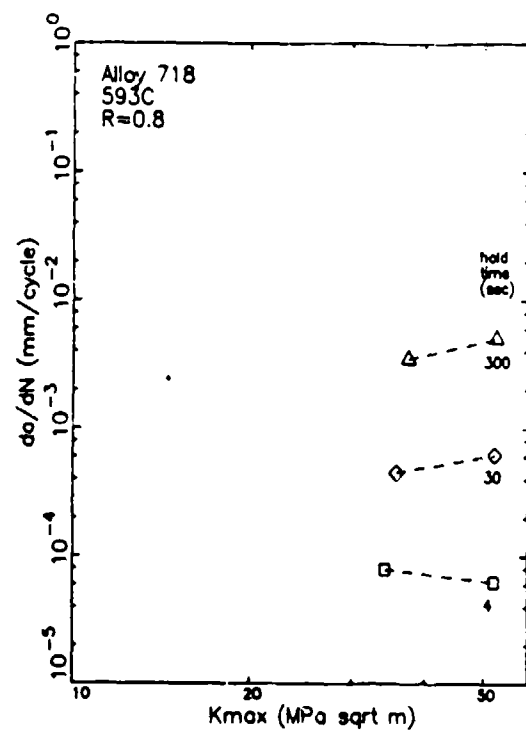
Figure 5.47 compares the results of the R=0, 0 second hold time tests performed at 593 and 649°C. There appears to be a relatively small influence



(a)



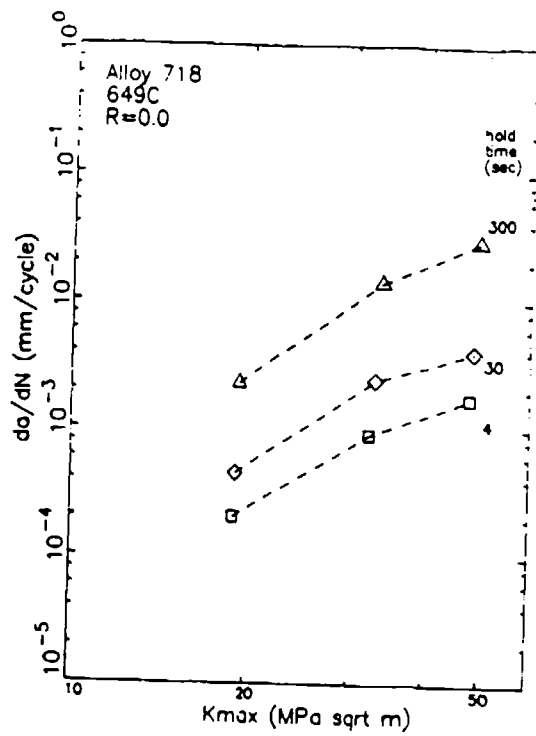
(b)



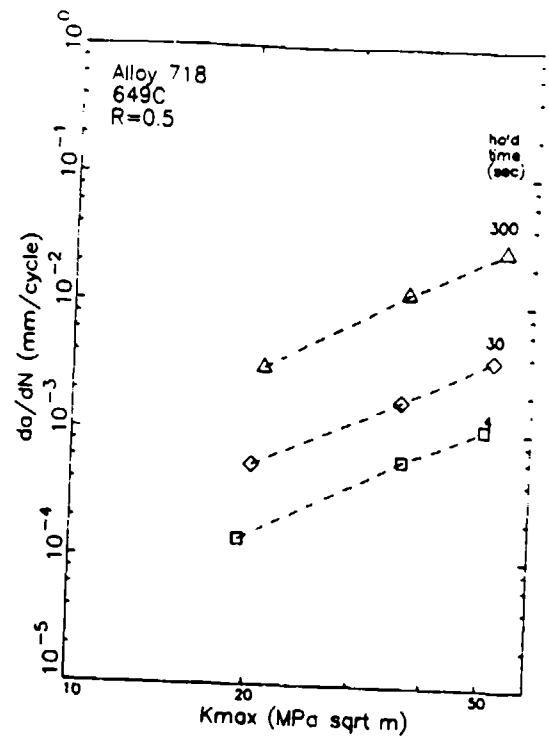
(c)

Figure 5.42:

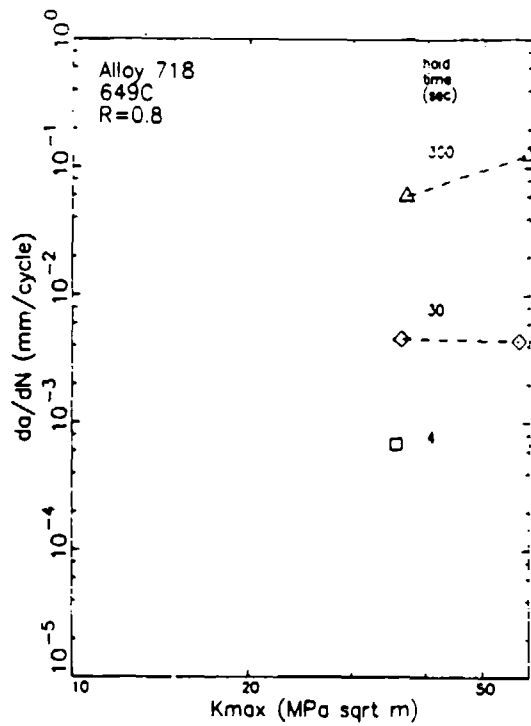
Results of the Constant  $\Delta K$  hold time tests on Alloy 718 at 593°C with (a) R=0.0, (b) R=0.5, and (c) R=0.8.



(a)



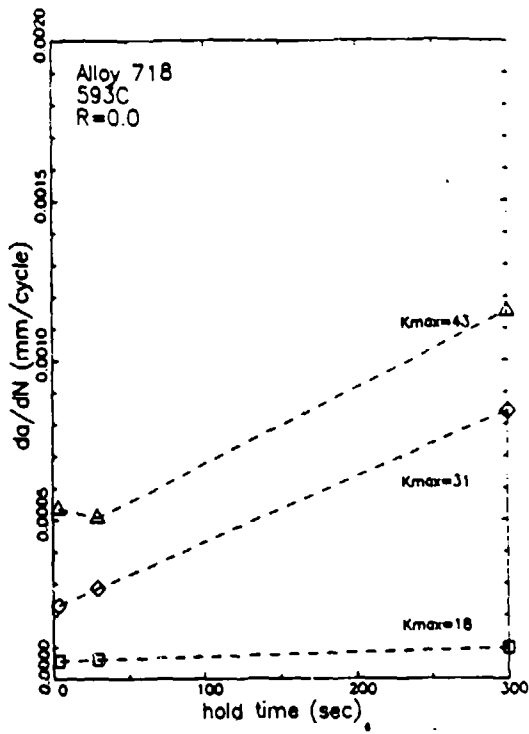
(b)



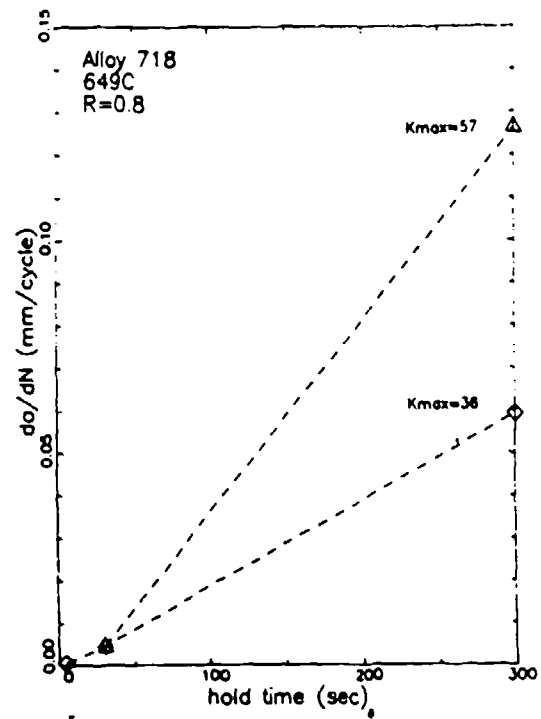
(c)

Figure 5.43:

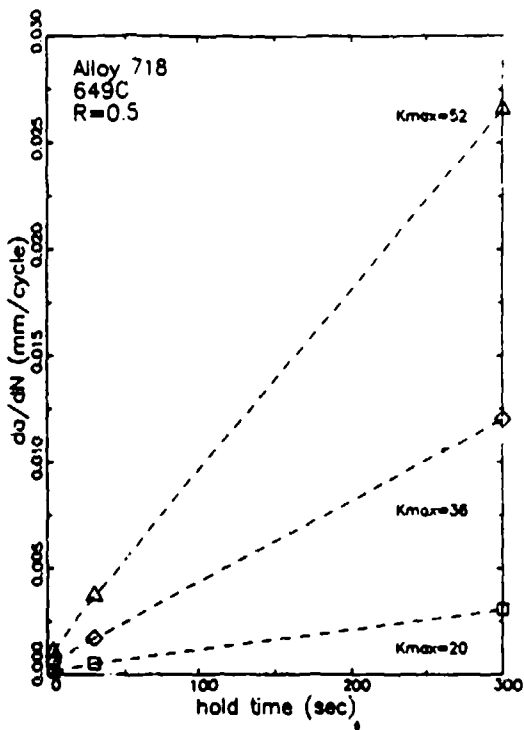
Results of the Constant  $\Delta K$  hold time tests on Alloy 718 at 649°C with (a) R=0.0, (b) R=0.5, and (c) R=0.8.



(a)



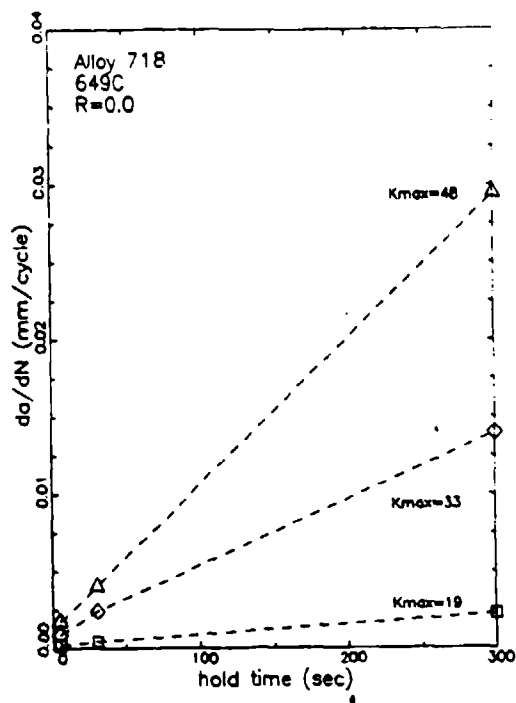
(b)



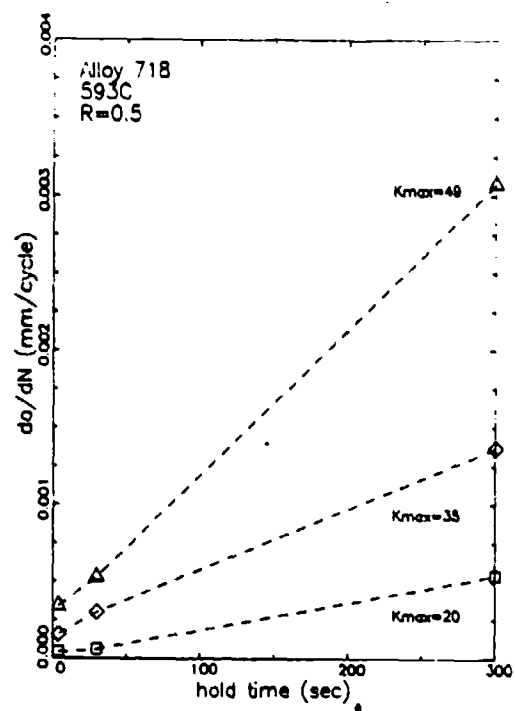
(c)

Figure 5.44:

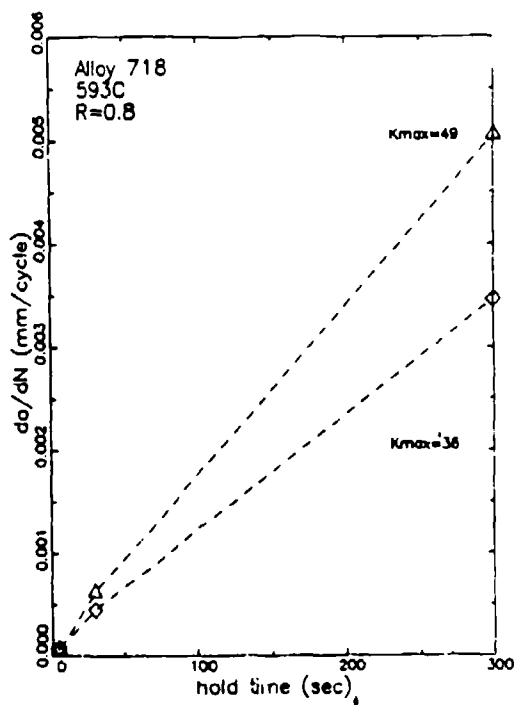
Variation of crack growth rate with hold time measured in Alloy 718 constant  $\Delta K$  tests at 593°C with (a)  $R=0.0$ , (b)  $R=0.5$ , and (c)  $R=0.8$ .



(a)



(b)



(c)

Figure 5.45:

Variation of crack growth rate with hold time measured in constant Alloy 718  $\Delta K$  tests at 649°C with (a) R=0, (b) R=0.5, and (c) R=0.8.

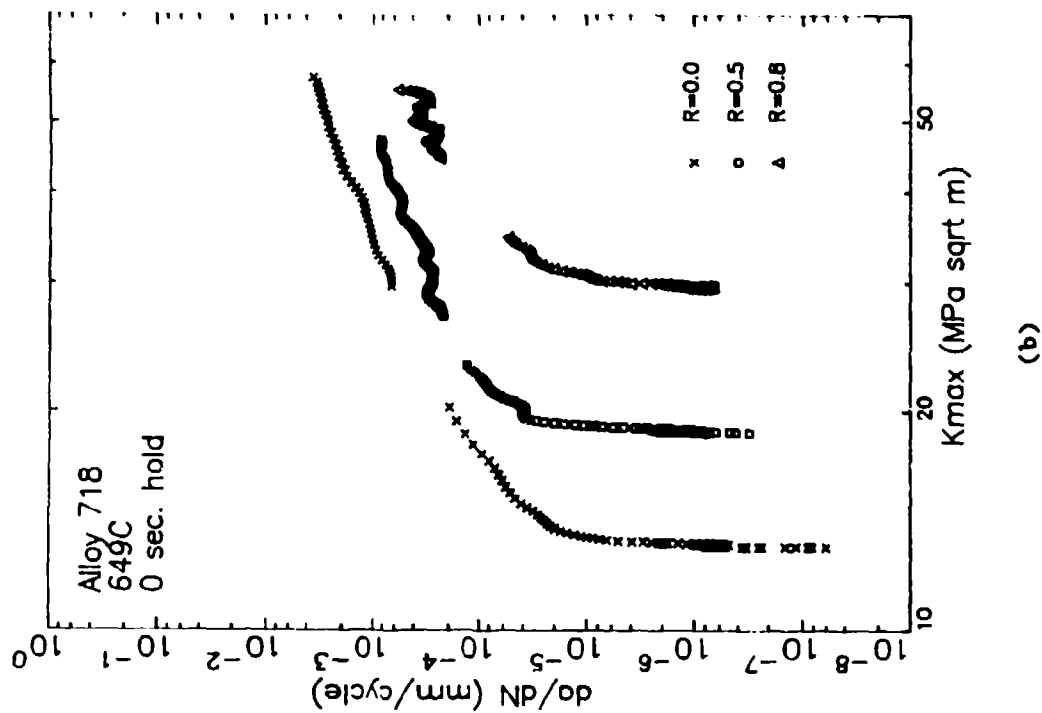
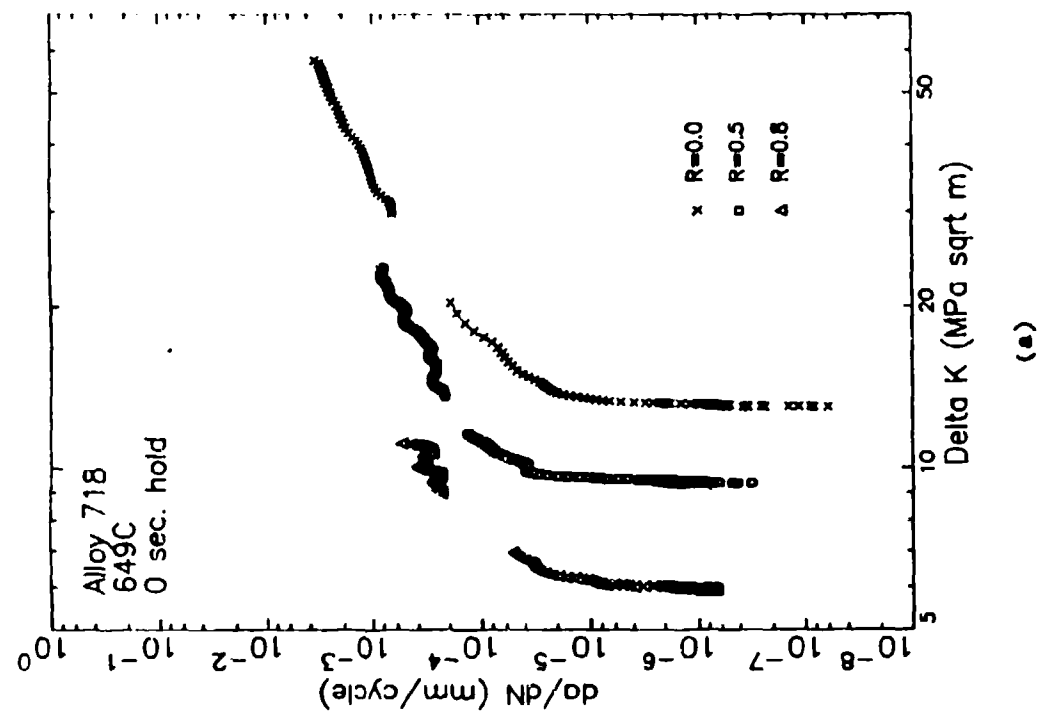


Figure 5.46: Results of 649°C Alloy 718 threshold tests with 3 second cycle period and different R-ratios as a function of (a)  $\Delta K$  and (b)  $K_{max}$ .

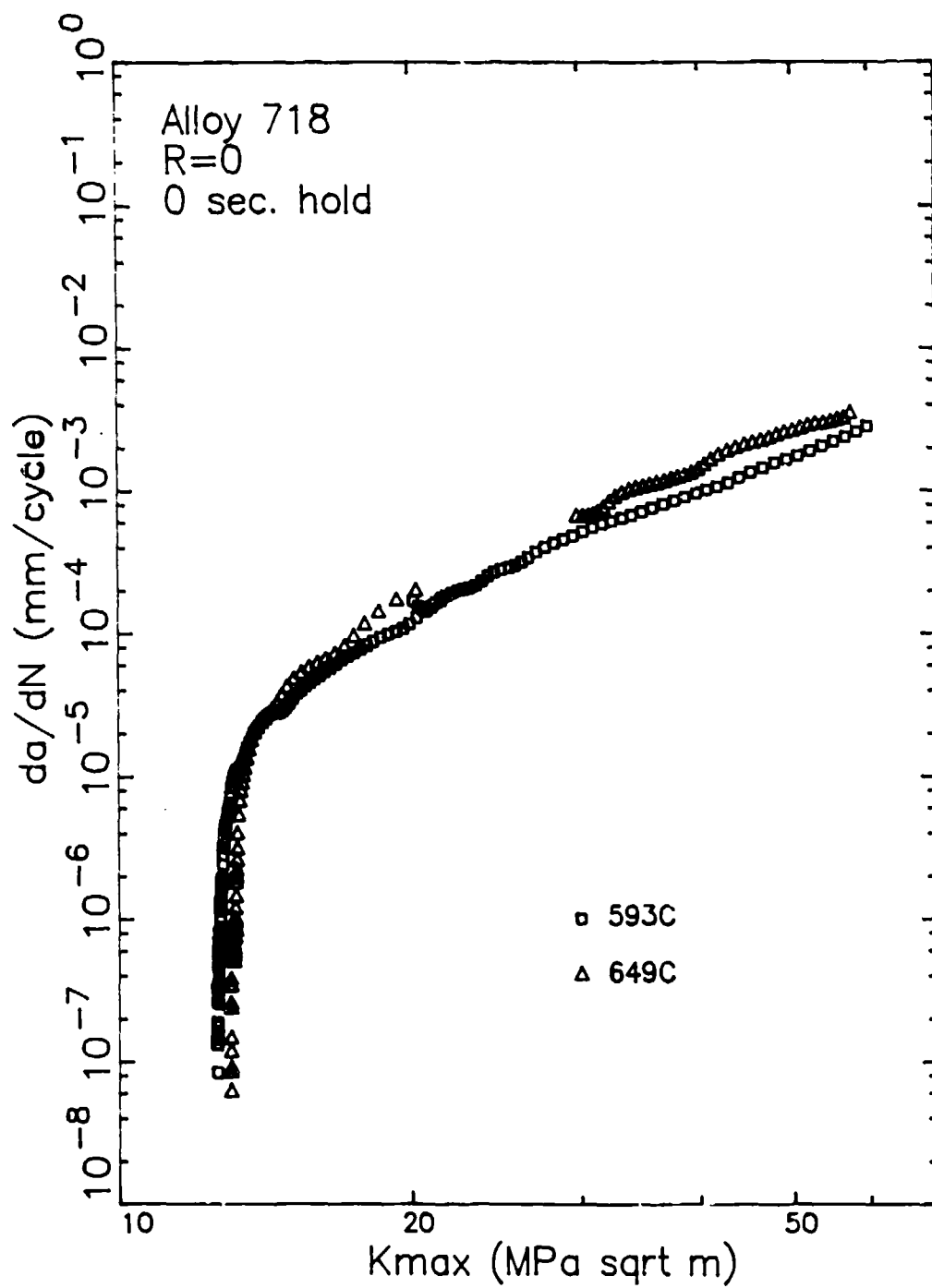


Figure 5.47: Comparison of 593 and 649°C Alloy 718 threshold tests with 3 second cycle period for R=0.0.

of temperature for this cycling condition.

The crack growth rates measured during R=0 threshold tests with hold times of 0 and 300 seconds are shown in Figure 5.48. These were the only threshold tests performed for the 649°C, R=0 cycling conditions. These data show the increase in threshold with increasing hold time, similar to that observed in Rene'95. The influence of R-ratio and hold times on the threshold values measured in Alloy 718 at 649°C are shown in Figure 5.49. As was the case for Rene'95, these data are presented as  $(K_{th})_{max}$  values. The asterisk on the right side of this figure shows the value of the static crack growth threshold. The only R=0.5 test was performed for a 0 second hold time. The R=0.8 data shows the same general behavior as observed for Rene'95 at this R-ratio where the threshold decreases rapidly with increasing hold time and then either saturates or increases slightly to a value much higher than the static crack growth threshold.

The remainder of this section will compare the results from the threshold and constant  $\Delta K$  tests. No comparisons are shown for 0 second hold time tests because no accurate data were obtained from the constant  $\Delta K$  tests. Figure 5.50 shows the results from the 649°C, R=0, 300 second hold time test. The crack growth rates measured in the constant  $\Delta K$  test are significantly lower than those measured during the increasing  $\Delta K$  portion of the threshold test.

The results from the R=0.8 threshold and constant  $\Delta K$  tests are shown in Figure 5.51. No Region II crack growth rates were measured under increasing  $\Delta K$ -control condition for any of these hold times. After the crack arrested and the increasing  $\Delta K$  portion of the test was started, there was a very rapid acceleration in crack growth rate making it almost impossible to measure the Region II crack growth rates. This behavior is very similar to that shown in Figure 5.41 for the transient behavior. This was observed to a lesser extent in the 649°C Rene'95 threshold tests. This type of behavior has also been observed after 20 cpm threshold tests of Alloy 718 at 427°C (800°F)<sup>(69)</sup>. The differences between the Region II data measured during the  $\Delta K$ -shed and constant  $\Delta K$  tests vary significantly. This may result from retardation during the  $\Delta K$ -shed because the static retardation behavior increases with  $K_{max}$  level.



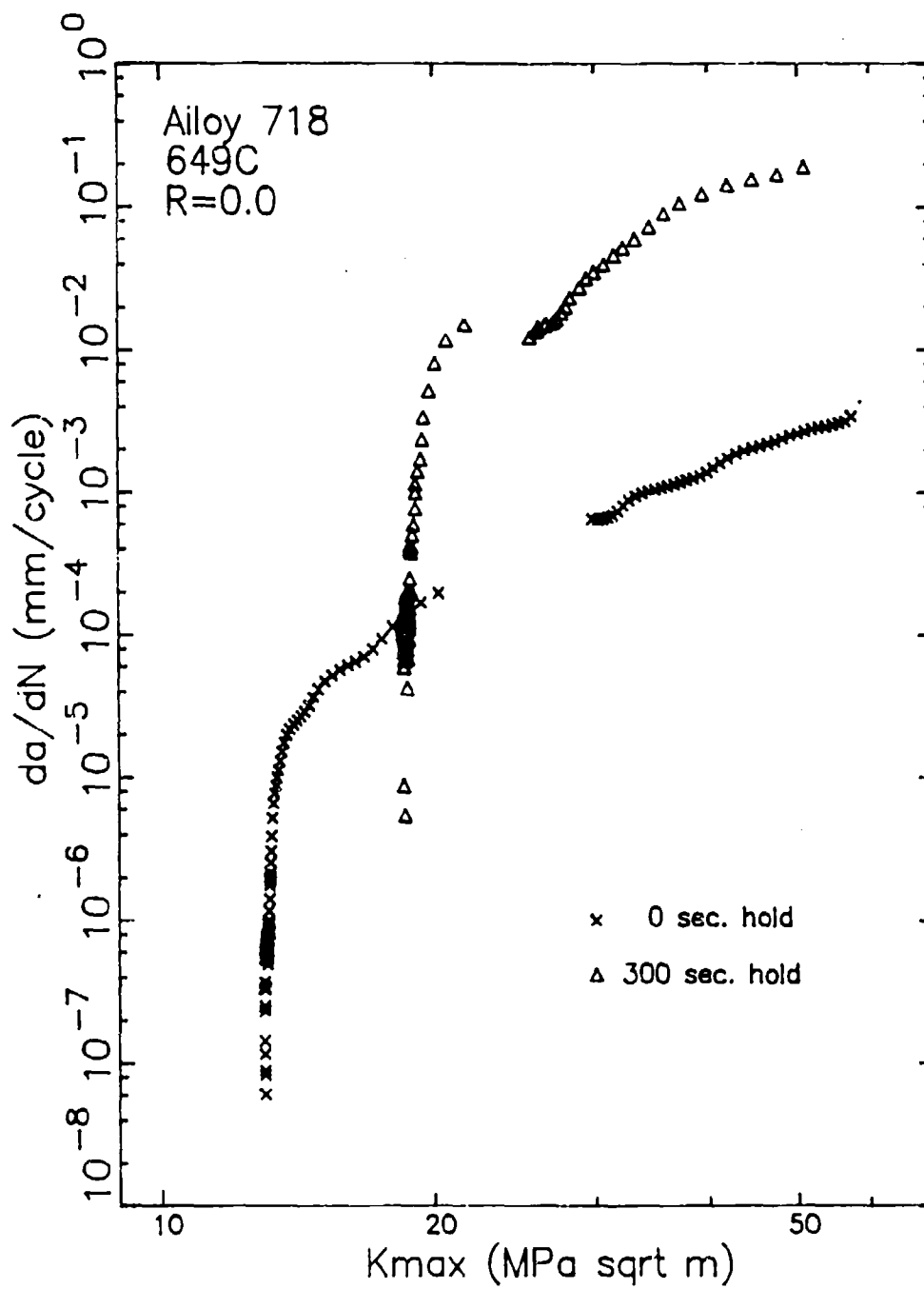


Figure 5.48: Results of Alloy 718 threshold tests with R=0 and different hold times at 649°C.

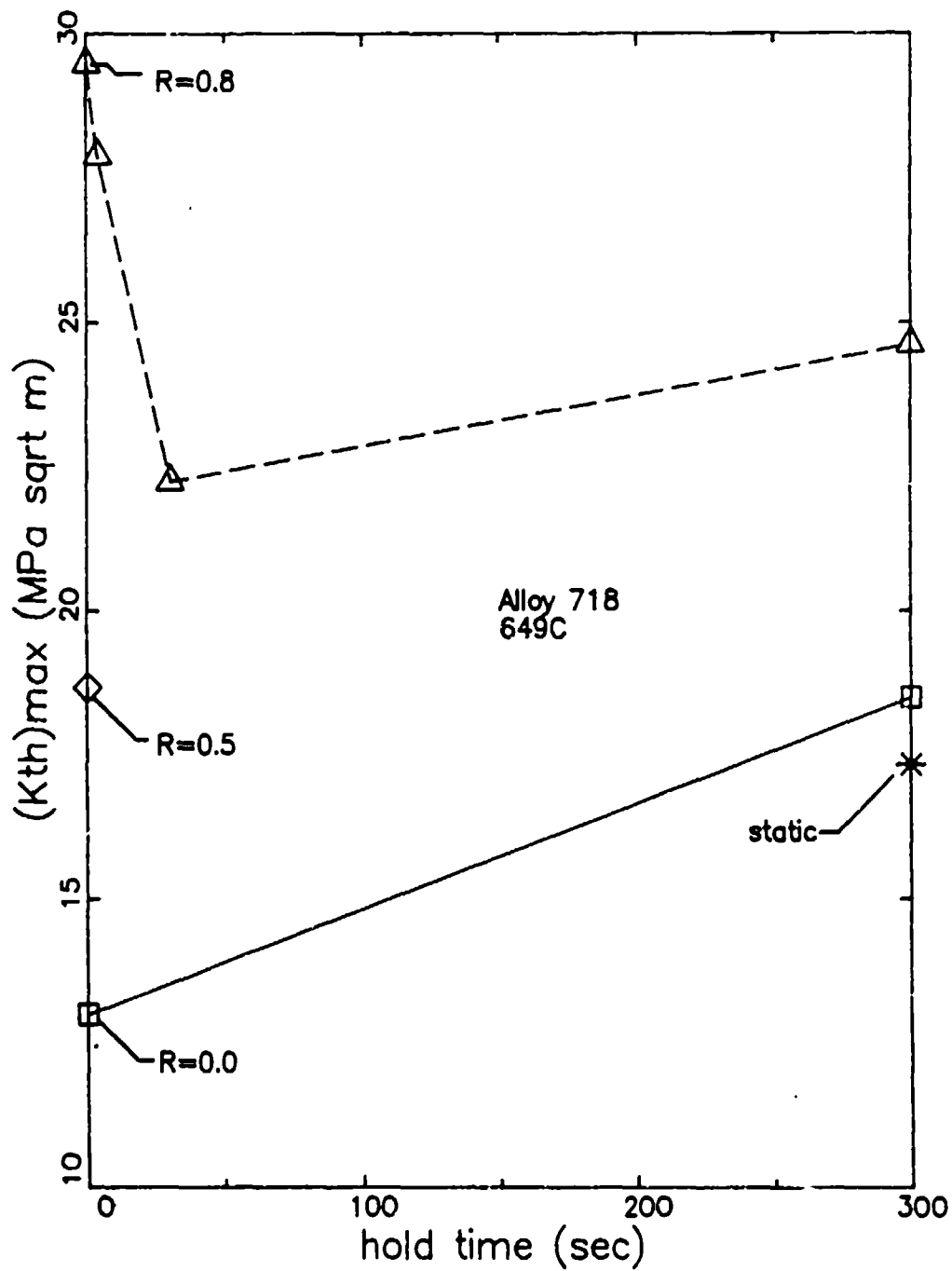


Figure 5.49: Variation of  $(K_{th})_{max}$  in Alloy 718 at 649°C with R-ratio and hold time.

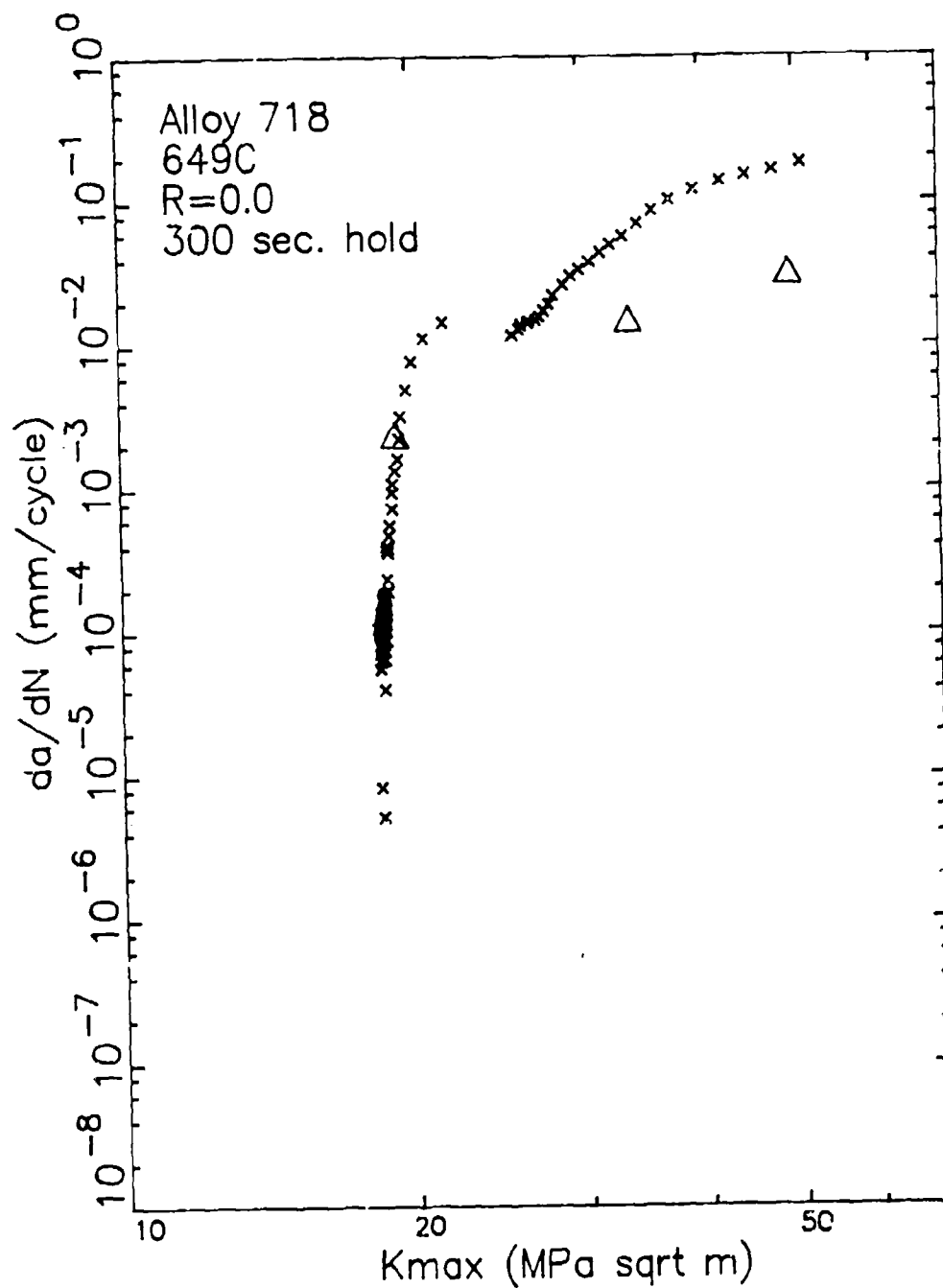
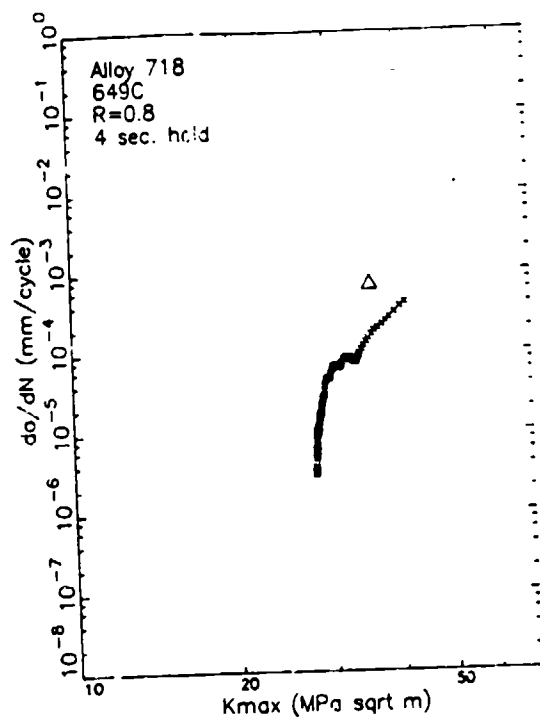
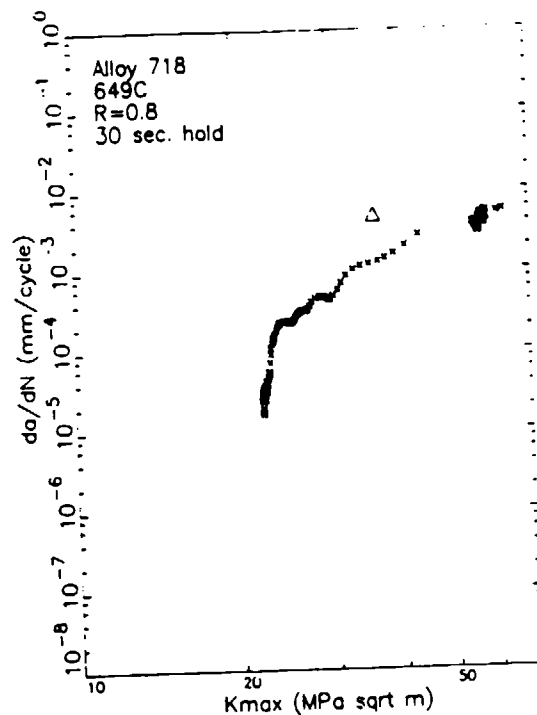


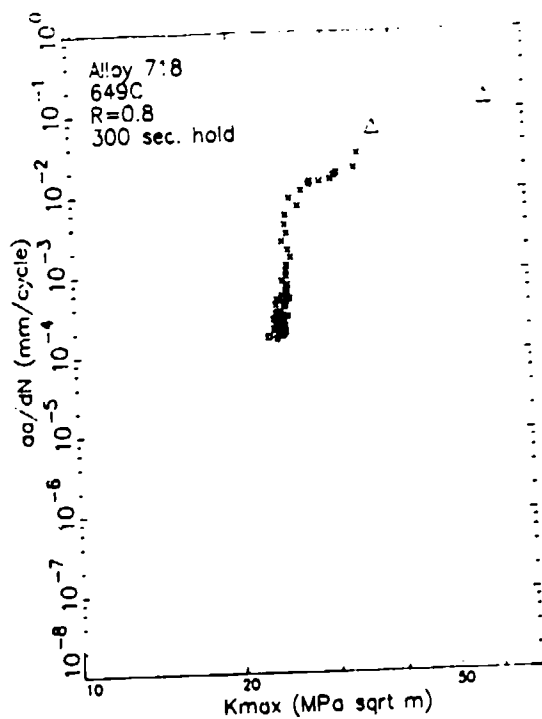
Figure 5.50: Comparison of crack growth rates measured in threshold and constant  $\Delta K$  tests of Alloy 718 at 649°C and R=0 for a 300 second hold time cycle.



(a)



(b)



(c)

Figure 5.51:

Comparison of crack growth rates measured in threshold and constant  $\Delta K$  tests of Alloy 718 at 649°C and  $R=0.8$  for hold times of (a) 4 seconds, (b) 30 seconds, and (c) 300 seconds.

### 5.2.3 Alloy 718. Static Crack Growth

The static crack growth properties of Alloy 718 were determined at 593 and 649°C using  $\Delta K$ -shed and constant load tests. The results of the 649°C tests are shown in Figure 5.52. The constant load test has an artificial threshold and there is a significant difference between the two types of tests. This is the same type of behavior observed in Rene'95. The near-threshold results shown in this figure were used to establish the value of the static threshold shown in Figure 5.49. Only one static crack growth test was performed on Alloy 718 at 593°C. The results of that constant load test are shown in Figure 5.53.

Comparison of the results shown in Figures 5.52 and 5.53 reveals that decreasing the test temperature from 649 to 593°C decreases static crack growth rates by approximately an order of magnitude. It is interesting that the static crack growth rates measured in Rene'95 (Figures 5.28 and 5.29) had a very distinct linear Region II which extended to K levels approaching 60 MPa/m. The companion tests on Alloy 718 showed a decreasing slope with increasing K. Alloy 718 has a lower creep capability and this may reflect the presence of larger amounts of creep deformation at the tip of the crack.

### 5.2.4 Alloy 718. Retardation Tests

Four overpeak hold time tests were performed on Alloy 718 specimens at 649°C. The test matrix was comprised of two R-ratios (0.0 and 0.5) and two overpeak ratios (10 and 20%) and is shown in Table 5.5. The overpeak cycles and test techniques for these tests were identical to those performed on Rene'95. The transient crack growth behavior observed during the constant  $\Delta K$  tests was also observed in the Alloy 718 overpeak hold time tests. As in the constant  $\Delta K$  tests, this prevented the use of the 0 second hold time data from the overpeak hold time tests. The results of these tests were analyzed identically to the Rene'95 constant  $\Delta K$  overpeak tests. Statistical analysis results for the Alloy 718 retardation tests are shown in Appendix D. The

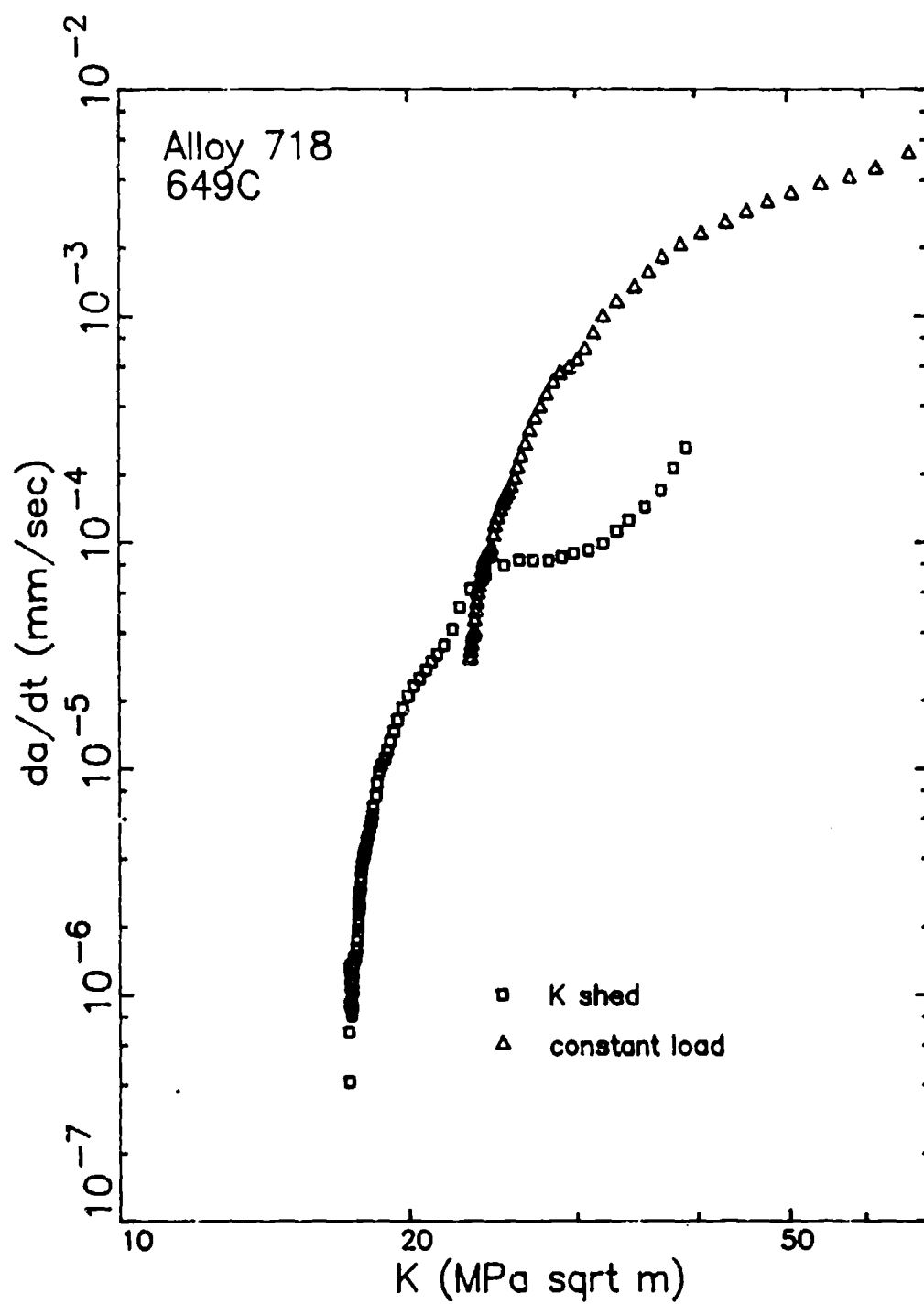


Figure 5.52: Results of Alloy 718 static crack growth tests at 649°C.

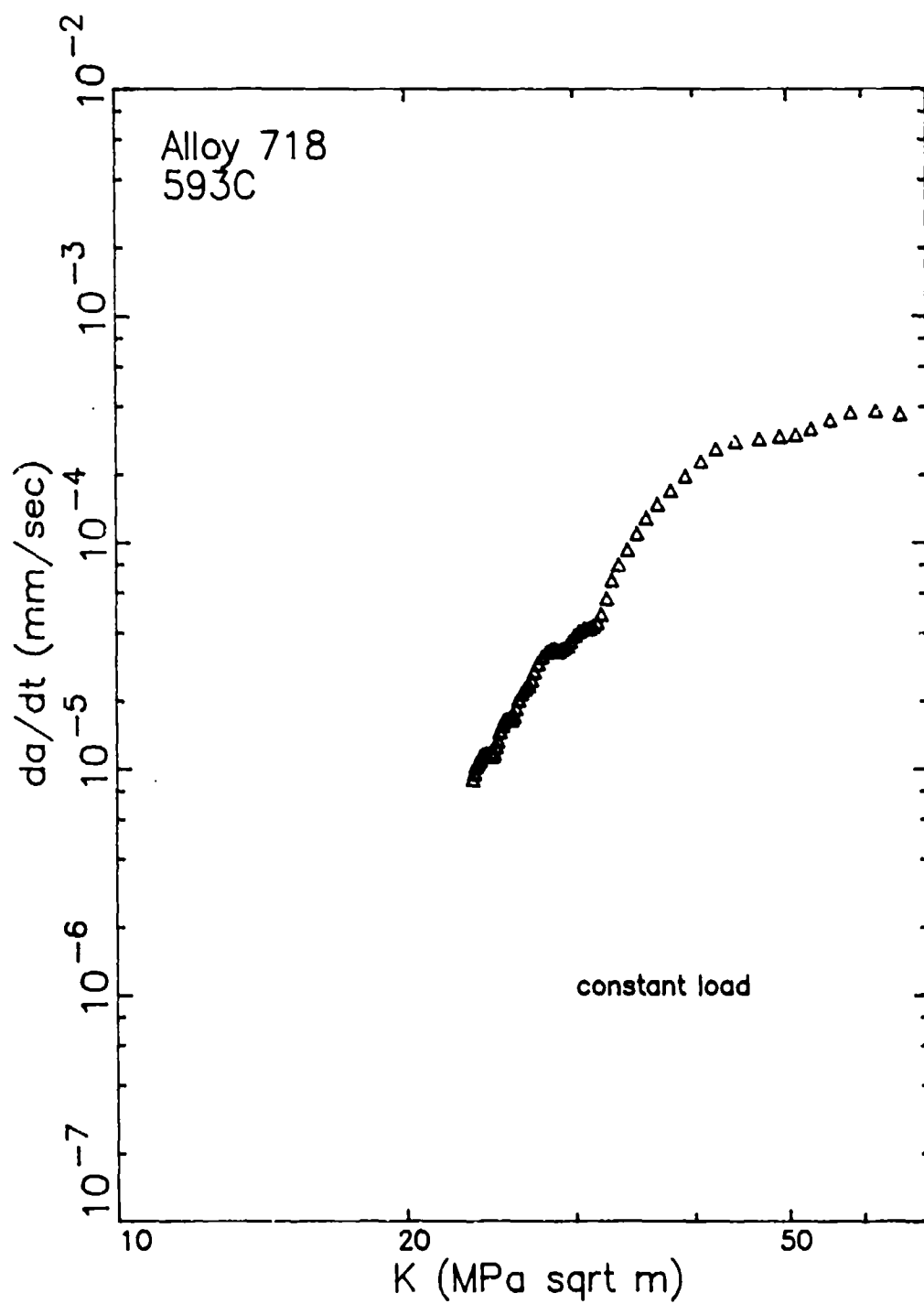


Figure 5.53: Results of Alloy 718 static crack growth tests at 593°C.

Table 5.5: Alloy 718 Overpeak Cycle Test Matrix

<u>Test Number</u>	<u>Temperature (°C)</u>	<u>R</u>	<u>Overpeak Ratio</u>
A13-18	649	0.0	1.1
A13-31	649	0.0	1.2
A13-36	649	0.5	1.1
A13-08	649	0.5	1.2



average values of  $K_{hold}$  and crack growth rate determined in these analyses are represented by large symbols in the following figures.

The results from the Alloy 718,  $R=0.0$  overpeak hold time tests are shown in Figure 5.54 where results for different hold times are indicated with different symbols. The dotted lines connect the results from cycles with the same hold time. Increasing the overpeak ratio results in suppression of time-dependent crack growth. For 20% overpeaks (Figure 5.54b), increasing  $K_{hold}$  results in a larger amount of retardation. This trend occurs for the 10% overpeaks with a 30 second hold time, but the effect is not clear for the 10% overpeak with 300 second hold times.

Figure 5.55 shows the data obtained from the 649°C  $R=0.5$  retardation tests. These results also show that increasing the amount of the overpeak suppresses the influence of hold time in these types of cycles.

The crack growth data shown in Figures 5.54 and 5.55 have been replotted on linear axes as a function of hold time for fixed values of  $K_{hold}$ . The results for the  $R=0.0$  and 0.5 tests are shown in Figures 5.56 and 5.57, respectively. These data can be compared to the constant  $\Delta K$  data which did not include overpeaks on each cycle. In the non-overpeak constant  $\Delta K$  tests, the crack growth rates varied linearly with hold time with the slope of the linear relationship increasing with  $K_{hold}$  level. The results from the  $R=0$ , 10% overpeak Alloy 718 test (Figure 5.56a) shows that there is a significant influence of hold time for  $K_{hold}$  values of 35 and 52 MPa/m, but that the slopes of the crack growth rate with hold time are similar for these two situations. This indicates that a significant amount of retardation is occurring at the higher  $K_{hold}$  levels. The results of the  $R=0$ , 20% overpeak (Figure 5.56b) show the slopes are similar independent of  $K_{hold}$  level which results from the larger amount of retardation associated with the higher overpeak.

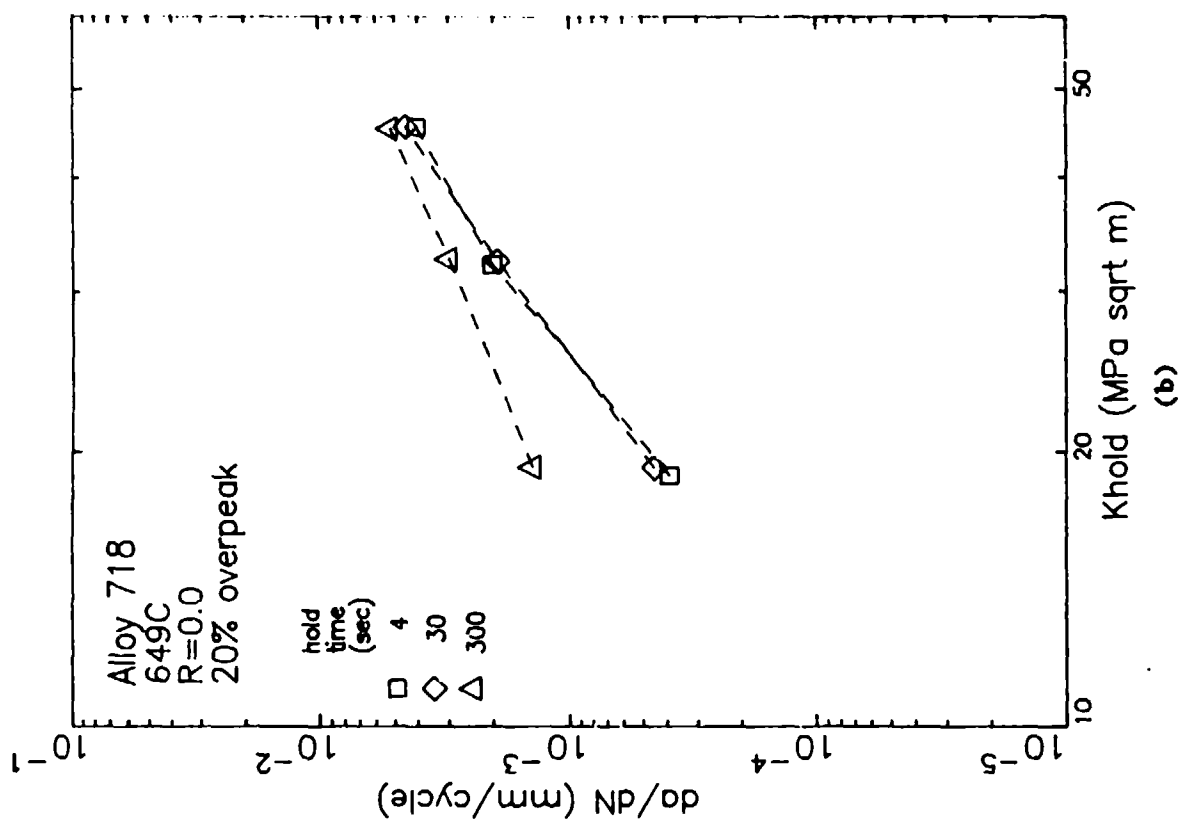
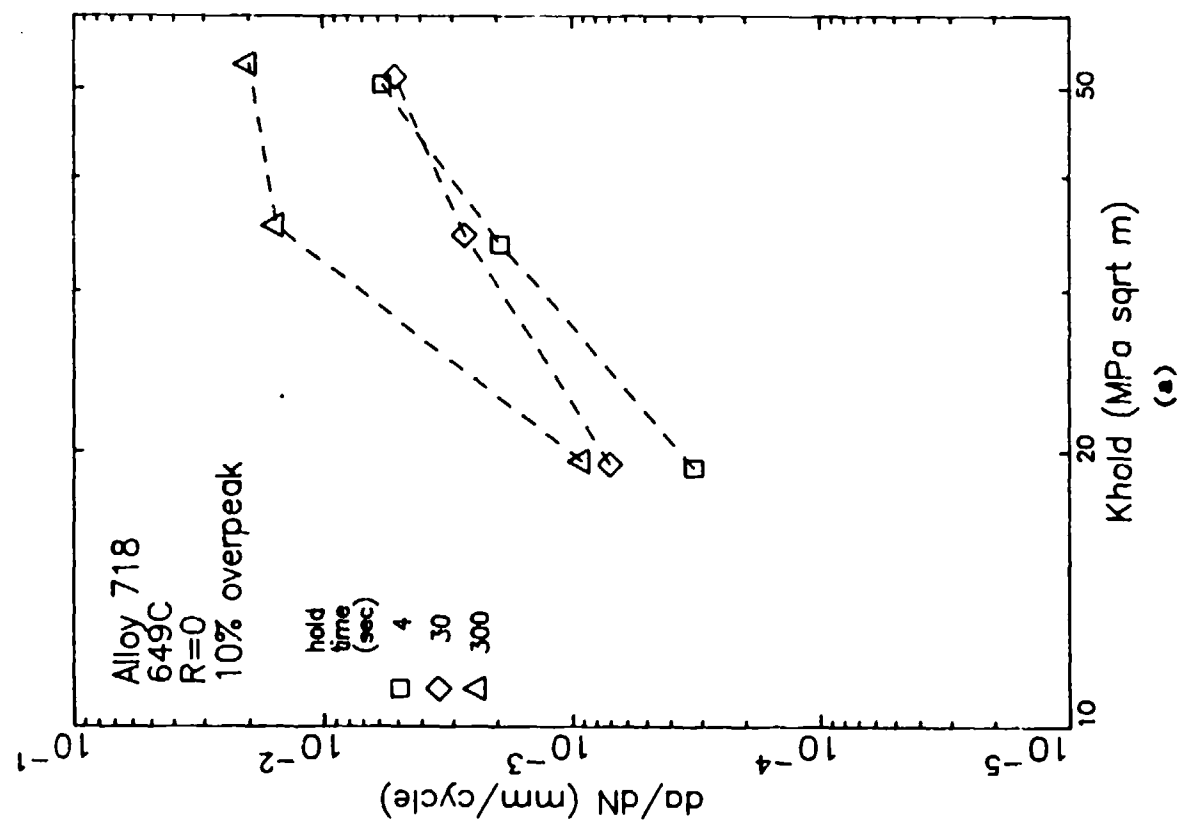


Figure 5.54: Results of 649°C multiple overpeak hold time tests on Alloy 718 with R=0 for overpeaks of (a) 10% and (b) 20%.

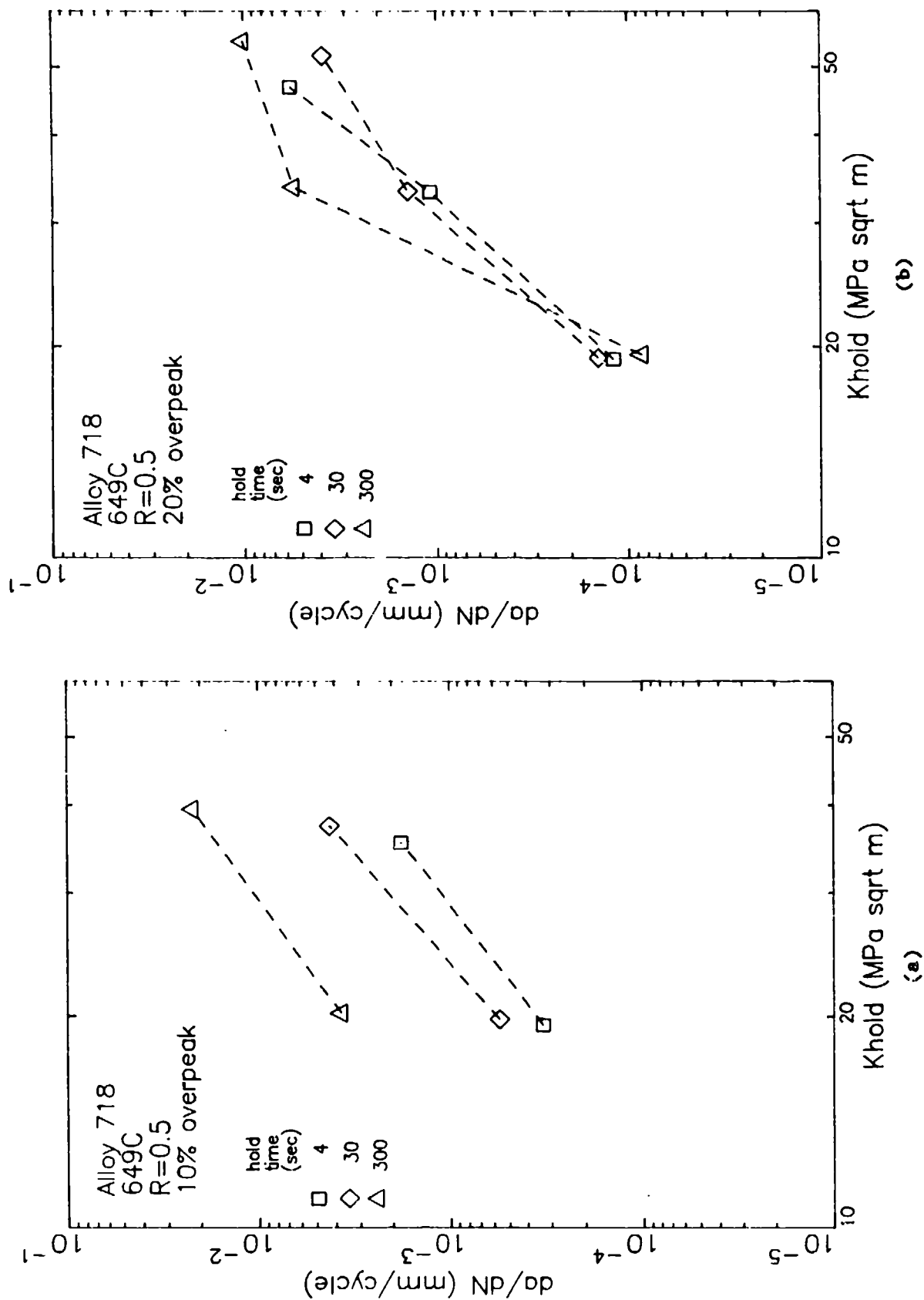


Figure 5.55: Results of 649°C multiple overpeak hold time tests on Alloy 718 with  $R=0.5$  for overpeaks of (a) 10% and (b) 20%.

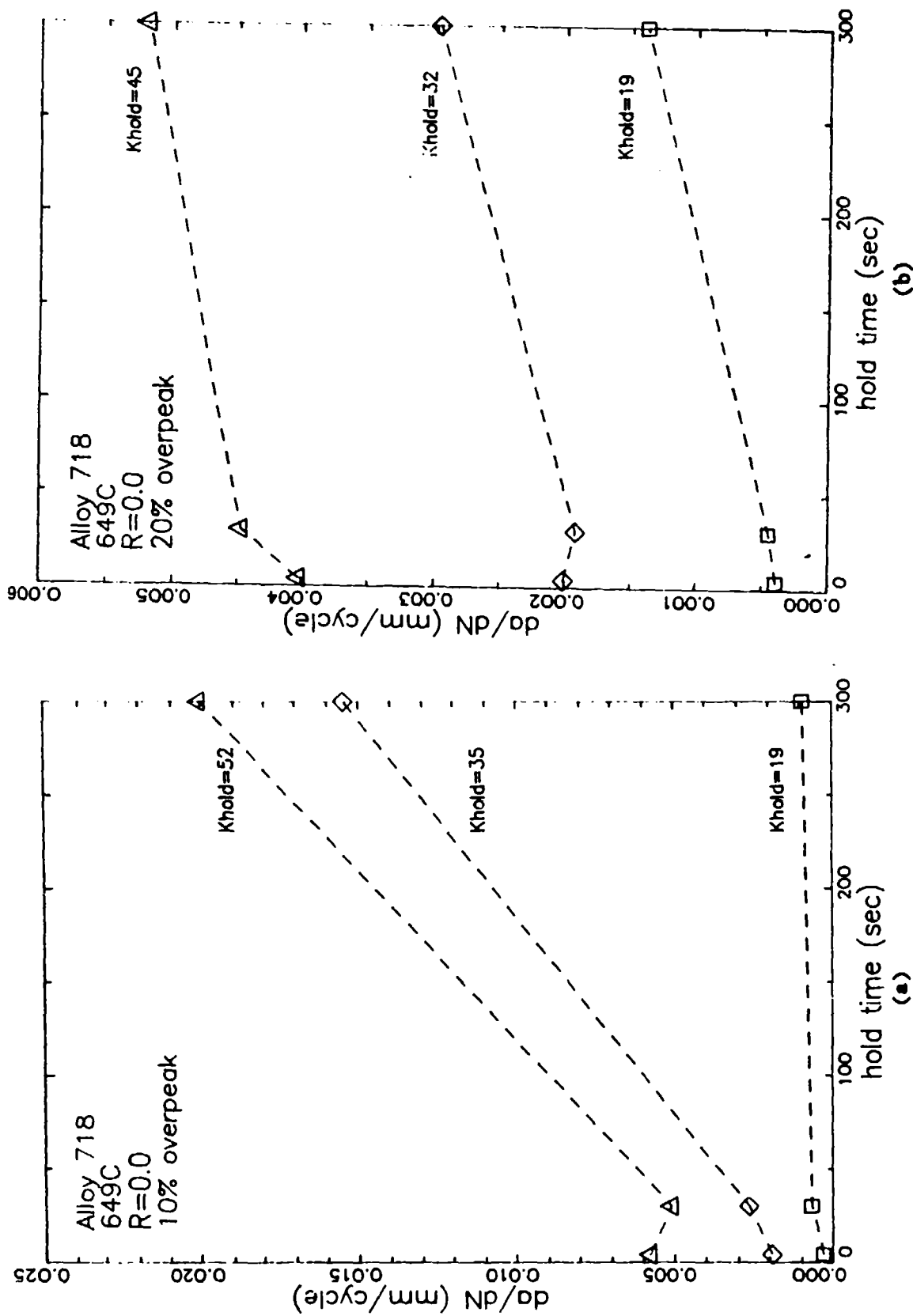


Figure 5.56: Variation of crack growth rate with hold time measured in 649°C multiple overpeak hold time tests on Alloy 718 with R=0 for overpeaks of (a) 10% and (b) 20%.

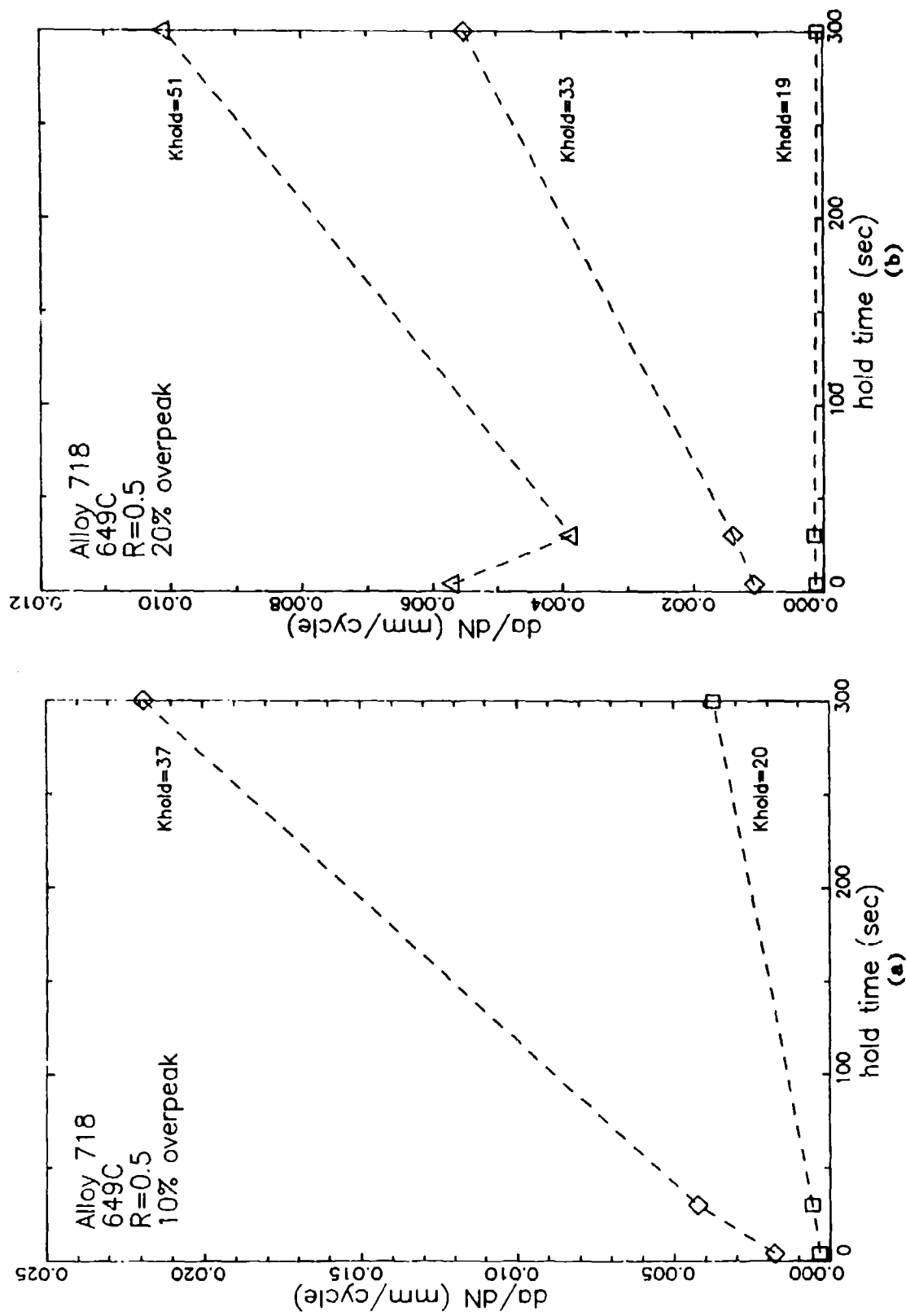


Figure 5.57: Variation of crack growth rate with hold time measured in 649°C multiple overpeak hold time tests on Alloy 718 with R=0.5 for overpeaks of (a) 10% and (b) 20%.

The results from the R-0.5 overpeak tests are shown on linear axes in Figure 5.57. The overall trends are similar to those shown for the R=0 tests; however, it appears that the amount of retardation is smaller with increasing R-ratio.

## 6.0 MECHANISM STUDIES

This section of the report describes the experimental work performed to better understand the mechanisms which control the time-dependent crack growth of Alloy 718 and Rene'95.

### 6.1 APPROACH OF MECHANISM STUDIES

These experiments were intended to aid in the interpretation and modeling of the crack growth behavior and can be divided into four areas:

1. fractographic examination
2. vacuum tests
3. metallographic sectioning experiments
4. characterization of crack tip damage zones

#### 6.1.1 Fractographic Examination

As a crack grows through a material, the resultant fracture surfaces leave a history of the deformation and fracture events. Although it is difficult to describe the entire fracture behavior from fractographic appearance, the changes in fracture mode with alloy, temperature, environment, and cycling conditions may provide clues as to the parameters which participate in the fracture events. Fractography was performed on selected specimens to better understand time-dependent crack growth.

#### 6.1.2 Vacuum Tests

As reported in the literature survey, the time-dependent crack growth process can be described in terms of creep-fatigue-environment interactions. It is almost impossible to separate creep-fatigue interactions; however the environmental part can be eliminated by performing crack growth tests in a high vacuum environment. Crack growth tests were performed in the high vacuum facility at GEAE to help understand the influence of environment on the

time-dependent crack growth process of these alloys. Fractography was also performed on many of the vacuum test specimens.

#### 6.1.3 Metallographic Sectioning Experiments

The threshold measurements showed that R=0, threshold values increase with longer hold times and lower test frequencies. When those data were presented, it was argued that this was consistent with creep-assisted crack tip blunting or stress redistribution near the crack tip. Several threshold tests were performed, duplicating selected conditions reported in Section 5, except the specimens were not broken after reaching the crack growth threshold. Metallographic sectioning was performed on these specimens to examine the morphology of the crack tip.

#### 6.1.4 Characterization of Crack Tip Damage Zones

During the Alloy 718 constant  $\Delta K$  tests, evidence of transient crack growth behavior was observed (Figure 5.41). These observations were often subjective in nature. During this part of the investigation, the size of the transient zone was measured in both Rene'95 and Alloy 718. Individual Alloy 718 specimens were also tested in solely in air, solely in vacuum, and sequentially in both air and vacuum to isolate the creep- and environmentally-induced damage at the crack tip.

### 6.2 FRACTOGRAPHY OF SPECIMENS TESTED IN AIR

Scanning electron microscopy (SEM) was used to study the fracture surface morphology of selected Rene'95 and Alloy 718 test specimens. For constant  $\Delta K$  hold time and frequency tests, fractographic examinations were performed at the specimen mid-thickness and crack depths corresponding to the midpoint of each  $K_{max}$ -cycle type segment. These midpoint positions were determined from post test crack length measurements and data analysis results. Accurate location of these positions for SEM study was achieved using a traveling stage controlled by a micrometer graduated in 0.001 mm increments. The region used to measure the crack growth threshold in decreasing  $\Delta K$  threshold tests



was located in a similar manner. Constant load tests were examined at the specimen mid-thickness for crack depths which sampled the entire region of static crack growth. These positions corresponded to regular intervals of crack length and were also located on the SEM using the traveling stage.

The fractographic results for tests performed in air are reported in four sections. The first three present the observations for Rene'95 constant  $\Delta K$  (Region II), threshold (Region I), and retardation tests. The fourth section describes the fracture appearance of the Alloy 718 constant  $\Delta K$  test specimens. Table 6.1 lists the Rene'95 specimens and associated test conditions used in the fractographic study. Fractographic observations for the vacuum tests are reported along with the vacuum data in Section 6.3.

#### 6.2.1 Rene'95: Constant $\Delta K$ (Region II) Observations

The examination of constant  $\Delta K$ ,  $R=0$ , hold time specimens tested at 538, 593, and 649°C revealed fracture morphologies that ranged from entirely transgranular to entirely intergranular. The results are summarized in Table 6.2 where the observations for all three hold times (4, 30, and 300 seconds) are generalized for each  $K_{max}$  level and temperature. T indicates a mode that is entirely transgranular, I indicates a mode that is entirely intergranular, and I + T indicates a mixed mode, where intergranular failure is prominent. As evident from the table, the combination of decreasing temperature and higher  $K_{max}$  resulted in an increased tendency for transgranular failure. It was also observed for mixed mode cases that the amount of transgranular failure decreased with increasing hold time. This behavior is illustrated in the SEM micrographs of Figure 6.1, where the morphology for hold times of 4 and 300 seconds is compared for the two mixed mode cases; 538°C and  $K_{max} = 20$  MPa/m, and 593°C and  $K_{max} = 44$  MPa/m. At both temperature -  $K_{max}$  combinations, the 300 second hold time has resulted in more pronounced intergranular failure.

As indicated by the asterisk in Table 6.2, slight evidence of transgranular failure was also observed for the 4 second hold time region of the 649°C test specimen. The SEM micrographs of Figure 6.2 compare the

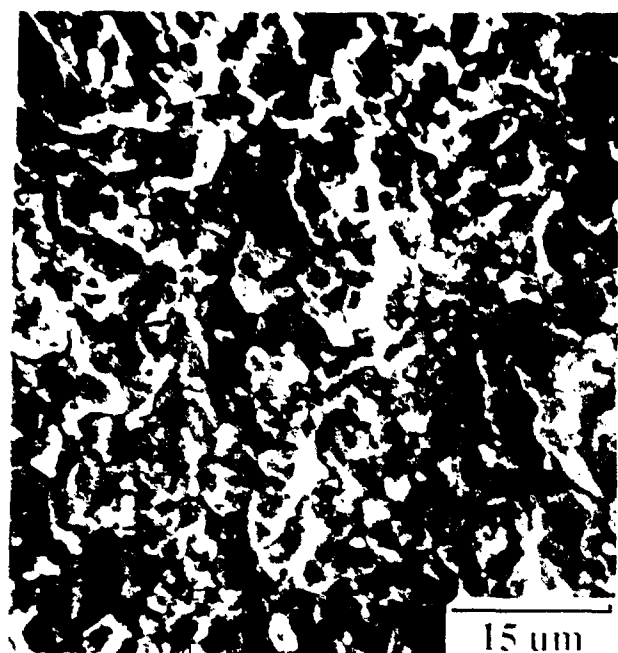
Table 6.1: Rene'95 Simple Cycle Specimens Evaluated in Fractographic Studies

Test Number	Temperature (°C)	R	Test Type	Variable
AF19	538	0.0	constant $\Delta K$	hold time
AF45	593	0.0	constant $\Delta K$	hold time
AF54	593	0.0	constant $\Delta K$	frequency
AF44	593	0.5	constant $\Delta K$	hold time
AF66	593	0.5	constant $\Delta K$	frequency
AF59	593	0.8	constant $\Delta K$	hold time
AF12	593	0.8	constant $\Delta K$	frequency
AF50	593	static	threshold	
AF70	593	static	constant load	
AF03	649	0.0	constant $\Delta K$	hold time
AF05	649	0.0	constant $\Delta K$	frequency
AF14	649	0.0	threshold	3 sec. cycle
AF63	649	0.0	threshold	30 sec. hold
AF06	649	0.0	threshold	300 sec. hold
AF18	649	0.0	threshold	30 sec. cycle
AF10	649	0.0	threshold	300 sec. cycle
AF15	649	0.5	constant $\Delta K$	hold time
AF09	649	0.5	threshold	3 sec. cycle
AF16	649	0.5	threshold	300 sec. hold
AF23	649	0.5	threshold	300 sec. cycle
AF72	649	0.8	constant $\Delta K$	hold time
AF55	649	0.8	threshold	3 sec. cycle
AF21	649	0.8	threshold	30 sec. hold
AF30	649	0.8	threshold	300 sec. hold
AF40	649	0.8	threshold	300 sec. hold
AF69	649	0.8	threshold	300 sec. cycle
AF17	649	static	threshold	
AF60	649	static	constant load	

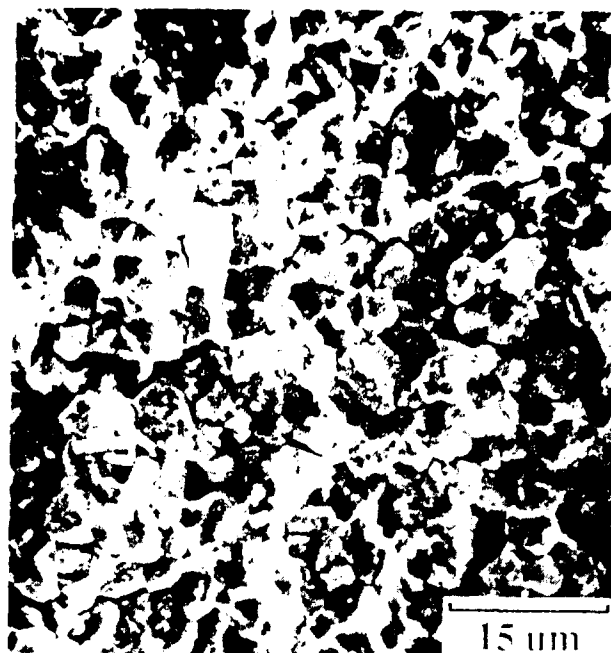
Table 6.2: Summary Of Rene'95 R-0 Fractography Results For Hold Time Test Specimens

Temperature (°C)	K <sub>max</sub> (MPa√m)		
	20	33	44
538	I+T	T	T
593	I	I	I+T
649	I	I	I*

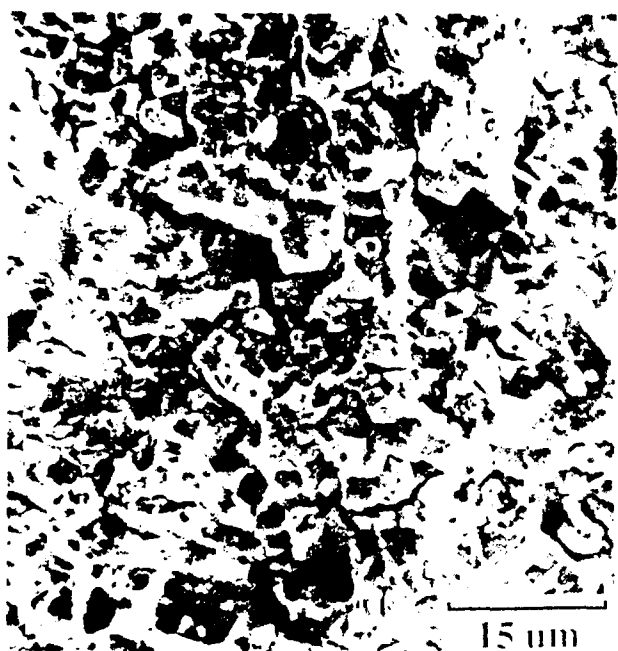
\* some evidence of transgranular failure



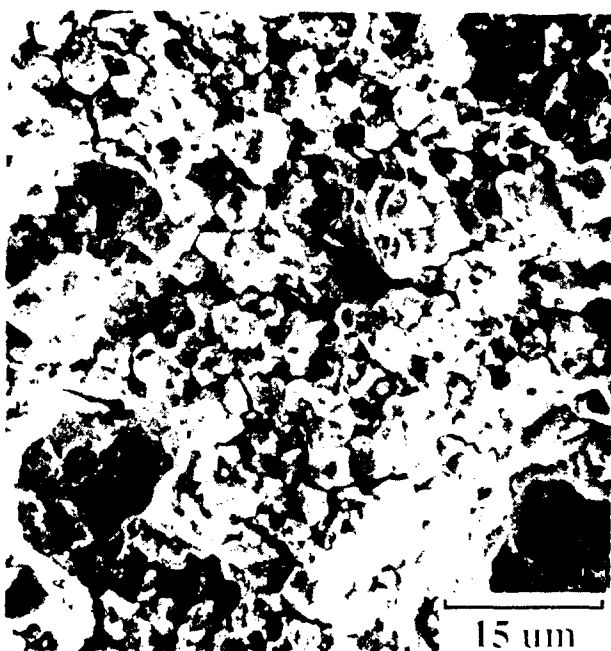
(a)



(b)

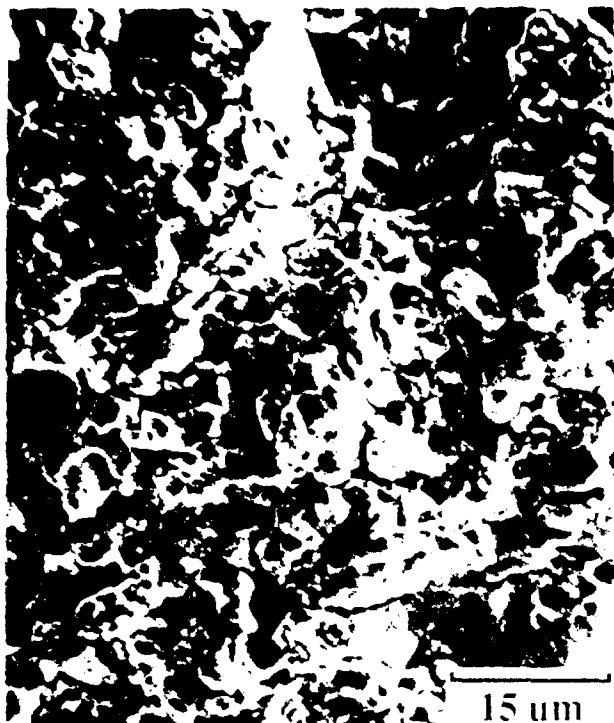


(c)

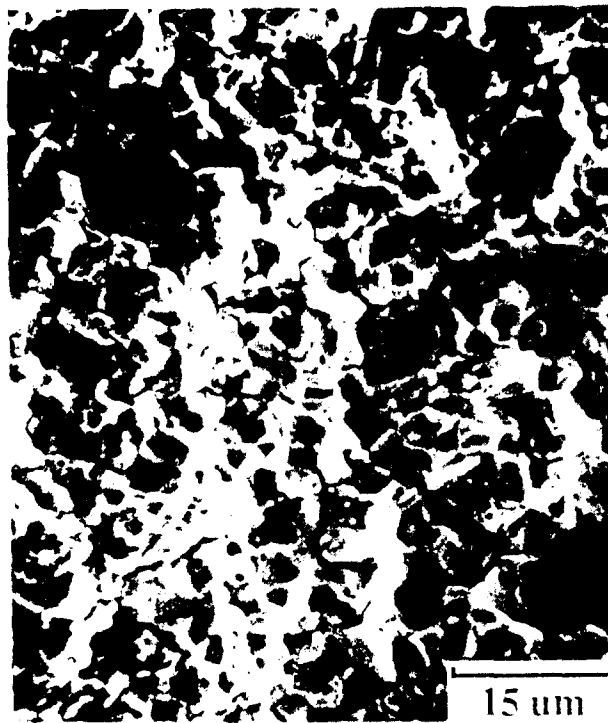


(d)

Figure 6.1 SEM micrographs showing Region II fracture morphology of constant  $\Delta E$ ,  $R=0$  Rene'95 specimens tested in air and conditions of (a) 538°C, low  $K_{max}$ , 4 second hold time cycle, (b) 538°C, low  $K_{max}$ , 300 second hold time cycle, (c) 593°C, high  $K_{max}$ , 4 second hold time cycle, and (d) 593°C, high  $K_{max}$ , 300 second hold time cycle



(a)



(b)



(c)

Figure 6.2:

SEM micrographs showing Region II fracture morphology of constant  $\Delta K$ , R=0 Rene 95 specimen tested in air at 640°C and conditions of (a) high  $K_{max}$ , 4 second hold time cycle, (b) high  $K_{max}$ , 30 second hold time cycle, and (c) high  $K_{max}$ , 300 second hold time cycle.

fracture appearance for the 4 second hold time segment of this specimen, which appears slightly transgranular, Figure 6.2a, with those for the 30 and 300 second hold times, which are clearly intergranular, Figures 6.2b and 6.2c. These detailed findings are consistent with the general trends described above.

The fractographic observations for the 538°C hold time specimen correlated with the peculiar trends observed in its crack growth behavior (Figure 5.4a). At low  $K_{max}$ , increasing hold time accelerated crack growth rates and could be associated with an increase in the amount of intergranular failure (compare Figures 6.1a and 6.1b). At the other  $K_{max}$  levels, there was either no hold time effect (intermediate  $K_{max}$ ), or a reversed effect (high  $K_{max}$ ) where increased hold time resulted in lower growth rates. The fracture morphology for each hold time segment at these higher  $K_{max}$  levels appeared to be entirely transgranular. SEM micrographs for the 4 and 300 second hold time regions at these  $K_{max}$  levels are shown in Figure 6.3.

One possible explanation for the reduction in crack growth rates with increased hold time at the high  $K_{max}$  condition is that localized crack tip blunting and/or stress redistribution is occurring. No evidence of this phenomenon was revealed by the fractography; the morphology for the 300 second hold time was similar to that of the 4 second hold time (Figures 6.3c and 6.3d).

There is also a correlation between fractographic observations and crack growth behavior for the 593°C test (Figure 5.4b). For the condition of mixed mode failure (high  $K_{max}$ ; see Table 6.2), the acceleration of growth rates with hold time could again be associated with an increase in the amount of intergranular fracture. Fractography-crack growth behavior correlations for the other  $K_{max}$  levels of this test, or the 649°C hold time test, Figure 5.3, are not possible since the fracture mode for these remaining conditions was predominantly intergranular. It should be pointed out, however, that the condition where slight evidence of transgranular failure was observed (649°C, 4 second hold time, high  $K_{max}$ ) again corresponds to the lowest growth rates at that  $K_{max}$  level.

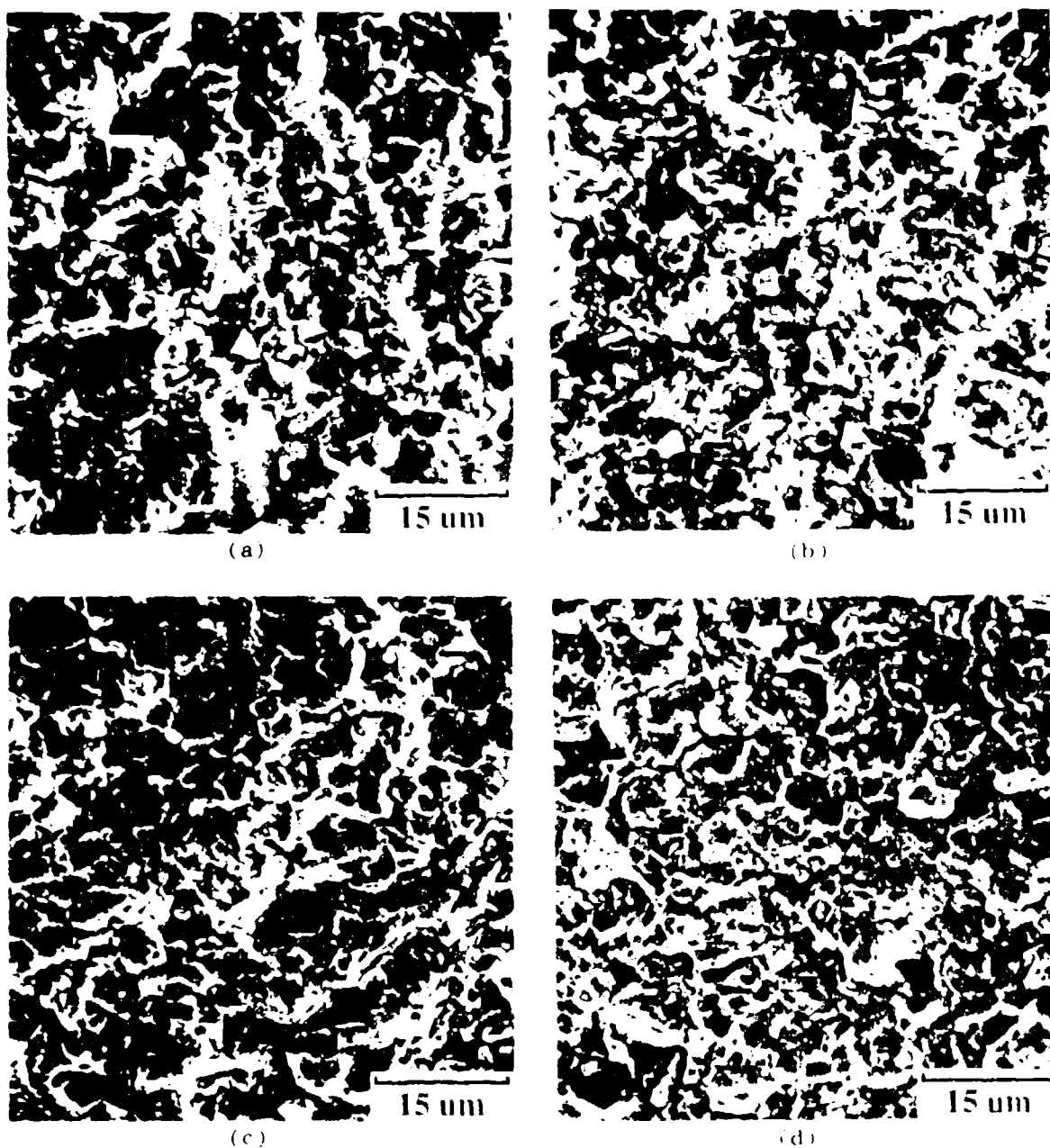


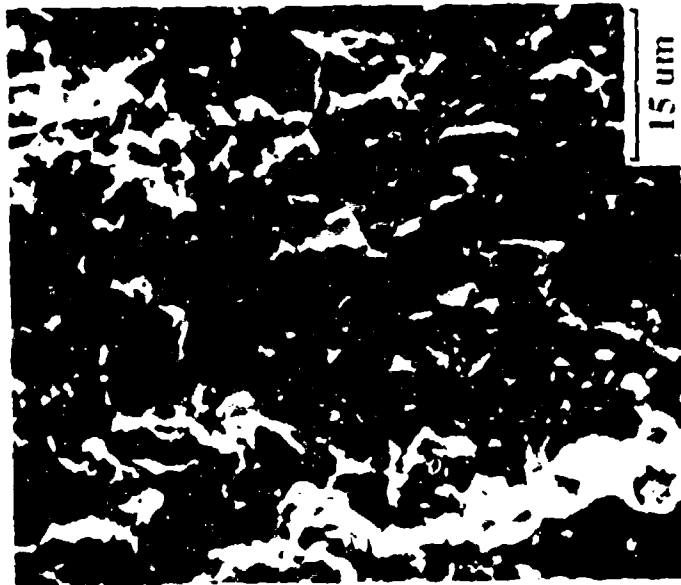
Figure 6.3: SEM micrographs showing Region II fracture morphology of constant  $\Delta K$ ,  $R=0$  Rene'95 specimen tested in air at  $538^{\circ}\text{C}$  and conditions of (a) intermediate  $K_{\text{max}}$ , 4 second hold time cycle, (b) intermediate  $K_{\text{max}}$ , 300 second hold time cycle, (c) high  $K_{\text{max}}$ , 4 second hold time cycle, and (d) high  $K_{\text{max}}$ , 300 second hold time cycle.

The study of constant  $\Delta K$ ,  $R=0$ , frequency specimens tested at 593 and 649°C also revealed a range in fracture morphology. Table 6.3 compares the fractographic observations for the 593°C frequency and hold time test specimens. In this table there are two designations for mixed mode fracture, I+T and T+I, representing more prominent intergranular or more prominent transgranular failure, respectively. As was the case for the hold time specimen, an increase in cycle duration typically promoted intergranular crack growth. A noticeable difference in fracture mode between the hold time and frequency cycled specimens, however, was observed at the low  $K_{max}$  condition. Table 6.3 shows that the frequency test specimen exhibited mixed mode fracture, while the companion hold time specimen exhibited intergranular fracture. These features are illustrated in Figure 6.4, where SEM micrographs for 30 second cycle period and 30 second hold time at the low  $K_{max}$  level are compared. Note that the transgranular regions for the frequency test specimen are distinguished by flat facets. As indicated in Table 6.3, the 30 second cycle period region contained the largest amount of transgranular fracture for the frequency test specimen at the low  $K_{max}$  level.

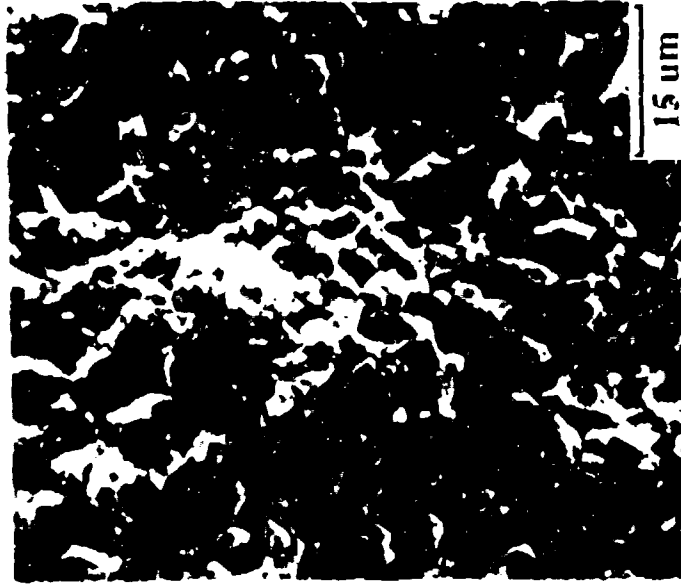
The fatigue mode characteristics of the frequency test can be correlated with the observed crack growth behavior, Figure 5.9a. At low  $K_{max}$ , there is little effect of cycle period, and mixed mode fracture was observed. These crack growth rates are also much slower than those observed for the hold time test at this  $K_{max}$  level, which exhibited intergranular failure for each hold time. At all other conditions for the frequency test, there is a clear influence of cycle period and a transition to completely intergranular failure.

Under most conditions, the 649°C, constant  $\Delta K$ , frequency specimen fracture was similar to that of the companion hold time test. At low frequency, however, mixed mode fracture was clearly evident at the high  $K_{max}$  level (the 4 second hold time segment exhibited very little transgranular failure), and the intermediate  $K_{max}$  level contained a slight amount of transgranular failure (the 4 second hold time segment exhibited intergranular failure). Figure 5.3 showed that the hold time test had faster growth rates at these  $K_{max}$  levels. The fractography results are again consistent with the





(a)



(b)

**Figure 6.4:** SEM micrographs showing Region II fracture morphology of constant  $\Delta K$ ,  $R=0$  Rene'95 specimens tested in air at  $593^{\circ}\text{C}$  and conditions of (a) low  $K_{\text{max}}$ , 30 second cycle period and (b) low  $K_{\text{max}}$ , 30 second hold time cycle.

Table 6.3: Summary Of Rene'95 593°C, R=0 Hold Time and Frequency  
Fractographic Observations

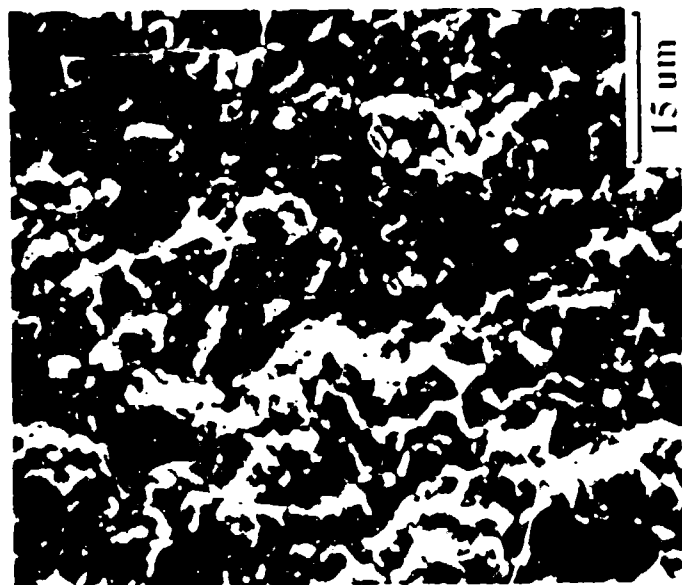
$K_{max}$ (MPa/m)	cycle period (sec)	fatigue mode	hold time (sec)	fatigue mode
19	3	I+T	4	I
	30	T+I	30	I
	300	I+T	300	I
21	3	I	4	I
	30	I	30	I
	300	I	300	I
44	3	T+I	4	T+I
	30	I	30	I+T
	300	I	300	I

trend for  $R=0$ , hold time and frequency test crack growth rates at a given  $K_{max}$  level to increase with increased amounts of intergranular fracture.

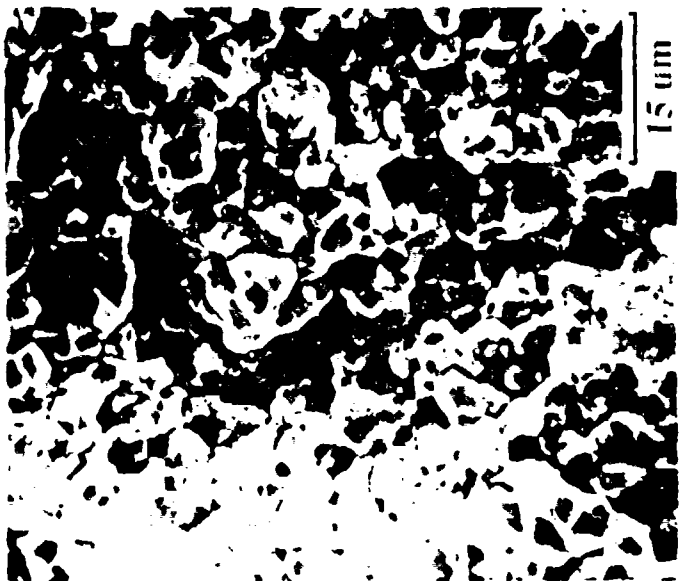
Increasing the R-ratio for 593 and 649°C hold time tests resulted in intergranular fracture for all hold times and  $K_{max}$  levels. As described previously, some mixed mode failure was observed for the  $R=0$  tests at these temperatures.

The effects of R-ratio and frequency on fracture mode were only studied for the 593°C tests. At an R-ratio of 0.5, the occurrence of transgranular fracture was again diminished with increasing R-ratio. Although predominantly intergranular, some transgranular failure appeared to be present at the conditions where mixed mode was observed for the  $R=0$  test (see Table 6.3). For the  $R=0.8$  test specimen, evidence of transgranular fracture was further diminished at the high  $K_{max}$  level, but some transgranular fracture was observed at the 3 and 30 second cycle periods for the intermediate  $K_{max}$  level. The  $R=0$  and 0.5 specimens exhibited intergranular failure under these conditions. The SEM micrographs of Figure 6.5, show the observed morphology for the 3 second cycle period of the  $R=0$  and  $R=0.8$  specimens at the intermediate  $K_{max}$  level. A comparison of frequency and hold time effects on crack growth rates for these R-ratios revealed that for comparable  $K_{max}$  - cycle time segments, the presence of some transgranular failure in the frequency test specimen was associated with similar or significantly reduced crack growth rates.

The remaining description of Region II fracture mode pertains to the 593 and 649°C static tests. Cracking for these specimens occurred in an intergranular mode, independent of the test control technique (constant load or decreasing  $\Delta K$ ). The 649°C constant load specimen selected for examination was precracked with a ramp period of 3 seconds to reduce the initial  $\Delta K$ . At this condition, the crack would not propagate under static loading. Subsequent 3 second ramp cycling was performed to grow the crack to a larger size. It was necessary to increase the  $\Delta K$  by nearly 50 percent to achieve static crack growth. Study of this region revealed an intergranular fracture mode both before and after the arrest position. This indicates that the



(a)



(b)

Figure 6.5: SEM micrographs showing Region II fracture morphology of constant  $\Delta K$  Rene'95 specimens tested in air at 593°C and conditions of (a)  $R=0$ , intermediate  $K_{max}$ , 3 second cycle period and (b)  $R=0.8$ , intermediate  $K_{max}$ , 3 second cycle period.

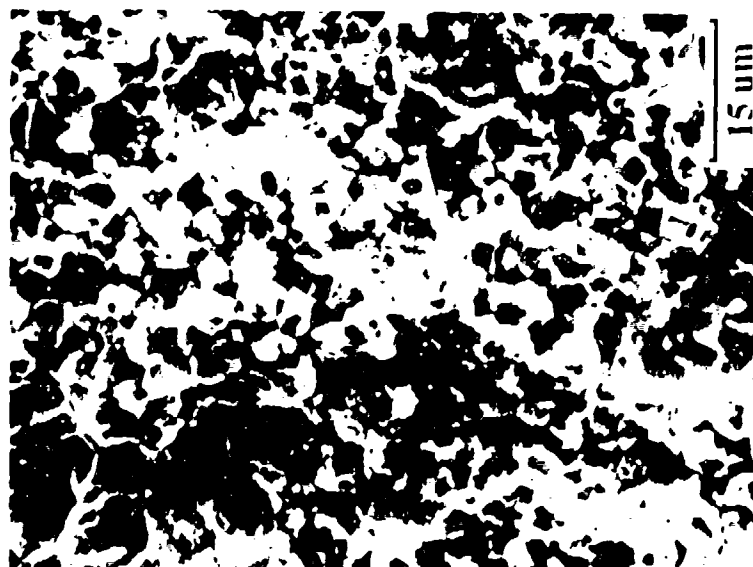
arrest was not caused by a change in fracture mode, and that again, the possible occurrence of local crack tip blunting and/or stress redistribution was not supported by fractographic observations.

#### 6.2.2 Rene'95: Region I Observations

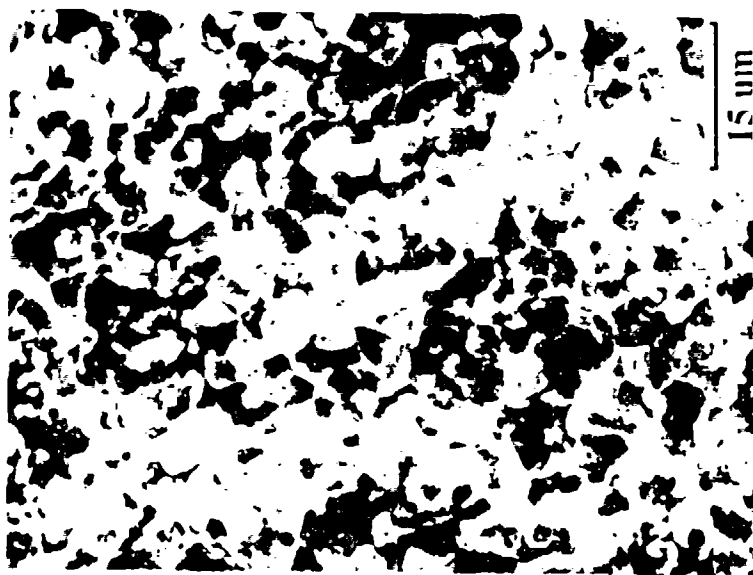
The fractographic study of Region I threshold specimens considered all 649°C conditions shown on Figure 5.19 except the 4 second hold time, R=0.8 condition. The fracture mode for all specimens except the 3 second cycle period specimen tested at R=0, was completely intergranular in the region of crack arrest. For this exception, some isolated transgranular-flat faceted areas were observed within a predominantly intergranular morphology. Figure 5.19 shows that this condition resulted in the lowest threshold of all cyclic tests. The SEM micrographs of Figure 6.6 show the fracture morphology in the region of crack arrest for the R=0, 3 second cycle period specimen, and the cyclic specimen having the next highest threshold. The latter specimen was tested at R=0 with a 30 second hold time and exhibited intergranular fracture.

#### 6.2.3 Rene'95: Retardation Test Observations

The 649°C, R=0, hold time specimen tested with a 20 percent overpeak was selected for SEM study of Region II retardation effects. The fracture mode for all  $K_{max}$ -hold time combinations was intergranular. As previously described, subtle transgranular fracture in a predominantly intergranular mode was observed for the companion non-overpeaked specimen at the high  $K_{max}$  level and 4 second hold time condition. For this condition, the overpeak thus promoted intergranular fracture. A much more noticeable difference between the hold time fracture regions of the overpeak specimen and the companion hold time specimen was observed at low magnification. The low magnifications SEM micrographs in Figure 6.7 show the entire region of crack growth for both of these specimens. As hold time duration increases at each  $K_{max}$  level, the non-overpeaked specimen exhibits a much more tortuous fracture surface.

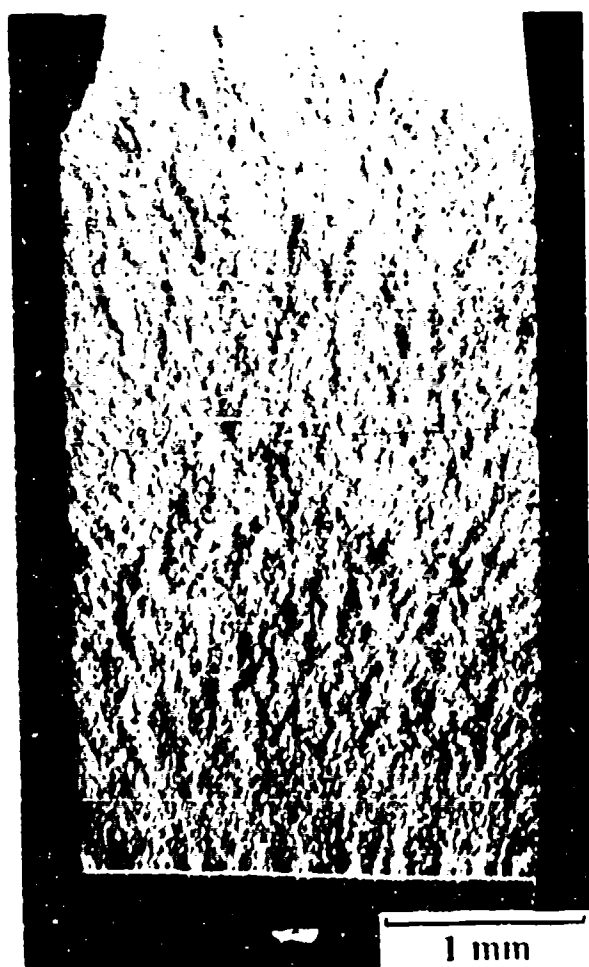


(a)



(b)

Figure 6.6: SEM micrographs showing threshold arrest morphology of K-shed, R=0 Rene'95 specimens tested in air at 649°C and conditions of (a) 3 second cycle period and (b) 30 second hold time cycle.



(a)



(b)

Figure 6.7: SEM micrographs showing the fracture surface of constant  $\Delta K$ , R=0 Rene'95 hold time specimens tested in air at 649°C and conditions of (a) 20% overpeak and (b) no overpeak.

#### 6.2.4 Alloy 718: Constant $\Delta K$ (Region II) Hold Time Observations

The R=0, constant  $K_{max}$ , hold time specimens tested at 593 and 649°C were selected for the SEM study of Alloy 718 Region II morphology. The fracture morphology at 593°C and the low  $K_{max}$  level transitioned from mixed mode to a predominantly intergranular mode as hold time increased. Figure 6.8 shows SEM micrographs which illustrate the morphology for each low  $K_{max}$  segment. As the  $K_{max}$  level increased, the tendency for intergranular failure with increasing hold time diminished. Figure 6.9 shows micrographs for the 4 and 300 second hold times at the intermediate and high  $K_{max}$  levels. For the high  $K_{max}$  level, the 300 second hold time has resulted in negligible intergranular failure.

At 649°C, a trend in fracture morphology transition like that of the 593°C test was observed at the low  $K_{max}$  level, but intergranular fracture became more prevalent with increasing  $K_{max}$  and hold time. The SEM micrographs of Figure 6.10 show the morphology for the 4 and 300 second hold times at the intermediate and high  $K_{max}$  levels for the 649°C specimen. Whereas the 593°C specimen had negligible intergranular failure for the high  $K_{max}$ , 300 second hold time, Figure 6.9d, the 649°C test exhibits complete intergranular failure, Figure 6.10d. The effects of hold time on fatigue crack growth rates were much more pronounced for the 649°C test at all  $K_{max}$  levels. This correlates with the pronounced increase in the amount of intergranular fracture, particularly at the high  $K_{max}$  level.

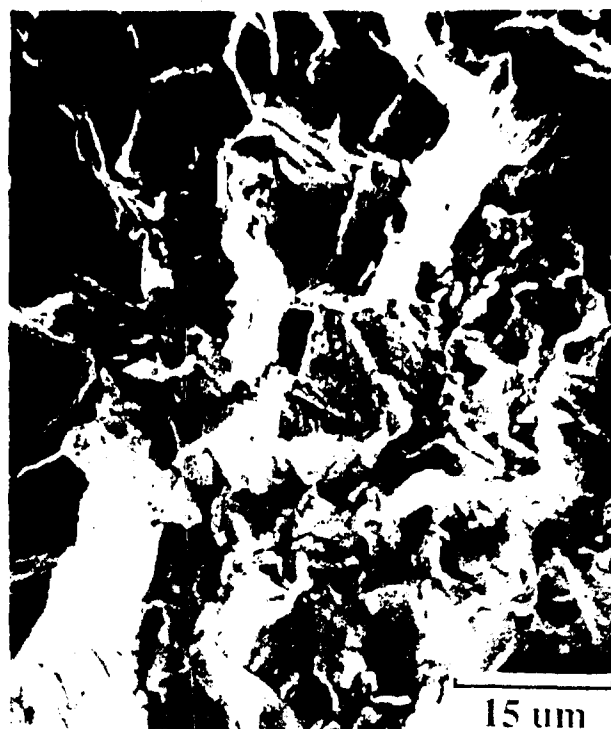
#### 6.3 VACUUM RESULTS

Region II vacuum crack growth tests were performed on both Rene'95 and Alloy 718. The selected test conditions are listed in Table 6.4. The intent of these tests was to determine the role of the environment on the crack growth rates and failure modes. This section will describe both the crack growth data and fractographic examination results of specimens tested in high vacuum.





(a)



(b)



(c)

Figure 6.8:

SEM micrographs showing Region II fracture morphology of constant  $\Delta K$ , R-0 Alloy 718 specimen tested in air at 593°C and conditions of (a) low  $K_{max}$ , 4 second hold time cycle, (b) low  $K_{max}$ , 30 second hold time cycle, and (c) low  $K_{max}$ , 300 second hold time cycle.

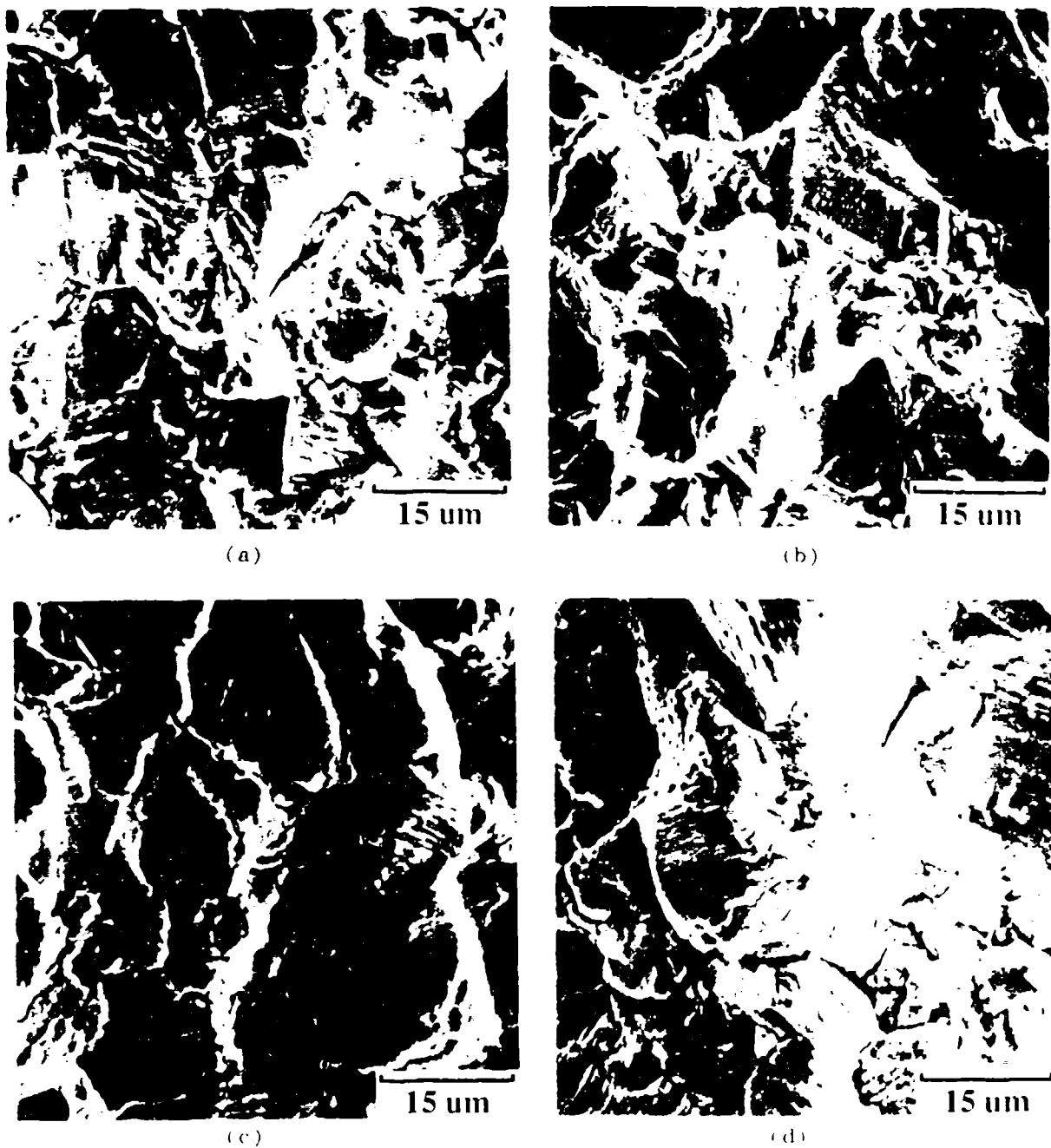
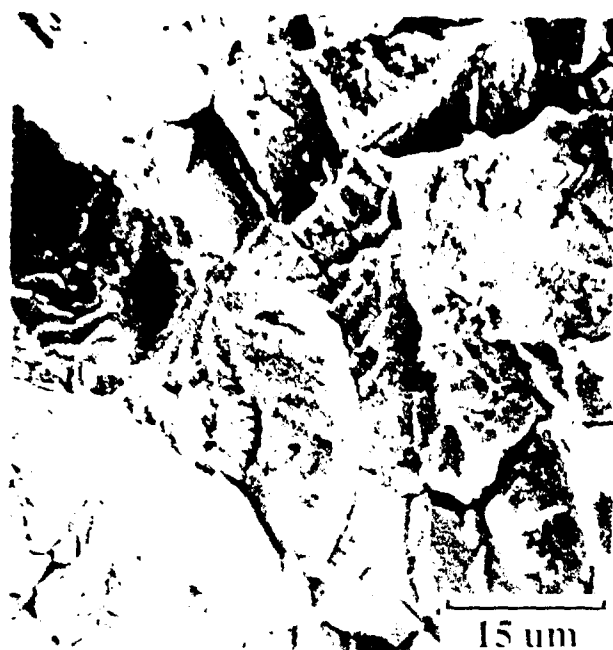


Figure 6.9: SEM micrographs showing Region II fracture morphology of constant  $\Delta K$ ,  $R=0$  Alloy 718 specimen tested in air at  $593^{\circ}\text{C}$  and conditions of (a) intermediate  $K_{\text{max}}$ , 4 second hold time cycle, (b) intermediate  $K_{\text{max}}$ , 300 second hold time cycle, (c) high  $K_{\text{max}}$ , 4 second hold time cycle, and (d) high  $K_{\text{max}}$ , 300 second hold time cycle.



(a)



(b)



(c)



(d)

Figure 6.10. SEM micrographs showing Region II fracture morphology of constant  $\Delta K$ , R-0 Alloy 718 specimen tested in air at 649°C and conditions of (a) intermediate  $K_{max}$ , 4 second hold time cycle, (b) intermediate  $K_{max}$ , 300 second hold time cycle, (c) high  $K_{max}$ , 4 second hold time cycle, and (d) high  $K_{max}$ , 300 second hold time cycle.

Table 6.4: Vacuum Crack Growth Specimens

<u>Material</u>	<u>Specimen</u>	<u>Temperature (°C)</u>	<u>R</u>	<u>Hold Time (sec)</u>
Rene'95	AF26	593	0.0	0
Rene'95	AF71	649	0.0	0
	AF78	649	0.0	0
	AF76	649	0.0	300
	AF37	649	0.8	0
Alloy 718	A13-18	649	0.0	0
	A13-01	649	0.0	300

### 6.3.1 Rene'95 Vacuum Crack Growth Results

All vacuum crack growth tests were performed with either a 3 second cycle or a 300 second hold time with 1.5 second loading and unloading ramps. These will be referred to as 0 and 300 second hold time cycles because they had the same ramp periods. These tests were performed using the controlled increasing  $\Delta K$  option in the potential drop software. Comparisons to tests performed in air will be done between tests performed using the same control mode.

The results of the 649°C tests with R-ratios of 0.0 and 0.8 are compared as a function of  $\Delta K$  and  $K_{max}$  in Figure 6.11a and 6.11b, respectively. These results show, like the 0 second hold time data in air, that increasing R-ratio accelerates crack growth rates. The significance of this comparison is that these data cannot be correlated using either  $\Delta K$  or  $K_{max}$ , indicating that an interpolative model, such as the Walker model, may be used to describe the crack growth behavior in vacuum.

Figure 6.12 compares the results of the 593°C R=0, 300 second hold time vacuum test with its companion test in air. The crack growth rates range from two to four times slower in vacuum than in air, depending on the  $\Delta K$  level.

Figure 6.13 compares the results of the air and vacuum tests for the three 649°C test conditions evaluated in vacuum. The cracks in the 0 second hold time tests in air grew approximately six times faster than the cracks in the vacuum tests independent of the R-ratio. The R=0, 300 second hold time tests (Figure 6.13c) in air grew approximately 100 times faster than the corresponding test in vacuum. These results show that laboratory air is an aggressive environment for Rene'95. It is especially aggressive for long hold times.

The influence of hold time on the crack growth rate of Rene'95 for R=0 cycling at 649°C is compared in Figure 6.14. In the presence of air, a 300 second hold time accelerates the crack growth by two orders of magnitude, while in vacuum the same hold time results in a four fold increase in the crack growth rate.

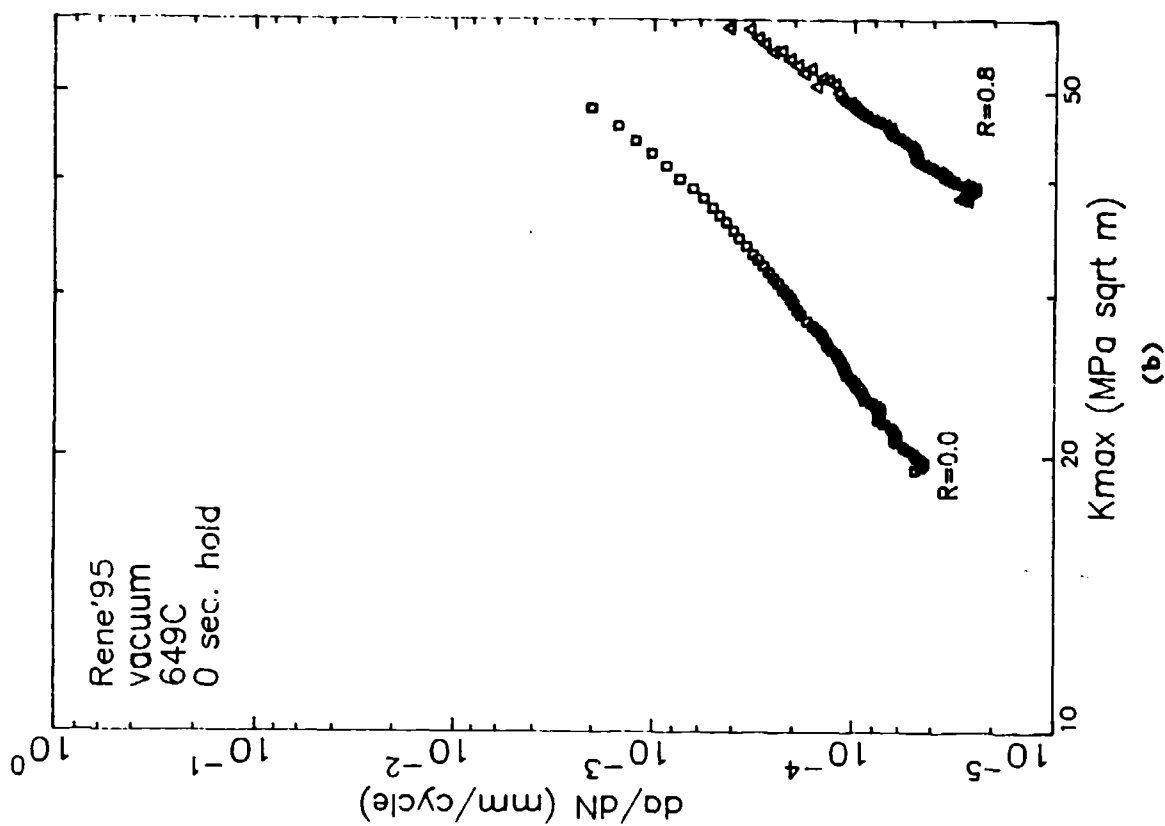
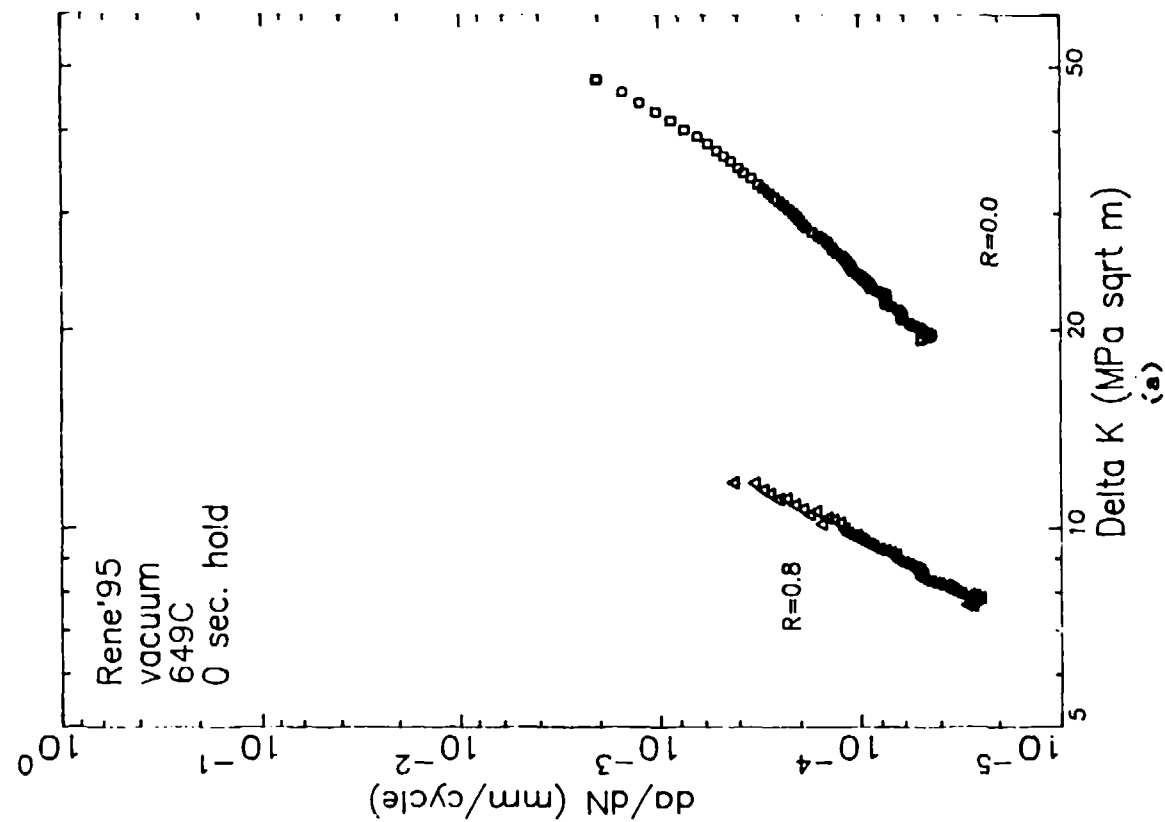


Figure 6.11: Crack growth data from 3 second period Rene'95 vacuum tests with different R-ratios as a function of (a)  $\Delta K$  and (b)  $K_{max}$ .

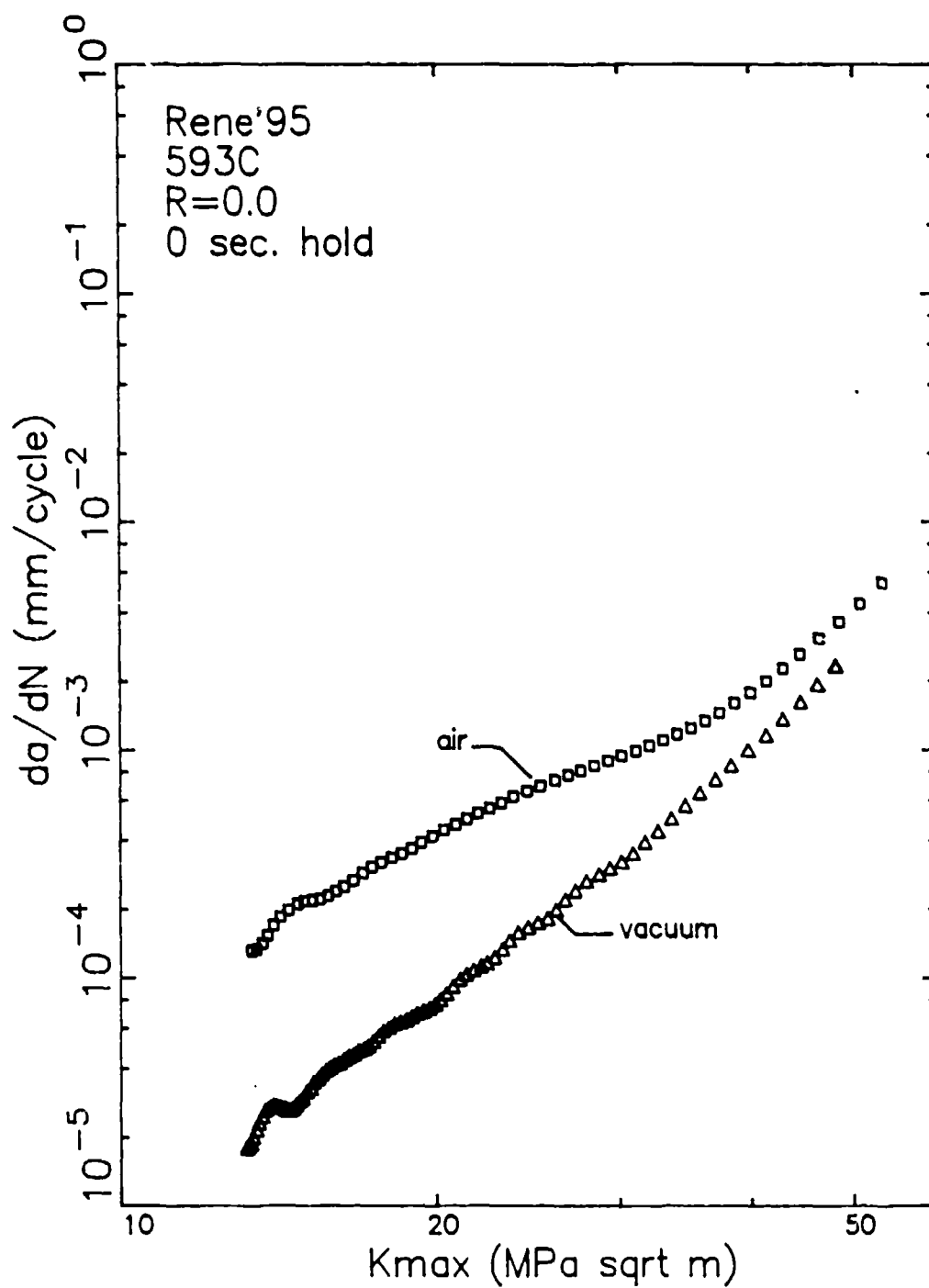
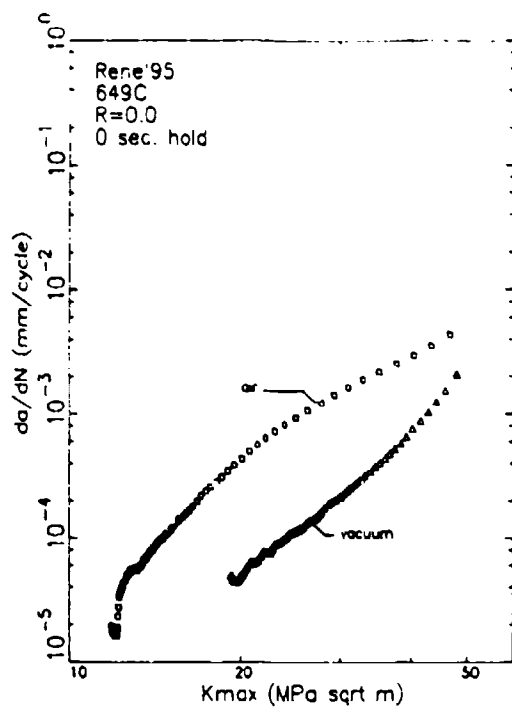
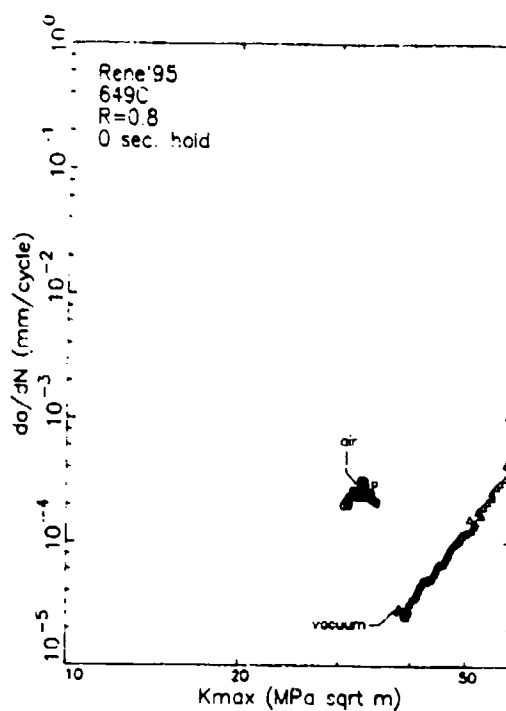


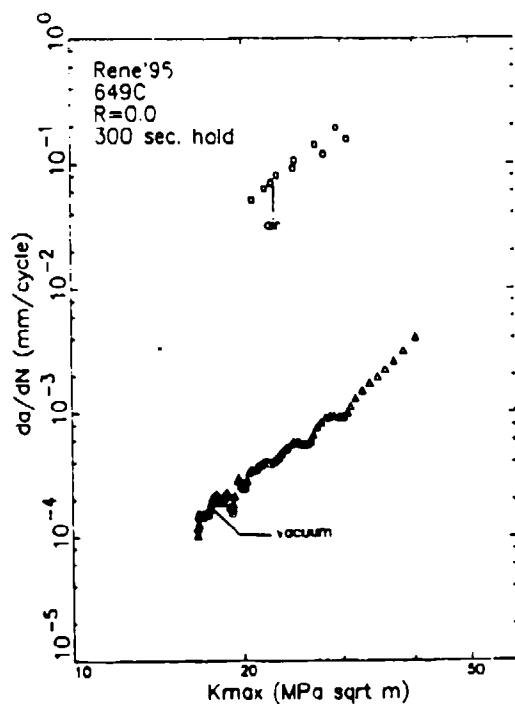
Figure 6.12: Comparison of Rene'95 crack growth rates measured in air and vacuum for tests cycled at 593°C with R=0 and 0 second hold time.



(a)



(b)



(c)

Figure 6.13:

Comparison of Rene'95 crack growth rates measured in air and vacuum for tests cycled at 649°C with (a) R=0 and 0 second hold time, (b) R=0.8 and 0 second hold time, and (c) R=0 and 300 second hold time.



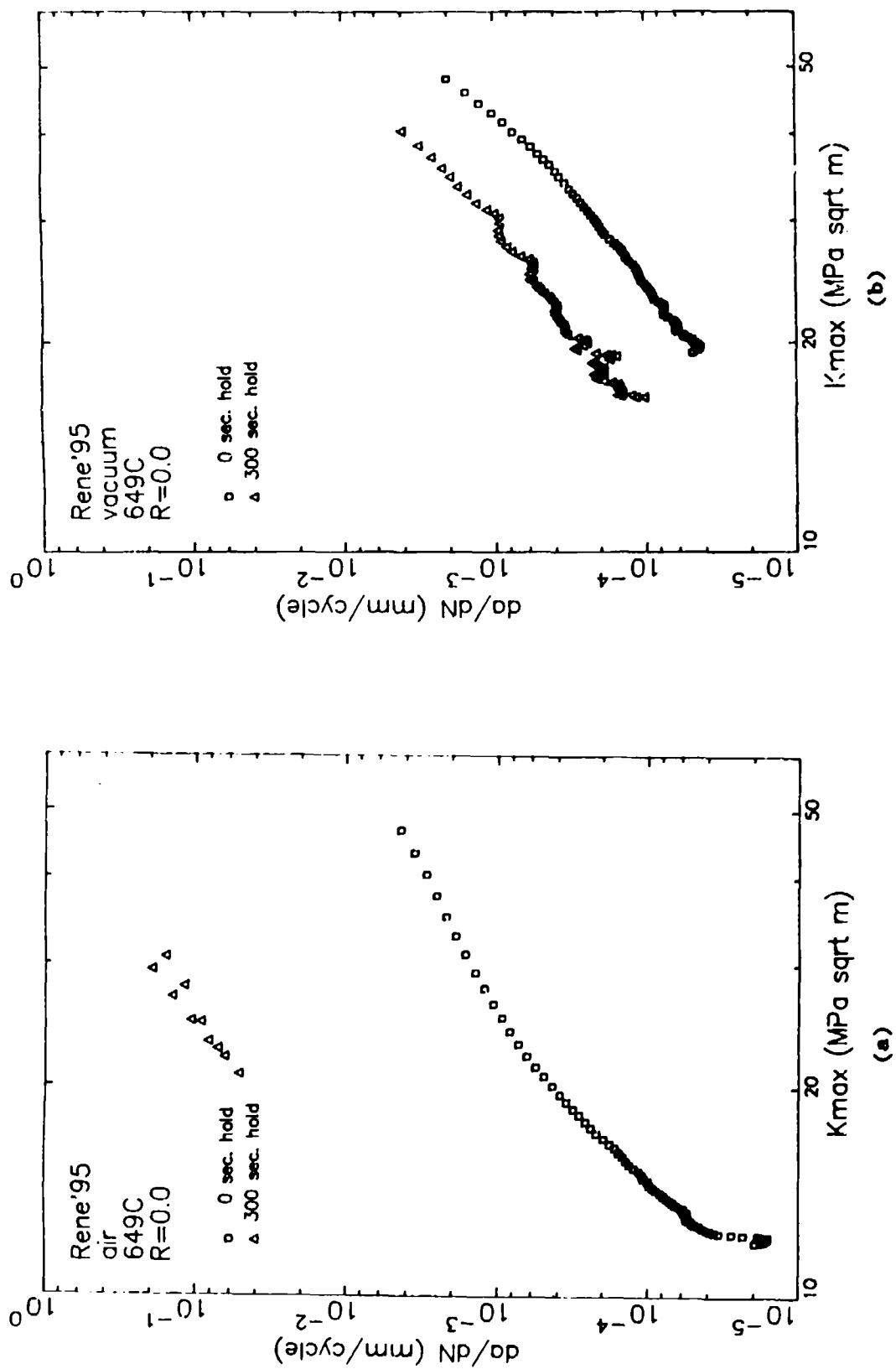


Figure 6.14: Influence of hold time on Rene'95 crack growth rates at 649°C with R=0 in (a) air and (b) vacuum.

The influence of test temperature on the R=0, 3 second cycle crack growth rates in air and vacuum are shown in Figure 6.15. The crack growth rates are faster in air, but the relative influence of temperature on the crack growth rates is similar.

#### 6.3.2 Alloy 718 Vacuum Crack Growth Results

The only vacuum crack growth tests performed on Alloy 718 specimens were at 649°C with R=0 and hold times of 0 and 300 seconds. Figure 6.16 compares the results of the vacuum tests to the corresponding tests performed in air. The presence of air accelerates the no hold time crack growth rates by a factor of approximately three, while for 300 second hold times, this factor is in excess of an order of magnitude.

Figure 6.17 compares these results as a function of the hold time. In air, a 300 second hold time accelerates the crack growth rate by a factor of approximately twenty. Hold time also accelerates the crack propagation rate in vacuum, but to a much smaller extent.

#### 6.3.3 Rene'95 Vacuum Test Fractographic Observations

Three Rene'95 specimens were selected for SEM study of Region II fracture morphology after vacuum testing: the 649°C, R=0, 3 second cycle period and 300 second hold time specimens, and the 593°C, R=0, 3 second cycle period specimen. Each was examined at  $K_{max}$  levels corresponding to the companion constant  $K_{max}$  air test specimens (low and intermediate  $K_{max}$  for the 649°C tests; all three  $K_{max}$  levels for the 593°C test). At 649°C, the vacuum tested, 3 second cycle period specimen exhibited transgranular fracture at the low  $K_{max}$  level and predominantly transgranular fracture at the intermediate  $K_{max}$  level. Under comparable conditions, the constant  $K_{max}$  air test exhibited predominantly intergranular failure (some minor evidence of transgranular cracking was observed at the intermediate  $K_{max}$  level). and similar crack growth rates. The 649°C, vacuum tested, 300 second hold time specimen showed intergranular failure, like the companion constant  $K_{max}$  air test, but crack growth rates were more than an order of magnitude slower. The growth rates

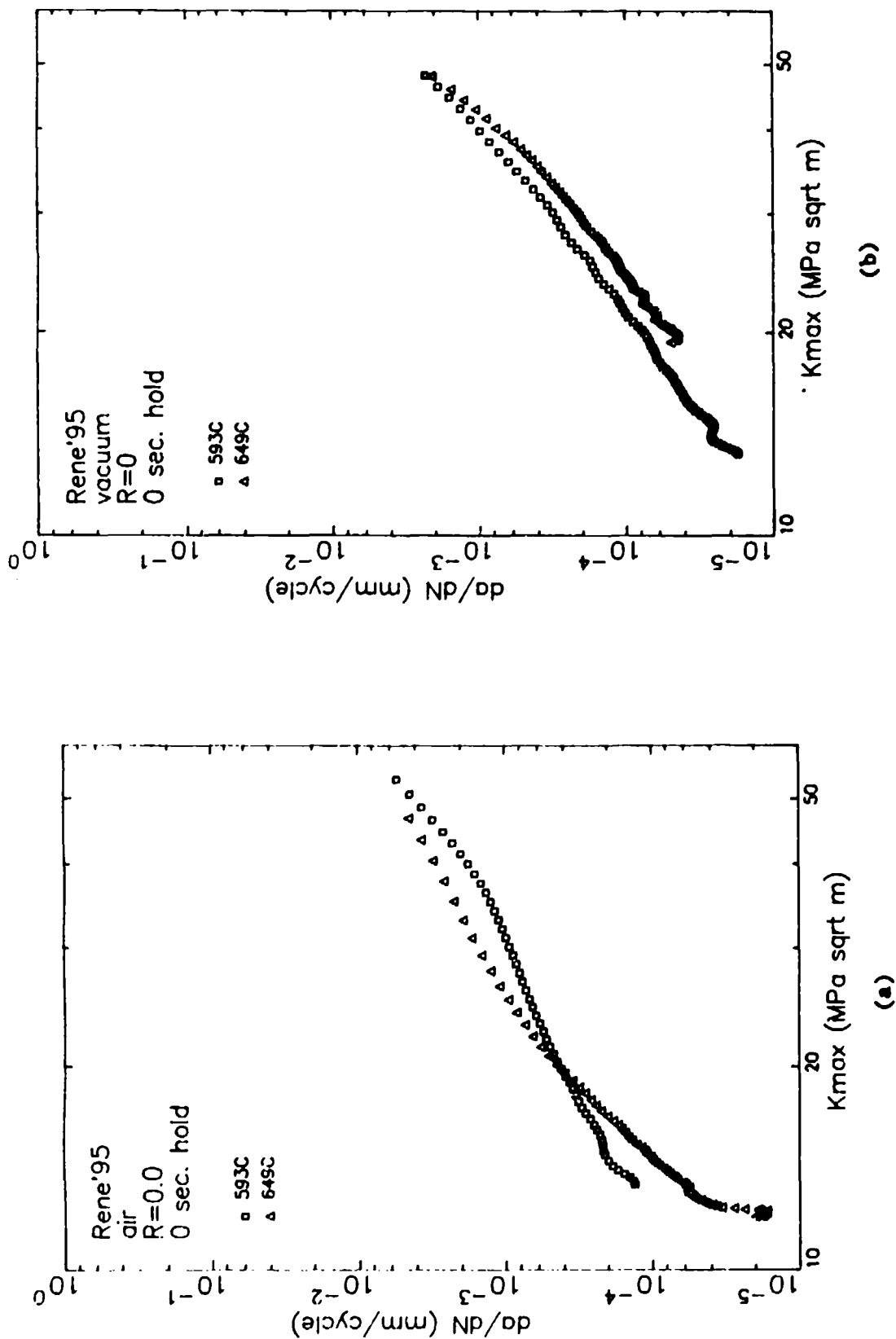


Figure 6.15: Influence of test temperature on Rene'95 crack growth rates at  $R=0$  and 0 second hold time in (a) air and (b) vacuum.

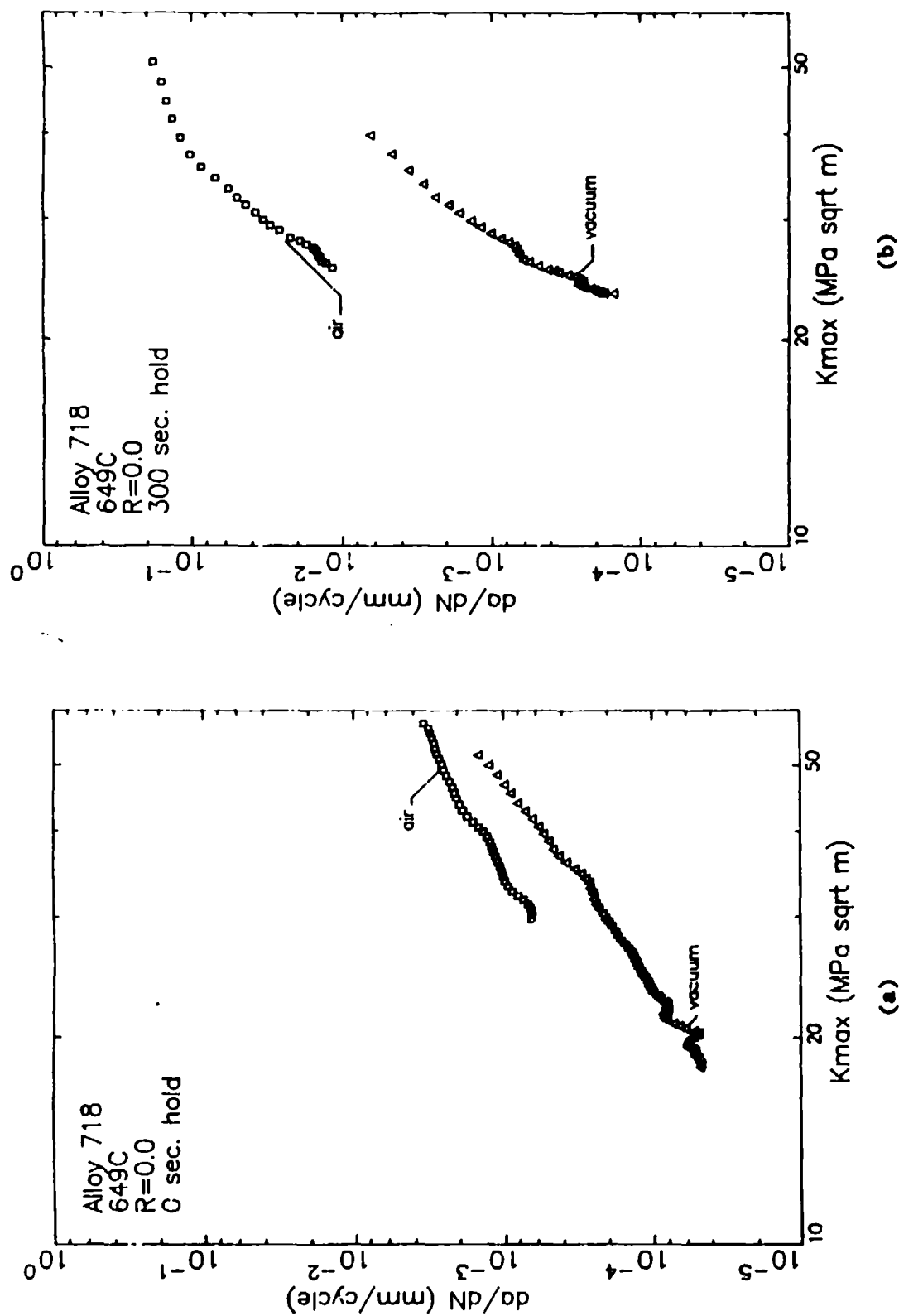


Figure 6.16: Comparison of Alloy 718 crack growth rates measured in air and vacuum for tests cycled at 649°C with R=0 and (a) 0 second hold time and (b) 300 second hold time.

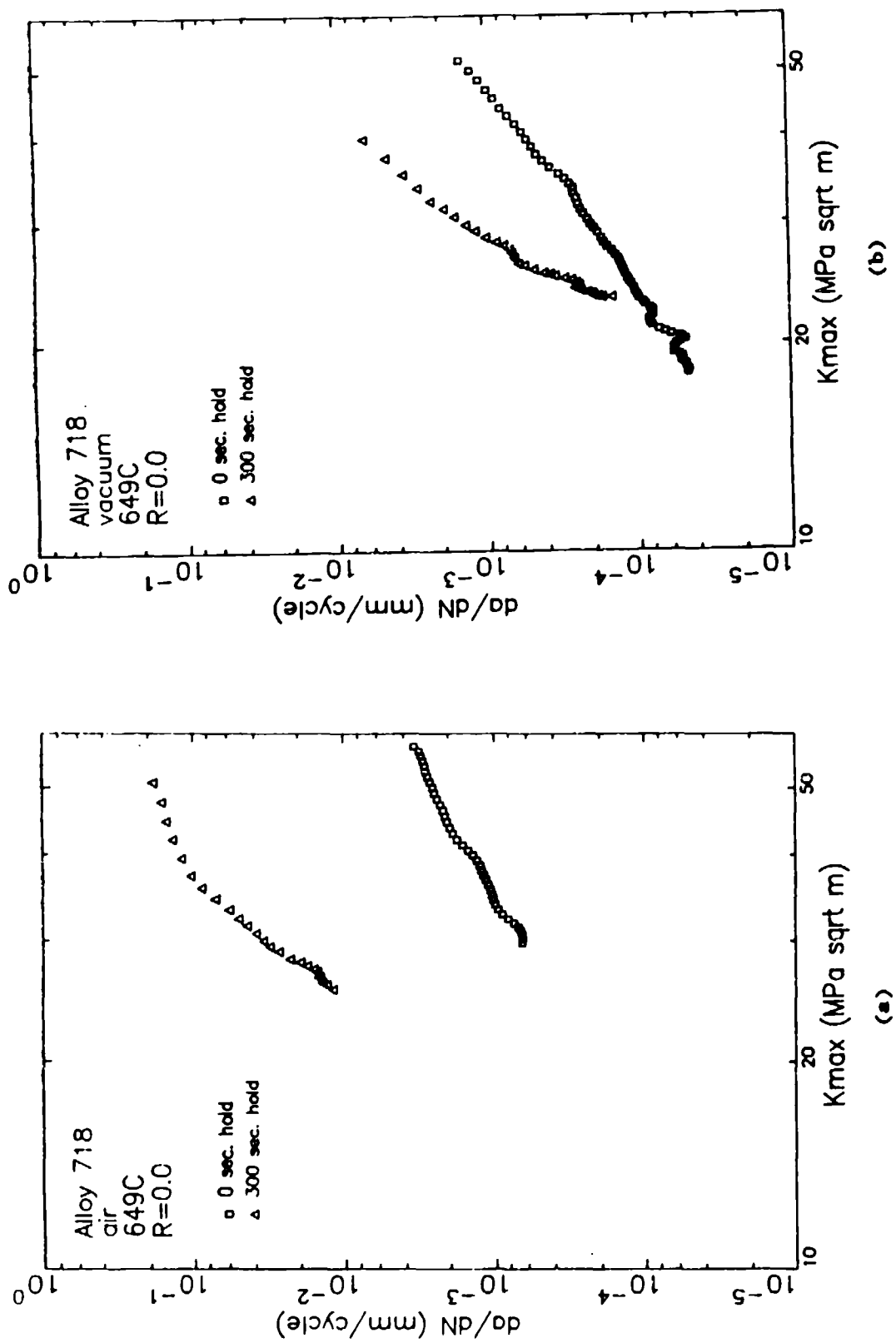


Figure 6.17: Influence of hold time on Alloy 718 crack growth rates at 649°C with R=0 in (a) air and (b) vacuum.

for the 300 second hold time vacuum test are only a factor of two faster than those of the 3 second cycle period vacuum test. These results indicate that the effects of environment on crack growth rates become much more significant with long hold times, whereas the accompanying effects on fracture morphology become negligible. The fracture morphology trends suggest the presence of either air or creep can induce the transition in crack propagation mode from transgranular to intergranular. Figure 6.18 shows SEM micrographs which illustrate the morphology observed at each  $K_{max}$  level for the two 649°C vacuum tests.

The 593°C vacuum specimen tested with a 3 second cycle exhibited transgranular failure at all three  $K_{max}$  levels. The crack growth rates were a factor of two to three slower than those of the 649°C vacuum specimen tested at the same conditions, which also fractured in a transgranular mode. Compared to the companion constant  $K_{max}$  air test, which fractured in a mixed mode at the low and high  $K_{max}$  levels and an intergranular mode at the intermediate  $K_{max}$  level (see Table 6.3), the vacuum testing resulted in similar crack growth rates.

#### 6.3.4 Alloy 718 Vacuum Test Fractographic Observations

SEM fractography of vacuum tested Alloy 718 was performed on the R-0, 649°C specimens tested with a 3 second cycle period and 300 second hold time segment. The specimen cycled with a 3 second period exhibited complete transgranular fracture. The SEM micrographs of Figure 6.19 illustrate the observed morphology at typical low, intermediate, and high  $K_{max}$  levels for constant  $K_{max}$  tests. This morphology is in sharp contrast to the intergranular appearance of the low  $K_{max}$  value in the constant  $\Delta K$  tests performed in air as shown in Figure 6.20. Fractography was not taken from the regions with the higher  $K_{max}$  values because they were preceded by hold time cycling and were possibly altered by the transient behavior described in Section 5.

The 300 second hold time specimen was examined at  $K_{max}$  levels corresponding to those of the 649°C hold time specimen tested in air

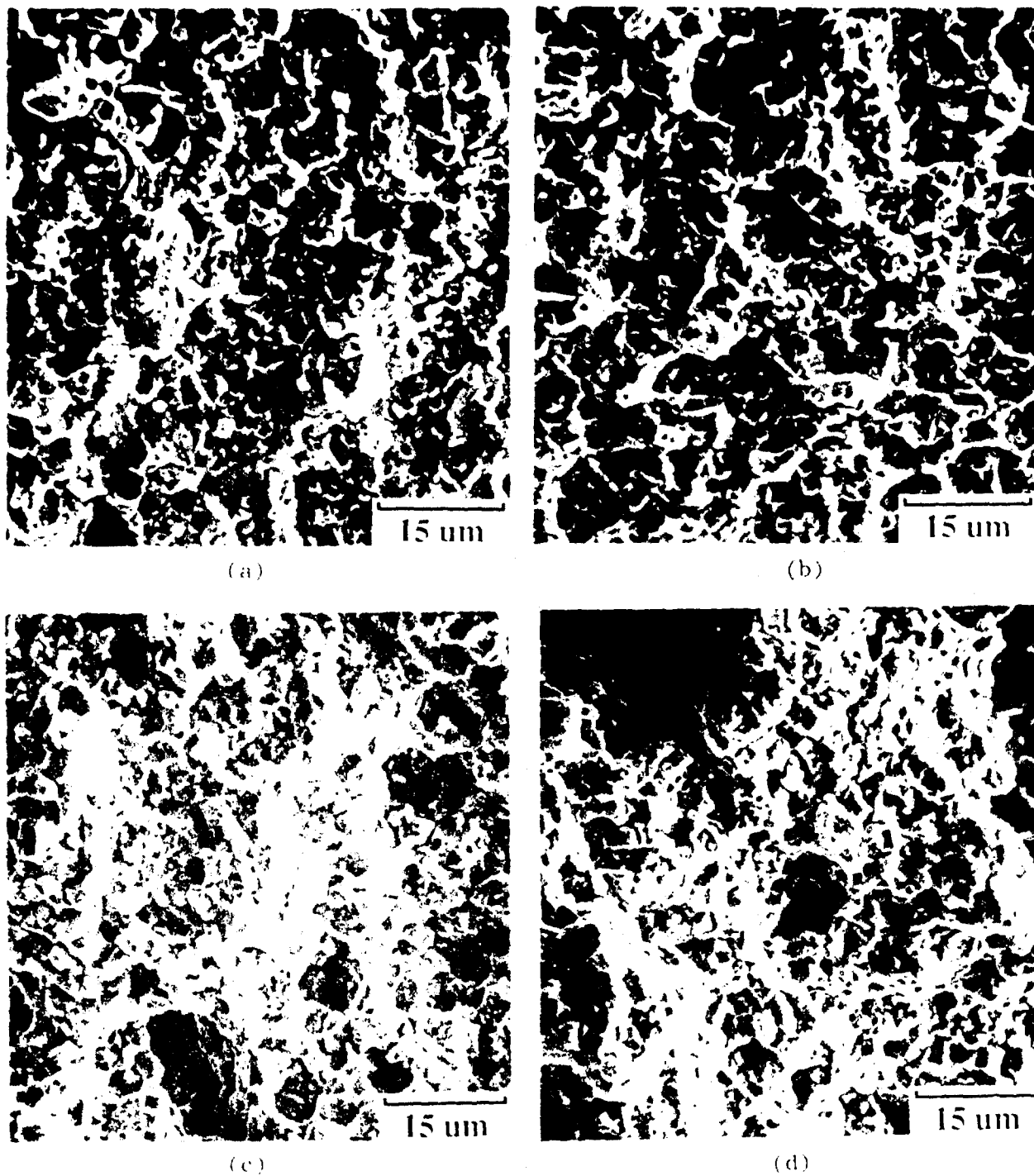


Figure 6.18: SEM micrographs showing Region II fracture morphology of K-Increase, R=0 Rene'95 specimens tested in vacuum at 649°C and conditions of (a) low  $K_{max}$ , 3 second cycle period, (b) intermediate  $K_{max}$ , 3 second cycle period, (c) low  $K_{max}$ , 300 second hold time cycle, and (d) intermediate  $K_{max}$ , 300 second hold time cycle.



(a)



(b)



(c)

Figure 6.19:

SEM micrographs showing Region II fracture morphology of  $K_{\text{max}}$ -increase,  $R=0$  Alloy 718 specimen tested in vacuum at  $649^{\circ}\text{C}$  with a 3 second cycle period; (a) low  $K_{\text{max}}$ , (b) intermediate  $K_{\text{max}}$ , and (c) high  $K_{\text{max}}$ .





Figure 6.20: SEM micrograph showing Region II fracture morphology for constant  $\Delta K$ , R=0 Alloy 718 specimen tested in air at 649°C with a 3 second cycle period (low  $K_{max}$  level).

(described in the previous section). Due the small range in  $K_{max}$  for the vacuum test, the comparison was limited to the intermediate  $K_{max}$  level. The SEM micrograph of Figure 6.21 shows that intergranular fracture occurred. Intergranular fracture was also observed for the 300 second hold time segment of the air test specimen at this  $K_{max}$  level.

#### 6.3.5 Discussion of Vacuum Results

The vacuum test results showed a strong influence of environment on the crack growth rates as has been reported by previous investigators (12-14,18,25,29). It was noteworthy that 300 second hold time cycling at 649°C in vacuum accelerated the crack growth rates relative to the no hold time (20 cpm) cycling and resulted in a transition from a transgranular to intergranular fracture mode for both Rene'95 and Alloy 718. A similar change in fracture mode and crack growth rates was observed when comparing zero hold time tests in air and vacuum. The Rene'95 crack growth rate data for these three cycling condition are shown in Figure 6.22. In the lowest crack growth rate condition, cracks grow in a transgranular mode. Increasing the hold time in vacuum or changing the environment to air results in a similar increase in crack growth rates and intergranular crack propagation. These results suggest that intergranular crack growth can be caused by either creep deformation or environmental damage. This behavior suggests that there is a strong creep-fatigue-environment interaction during the time-dependent crack growth in nickel-base superalloys. The five fold acceleration in crack growth rate shown in Figure 6.22 is larger than anticipated from the superposition concept and may suggest that intergranular crack propagation is inherently faster than transgranular propagation.

Figure 6.23 shows the 649°C crack growth data for the same three cycling conditions in Alloy 718. Again the condition with the lowest propagation rates has a transgranular crack growth mode. Increasing the hold time in vacuum or adding the influence of air increases the crack growth rate and causes a transition from transgranular to intergranular failure. The crack growth rates are not as similar for the latter two conditions in Alloy 718 as compared to Rene'95; however, the overall trends are the same.

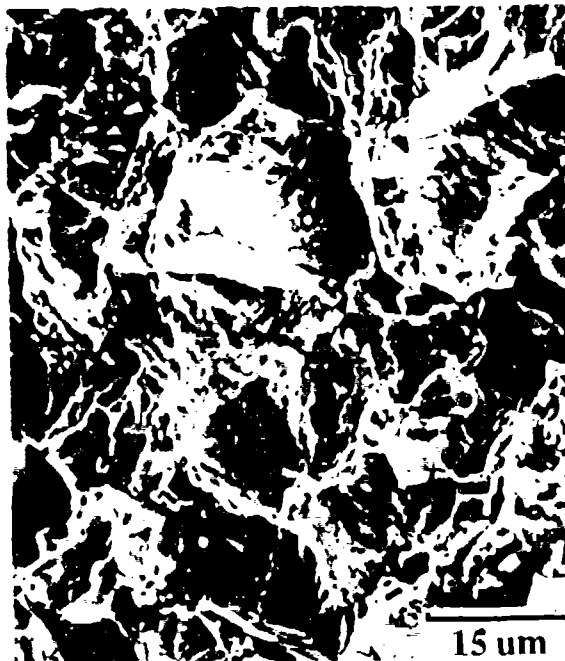


Figure 6.21: SEM micrograph showing Region II fracture morphology of K-increase, R-O Alloy 718 specimen tested in vacuum at 649°C with a 300 second hold time cycle (intermediate K level).

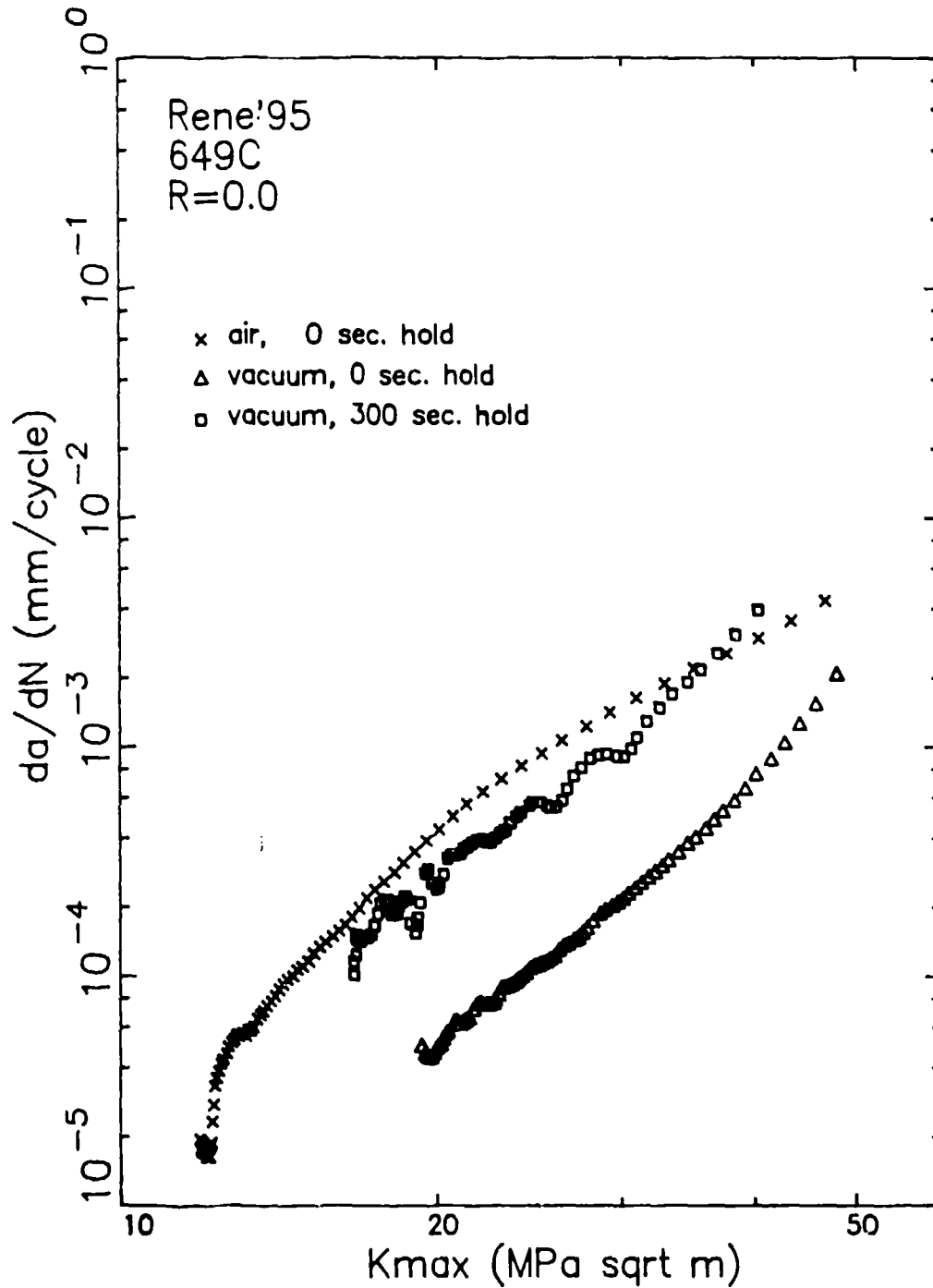


Figure 6.22: Comparison of Rene'95 crack growth rates measured at 649°C for R=0 cycling with 0 second hold time in air and vacuum and 300 second hold time in vacuum.

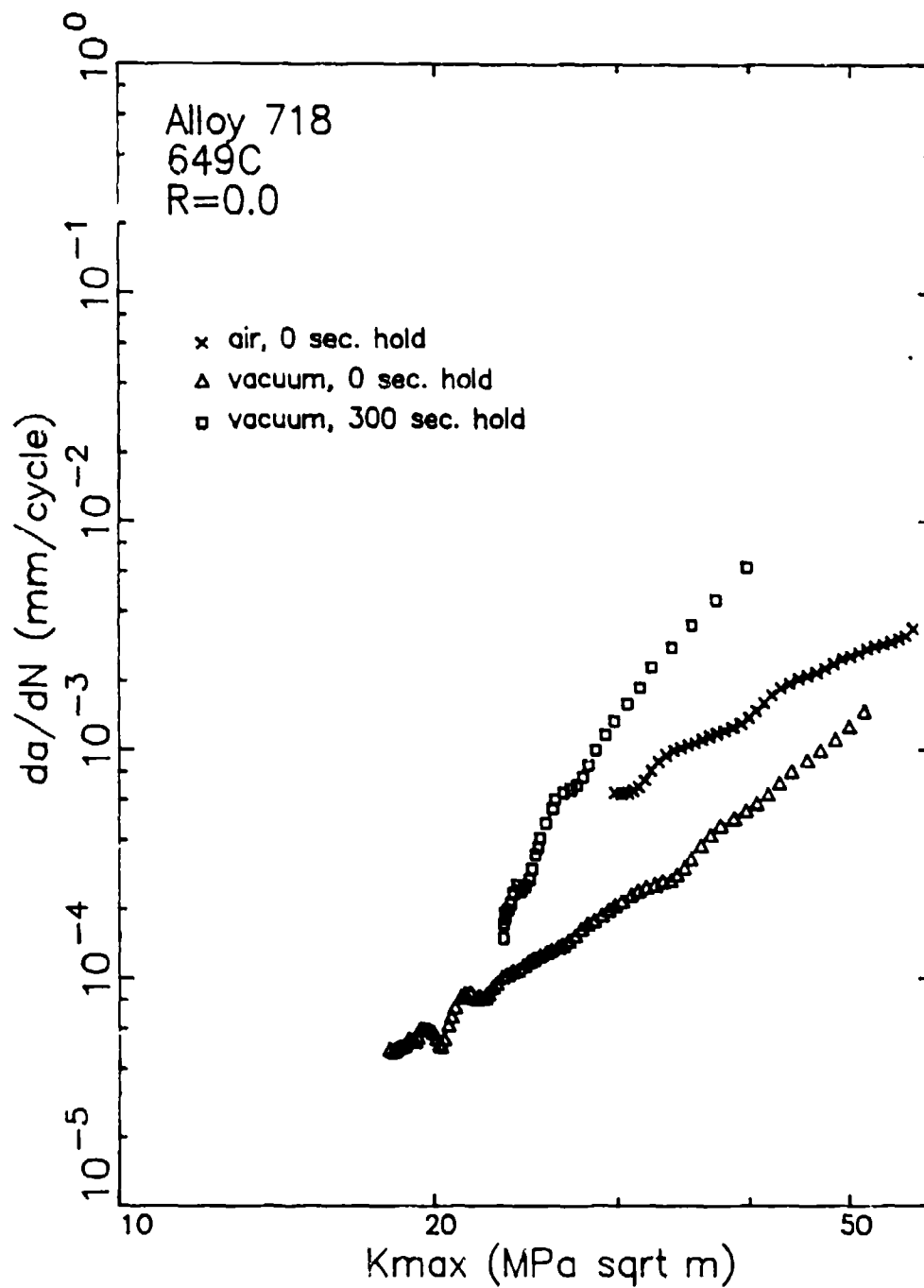


Figure 6.23: Comparison of Alloy 718 crack growth rates measured at 649°C for R=0 cycling with 0 second hold time in air and vacuum and 300 second hold time in vacuum.

#### 6.4 METALLOGRAPHIC SECTIONING STUDIES

A metallographic study was performed to determine whether crack tip blunting could be detected through metallographic examination of a crack. For this study, Rene'95 and Alloy 718 specimens were subjected to threshold testing using a R=0, 300 second hold time cycle. This test condition was expected to promote blunting. Both specimens were left intact after the crack arrested. The crack tip region was studied after step polishing in the specimen thickness direction.

The optical micrographs of Figure 6.24a show the entire crack observed for the Rene'95 specimen at approximately mid-thickness in a low magnification montage. Figures 6.24b and 6.24c show high magnification optical micrographs of the crack tip region before and after etching, respectively. From Figure 6.24a, it can be seen that the crack faces remain relatively tightly spaced over the entire crack length. Near the position of crack arrest, several discontinuous segments of cracking are present, Figure 6.24b, and the crack tips of each of these segments, as well as short branched segments, appear relatively sharp. The etched micrograph of Figure 6.24c shows that the crack was following an intergranular path.

The optical micrographs of Figure 6.25 illustrate characteristics of the crack and crack tip region for the Alloy 718 specimen at approximately mid thickness. The low magnification montage, Figure 6.25a, shows a relatively large separation between the crack faces over the entire pre-arrest, steady state growth area. From the high magnification micrographs showing the crack arrest region, Figures 6.25b, 6.25c, and 6.25d, it can be seen that the cracking is discontinuous and that prior to the end of the cracking, a large grain has acted as an obstacle in the general propagation path. These micrographs (Figures 6.25c and 6.25d) also show that the crack is following an intergranular path and that the crack tips of various segments appear relatively sharp (Figure 6.25b). It is evident, however, that the separation between crack faces in the region of crack arrest is still relatively large.

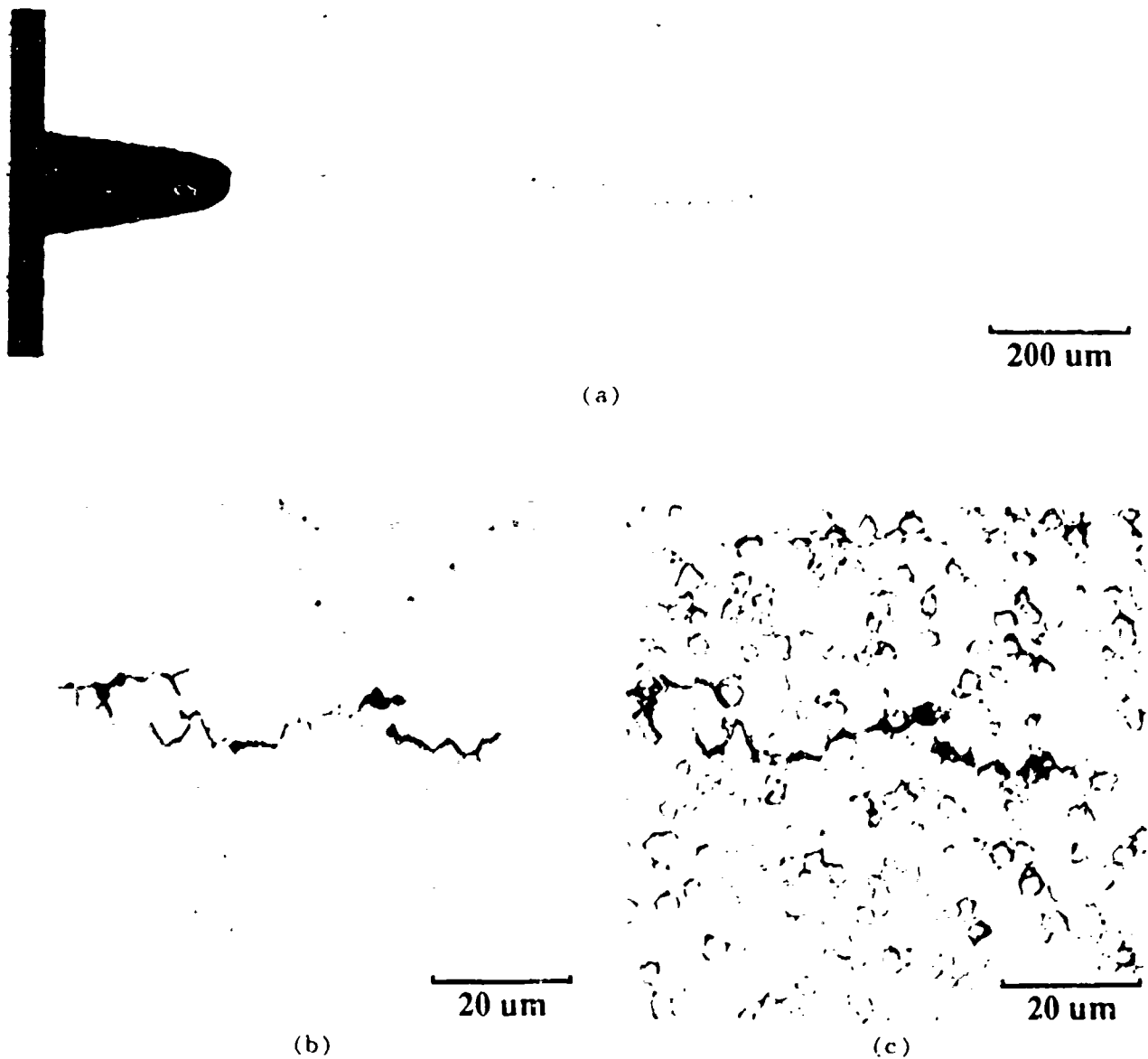


Figure 6.24: Optical micrographs showing crack in K-shed, R=0 Kene'95 specimen tested in air at 649°C with a 300 second hold time cycle; (a) low magnification view of entire crack, (b) high magnification view of crack in arrest region (unetched microstructure), and (c) high magnification view of crack in arrest region (etched microstructure).

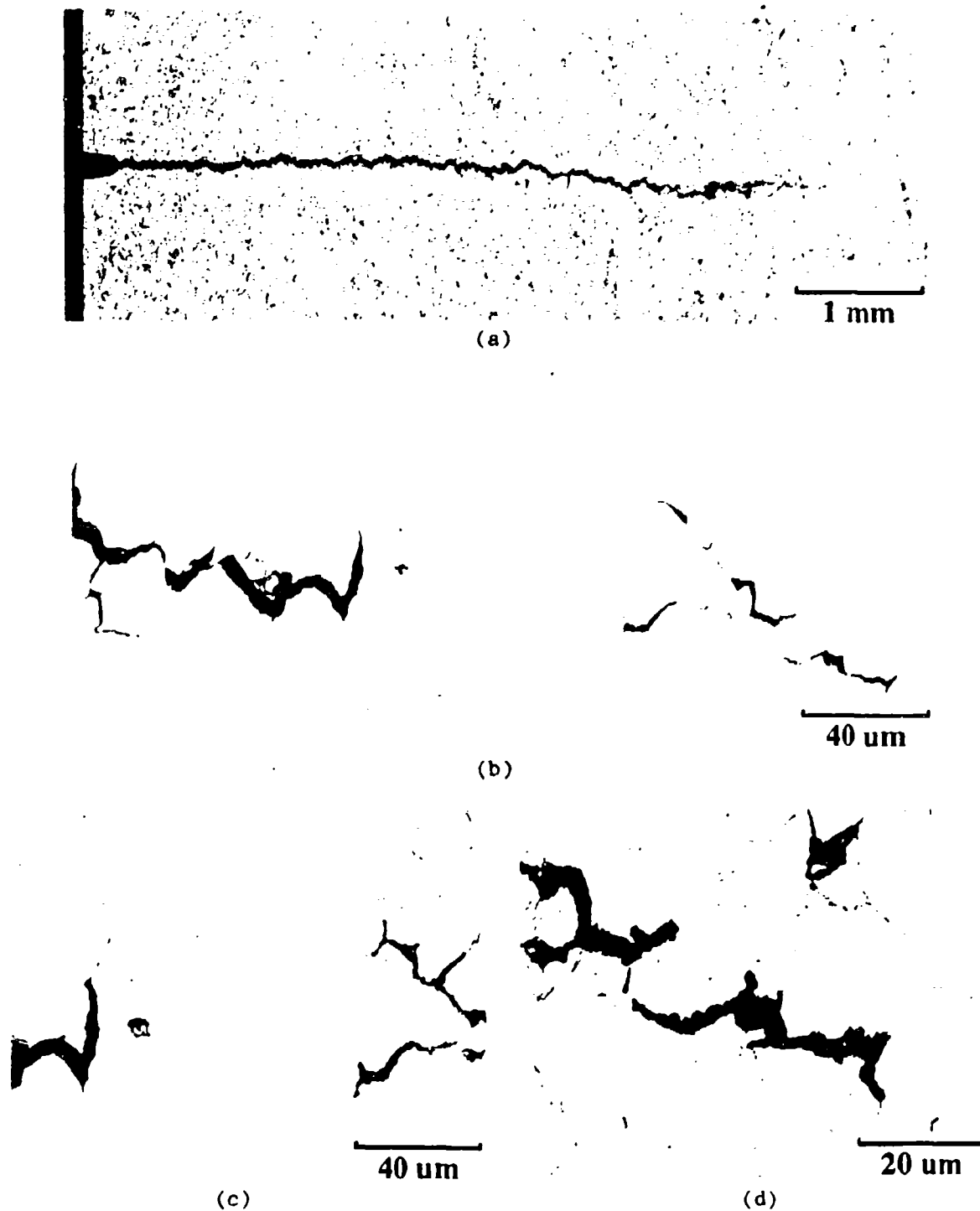


Figure 6.25: Optical micrographs showing crack in K-shed, R-0 Alloy 718 specimen tested in air at 649°C with a 300 second hold time cycle; (a) low magnification view of entire crack, (b) high magnification view of crack in arrest region (unetched microstructure), and (c) and (d) high magnification views of crack in arrest region (etched microstructure).



Although evidence of blunted crack tips was not detected by the metallographic study, several differences between the Rene'95 and Alloy 718 specimens were observed. The crack in the Alloy 718 specimen showed a larger separation between its two faces and was subject to large grains acting as obstacles for the preferred intergranular growth mode. Possible explanations for the large separation include massive Mode II displacement giving rise to a shifting of the crack faces (ie., one of the mechanisms believed to promote roughness-induced closure), a large bending component for this specimen geometry and loading condition, or a large amount of localized creep deformation in the vicinity of the crack as it propagates and eventually arrests. Since the separation appears too large for the Mode II related explanation, and the bending component would be both small and elastic, it is believed that localized creep was principally responsible for the wide crack face separation. The large difference between the Rene'95 and Alloy 718 specimens is consistent with the lower creep capability of Alloy 718.

#### 6.5 MECHANISM TESTING PROGRAM

As shown in Section 5, the constant  $\Delta K$  testing of Alloy 718 resulted in some peculiar transients in crack growth rates when transitioning from 300 second hold time cycles to 3 second cycle periods. This section will describe several additional experiments performed to investigate this behavior.

Examination of the data from Alloy 718 tests described in Section 5 showed that the transient zone could be described by the distance over which the crack growth rate was accelerated. In this report, that distance will be called a damage zone. This terminology does not imply anything about the damage or the mechanism leading to the more rapid crack growth, but only that there apparently is a zone of damage where the crack growth is more rapid. Figure 6.26 shows the size of this zone as a function of  $K_{max}$  and R ratio for the 593°C tests previously described in Section 5. These data show that the zone increases in size with K level and R-ratio. The dependency on K suggests that it is somehow related to the size of the plastic or creep zone around the crack tip. The R-ratio dependency may suggest a high sensitivity to creep deformation. The creep process would be interrupted with large amounts of

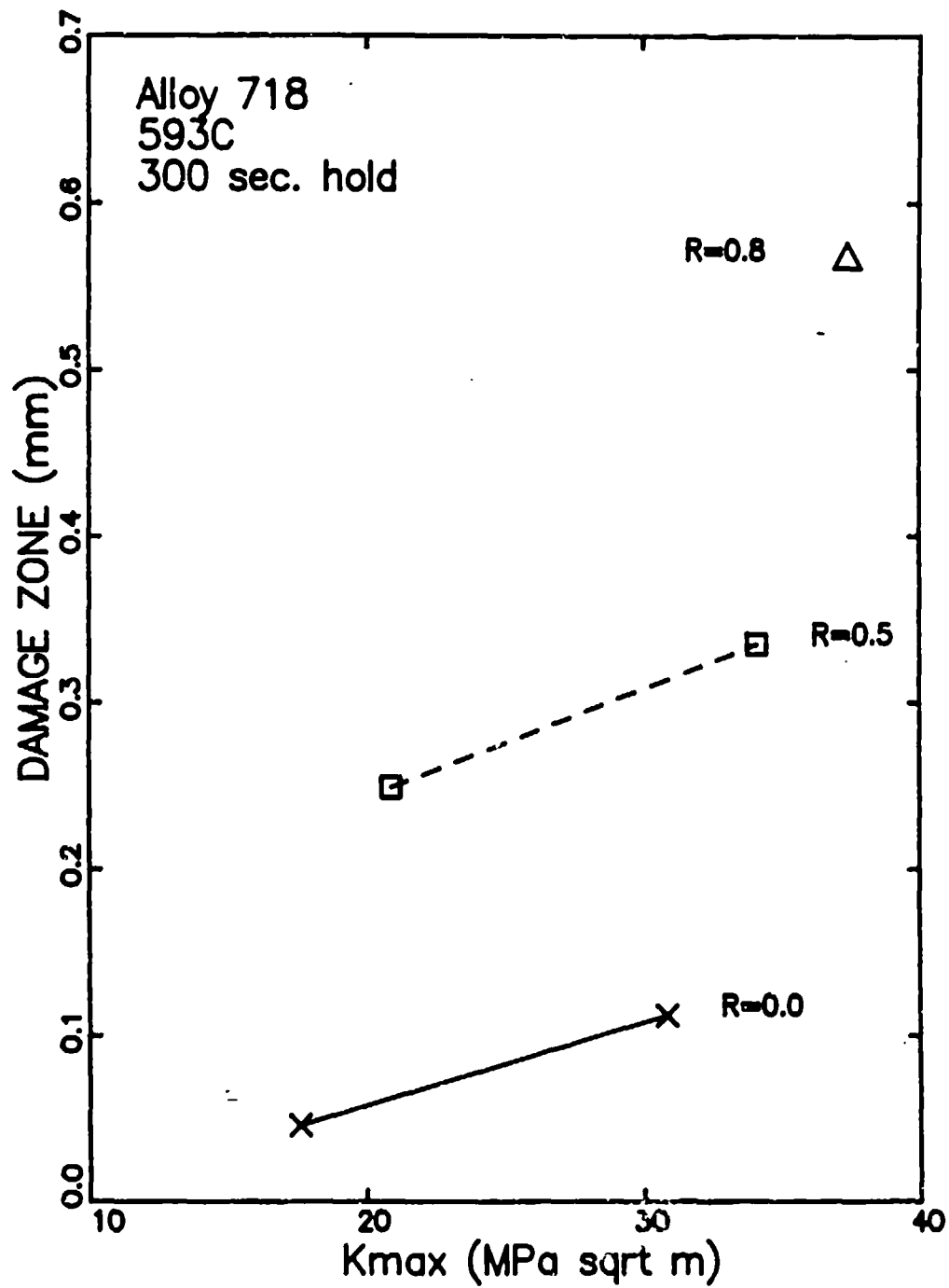


Figure 6.26: Variation of damage zone size with R-ratio and  $K_{max}$  for Alloy 718 cycled at 593°C with a 300 second hold time.

cyclic loading (low R) and therefore the size of this zone would be small. This size effect trend does not rule out the possibility of a high diffusivity zone where an embrittling species (presumably oxygen) could create a low ductility region at the tip of the crack.

To further investigate the development of this zone, crack growth experiments were performed where constant  $\Delta K$  segments with hold times of 4, 30, and 300 seconds were separated by segments with 3 second cycles. This is shown in Figure 6.27 for an Alloy 718 test performed at 649°C with a R-ratio of 0.0. After the 300 second hold time segment, another 3 second cycling segment was performed. The specimen was then held at zero load for a period of six to eight hours. The intent of this zero load hold time was to determine if a damage zone would form by diffusion of the damaging species into the crack tip zone. It would have been more desirable to do this under a small load, but concern about static crack growth ruled out the use of applied loads. After the zero load hold, a final 3 second cycle period was performed. Tests of this type were conducted using Rene'95 and Alloy 718 specimens heated to 593 and 649°C. The specimens were cycled at R=0 with a  $K_{max}$  of approximately 30 MPa/m. The size of the damage zone was measured after each hold time segment. These results are shown in Figure 6.28. Increasing temperature and hold time duration increased the size of the damage zone. The zones were much larger in Alloy 718 than in Rene'95. No damage zones could be detected in the Rene'95 test performed at 593°C. No damage was detected after any of the zero load hold time exposures independent of test temperature or material. These results further suggest that the zone is related to time dependent deformation (creep) and not to the diffusion of some embrittling species into the deformed zone at the tip of the crack; however, crack closure could prevent the crack tip from being exposed to the environment.

The environment can be eliminated by performing tests in vacuum, so the transition from 300 second hold time cycling to 3 second period cycling was investigated using all four combinations of air and vacuum on Alloy 718 specimens cycled at R=0 with  $K_{max}$  = 40 MPa/m. These results are shown in Figure 6.29. The damage zone was only observed when the 20 cpm cycling was performed in air, independent of whether the hold time cycling was performed

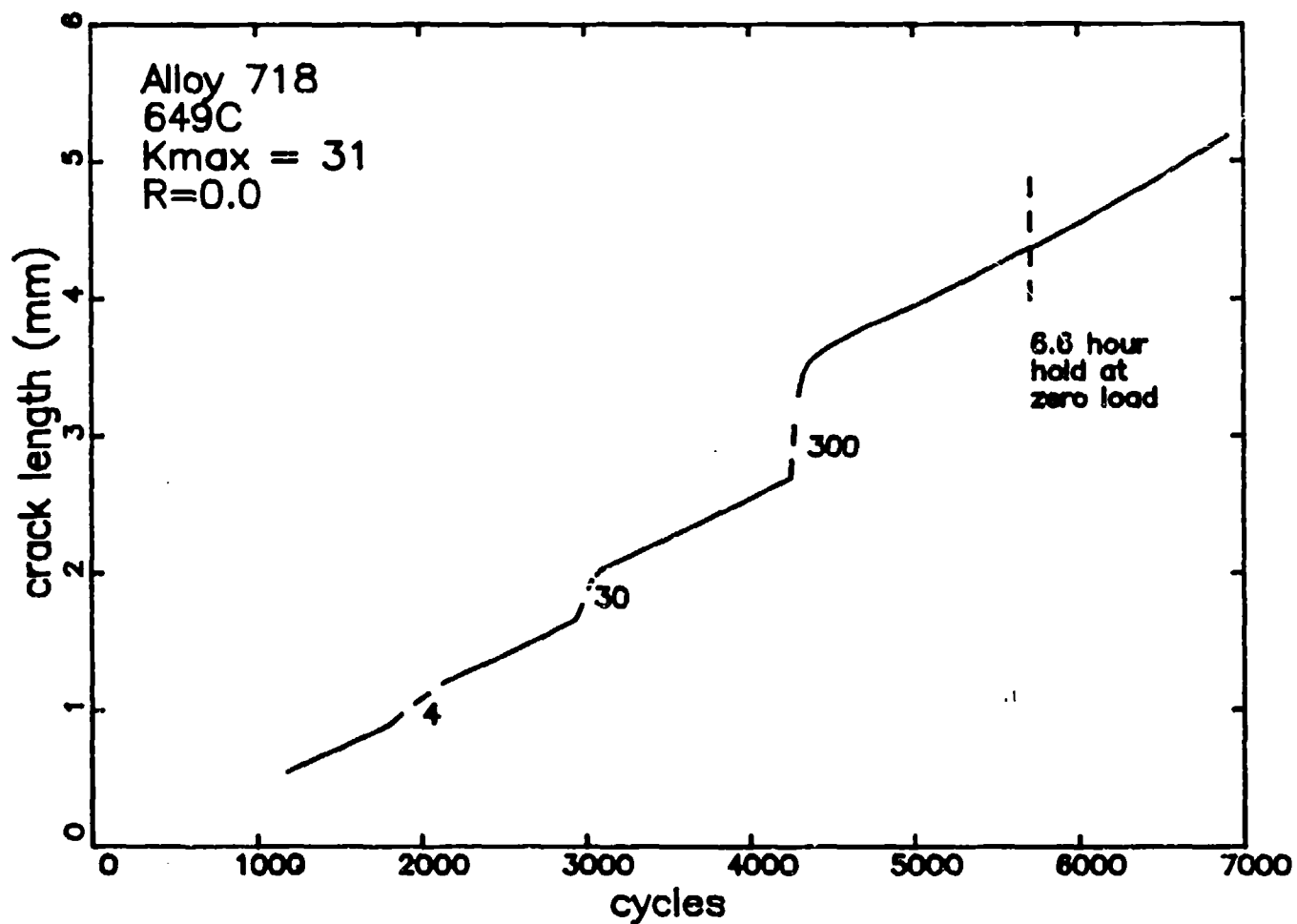


Figure 6.27: Variation of crack length with cycles for damage zone experiment in air.

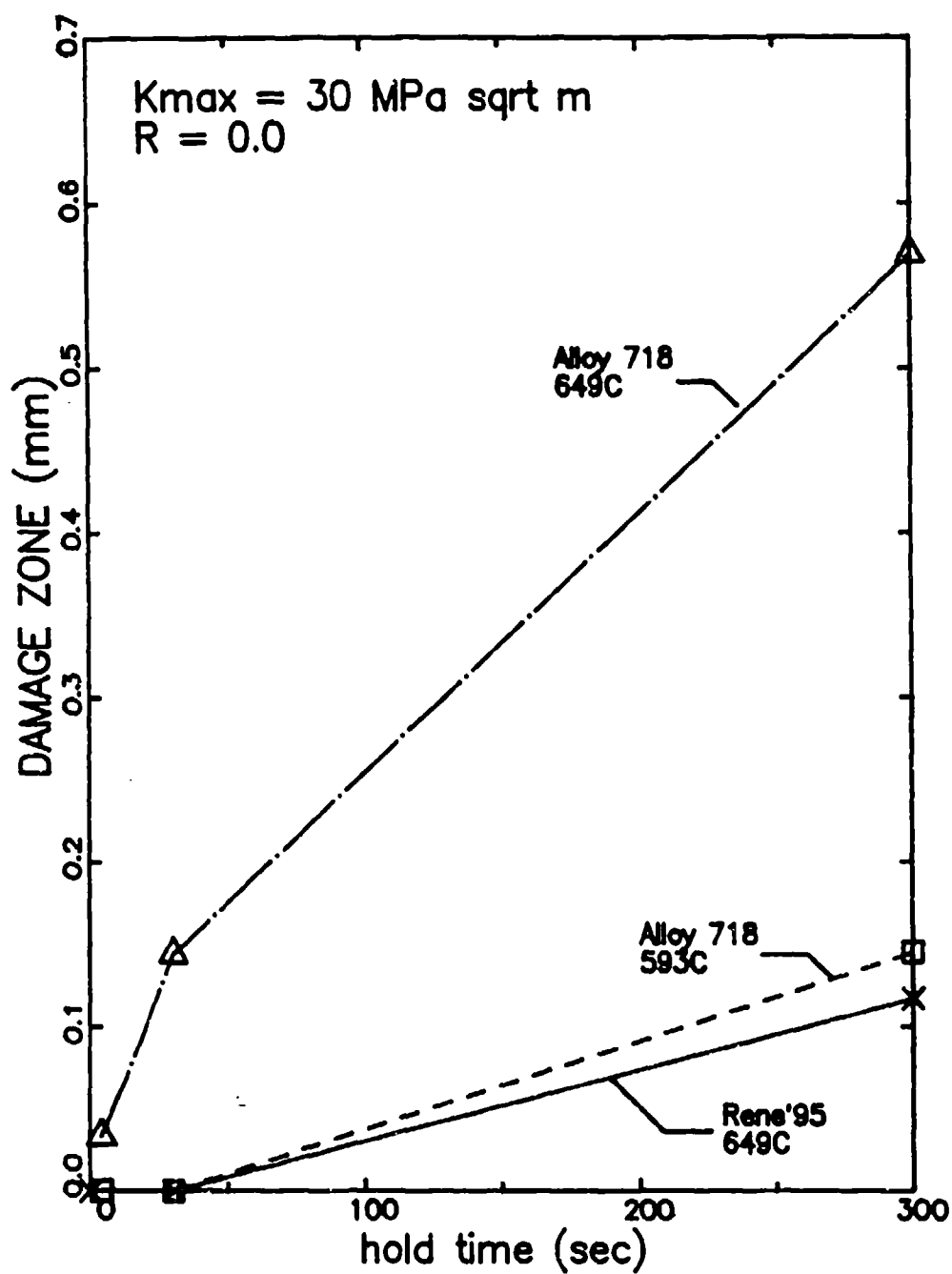


Figure 6.28: Variation of damage zone size with hold time, material, and test temperature as measured in damage zone experiment in air.

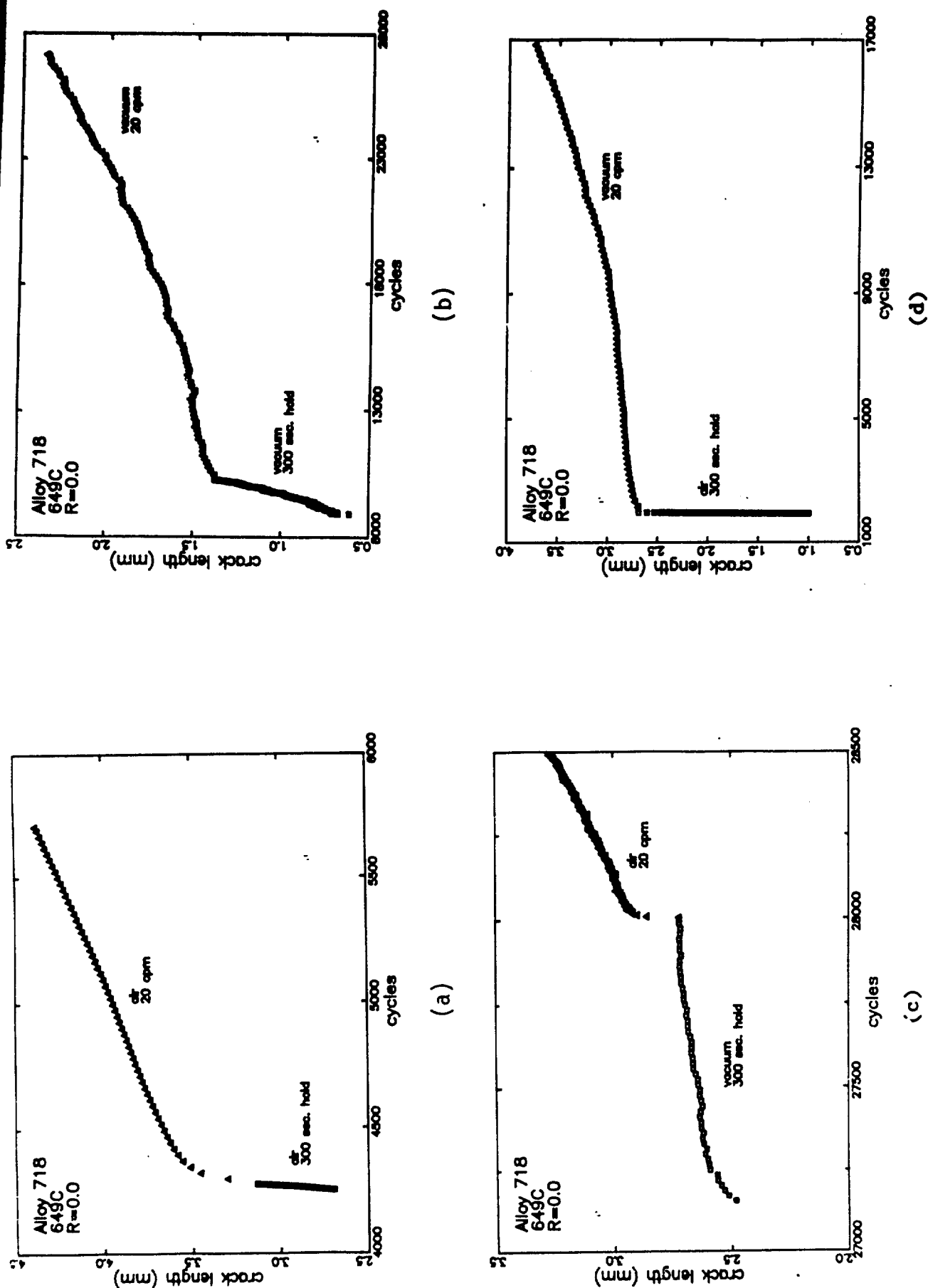


Figure 6.29: Variation of crack length with cycles for the transition from 300 second hold time to 20 cpm cycling for (a) air/air cycling, (b) vacuum/vacuum cycling, (c) vacuum/air cycling, and (d) air/vacuum cycling.

in air or vacuum. The damage zone was never observed when the rapid cycling was performed in vacuum. These data suggest that a damage zone is created during the 300 second hold time cycling no matter what the environment, but for the accelerated crack growth to occur oxygen must be present at the crack tip during the rapid cycling. These experiments further document the close interaction between creep and environment in the mechanisms of time-dependent crack growth.

Another interesting behavior which occurred in the tests performed in this investigation was the tunneling of the cracks where crack growth was faster in the interior of the specimens relative to that along the specimen surface. The amount of tunneling was quantified by measuring the difference between the crack length at the mid-thickness position and the average of the two surface crack length measurements. An increase in this value corresponds to a larger difference between the surface and center crack lengths and thus more tunneling. The results for the R=0 and R=0.5 constant  $\Delta K$  and retardation tests are reported in Table 6.5. These measurements came after the highest  $K_{max}$  or  $K_{01}$  300 second hold time segment and have similar values of  $K_{max}$  or  $K_{hold}$ . These results show that increasing temperature and R-ratio increases the amount of tunneling. The tunneling is also more pronounced in Alloy 718 than Rene'95, the more creep resistant material. These data also show that a 10% overpeak has either little effect or increases the amount of tunneling relative to the non-overpeak, constant  $\Delta K$  results. The 20% overpeak tests exhibit less tunneling than the 10% overpeak tests. It was also noted in the threshold tests that the amount of tunneling increased with hold time, cycle period and  $K_{max}$  level.

The non-overpeak results show that increasing the amount of time for creep deformation results in more tunneling. This trend is identical to the damage zone sizes. This suggests that the criterion for crack advance is very sensitive to state of stress. The center of a through crack specimen is much closer to a plane strain condition than the surface location which is very close to a plane stress condition. The lack of constraint in the plane stress loading apparently results in significantly lower crack growth rates. This suggests that the models developed in this investigation for the growth of

Table 6.5: Crack Curvature Data

		<u>Rene '95</u>		<u>Alloy 718</u>	
		<u>593°C</u>	<u>649°C</u>	<u>593°C</u>	<u>649°C</u>
R=0.0	simple cycle	0.45	0.89	0.37	1.72
	10% overpeak	0.43	0.84		1.80
	20% overpeak	0.40	0.29		0.55
R=0.5	simple cycle	1.06	1.18	1.18	1.63
	10% overpeak	0.96	1.64		3.61
	20% overpeak	0.66	0.38		2.12



through cracks may have to be modified significantly if they are to be applied to surface cracks.

The amount of tunneling in the retardation tests is very interesting. The value of  $K_{hold}$  in these tests were similar to the  $K_{max}$  values in the constant  $\Delta K$  tests, so the values of  $K_{01}$  were higher. The larger amount of tunneling sometimes observed in the 10% overpeak tests suggests that creep deformation is related to the maximum value of  $K$  in the cycle and not necessarily the  $K$  during the hold time. The decreased amount of tunneling in the 20% overpeak tests combined with the detection of the transient damage zones in the Alloy 718 retardation tests suggests that although creep deformation is occurring during hold time following the overpeaks, but that the retardation is suppressing the static crack growth. The possibility of creep-induced stress relaxation during this type of cycle may help to rationalize the larger effect of small overpeaks on static crack growth relative to cyclic crack growth.

## 6.6 DISCUSSION

fractographic study of Rene'95 specimens tested in air indicated that cyclic crack growth is associated with transgranular fracture while static or time dependent crack growth is associated with intergranular fracture. Transgranular fracture was observed for the 538°C, 20 cpm test, which represents nominally cyclic behavior, while intergranular fracture was observed for the 593 and 649°C static tests. The fractographic study of specimens tested under a wide range of test conditions at 593 and 649°C showed trends in fracture morphology that were consistent with these results. As hold time or cycle period increased for a given  $K_{max}$ , it was typically observed that transgranular fracture diminished. In the comparison of frequency and hold time effects, it was also typically observed that the hold time cycle promoted intergranular fracture. The difference in fracture mode under cyclic and static conditions suggests that superposition is the appropriate approach for modeling time dependent crack growth.

The fractographic studies also revealed evidence of a competition between static crack growth damage mechanisms and creep-induced crack tip blunting or stress redistribution. As  $K_{max}$  level increased for the 538°C test, the fracture morphology for the 300 second hold time cycle transitioned from predominantly intergranular to entirely transgranular. It was also observed that the high R-ratio, 593°C frequency test showed increased evidence of transgranular fracture. In all other cases, increasing the R-ratio diminished transgranular fracture. These findings indicate that cyclic behavior has dominated conditions where more pronounced static behavior would be expected. The trends in R=0.8 threshold behavior also suggested the presence of competing mechanisms. As hold time increased, the threshold initially diminished as expected for a more pronounced influence of static damage, but reversed this trend for the 300 second hold time condition. This suggests that a creep-induced blunting or stress redistribution mechanism may become more dominant than a static damage mechanism for cycles with long hold times. Metallographic sectioning of an Alloy 718 threshold crack growth specimen cycled at 649°C with a 300 second hold time showed no evidence of localized crack tip blunting, but there was a relatively large crack opening over the entire length of the crack. This suggests that creep-induced stress redistribution may be more important than localized blunting. Stress redistribution would locally relax the stresses at the crack tip so that larger applied loads would be necessary to propagate a crack. The influence of this type of mechanism would be most easily observed for low crack growth rates where the relaxation can occur over a significant period of time without the crack growing through the relaxation zone. This is a potential explanation for the trend of increasing threshold values with increasing frequency or hold time for the R=0 tests. Further evidence of stress relaxation and redistribution was observed in a 649°C static test where a significant increase in  $\Delta K$  after steady growth in a 20 cpm precrack was necessary to promote static crack growth.

Hold time crack growth experiments on both Alloy 718 and Rene'95 specimens resulted in accelerated crack growth and intergranular fracture modes. The damage zone experiments strongly suggest that damage is created by creep, but must be activated by the environment. Both sets of experiments

suggest that the time dependent crack growth process in nickel-base superalloys is caused by a complex interactions between creep, fatigue, and environment.

The results of the mechanism tests strongly suggest that creep induced deformation can result in both localized stress relaxation and damage zones. Linear elastic fracture mechanics does not describe the apparent stress relaxation behavior. It may be necessary to use nonlinear fracture mechanics parameters to model the time dependent crack growth for situations which are dominated by the stress relaxation phenomenon.

## 7.0 CRACK GROWTH MODELING

This section of the report will describe the models used to determine the time-dependent crack growth behavior and their application to predict the 649°C crack growth data of Alloy 718 and Rene'95. A description of a computer code which implements the models will also be described. This description preceeds the comparison of the predictions and experimental data because the code was used extensively throughout those evaluations.

### 7.1 CRACK GROWTH MODELS

Four basic models were developed or utilized during this investigation:

1. interpolation model of the threshold behavior
2. interpolation model of time-dependent crack growth
3. superposition model of crack growth
4. retardation model

Each of these will be discussed in separate sections. The threshold model was common to both the interpolation and superposition model and the retardation model is applicable only to the superposition model.

The sigmoidal (Knaus) crack growth equation was selected for describing the crack growth behavior in both the interpolative model and the cyclic portion of the superposition model. This selection was made because of the ability of the sigmoidal equation to independently adjust the portions of the crack growth curves (Regions I, II, and III). The Sinh curve is symmetric relative to its inflection point, so as the threshold is increased, the apparent toughness (onset of Region III) is also reduced. Based on the observed changes in threshold with R-ratio, cycle period, and hold time, it does not appear that the Sinh model can accurately model this behavior. The inability of the Sinh equation to adequately treat these phenomena primarily results from having four constants rather than the six in the sigmoidal equation. The number of variables in the Sinh equation could be increased to obtain the additional flexibility which already exists in the sigmoidal

equation. This approach was not taken because the resulting equation would probably have many of the same characteristics as the sigmoidal equation. In addition, there is a relatively large experience base with the sigmoidal equation to model the transitions between the various parts of the crack growth curve.

#### 7.1.1 Interpolation Model Of Threshold Values

Variation of the threshold behavior with hold time and cycle period were highly dependent on the R-ratio of the cycle. It appears that this results from the competition between static crack growth and stress redistribution near the crack tip. This competition cannot be treated explicitly using linear elastic fracture mechanics (LEFM) principles, so it was approximated using an interpolative model with LEFM parameters.

The model was developed in terms of the R-ratio ( $R$ ), the cycle ramp time ( $V$ ) and the hold time ( $T$ ). Using this nomenclature,  $T$  equals zero for the frequency tests and  $V$  equals 3 seconds for the constant  $\Delta K$  hold time tests. The form of the interpolation model equation was developed based on several limiting cases:

1. As  $V$  and  $T$  approach zero, the influence of  $R$  will follow a Walker type relationship.
2. For static crack growth ( $V=0$ ,  $T$  approaches infinity, and  $R$  approaches unity), the threshold value should approach the static threshold  $(K_{th})_s$ .
3. The increase in threshold with  $V$  or  $T$  should increase with  $R$  ratio as was observed in experiments.

The equation developed to meet these boundary conditions is:

$$(K_{th})_{max} = (K_{th})_s + [K_0(1-R)^{-m} - (K_{th})_s] \exp(-AV-BT) + C(1-R) \ln(1+DV+ET) \quad (7.1)$$

where  $K_0 = (K_{th})_{eff}$  for cyclic (non time dependent) loading

$(K_{th})_s$  = static crack growth rate threshold

A, B, C, D, E = material constants

The second term of this expression diminishes with more time-dependent conditions (increasing V and/or T) so that  $(K_{th})_{max}$  approaches  $(K_{th})_s$ . The third term results in an increase of  $(K_{th})_{max}$  with more time-dependent conditions. The amount of this increase diminishes with increasing R-ratio. The concept behind this approach is that cyclic plasticity will generate mobile dislocations which may then enhance the ability of the material to creep. Although this seems correct, it is not known to have been demonstrated experimentally for this materials.

This expression meets the three boundary conditions described above. For non time dependent conditions ( $V=0$ ,  $T=0$ ), the exponential term is unity and the logarithmic term is zero so Equation 7.1 reduces to

$$(K_{th})_{max} = K_0(1-R)^{-m} \quad (7.2)$$

which is identical to the Walker relationship. For static crack growth, the second and third terms in Equation 7.1 are zero so  $(K_{th})_{max}$  is equal to  $(K_{th})_s$ .

The values of the constants  $K_0$ ,  $m$ , and A through E were evaluated using nonlinear optimization techniques. This value of  $(K_{th})_{max}$  was then used in the interpolation model.

The threshold value calculated using the interpolation threshold model was used as the threshold value for the cyclic crack growth curve. This required adjustment of the cyclic crack growth constants so not to alter the

Region II cyclic crack growth rates. The values of B and Q were changed so that the position of the inflection point and the crack growth rate at the inflection point did not change. The values of P, D and  $K_C$  were not altered. Using the nomenclature introduced during the literature review (Section 2.0), the log of the inflection point ( $x_i$ ) can be expressed in terms of the log of  $K_{th}$  ( $x_0$ ) and the log of  $K_C$  ( $x_f$ )

$$x_i = [x_f \sqrt{Q} + x_0 \sqrt{(-D)}] / [\sqrt{Q} + \sqrt{(-D)}] \quad (7.3)$$

By fixing the inflection point ( $x_i$ ) and adjusting the threshold according to the threshold interpolation model to  $x_0'$ , a new value of Q ( $Q'$ ) can be calculated by rearranging Equation 7.3:

$$\sqrt{Q'} = [(x_f - x_0') \sqrt{Q} + (x_0 - x_0') \sqrt{(-D)}] / (x_f - x_0) \quad (7.4)$$

The log of the crack growth rate ( $y$ ) is expressed as

$$y = B + P (x - x_0) + Q [\log(x - x_0)] + D [\log(x_f - x)] \quad (7.5)$$

The new value of B ( $B'$ ) can be determined by setting  $x$  equal to  $x_i$  and requiring that  $y$  at the inflection point ( $y_i$ ) be identical with the new and old values of  $K_{th}$ , B, and Q. It can be shown that

$$B' = y_i + PZ/\sqrt{Q'} + Q' \log(Z/\sqrt{Q'}) - D \log(Z/\sqrt{(-D)}) \quad (7.6)$$

$$\text{where } Z = (x_f - x_0') / (\sqrt{Q'} + \sqrt{(-D)})$$

This approach was utilized to adjust the cyclic crack growth curve for the changes in time-dependent threshold. Sample calculations were performed using the cyclic curve generated for Rene'95 at 649°C with several higher values of thresholds. The results of these alterations are shown in Figure 7.1. The ability of this approach to increase the threshold without significantly influencing the Region II crack growth rates illustrates the flexibility of the sigmoidal crack growth equation.

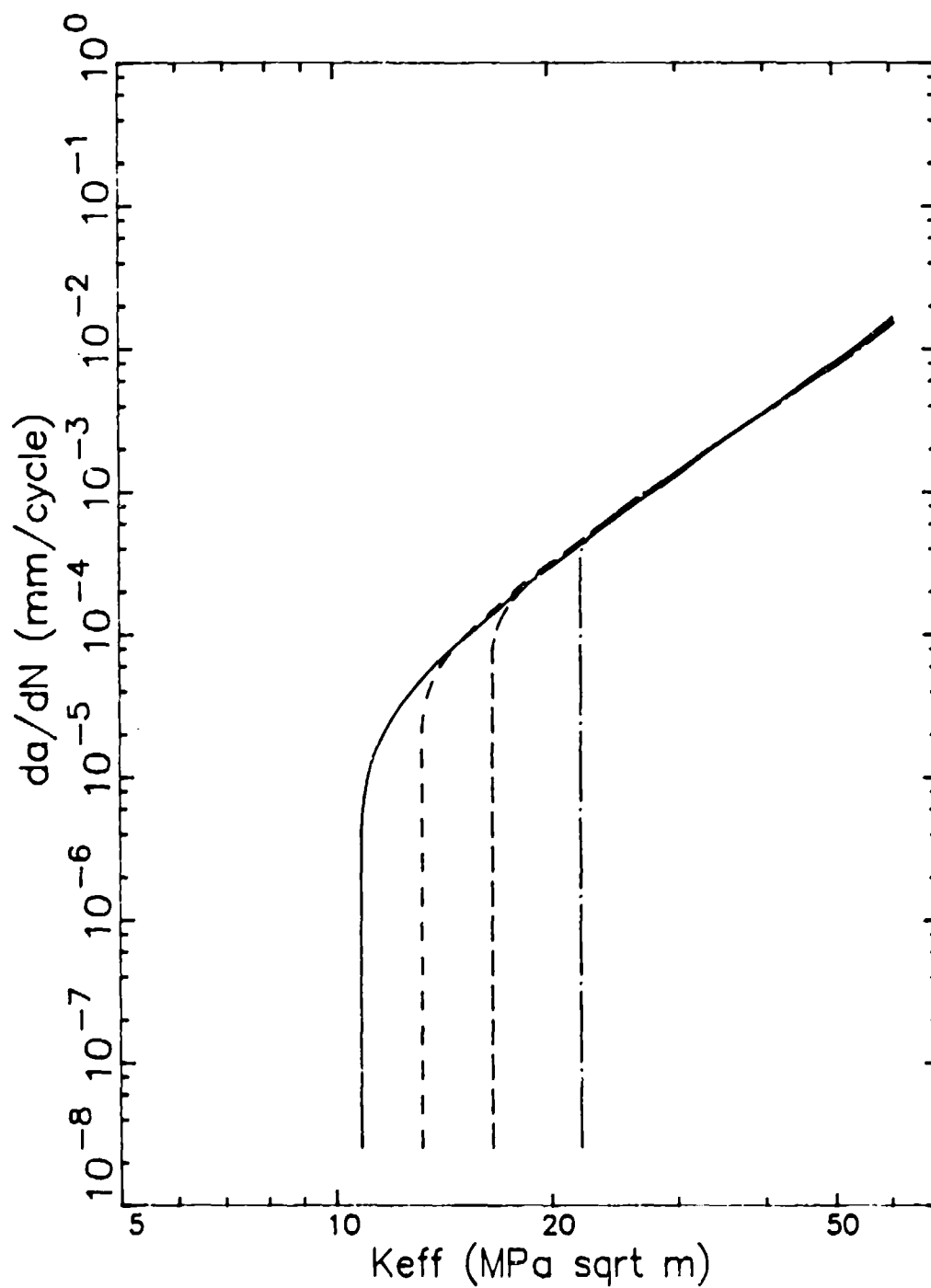


Figure 7.1: Sigmoidal crack growth rate curve adjusted to permit static crack growth below the static crack growth threshold.



### 7.1.2 Interpolation Model

The interpolative model developed in this program was based on the sigmoidal (Knaus) crack growth equation where the value of  $K$  was replaced by the maximum value of  $K$  in a cycle ( $K_{\max}$ ). The expression developed in the interpolative threshold model was used for  $(K_{th})_{\max}$ . The values of  $K_c$  and  $D$  were held constant.  $K_c$  sets the cyclic toughness and  $D$  controls the transition between Region II and III crack growth. Neither of these will influence the portion of the crack growth curve which has a significant influence on residual life.

The values of  $B$ ,  $P$ , and  $Q$  were permitted to vary according to the following equations:

$$\begin{aligned} B &= B_1 + B_2 \ln(1-R) + B_3 \ln(1+V) + B_4 \ln(1+T) \\ P &= P_1 + P_2 \ln(1-R) + P_3 \ln(1+V) + P_4 \ln(1+T) \\ Q &= Q_1 + Q_2 \ln(1-R) + Q_3 \ln(1+V) + Q_4 \ln(1+T) \end{aligned} \quad (7.7)$$

This formalism was the same formalism used in the Sinh interpolation model developed in previous investigations.(36-38). The constants for  $B$ ,  $P$ , and  $Q$  comprise an array of 12 coefficients. The values of the array were determined from the available crack growth data using nonlinear optimization techniques. It should be noted that in essence, this type of model is primarily an empirical curve fitting approach. The interpolative models for  $B$ ,  $P$ , and  $Q$  do not directly consider the mechanisms which control time-dependent crack growth.

### 7.1.3 Superposition Model

The superposition used in this investigation is based on the linear superposition approach reported by Wei and coworkers(45,46). This model was evaluated by using the static crack growth data to model time-dependent crack growth. It should be noted that with this approach, no hold time or low frequency test data were used to determine any material properties.

The static crack growth rate curve was represented using a Paris relationship. This permitted closed form integration as first reported by Christoff<sup>(21)</sup> and presented in the literature review section of this report. Two modifications were made to this approach. The first was the inclusion of the static threshold and not permitting static crack growth below  $(K_{th})_s$ . This process is shown in Figure 7.2 for a triangular shaped cycle with a R-ratio of zero. The entire loading cycle is indicated by dashed lines. Only the portion above the static threshold (indicated by the solid line), will be permitted to contribute to static crack growth. This is rather easily accomplished by adjusting the R ratio and changing the time integration interval.

The second modification was a slight change in the integration procedure developed by Christoff<sup>(21)</sup>. The modification included the fact that K increases as the crack grows. This has an almost negligible effect when the time-dependent portion of the calculation is small. This is not the case for some of the very rapid crack growth rates measured during long hold time and low frequency tests in this investigation. This was accomplished by assuming that for any specific loading situation, K is proportional to the square root of the crack length.

$$K = (K_1 + \Delta K \tau) \sqrt{a/a_0} \quad (7.8)$$

where a - current crack length

$a_0$  - crack length at the start of the loading segment

$K_1$  - K at the start of the loading segment

$\Delta K$  - the change in K during the loading segment

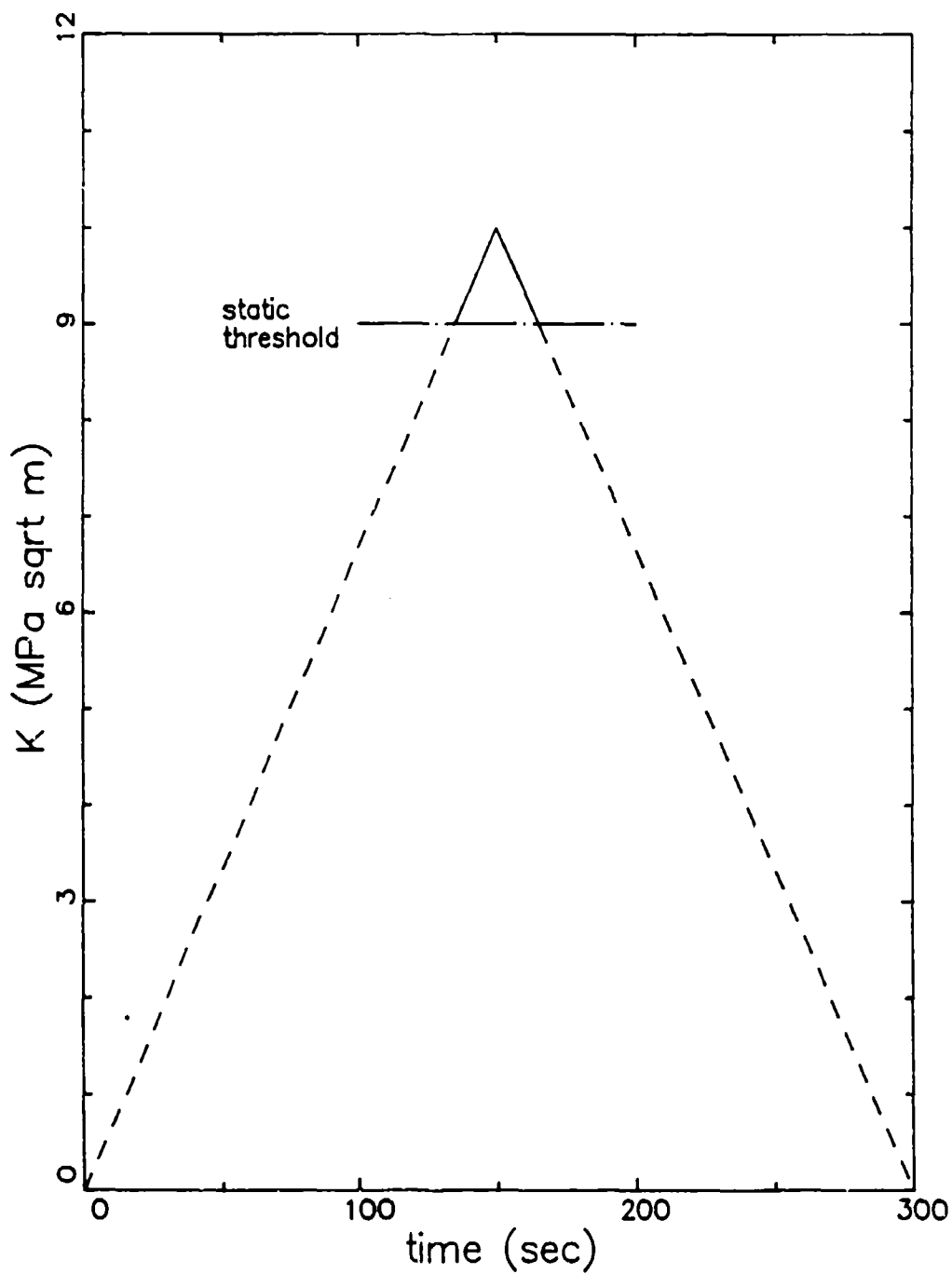


Figure 7.2: Schematic diagram of superposition model including a static crack growth threshold.

Integration of Equation 7.8 results in

$$\Delta a/a_0 = [1 + (2-n) CF K_{\max}^n T]^{2/(2-n)} - 1 \quad (7.9)$$

where  $F = 1$  for hold times

$F = [(1 - R(1+n)) / (1 - R)] / (1 + n)$  for ramps

$T =$  time duration of loading segment above  $(K_{th})_s$

$K_{\max} =$  the maximum  $K$  in the loading segment

$R =$  actual or adjusted  $R$  ratio

and  $C, n =$  Paris constants for static crack growth

It can be shown by series expansion that as the second term in the brackets of Equation 7.9 approaches zero, this expression is identical to those developed by Christoff(21). The function  $F$  in Equation 7.9 has the same effective time relationship for loading ramps as shown in Figure 2.4.

#### 7.1.4 Retardation Model

The retardation model used in this investigation was a modified Willenborg model developed for cyclic retardation of nickel-base superalloys<sup>(49)</sup>. The Willenborg model described in the literature review section was modified reflecting some of the experimentally observed behavior. The two most significant changes were that the distance over which retardation was observed was equal to twice the overpeak plastic zone ( $r_{01}$ ) where  $r_{01}$  was defined to be

$$r_{01} = (1 / 2\pi) (K_{01}/\sigma_y)^2 \quad (7.10)$$

This result was very similar to that reported by Mills and Hertzberg<sup>(71)</sup> in aluminum alloys.

Another frequently reported event was observed immediately after the overpeak, where the crack growth rates decreased rapidly to a minimum followed by a gradual increase to the non-retarded value such as previously shown in Figure 5.31. The original Willenborg model predicts an instantaneous drop in

K following the overpeak, but data like that shown in Figure 5.31 indicates that the drop is more gradual. Examination of data of this type for several materials, test temperatures, overpeak ratios, and  $K_{\max}$  levels showed that the distance of the minimum in crack growth rate occurred at  $((r_p)_{\text{old}})/2$ , half the plastic zone size as calculated with the K prior to the overpeak. Presumably this is a zone which had been damaged prior to the application of the overpeak.

The modified Willenborg model developed for nickel-base superalloys altered the distance  $\Delta_{\max}$  over which the retardation would occur and included the gradual rather than instantaneous drop in  $K_{\text{red}}$ . The modified Willenborg equation reflecting the change in  $\Delta_{\max}$  is

$$K_{\text{red}} = (K_{01} [2 r_{01}^2 - (r_{01} - (r_p)_n) \Delta] / [2 r_{01}^2 - K_{\max}]^{\frac{1}{2}} \quad (7.11)$$

The maximum value of  $K_{\text{red}}$  occurs when  $\Delta = ((r_p)_{\text{old}})/2$  and equals

$$(K_{\text{red}})_{\min} = (K_{01} (2 r_{01}^2 - (r_{01} - (r_p)_n)((r_p)_{\text{old}})/2) / 2 r_{01}^2 - K_{\max})^{\frac{1}{2}} \quad (7.12)$$

It is more convenient to represent these expressions in terms of the terms  $T_1$  and  $T_2$

$$K_{\text{red}} = (T_1 - T_2 K_{\max})^{\frac{1}{2}} \quad (7.13)$$

When  $\Delta$  is greater than  $((r_p)_{\text{old}})/2$

$$T_1 = K_{01} (2 r_{01}^2 - (r_{01} - (r_p)_n) \Delta / 2 r_{01}^2$$

and  $T_2 = 1$  (7.14)

At  $\Delta = ((r_p)_{\text{old}})/2$

$$(T_1)_{\min} = K_{01} (2 r_{01}^2 - (r_{01} - (r_p)_n)((r_p)_{\text{old}})/2) / 2 r_{01}^2$$

and  $(T_2)_{\min} = 1$  (7.15)

As a mission analysis is performed, the values of  $T_1$  and  $T_2$  are saved for later use. When a new overpeak is applied the values of  $T_1$  and  $T_2$  vary linearly with  $\Delta$  starting with the old values  $((T_1)_{\text{old}}$  and  $(T_2)_{\text{old}}$ ) for  $\Delta$

equals zero and equalling  $(T_1)_{\min}$  and  $(T_2)_{\min}$  when  $\Delta$  equals  $(r_p)_{\text{old}}/2$ . When  $\Delta$  is less than  $(r_p)_{\text{old}}/2$

$$\begin{aligned} T_1 &= (T_1)_{\text{old}} (1 - 2\Delta/(r_p)_{\text{old}}) + (T_1)_{\min} 2\Delta/(r_p)_{\text{old}} \\ \text{and } T_2 &= (T_2)_{\text{old}} (1 - 2\Delta/(r_p)_{\text{old}}) + 2\Delta/(r_p)_{\text{old}} \end{aligned} \quad (7.16)$$

With frequent repetitious overpeaks so that the crack growth increment is less than  $(r_p)_{\text{old}}/2$ , the value of  $(T_2)_{\text{old}}$  approaches unity. Under this circumstance the value of  $K_{\text{red}}$  can be approximated by  $(K_{\text{ol}} - K_{\text{max}}) \Phi$ .

The solid lines in Figure 7.3 illustrates the variation in  $K$  predicted by this model for a single overpeak. The dashed line illustrates the case for closely spaced multiple overpeaks.

The modified Willenborg model has been applied to tests of nickel base superalloys which received a single overpeak after approximately 0.25 mm (0.01 inch) of growth<sup>(49)</sup>. For these materials, the value of  $\Phi$  is not a constant but a function of  $K_{\text{max}}$ . Based on the experimental data, the following expression was developed for  $\Phi$ :

$$\Phi = \Phi_1 + \Phi_2 K_{\text{max}} \quad (7.17)$$

For cyclic crack growth the value of  $\Phi_1$  was zero. The impact this behavior is that the relative retardation increases with  $K_{\text{max}}$ . The constants  $\Phi_1$  and  $\Phi_2$  are the only adjustable constants in this model. As noted in the literature review section, the value of  $\Phi$  should always be less than unity.

This model has also been applied to specimens with simple missions without hold times and adequately predicted their lives. The amount of relative retardation diminished as the R-ratio increased because, for the most part, the cyclic crack growth rates for nickel base superalloys are controlled by  $\Delta K$  for high R-ratios ( $m^+ = 1$ ) while for negative R-ratios the growth is controlled by  $K_{\text{max}}$ .

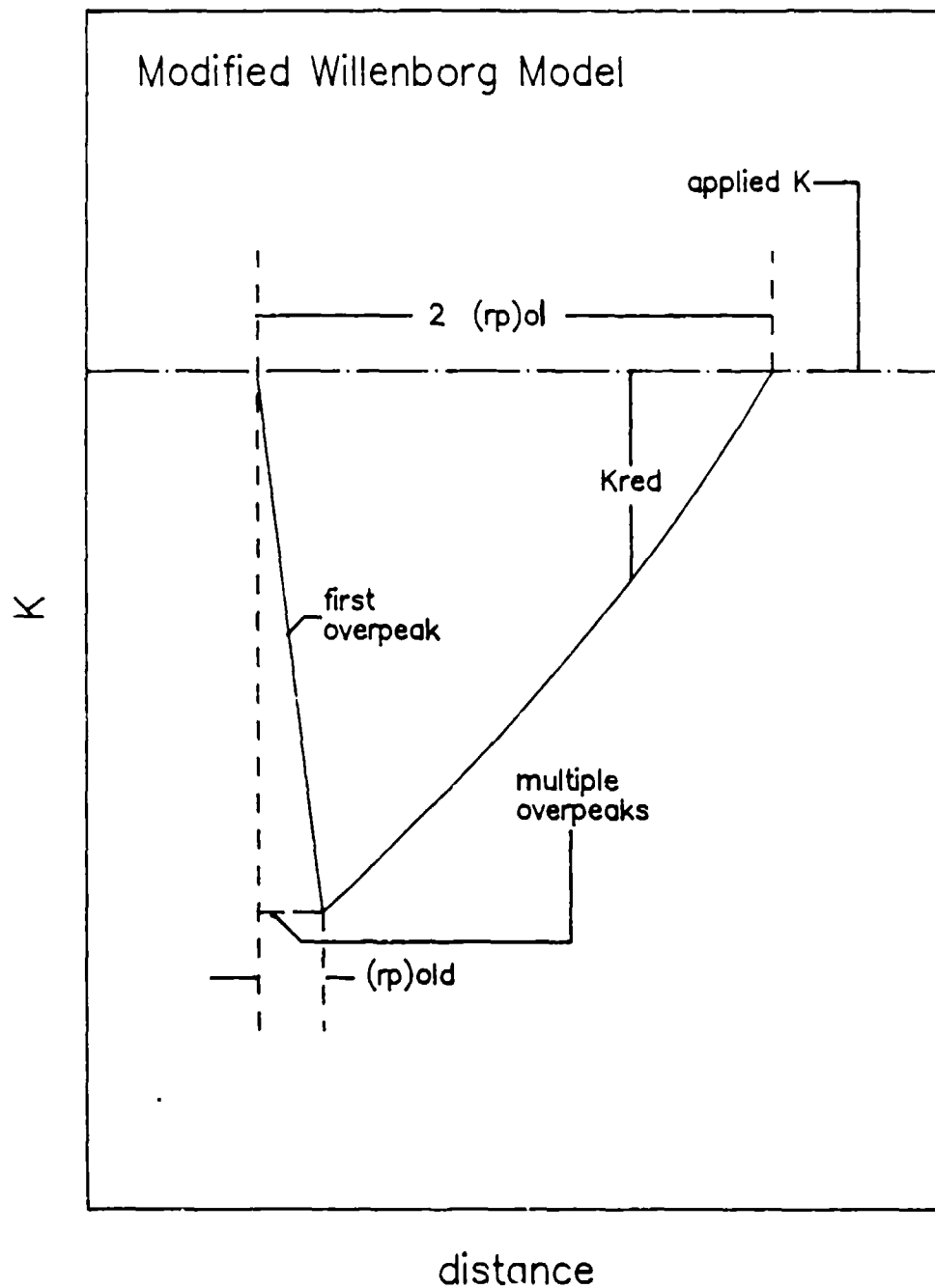


Figure 7.3: Schematic diagram of modified Willenborg retardation model

Weerasooriya and Micholas<sup>(50)</sup> used a Willenborg type model to predict the crack growth rates in Alloy 718 during overpeak hold time cycles so it seems reasonable to use the modified Willenborg model discussed above to model retardation during static crack growth. The data shown in Figure 5.31 illustrates that the modified Willenborg model accurately predicts the position of the minimum in crack growth rate and the extent of the retardation zone. The only difference between the cyclic and static crack retardation models is that the value of  $\phi$  was defined in terms of  $K_{01}$  rather than  $K_{max}$  for static retardation.

$$\phi = \phi_1 + \phi_2 K_{01} \quad (7.18)$$

The application of cyclic and static retardation result in some rather different conclusions. Cyclic retardation should be applied for those cycles where  $K_{max}$  is less than  $K_{01}$ . The combination of static retardation with the linear superposition model requires that static retardation should be applied at all values of  $K$  less than  $K_{01}$ . Consider, for example, a load controlled,  $R=0$ , constant amplitude, constant frequency test. The  $K$  at the maximum load ( $K_{max}$ ) would increase with each cycle due to the increase in crack length. This would result in no cyclic retardation. If static retardation is applied to the same cycle, there are benefits because the value of  $K$  should be reduced at all  $K$  levels below  $K_{max}$ . Figure 7.4 illustrates the application of the modified Willenborg model to this type of cycle. For simplicity sake it is assumed that  $\phi$  equals unity so that  $K_{red}$  equals  $K_{max} - K$ . Combination of the static retardation with the static threshold results in a significant decrease of the time period over which static crack growth would be calculated. The use of Equation 7.19 also dictates that linear loading segments remain linear after the application of the retardation model so that the superposition model equations developed in Section 7.1.3 can still be used.

The experimental data in Section 5 showed that 20% overpeaks in combination with hold times resulted in unmeasurable amounts of static crack growth during the hold time loading at high levels of  $K$ . For this to occur, the effective  $K$  during the hold time ( $K_{hold} - K_{red}$ ) must be below the static threshold. The retardation model is applied to a  $R=0$ , 20% overpeak, with  $K_{01}$



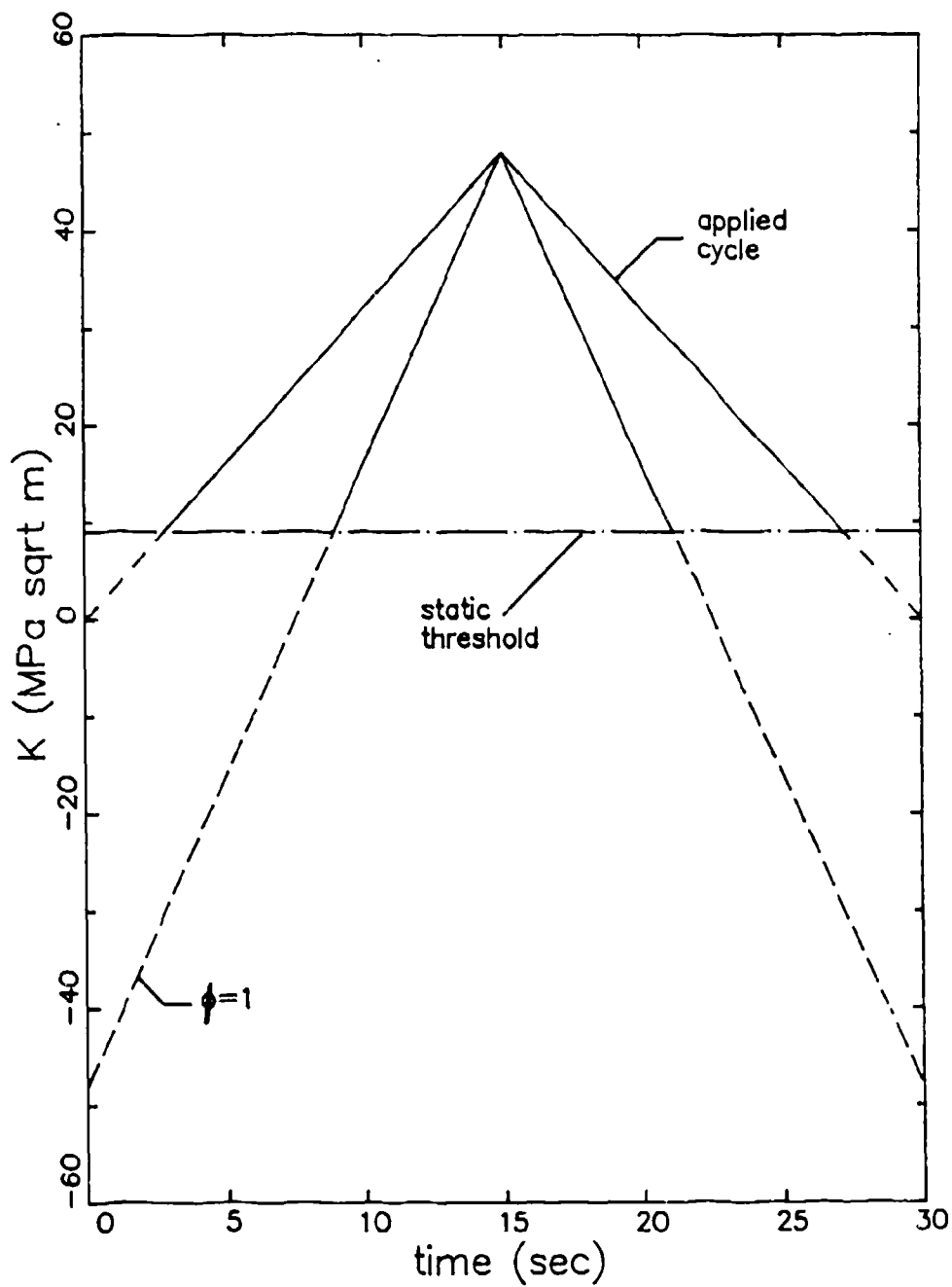


Figure 7.4: Application of static retardation to constant amplitude, constant frequency tests.

- 48 MPa/m in Figure 7.5. It is assumed that  $K_{red}$  equals  $(K_{01}-K)\Phi$ , and that the static threshold is 9 MPa/m, which seems reasonable based on the static crack growth thresholds shown in Section 5. The retardation model was applied using retardation constants of 1 and 4. Crack growth would be expected in the former case but suppressed for any case where  $\Phi$  is in excess of 4. This simple case illustrates that the values of  $\Phi$  necessary to predict the static crack growth are in excess often in excess of unity. These seem like unreasonable values, but may reflect the time-dependent relaxation of stresses. This may be related to the significance of creep deformation associated with creep-fatigue-environment interactions.

These large values of  $\Phi$  were necessary to predict the retardation of hold times at intermediate K levels. If these same constants were applied to constant amplitude low frequency tests, very little time-dependent crack growth was predicted. This issue was resolved by applying the cyclic retardation constants to loading ramps and using static retardation constants for hold time segments.

Table 7.1 summarizes the approach taken to calculate  $\Phi$  ( $K_{max}$  or  $K_{01}$ ) and which set of  $\Phi_1$  and  $\Phi_2$  constants are used to calculate  $\Phi$ .

## 7.2 ADVANCED CUMULATIVE DAMAGE CYCLE (ACDCYCLE) COMPUTER CODE

This section of the report describes the residual life prediction code which implements the models described in the previous sections. This code is restricted to through crack analyses in compact specimens and two types of single edge notch specimens. This program is known as ACDCYCLE (Advanced Cumulative Damage CYCLE) and was written using Fortran 77 and compiled on an IBM XT with an 8087 math coprocessor chip. This program was delivered to the Air Force Material Laboratory in a compiled form for their use and distribution. The program was written to be extremely user friendly and permits input of necessary data (material properties, specimen geometry, and mission) with either data files or manual entry. There are checks within the code to prevent the use of non-existent data files as well as prevention of writing on top of already existing files.

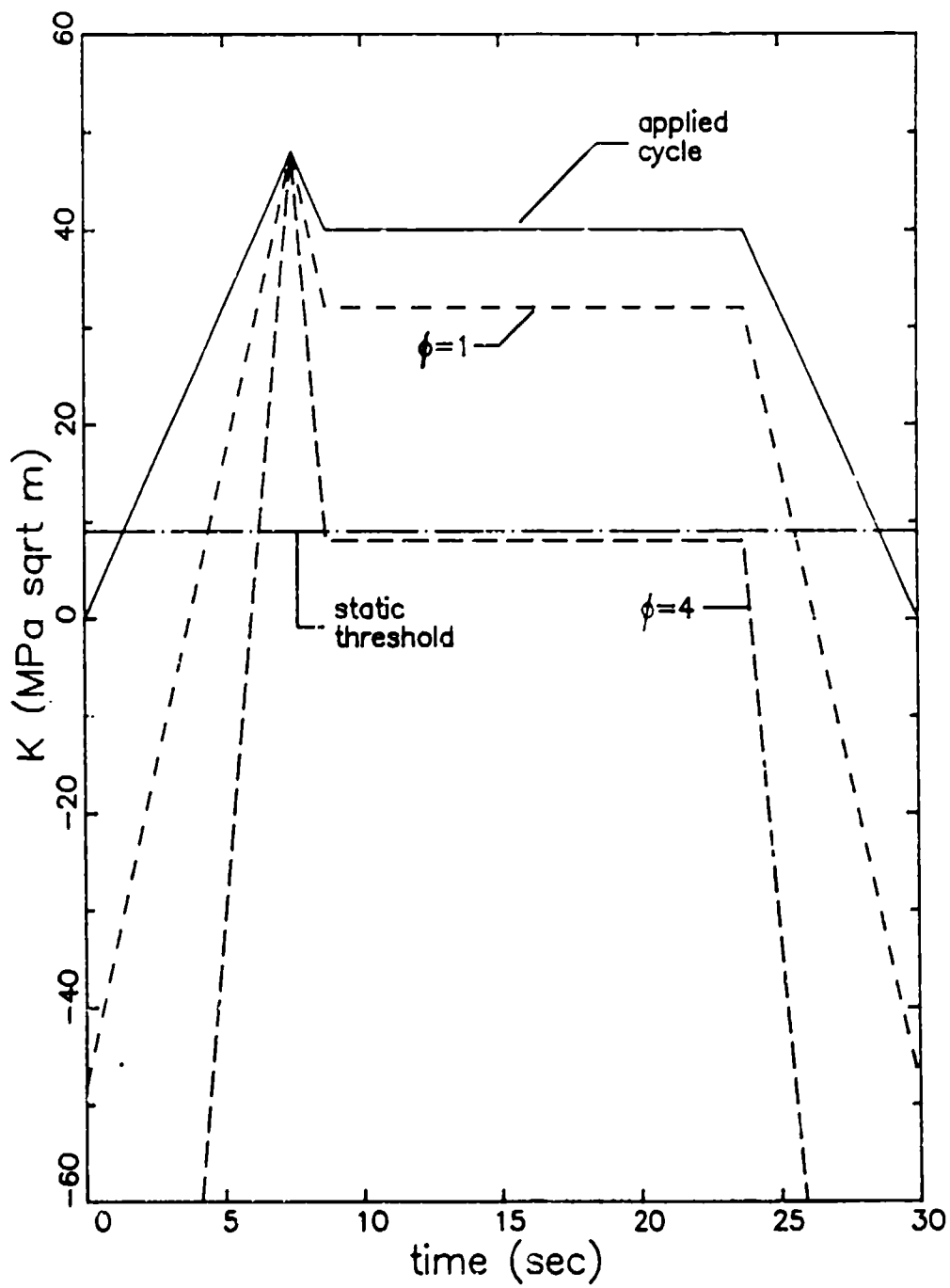


Figure 7.5: Application of static retardation to overpeak hold time test cycle.

Table 7.1: Application of Retardation Constants

<u>Cycle Type</u>	<u>Calculation of <math>\ddagger</math> (<math>K_{ol}</math> or <math>K_{max}</math>)</u>	<u>Retardation Constants</u>
cyclic	$K_{max}$	cyclic
static ramp	$K_{ol}$	cyclic
static hold	$K_{ol}$	static

The following sections will describe the basic options, input/output capabilities, and details of performing a residual life estimate.

#### 7.2.1 ACDCYCLE Opt

The program was written using a menu format which has the following seven options:

1. Calculate a crack growth rate
2. Estimate a residual life
3. Calculate the crack growth increment for one cycle
4. Restart the residual life estimate
5. Perform analysis from stacked files
6. Calculate a crack growth curve
7. Stop

Option 1 calculates the crack growth rate for a specified mission. This feature does not permit the use of retardation models because the retardation constants are dependent on the previous loading history of the specimen.

Option 2 calculates the number of cycles required to grow a given amount for a specified mission and material properties. This life is terminated by either a final crack length or when  $K_{max}$  approaches the material toughness ( $K_C$ ).

Option 3 calculates the crack growth increment for one cycle. The chief purpose of this option is to permit the inclusion of a single overpeak prior to subsequent cycling.

Option 4 permits a continuation of a residual life estimate using a different set of material properties and/or mission types. The restart option retains the history dependent constants such as those used to perform retardation modeling. This option, when combined with option 3, can calculate the number of cycles necessary to grow a crack a specified distance following an overpeak.

Option 5 allows the program to be run many times from a file constructed with the desired parameters. This option was included for use in predicting the lives of the constant K hold time-overpeak tests.

Option 6 permits the calculation of the crack growth rate for a given mission. The crack growth rates are calculated using the same parts of the program used in Option 1 and do not include the effects of retardation. The calculations are initiated at a value of  $K_{max}$  which is 0.5 percent greater than  $(K_{th})_{max}$  for that mission. The crack growth rates are then calculated for values of K higher by one percent over the previous value. This procedure is terminated when either (1)  $K_{max}$  approaches  $K_c$  or when the crack growth rate exceeds  $2.5 \times 10^{-1}$  mm/cycle ( $1 \times 10^{-2}$  inch/cycle).

After completion of the desired option the software returns to the main menu for another calculation (Option 1 through 6) or termination of its activities (Option 7).

#### 7.2.2 ACDCYCLE Input and Output

After selection of one of the six options described in the previous section, the crack growth model, material properties, specimen geometry, and mission profile must be selected. The material, specimen, and mission data, once input, are stored in computer files to facilitate their use in future computations.

After selection of the option, the first information selected is which crack growth model. ACDCYCLE was written to perform the evaluations using either (1) the interpolation or (2) the combined interpolation-superposition models described in the previous section. If the interpolative model is selected, the retardation model cannot be applied.

The material constants are different for each of the crack growth models so a separate materials data file must be maintained for each material/temperature/model combination. When ACDCYCLE is used with the interpolation-superposition model, the static crack growth, cyclic

retardation, and static retardation options can be selected (on or off) without setting up a separate data file for each of these combinations.

ACDCYCLE can perform crack growth analyses for three through crack type of laboratory specimens. The K-solution used for the buttonhead single edge notch (SEN) specimen is the Harris solution<sup>(61)</sup>. The Tada solution<sup>(72)</sup> was used for the pin-loaded SEN specimen and the K-solution recommended by ASTM<sup>(68)</sup> was used for the compact specimen. In addition to the type of specimen, the initial crack length, specimen width (W), and final crack length are input. The final crack length is used to terminate a residual life option. This is particularly useful in combination with the restart / stacked case option to predict the behavior in a specimen which has been cycled in several different ways.

ACDCYCLE permits prediction of crack growth under either stress-controlled or K-controlled conditions. Several unique features have been built into this computer code to (1) facilitate easy use of simple missions, (2) to permit the use of a single mission files for cases where only the level of stress or K changes, and (3) to permit the repetition of a mission block. A simple mission is considered to be comprised of a loading ramp with a time increment  $V/2$ , a hold time of length T, and an unloading ramp with a time increment of  $V/2$ . This mission can be described in terms of a ramp time (V which is the sum of increasing and decreasing time), a hold time (T), and R-ratio. ACDCYCLE permits the user to input the values of V, T, and R and the code creates a mission file with the appropriate stress (or K) pairs. The stress or K levels can be changed by specifying the maximum level of stress or K multiplier for a mission which had the proper time and relative loading sequence. The multiple mission block is introduced by giving the number of times a mission should be repeated (a value of one in just a single mission). This option is useful in modeling constant K tests where retardation may have occurred between blocks of load-controlled cycling.

After the model, material, specimen, and mission information is input, the user has the option of having the output stored in a data file as well as appearing on the PC monitor (and printer if so desired). The output lists all

the model, material, specimen, and mission input data as well as the results. The advantage of having the output stored on a data file is that it can be edited for subsequent computer plotting. For example, the predicted crack growth rate curves shown in this section were computer plotted from files created using Option 6 of ACDCYCLE.

### 7.2.3 Residual Life Calculations

The residual life calculations performed in ACDCYCLE use three subroutines - RESLIF, ONECYCLE, AND MODWIL. The residual life calculation is monitored and controlled in RESLIF. The numerical integration is performed using the increment of crack growth in one mission cycle and numerically integrating it with respect to mission cycles using a second order Runge-Kutta technique. Each time the increment in crack length is required, RESLIF calls the subroutine ONECYCLE. Within this subroutine, the current crack length and the loads for that mission cycle (adjusted for K-controlled tests, if appropriate) are used to calculate the corresponding increment in crack length. The calculations within ONECYCLE will be described using the 10 point mission shown schematically in Figure 7.6. The calculations will be described separately for the interpolation and the interpolation-superposition model.

A single cyclic loading was considered to end when the load reaches a local minimum such as at mission points 1, 4, 6, and 10 in Figure 7.6. The interpolation model considers only the ramp times (V), hold times (T) and R-ratio (R) for each cyclic loading. The crack advance during a given mission cycle was calculated by determining the values of V, T, and R for each cyclic load. The interpolative crack growth equation then calculates the crack growth increment ( $da/dN$ ). The crack length is then incremented, the values of K are updated, and this procedure is repeated until the end of one mission cycle. This steps in this procedure for the mission shown in Figure 7.6 are listed in Table 7.2.

The interpolative-superposition model was applied in a slightly different fashion. The cyclic crack growth rate was applied for each loading cycle, then the amount of static crack growth was calculated for the segment between



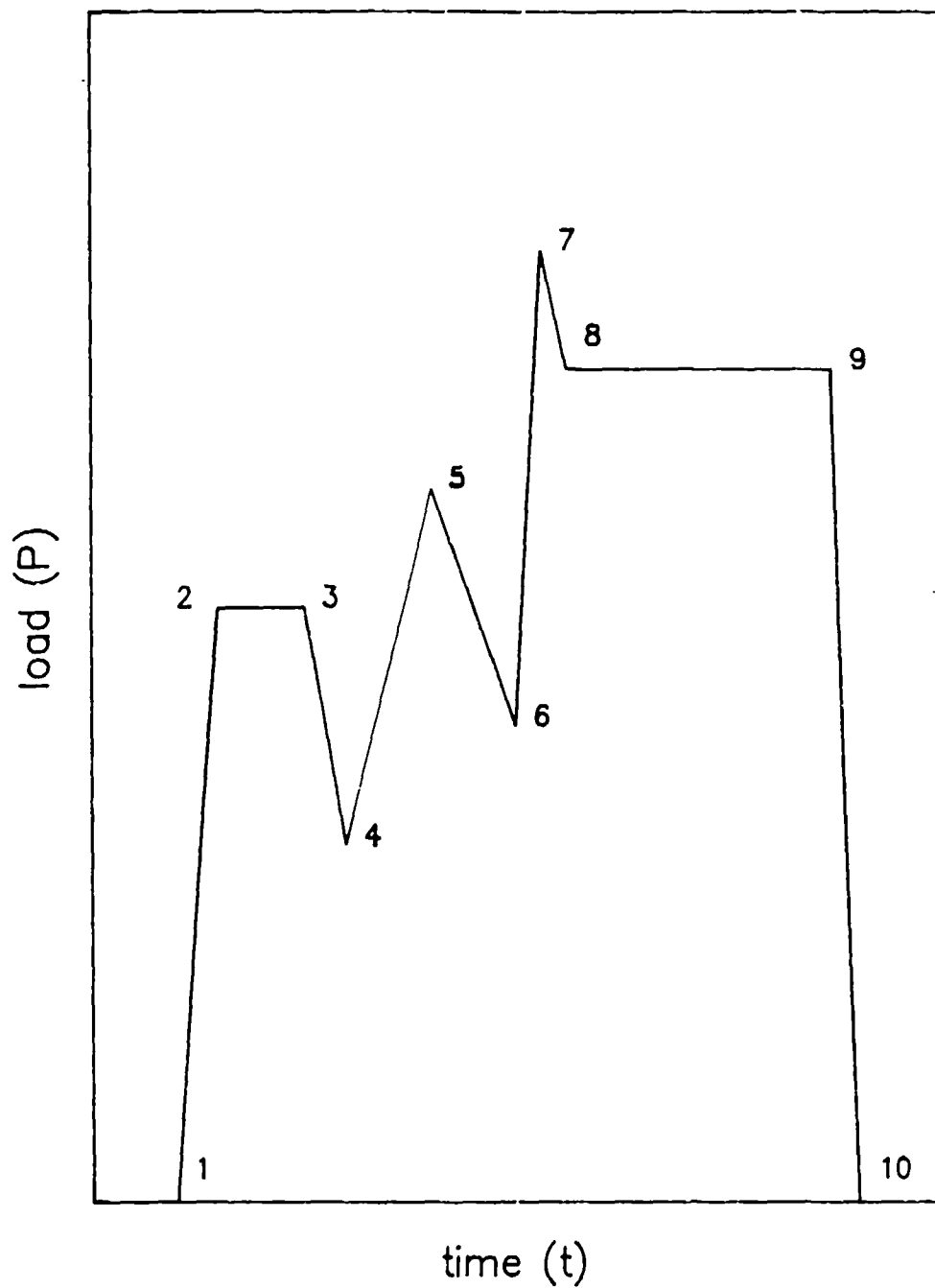


Figure 7.6: Schematic example of a mission analyzed by ACDCYCLE.

Table 7.2: Sequence Of Mission Analysis In ACDCYCLE Using Interpolation Crack Growth Model

<u>Step</u>	<u>Mission Point Range</u>	<u>R</u>	<u>V</u>	<u>T</u>
1	1 to 4	P1/P3	$(t_4 - t_1) + (t_4 - t_3)$	$(t_3 - t_2)$
2	4 to 6	P5/P4	$(t_6 - t_4)$	0
3	6 to 10	P6/P7	$(t_8 - t_6) + (t_{10} - t_9)$	$(t_9 - t_8)$

adjacent mission points. This process was repeated until the end of the entire mission cycle. If the maximum value of  $K$  in one load-unload cycle was less than that calculated for  $(K_{th})_{max}$  according to the interpolative threshold model, no cyclic or static crack growth was attributed to that loading cycle. The steps in this procedure are described in Table 7.3. Not shown in the table are the calculations for  $V$ ,  $T$ , and  $R$  for steps 1, 5, and 8. These were identical to those shown in Table 7.2 for the interpolative model.

In both models, the crack lengths were updated and the values of  $K$  were recalculated before each step listed in Tables 7.2 and 7.3. If retardation was used in the interpolation-superposition model, each time the values of  $K$  were updated the retardation model was applied using a subroutine called MODWIL. The values of  $K$  were reduced, and for loading ramps, the value of  $R$  was recalculated using the  $K$  values as modified by the retardation model. It should be noted that the values of the history dependent retardation values were stored at several points during these calculations. If it was necessary to reduce the mission cycle increment in RESLIF or the time increment for static calculations in ONECYCLE, the integration was repeated using a smaller cycle or time increment along with the old values of the crack length and retardation terms.

### 7.3 MODELING OF RENE'95 AT 649°C

The most extensive modeling was performed on Rene'95 at 649°C because of the larger data base at this temperature - material combination. The following sections will describe the application of the models described in Section 7.1 to these data and critique their ability to predict the experimental data.

All the data in this investigation were obtained in English units (ksi, ksi/in, inch, inch/cycle, and inch/sec). The constants for the time-dependent crack growth models were also determined using these units. The materials constants listed in the tables in this section are also in English units, however all comparisons are made in SI units.

Table 7.3: Sequence Of Mission Analysis In ACDCYCLE Using Interpolation + Superposition Crack Growth Model

<u>Step</u>	<u>Mission Point Range</u>	<u>Type of Analysis</u>
1	1 to 4	cyclic
2	1 to 2	static
3	2 to 3	static
4	3 to 4	static
5	4 to 6	cyclic
6	4 to 5	static
7	5 to 6	static
8	6 to 10	cyclic
9	6 to 7	static
10	7 to 8	static
11	8 to 9	static
12	9 to 10	static

There was very little near toughness crack growth data generated in this investigation. Therefore, the value of  $K_{IC}$  in both the interpolative and superposition models was set to 65.9 MPa/m (60 ksi/in). This value was selected based on extensive residual life estimations for Rene'95. Increasing the value of  $K_{IC}$  above this level does not significantly improve the calculated residual lives because of the rapid crack growth rates at the upper end of the Region II portion of the curve.

#### 7.3.1 Rene'95 Threshold model

The material constants for the interpolation threshold model (Equation 7.1) were determined using nonlinear optimization techniques in order to minimize the error between the predictions and the experimental data previously shown in Figure 5.19. The constants for the threshold interpolation model are listed in Table 7.4. The results of this model are compared to the data in Figure 7.7. The comparison of the hold time threshold tests are shown in Figure 7.7a. The model accurately predicts the influence of hold times for R ratios of 0 and 0.5. The sudden decrease in threshold with hold time for R=0.8 is predicted well, but does not adequately increase for longer hold times to predict the R=0.8, 300 second hold time data point. This was the most poorly predicted threshold data point for Rene'95 at 649°C. Figure 7.7b shows a similar comparison for the 649°C low frequency tests on Rene'95. This model predicts most of these threshold values within 1 MPa/m.

This model was used in both the interpolative and superposition, so from this point on the superposition model will be called the interpolation + superposition model.

#### 7.3.2 Rene'95 Interpolation Model

Nonlinear optimization techniques were used to determine the 649°C Rene'95 experimental data presented in Section 5.2 were used to determine the value of D and the 12 constants necessary to describe B, P, and Q. The values of these constants are listed in Table 7.5. The comparison between this model

Table 7.4: Constants for 649°C Rene'95 Interpolation Threshold Model

$$K_0 = 10.148$$

$$K_g = 9.302$$

$$m = 0.23386$$

$$A = 2.8862 \times 10^{-3}$$

$$B = 6.0360 \times 10^{-2}$$

$$C = 1.7172$$

$$D = 4.2790 \times 10^{-2}$$

$$E = 6.7776 \times 10^{-2}$$

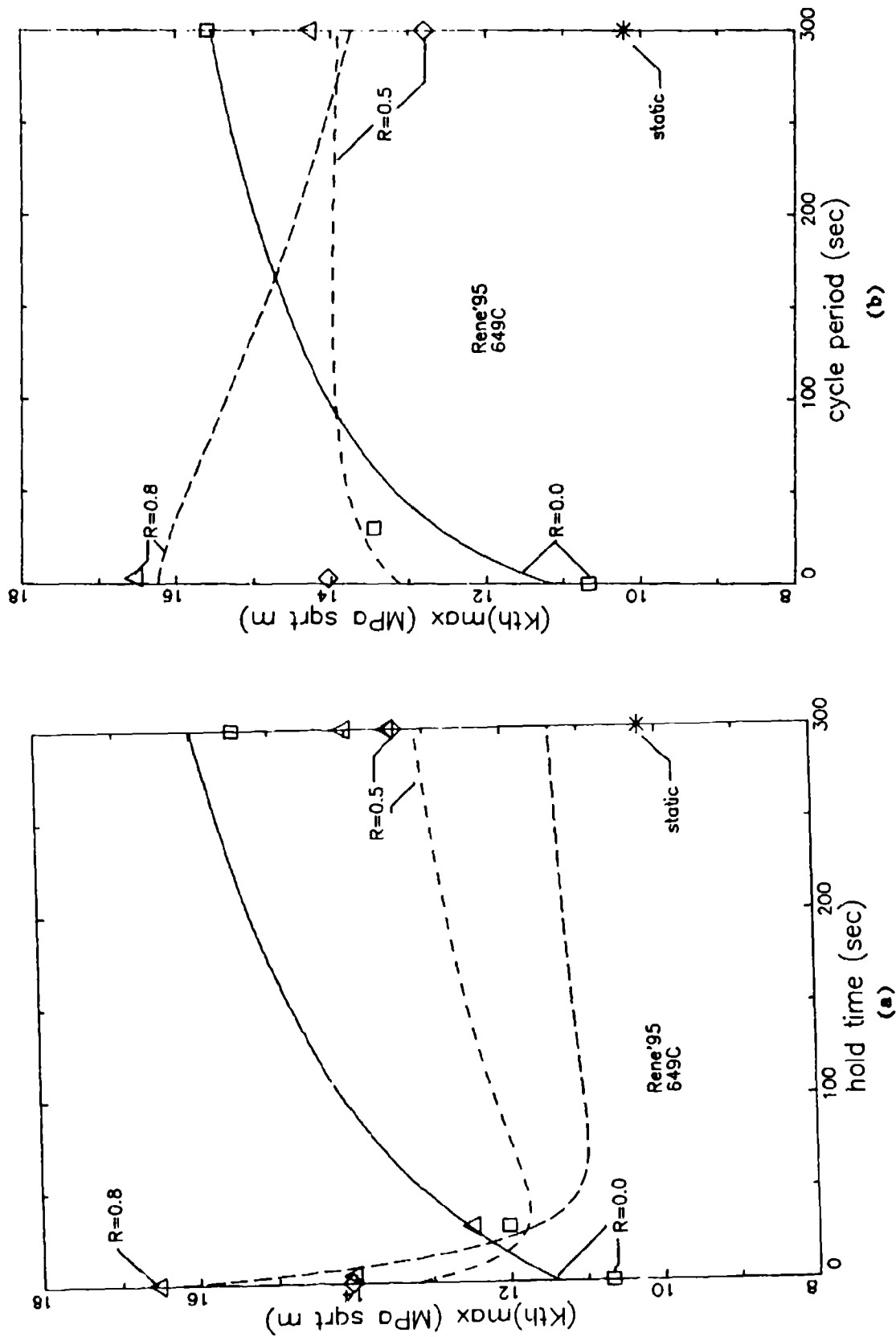


Figure 7.7: Comparison of 649°C Rene'95 (a) hold time and (b) frequency threshold data with predictions from the interpolation threshold model.

Table 7.5: Constants for 649°C Rene'95 Interpolation Model

$B_1 = -14.461$	$P_1 = 3.0128$	$Q_1 = -1.8029 \times 10^{-2}$
$B_2 = 0.74195$	$P_2 = 9.01582 \times 10^{-4}$	$Q_2 = 0.13197$
$B_3 = 0.83684$	$P_3 = -4.53246 \times 10^{-2}$	$Q_3 = 7.7415 \times 10^{-2}$
$B_4 = 0.42214$	$P_4 = 0.19634$	$Q_4 = 1.64676 \times 10^{-3}$

$$D = -4.17871 \times 10^{-5}$$

$$K_c = 60$$



and the experimental data will be presented in Section 7.3.4 along with the results of the interpolation+superposition model.

### 7.3.3 Rene'95 Interpolation + Superposition Model

The time-dependent contribution of this model is determined using the superposition of cyclic and static crack growth; however, interpolation models were used to model the threshold (Section 7.3.1) and the Walker model was used to model the influence of R-ratio on the cyclic crack growth rates.

As noted in Section 6, it appears that intergranular crack growth is faster than transgranular growth even in the absence of environment. Most of the time-dependent crack growth occurred in an intergranular mode, so data from specimens which resulted in intergranular crack growth were used to develop the cyclic crack growth rate curve. The test specimen used to collect near threshold data which had the least amount of time-dependent crack growth was the specimen tested with an R ratio of zero and a cycle period of 3 seconds. As described in Section 6, the crack growth in this tests was just slightly higher than determined in vacuum with a 30 second hold time, a conditions which also had intergranular crack propagation.

The influence of R-ratio was treated using the Walker model, as discussed in the literature review. High R-ratio tests performed in air appeared to have some amount of time-dependent crack growth because of the difference in the near-threshold regime. As a result, the vacuum test performed with a 3 second cycle period and a R-ratio of 0.8 was used to determine the Walker exponent.

Nonlinear optimization was performed on the data from these two test specimens to determine the values of  $K_{th}$ ,  $D$ ,  $P$ ,  $Q$ ,  $D$ , and  $m^+$ . The values of these constants are listed in Table 7.6. Figure 7.8 shows the crack growth data from the two test specimen discussed above plotted against to effective value of  $K$  ( $K_{eff}$ ) as defined by the Walker relationship (Equation 2.14). Also shown in this figure is the curve represented by the constants listed in Table 7.6. The agreement between the tests data and the curve is excellent.

Table 7.6: Constants for 649°C Rene'95 Superposition Model

Cyclic Constants

$$K_{th} = 9.8329$$

$$Q = 0.49779$$

$$K_c = 60.0$$

$$D = -9.8968 \times 10^{-2}$$

$$B = -12.924$$

$$m^+ = 0.72032$$

$$P = 2.9466$$

Static Constants

$$K_B = 9.302$$

$$C = 6.098 \times 10^{-11}$$

$$n = 3.63$$

Static Retardation Constants

$$\phi_1 = 0.9566$$

$$\phi_2 = 0.1867$$

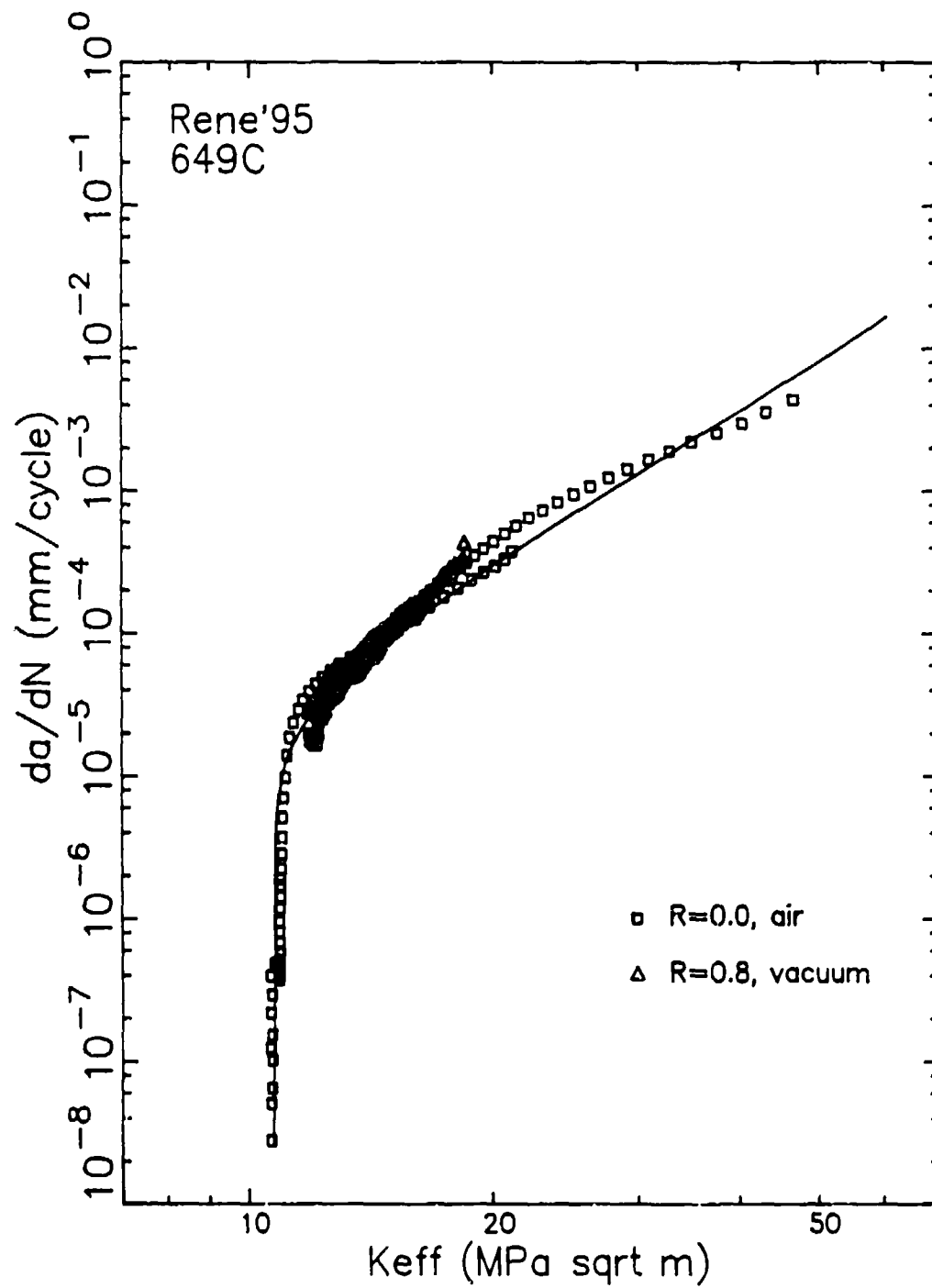


Figure 7.8: Cyclic crack growth curve used in the 649°C Rene'95 superposition model.

The static crack growth curve used in the superposition model is represented by a Paris equation truncated at the lower end by a threshold value. The static threshold value was taken to be the lowest value of  $K$  at which crack growth was measured in the 649°C Rene'95 static K-shed test. The 649°C static crack growth data shown in Figure 5.28 were edited to eliminate the near-threshold regime in the K-shed test and the artificial threshold data or "tails" in the constant load tests. Linear regression analysis to the logarithmic form of the Paris equation was performed to determine the best fit through the edited data. The static threshold and Paris equation constants are listed in Table 7.6. This curve is shown through the 649°C Rene'95 static crack growth data in Figure 7.9. This looks to be a good fit to the data, but as noted in Section 5, there is a rather wide amount of scatter in these data. The scatter may affect the establishment of a reliable static crack growth curve. The quality of this curve is extremely important because it is the source of the time-dependent contribution to the superposition model.

The correlation between the superposition model predictions and the experimental data are presented in the next section.

#### 7.3.4 Comparison of Predicted and Measured Crack Growth

The constants listed in Tables 7.4 through 7.6 were entered in materials data files and the crack growth option in ACDCYCLE was used to generate crack growth curves for the 18 different testing conditions evaluated in this program (3 R-ratios x 3 frequencies and 3 R-ratios x 3 hold times). It is important to note that these data were used to establish the material constants for the interpolation model but data from only one of the eighteen conditions were used to determine the superposition model constants.

It should also be remembered that these calculations do not include any benefit of retardation. Retardation can significantly slow down the crack growth rates in frequency tests and any type of tests with very rapid crack growth. This will be discussed and treated later in this section.

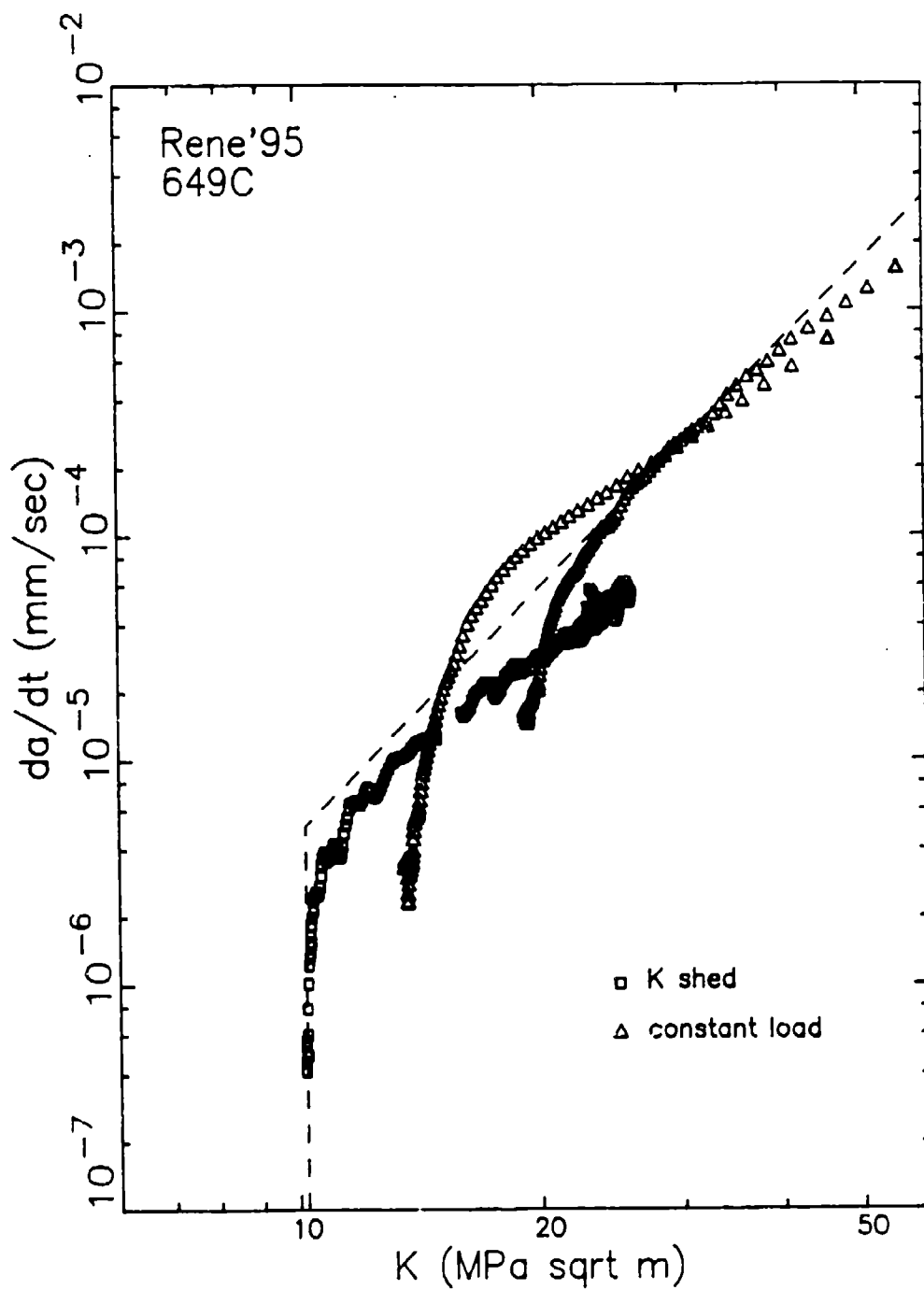
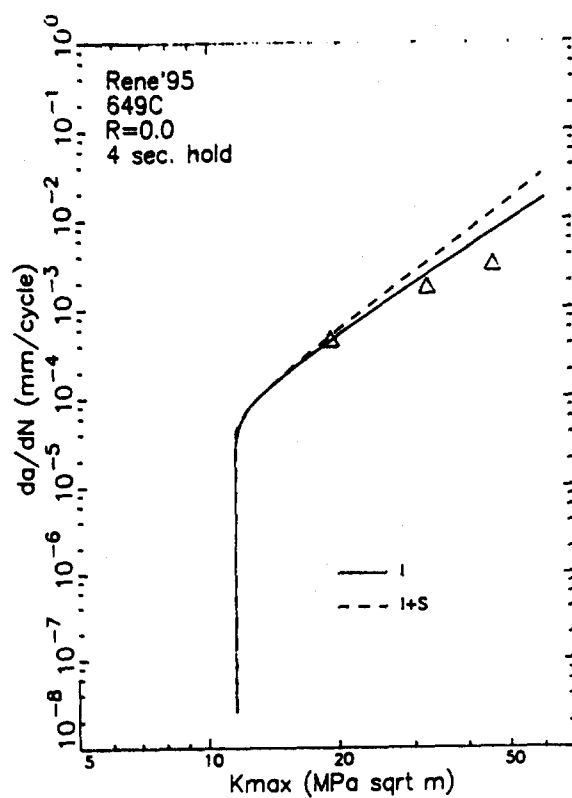


Figure 7.9: Static crack growth curve used in the 649°C Rene'95 superposition model.

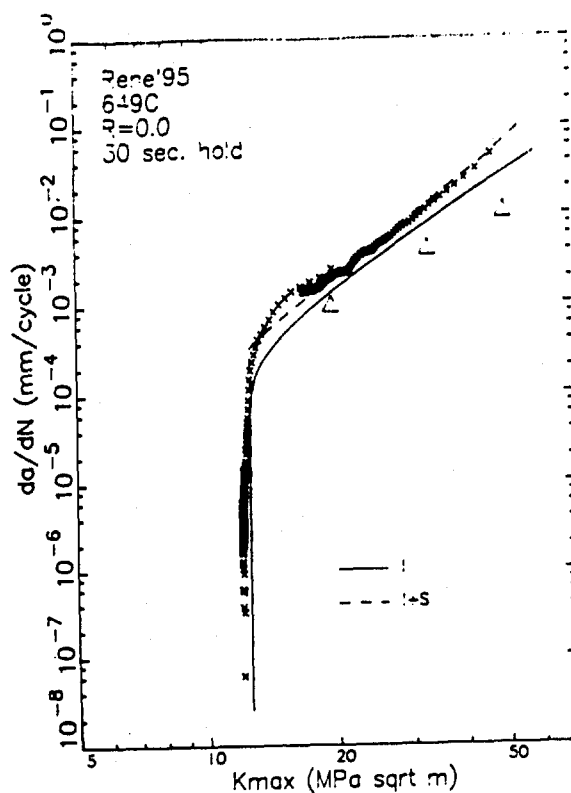
The prediction of the hold time tests will be discussed before the frequency tests because there is little influence of retardation on the increasing K hold time data. Figure 7.10 shows the comparison of the experimental data with the predictions of both models for 649°C, R=0 hold time tests on Rene'95. In these figures the small symbols represent the results from the threshold tests while the large symbols represent the data from the constant  $\Delta K$  tests. The solid line is the prediction from the interpolation model (I) while the dashed line represents the interpolation + superposition (I+S) model prediction. The results of the constant  $\Delta K$  tests were lower than the increasing K tests, particularly for the hold time tests due to retardation between constant load cycling segments so the increasing K portions of the threshold tests are considered to be a better indicator or provide more accurate crack growth rates. In all cases the predictions of the totally interpolative model are below those of the I+S model. This results primarily from the inclusion of the constant  $\Delta K$  data in determining the material constants. Exclusion of these data would undoubtedly increase the predicted crack growth rates but would lead to other errors for situations such as R=0, 4 second hold time (Figure 7.10) where there are no increasing K data from the threshold tests. The I+S model accurately predicts the R=0, 30 second hold time data and is less than 2 times lower than the 300 second hold time data. In the case of the R=0, 300 second hold time, the prediction of the I model is almost six times lower than the I+S prediction and over ten times lower than the experimental data.

The comparison of the R=0.5 hold time experiments and predictions are shown in Figure 7.11. For the two lower hold times, both models lie above the constant  $\Delta K$  data. The only R=0.5 hold time tests with increasing K data from the threshold test was one with a 300 second hold time (Figure 7.11c). In that case, the predictions from the two models bracket the experimental Region II data. The I+S model more accurately predict the response at lower K levels relative to the predictions at higher K levels.

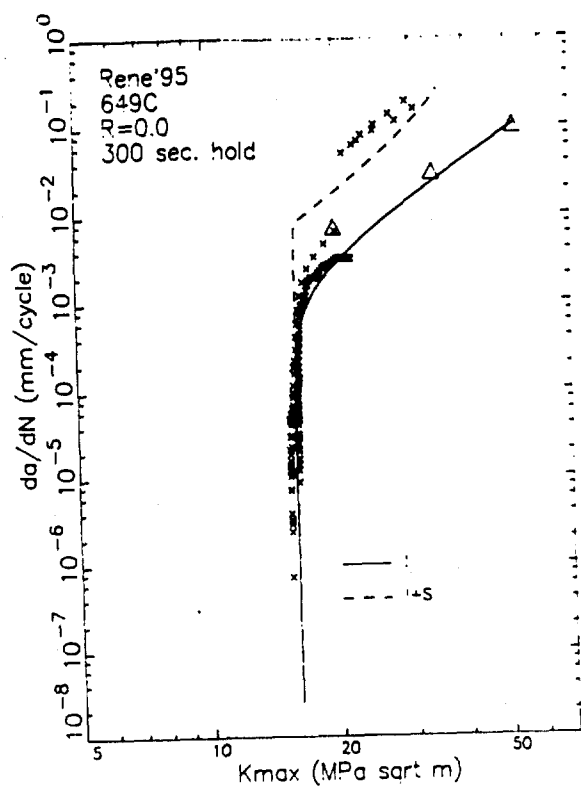
One reason for this influence of K on the predicted crack growth rates might be the way in which these predictions are performed in ACDCYCLE. For simple cycles like those predicted in Figure 7.11, the interpolation model



(a)



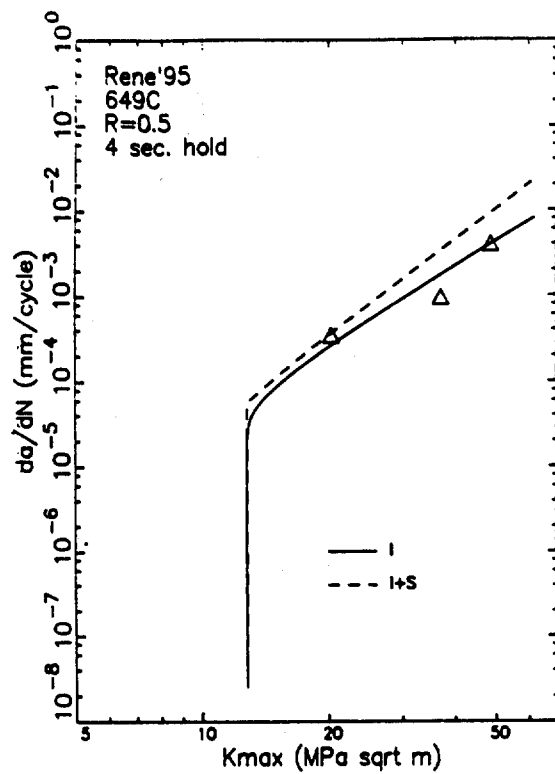
(b)



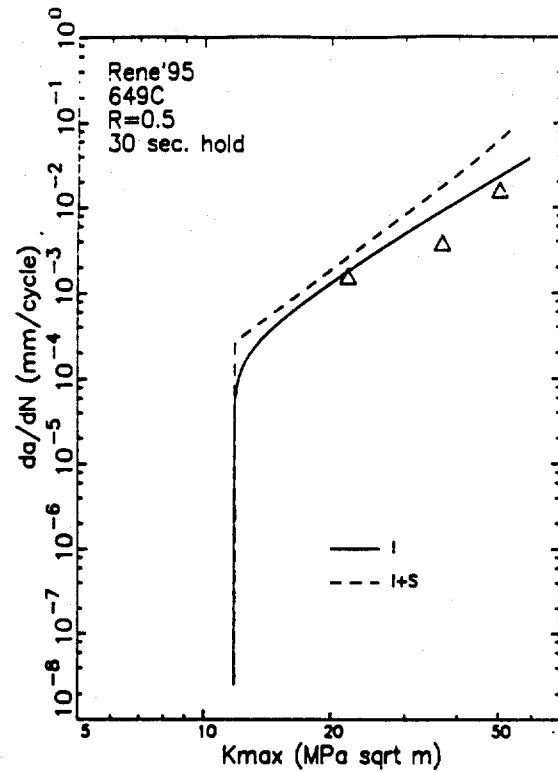
(c)

Figure 7.10:

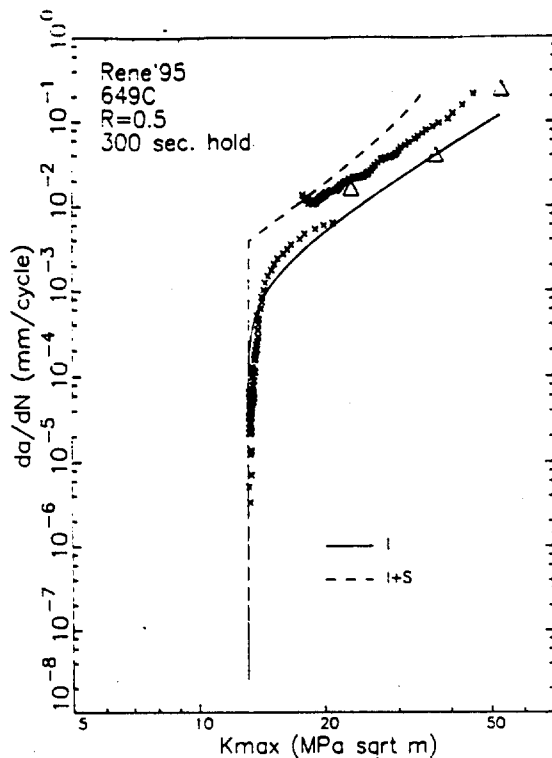
Comparison of experimental data with predictions from interpolation model (I) and interpolation + superposition model (I+S) for Rene'95 tested at 649°C with R=0.0 and hold times of (a) 4 seconds, (b) 30 seconds, and (c) 300 seconds.



(a)



(b)



(c)

Figure 7.11:

Comparison of experimental data with predictions from interpolation model (I) and interpolation + superposition model (I+S) for Rene'95 tested at 649°C with R=0.5 and hold times of (a) 4 seconds, (b) 30 seconds, and (c) 300 seconds.



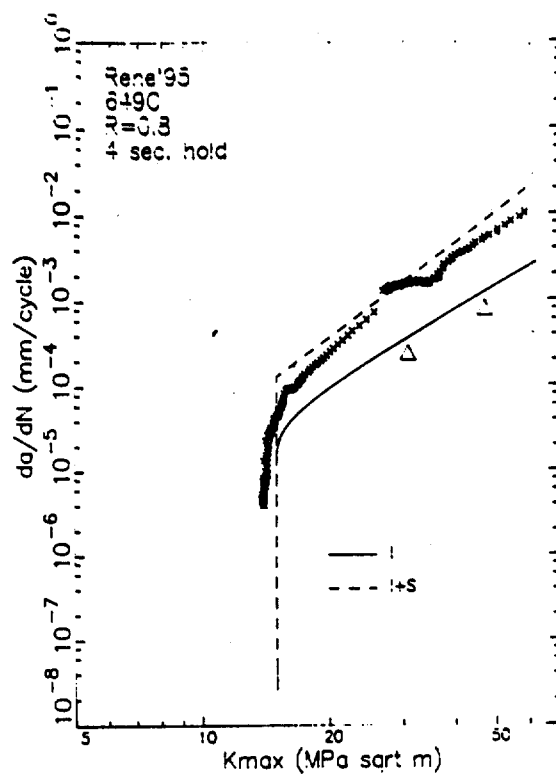
calculates a crack growth rate based on the initial crack length. When the interpolation model is applied, the crack length is incremented after each cyclic and static calculation. During long hold times this results in  $K$  levels higher than specified at the start of the cycle. This also occurs during the testing as well.

Figure 7.12 shows the predictions and the data for the 649°C,  $R=0.8$  hold time tests on Rene'95. In general both models adequately predict the Region II crack growth response. The largest deviation occur in the near threshold regime. Both models use the same threshold interpolation model. As noted earlier, the threshold model fairly accurately predicts the initial drop in threshold with increasing hold times but does not predict the increased threshold for a 300 second hold time as shown in Figure 7.12c.

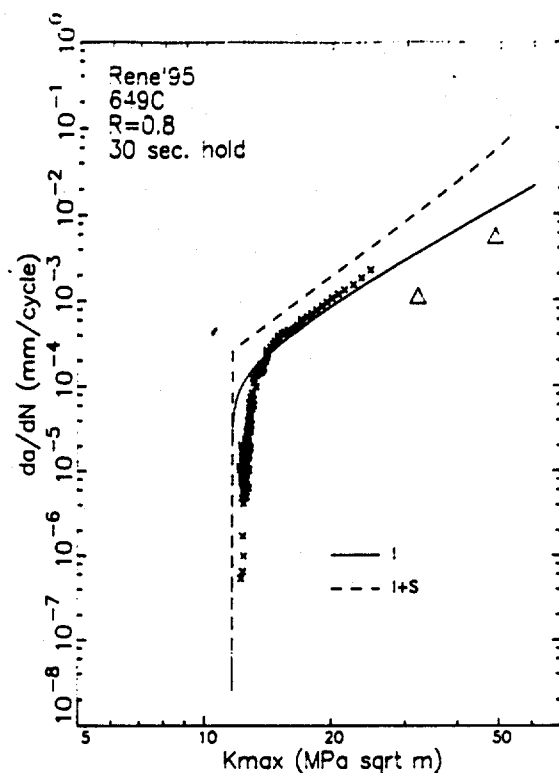
The comparison of the models and experimental data for the  $R=0$  frequency tests are shown in Figure 7.13. The test results shown in Figure 7.13a represent one of the tests used to establish the cyclic crack growth curve for the I+S model. Both models accurately predict the results for the lower two frequencies. For a 300 second cycle period, the totally interpolative model predicts the response much better than the I+S model which overpredicts the crack growth rates by a factor of four.

Figure 7.14 shows the predictions and data from the 649°C,  $R=0.5$  frequency tests. The crack growth data from the 300 second cycle period threshold test shown in Figure 7.14c were from the K-shed portion of that test. No increasing  $K$  data were obtained in that specimen. It would be expected that the true crack growth rates would lie slightly higher than those shown for the constant  $\Delta K$  data. The predictions of the interpolation model seem to fall below the data, while the superposition model appears to accurately predict the response.

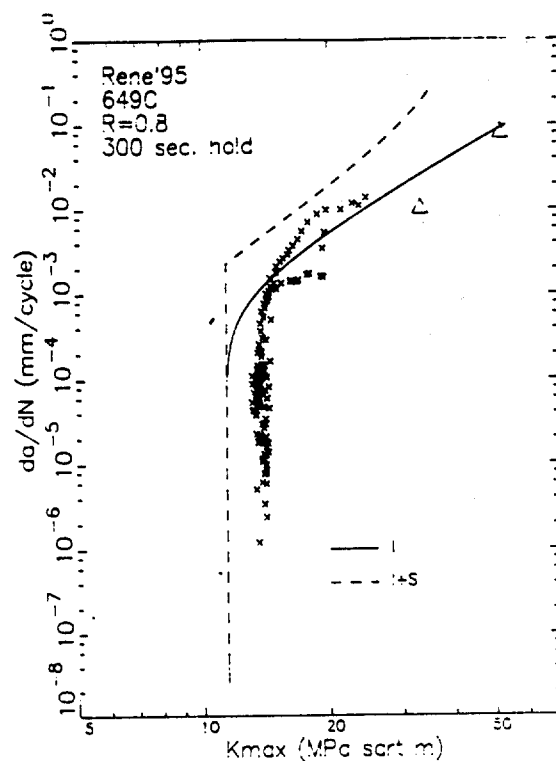
The comparisons for the  $R=0.8$  frequency tests are shown in Figure 7.15. For these test conditions, the I and I+S model predictions of the Region II crack growth rates are different by at least an order of magnitude. Based on the data from the threshold tests (small symbols), the superposition model



(a)



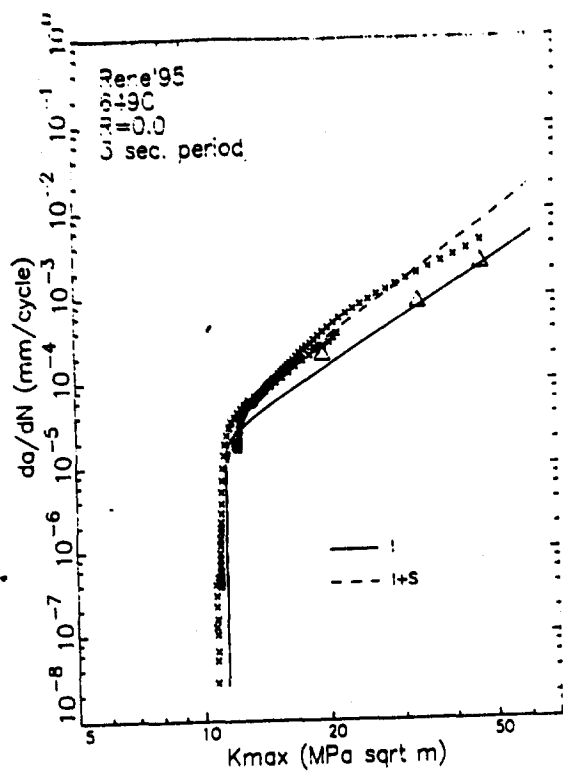
(b)



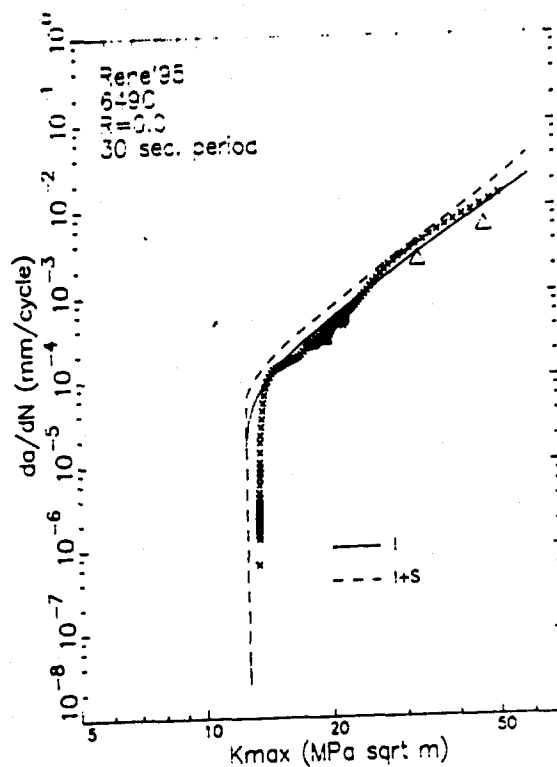
(c)

Figure 7.12:

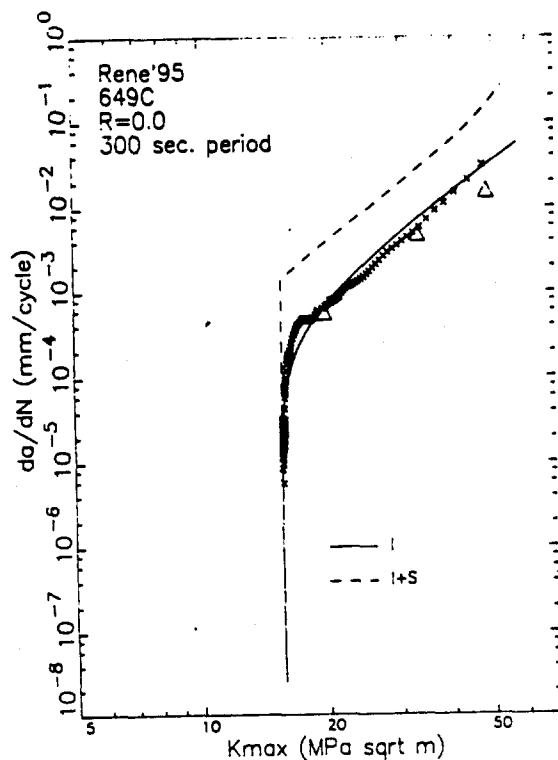
Comparison of experimental data with predictions from interpolation model (I) and interpolation + superposition model (I+S) for Rene'95 tested at 649°C with R=0.8 and hold times of (a) 4 seconds, (b) 30 seconds, and (c) 300 seconds.



(a)



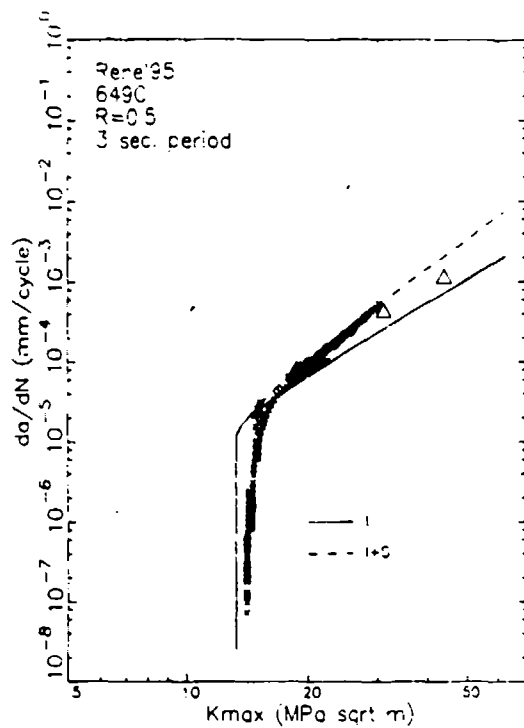
(b)



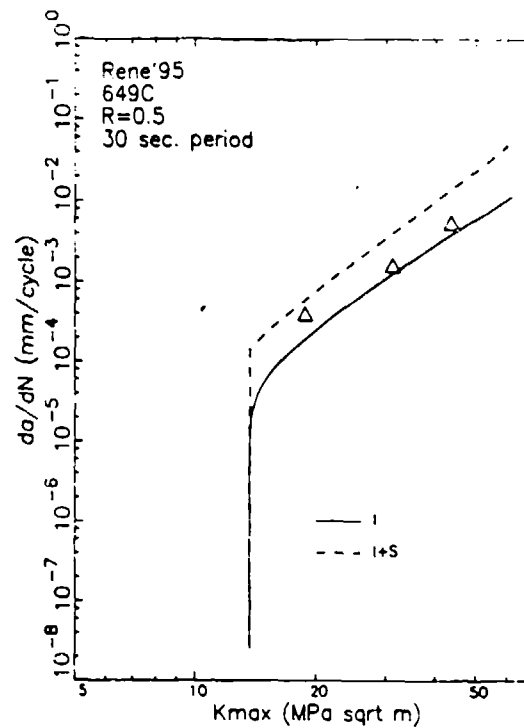
(c)

Figure 7.13:

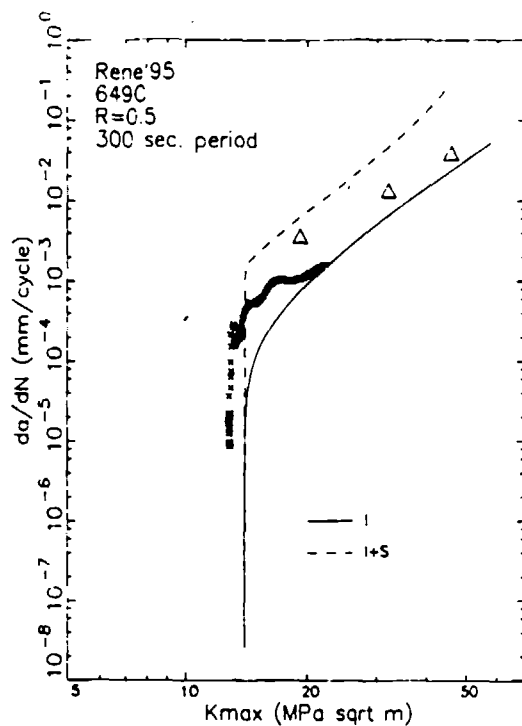
Comparison of experimental data with  
 predictions from interpolation model  
 (I) and interpolation +  
 superposition model (I+S) for  
 Rene'95 tested at 649°C with R=0.0  
 and cycle periods of (a) 3 seconds,  
 (b) 30 seconds, and (c) 300 seconds.



(a)



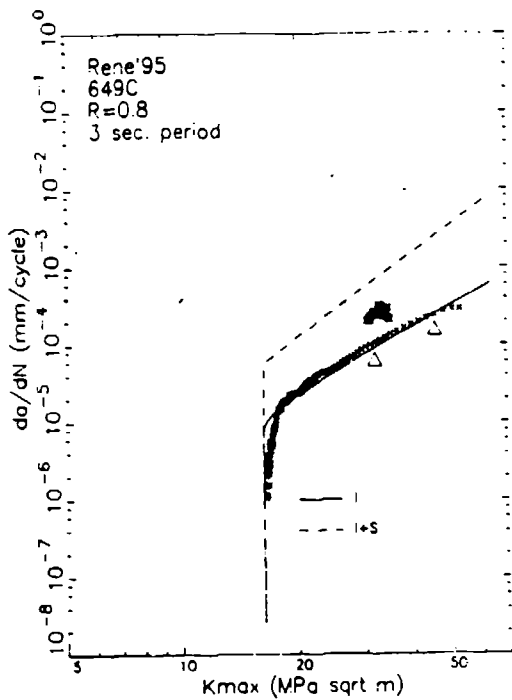
(b)



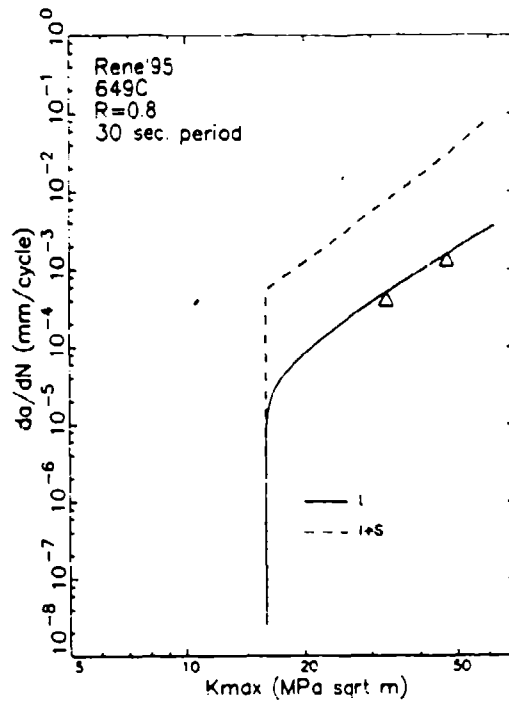
(c)

Figure 7.14:

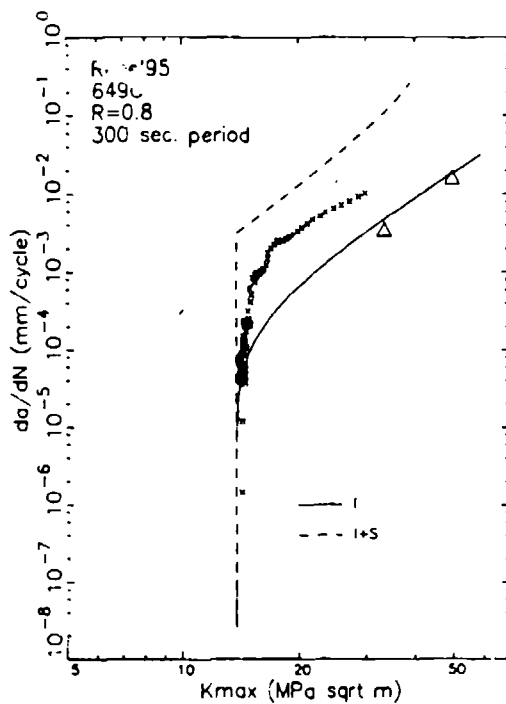
Comparison of experimental data with predictions from interpolation model (I) and interpolation + superposition model (I+S) for Rene'95 tested at 649°C with R=0.5 and cycle periods of (a) 3 seconds, (b) 30 seconds, and (c) 300 seconds.



(a)



(b)



(c)

Figure 7.15:

Comparison of experimental data with predictions from interpolation model (I) and interpolation + superposition model (I+S) for Rene'95 tested at 649°C with R=0.8 and cycle periods of (a) 3 seconds, (b) 30 seconds, and (c) 300 seconds.

appears to be overpredicting the lives by a factor of two or three while the interpolation model is underpredicting the lives by a similar amount.

Both models accurately predict the general trends in the crack growth response. The interpolation model suffers from consideration of some of the artificially low constant  $\Delta K$  test data. It is very encouraging to observe the ability of the superposition model to predict the long hold time and cycle period data because none of those data were used to develop the non-threshold time dependent contribution to the crack growth rates.

One of the major concerns with interpolation models is the ability of that model to predict the response outside the range of conditions over which the model was calibrated. There was no additional data available from this investigation to compare with these models but work by Weesooriya<sup>(24)</sup> has clearly established that there is a transition from cycle dependent to time dependent growth with increasing cycle period or hold time. The interpolation and superposition model developed for Rene'95 at 649°C was evaluated for R-ratios of 0, 0.5, and 0.8 and for hold times and cycle periods ranging from 0.01 to 1000 seconds. The loading ramps associated with the hold time cycles were each 0.005 seconds long resulting in a cyclic time (V) of 0.01 seconds or a cycle 0.01 seconds longer than the hold time. This rapid loading was used so that the influence of loading rate would be small compared to the hold time effect. Predictions were performed for cycles with a maximum K ( $K_{max}$ ) of 40 MPa/m using the crack growth option in ACDCYCLE. This value of  $K_{max}$  was selected so that the cyclic threshold was exceeded.

Figure 7.16 show the predictions of the superposition model for hold times and cycle periods. The transition from cycle to time dependency with increasing cycle time is observed for both types of cycles. There is a strong influence of R-ratio at rapid cycling due to the impact of R on  $\Delta K$  which to a large extent controls the cyclic crack growth rates. As hold time increases (Figure 7.16a), there is no longer any influence of R on the crack growth rates. The influence of R reverses from the cyclic to time dependent portion. This response is qualitatively similar to the results of Weerasooriya<sup>(24)</sup> for Alloy 718.

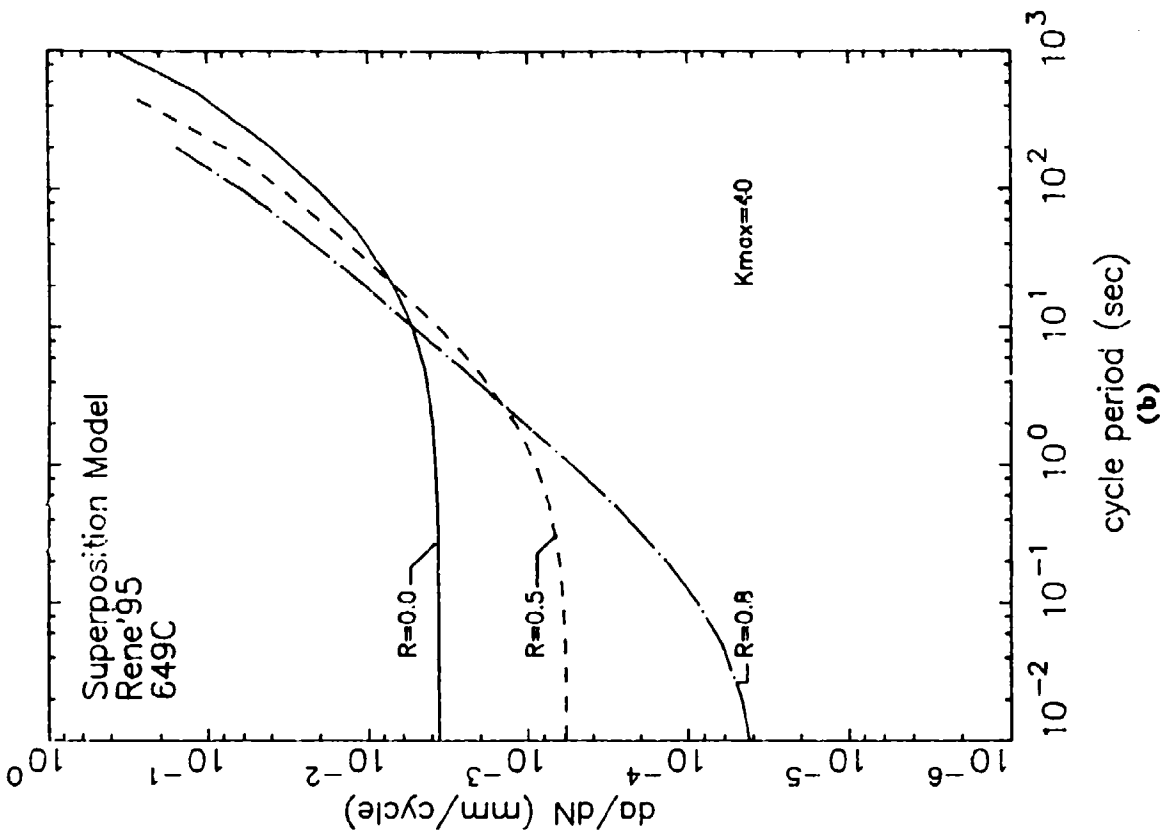
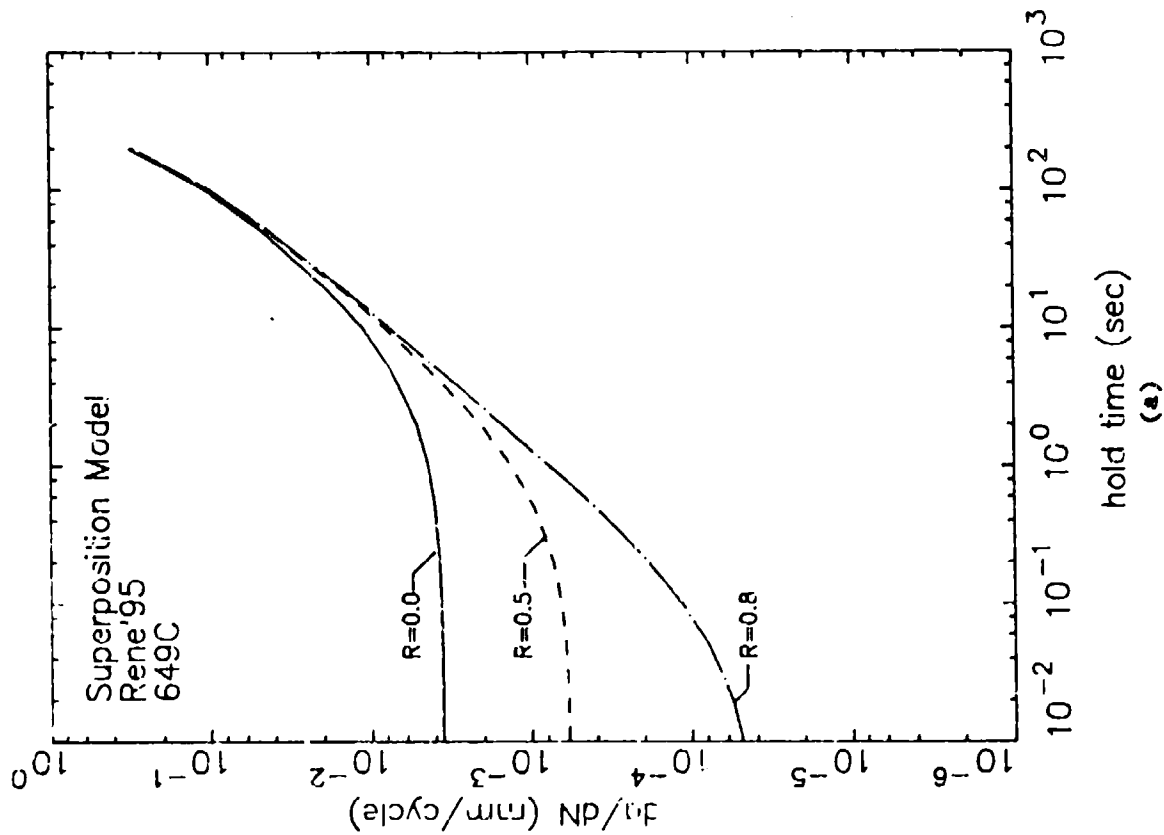


Figure 7.16: Predictions of crack growth rates in Rene'95 at 649°C with (a) hold time and (b) cycle period (frequency) using the superposition model.

These predictions illustrate that the conditions where the transition between cycle and time dependent conditions are a measure of the relative contributions of the cyclic and static crack growth rather than the absolute time-dependent contribution. If one ignores the static contribution from the rapid loading ramps, the static contribution to the hold time cycles (Figure 7.16a) is identical. The time required for the transition from cycle to time dependent conditions decreases with increasing R-ratio due to the influence of R on the cyclic crack growth rates.

The predictions of the totally interpolative model for the same cycles are shown in Figure 7.17. In this case the transition is shown for the hold time cycles (Figure 7.17a), but not for the frequency cycles (Figure 7.17b). The latter result is possible based on the experimental data but seems unreasonable. The crack growth rates measured for Rene'95 at R=0 with a three second cycle period in vacuum were about four times lower than those measured in air under the same conditions (Figure 6.16a). In addition, the cracks in vacuum propagated in a transgranular mode. It is reasonable to think that this is close to a lower bound crack growth rate in Rene'95. The crack growth rates predicted by the interpolation model (Figure 7.17b) decrease two orders of magnitude for cyclic periods between 0.01 and 3 seconds.

The crack growth rates predicted for hold time cycles are significantly lower for the interpolation model than for the superposition model. The hold time and frequency predictions for the R=0 cycles are replotted in Figure 7.18. Figure 7.18a shows that the superposition model predicts that a 300 second cycle period frequency test would have a crack growth rate approximately four times lower than a 300 second hold time cycle. That is very similar to the experimentally observed data (Figure 5.13a) for 1.5 second loading ramps relative to the 0.005 second ramps used in the predictions shown in Figure 7.18a. The predictions of the interpolation model (Figure 7.18b) show that for the longer cycle periods, cracks experiencing hold times grow a factor of 20 slower than cracks in frequency tests. This also seems to be physically unreasonable.



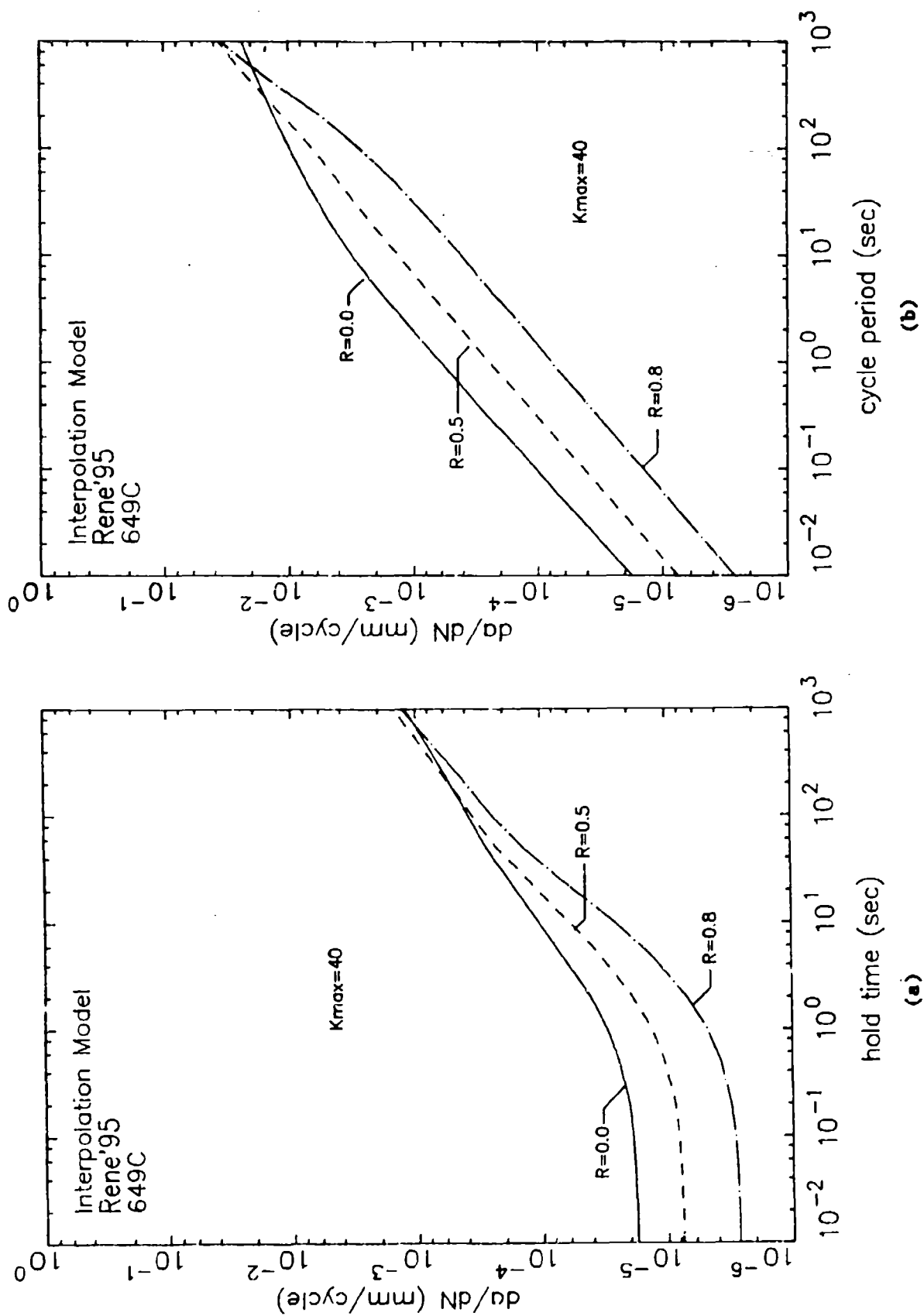


Figure 7.17: Predictions of crack growth rates in Rene'95 at 649°C with (a) hold time and (b) cycle period (frequency) using the interpolation model.

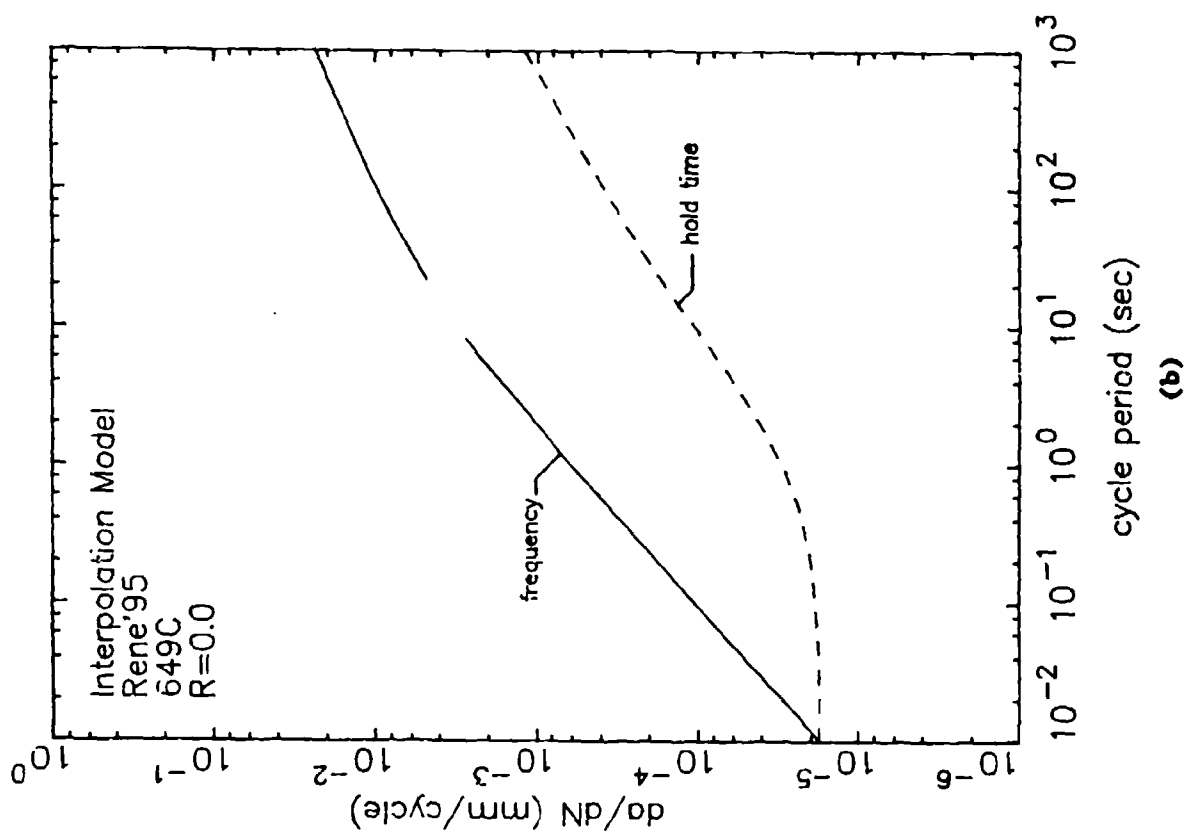
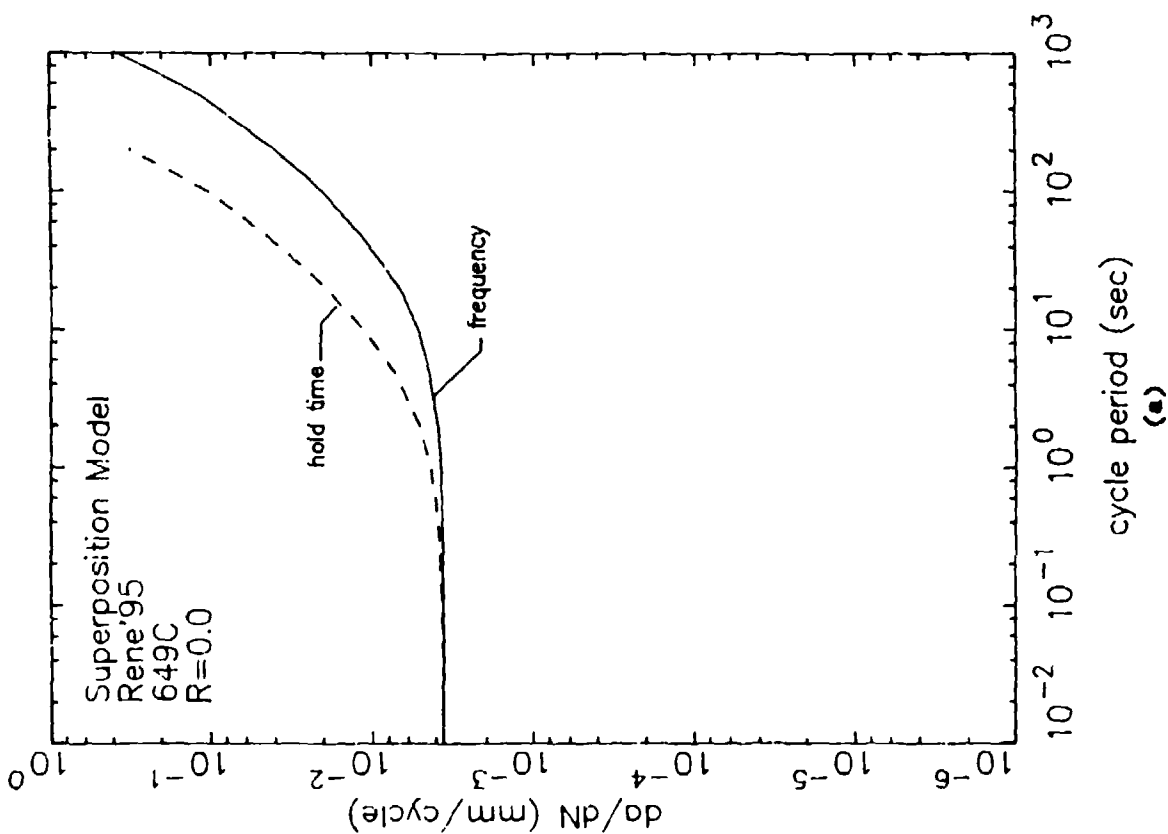


Figure 7.18: Comparison of crack growth predictions for R=0 hold time and frequency cycling of Rene'95 at 649°C using the (a) superposition and (b) interpolation models.

The reason for this behavior is an extreme sensitivity of the interpolation model to low frequencies. A second set of hold time predictions was performed with a loading and unloading ramp of 1.5 seconds, the experimental conditions used in this investigation. Figures 7.10 through 7.12 demonstrated that the interpolation model adequately predicts crack growth during this type of cycle. Figure 7.19 compares the predictions for the 0.005 second and 1.5 second loading ramps. The superposition model (Figure 7.19a) predicts a very small influence of loading ramp and only when the crack growth rate is dominated by the crack growth associated with the loading ramps. The interpolation model (Figure 7.19b) predicts sixty fold difference in crack growth rates over the entire range of hold times.

The excessive sensitivity of the interpolation model to frequencies could be remedied by collecting data over a wider range of conditions or reformulating the equations describing B, P, and Q. This sensitivity demonstrates a basic weakness of any interpolation methodology. The interpolation approach is basically a curve fitting technique and if the range of input data or the constructions of the crack growth constants do not adequately cover all conditions over which the crack growth predictions must be performed, this type of model can lead to extremely erroneous predictions.

On this basis, the remaining effort in this investigation will consider only superposition models. This approach has the additional benefit that the concept behind the model reflects the underlying mechanisms of time dependent crack growth as reported in Section 6. By the basic nature of the model, it will always show the transition from cycle to time dependent behavior.

#### 7.3.5 Retardation model

The retardation model discussed in Section 7.2 was applied the 649°C Rene'95 hold time retardation tests. Retardation is history dependent so the static retardation constants were determined by predicting the entire crack length history of each of the five 649°C Rene'95 hold time retardation tests. This was accomplished using the stacked case option in AGDCYCLE. Figure 7.5 schematically illustrates that if the value of K is reduced to below the

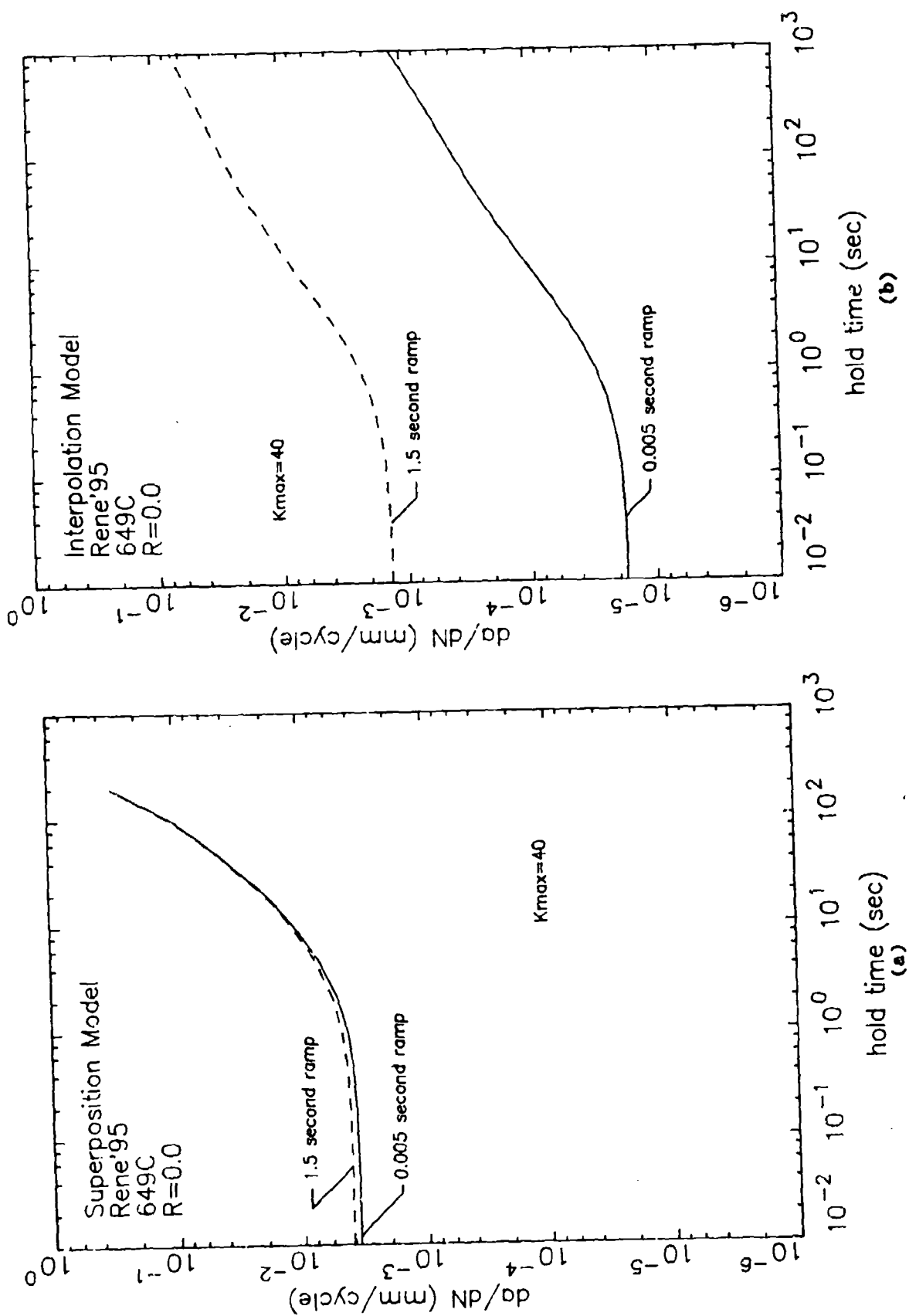


Figure 7.19: Comparison of 649°C Rene'95 crack growth predictions for R=0 hold time cycles with 0.005 and 1.5 second loading ramps using the (a) superposition and (b) interpolation models.

static threshold and the crack growth rate is independent of the hold time, only a lower bound for  $\Phi$  can be determined. This required that the value of  $\Phi$  be evaluated for testing conditions which showed time-dependent behavior, so the static retardation constants were determined using the 10 percent overpeak tests. In each of the two 10 percent overpeak tests ( $R=0.0$  and  $0.5$ ), there were four hold time segments (0, 4, 30, and 300 seconds) at a constant value of  $K_{01}$ . Repetitive ACDCYCLE analyses were performed to determine the value of  $\Phi$ , which best predicted the number of cycles for all four hold times. The longer the hold time, the more sensitive the result was to  $\Phi$ . Figure 7.20 shows the resulting values of  $\Phi$  for the six segments in these two tests. It appears that  $\Phi$  is linear with  $K_{01}$  and does not seem to be very sensitive to  $R$  ratio. The line in this figure is the best fit through the data. The slope and intercept determined the values of  $\Phi_1$  and  $\Phi_2$ . The values of the retardation constants are listed in Table 7.6.

The values of  $\Phi$  are much larger than unity as anticipated from Figure 7.5. Consideration of elastic unloading requires that  $\Phi$  not exceed 1. The fact that  $\Phi$  must exceed 1 suggests that this is not a good retardation model and/or that other complex stress relaxation processes are occurring. The strong influence of creep in time dependent crack growth suggests that the latter may be true. Complicated creep-assisted stress redistribution probably plays an important role in the retardation of static crack growth after only relatively small overpeaks.

The values of  $\Phi_1$  and  $\Phi_2$  were used to predict the number of cycles required to propagate through all the individual segments in the 649°C overpeak hold time test specimens. These results are compared with the experimentally measured values in Figure 7.21. The solid line in these figures represents perfect agreement. The dashed lines enclose a region which is within a factor of two of the perfect agreement. In all but a few occasions, the predictions agree within a factor of two of the experimental data. Most of those exceptions occurred for test conditions with 300 second hold times.

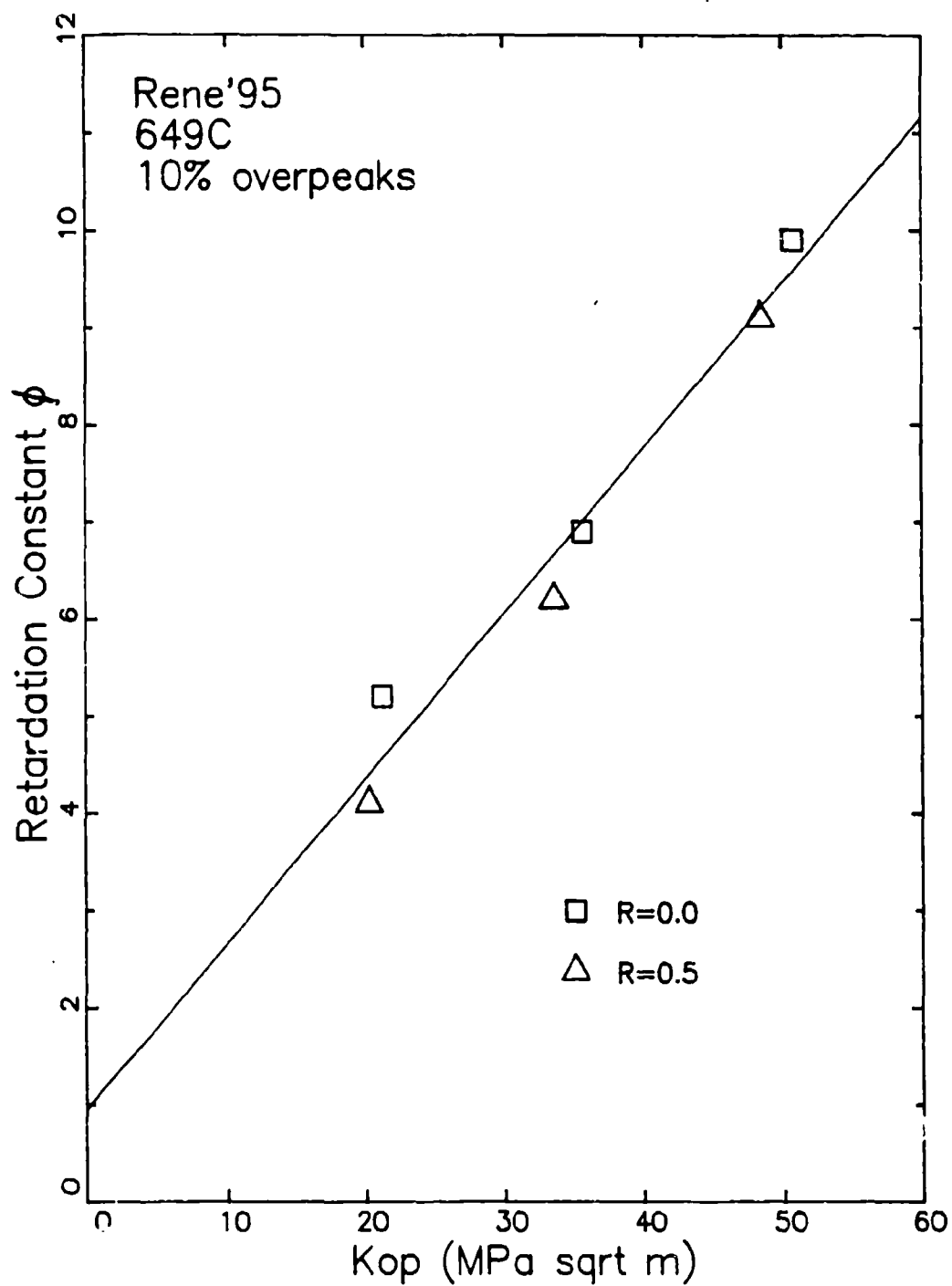
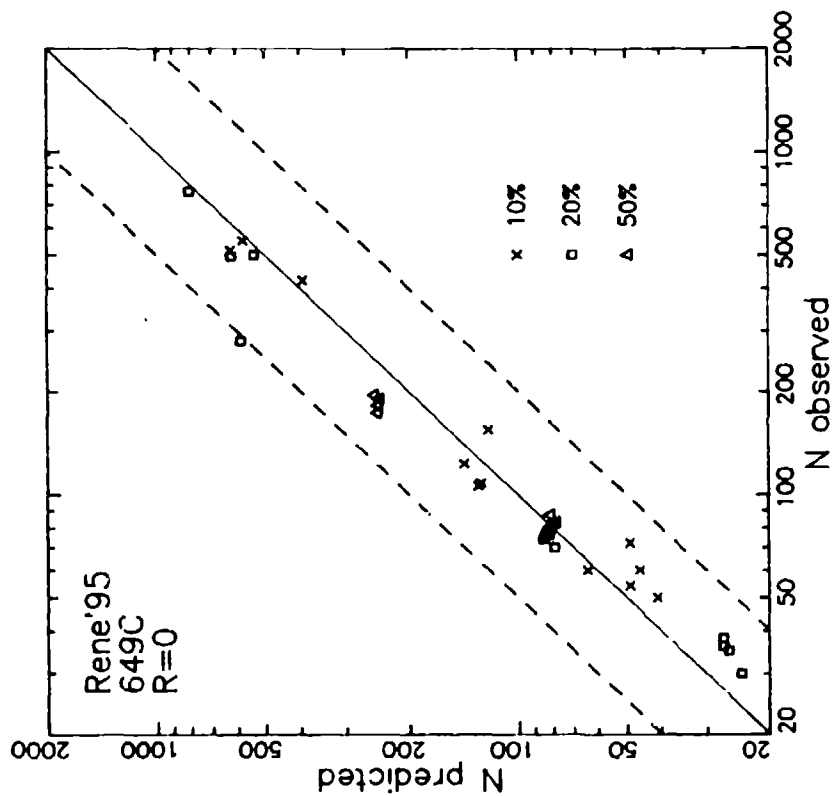
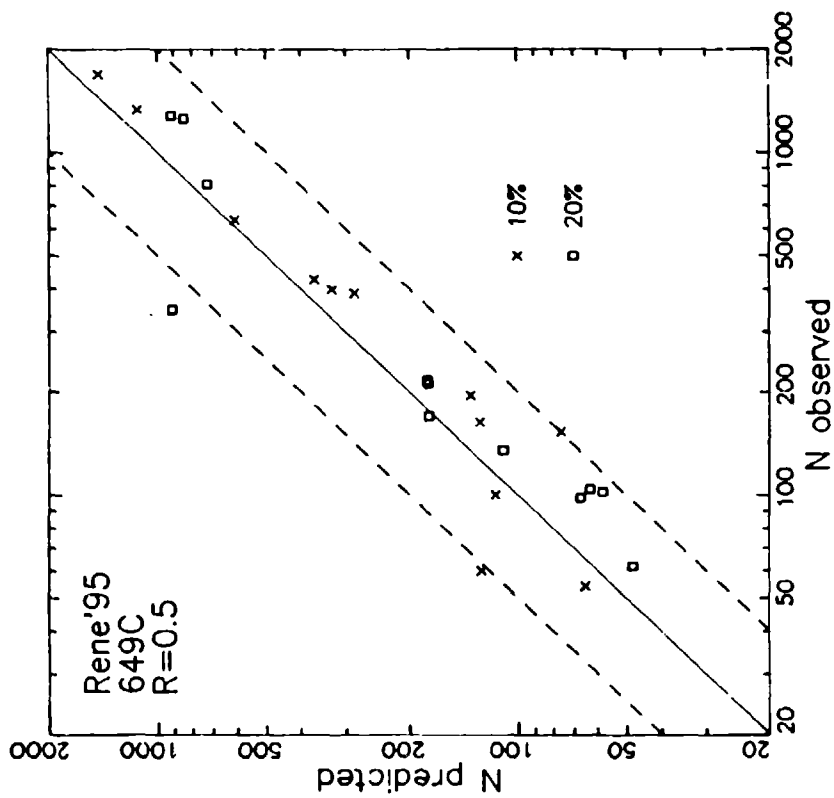


Figure 7.20: Variation of  $\phi$  with  $K_{01}$  for 649°C Rene'95 hold time overpeak tests with 10% overpeaks.



(a)



(b)

Figure 7.21: Comparison of predicted and observed cycles to propagate through individual segments of 649°C  
Rene'95 hold time overpeak tests with R-ratios of (a) 0.0 and (b) 0.5.

The results of these tests were treated using an effective crack growth rate; that is, the crack length increment of a given segment (constant R,  $K_{01}$ , and hold time) divided by the cycles to propagate through that segment. To illustrate the beneficial effects of static retardation, the effective crack growth rates determined from the test specimen data was compared to the analyzed lives. The analyses were performed using three different options available in ACDCYCLE:

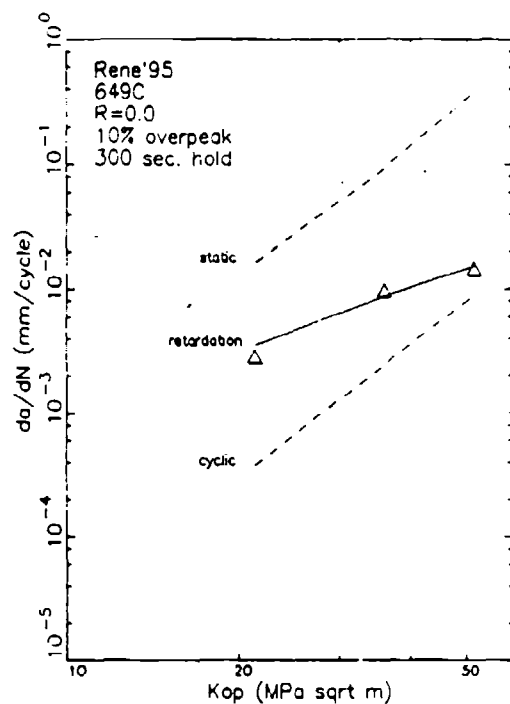
1. cyclic analysis (no static crack growth)
2. static analysis (no retardation)
3. retardation (permit static growth and retardation)

The effective crack growth rates determined from the 649°C, Rene'95 tests and the three types of ACDCYCLE analyses. The results for the R=0, 300 second hold time tests are compared in Figure 7.22. These results show excellent agreement between the experimental data and the retardation predictions. One of the segments which fell outside of the 2 fold scatter band was the 20% overpeak condition at the lowest value of  $K_{01}$ . The comparison with the various analyses show that even with a 10% overpeak, there is a significant benefit from static retardation. This benefit increases with increasing K levels and overpeak ratios. The retardation results never totally eliminate a time dependent effect due to the influence of the 15 second loading and unloading cycle in these tests.

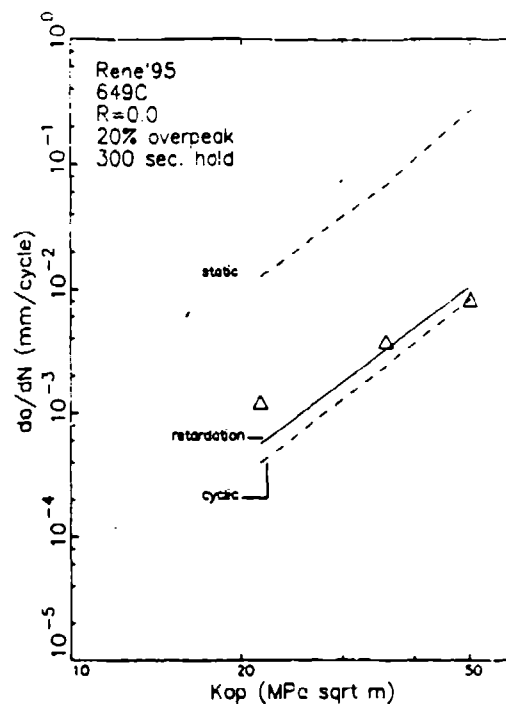
A similar comparison for the 649°C, R=0.5 Rene'95 overpeak tests are shown in Figure 7.23. As in the lower R ratio tests, the 20% overpeak condition at the lowest value of  $K_{01}$  fell outside the two fold scatter band. These results also show the same general trend of increasing benefit with higher overpeaks and higher K values.

This retardation model accurately predicts the lives of the constant K test results. This is extremely remarkable considering the very complex behavior of these materials and the fact that there are just two adjustable constants in the model ( $\Phi_1$  and  $\Phi_2$ ).

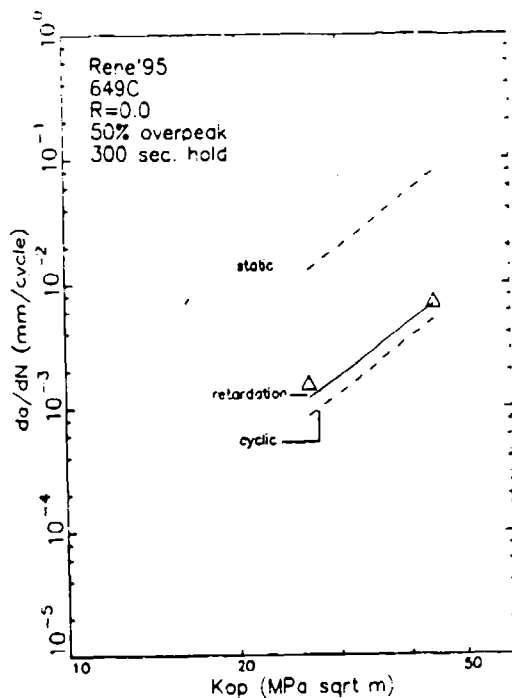




(a)



(b)



(c)

Figure 7.22:

Comparison of ACDCYCLE predictions  
 with experimental crack growth rates  
 in 649°C, R=0.0 Rene'95 hold time  
 overpeak tests with 300 second hold  
 times and (a) 10%, (b) 20%, and (c)  
 50% overpeaks.

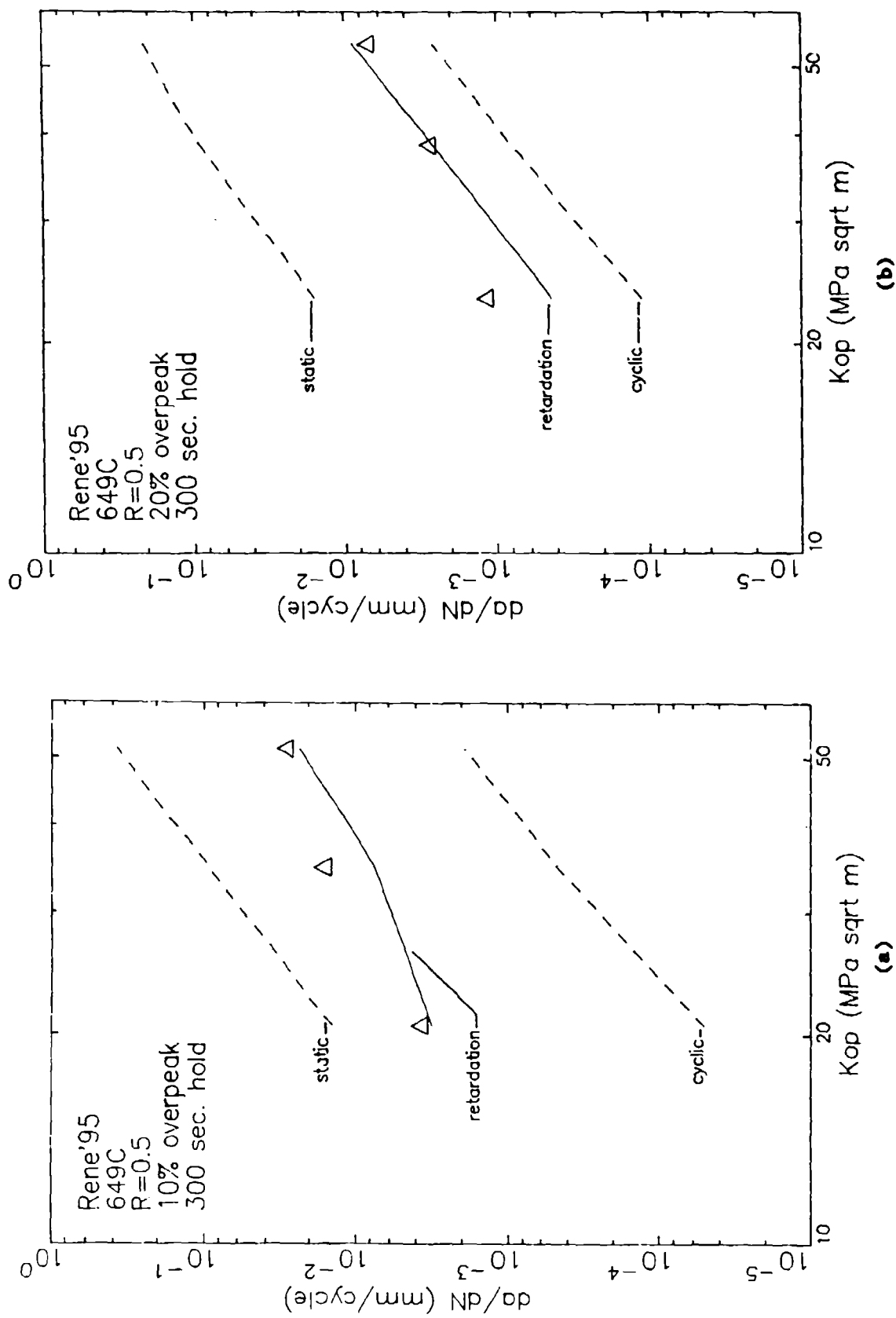


**Figure 7.23: Comparison of ACDYCLE predictions with experimental crack growth rates in 649°C, R=0.5 Rene'95 hold time overpeak tests with 300 second hold times and (a) 10% and (b) 20%.**

The retardation model was used predict two situations encountered during the prediction of the experimental data where there may be a significant effect of retardation. Effective crack growth rates were determined by permitting a crack to propagate 2.5 mm (0.1 inch) after it had fully developed its retardation zone. These analyses were performed using the stacked case option in ACDCYCLE. The first situation modeled was the R=0, 300 second cycle period (frequency). It was previously shown (Figure 7.13c), that the superposition model overpredicted this condition by about a factor of four. The benefits of static retardation for loading ramps was shown in Figure 7.4. This loading situation was modeled in three different ways:

1. no retardation
2. retardation with a block size of 1
3. retardation with a block size of 5

The block size is the number of cycles between load changes in these constant  $\Delta K$  tests. The block size of 5 was selected because that was the block size for all three 300 second cycle segments in the R=0 test at 649°C. Figure 7.24 shows these three types of predictions along with the experimentally measured crack growth rates. Static retardation reduces the predicted crack growth rates by approximately 50 percent. There is relatively little influence of block size until the crack growth rates get to high levels where there would be a relatively large increment in crack growth between load adjustments. Once this level is reached there is a rapid drop in the predicted crack growth rates as indicated in Figure 7.24. It is difficult to perform these types of analyses because ACDCYCLE terminates the analysis when  $K_{max}$  reaches 96% of  $K_c$ . There needs to be a significant increase in  $K$  during the cycle in order to result in significant additional retardation.

The retardation constants used during loading ramps are the cyclic constants and  $\phi$  cannot exceed 1. For hold time segments, the static constants are used and there is no maximum value cap on  $\phi$ . Under this situation, the amount of retardation predicted for constant  $\Delta K$  testing cycles may be different for different block sizes. This concept was evaluated for the R=0, 300 second hold time tests which showed an order of magnitude difference in

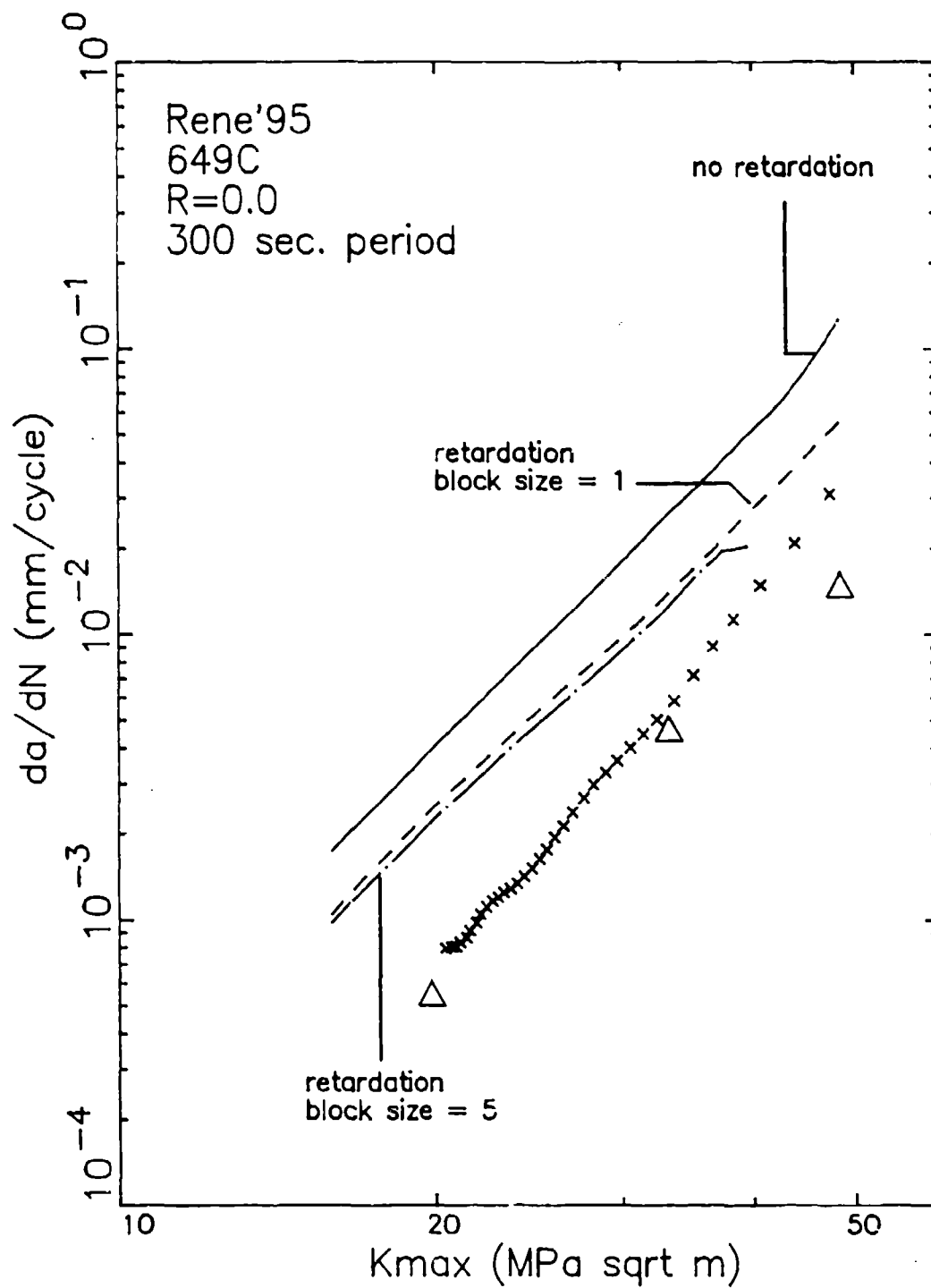


Figure 7.24: Comparison of ACDCYCLE predictions with experimental crack growth rates in 649°C, R=0.0 Rene'95 test with a cycle period of 300 seconds.

crack growth rate between constant load or increasing K tests and constant  $\Delta K$  tests. The results of the analysis with no retardation and retardation with a block size of one is shown in Figure 7.25. Increasing K value results in more retardation for the block size of 1. Once the critical value is reached the predicted crack growth rate drops precipitously. It is interesting that the block sizes used in the constant  $\Delta K$  segments shown in Figure 7.25 were 5 for the lowest  $K_{max}$ , 3 for the intermediate  $K_{max}$ , and 1 for the highest  $K_{max}$ . It is interesting to note that the precipitous drop in K occurred between the data points measured with block sizes of 3 and 1.

The results of the analyses shown in Figures 7.24 and 7.25 suggest that static retardation can have a significant effect on the crack growth rates measured in the constant  $\Delta K$  tests. The observation that there was a much larger difference between the two types of test data (constant  $\Delta K$  vs. increasing  $\Delta K$ ) in the hold time tests is also consistent with the formulation of the retardation model.

The different treatment of ramps and hold times is no problem for the simple cycles evaluated in this investigation; however, as one performs mission analyses, the difference between a hold time segment and a high R-ratio ramp becomes almost indistinguishable. A similar problem exists for other time-dependent crack growth models where no static crack growth is assumed to occur for decreasing load ramps. If they are not counted, neither should hold time segments which might interrupt those ramps. The latter type of cycle is identical to those in the overpeak hold time tests where significant time dependent crack growth was observed for small values of the overpeak ratio. The potential difficulties suggest that this is a good engineering approach to static retardation, but the process is poorly understood, and the concept behind the retardation model may not reflect the operating retardation mechanism.

#### 7.4 MODELING OF ALLOY 718 AT 649°C

The crack growth data determined for Alloy 718 at 649°C were modeled using procedures similar to those described in Section 7.3 for Rene'95. There

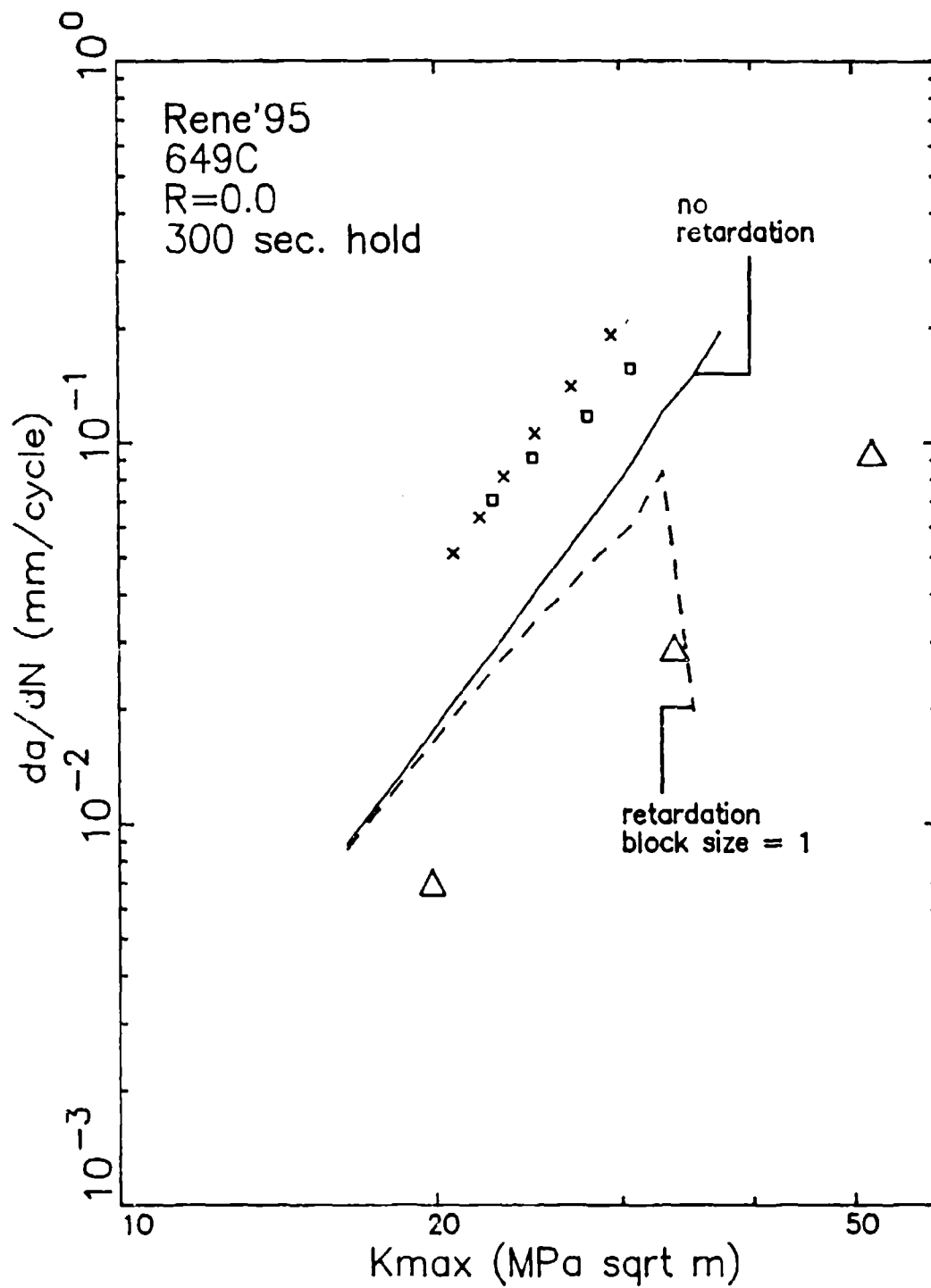


Figure 7.25: Comparison of ACDCYCLE predictions with experimental crack growth rates in 649°C, R=0.0 Rene'95 test with a hold time of 300 seconds.

were two major exceptions - no Alloy 718 threshold data were obtained as a function of frequency so only the hold time portion of the threshold model was derived and a totally interpolative model for Alloy 718 was not developed for the reasons demonstrated in Section 7.3.4.

#### 7.4.1 Alloy 718 Threshold Model

The material constants for the interpolation threshold model (Equation 7.1) were determined using the same nonlinear optimization techniques used for Rene'95. An additional restriction was placed on the Alloy 718 model where all constants related to testing frequency were set to zero because Alloy 718 threshold data was not collected as a function of test frequency. The constants for the threshold interpolation model are listed in Table 7.7. The results of this model are compared to the hold time threshold data as shown in Figure 7.26. The model accurately predicts the influence of hold times for R ratios of 0 and 0.5. The sudden decrease in threshold at hold time of 30 seconds for a R-ratio of 0.8 was not modeled well, however the threshold at all other conditions were predicted reasonably well. This model predicts most of these threshold values within 5 MPa/m. The interpolative threshold model comprised the interpolative portion of the Alloy 718 interpolation + superposition model.

#### 7.4.2 Alloy 718 Interpolation + Superposition Model

The time-dependent contribution to Alloy 718 crack growth (non-threshold) was determined using the superposition of cyclic and static crack growth. The static crack growth curve used in the superposition model is represented by a Paris equation truncated at the lower end by a threshold value. The static threshold value was taken to be the lowest value of K at which crack growth was measured in the 649°C Alloy 718 static K-shed test. The 649°C static crack growth data shown in Figure 5.52 were edited to eliminate the near-threshold regime in the K-shed test and the artificial threshold data or "tails" in the constant load tests. Linear regression analysis to the logarithmic form of the Paris equation was performed to determine the best fit through the edited data. The static threshold and Paris equation constants

Table 7.7: Constants for 649°C Alloy 718 Interpolation Threshold Model

$$K_o = 12.059$$

$$K_s = 15.78$$

$$m = 0.43892$$

$$A = 0.0$$

$$B = 1.5964 \times 10^{-2}$$

$$C = 1.3355$$

$$D = 0.0$$

$$E = 3.5524 \times 10^{-2}$$



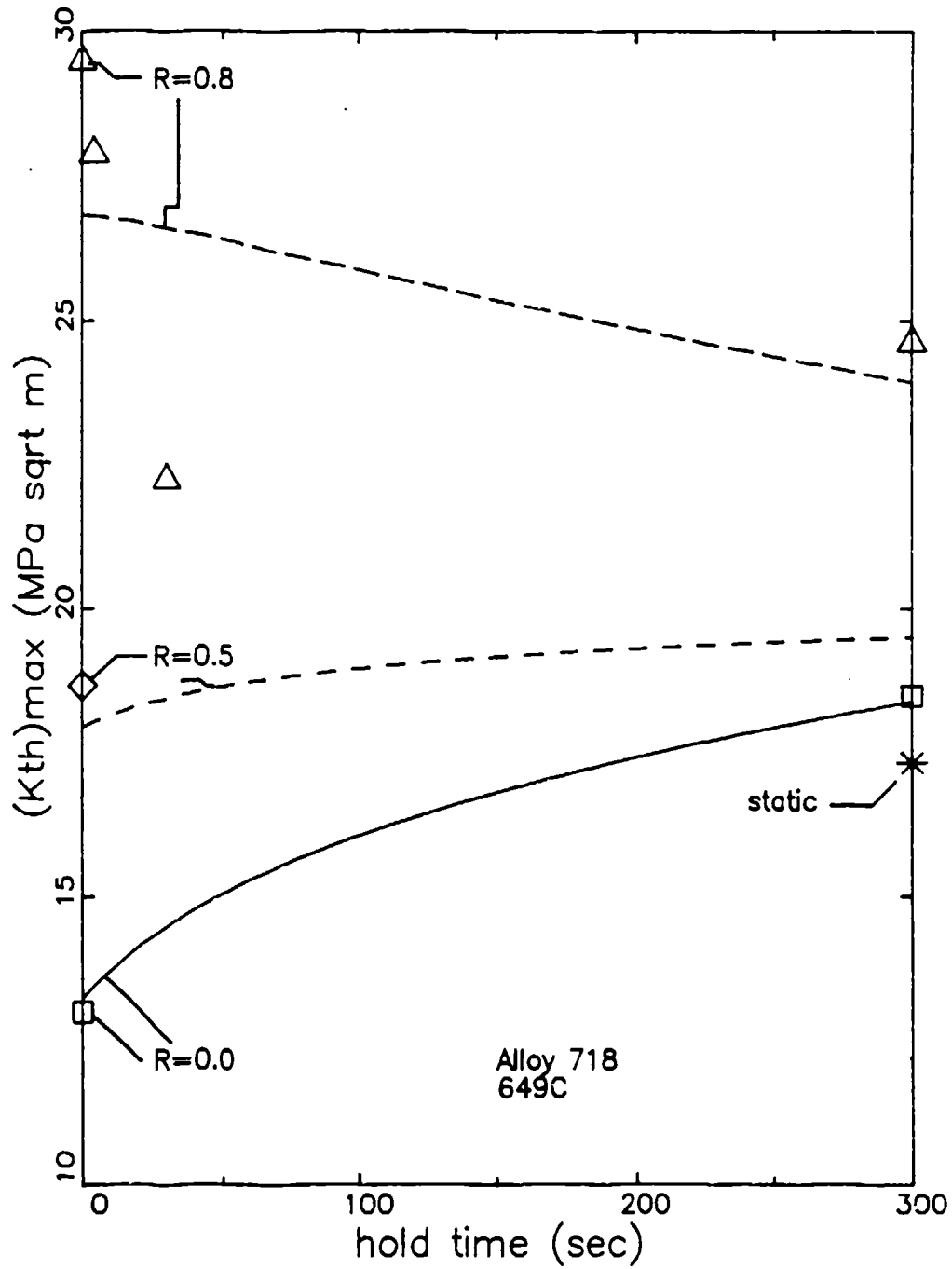


Figure 7.26: Comparison of 649°C Alloy 718 hold time threshold data with predictions from the interpolation threshold model.

are listed in Table 7.8. This curve is shown along with the 649°C Alloy 718 static crack growth data in Figure 7.27. This looks to be a good fit to the data, but similar to the observed behavior in Rene'95, there is a large amount of scatter in these data. The scatter may affect the establishment of a reliable static crack growth curve. The quality of this curve is extremely important because it is the source of the time-dependent contribution to the superposition model.

The 0 second hold time (3 second period) test data were used to determine the cyclic crack growth constants. The procedure used for Alloy 718 was different than that used for Rene'95. In Alloy 718, a cyclic crack growth curve was drawn through the R=0 continuously cycled data. The constants of the sigmoidal curve ( $K_{th}$ , B, P, Q, and D) were determined using nonlinear optimization analysis of the R=0, 0 second hold time tests. As in the case of Rene'95, the value of  $K_C$  was set to be 65.88 MPa/m (60 ksi/in.). ACDCYCLE was then used to combine the effect of the cyclic and static crack growth. The resultant curve was above the R=0 cyclic data and had a slightly higher slope. The slope of the calculated cyclic curve was decreased by adjusting the value of P in the sigmoidal equation which controls the slope of the curve at the inflection point which occurs in Region II. The totally cyclic curve, superposition (cyclic + superposition) curve, and R=0, 0 second hold time data are shown in Figure 7-28. These data show that the calculated superposition curve falls through the experimental data.

The value of the Walker exponent ( $m^+$ ) was determined from the R=0.5, 0 second hold time test data using an iteration approach. The cyclic curve, superposition curve, and experimental data for the R=0.5, 3 second cycle are shown in Figure 7-29 along with the crack growth data from the R=0.5, 0 second hold time tests. The agreement is quite good at low K values and diminishes with increasing stress intensity. The values of the cyclic crack growth constants are listed in Table 7.8.

Table 7.8: Constants for 649°C Alloy Superposition Model

Cyclic Constants

$K_{th}$	=	11.848	$Q$	=	0.85339
$K_c$	=	60.0	$D$	=	$-1.248 \times 10^{-2}$
$B$	=	-11.939	$m^+$	=	0.50
$P$	=	1.2129			

Static Constants

$K_g$	=	15.78
$C$	=	$5.517 \times 10^{-13}$
$n$	=	5.023

Static Retardation Constants

$\phi_1$	=	-3.237
$\phi_2$	=	0.241

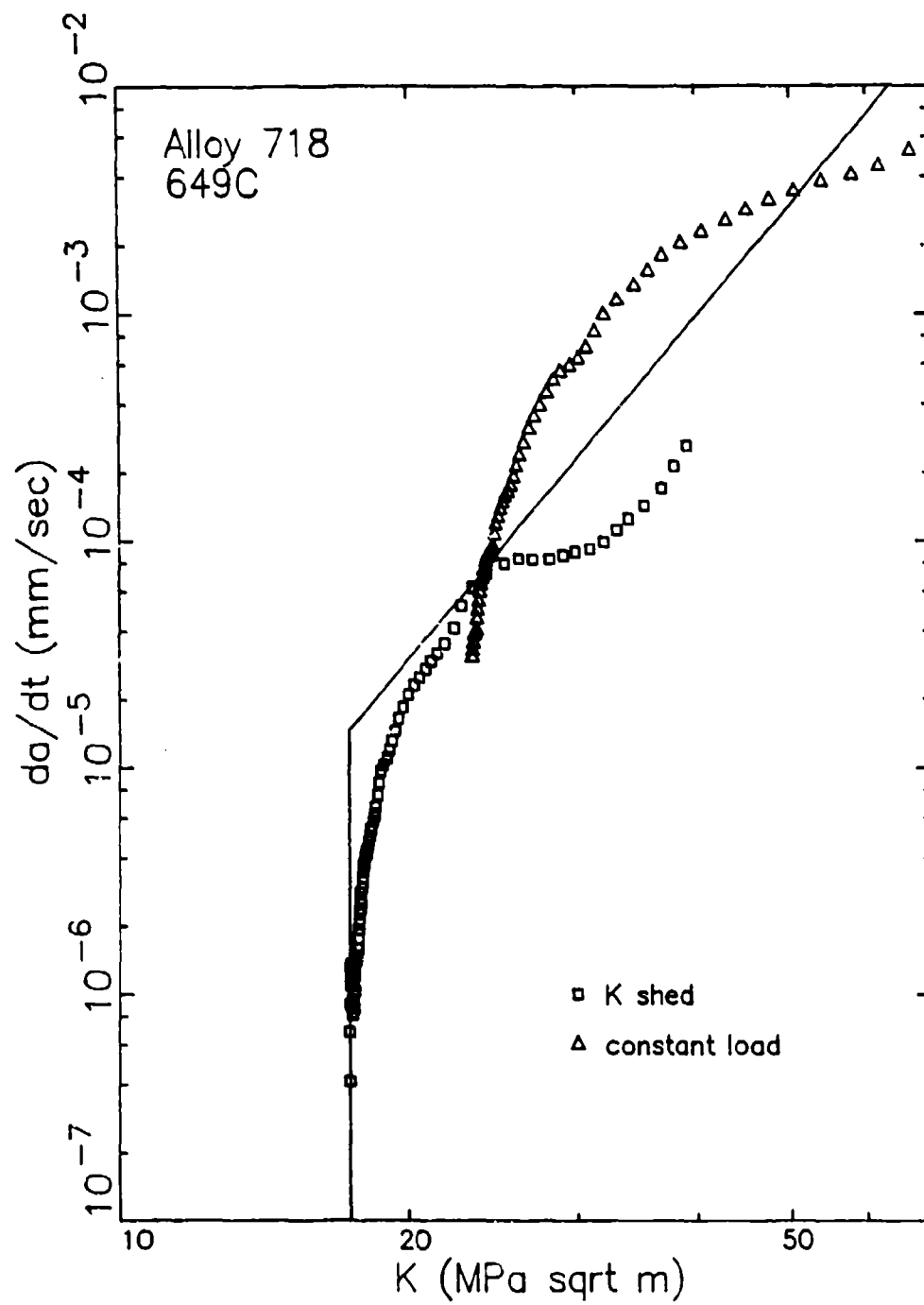


Figure 7.27: Static crack growth curve used in the 649°C Alloy 718 superposition model.

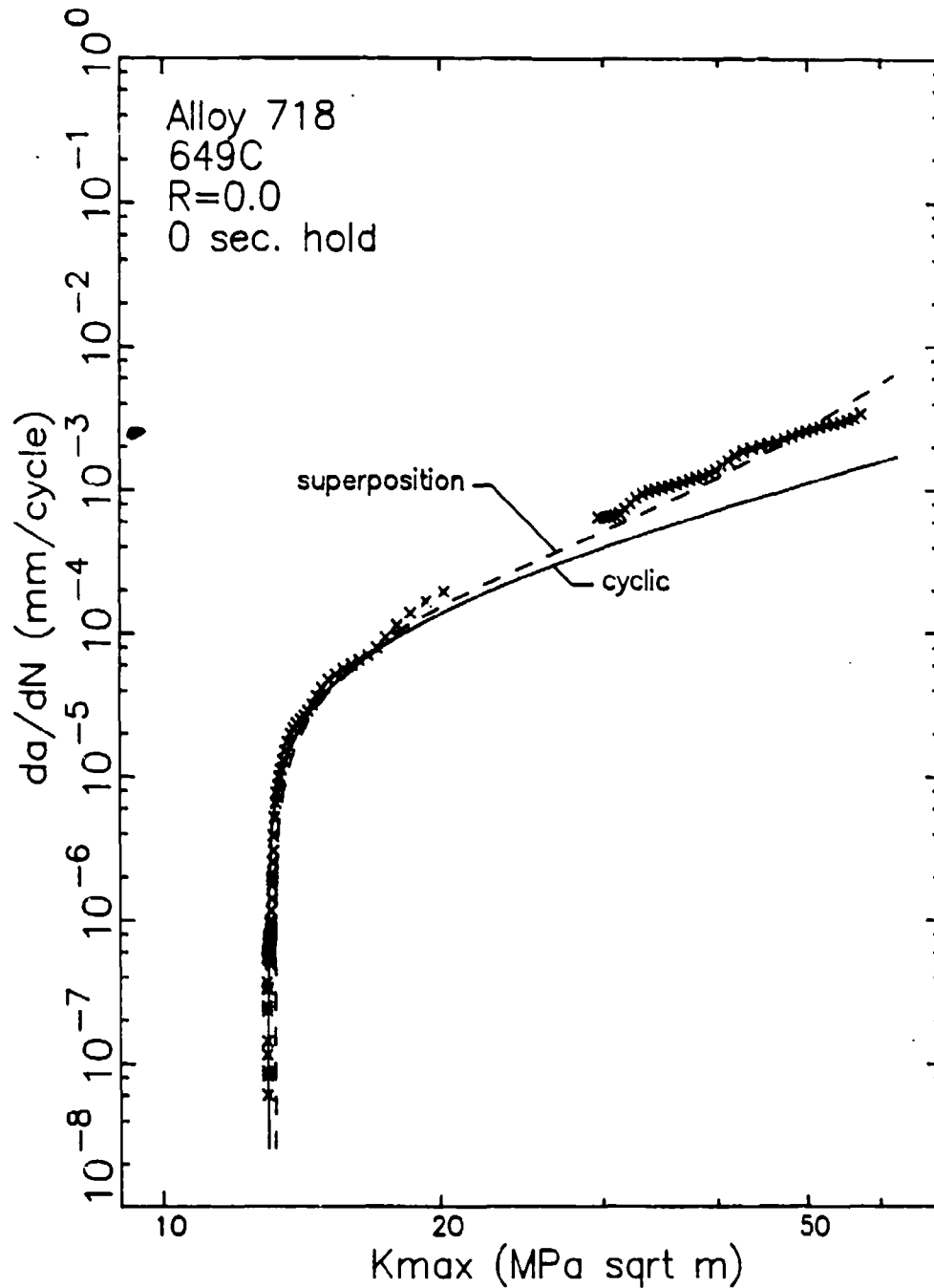


Figure 7.28: Comparison of cyclic and superposition ACDCYCLE predictions with Alloy 718 crack growth data measured during a R=0, 0 second hold time test in air.

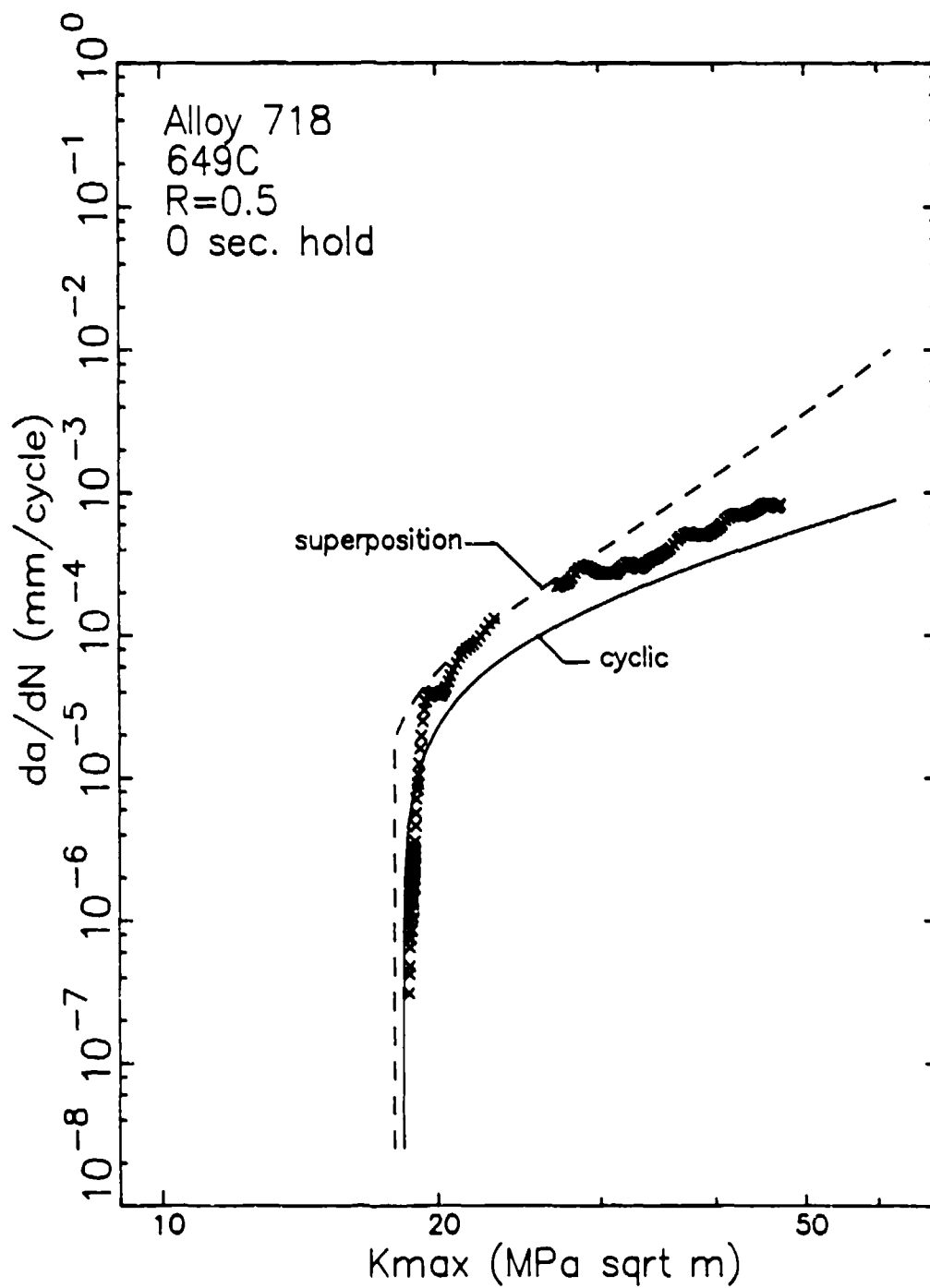
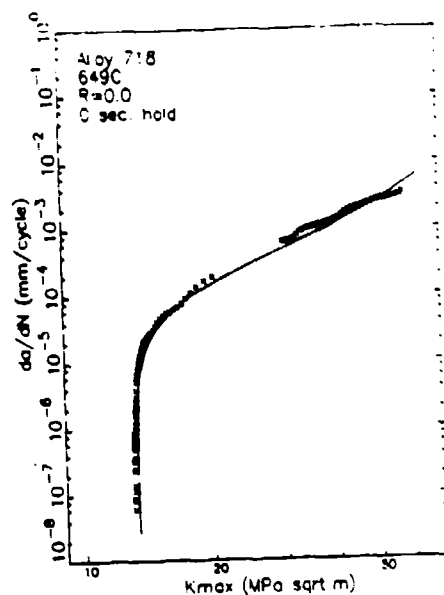


Figure 7.29: Comparison of cyclic and superposition ACDCYCLE predictions with Alloy 718 crack growth data measured during a R=0.5, 0 second hold time test in air.

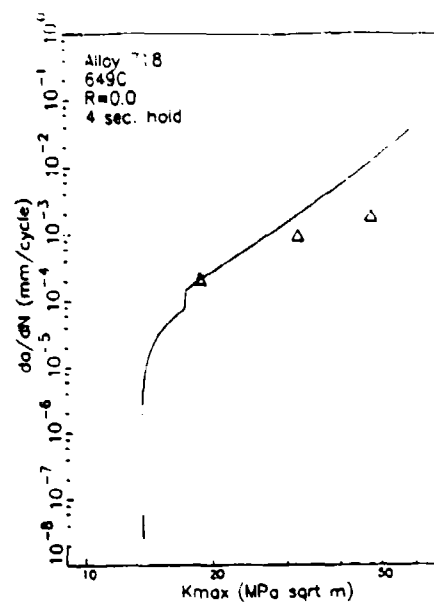
#### 7.4.3 Comparison of Predicted and Measured Crack Growth

The constants listed in Tables 7.7 and 7.8 were entered in materials data files and the crack growth option in ACDCYCLE was used to generate crack growth curves for the 12 different testing conditions evaluated in this program (3 R-ratios x 4 hold times). Figure 7.30 shows the comparison of the experimental data with the prediction of interpolation + superposition model for 649°C, R=0 hold time tests on Alloy 718. As in the previous figures for Rene'95, the small symbols represent the results from the threshold tests while the large symbols represent the data from the constant  $\Delta K$  tests. The solid line is the prediction from the interpolation + superposition model. The results of the constant  $\Delta K$  tests were lower than the increasing K tests, particularly for the hold time tests due to retardation between constant load cycling segments. Thus, the increasing K portion on the threshold tests are considered to be a better indicator or provide more accurate crack growth rates.

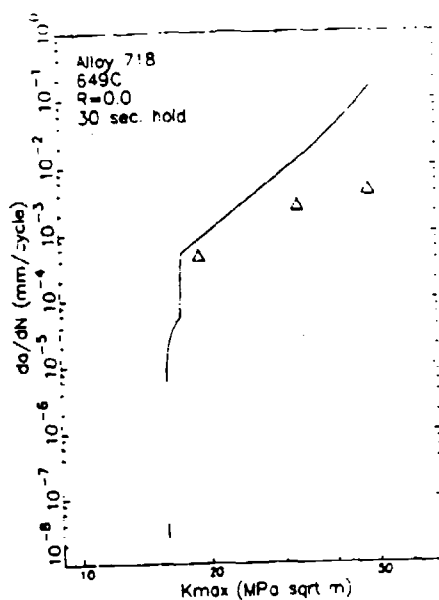
The interpolation + superposition model seems to adequately predict the crack growth behavior for these R=0 hold time tests. The predictions for the 0, 4, and 30 second hold time tests show a step function increase in the crack growth rates at K-levels slightly above the transition between Regions I and II. This sudden increase occurs at the static threshold values. This behavior occurs because the threshold values calculated for R=0 tests with hold times less than approximately 200 seconds are less than the static crack growth threshold (Figure 7.26). The only comparisons in this report will be for the three R-ratios evaluated experimentally, however this type of a step increase would also be predicted for other near-zero positive R-ratios for low hold times. For the cases shown in Figure 7.30, either the changes in crack growth rate are relatively small (hold times of 0 and 4 seconds) or the cyclic and static threshold values are similar (30 second hold time) so that the experimental data neither substantiate nor refutes this type of behavior. More experimental work is required to evaluate the crack growth behavior in this regime.



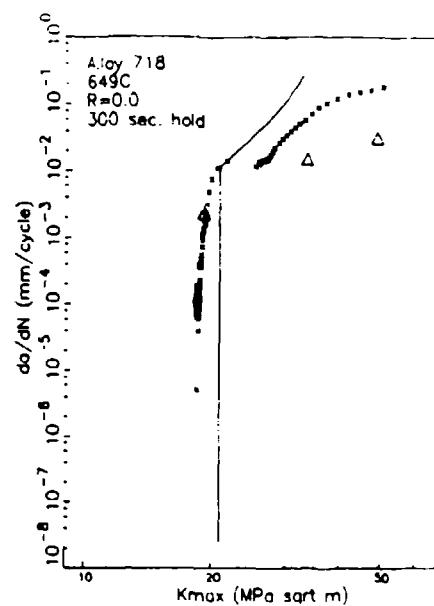
(a)



(b)



(c)



(d)

Figure 7.30: Comparison of experimental data with predictions from interpolation + superposition model for Alloy 718 tested at 649°C with R=0.0 and hold times of (a) 0 seconds, (b) 4 seconds, (c) 30 seconds, and (d) 300 seconds.

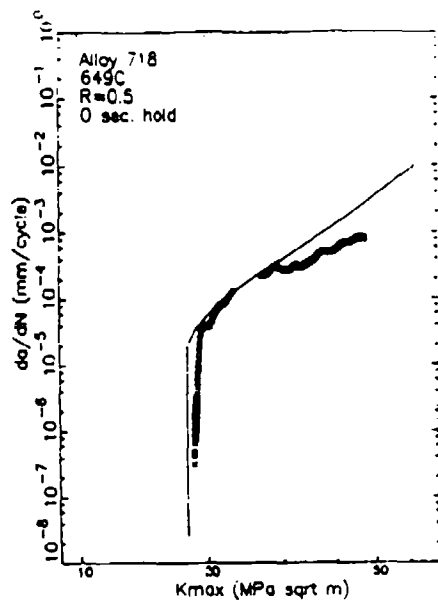


Figure 7.31 compares the predictions between the interpolation + superposition model and the Alloy 718 R=0.5 tests. With the exception of the 0 second hold time condition, no threshold tests were performed at this R-ratio. The longer hold time tests show that the predictions are much higher than the results from the constant  $\Delta K$  tests. It is not known if these discrepancies result from inadequacies of the model or large amounts of retardation during the constant  $\Delta K$  tests. As anticipated, the R=0.5 predictions do not show the step function in crack growth rates because the calculated  $(K_{th})_{max}$  values exceed the static threshold.

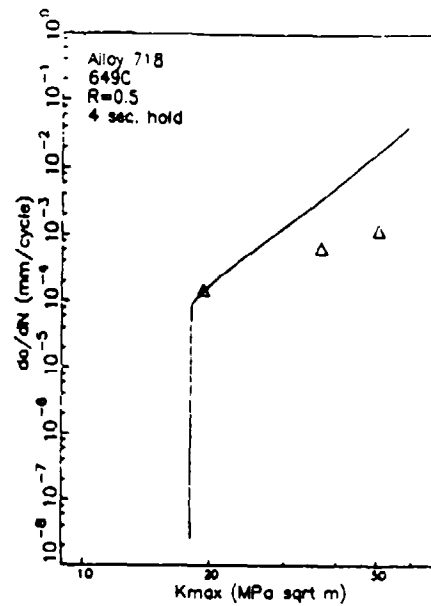
The R=0.8 test data are compared to the interpolation + superposition predictions in Figure 7.32. For all hold times, the predictions are approximately 2 to 4 times greater than the experimentally measured crack growth rates. This type of model also overpredicted the crack growth rates measured in Rene'95. This model correctly predicts the relative effects of hold times, but appears to be inaccurate by a constant factor. This problem could be alleviated by using an effective static crack growth curve determined from hold time data, rather than from static crack growth tests. The combined influence of cyclic and static loads may result in changes in the deformation and stress fields near the crack tip and thus different crack growth rates relative to those measured in specimens under static loads.

#### 7.4.4 Retardation Model

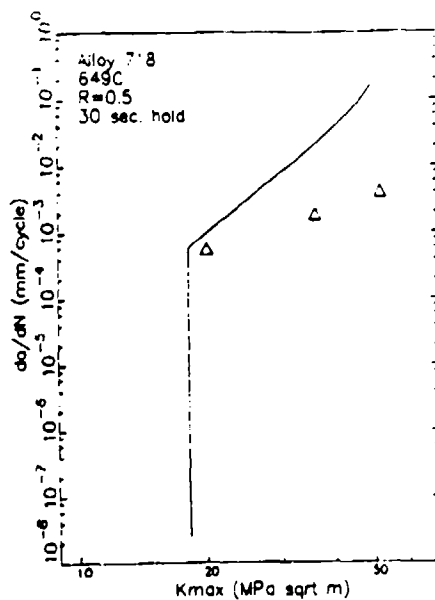
The modified Willenborg retardation model was used to model the overpeak retardation behavior measured in Alloy 718 at 649°C. The Alloy 718 retardation constants were determined for ACDYCLE analyses of the experimental results from the 10% overpeak tests using the same approach as described for Rene'95 in Section 7.3.5. Figure 7.33 shows the resulting values of  $\phi$  determined from the 10% overpeak tests. As in the case of Rene'95, it appears that  $\phi$  is linear with  $K_{O1}$  and does not seem to be very sensitive to R ratio. The line in this figure is the best fit through the data. The slope and intercept determined the values of  $\phi_1$  and  $\phi_2$ . The values of the retardation constants are listed in Table 7.8. The major difference between the Rene'95 and Alloy 718 retardation constants occur at low values of



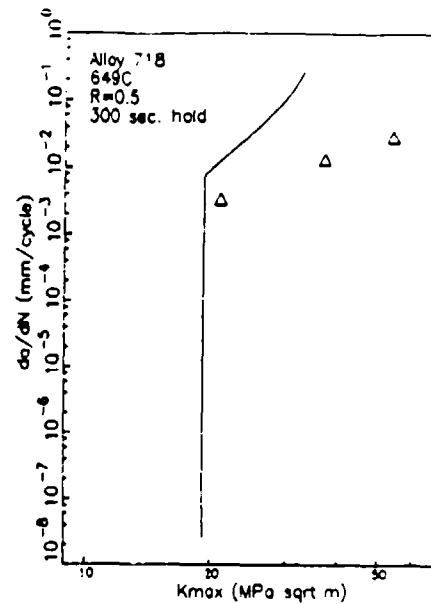
(a)



(b)

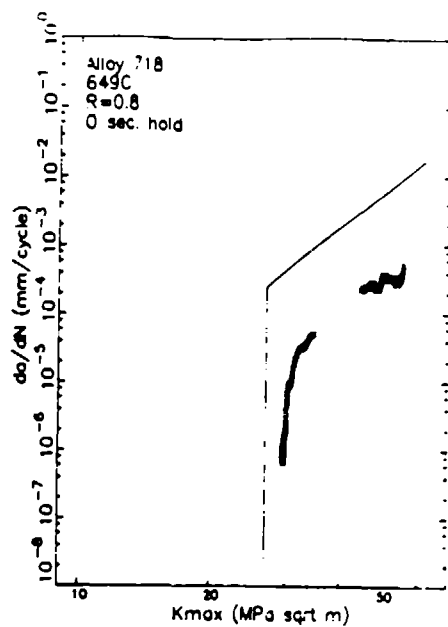


(c)

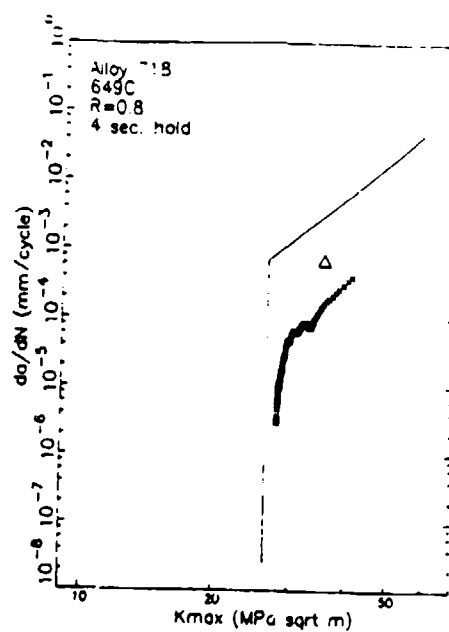


(d)

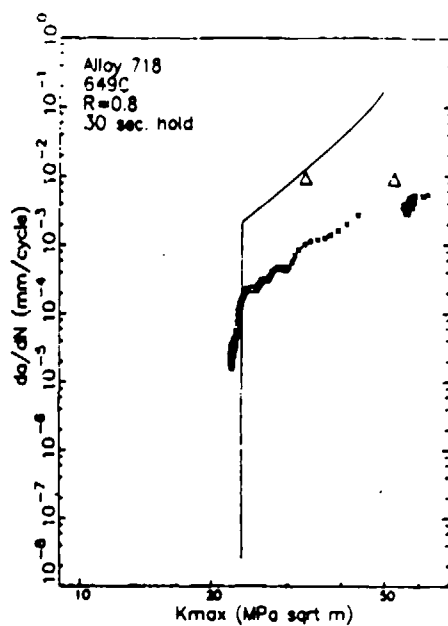
Figure 7.31: Comparison of experimental data with predictions from interpolation + superposition model for Alloy 718 tested at 649°C with  $R=0.5$  and hold times of (a) 0 seconds, (b) 4 seconds, (c) 30 seconds, and (d) 300 seconds.



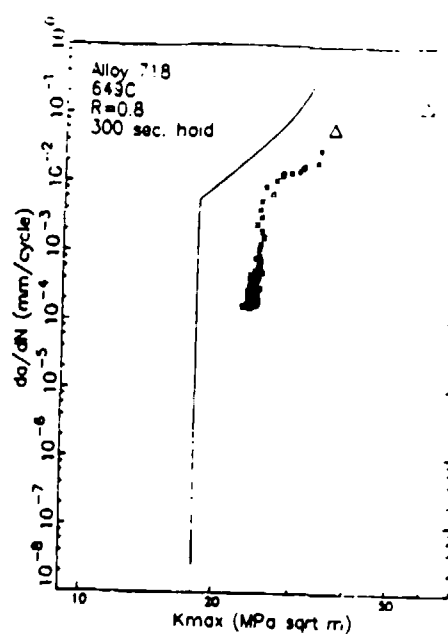
(a)



(b)



(c)



(d)

Figure 7.32: Comparison of experimental data with predictions from interpolation + superposition model for Alloy 718 tested at 649°C with R=0.8 and hold times of (a) 0 seconds, (b) 4 seconds, (c) 30 seconds, and (d) 300 seconds.

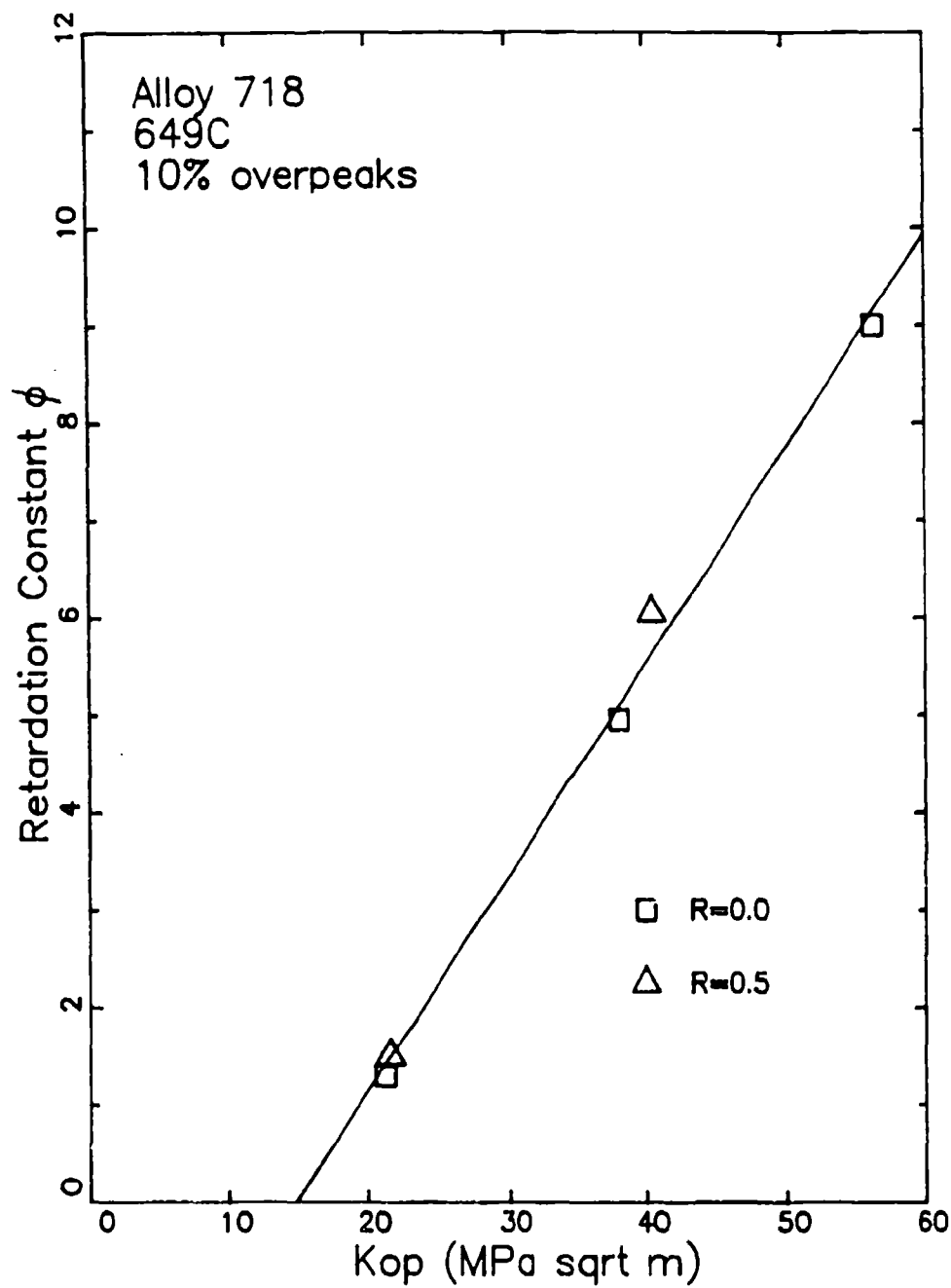
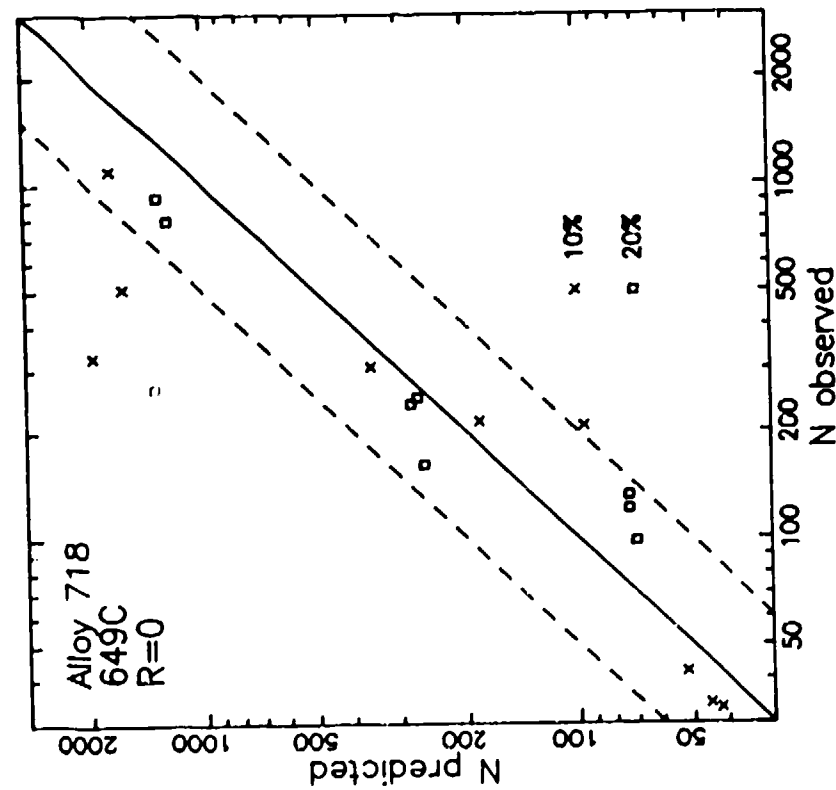


Figure 7.33: Variation of  $\phi$  with  $K_{O1}$  for 649°C Alloy 718 hold time overpeak tests with 10% overpeaks.

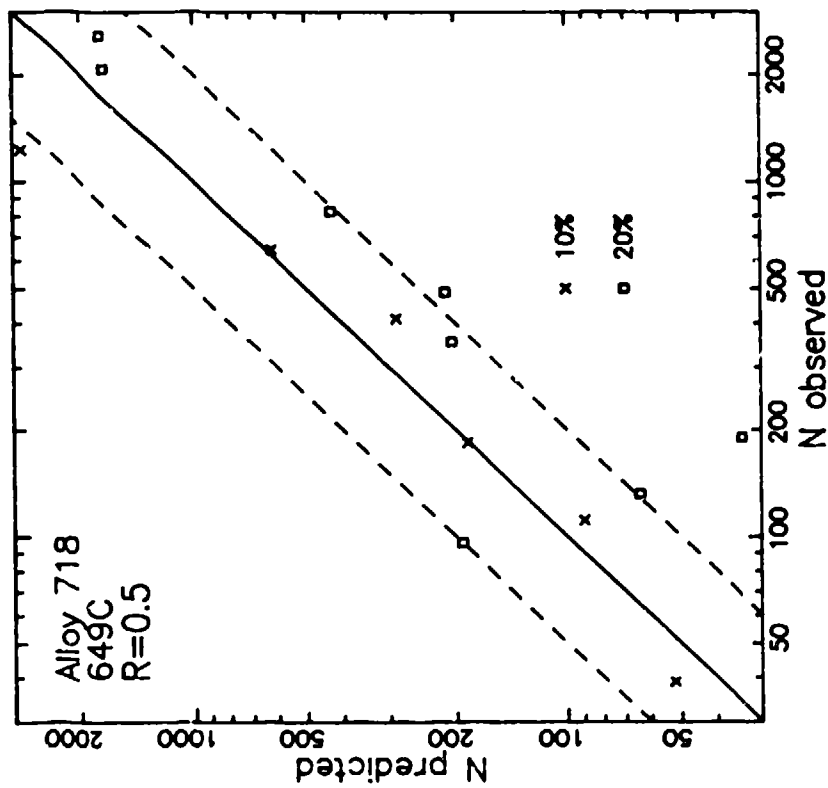
$K_{01}$ . The value of  $\Phi_1$  was positive for Rene'95 but is negative for Alloy 718. For Alloy 718, the value of  $\Phi$  is positive only for  $K_{01}$  values greater than 14.75 MPa/m (13.43 ksi/in.). This will probably have little effect on the ability to predict the crack growth rates of Alloy 718 because in almost every case, the cyclic and static threshold values (Figure 7.26) exceed this value. The values of  $\Phi$  for both Rene'95 and Alloy 718 can be much greater than unity. As discussed in Section 7.3.5, this suggests that the strong influence of overpeaks on retarding hold time crack growth results from complex stress relaxation processes.

The values of  $\Phi_1$  and  $\Phi_2$  were used to predict the number of cycles required to propagate through all the individual segments in the 649°C Alloy 718 overpeak hold time test specimens. These results are compared with the experimentally measured values in Figure 7.34. The solid line in these figures represents perfect agreement. The dashed lines enclose a region which is within a factor of two of the perfect agreement. In general, the agreement is quite good; however, the model predicts longer lives than experienced experimentally for R=0 long live segments as shown in Figure 7.34a. The three outliers correspond to long hold time situations at low values of  $K_{01}$  (21 to 24 MPa/m). The longer predicted lives result from suppression of  $K$  to below the static threshold where no hold time effect is calculated. This type of an effect was observed to a lesser extent in the prediction of the R=0.5 overpeak tests (Figure 7.34b). This may suggest that the static threshold should be lower than that measured in the single static threshold tests performed on Alloy 718 at 649°C. For most other cases, the retardation model combined with the interpolation + superposition model accurately predicted the lives of the Alloy 718 overpeak tests.

The effective crack growth rates calculated using cyclic (no static or retardation), static (no retardation), and retardation (including static) analysis of the Alloy 718 overpeak tests was performed. The results of the analysis and experimental data for the R=0, 300 second hold time tests are shown in Figures 7.35 and 7.36. These results show excellent agreement between the experimental data and the retardation predictions for all cases except those with low values of  $K_{01}$  as discussed previously. As observed for



(a)



(b)

Figure 7.34: Comparison of predicted and observed cycles to propagate through individual segments of 649°C Alloy 718 hold time overpeak tests with R-ratios of (a) 0.0 and (b) 0.5.

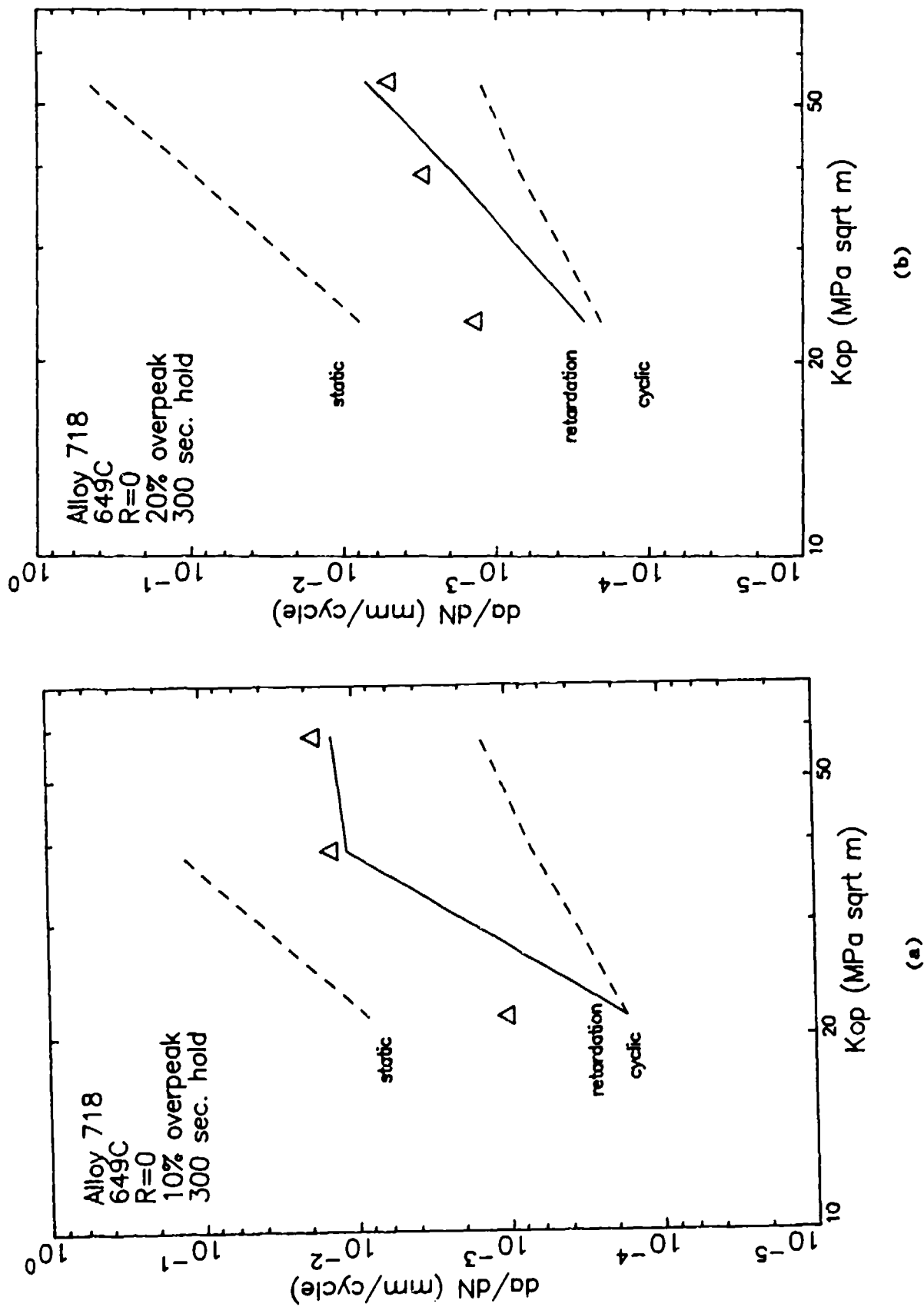


Figure 7.35: Comparison of ACDCYCLE predictions with experimental crack growth rates in 649°C, R=0.0 Alloy 718 hold time overpeak test with 300 second hold times and (a) 10% and (b) 20% overpeaks.

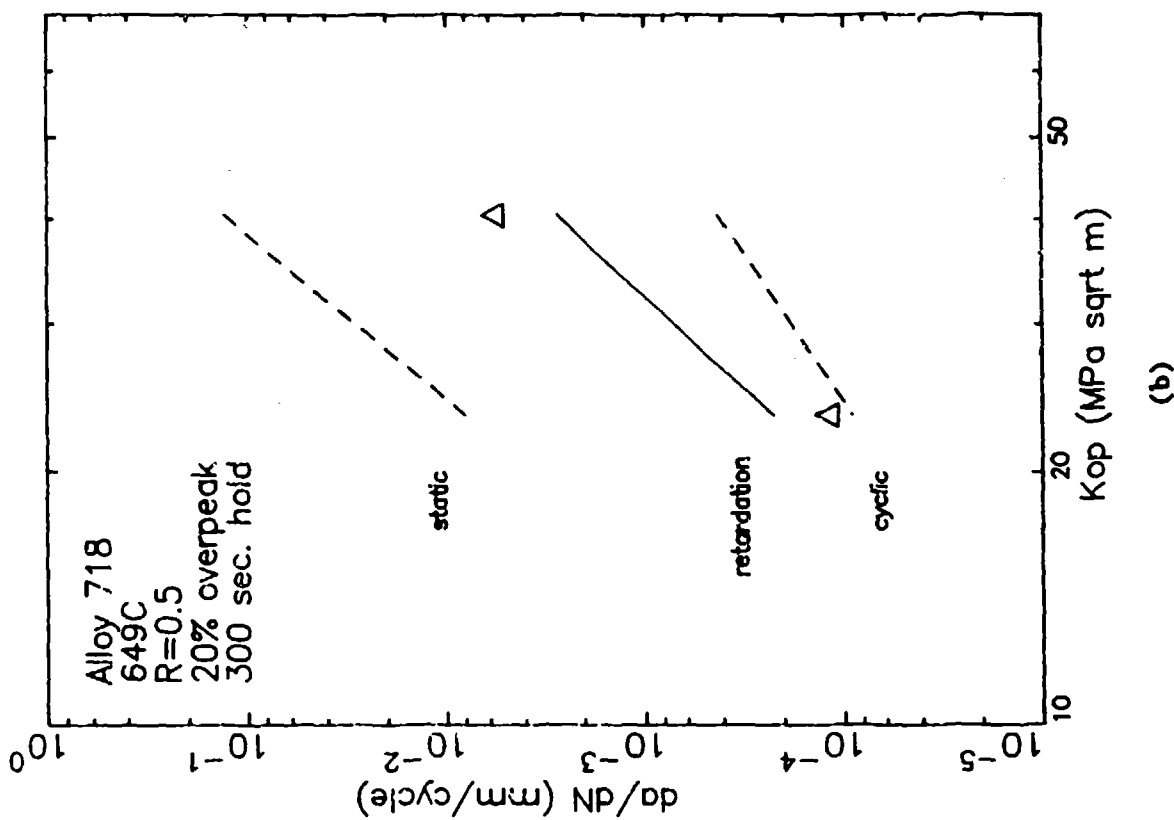
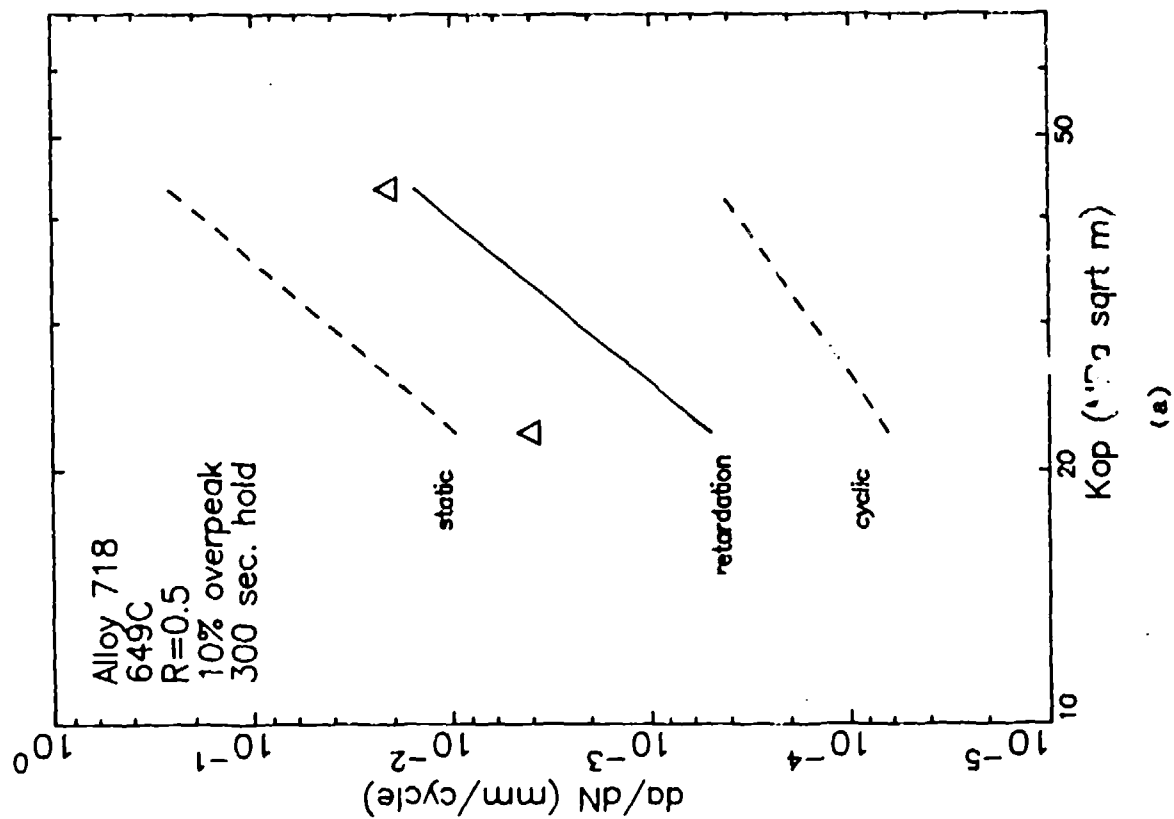


Figure 7.36: Comparison of ACDCYCLE predictions with experimental crack growth rates in 649°C, R=0.5 Alloy 718 hold time overpeak tests with 300 second hold times and (a) 10% and (b) 20%.



Rene'95, there is a significant benefit from static retardation. This benefit increases with increasing K levels and overpeak ratios. The retardation results never totally eliminate a time dependent effect due to the influence of the 15 second loading and unloading cycle in these tests.

A similar comparison for the 649°C, R=0.5, 300 second hold time Alloy 718 overpeak tests are shown in Figure 7.23. The prediction of the low  $K_{01}$ , 10% overpeak condition was much lower than the experimentally measured crack growth rate. This result also suggests the effective static threshold of Alloy 718 is lower than that measured in the static threshold test. These results also show the same general trend of increasing benefit with higher overpeaks and higher K values.

These retardation model predictions for Alloy 718 were not as accurate as those shown for Rene'95, but are still quite good. It appears that some fine tuning of the static threshold could improve the quality of these predictions. These results show that this retardation model can provide relatively accurate estimates of the suppression of hold time crack growth resulting from overpeaks.

## 8.0 SUMMARY AND CONCLUSIONS

An extensive crack growth data base was generated on both Rene'95 and Alloy 718. These data covered eight orders of magnitude in crack growth rate and included the influence of hold time, test frequency, R ratio, and overpeak ratio. In general, Region II crack growth rates were proportional to the hold time suggesting that these data can be predicted using a linear superposition model. Increasing test temperature increased the acceleration in crack growth rates due to time dependent crack growth.

The crack growth data measured in this investigation followed these trends; however, there were some surprising low temperature Region II Rene'95 results and higher temperature near-threshold data for both materials which suggest that localized crack tip blunting or stress redistribution can result in lower crack growth rates than those anticipated from the static component of crack growth. Sectioning experiments on an interrupted 649°C 300 second hold time threshold test of Alloy 718 showed that the crack was open over the entire range of crack length, but there was not evidence of localized blunting. This suggested that creep-assisted stress relaxation and redistribution may help to lower the crack tip stress concentration for situations of relatively slow static crack growth (low temperatures and near-threshold crack growth).

A very strong retardation effect was observed where relatively small overpeaks could totally suppress time dependent crack growth. The strong retardation effects combined with very rapid, time dependent crack growth rates resulted in artificially low crack growth rates during constant  $\Delta K$  testing. This type of testing should be avoided in future test programs.

Extensive fractography was performed on the fractured tests specimens. The fracture mode of cyclic crack growth was transgranular; however, as the amount of static crack growth increased, the fracture mode transitioned to an intergranular mode. Qualitatively this supported the use of a superposition model which separately considers the components of cyclic and static crack growth. It was also shown that hold time cycling in vacuum resulted in higher

crack growth rates than continuous cycling in vacuum and a transition from transgranular to intergranular crack growth. These results show the strong influence of creep on time dependent crack growth. The faster crack growth rates may suggest that intergranular crack propagation is inherently faster than growth in a transgranular mode.

Transient crack growth behavior was observed between hold time cycling and more rapid constant frequency testing. It was shown that a damage zone was created at the crack tip which increased in size with reductions in creep resistance (Alloy 718 vs. Rene'95), increasing temperature, increasing R-ratio, and increasing hold time. These types of tests were also performed on Alloy 718 at 649°C in air and vacuum. These results showed that the damage zone was formed by creep, independent of environment; however, air was necessary at the crack tip in order to cause accelerated crack growth. The transient and vacuum crack growth tests showed that the time dependent crack growth mechanism in nickel-base superalloys is a complex interaction between creep, fatigue, and environment.

The crack growth data obtained in this investigation were modeled using a sigmoidal (Knaus) crack growth equation due to the ability of this equation to independently adjust the near-threshold and Paris regimes (Regions I and II). The near-threshold crack growth data in this program were modeled using an interpolative model to predict the influence of R-ratio, frequency, and hold time. This model was then combined with either a totally interpolative model or a linear superposition model to predict the time dependent crack growth rates. The linear superposition approach included the Walker model to account for the influence of R on the cyclic crack growth rates. Only the 649°C Rene'95 data were modeled using both an interpolation and an interpolation + superposition models. These models adequately predicted the entire data base, but the interpolation model made what appeared to be unreasonable estimates of crack growth rates outside the range covered by the data base. On this basis, the superposition model was selected as the best model.

The 649°C Alloy 718 data were also modeled using the linear superposition model. For both materials the static crack growth component was predicted from a curve constructed through the static crack growth data which showed a relatively large amount of scatter. It may be possible to improve the quality of the predictions by using an inferred static crack growth curve as determined from hold time tests.

A modified Willenborg retardation model developed for cyclic retardation was successfully applied to the overpeak hold time tests. It was necessary to use material constants in excess of those considered reasonable. The large amount of static crack growth retardation may be related to localized creep deformation at the crack tip.

A computer code called ACDCYCLE was developed which can access all these models and perform a variety of functions including residual life predictions and the generation of crack growth rate curves. This code can be run on IBM XT personal computers with an 8087 math coprocessor chip. This code was delivered to the Air Force Materials Laboratory.

A superposition model was successfully developed but some of the experimental data suggests that nonlinear has the potential for both accelerating time-dependent crack growth through creep-induced damage or slowing it down by creep-induced stress redistribution. It was necessary to include an interpolation threshold model and a largely empirical retardation model to accurately predict conditions which are believed to be highly dependent on the stress redistribution. The superposition model worked well for the situations considered in this investigation, but the development of alloys with lower time dependent crack growth rates and / or application of the current materials to higher temperatures with the resultant lower creep resistance may require the development and application of non linear fracture mechanics parameters to better describe time dependent crack growth behavior.

## 9.0 REFERENCES

1. L.F. Coffin, Jr., "The Effect of Vacuum on the High Temperature Low Cycle Fatigue Behavior of Structural Metals", Corrosion Fatigue: Chemistry, Mechanics, Microstructure, Proceedings of the International Conference on Corrosion Fatigue, NACE, Houston, 1972, pp. 590-600
2. L.F. Coffin, Jr., "The Effect of High Vacuum on the Low Cycle Fatigue Law", Met. Trans., 3, 1972, pp. 1777-1788
3. L.F. Coffin, Jr., Fracture 1969, Proceedings of Second International Conference on Fracture, Brighton, 1969, Chapman and Hall, London, 1969, p.643
4. L.F. Coffin, Jr., Proceedings of the Air Force Conference on Fatigue and Fracture of Aircraft Structures and Materials, AFFDL TR 70-144, Air Force Flight Dynamics Laboratory, Wright-Patterson AFB, Wright-Patterson, Ohio, 1970, p.301
5. W.J. Ostergren, ASME-MPC Symposium of Creep-Fatigue Interaction, MPC-3, ASME, pp.170-202
6. S.S. Manson, G.R. Halford, and M.H. Hirschberg, Design for Elevated Temperature Environment, S.Y. Zamrik, editor, ASME, 1971, pp.12-28.
7. G.R. Halford and J.F. Saltsman, Proceedings of ASME International Conference on Advances in Life Prediction Methods, D.A. Woodford and J.R. Whitehead, editors, ASME, 1963, pp. 17-26.
8. J.F. Saltsman and G.R. Halford, ASTM STP 942, ASTM, 1987, pp. xxx-xxx.
9. W.H. Chang, Superalloys - Processing, AIME, 1972, MCIC-72-10
10. D.A. Woodford and R.H. Bricknell, Embrittlement of Alloys, Academic Press, 1982

11. Clavel and Pineau, Met. Trans., 9A, 1978, pp.471-480
12. R.M. Felloux and J.S. Huang, Creep-Fatigue-Environment Interactions, R.M. Pelloux and N.S. Stoloff, editors, TMS-AIME, 1980, p. 151.
13. J.P. Pedron and A. Pineau, Mat. Sci. Eng., 56, 1982, pp.143-156
14. K.R. Bain and R.M. Pelloux, Met. Trans., 15A, 1984, pp. 381-388
15. A. Diboine and A. Pineau, Fat. Fract. Eng. Mat. Str., 10, 1987, pp. 141-151
16. K. Sadananda and S. Shahinian, Met. Trans., 8A, 1977, pp. 439-449
17. K. Sadananda and S. Shahinian, Characterization of Materials for Service at Elevated Temperatures, ASME, Series MPC-7, George V. Smith, editor, 1978, pp.107-127
18. S. Shahinian and K. Sadanadna, Engineering Aspects of Creep, 2, 1980, pp. 1
19. K. Sadananda and S. Shahinian, Metals Tech., 1982, pp. 18-25
20. James M. Larsen and Theodore Nicholas, "Cumulative-Damage Modeling of Fatigue Crack Growth in Turbine Engine Materials", Engineering Fracture Mechanics, 22, 1985, pp. 713-730
21. Jeffrey R. Christoff, "Evaluation of Fatigue-Creep Crack Growth in an Engine Alloy", M.S. Thesis, Air Force Institute of Technology, Wright-Patterson Air Force Base, Ohio, 1983.
22. T. Nicholas, T. Weerasooriya, and N.E. Ashbaugh, "A Model for Creep/Fatigue Interaction in Alloy 718", ASTM STP 905, Fracture Mechanics: Sixteenth Volume, ASTM, 1986, Philadelphia, Pa., pp.167-180

23. T. Nicholas and T. Weerasooriya, "Hold-Time Effects in Elevated Temperature Fatigue Crack Propagation", ASTM STP 905, Fracture Mechanics: Sixteenth Volume, ASTM, 1986, Philadelphia, Pa., pp.155-168
24. Tusit Weerasooriya, "Effect of Frequency on Fatigue Crack Growth Rate of Inconel 718 at High Temperature", AFWAL-TR-87-4038, University of Dayton, Dayton, Ohio. 45469, June 1987
25. H.D. Solomon and L.F. Coffin, Jr., ASTM STP 520, ASTM, 1973, pp.112-122.
26. H. D. Solomon, Met. Trans., 4, 1973, pp.341-347
27. S. Floreen, Met. Trans., 6A, 1975, pp. 1741-1749
28. A. Coles, R.E. Johnson, and H.G. Popp, J. of Eng. Mat. Tech., 98, 1976, pp. 305-315
29. S. Floreen and R.H. Kane, Met. Trans., 10A, 1979, pp.1745-1751
30. Lee A. James and W.J. Mills, Eng. Frac. Mech., 22, 1985, pp. 797-818
31. B.A. Cowles, D.L. Sims, and J.R. Warren, "Evaluation of the Cyclic Behavior of Aircraft Turbine Disk Alloys", NASA-CR-1594039, October 1978
32. D.A. Utah, "Crack Modeling in An Advance Powder Metallurgy Alloy", AFWAL-TR-80-4098, July 1981
33. Robert C. Donath, "Crack Growth Behavior of Alloy IN100 Under Sustained Load at 732°C (1350°F)", AFWAL-TR-80-4131, Air Force Materials Laboratory, Wright-Patterson Air Force Base, Ohio 45433, April 1981
34. J.M. Larsen and T. Nicholas, ASTM STP 721, ASTM, 1983, pp. II-536 - II-552.

35. P.C. Paris, "Fatigue - An Interdisciplinary Approach", Proceedings 10<sup>th</sup> Sagamore Conference, Syracuse University Press, Syracuse, N.Y., 1964, p. 107
36. R.M. Wallace, C.G. Annis, Jr., and D.L. Sims, "Application of Fracture Mechanics at Elevated Temperatures", AFML-TR-76-176 Part II, Wright-Patterson Air Force Base, April 1977
37. J.M. Larsen, B.J. Schwartz, and C.G. Annis, "Cumulative Damage Fracture Mechanics Under Engine Spectra", Technical Report AFML-TR-79-4159, Wright-Patterson AFB, Ohio January 1980
38. D.L. Sims and F.K. Haake, "Evaluation of Crack Growth in Advanced P/M Alloys", AWWAL-TR-79-4160, Wright-Patterson Air Force Base, March 1980
39. W. Knaus, General Electric Aircraft Engines, unpublished research, 1965
40. K. Walker, "The Effect of Stress Ratio During Crack Propagation and Fatigue for 2024-T3 and 7075-T6 Aluminum", Effects of Environment and Complex Load History on Fatigue Life, ASTM STP 621, ASTM, 1970, pp.1-14
41. R.H. Van Stone, "The Influence of Temperature and Stress Ratio on the Crack Growth Behavior of Rene'95", GE Aircraft Engines Report 82-640, Cincinnati, Ohio 45215, 1982
42. R.H. Van Stone and D.D. Krueger, "Investigation of Direct Aged Inconel 718 Fatigue Behavior", Contract N00019-82-C-0373, Final Report, General Electric Aircraft Engine Business Group, Cincinnati, Ohio 45215, December 1984.
43. R.H. Van Stone, M.S. Gilbert, O.C. Gooden, and J.H. Laflen, ASTM STP 969, ASTM, 1988, pp. 637-656
44. R.H. Van Stone and D.D. Krueger, ASTM STP 969, ASTM, 1988, pp. 883-906



45. R.P. Wei and J.D. Landes, Mat. Res. Std., 2, 1969, pp. 25-46
46. J.P. Gallagher and R.P. Wei, Corrosion Fatigue, NACE-2, NACE, 1972, pp. 409-423.
47. H.D. Solomon, Corrosion Fatigue, NACE-2, NACE, 1972, pp. 420-421
48. M.O. Spiedel, High Temperature Materials in Gas Turbines, 1974, p. 206
49. R.H. Van Stone, GE Aircraft Engines, Cincinnati, Ohio 45215, unpublished research, 1987
50. T. Weerasooriya and T. Nicholas, "Overload Effects in Sustained Load Crack Growth in Inconel 718", Fracture Mechanics: Eighteenth Symposium, ASTM STP 945, ASTM, Philadelphia, 1987, to be published
51. J. Willenborg, R. Engle, and H. Wood, "A Crack Growth Retardation Model Using an Effective Stress Concept", AFFDL-TM-71-1-FBR, Wright-Patterson Air Force Base, Ohio, January 1971
52. D.R. Chang, D.D. Krueger, and R.A. Sprague, "Superalloy Powder Processing, Properties, and Turbine Disk Application", published in Superalloy 1984, ASM
53. D.D. Krueger, R.H. Van Stone, and M.F. Henry, "Metallurgical Effects on Fatigue Behavior of Gas Turbine Disk Alloys", NAVAIR Contract N00019-82-C-0226, Final Report, General Electric Aircraft Engine Business Group, Cincinnati, Ohio 45215, 1985
54. L.A. James, J. of Eng. Mat. Tech., 1973, pp. 254-256
55. D.D. Krueger, Stephen D. Antolovich, and R.H. Van Stone, Met. Trans., 18A, 1987, pp. 1431-1449

56. R.H. Van Stone, D.D. Krueger, and L.T. Duvelius, ASTM STP 791, ASTM, Philadelphia, 1983, pp.553-558
57. J.I. Yuen, P. Roy, and W.D. Nix, Met. Trans., A15, 1985, pp. 1769-1775
58. K.S. Kim, R.H. Van Stone, S.N. Malik, and J.H. Laflen, "Elevated Temperature Crack Growth", Contract NAS3-23940, Final Report, GE Aircraft Engines, Cincinnati, Ohio 45215, 1988
59. D.F. Paulonis, J.M. Oblak, and D.S. Duvall, Transactions ASM, 62, 1969, pp. 611-622.
60. P.K. Wright, H. Jang, and H.G. Popp, "Fatigue and Fracture of Advanced Blade Materials", AFWAL-TR-84-4166, GE Aircraft Engines, Cincinnati, Ohio 45215, February 1985
61. D.O. Harris, J. Bas. Eng., 89, 1967, p.49.
62. S.N. Malik and M.S. Gilbert, GE Aircraft Engines, Cincinnati, Ohio 45215, private communication, 1986
63. R.P. Gangloff, Fat. Eng. Mat. and Structures, 4, 1981, pp. 15-33
64. J.R. Wilcox and M.F. Henry, General Electric Corporate Research and Development, Schenectady, New York 12301, unpublished literature, 1984.
65. W.R. Catlin, D.C. Lord, T.A. Prater, and L.F. Coffin, "The Reversing DC Potential Method", General Electric Corporate Research and Development, Schenectady, New York 12301, accepted for publication by ASTM.
66. H.H. Johnson, Materials Research and Standards, 5, 1965, pp. 442-445.
67. M.F. Henry, General Electric Corporate Research and Development, Schenectady, New York 12301, unpublished research, 1986.

68. "Standard Test Method For Measurement of Fatigue Crack Growth Rates", E647-86a, 1987 Annual Book of ASTM Standards, 03.01, ASTM, 1987, pp. 899-926
69. D.D. Krueger, "Effects of Grain Size and Precipitate Size on the Fatigue Crack Behavior of Alloy 718 at 427C", M.S. Thesis, University of Cincinnati, Cincinnati, Ohio 45215, 1984
70. L.P. Zawada and T. Nicholas, ASTM STP 945, ASTM, 1987,
71. W.J. Mills and R.W. Hertzberg, Eng. Frac. Mech., 7, 1975, pp. 705-711
72. H. Tada, P.C. Paris, and G.R. Irwin, The Stress Analysis of Cracks Handbook, Del Research Corporation, Hellertown, Pa. 1973

#### APPENDIX A: STATISTICAL ANALYSIS OF RENE'95 CONSTANT $\Delta K$ DATA

The figures in this appendix show the results of the statistical analysis of the Rene'95 constant  $\Delta K$  tests. The small rectangles in the figures enclose a region of plus and minus one standard deviation in crack growth rate ( $da/dN$ ) and  $K_{max}$ . The techniques used to establish these values were described in Section 4.4.2. The dashed lines in these figures connect the mean values of  $da/dN$  and  $K_{max}$  for cycles with constant hold times and R-ratio.

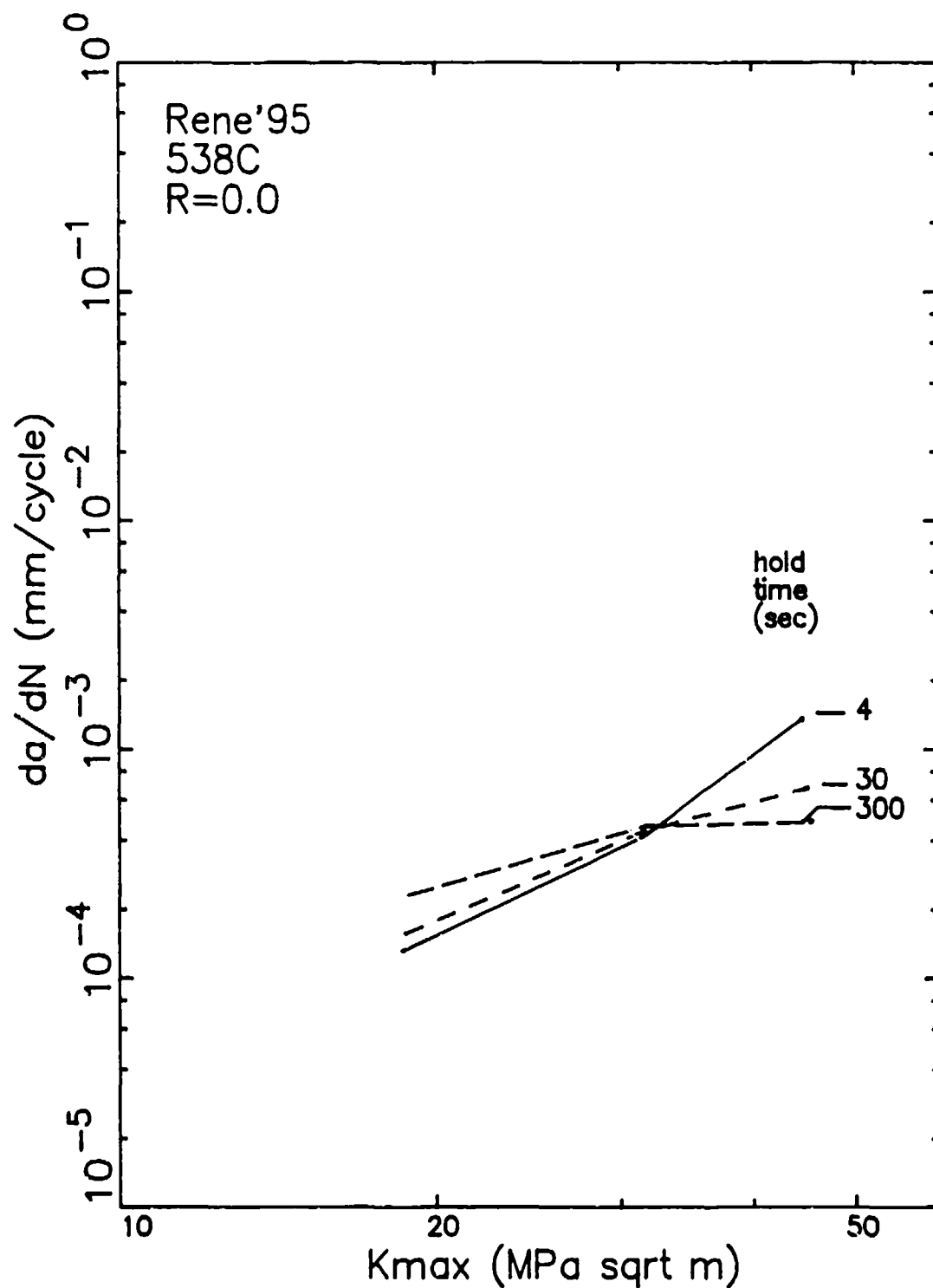
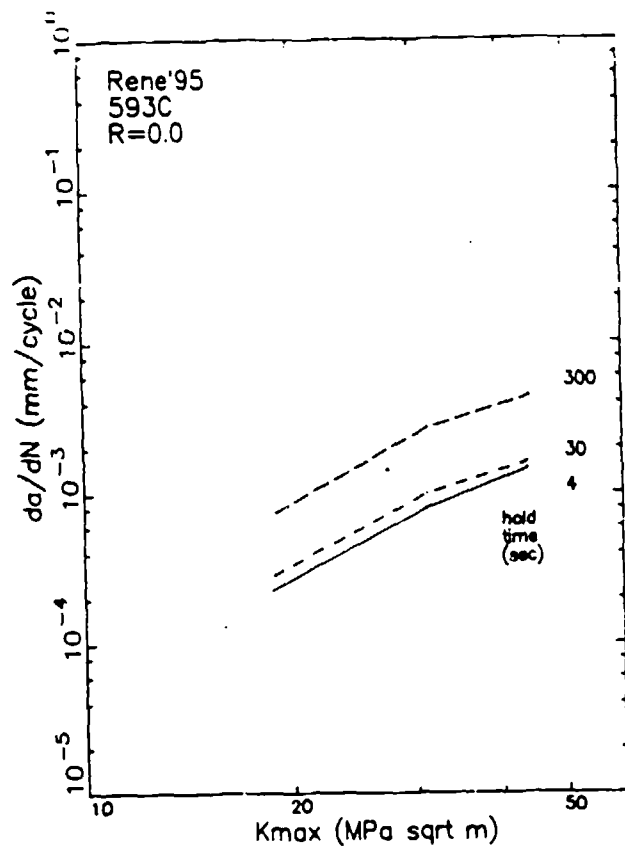
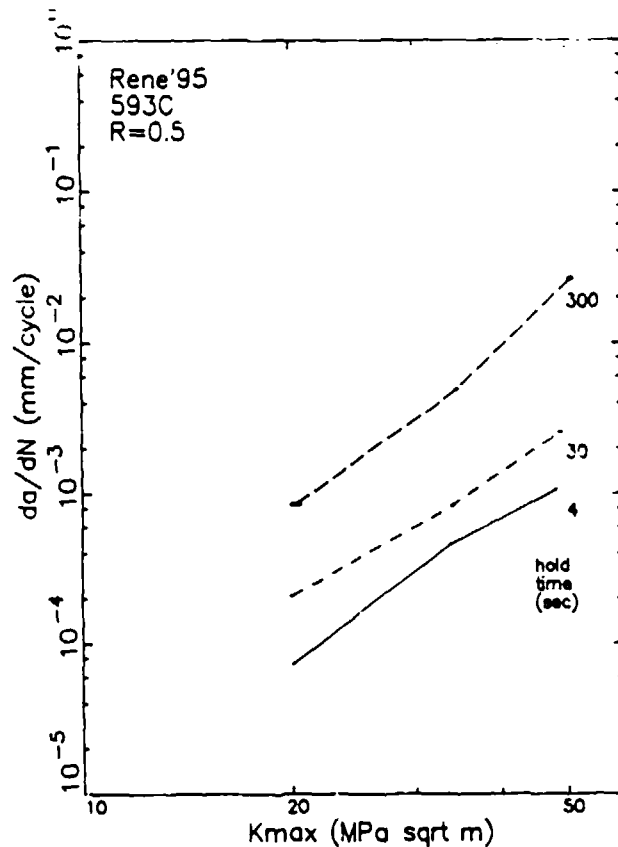


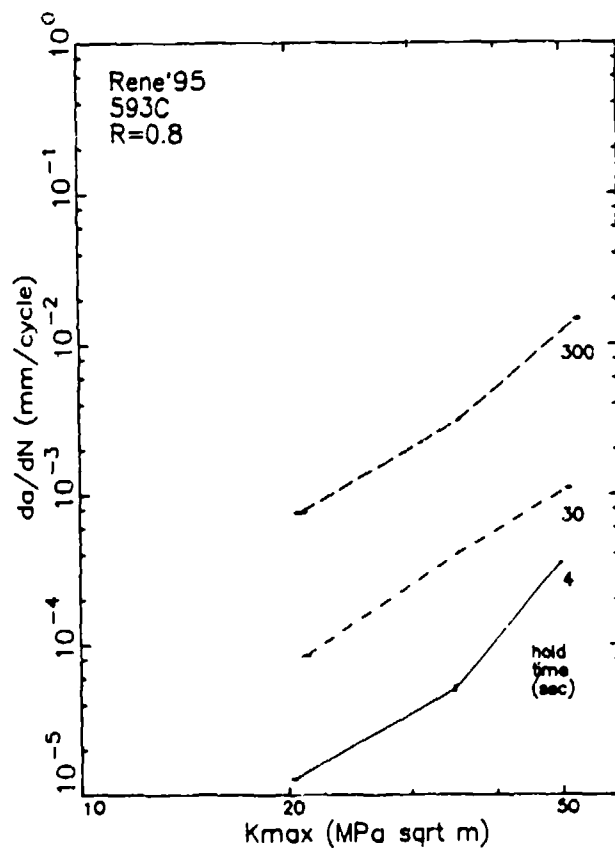
Figure A.1: Statistical analysis results of Rene'95 constant  $\Delta K$  hold time crack growth data from specimen cycled at 538°C with a R-ratio of 0.0.



(a)



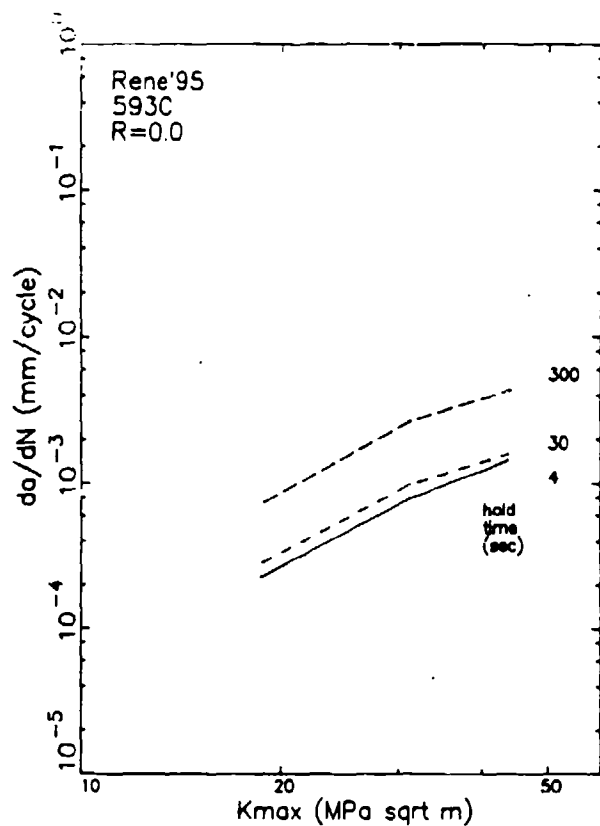
(b)



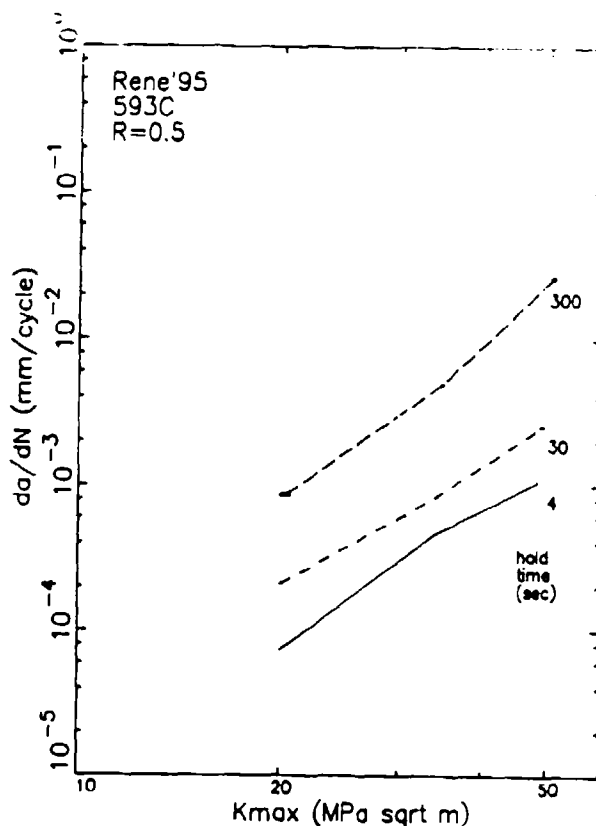
(c)

Figure A.2:

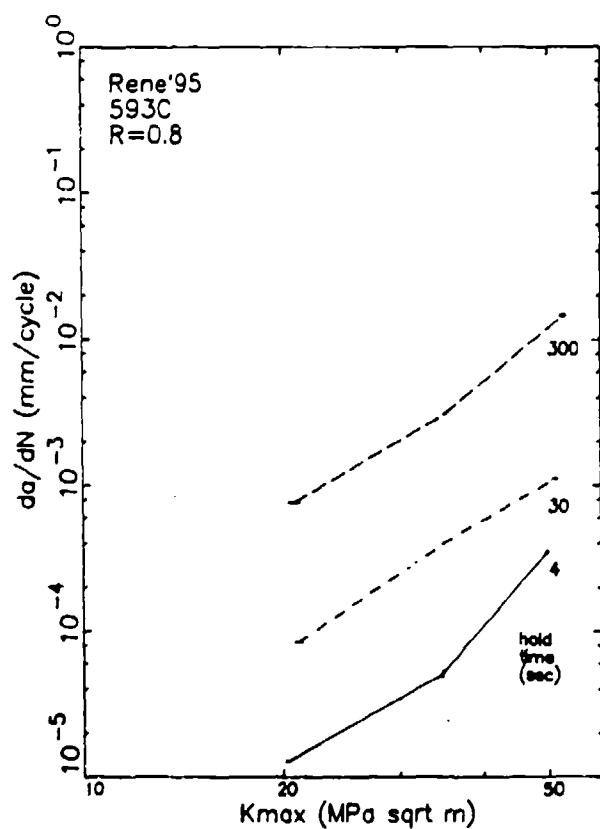
Statistical analysis results of  
Rene'95 constant  $\Delta K$  hold time crack  
growth data from specimens cycled at  
593°C with R-ratios of (a) 0.0, (b)  
0.5, and (c) 0.8.



(a)



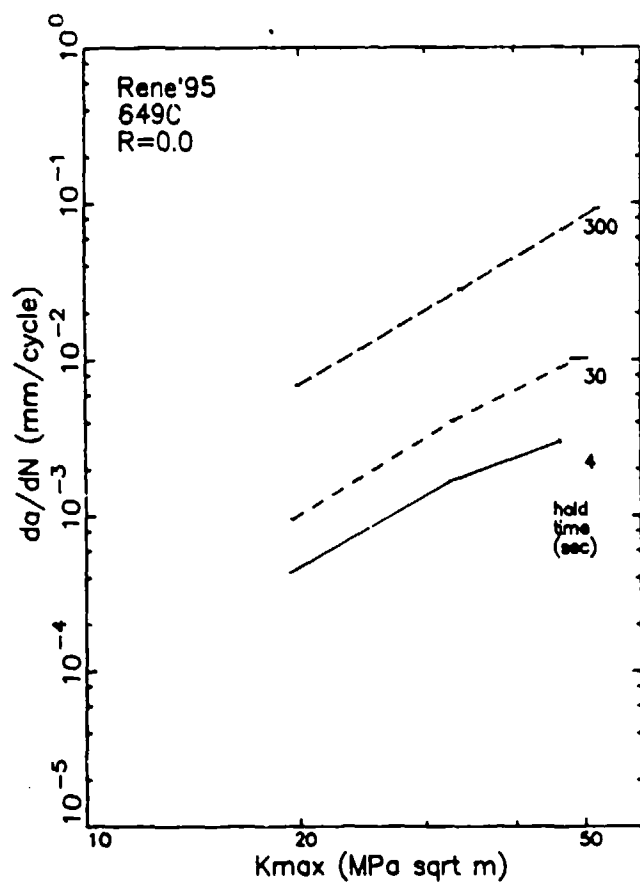
(b)



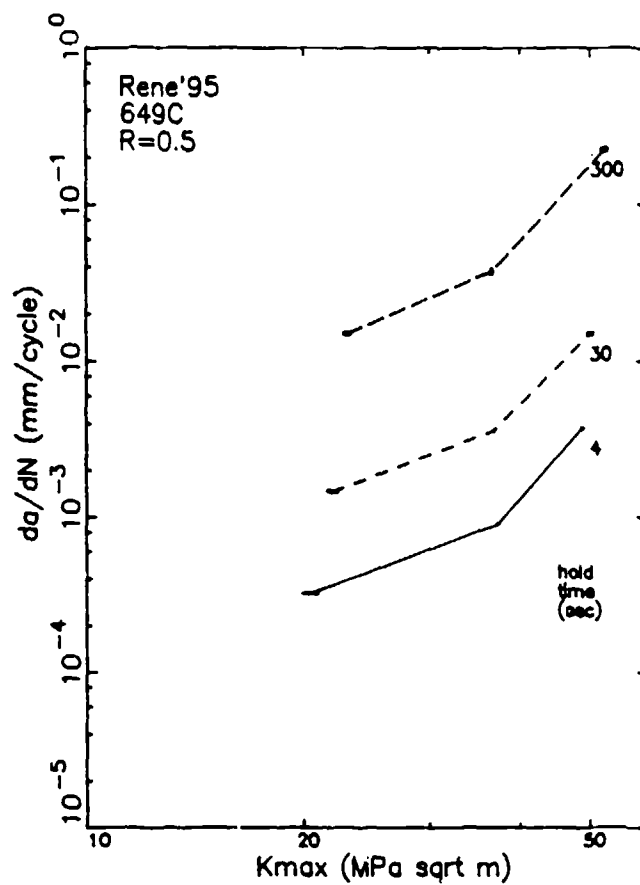
(c)

Figure A.3:

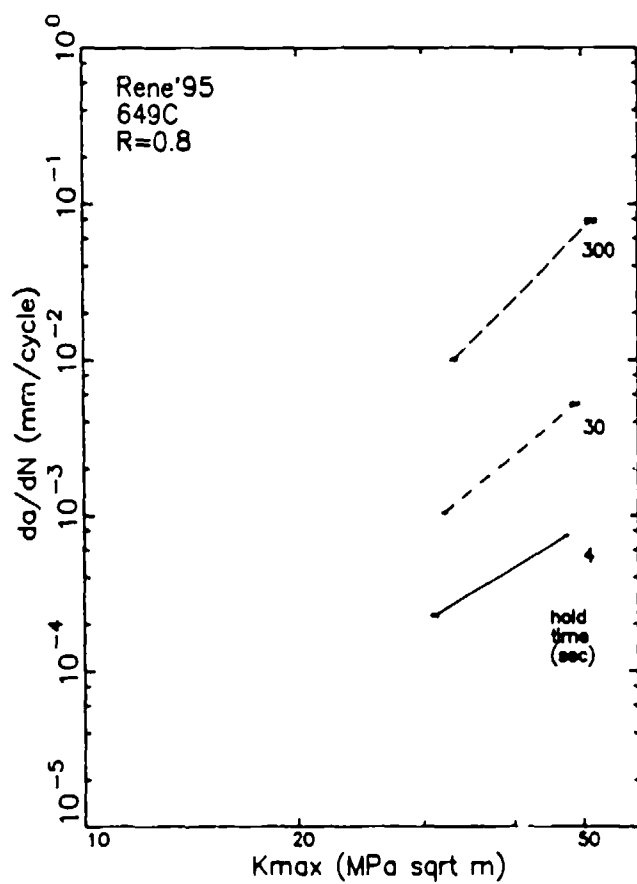
Statistical analysis results of  
Rene'95 constant  $\Delta K$  frequency crack  
growth data from specimens cycled at  
593°C with R-ratios of (a) 0.0, (b)  
0.5, and (c) 0.8.



(a)



(b)

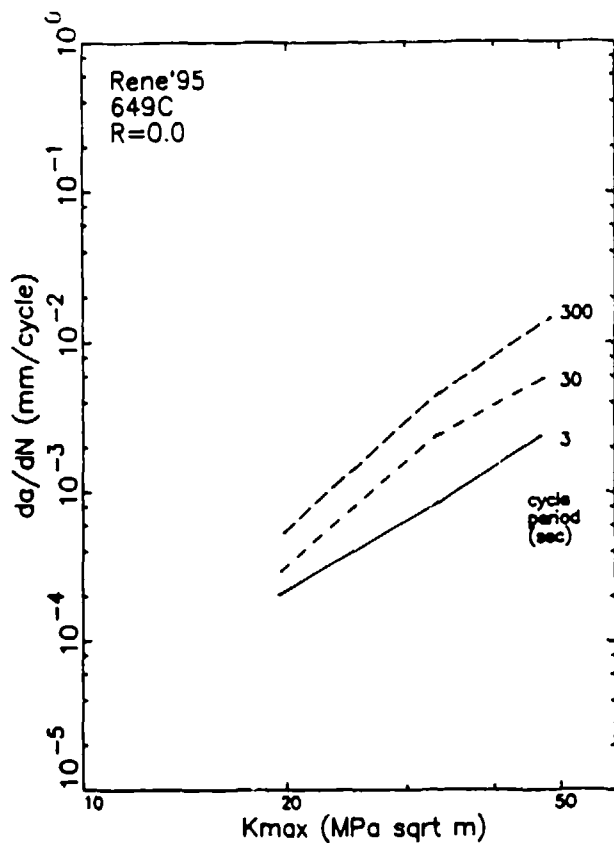


(c)

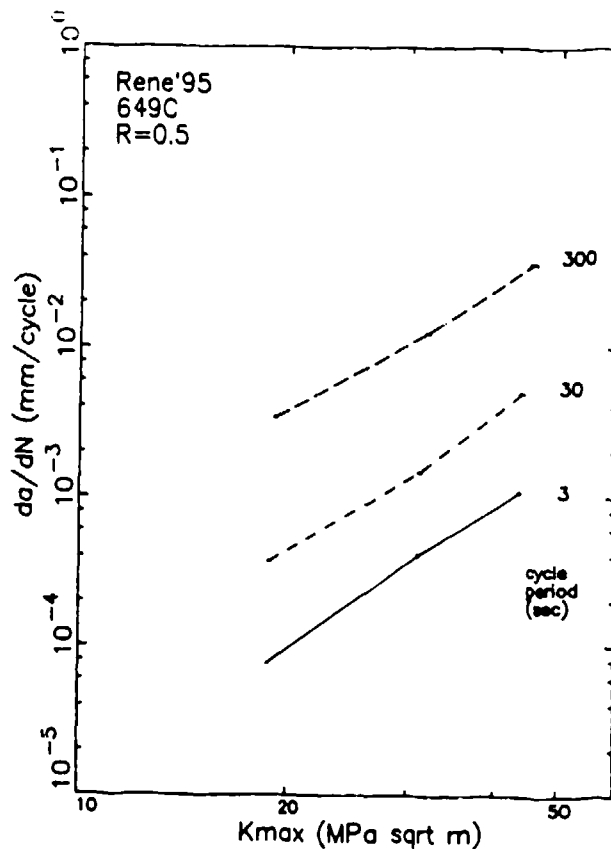
Figure A.4:

Statistical analysis results of Rene'95 constant  $\Delta K$  hold time crack growth data from specimens cycled at 649°C with R-ratios of (a) 0.0, (b) 0.5, and (c) 0.8.

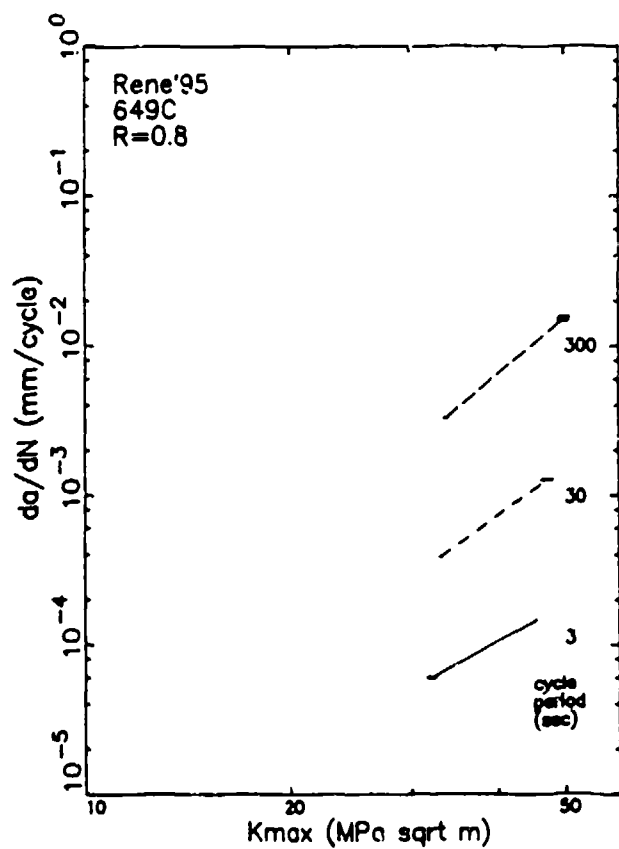




(a)



(b)



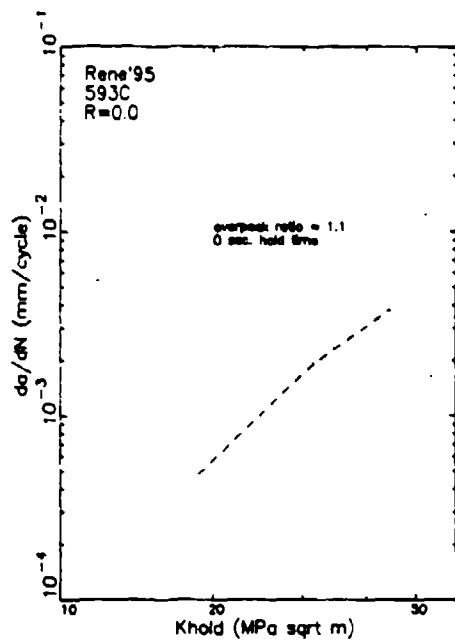
(c)

Figure A.5:

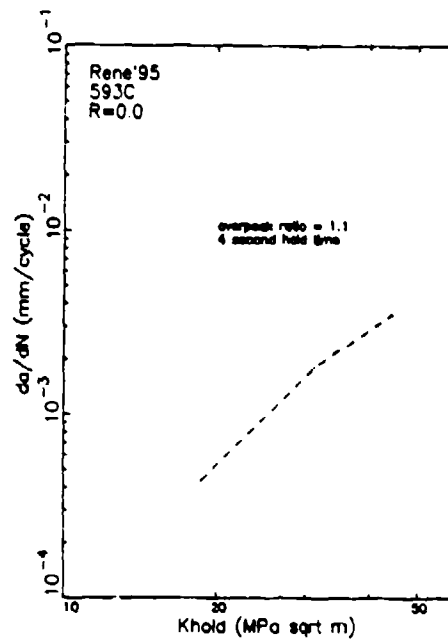
Statistical analysis results of  
Rene'95 constant  $\Delta K$  frequency crack  
growth data from specimens cycled at  
649°C with R-ratios of (a) 0.0, (b)  
0.5, and (c) 0.8.

## APPENDIX B: STATISTICAL ANALYSIS OF RENE'95 OVERPEAK HOLD TIME DATA

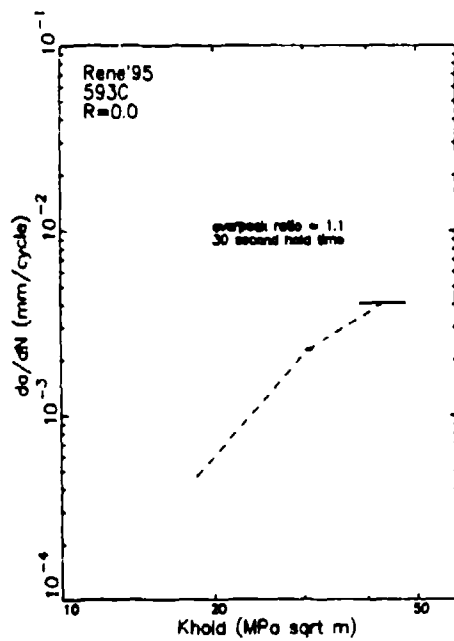
The figures in this appendix show the results of the statistical analysis of the Rene'95 overpeak hold time tests. The small rectangles in the figures enclose a region of plus and minus one standard deviation in crack growth rate ( $da/dN$ ) and  $K_{max}$ . The techniques used to establish these values were described in Section 4.4.2. The dashed lines in these figures connect the mean values of  $da/dN$  and  $K_{max}$  for cycles with constant hold times and R-ratio.



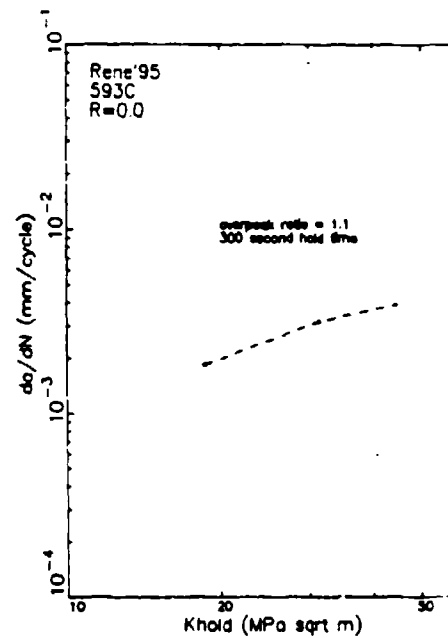
(a)



(b)

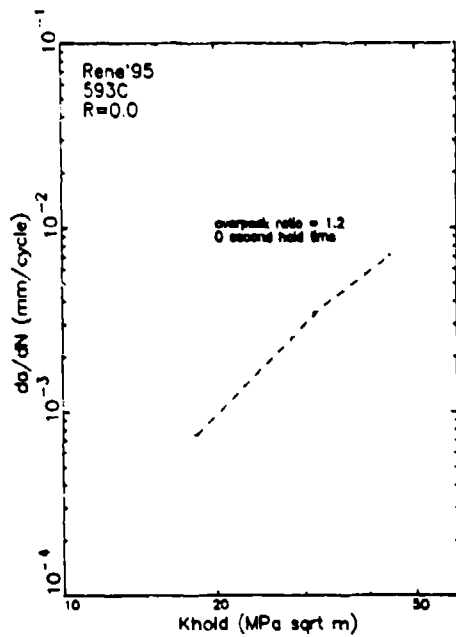


(c)

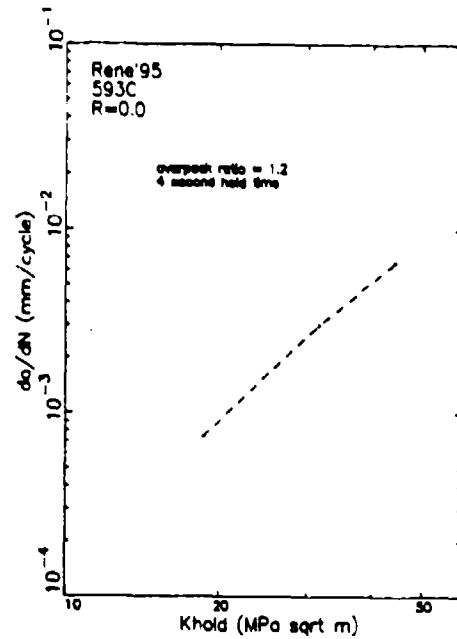


(d)

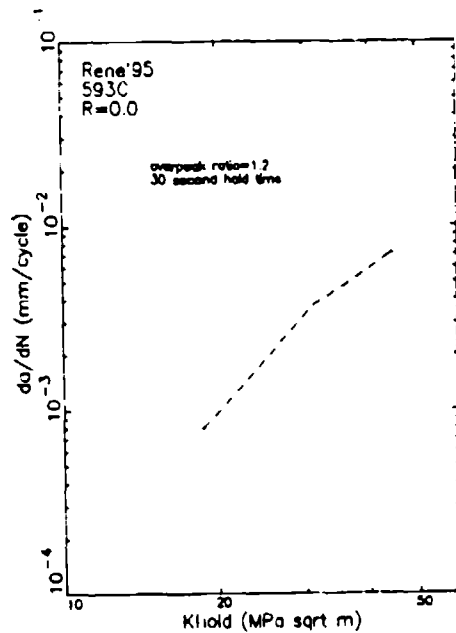
Figure B.1: Statistical analysis results of crack growth data from Rene'95 specimen AF73 cycled at 593°C with a 10% overpeak and R-ratio of 0.0 having hold times of (a) 0, (b) 4, (c) 30, and (d) 300 seconds.



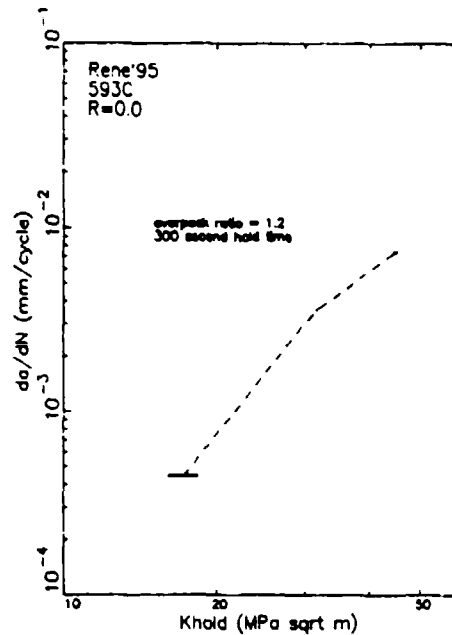
(a)



(b)

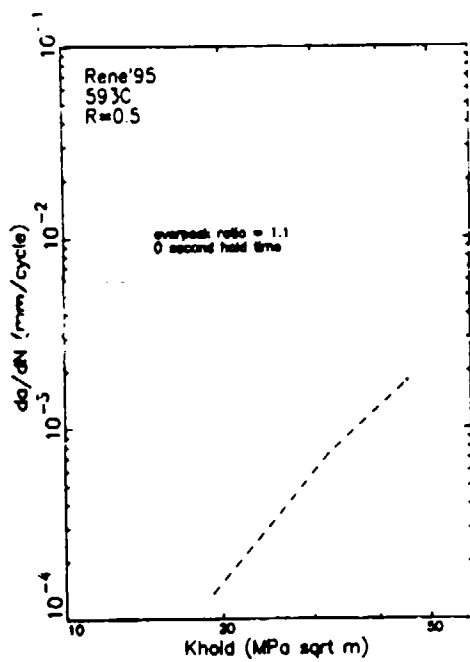


(c)

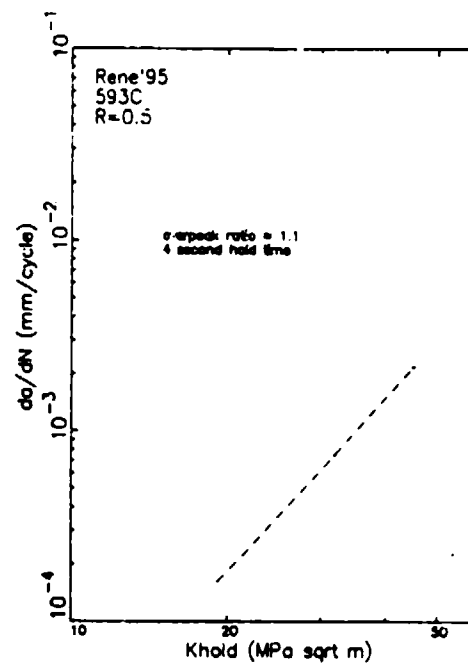


(d)

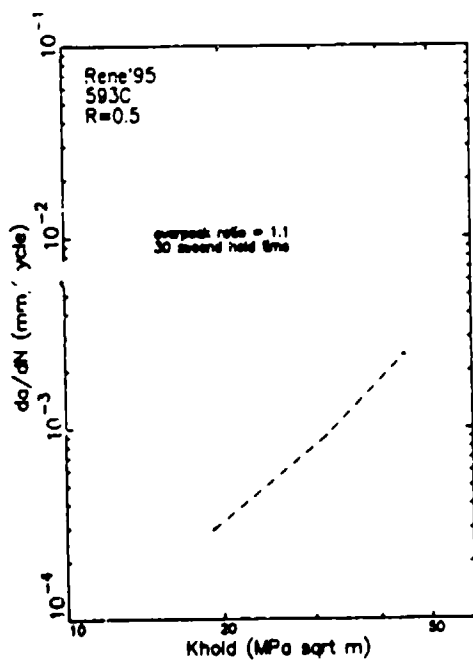
Figure B.2: Statistical analysis results of crack growth data from Rene'95 specimen AF28 cycled at 593°C with a 20% overpeak and R-ratio of 0.1 having hold times of (a) 0, (b) 4, (c) 30, and (d) 300 seconds.



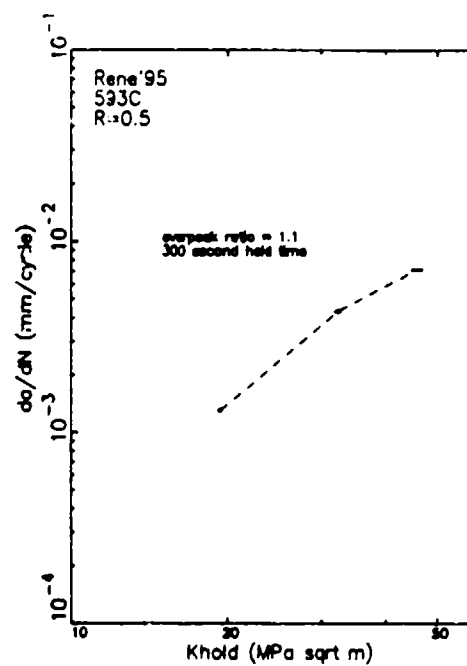
(a)



(b)

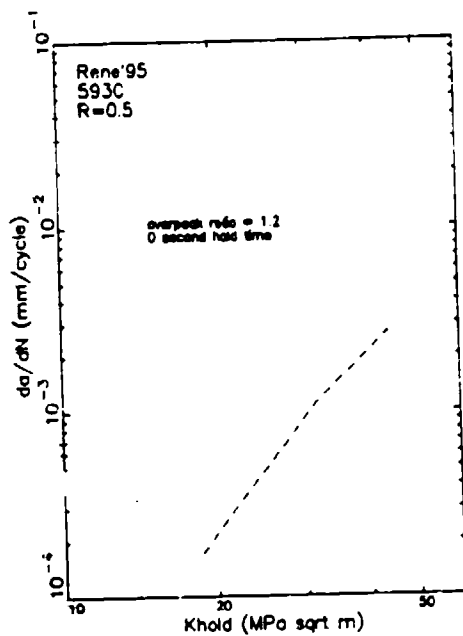


(c)

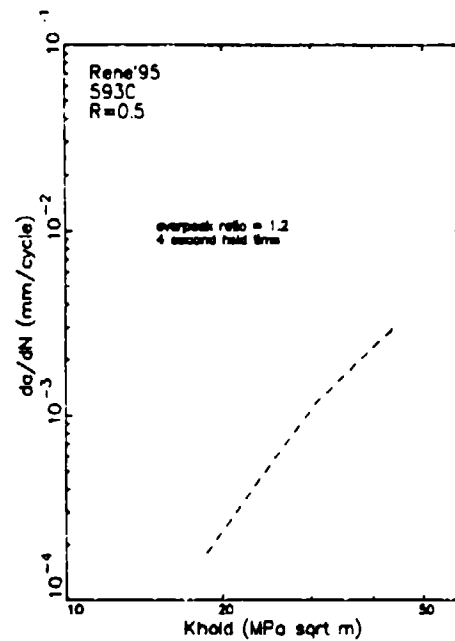


(d)

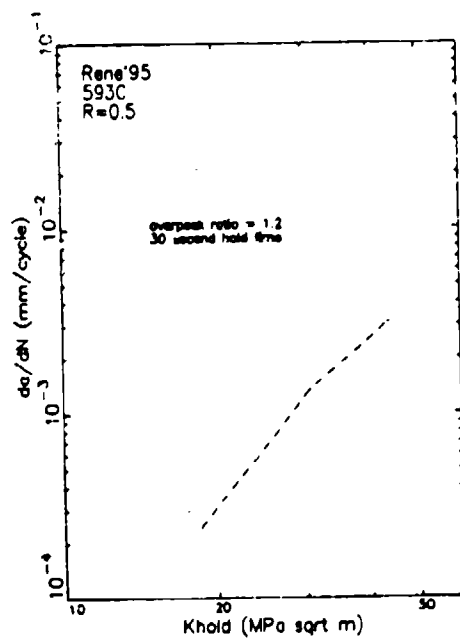
Figure B.3: Statistical analysis results of crack growth data from Rene'95 specimen AF73 cycled at 593°C with a 10% overpeak and R-ratio of 0.5 having hold times of (a) 0, (b) 4, (c) 30, and (d) 300 seconds.



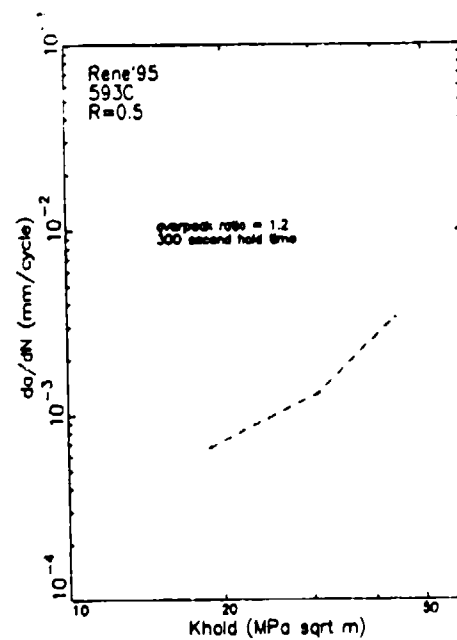
(a)



(b)

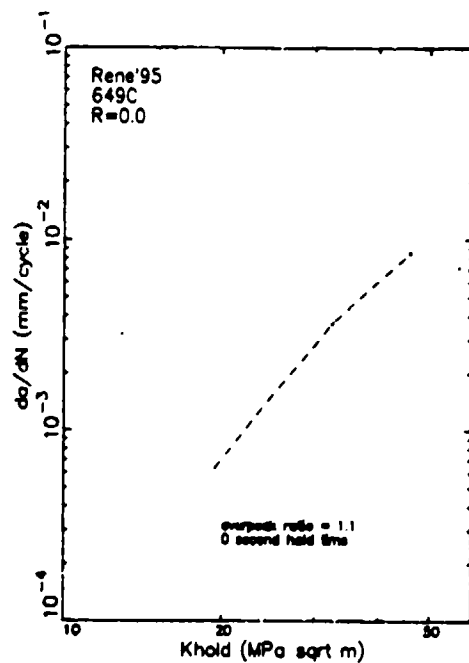


(c)

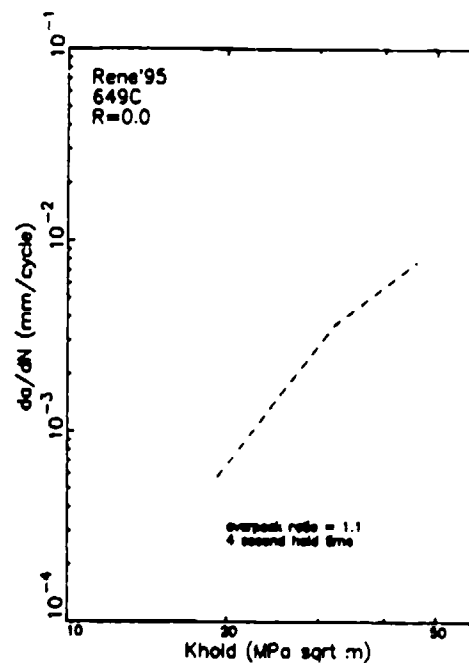


(d)

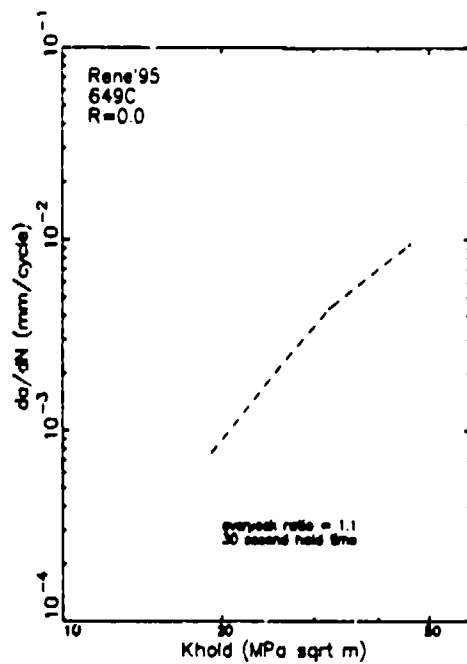
Figure B.4: Statistical analysis results of crack growth data from Rene'95 specimen AF43 cycled at 593°C with a 20% overpeak and R-ratio of 0.5 having hold times of (a) 0, (b) 4, (c) 30, and (d) 300 seconds.



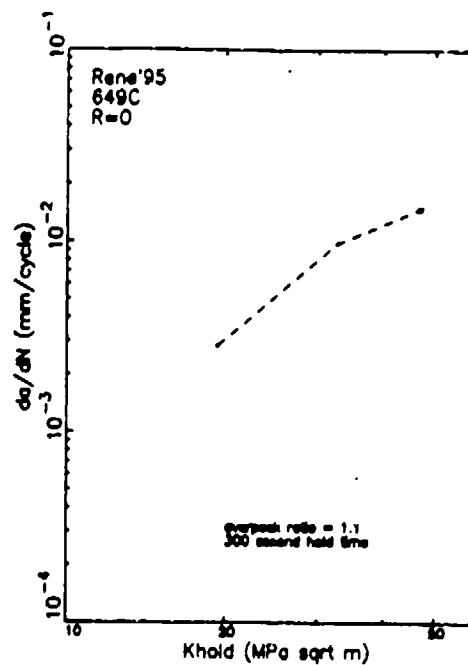
(a)



(b)

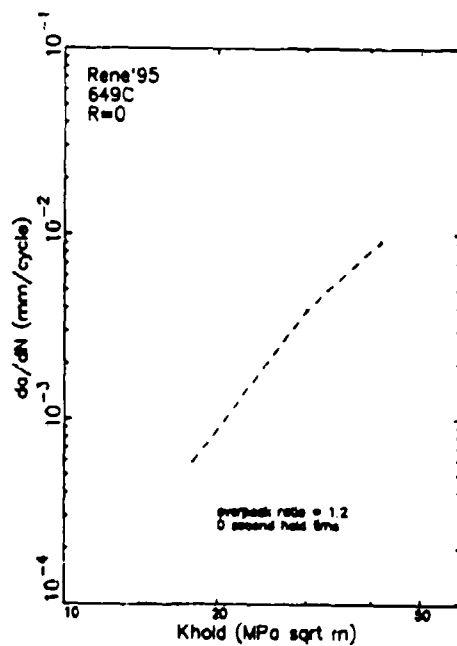


(c)

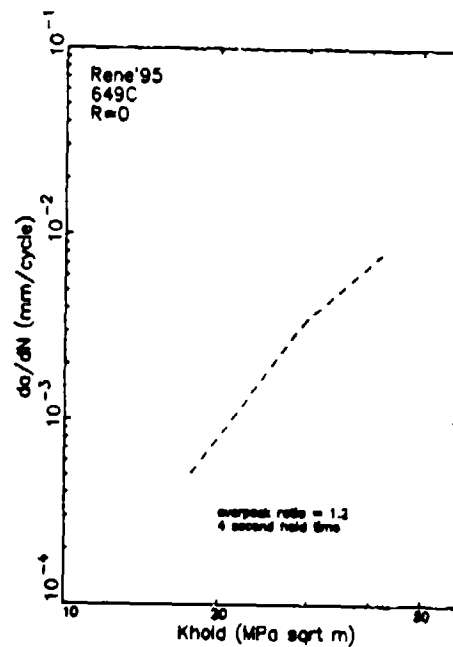


(d)

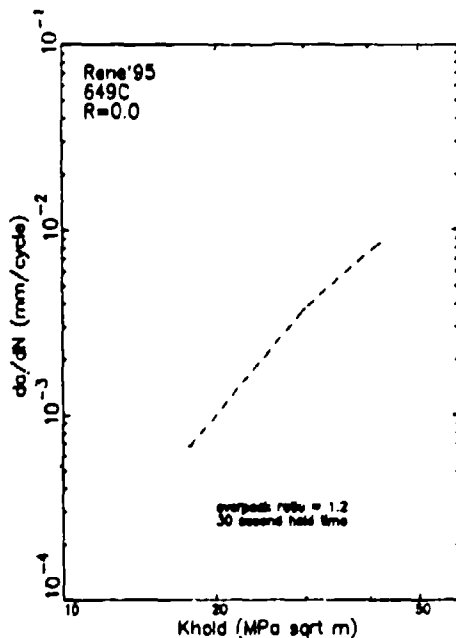
**Figure B.5:** Statistical analysis results of crack growth data from Rene'95 specimen AF68 cycled at 649°C with a 10% overpeak and R-ratio of 0.0 having hold times of (a) 0, (b) 4, (c) 30, and (d) 300 seconds.



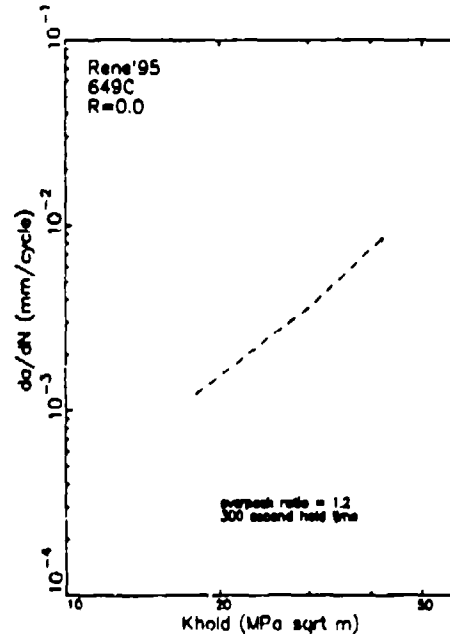
(a)



(b)



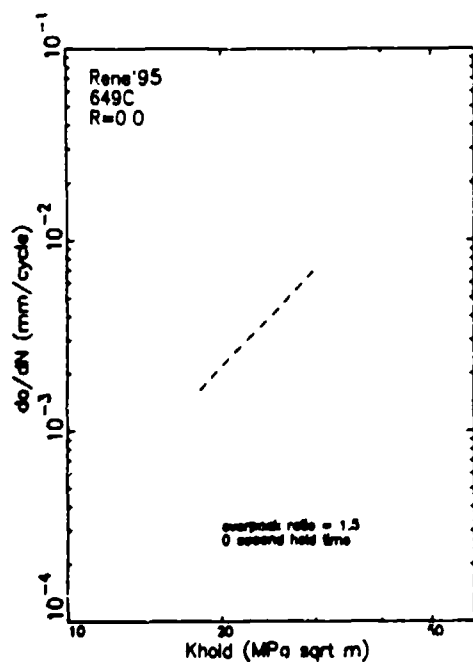
(c)



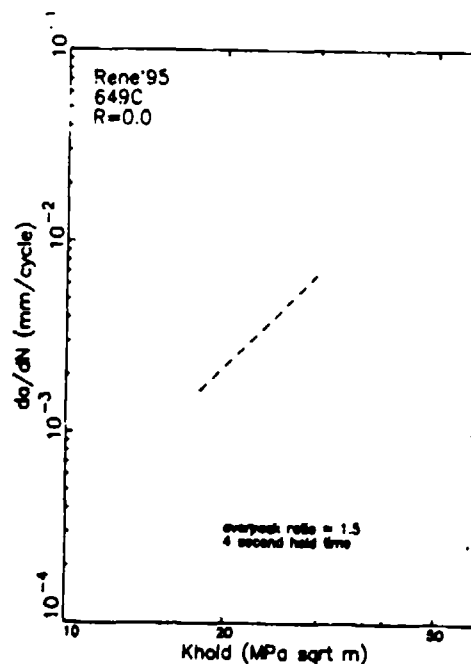
(d)

Figure B.6: Statistical analysis results of crack growth data from Rene'95 specimen AF29 cycled at 649°C with a 20% overpeak and R-ratio of 0.0 having hold times of (a) 0, (b) 4, (c) 30, and (d) 300 seconds.

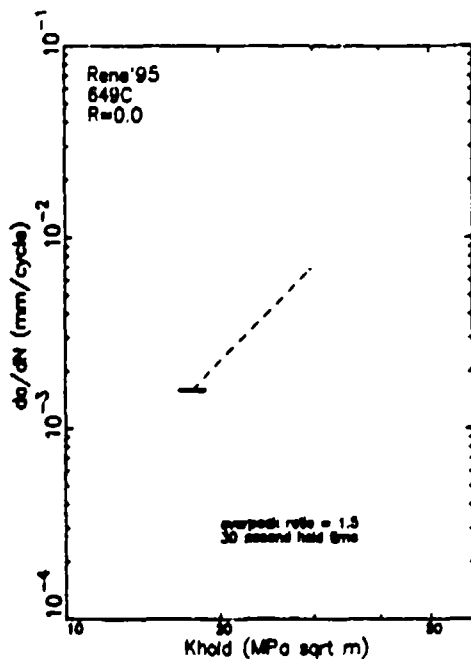




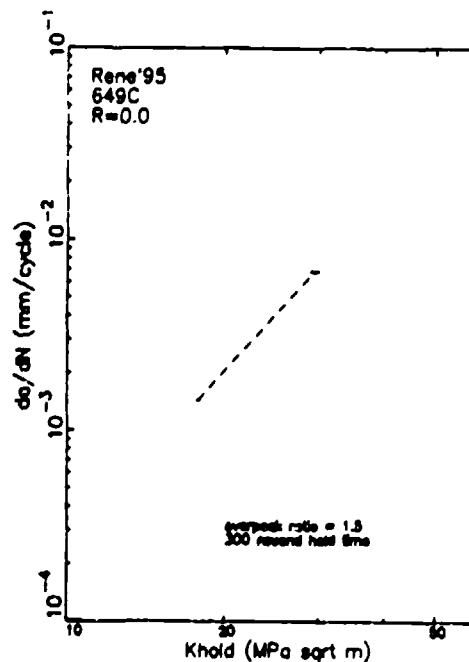
(a)



(b)

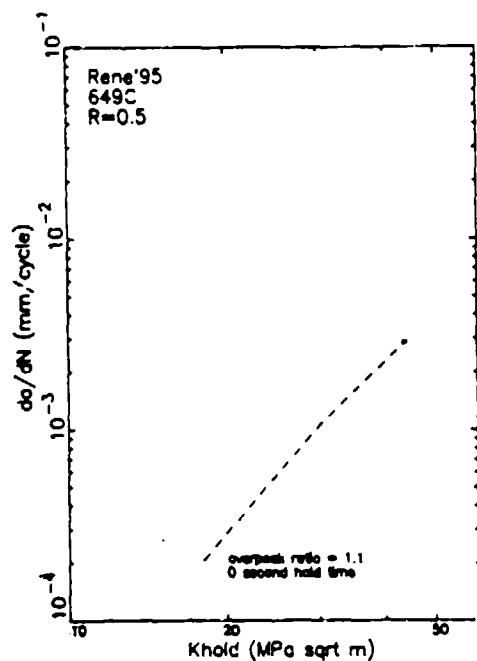


(c)

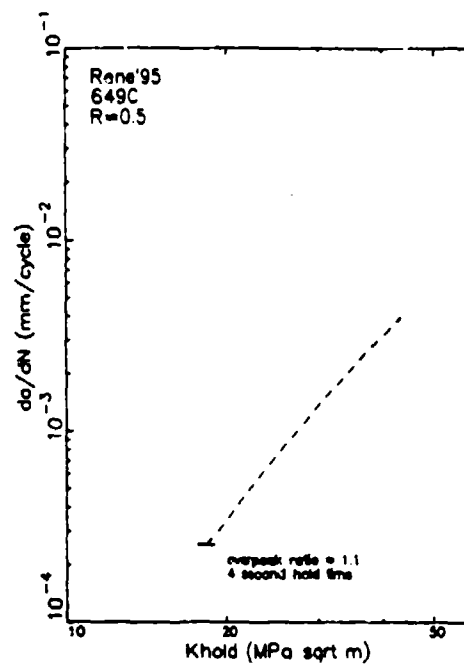


(d)

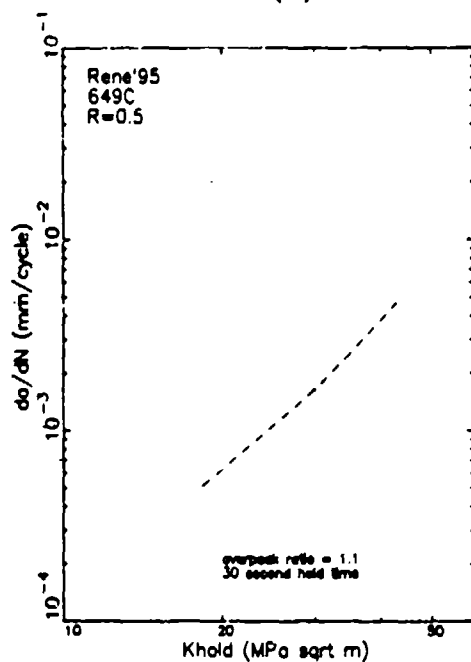
**Figure B.7:** Statistical analysis results of crack growth data from Rene'95 specimen AF34 cycled at 649°C with a 50% overpeak and R-ratio of 0.0 having hold times of (a) 0, (b) 4, (c) 30, and (d) 300 seconds.



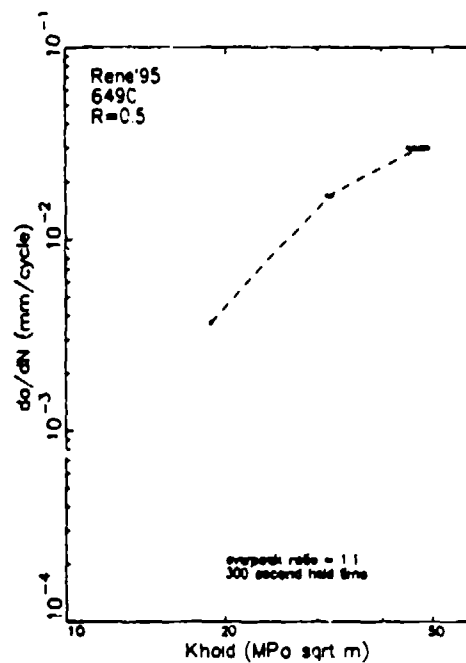
(a)



(b)

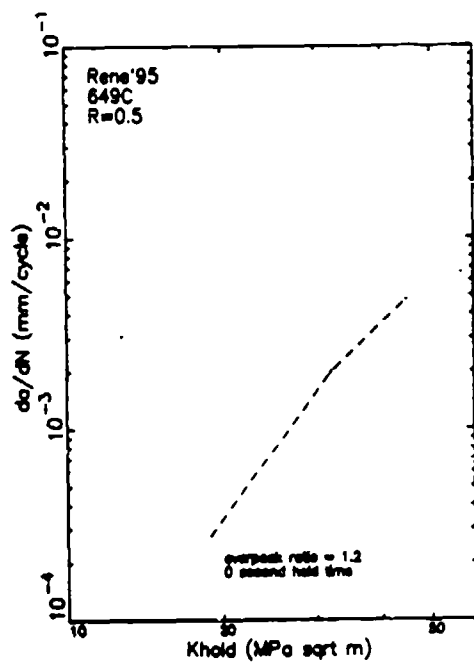


(c)

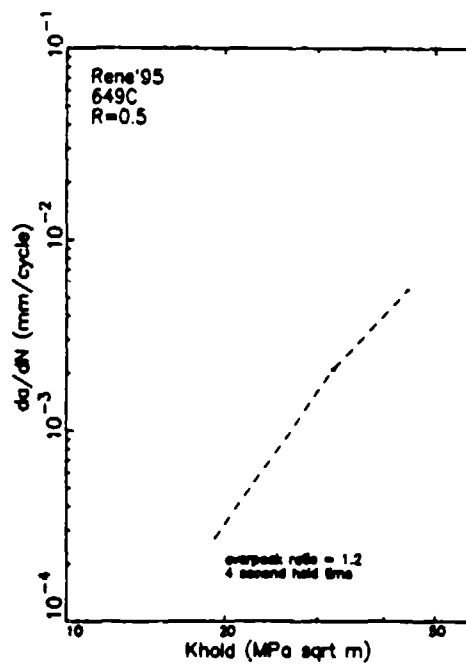


(d)

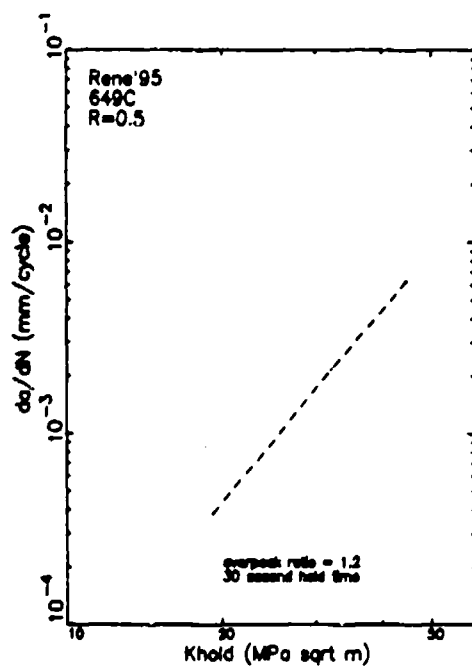
Figure B.8: Statistical analysis results of crack growth data from Rene'95 specimen AF75 cycled at 649°C with a 10% overpeak and R-ratio of 0.5 having hold times of (a) 0, (b) 4, (c) 30, and (d) 300 seconds.



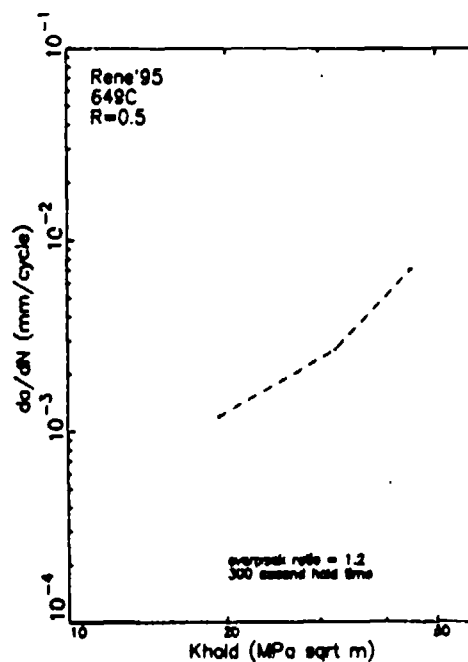
(a)



(b)



(c)

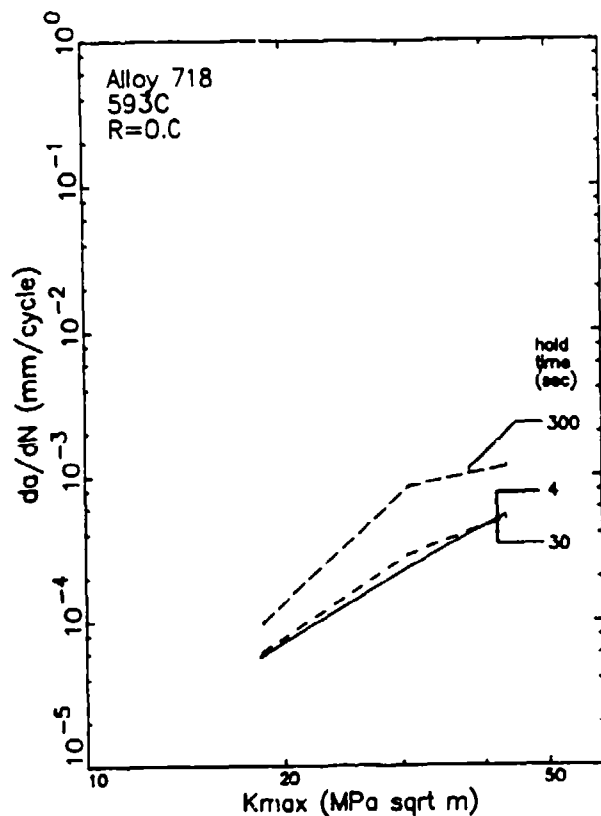


(d)

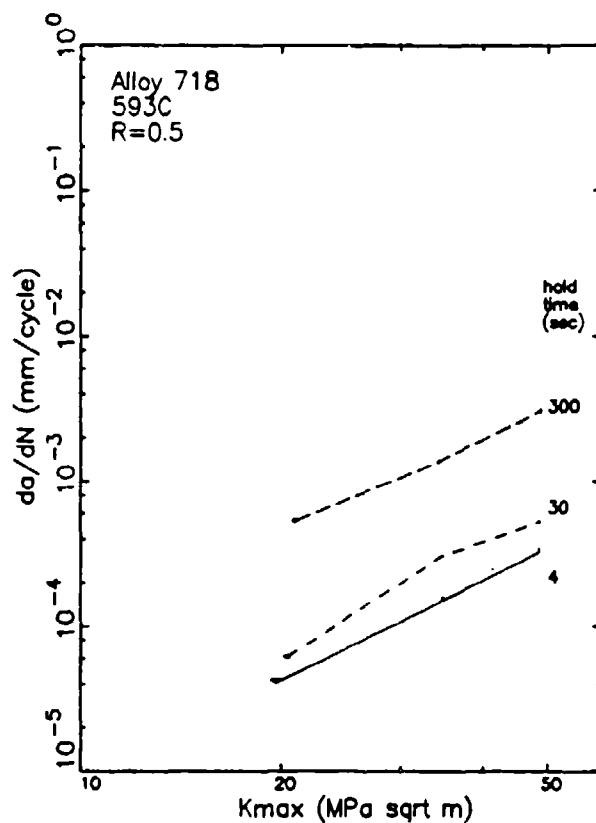
Figure B.9: Statistical analysis results of crack growth data from Rene'95 specimen AF35 cycled at 649°C with a 20% overpeak and R-ratio of 0.5 having hold times of (a) 0, (b) 4, (c) 30, and (d) 300 seconds.

#### APPENDIX C: STATISTICAL ANALYSIS OF ALLOY 718 CONSTANT $\Delta K$ DATA

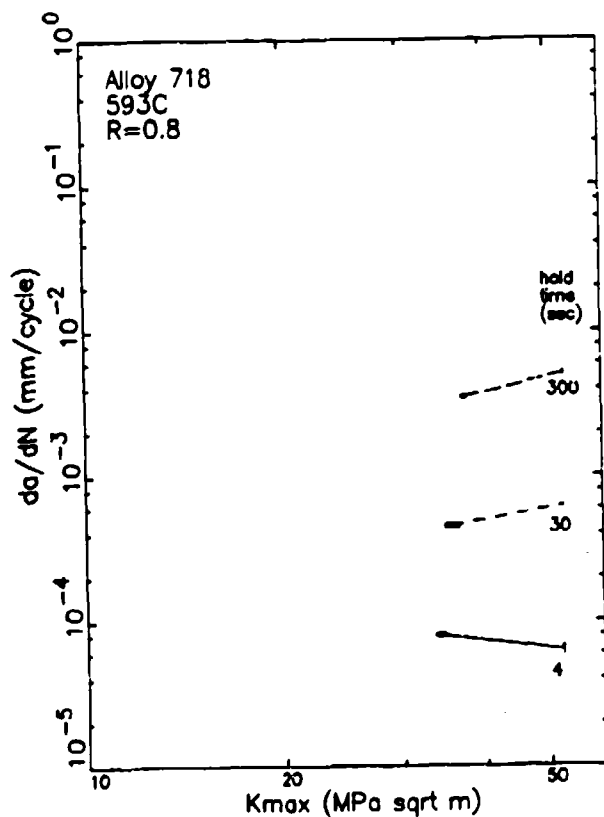
The figures in this appendix show the results of the statistical analysis of the Alloy 718 constant  $\Delta K$  tests. The small rectangles in the figures enclose a region of plus and minus one standard deviation in crack growth rate ( $da/dN$ ) and  $K_{max}$ . The techniques used to establish these values were described in Section 4.4.2. The dashed lines in these figures connect the mean values of  $da/dN$  and  $K_{max}$  for cycles with constant hold times and R-ratio.



(a)



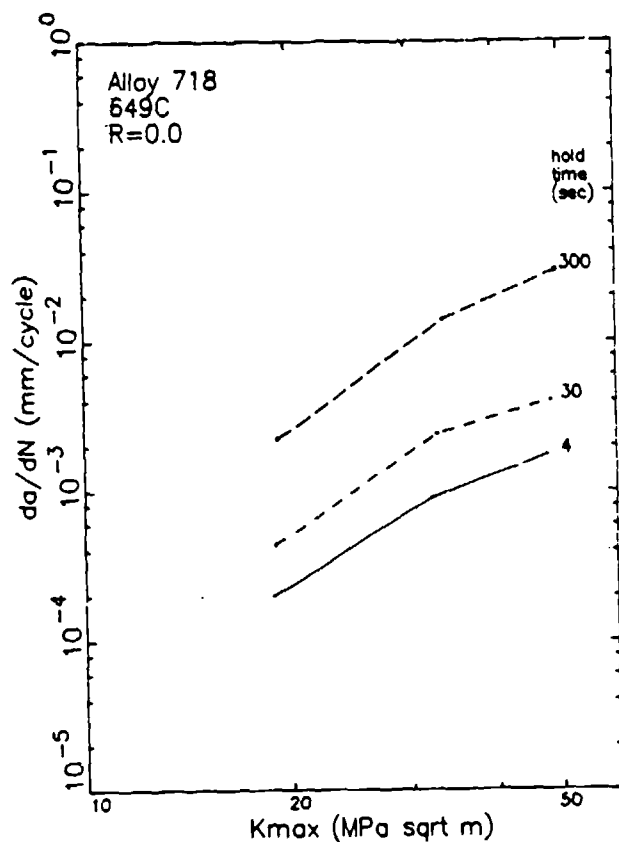
(b)



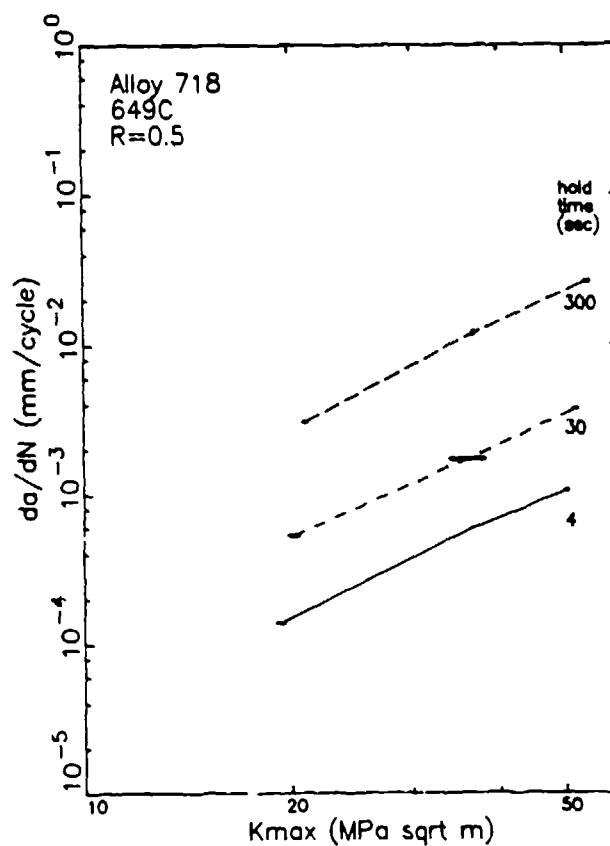
(c)

Figure C.1:

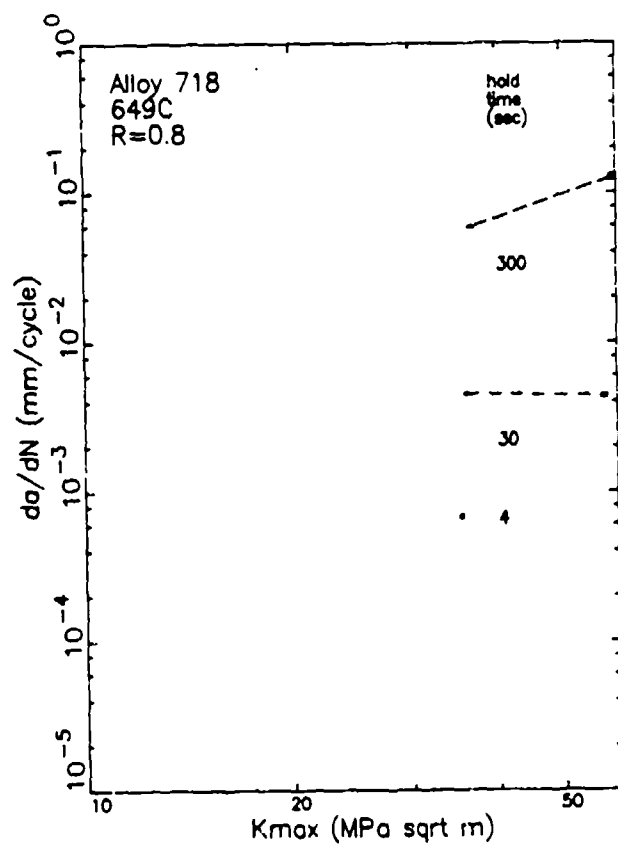
Statistical analysis results of Alloy 718 constant  $\Delta K$  hold time crack growth data from specimens cycled at 593°C with R-ratios of (a) 0.0, (b) 0.5, and (c) 0.8.



(a)



(b)



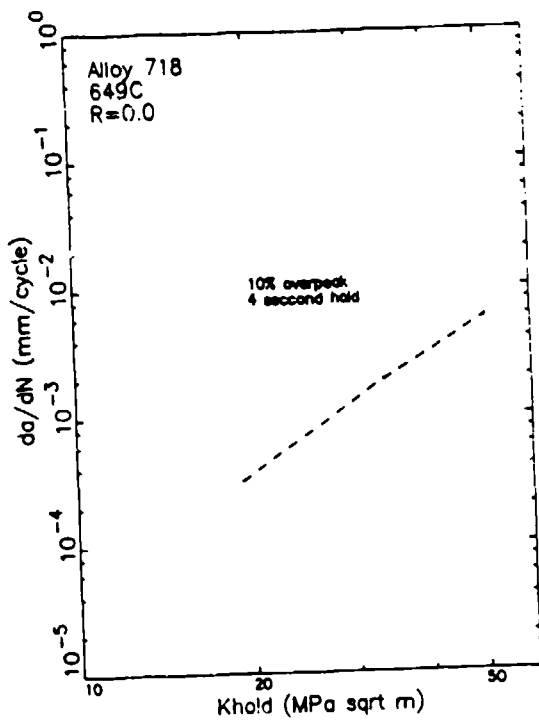
(c)

Figure C.2:

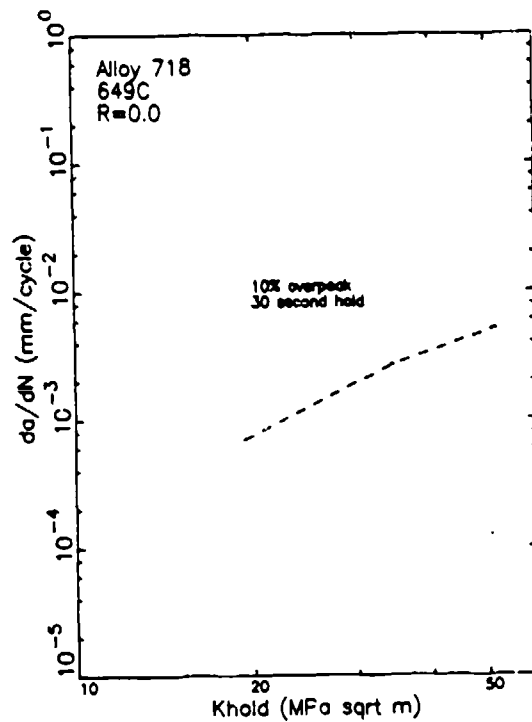
Statistical analysis results of Alloy 718 constant  $\Delta K$  hold time crack growth data from specimens cycled at 649°C with R-ratios of (a) 0.0, (b) 0.5, and (c) 0.8.

#### APPENDIX D: STATISTICAL ANALYSIS OF ALLOY 718 OVERPEAK HOLD TIME DATA

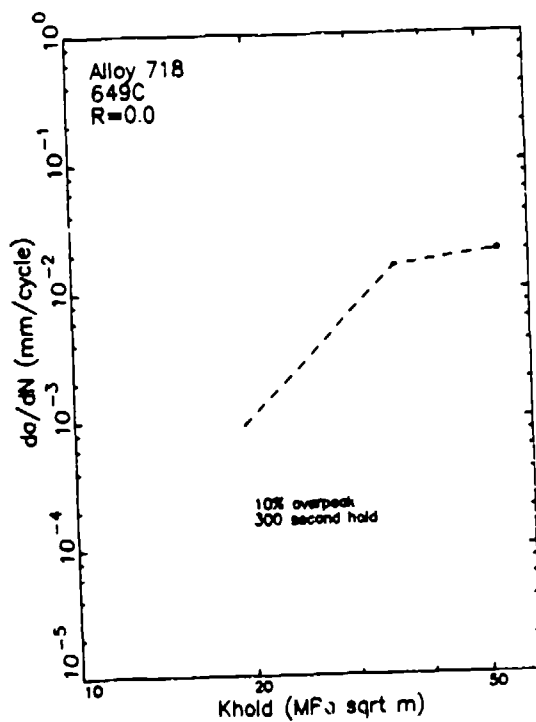
The figures in this appendix show the results of the statistical analysis of the Alloy 718 overpeak hold time tests. The small rectangles in the figures enclose a region of plus and minus one standard deviation in crack growth rate ( $da/dN$ ) and  $K_{max}$ . The techniques used to establish these values were described in Section 4.4.2. The dashed lines in these figures connect the mean values of  $da/dN$  and  $K_{max}$  for cycles with constant hold times and R-ratio.



(a)



(b)

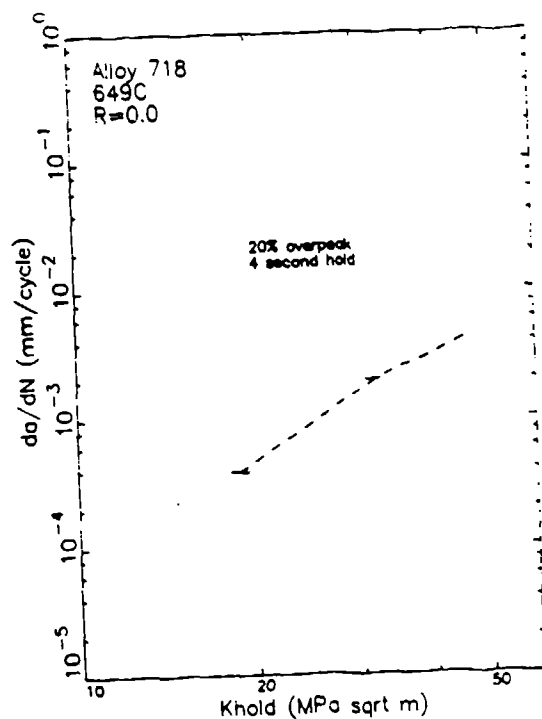


(c)

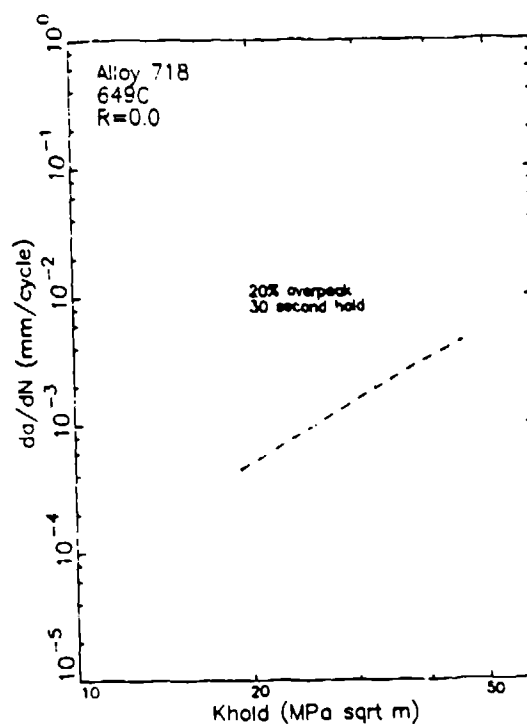
Figure D.1:

Statistical analysis results of crack growth data from Alloy 718 specimen A13-02 cycled at 649°C with a 10% overpeak and R.ratio of 0.0 having hold times of (a) 4, (b) 30, and (c) 300 seconds.

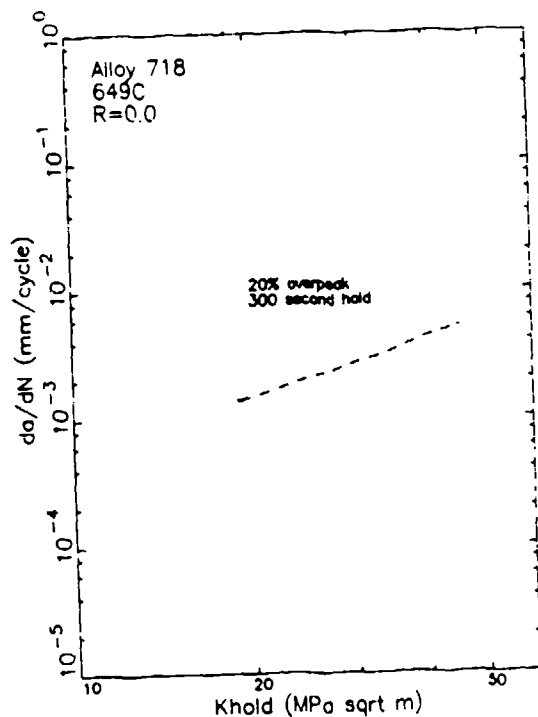




(a)



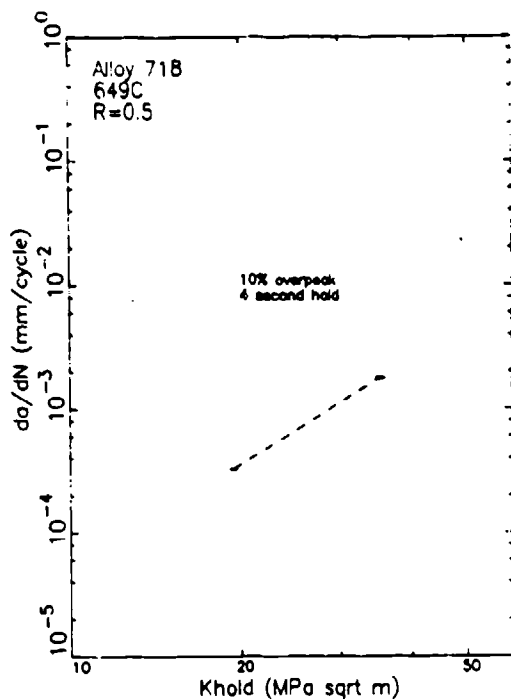
(b)



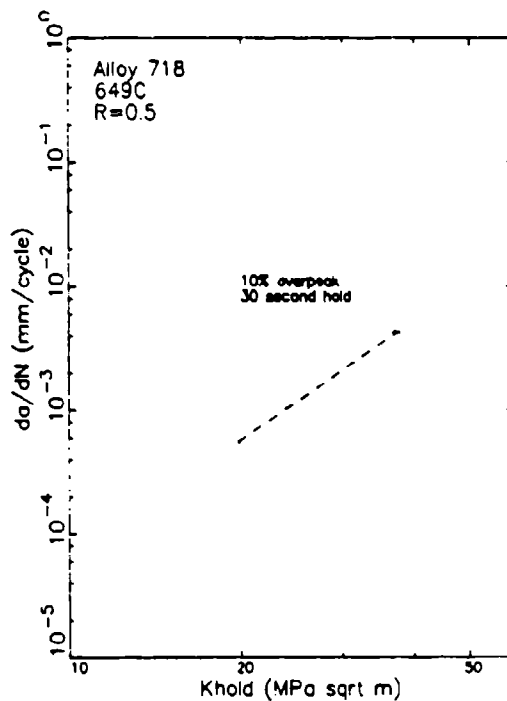
(c)

Figure D.2:

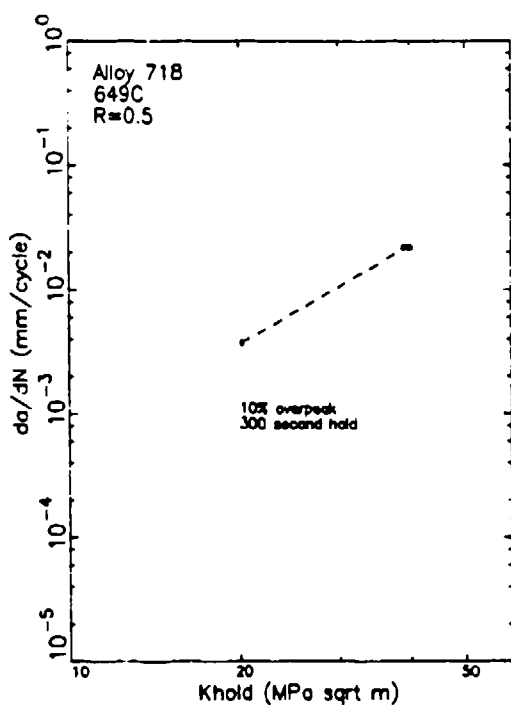
Statistical analysis results of crack growth data from Alloy 718 specimen A13-14 cycled at 649°C with a 20% overpeak and R-ratio of 0.0 having hold times of (a) 4, (b) 30, and (c) 300 seconds.



(a)



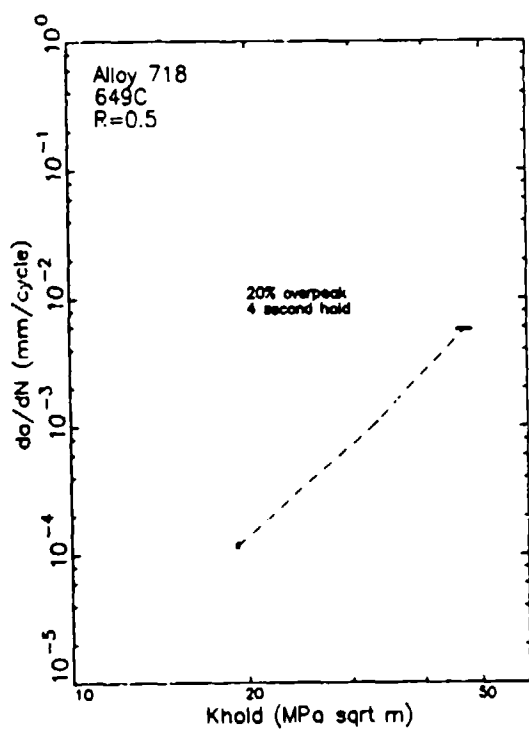
(b)



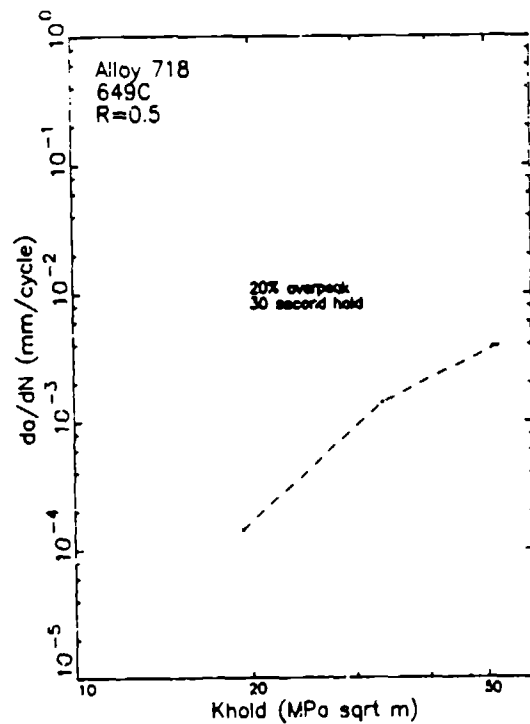
(c)

Figure D.3:

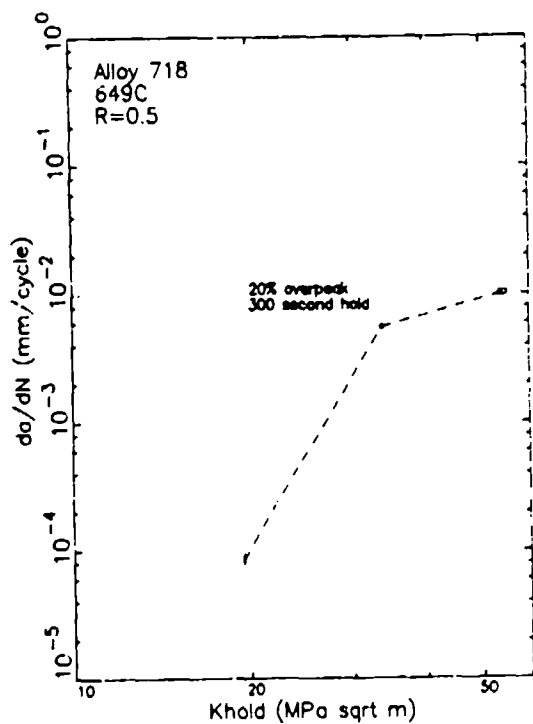
Statistical analysis results of crack growth data from Alloy 718 specimen A13-32 cycled at 649°C (1200°F) with a 10% overpeak and R-ratio of 0.5 having hold times of (a) 4, (b) 30, and (c) 300 seconds.



(a)



(b)



(c)

Figure D.4:

Statistical analysis results of crack growth data from Alloy 718 specimen A13-05 cycled at 649°C (1200°F) with a 20% overpeak and R-ratio of 0.5 having hold times of (a) 4, (b) 30, and (c) 300 seconds.